THE MARQUARDT CORPORATION

15 JULY 1963

FINAL REPORT

THRUST CHAMBER COOLING TECHNIQUES FOR SPACECRAFT ENGINES

CONTRACT NUMBER NAS-7-103
PROJECT NUMBER 278

REPORT 5981

VOLUME II

UNCLASSIFIED

(Title -- Unclassified)

FINAL REPORT
THRUST CHAMBER COOLING TECHNIQUES FOR SPACECRAFT ENGINES

For the Period
13 February 1962 to 12 February 1963

VOLUME II

Contract NAS 7-103

Project 278

PREPARED BY

J.G. Campbell, D.R. Batha,
M.D. Carey, A.R. Nagy, R.C. Stechman

APPROVED BY

M. E. Goodhart, Manager
Advanced Technology Development

CHECKED BY

C. D. Coulbert
Project Engineer

UNCLASSIFIED

THE Marquardt CORPORATION
VAN NUYS, CALIFORNIA

MAC A1198

CONTENTS

MAC A673

LIST OF TABLES

MAC A673

LIST OF ILLUSTRATIONS

LIST OF ILLUSTRATIONS (Continued)

MAC A678

LIST OF ILLUSTRATIONS (Continued)

MAC A673

LIST OF ILLUSTRATIONS (Continued)

MAC A673

LIST OF ILLUSTRATIONS (Continued)

MAC A673

LIST OF ILLUSTRATIONS (Continued)

MAC A673

LIST OF ILLUSTRATIONS (Continued)

MAC A673

LIST OF ILLUSTRATIONS (Continued)

MAC A673

LIST OF ILLUSTRATIONS (Continued)

MAC A633

LIST OF ILLUSTRATIONS (Continued)

I. SUMMARY

This is Volume II of the two volume final report on NASA Contract NAS 7-103. This volume presents thrust chamber design data and design approaches for the basic engine cooling techniques described in Volume I. Data on propellants and thrust chamber materials are included as well as additional data on space mission propulsion requirements and a bibliography of reports on rocket cooling and related topics.

This report supplements the studies presented in Volume I by facilitating more detailed design studies of promising thrust chamber cooling techniques. The readily available material referenced herein may be used to supplement this report by providing additional detailed design and test data for specific areas of interest. Some of the more recent and advanced research on thrust chamber cooling is reported in the technical journals listed in the bibliography.

II. INTRODUCTION

The objectives of the program conducted under this contract were:

1. To determine the applicability and limitations of the various thrust chamber cooling methods for liquid propellant rocket engines used to fulfill spacecraft propulsion requirements.

2. To present thrust chamber design procedures for each cooling technique and to provide a basis for comparing different cooling designs on the basis of applicability, weight, performance, etc.

3. To develop and present a rapid and convenient procedure for selecting the most suitable cooling method for the various spacecraft engine applications.

Volume I has presented the procedure for selecting the most promising cooling techniques along with preliminary design data to facilitate an evaluation of the limitations on each cooling method as well as permitting a thrust chamber weight comparison to be made.

This volume presents the analytical background for these studies. Answers are provided to such design problems as:

1. Over what thrust range can a regeneratively cooled thrust chamber be throttled?

2. What are the effects in a radiation cooled thrust chamber of surface emissivity, external fins, axial heat conduction and internal reradiation?

3. How does char depth in an ablative chamber vary with pressure, duty cycle and material formulation?

4. What are the theoretical capabilities of film and transpiration cooling at different thrust levels and chamber pressures?

To assist in making the required heat transfer and design calculations, physical and thermal property data are presented for the various propellants and structural materials of greatest interest. The bibliography, which is organized by subject entries, refers to reports and articles readily available which contain supplementary design data and test results.

Background information on space mission maneuvers and propulsion requirements are included to describe the typical operational and environmental conditions under which a cooling technique must operate.

III. THRUST CHAMBER COOLING METHODS

A. Regenerative Cooling

In the design of rocket thrust chambers for space mission applications, regenerative cooling is one of the foremost methods for insuring structural integrity of the components. This method is particularly well suited for long durations of operation above the chamber pressure limit of satisfactory radiation cooling. As a general rule, the regenerative designs require less exotic materials than do alternate methods, and at the present state of the art exhibit a higher reliability. They are compromised, however, by a certain degree of manufacturing complexity associated with the cooling passage geometry. The inherently higher propellant system pressure requirement and the attendant weight factor are also important considerations in a thorough analysis.

Regenerative cooling of chemical rocket engine thrust chambers, in its simplest form, consists of equating the heat energy rejected by the combustion products to their enclosing walls to the heat energy that is absorbed by the cooling fluid. The term regenerative implies that the cooling fluid is one or both of the propellants used prior to injection, although the coolant flow rate need not be the same as that supplied to the injection plate. In most instances, the fuel is used as the cooling fluid since, for the propellant combinations under consideration for space application, the only oxidizers which have any appreciable cooling potential are nitric acid (IRFNA) and nitrogen tetroxide (N_2O_4). (Figure 1) There may be, however, specific applications where the use of the oxidizer as a primary or auxiliary coolant can be shown to be advantageous.

To produce a successful regeneratively cooled design, it is necessary to balance the factors affecting the rejection and absorption of heat so as to result in sound structural temperatures along with pressure losses and component weights that are in line with the mission requirements. Among the parameters that have to be considered in predicting heat rejection are the nozzle thrust (F), chamber pressure (P_c), expansion area ratio (ϵ), combustion zone characteristic length (L^*), and the propellant combination with its associated mixture ratio, performance, thermodynamic and transport properties. The flow of heat into the coolant fluid is affected by the coolant mass velocity (flow rate per cross-sectional area for coolant flow), temperature, fluid properties, the degree of subcooling, and for some fluids the ratio of the wall temperature to the bulk fluid temperature. Conditions existing across the wall of the thrust chamber are determined by the material, its thermal conductivity, and the thickness of the wall.

The general equation covering the situation is the Newton equation for heating or cooling, which is:

$$Q_x = U_x A_x (T_g - T_c)_x \qquad (1)$$

where

Q = Heat flux

A = Area for heat transfer

U = Overall coefficient for heat transfer

T_g = Forcing temperature of the heat rejecting fluid

T_c = Temperature of the heat absorbing fluid and x refers to values at a specific location

The overall coefficient for heat transfer U is usually given by the following relationship:

$$U = \frac{1}{\sum_{1}^{n} R_i} \tag{2}$$

where the R_i are the resistances to heat transfer.

Or the familiar case of two convective films separated by a single wall, shown by the following equation:

$$U = \frac{1}{\frac{1}{h_1} + \frac{1}{k/t} + \frac{1}{h_2}} \tag{3}$$

where

h = Convection coefficient

k = Wall thermal conductivity

t = Wall thickness

This representation is strictly true only for situations wherein the heat transfer paths are in series. This is not the case for radiation heat transfer in combination with convective heat transfer. Thus, whenever a surface has a radiation component that represents an appreciable fraction of the convective components, as in very low chamber pressure applications, a slight modification must be made to the method of analysis. This will be illustrated in the succeeding work.

In order to show qualitatively the cross-effects of the parameters referred to previously for regenerative cooling, it is necessary to look further into the mechanisms of heat transfer and the correlating equations that are used to describe them, and to examine the rocket performance equations that determine the geometry and operating range of the thrust chamber.

Considering first the cooling side (inside the cooling passages) of the problem, two different mechanisms of heat transfer are evident: forced convection and nucleate boiling, and three different types of fluids; stable liquids, cryogenics, and two-phase mixtures. The forced convection to liquids and gases is characterized by the familiar heat transfer coefficient concept. Here empirical or semiempirical formulas are used to predict local values of the heat transfer coefficient based on the parameters of fluid flow, passage geometry, and fluid properties. For example, liquids are often correlated by the following Seider-Tate equation:

$$h_c = 0.023 \frac{k}{D} (Re)^{0.8} (Pr)^{0.33} (\mu_b/\mu_w)^{0.14} \qquad (4)$$

while for cryogenic fluids (H_2) the equation is:

$$h_c = 0.025 \frac{k}{D} (Re)^{0.8} (Pr)^{0.4} (T_b/T_w)^{0.55} \qquad (5)$$

By reducing these equations to groups involving properties, geometry, and flow factors, we can examine the trends that would result from changes in various design parameters for liquids, as follows:

$$h_c = C \left(\frac{k^{0.67} C_p^{0.33}}{\mu^{0.47}} \right)_b \frac{G^{0.8}}{D^{0.2}} \left(\frac{\mu_b}{\mu_w} \right)^{0.14} \qquad (6)$$

and for cryogenic fluids, the equation is:

$$h_c = C \left(\frac{k^{0.6} C_p^{0.4}}{\mu^{0.4}} \right)_b \frac{G^{0.8}}{D^{0.2}} \left(\frac{T_b}{T_w} \right)^{0.55} \qquad (7)$$

Equations (6) and (7) indicate that convective coefficients are increased by increasing the mass velocity and the fluid temperature. It is important to note, however, the effect of increased wall to fluid temperature ratios. Here, the tendency is to increase the liquid coefficients while reducing the gaseous ones. This result follows directly from the way in which the viscosity varies as a function of temperature. Thus parametric curves indicating the effect of a single parameter on the convective heat transfer coefficients are represented by the following sketches:

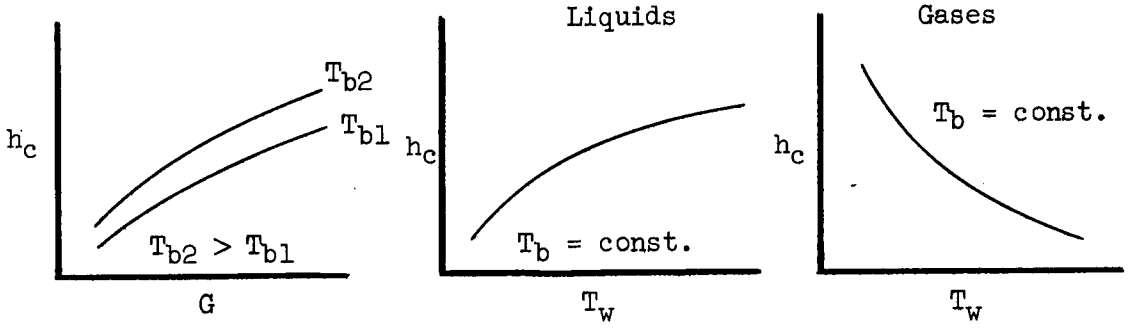

When the local heat transfer rates are so high as to produce wall temperatures in excess of the coolant fluids saturation temperature, a heat transfer mechanism known as nucleate boiling comes into play. Here vapor bubbles are formed on the hot surface, they detach and migrate toward the cooler regions of the flowing fluid, where they are then condensed. In this situation, the temperature of the wall is characterized by the coolant's saturation temperature over a wide range of nucleate boiling heat transfer rates. The line segment BB'C in the sketch below represents the nucleate boiling range.

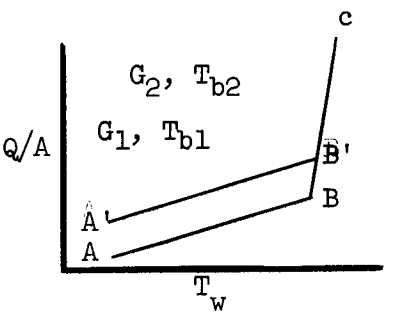

Neither the coolant mass velocity (G), nor its bulk temperature have any appreciable effect on the value of the wall temperature. Line segments AB and A'B' represent the forced convection regime and illustrate the effect of these parameters. The point C corresponds to the upper limit heat flux. This point is envisioned as that at which bubbles are formed at such a rate that a blanket of vapor tends to cover the wall completely forcing its temperature to rise drastically and usually resulting in failure. The method of design in a component utilizing

nucleate boiling as the heat transfer mechanism is to provide values of the upper limit heat flux capability that are everywhere in excess of the predicted local heat rejection rates. This is a difficult procedure to describe mathematically as there are very few correlating equations for the prediction of the upper limit heat flux. However, a great deal of experimental information is available in chart and tabular form that serves to illustrate the importance of fluid velocity, subcooling (saturation temperature minus bulk temperature) and pressure, as in the sketches shown below and in Figure 1.

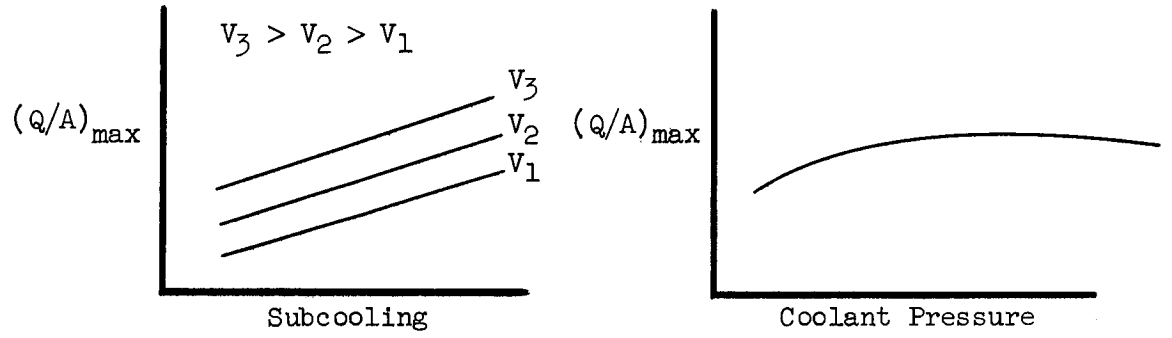

The two-phase mixtures where the fluid undergoes a change of phase during the cooling cycle are usually treated with convection equations modified to account for the quality of the fluid.

Heat rejection to the walls from the combustion gases is again a case of forced convection. The coefficient of heat transfer is predicted by the following modified Bartz equation:

$$h_g = 0.026 \frac{G^{0.8}}{D^{0.2}} \frac{\mu_s^{0.2}}{(Pr)^{0.6}} \left(\frac{H_r - H_w}{T_r - T_w}\right) \left(\frac{H_s}{H_f}\right)^{0.68} \qquad (8)$$

As with the previous equation for forced convection, the coefficient is seen to increase with increases in the mass velocity and fluid temperatures and to be affected by temperature difference across the boundary layer.

1. Regenerative Cooling Considerations

a. Performance Efficiency

For the regenerative cooling parameter studies in this program a performance efficiency of 100% shifting equilibrium was utilized. Reductions in performance level have, in general, only minor effect on the cooling circuit design features. For instance, a 5% loss in C* efficiency would bring about approximately 8% lower heat transfer rates and 5% greater total heat absorbing capacity. Hot wall designs, i.e., radiation and ablative cooling, exhibit greater sensitivity to efficiency due to the proportionately smaller temperature difference across the boundary layer.

MAC A 673

b. Mixture Ratio (O/F by Weight)

Selection of a rocket engine operating mixture ratio is the result of a careful balancing of the propellant performance characteristics and the overall spacecraft system and mission requirements. Thus each specific undertaking is quite likely to produce a slightly different ideal mixture ratio. Due to this flexibility the mixture ratio of 1.2 selected for the N_2O_4/N_2H_4 propellant combination represents only a single example of many possible realistic solutions. For this propellant combination the value of 1.2 corresponds to the near maximum levels of performance (I_{sp}) and combustion temperature. Table I illustrates the effect of changes in the mixture ratio on the local heat flux rates and total cooling potential for the propellant combinations considered herein. For a temperature limited coolant, such as hydrazine, the allowable heat rejection rate is limited by the total cooling potential, and hence, the nozzle size, or surface area cooled is limited.

c. Chamber Characteristic Length - L*

The combustion chamber characteristic length, defined as the chamber volume divided by the nozzle throat area, is an empirical factor frequently used in the design of rocket engines. Since this factor affects directly the geometry of a combustion zone some systematic method of L* selection is necessary to permit further investigations. Data pertaining to many thrust chamber designs were correlated in Figure 13 of Volume I, by a plot of L* as a function of nozzle throat area. It is not possible at this time to analytically predict L* requirements or to correlate them empirically for such factors as mixture ratio, chamber pressure, propellant, etc. However, the available data did seem to point out that the L* falls between 15 and 35 inches and generally increases with nozzle throat area. For this reason Figure 13 of Volume I was taken as the basis for all calculations dealing with combustion chamber geometry. For temperature limited coolants an increase in L* requires a corresponding reduction of the exit nozzle surface area which can be cooled so as to maintain a maximum heat transfer.

d. Nozzle Expansion Area Ratio - ϵ

In preparing this report a large number of combinations of thrust and chamber pressure were considered. So that a discrete value of nozzle throat area could be assigned to each combination, a standard nozzle expansion ratio, and hence, thrust coefficient had to be assumed. Thus, a nozzle ϵ of 40:1 was taken as the basis for all calculations. If, for a temperature limited coolant such as hydrazine, an ϵ of 40:1 is not attainable by regenerative cooling some form of uncooled nozzle extension is postulated.

e. Nozzle Surface Area

All nozzles considered in this study were 75% bells having an initial expansion angle of 30° and an exit divergence angle of 10°. The surface areas of all nozzle satisfying these requirements are given in Figure 2 as a function of throat area and expansion ratio. Incremental surface areas are obtained by subtraction of the corresponding values. Surface areas upstream from the nozzle throat are correlated in Figure 3 as functions of contraction ratio and nozzle throat area. The combustion chamber L* relations, as previously discussed, are inherent in this set of curves.

f. Cooling Circuit Configuration

The coolant passage flow configuration must be tailored to the specific requirements of the propellant combination. For incompressible coolants such as hydrazine and Aerozine 50 a two-pass system is usually employed. In a two-pass system, one half of the surface area is cooled by the coolant as it flows through alternating tubular passages from the injection end of the thrust chamber toward the nozzle exit plane where the flow reverses and cools the remaining half of the surface area on the return pass to the injector plate. Primary advantages of the two-pass cooling system are an effective doubling of the flow area for the same coolant velocity resulting in larger passage dimensions, and the elimination of large manifolds on the expansion nozzle bell. The disadvantages of this system are limited to a larger pressure drop due to the longer effective length of passage.

Compressible coolants, such as hydrogen, requiring much higher velocities have a correspondingly higher pressure drop for two-pass cooling systems. In addition, the heat transfer coefficient for hydrogen increases as the fluid temperature rises. Since hydrogen is normally tanked at sub-critical temperatures (60°R) the cooling of high heat fluxes associated with nozzle throats would not be feasible at this inlet temperature. For these reasons, the hydrogen coolant is introduced downstream of the nozzle throat at as low an expansion area ratio as is practical from the standpoint of local heat transfer rates. The fluid cools a portion of the expansion nozzle, reverses direction, and cools the remaining nozzle area as it passes on to the injector plate. Thus the hydrogen is well removed from the critical temperature region when exposed to the high heat fluxes at the nozzle throat.

Since the supply and distribution manifolding for hydrogen are much larger than the similar items for denser fluids placing of the manifolding at the lowest possible expansion area ratio is relatively important from a weight standpoint.

In summary, for the purposes of this study a two-pass cooling system was assumed for hydrazine and Aerozine-50 while a pass and one-half flow system was used for the hydrogen cooled motors.

MAC A673

g. Pressure Losses

An accurate calculation of the cooling circuit pressure drop cannot be made without specifying in some detail the cooling passage geometry. This detail would include not only the passage configuration at the critical nozzle throat region but at several intermediate positions along the length of nozzle and combustion chamber as well. Since the specification of such a vast amount of detailed design information is beyond the intention of this study a rule of thumb approximation has been substituted for actual pressure drop calculations. This approximation considers that the coolant circuit pressure loss is equal to twice the coolant velocity head at the nozzle throat. Figure 4 shows the velocity head, expressed in lb/sq in. as a function of the coolant velocity in ft/sec, for a density of 56 lb/ft^3. Correction for other densities is accomplished by inverse ratio. When limited to incompressible fluids the method should have an accuracy of about 10 to 20%.

An IBM 704 computer program, available for the hydrogen cooling phase of this program, allowed accurate calculations to be made for the compressible flow pressure drops. Both total pressure and Mach number distributions were available for all hydrogen cooling correlations.

Whenever the pressure loss through the injector plate was of any significance, as for the prediction of coolant supply pressure, it was assumed for comparison purposes that a satisfactory injector design could be produced having a pressure drop of 10% of the combustion chamber pressure. This assumption may be modified as warranted by specific considerations discussed later in this report.

2. Specific Considerations for the N_2O_4/N_2H_4 Propellant Combination

a. Local Heat Rejection Rates

As stated previously the wall temperatures of a cooling jacket transferring heat by nucleate boiling is characterized by the saturation temperature. Therefore, the Bartz (Reference 190) relationship for film coefficient can be solved directly without iterative procedures. Since the coolant saturation temperatures are very low in respect to the combustion temperatures, small errors in wall temperature will have a very negligible effect on film temperature drop and hence heat transfer rates. In the areas of the coolant jacket where nucleate boiling does not exist, the wall temperatures produced by the convective cooling coefficients are by nature below the saturation temperature. So the difference between combustion temperature and wall temperature is even greater and slight errors have even less of an effect on heat transfer rates.

Thus it is apparent that whenever the primary mode of heat transfer to the coolant is nucleate boiling the calculation of local heat transfer rates becomes a direct solution of the combustion gas film coefficient using the Bartz, or some other suitable relationship.

b. Total Heat Capacity

One well known feature of hydrazine is its monopropellant capability. Its tendency toward self-propelled, explosive decomposition at elevated temperatures makes its use as a coolant for rocket engines a difficult problem. Due to these characteristics, the overriding consideration in a cooling system design with hydrazine is the maximum coolant temperature. Since it is a temperature limited fluid the conclusion follows that there exists a maximum total heat absorbing capacity.

When this property is related to specific chamber parameters such as thrust, chamber pressure, and performance the limit can be expressed in terms of maximum motor surface area. Two parameters necessary in determining the maximum cooled surface area are the nozzle contraction and expansion area ratios. The chamber L*, as determined from the nozzle throat area, coupled with the contraction ratio specifies the surface area upstream from the throat while the expansion area ratio fixes the surface area downstream from the throat.

To accomplish the above results it was necessary to complete a stepwise integration process of the motor surface area and the local heat flux values. Computations were made for two different contraction area ratios and that with the lowest total heat transfer was selected. Using combustion chamber surface areas as defined in Figure 3 it was determined that the total heat transfer to contraction area ratio chambers of 2 and 4 were identical at a nozzle throat area of 200 $in.^2$. Thus a contraction area ratio of 4:1 was used for throat areas less than 200 $in.^2$ while 2:1 was used whenever the throat area exceeded 200 $in.^2$. This serves to minimize heat transfer to the combustion chamber thereby allowing for larger nozzle expansion area ratios. The resulting maximum coolable nozzle expansion area ratios are presented in Figure 5 as a function of thrust and chamber pressure.

A great many factors have bearing on the maximum temperature to which hydrazine can be heated. Among them are the pressure, materials in contact with the fluid, contaminants that may be present, and local heating rate. A value of 350°F has been established as the upper limit for purposes of this study. At chamber pressures below 100 psia a modification has to be made in the maximum hydrazine temperature limit. Since, at these low pressures the saturation temperature is less than 350°F, it must be used as the criteria for establishing the maximum heat capacity of the coolant rather than the higher thermal decomposition value.

The effect of additives to inhibit the thermal and catalytic decomposition of hydrazine has received much study in recent years. Most promising among those additives extensively reported is ethylenediamine (EDA). A mixture of 90% hydrazine and 10% EDA serves to effectively inhibit thermal decomposition without seriously compromising either performance or heat transfer. While all conclusions of this study are based on commercially pure hydrazine, substitution of a 90/10 mixture should produce no major changes.

MAC A673

c. Designing for Local Heat Transfer Rates

A second characteristic feature of a hydrazine cooled rocket engine is the absorbing of heat through the mechanism of nucleate boiling. As previously described, nucleate boiling consists of the formation of vapor bubbles on a heated surface followed immediately by their rapid collapse in the surrounding sub-cooled liquid. Since, due to the nature of the heat transfer mechanism, the temperature of the heated surface is maintained at or slightly above the coolant saturation temperature, design of the cooling circuit reduces to the matching of local coolant velocity and heat transfer rates.

A great amount of experiment has gone into the graphical and mathematical correlation of nucleate boiling data. In general, each is valid for only a limited range of conditions. The JPL correlation for hydrazine has been used throughout this study. It consists of the following equation:

$$\frac{Qul}{A} = \left[1 - 0.236 \left(\frac{P - 675}{675} \right)^2 \right] \left[6.0 + 0.246V - T_b \left(0.015 + 2.7 \times 10^{-4} V \right) \right] \quad (9)$$

For

$100 < P < 1200$ psia

$1.0 < V < 93$ ft/sec

$67 < T < 347$°F

Where

$\frac{Qul}{A}$ = Maximum heat flux to coolant Btu/sq in. sec

P = Local pressure psia

V = Local velocity ft/sec

T = Local coolant temperature °F

Before a comparison is made with the predicted local heat rejection rate from the combustion gases, the maximum local heat flux to the coolant should be divided by a safety factor of 1.7. This factor stems from a combination of the uncertainties associated with both the film coefficient and upper limit heat flux correlations.

MAC A673

Coolant velocity requirements at the nozzle throat as determined from Equation (9) are presented in Figure 6 as a function of thrust and chamber pressure.

Of primary importance in selecting a coolant technique for a rocket engine system is knowledge of the required propellant supply pressure. The cooling jacket pressure drop is a parameter associated with regeneratively cooled systems that has strong bearing on the entire design procedure. As previously discussed the jacket pressure loss has been assigned a value equal to two velocity heads at the maximum coolant velocity. This relationship is shown in Figure 4 for a fluid density of 56 lb/ft^3. Based on the requirements for maximum cooling velocity as stated above, Figure 7 illustrates the coolant (fuel) supply pressure as a function of thrust and chamber pressure. An injector pressure drop of 10% of chamber pressure level has been included in the figures.

d. Coolant Jacket Geometry

Once the coolant flow rate, velocity, temperature, and pressure have been established, the required cross-sectional area of the cooling jacket follows directly from the continuity equation. The problem of designing a cooling jacket consists simply of distributing the total area around the circumference of the nozzle in a manner consistent with manufacturing capabilities.

The actual passage shape (minimum width and width to height ratio) has little effect on heat transfer. Secondary effects such as two-dimensional heat conduction in passage walls and boundary layer variations in corners have been ignored in this study. Consequently, all considerations leading to limits on coolant passage shape are derived from stress and manufacturing criteria. The primary limitations bearing on all passage shapes are the minimum height to width ratio of 1.0 (square passages), a minimum dimension of 0.06 inch and a minimum wall thickness of 0.01 inch.

Based on these limitations an expression can be developed to relate basic thrust chamber dimensions to basic coolant passage dimensions. This expression is:

$$\frac{Acj}{\pi D} = X + 4t\left(\frac{t - X}{X}\right) = X - 4t\left(1 - \frac{t}{X}\right) \qquad (10)$$

Where

Acj = Coolant jacket cross-sectional flow area

D = Chamber diameter

X = Coolant passage external dimension

t = Coolant passage wall thickness

MAC A673

Equation (10) is based on square passages having a wall thickness of 0.01 inch. The variation of these factors is illustrated in Figure 8 where a plot of Equation (10) is shown. Considering the basic assumption of 0.06 inch minimum passage dimension, and a two-pass flow system, a minimum passage factor of 0.0265 is indicated. Regions of passage height greater than width (B > X) and less than width (B < X) are also shown.

This illustration defines, without the need for detailed analysis, the coolant jacket construction limitations in terms of available thrust chamber design information. Continuing one step further, the passage factor ($Acj/\pi D$) can be correlated against chamber pressure and thrust as shown in Figure 9. All points in the region above $Acj/\pi D = 0.0265$ are possible from a cooling jacket geometry standpoint. Given a value of passage factor from Figure 9 based on a thrust and chamber pressure combination, the individual passage dimension can be determined by the data in Figure 8. Possible solutions lie in the range B > X, between the minimum practical dimension (assumed) and the maximum allowable dimension (B = X).

All of the above discussion is based on longitudinal, two-pass cooling systems. Minor considerations given to helical wrap cooling jackets did not point out any areas of operation forbidden to longitudinal designs. The inherent disadvantages of helical wrap chambers for high pressures and large nozzle expansion area ratios seem to preclude further investigation.

e. Effect of Cooling Smaller Expansion Area Ratios

Referring back to Figure 5 it is apparent that at thrusts of 10K and above, nozzle expansion area ratios greater than 30:1 can be regeneratively cooled. There are many reasons why the desire should exist (reduction of pressure drop, cost, etc.) to only cool smaller expansion ratios, 10:1 or 15:1 for instance. What will be the effect of this on the results of this study?

The lower coolant temperature rise, as a consequence of less total heat transfer, will result in a lower velocity requirement, which in turn allows a larger more easily constructed coolant passage. Two examples of the reduction in coolant velocity that can result from reductions in the cooled area ratio are shown in Figure 10.

f. Applicability Map for N_2O_4/N_2H_4

To better illustrate the limits imposed on regenerative cooling by the previous discussion the major parameters are plotted jointly on a grid of chamber pressure and thrust. Lines of maximum coolable nozzle expansion area ratio, required coolant supply pressure, and the lines of maximum coolant passage width are superimposed in Figure 11.

The area above and to the left of the line of minimum passage width represents a region that is not possible for the N_2O_4/N_2H_4 propellant combination. A supply pressure of 700 psia is considered as the maximum practical for the type of propulsion systems under consideration here. Since nozzles cooled to expansion area ratios of less than 5:1 will have limited application in space propulsion programs, this represents a third limit on the envelope of feasible regenerative cooling with N_2O_4/N_2H_4.

g. Throttling Potential

(1) Heat Transfer

In the investigation of throttling for an N_2H_4 cooled thrust chamber several items became apparent. First was that the thrust chamber design should be based on the minimum thrust, and chamber pressure, and the thrust range capability based on uprating the engine. Limits of throttling potential from a heat transfer standpoint are shown in Figure 12. Thrust level was seen to play only a minor role. Uprating of an engine is basically a coolant pressure limited process. At coolant pressures sufficiently high the pressure term in Equation (4) caused the cooling margin safety factor to fall below 1.7, thereby establishing the limit illustrated in Figure 12.

(2) Supply Pressure

Of equal importance in limiting throttling is the supply pressure requirements. These are given in Figure 13 at the 4K thrust level as a function of chamber pressure and throttling (uprating) factor. Depending on the maximum desired supply pressure this limit can be more restrictive than the heat transfer limit.

3. Specific Considerations for the N_2O_4/Aerozine-50 Propellant Combination

In general, Aerozine-50 (50% UDMH/50% N_2H_4) exhibits the same properties and limitations as N_2H_4. Both utilize nucleate boiling as the primary mode of heat transfer and both are heat capacity limited coolants. All of the design plots discussed in the previous section as necessary for N_2H_4 cooling are also required for an Aerozine-50 cooling design. Specific reference, in this section, will be limited to the difference between the two coolants.

a. Local Heat Rejection Rates

Due to the properties of the combustion products (primarily specific heat) the local heat transfer rates for N_2O_4/Aerozine-50 are less than those of N_2O_4/N_2H_4. The higher vapor pressure of Aerozine-50 results in lower wall temperatures within that portion of the cooling jacket undergoing nucleate boiling heat transfer.

b. Total Heat Capacity

Since liquid Aerozine-50 exhibits no thermal decomposition temperature within the range of interest its maximum temperature is determined directly from its vapor pressure and saturation temperature relationship. This fluid property is included in the section on fluid properties.

c. Designing for Local Heat Transfer Rates

The correlation of coolant velocity requirement with local heat transfer rate, temperature, and pressure for Aerozine-50 was accomplished by the use of graphical rather than mathematical data. These plots are considerably limited in the temperature and pressure range to which they apply. Extrapolations, particularly to low pressures (below 200 psia) and high temperature (above 250°F) will introduce uncertainties based on current data. The safety factor as based on coolant capability and local heat rejection rate has been maintained at a level of 1.7. For regions requiring large data extrapolation an increase in this safety factor might be warranted.

Since Aerozine-50 is a less efficient coolant than N_2H_4 based on coolant velocity requirement, the cooling jacket pressure loss and hence supply pressure requirements are greater. Supply pressure as a function of chamber pressure and thrust is given in Figure 16.

d. Applicability Map For N_2O_4/Aerozine-50

The coolant supply pressure requirement, maximum coolable nozzle area ratio, and the minimum allowable coolant passage width have been superimposed onto a grid of nozzle thrust and chamber pressure in Figure 18. As for the previous propellant combination this illustration clearly indicates the regions wherein regeneratively cooled chambers are not feasible.

e. Throttling Potential

Very little throttling potential is evident for Aerozine-50 cooled thrust chambers over the range investigated. In all cases the coolant capability failed to keep pace with the rise in heat transfer rate as the chamber pressure was increased. Limited derating may be possible when the design nozzle expansion ratio is only a small part of the maximum allowable expansion area ratio.

4. Specific Considerations for the O_2H_2 Propellant Combination

a. Local Heat Rejection Rates

Regenerative cooling with hydrogen utilizes the convection mechanism of heat transfer. Since neither the wall temperature nor the heat flux can be assumed beforehand, an iterative solution of the problem is required. A simplification can be achieved by assuming a maximum wall temperature value and designing on that basis. An IBM 704 computer program was used to conduct the analysis.

MAC A 673

b. Total Heat Capacity

Hydrogen is not a heat capacity limited coolant. That is, the temperature of hydrogen can be raised to any desired level without degradation of its cooling potential. Practically, of course, the fluid temperature must be lower than the desired maximum structural temperature. A value of 1000°R, as a maximum hydrogen temperature for regenerative cooling, and a 2000°R wall temperature adjusted for temperature drops across the passage wall and film were chosen for the parametric studies. Values of hydrogen enthalpy rise greater than the value corresponding to 1000°R would indicate regions wherein regenerative cooling with hydrogen would be undesirable. Enthalpies are used rather than temperatures due to the variation of specific heat with pressure and temperature. Values of this cooling potential factor are plotted on the applicability map for hydrogen to be discussed later in this report.

The degradation of cooling potential at elevated coolant temperatures is a common property among coolant fluids. However, an interesting feature of hydrogen regenerative cooling involves the difficulties resulting from too low rather than too high a coolant temperature. At local coolant temperatures below 300°R, the convective film coefficient is very sensitive to changes in coolant temperature. So sensitive, in fact, that a small reduction in coolant temperature at a fixed design condition will reduce film coefficients sufficiently to bring about a rise in local wall temperatures. Thus, any change in operation or design parameters causing a reduction in inlet coolant temperature would, if not compensated for, result in increased wall temperatures. This is in direct contrast to most coolants (hydrazine, RP-1, water) where the coolant temperature has little effect on nozzle wall temperatures. An example of the effect on nozzle throat wall temperatures of changes in the cooled nozzle expansion area ratio is given in Figure 19. All factors are held constant including the coolant flow rate per unit area. Only the inlet coolant temperature profile is varied.

Some indication of the rapid rise in wall temperatures at very high fluid temperature is given in Figure 24. Above 700°R fluid temperature, the wall temperature rises rapidly with further increases of coolant temperature, whereas below 700°R it had been decreasing. This plot was introduced to show the effect of throttling, as discussed later, but also serves to illustrate this point.

c. Designing for Local Heat Transfer Rates

In designing for convective cooling, the coolant velocity is varied until a satisfactory wall temperature is produced. For a compressible fluid, such as hydrogen, it is more convenient to use the mass velocity term (coolant flow per unit cross section area) rather than the velocity. A correlation of coolant mass velocity versus chamber pressure is shown in Figure 20 and is seen to be independent of nozzle thrust level.

MAC A673

Frictional pressure drop and coolant velocity were calculated by the IBM 704 computer program referred to previously. It is assumed that the entire momentum of the coolant discharged from the coolant jacket is lost in the form of pressure drop. Injector pressure drops continue on the same basis as before, being 10% of design chamber pressure. The required hydrogen supply pressure is given in Figure 21 as a function of chamber pressure and thrust.

d. Coolant Jacket Geometry

Individual coolant passage geometry is correlated in the same manner as before and presented in Figure 22.

e. Applicability Map for O_2H_2

Supply pressure, coolant enthalpy rise factor, and coolant passage dimension illustrate reasonable design solutions for O_2H_2 systems in Figure 23.

f. Throttling Potential

A thrust chamber designed to operate at a maximum level of wall temperature will have no capacity for increases in chamber pressure. Derating, however, is quite feasible and over a wide range of pressure. Shown in Figure 24 is the derate throttling capability of a specific design. A chamber pressure reduction by a factor of ten is possible before the wall temperature again starts to rise.

Chambers designed to operate nominally at wall temperatures less than 2000°R will exhibit both uprate and derate capabilities. This is illustrated in Figure 25 where variations in wall temperature for several designs are presented over a wide range of chamber pressures.

B. Radiation Cooling

1. Design Concept

The principle of radiation cooling is quite simple. It depends on the use of a thin combustion chamber wall which is heated by the combustion gas to an equilibrium temperature at which the heat radiated to space from the wall equals the heat transferred to the wall from the combustion gas. Materials with fairly high thermal conductivity are desirable to avoid overheating the inner surface of the wall.

The limits of applicability of radiation cooling, as affected by motor thrust, burning time, chamber pressure, propellant combination, and mixture ratio, depend on the maximum permissible temperature of available structural materials. Except for the expansion skirt, most portions of a radiation cooled motor will be above 2200°F. With the exception of pyrolytic materials, such as pyrolytic graphite, the only materials with the necessary ductility, strength, and thermal

conductivity to meet the requirements of a radiation cooled motor above 2200°F are the refractory metals, such as tungsten, molybdenum, and columbium. These metals, however, will be rapidly oxidized by liquid rocket exhausts containing water vapor, carbon dioxide, or any free oxygen, unless protected by a suitable coating. Therefore, one of the most important limits for radiation cooled motors is found to be the operating temperature limit of these coatings (See Figures 152 and 153 and Table XIV).

Equilibrium wall temperatures of a radiation cooled motor can be easily calculated, as a first approximation, by assuming that all portions of the motor wall have a shape factor of 1.0 for radiation to space, do not exchange radiation with other portions of the motor, and are not affected by conduction in the motor walls. Using these assumptions, a convenient way of predicting equilibrium wall temperatures is by cross-plotting the combustion gas convective heat flux to the motor walls and radiation from the walls to space versus wall temperature. Such cross-plots are shown in Figures 26 through 39. The intersection points represent equilibrium wall temperature for various expansion ratios and for various values of the radiation factor, which is defined as follows:

$$F_r = F_e F_a \quad \text{(dimensionless)} \tag{11}$$

Where

F_e = Emissivity factor

F_a = Effective shape factor

The emissivity factor will equal the emissivity of the outer surface for radiation to space, but will be affected also by the emissivity of the surroundings if a radiation shield or heat sink is placed near the motor.

The effective shape factor is 1.0 for a thin wall without internal radiation and axial conduction. For symmetrically thick walls, the effective shape factor would be increased by the ratio of outside to inside diameter. Except for very small motors (less than 1.0 inch diameter) the advantage of a thick wall would be more than offset by the increase in weight and wall temperature gradient.

Axial heat conduction can appreciably reduce wall temperatures, at the throat, and this effect could also be thought of as an increase of effective shape factor.

Internal radiation exchange also effects the equilibrium wall temperature, and this has been evaluated in terms of effective shape factors for the expansion nozzle.

2. Conduction Effects

a. Radiation Fins

One way to increase the effective shape factor is by use of external radiation fins. Two radiation fin configurations which were analyzed are shown in Figure 40.

The thermal conductivities of several refractory metals of interest for radiation cooled motors are shown in Figure 40 . There is a large difference in the reported values for pure molybdenum and 0.5% titanium-molybdenum alloy.

Maximum equilibrium temperatures of the combustion chamber when using the two fin configurations are compared in the table below with the temperature which would be predicted for a very thin wall (i.e., a perfect conductor).

Configuration	Material	Maximum Chamber Temperature (°F)
Thin wall	Perfect Conductor	3076
No. 1 (Six fins)	0.5% Ti-molybdenum	2957
	Pure Tungsten	2908
	Pure Molybdenum	2902
No. 2 (Equilateral triangle)	0.5% Ti-molybdenum	2963
	Pure Molybdenum	2876

The two fin configurations analyzed are not necessarily the most effective in improving radiation cooling, but a reduction of 200°F is shown.

b. Axial Conduction

Reduction of maximum motor temperatures at the throat is possible by distribution of some of the throat heat flux to other parts of the motor by thermal conduction in the motor wall, followed by radiation to space. This results in a somewhat higher temperature at locations adjacent to the throat, but this is more than offset by the advantage of lowering the maximum temperature, which is usually the limiting factor in the operation of radiation cooled motors.

The effectiveness of this distribution of heat by conduction is greatest for those cases in which the local heat flux from the combustion gas to the motor wall changes most rapidly with axial distance from the throat, which means that this effect will increase with decreasing throat diameter.

3. Study of a 100-Pound Thrust Motor

A motor which delivers 100 pounds thrust at a chamber pressure of 100 psia was analyzed, using three different wall thicknesses at the throat, as shown in Figure 41. Calculations with the IBM 704 thermal analyzer program were made for two metals: 0.5% Ti-molybdenum alloy, and pure tungsten. The results are shown in Figure 42. Tungsten has a decidedly lower maximum temperature because of its much higher thermal conductivity. However, the thermal conductivity of the 0.5% Ti-molybdenum alloy is based on extrapolated data above 3000°F. The thermal conductivity data for pure molybdenum, on the other hand, show values as high or higher than those for pure tungsten. Therefore, the temperatures for tungsten in Figure 42 are good approximations for pure molybdenum.

4. Two-Dimensional Flow Motor

The two-dimensional flow motor shown in Figure 43 was also analyzed on the thermal analyzer, using a 0.1 inch pure tungsten wall throughout. The same combustion chamber conditions were used as for the 100-pound thrust motor, and the maximum wall temperature was calculated to be 3236°F, as contrasted to a thin wall temperature, ignoring conduction distribution, of 4309°F. This very large decrease in maximum wall temperature was caused by the rapid change in the local heating rate resulting from the very small diameter. This scheme may be of importance in plug or separation nozzles as shown in Figure 44 , and also indicates that very small thrust motors could be radiation cooled even though the theoretical temperature at the throat, ignoring the conduction effect, might be far in excess of allowable temperatures for available materials.

It was taken for granted that the largest obtainable emissivity of the outer motor surface would be used. An emissivity of 0.8 was used for all of the conduction studies.

5. Internal Radiation

The effect of internal radiation exchange within the expansion nozzle for a 40:1 expansion ratio was determined by calculating effective radiation shape factors for heating rates which would produce throat temperatures from 2500°F to 4500°F. Two flame temperatures, 4640°F and 6000°F were used, and it was found that the effective shape factors were greater than 1.0 and almost constant at any expansion ratio, being only slightly affected by heating rate, as shown in Figure 45. Effective shape factors for 4640°F and 6000°F flame temperatures are practically identical. Wall temperatures with and without consideration of internal radiation exchange are shown in Figures 46 and 47 for flame temperatures of 4640°F and 6000°F, respectively. The throat convective heating rates were chosen arbitrarily, and the local heating rates in the nozzle were assumed to be proportional to the factor $(A_*/A)^{0.9}$. Shape factors for internal radiation between various parts of the nozzle were calculated by an IBM program based on shape factor relationships derived from Reference 211.

6. Experimental Data

Experimentally measured wall temperatures are available for two radiation cooled motor configurations: a 25-pound thrust motor operating at a chamber pressure of 100 psia and a 100-pound thrust motor (Figure 48) operating at a chamber pressure of 90 psia. The combustion chamber and throat temperatures were about equal (2700°F) for C* efficiencies of about 90%. Much higher wall temperatures would be predicted analytically, even including the axial conduction and internal radiation effects. The differences between predicted and measured temperatures in small thrust chambers is attributed to the local flow conditions in the vicinity of the injectors. Here, local O/F mixture variations, temperatures, velocities, and boundary layer structure cannot be characterized by the normal heat transfer analytical equations.

Measured temperatures in the expansion nozzle were close to predicted temperatures.

C. Ablative Cooling

1. Design Concept

The two types of ablative thrust chamber liners which are usually considered are as follows:

a. Plastic materials embedded in a structural matrix or plastics which themselves form the inner thrust chamber contour and which ablate at a fairly fast rate so as to act as an insulator and also as a protective film for the rocket throat downstream from the ablative material.

This concept has been studied and tested for a number of years (References 91, 111, 114, and 203) particularly for solid rocket application. This concept, although simple, involves relatively large mass ablation rates and run times for significant cooling have been limited to 15 to 30 seconds.

b. The more promising concept is the ablative liner of reinforced plastic that performs well as an insulator while resisting erosion and melting in a high temperature gas environment. This type of liner has been tested extensively at Marquardt (References 173 and 176) as well as at other agencies (References 89, 109, 114, and 204) for use with liquid propellants.

Using oriented silica reinforced phenolic as a liner material, burning time of over 300 seconds and even up to 22 minutes have been reported by other agencies. However, the requirement, for careful design of the injector is indicated by reports of burnouts in 2 seconds with a hydrogen-oxygen motor Reference 121).

A large variety of reinforced plastic combinations have been developed by the plastic industry and many combinations have been tested including phenolics, silicones, epoxies, and rubbers reinforced with silica, glass, zirconia, graphite cloth, and carbon cloth. However, for liquid engine application, the oriented silica fibers in phenolic have consistently shown superior performance. This has been attributed to the very viscous molten silica film which forms over the charred surface*.

Silica reinforced phenolic has been tested as a throat material and has shown considerable promise (Reference 204) for particular injector configurations. Normal erosion for small motors would be quite serious, while in tests on the larger motors, such as those reported in Reference 89 for lower pressures, the effect of small erosion rates in the throat could be acceptable.

A number of studies have provided an analytical approach to the ablation phenomena (References 103 and 112). Using these analyses to correlate the available data with the proper operational parameters such as pressure, local velocity, gas temperature, and plastic composition, it is believed that a rational design can be developed. The current method of calculating reinforced phenolic wall thickness is to use a predicted char depth, plus erosion rate, plus an uncharred material thickness at the end of burning.

The state of the art is such that each material vendor and engine fabricator has developed his own recommended design criteria, while improvements in resin systems and fabrication techniques cause continuing changes in design approaches. However, most of the recent developments have not increased the basic capabilities of the reinforced plastics, but rather have provided solutions to particular design probelms. A discussion of these problems and their possible solutions are presented below for the silica-phenolic ablatives and others as indicated.

2. Ablative Thrust Chamber Design Approaches

a. Influence of Operational Parameters

(1) Propellant

The most satisfactory ablative performance with silica-phenolic has been attained with the N_2O_4/hydrazine based fuel combinations. Grooving and eroding of nozzles and chamber walls appears to be sensitive to oxidizer

- - - - - - - - - - - - -

Note:

* Char and char depth as discussed in this section refers to the stable carbon residue resulting from the thermal degradation of the phenolic resin. The char depth refers to the boundary between the virgin phenolic and the completely degraded carbon residue which may in turn be reinforced with the silica fibers. This is indicated by temperature measurements of approximately 800°F for typical phenolic systems.

MAC A 623

and fuel distribution so that local O/F ratios do have an effect on ablative performance. The thermal pyrolysis products of phenolic charring include hydrogen and methane in addition to the carbon char residue. Therefore, the heating rate of the ablative surface could be affected by reaction with a local oxidizer rich mixture at the wall.

Carbon cloth and nylon reinforced phenolics are being evaluated for use with fluorine based oxidizer systems (Reference 207).

(2) Chamber Pressure

Although increasing chamber pressure increases the local heat transfer rates almost proportionately and heat transfer rates in a nozzle throat may be four times greater than in the combustion chamber, charring rates appear to be almost constant over a wide range of chamber pressures and local heat transfer coefficients. However, on the same basis, erosion rates or surface regression rates are influenced by these parameters and limit the applicability of these materials in nozzle throat sections.

(3) Thrust (Or Engine Size)

Char rates and surface erosion effects in the combustion region ahead of the throat are applicable over a wide range of chamber sizes (thrust levels of 25 to 2000 pounds under development at Marquardt). A char rate correction factor applicable to very small chamber diameters has been developed in Reference 88 and is shown in Figure 49. Of course, identical linear erosion rates in a small or a large thrust chamber throat would have a markedly different effect on relative throat area increase, and thus chamber size becomes a design factor for ablative throat applications.

(4) Run Time and Duty Cycle

Char depth versus running time is presented in Figures 50, 51, and 52 also Figure 8 of Volume I. The accumulated run time may be distributed in a variety of ways as suggested by the thrust versus time graphs in Figure 2 of Volume I. For steady state continuous operation, the char depth is approximately proportional to the 0.5 power of run time ($X = C\sqrt{t}$). Although there appears to be a great deal of scatter in the data of Figure 8 of Volume I, the design curve shown correlates very closely the latest experimental data in the 25 to 2000-pound thrust range.

Three other general classes of duty cycle have been evaluated experimentally, with results as follows:

1. Few Restarts with Long "Off" Times

Data from Marquardt tests and from Reference 89 indicate that if the thrust chamber liner is allowed to cool completely before being

refired, the time delay after restarting but before charring resumes just about balances the post run charring of the previous run. The net result is that the accumulated char depth is equal to the continuous run char depth.

2. Continuously Pulsed Duty Cycle

Data from tests on 100-pound thrust ablative chambers with duty cycles having "off" times of less than 10 seconds, resulted in accumulated char depths double those for identical thrust chambers with the same accumulated burn time. The results are presented in Figures 53 and 54.

3. Several Restarts with "Off" Times of 200 Seconds

Data from tests of 25 and 2000-pound thrust chambers has been obtained on the effect of a duty cycle consisting of "on" times of 13 seconds with "off" times of 200 seconds for 20 cycles. In the combustion chamber of the 2000-pound thrust engine, the effect was an increase in char depth of about 30% because in the 200 seconds "off" time, the chamber surface temperature was reduced but most of the heat absorbed was still contained in the chamber walls and on successive heat pulses, the total heat transfer to the walls was greater than for steady state running. During steady state running the wall temperature rises to a high value quickly and stays there, thus reducing the net heat flux over that for the pulsing mode.

The opposite effect on charring was noted for the 25-pound thrust chamber locations downstream from the throat and in the chamber wall adjacent to the injector face (Figure 55). This is attributed to the fact that for these components, heat can be effectively dissipated by radiation or conduction to the surroundings between pulses.

b. Choice of Ablative Materials

As noted above, a great number of plastic resin systems and reinforcements have been developed and tested for liquid motor application. It is apparent in current development programs that complete optimization has not yet been achieved in the choice of resin, in reinforcement or in fabrication techniques. Some of the variables involved in these choices are listed below with comments on their importance.

(1). Resins and Reinforcements

The most widely used resin system is the phenolic with and without filler materials. The standard phenolic resins include:

1. SC 1008 - Monsanto Chemical Co.
2. 91 LD - Cincinnati Testing Lab.
3. BLL-3085 - Bakelite Co.

MAC A673

The high-silica reinforcements include cloth and tape of the following:

1. Refrasil - H. I. Thompson Co.
2. Sil-Temp - Haveg Industries Inc.
3. Thermo-Sil - Aerothermal Industries Inc.

Silica-phenolic laminates using the silica cloth or tape preimpregnated with standard or modified phenolics and possibly fillers include the following:

1. HITCO-1401 P - Refrasil fabric impregnated with SC 1008 resin. Resin content runs about 33% by weight.
2. USP 5504 (formerly XAO 34-2) - Refrasil fabric impregnated with standard phenolic modified by addition of inorganic fillers (U. S. Polymeric).
3. USP 5067 - Refrasil fabric impregnated with USP 39 resin (proprietary system of phenolic plus fillers). Resin content runs 33% by weight with a density of 108 lb/ft^3.
4. Fiberite MX 2600 - Silica-phenolic equivalent to USP 5504 (MX 2625 system in tape form). Fiberite Corp. generally uses Sil-Temp reinforcement. Resin content runs about 29 to 33% by weight.

Other ablative laminate systems which appear interesting and are being evaluated by various agencies include the following:

1. Zirconia Phenoxy Aldehyde-Aerothermal Ind. This material is a chemically modified phenolic resin. It may be used with silica or carbon cloth reinforcement.

   Tests run by Aerothermal Industries with a gaseous O_2/H_2 rocket engine chamber showed only a 5% throat area change for a 300-second run. The chamber pressure was 300 psia and the throat diameter was 0.375 inch. Reinforcement was silica fabric.

2. Silicon Carbide Coated Carbon Cloth (Aerothermal Industries). This reinforcement has a high potential of erosion resistance for use with any standard resin system. Development is at present delayed due to fabrication difficulties causing embrittlement.

3. Silicone Rubber - Silica Cloth Impregnate (Aerothermal Industries - Dow Corning). Silicone Rubber is a highly cross-linked polymer which is reported to have excellent high temperature stability and charring characteristics.

4. FM 5311 (U. S. Polymeric Co.). This material is a high silica fabric molding compound formulated from a phenyl silane resin plus an additive.

   Recent high temperature and high heat flux testing indicates a substantial improvement in mass loss rate when tested against standard phenolic systems with similar reinforcements (USP tests).

5. X 2001 (Epoxy Novolac-Avco Manufacturing Co.). X 2001 is an epoxy-phenolic blend with silica fabric reinforcement plus the addition of inorganic fillers. Preliminary rocket firing tests have been made by Marquardt and other agencies with superior results in erosion resistance. Char rates and conductivity have proven to be higher.

6. MX S-19 (Fiberite Corporation). This is an unfilled silica phenolic laminate with a 40% higher resin content than their standard material MX 2646.

7. Moldable Silicon Carbide (Aerothermal Industries). This system is formulated from silicon carbide coated graphite powder which is mixed with a styrene phenolic, press molded and then pre-charred leaving a high density mixture of graphite and silicon carbide. It may be used for fabrication of throat and chamber sections.

   Tests performed by Aerothermal Industries with a gaseous O_2/H_2 rocket engine showed excellent results. Reported erosion is 0.013 mils/second for a 300-second run with a 0.375 inch throat and P_c = 300 psi.

8. Precharred Reinforced Plastics Impregnated with Subliming Salts or Polymers (Chance-Vought).

For parts of the thrust chamber not in contact with the combustion gases, still other resins and reinforcements may prove more suitable from the standpoint of lower density, lower thermal conductivity, higher strength, ease of fabrication or lower cost. These materials include the rubbers and epoxies as resins and such reinforcements as glass and asbestos.

The use of zirconia fibers for reinforcement has shown promise in some applications according to vendors, but due to the brittleness of the materials and the shortness of the resulting strands of fiber after molding, the ability of the zirconia to anchor and reinforce the char is greatly decreased. Research is continuing on the use of this type of reinforcement.

Carbon cloth has proven less satisfactory than silica for liquid propellants because no viscous molten film is formed. Also the carbon rapidly oxidizes with the storable hypergolics as compared to their performance with solid propellants.

Various types of torch and nozzle test programs to screen a large number of plastic-reinforcement combinations are reported in References 87, 94, 101, 102, and 107.

c. Ablative Thrust Chamber Fabrication Parameters

(1). Reinforcement Cloth Orientation

Preimpregnated reinforcement cloth orientation may be made parallel to the chamber centerline by wrapping it on a mandrel to build up the required wall thickness; or the orientation may be made perpendicular to the chamber centerline (90° orientation) by stacking and pressing discs of the cloth. Orientations in between may be achieved by modification of these basic techniques using tape or conical discs. Fiber orientations from 15° to 60° to centerline have been proposed as being optimum. Factors affected by orientation are several and optimization is not straightforward. They include the following:

1. Erosion resistance due to the shingle effect and fiber anchoring.

2. Reduced thermal conductivity due to higher conductivity along the direction of fibers rather than across them.

3. Reduced delamination. Swelling and out-gassing may cause serious delaminations if a short gas flow path is not provided.

4. Fabrication technique. Angle of orientation affects the choice of bias tape wrapping versus disc layup.

MAC A673

(2). Composite Wall Design

The designer must solve many detailed structural problems relative to attachment, insulation, pressure stresses, vibration, acceleration loads, etc. A typical structure assumed for the weight studies of Volume I is shown in Figure 56. In this design the thickness of the 45° oriented silica fiber was taken directly from the char depth plot in Figure 8 of Volume I. The temperature of the phenolic at the end of running time and maximum heat soak is assumed to be 800°F. The structural shell designed to take the pressure loads may be either a metal can or an overwrap of resin bonded glass filament or tape. An additional insulating layer of low conductivity plastic may be incorporated between the char layer and the structural shell. The insulating layer is designed to drop the outside temperature from 800°F to 500°F.

A typical phenolic bonded overwrap of 0.15 inch with alternating layers of longitudinal tape and circumferential filament glass windings constitutes a structural shell capable of carrying over 500 psia pressure at an operating temperature of 500°F. An alternate overwrap technique is the continuous helically or convolutely wound fiberglass winding designed to carry both the axial and hoop stresses.

One approach to the determination of proper wall thickness for chambers of reasonable size is to construct a test chamber with extra thick walls to preclude a possible burn out or structural failure. This chamber can then be run over the most severe duty cycle. When the chamber is cut open the char depth distribution along the walls from the injector head and throughout the nozzle expansion section can be used as a guide in contouring the required wall thickness. Figure 55 shows how the char depth is influenced by the presence of a graphite throat insert and also the effect of steady state and intermittent duty cycles. Thermocouples revealed transient temperature distributions during and after the run. Of course, reducing the ablative wall thickness for subsequent test chamber designs will influence the final temperature response at the char boundary.

In the overall design, it has been found that the configuration and distribution of materials give rise to problems of delaminations during fabrication, curing, firing and postrun soaking. This problem and the problems of swelling and differential thermal expansions between dissimilar materials and the sealing of throat inserts can be solved by careful material selection and structural design. Material suppliers provide an excellent source of data in this area. This report provides a summary of design data adequate for preliminary design purposes. Typical data included the following:

1. Temperature response of interior and back face of ablative walls (Figures 57 and 58)

2. Behavior of materials in a vacuum (Figures 59 and 60)

MAC A673

3. Reinforced phenolic strength versus temperature and soak time (Figure 61)

4. Weight of thermally degraded resins versus temperature (Figure 62)

5. Thermal conductivity of silica-phenolic laminates (Figures 63 and 64)

6. Effect of molding pressure on physical properties (Figure 65)

7. Effect of heat and vacuum on weight and dimension changes in silica-phenolic laminate (Table II)

8. Typical physical and thermal properties of ablative materials (Tables III and IV)

3. Experimental Studies

To investigate the effects of a vacuum environment on the thermal degradation of laminated refrasil phenolic, a series of laboratory tests were conducted at Marquardt during April 1962. Sample cylinders were cut of this material to approximate that of ablative chambers to be tested as attitude control motors. The inner surface of the cylinders were heated by a flat tungsten filament for periods of 3 to 4 minutes in an evacuated bell jar and they were then soaked in the vacuum for 2 hours as they cooled to ambient temperature. The results of these tests, and of identical control samples heated at ambient pressure, are given in Table II. It appears from these data that the vacuum environment has only a very small effect on the total outgassing rate of the material. Hoop strength tests performed on the twice-fired samples after the test runs indicated no difference in structural integrity. A cross section of the 60° axis samples as shown in Figure 66 exhibited no difference in char layer depth or strata delamination.

A second effect studied was the swelling of the sample after outgassing. There appeared to be no significant difference in behavior between the vacuum and nonvacuum samples in this effect, however, some insight can be gained into this problem by considering the manner in which the swelling took place. In all cases, the material swelled in a direction perpendicular to the lamina and contracted in the parallel direction. This type of dimensional change may be caused by the warping of the silica fibers.

An investigation into the swelling problem encountered was conducted under another test program. In one such test, a sample of laminated refrasil phenolic material was heated by radiant lamps from ambient temperature to 1000°F in increments of 100° for 45 minutes. The recorded linear expansions are plotted in Figure 67. The behavior of the material was linear in expansion to 300°F at which point outgassing effects caused a sharp increase in the rate of change in length with temperature. After reaching a maximum length, the expansion assumed an erratic up and down character due to apparent spasmodic outgassing of individual layers in the lamina. Popping noises were heard as individual pockets of gas were liberated.

Another similar test was conducted by soaking the sample for 1 hour at several significant temperature levels and allowing the sample to cool before proceeding to the next condition. The results of this test are shown in Table V.

D. Film and Transpiration Cooling

1. Liquid Film Cooling Analysis

An attractive means of rocket motor cooling is by use of a liquid or gas film interposed between the hot working fluid and the container wall. This process is called film cooling. Since liquid rockets are being considered, the possibility exists of injecting either of the propellants along the containing wall in the combustion chamber and in the nozzle itself. When care is taken to assure that the cooling film does not penetrate the main gas stream it can act as an efficient heat insulator. The application of film cooling can be divided into that in which the coolant is a liquid and that in which the coolant is a vapor.

Perhaps the most extensive survey of liquid film cooling in theory and practice is found in Reference 130. The theoretical developments of Sellers, Crocco, and Rannie are all discussed. Each essentially takes an ideal case in which the liquid is flowing smoothly along a flat surface. Mass, momentum, and energy balances were made for a differential volume of a laminar sublayer of the main gas stream, which builds up on a smooth layer of liquid. Since the entire container wall is considered to be covered with liquid, the boiling temperature of the liquid sets the wall temperature.

Crocco assumed a chemical reaction between the coolant and the main gas stream with the result of heat transfer rates 1.5 times higher than for the nonreactive case. Sellers and Rannie gave essentially the same results with Sellers derivation being easier to use. Sellers equation was the following:

$$\frac{1}{St_b} = 37\,(Re_b)^{0.1}\,1.475\,(Re_b)^{0.1} + Pr_m - 1 \qquad (12)$$

where St_b is the Stanton number of the bulk gas stream, Re is the Reynolds number of the bulk stream and Pr_m is the Prandtl number of the mixture. Sellers, by employing the data from Reference 135 for smooth surface ducts, rearranged his derivation to the following form:

$$St_b = \frac{0.0093}{Pr_b + 3.53} \qquad (13)$$

with Pr_b close to unity, $St_b = 0.002$.

MAC A673

Earlier tests at NACA (Reference 124) attempted to correlate this film cooling phenomena by measuring the film cooling process using hot air and water flowing in a horizontal smooth tube. Injection was made essentially parallel to the air flow. Thermocouples were installed to measure the wall temperature. Figure 68 shows the temperature distribution of the tube. It can be seen that the cooled length indicated by a wall temperature less than the boiling point of water does not vary appreciably with circumferential position, and that the wall temperature rose rapidly once past the cooled length. From a heat balance across the air coolant vapor film an effective heat transfer coefficient was computed from the following:

$$h = \frac{\dot{W}_c \Delta H_c}{(T_g - T_w)\, \pi D L} \qquad (14)$$

where

$\dot{W}_c$ = Coolant flow

ΔH_c = Enthalpy rise of coolant

T_g = Air temperature

T_w = Wall temperature, equal to saturation temperature

These calculations are correlated in Figure 69. The dotted line represents the well known correlation for single phase flow in a tube. The data indicate approximately twice the heat transfer rate for film cooling. For a Reynolds number of about 10^5, the Stanton number was 0.003 which is 50% greater than the Sellers experimental correlation. Further experiments on liquid film cooling were reported in Reference 128 in which a vertical tube containing a flow of hydrogen-oxygen combustion products was cooled with water. In this, a coolant flow rate was computed based on turbulent flow in a smooth tube. The experimental value of the coolant flow rate for the cooled length considered was twice that of the computed value. Recently (Reference 126) an experimental study was made to investigate the effect of different cooling liquids on the film cooling rates. A horizontal 3 inch I.D. film cooled chamber was placed between two convectively cooled chambers. Hydrogen-air combustion gas was used at pressures from 250 to 750 psia and temperatures from 2600°R to 4100°R with a gas stream Reynolds number of about 10^5. The liquids employed as film coolants were water, anhydrous ammonia, ethyl alcohol, and Freon 113. The coolants were introduced tangentially. The film cooled chamber was instrumented so that the wall temperature could be determined. Figure 70 is typical of the data obtained, which shows how the wall temperature varies with coolant flow rate. Figure 71 shows the linear dependence of the cooled length, which is defined as the chamber length, which is below the boiling point of the coolant, on coolant flow. This relationship is consistent with Equation (3).

Equation (3) also indicates that if the heat transfer coefficients are equal, the coolant flow rate will be inversely proportional to the enthalpy change of the coolant, which is the heat of vaporization plus any subcooling present, for the same cooled length. In general, this is born out by Figure 71 except that the plots for ethyl alcohol and ammonia are reversed. The authors claim that this reversal coincides with a theoretical result obtained from a laminar boundary layer analysis developed by Reference 136. Using Equation (3) the authors of Reference 136 computed h and compared it with the h obtained experimentally in the convectively cooled chamber upstream of the film cooled section. In every case, the film h was less than that for the upstream chamber. Also, these results were compared with the theoretical development of Graham (Reference 137), who modified the theory of Sellers (Reference 133) with the following equation:

$$Nu = \frac{0.8\, Pr_b\, Re\, (f/2)}{1 + 4\,(Pr_b - 1)\, f/2} \tag{15}$$

where f is the friction factor. The authors (Reference 126) state that the experimental data are considerably higher than Equation (4) but do not say by how much.

In addition to this, data obtained from the convectively cooled chamber downstream of the film cooled unit indicated that a cooling effect occurred even though no liquid was present. Apparently the cold vapor remained close to the wall for a distance, blanketing it from the hot gas stream. Investigation of this additional cooling effect was carried out further and reported in Reference 149. By making an energy balance about an element of vapor (assuming a nonadiabatic wall) the following equation was derived:

$$\ln \eta = \ln \frac{T_g - T_w - 2\, q_w/h}{T_g + T_w - 2\, T_v} = \frac{2\pi hD\, L}{\dot{W}_c\, C_{p_c}} \tag{16}$$

Cooling experiments were performed using water and ammonia in a cylindrical combustion chamber. Figure 72 shows a typical data correlation of the test results. A curve fit through the data gives the following equation:

$$\ln \eta = \frac{-2\pi hD\, L}{\dot{W}_c\, C_{p_c}}\; f\,(\dot{W}_g/\dot{W}_c) \tag{17}$$

where

$$f\,(\dot{W}_g/\dot{W}_c) = 1 + 0.25 \arctan\,(15 - \dot{W}_g/\dot{W}_c) \tag{18}$$

MAC A673

It must be noted, however, that only a few data points exist and these are considerably scattered.

The examination of film cooling effects was expanded by Reference 149 to include combined results of both film and regenerative cooling. In this instance, a liquid was injected just upstream of a cylindrical test section which contained passages for the regenerative coolant. Water was used as the film coolant. An analytical flow model was set up with the assumption of linear vaporization rate for the film coolant. The integrated equation is as follows:

$$\ln \beta = \frac{\frac{h_f}{h_w}(T_g - T_v) + \frac{\dot{W}_c \Delta H_v}{\pi D L h_w} = \frac{q_w}{h_w}}{\frac{h_f}{h_w}(T_g - T_v) + \frac{\dot{W}_c \Delta H_v}{\pi D L h_w} + T_w - T_c} = \frac{\pi D L h_w}{\dot{W}_c C_{p_c}} \ln (1 - X/L) \qquad (19)$$

where

q_w = Heat flux through wall per unit area

h_f = Heat transfer coefficient between gas stream and liquid film

h_w = Heat transfer coefficient between liquid film and wall

T_v = Boiling temperature of liquid film

T_c = Inlet coolant temperature

ΔH_v = Heat of vaporization of coolant

L = Length of coolant film

X = Axial distance

The test results are presented in Figure 73, indicating poor correlation with prediction by use of the previous equation. The apparent nonlinear vaporization rate was indicated as the possible reason for poor correlation. Rather than modify the vaporization rate approximation, the author correlated the results semiempirically as shown in Figure 74. The correlating equation shows the following:

$$\ln \beta = \frac{0.1 \pi D h_w L}{\dot{W}_c C_{p_c}} \ln (1 - X/L) - 0.5 \qquad (20)$$

MAC A673

Reference 125 reviews some earlier work done on a film cooled motor that had injection points in the combustion chamber and the convergent section of the nozzle. Figure 75 shows a plot of the Stanton numbers obtained for various injection points. It can be seen that a wide range of values exists from 0.004 up. Figure 76 shows the performance penalty that was obtained by use of the liquid coolant.

It should be noted that the above work neglected the effect of thermal radiation from the combustion species to the wall. This will increase the effective heat transfer coefficient. From this standpoint it would be desirable to have the coolant opaque to the radiation so it will not be transmitted to the wall.

Another interesting point brought out in Reference 126 was the low coolant requirement for Freon 113. Inspection of the test item showed a carbonaceous deposit downstream of the liquid film. This deposit resulting from decomposition of the Freon 113 added a heat transfer resistance to the system and reduced the overall heat transfer rate. This phenomena was also reported by Reference 131 in which an RP-1 lox motor was cooled with the fuel. Analysis of the data showed an intermittent peaking of the heat flux accompanied by a following dropoff. The explanation is that the carbon deposit builds up to an unstable thickness, flakes off, and then builds up again. Reductions in heat flux from a calculated 6 to 8 Btu/in.^{2}-sec with no deposit to a measured 2 Btu/in.^{2}-sec with deposits were reported.

One important consideration that must be taken into account in liquid film cooling is the hydrodynamics of the liquid as it flows along the wall. The main gas stream as it flows, exerts a shear at the liquid gas interface tending to set up small disturbances. If conditions are right, the gas can actually tear off droplets of liquid and remove them from the wall. This liquid which is removed will not help cool the wall and results in poor efficiency. In addition, if the velocity and injection angle of the liquid exceeds certain critical values, the stream will penetrate the gas stream rather than flow along the wall. Graham and Zucrow (Reference 130) have summarized information in this area. In regard to the problem of liquid penetration into the gas stream considerable work has been done by Beighley, Knuth, Greenberg, and Lauden (References 138 through 141, respectively) at Purdue University. Numerous physical parameters were varied in experimental work to determine the critical injection velocity at which liquid flow separation from the wall is visually observed. The parameters varied were liquid density, viscosity, surface tension, gas Reynolds number, injection angle, injection geometry, and hydraulic diameter. The area of application was investigated also, such as the combustion chamber, the junction between the combustion chamber and the nozzle, the divergent and convergent nozzle sections. Based on numerous data points the critical velocity was nearly independent of liquid surface tension and viscosity and slot depth. The final correlation showed for right angle injection that:

$$\frac{V+}{U_b}\sqrt{\frac{\rho_L}{\rho_b}}\left(\frac{b}{D}\right)^{(0.404 - 1.2 \times 10^{7}\, Re_b)} = 274\, Re_b^{-0.65} \qquad (21)$$

for

$$0.5 \times 10^5 < Re_b < 2.5 \times 10^5$$

and

$$\frac{V+}{U_b}\sqrt{\frac{\rho_L}{\rho_b}}\left(\frac{b}{D}\right)^{(0.404 - 1.2 \times 10^{7}\, Re_b)} = 0.085 \qquad (22)$$

for $2.5 \times 10^5 < Re_b < 12 \times 10^5$

where

b = Slot width

D = Diameter of chamber

$V+$ = Critical velocity

U_b = Gas stream velocity

Further work in this area was done by Knuth (Reference 142) in a circular duct in which the coolant was injected through radial holes. Liquid properties were again widely varied and the data were correlated by the following equation:

$$\frac{\rho_b U_b^2}{\rho_L (V+)^2} = 7.65 \times 10^{-5}\, Re_b^{0.79}\, (Re+\, Ca+)^{0.395} \qquad (23)$$

where

$Ca+ = \rho_L (V+)^2/(P_b - P_v)$

P_b = Static pressure of gas stream

P_v = Partial pressure of coolant vapors in gas stream

MAC A673

In summary then, the above work shows how, if the injection velocity is kept below the critical velocity, the liquid flow will not penetrate the gas stream.

A number of investigators have studied the stability of the film as it flows along the wall. Graham and Zucrow (Reference 130) give a summary of the work done up to 1957. By using different types of injectors it was concluded that the method of injection had no influence on the stability of the film so long as the critical injection velocity was not exceeded. Also, it was observed that the liquid flow goes through three regimes. In the first, the surface of the liquid appeared to be smooth for low flow rates. As the flow was increased the second regime was encountered in which waves began to form on the liquid surface. These waves became greater in amplitude and frequency as the flow was increased. As the liquid flow rate was increased still further, the waves continued to increase in number and amplitude but at a much slower rate than the second regime. It was noted that surface tension had only a minor effect in changing the transition regime. Viscosity had a strong influence in maintaining stability. Increased gas mass velocity tended to reduce the amplitude but increase the frequency of the waves. Gas stream temperature had little effect.

In order to develop some quantitative method for film stability comparison, a semiempirical method was used by Graham and Zucrow by employing the data of Reference 143. A stability effectiveness factor E_s was defined as follows:

$$E_s = \frac{\dot{W}_c \text{ ideal}}{\dot{W}_c \text{ actual}} \tag{24}$$

Another method of viewing this would be to consider this factor as a correction the heat transfer coefficient as expressed in Equation (14) such that,

$$E_s = \frac{h \text{ ideal}}{h \text{ actual}} \tag{25}$$

where h ideal would be that coefficient derived from flow along a smooth surface. By using the data of Reference 143 a functional relationship between E_s and $\dot{W}_c+$, which is defined as the dimensionless coolant flow equal to $\dot{W}_c/\pi D \mu_L$), was developed and is shown in Figure 77.

MAC A 673

By staying below a $\dot{W}_c+$ value of 300, the effectiveness should remain unity. Therefore, if the film cooled length is plotted against coolant flow rate a straight line will result as shown in Figure 71. However, if the critical value of $\dot{W}_c+$ is exceeded, droplet breakaway will occur and a knee will appear in the plot as shown in Figure 78. It must be kept in mind that this work was done in a smooth tube. Adverse pressure gradients in the nozzle section may greatly affect the stability.

One additional factor to be considered in liquid film cooling is the even distribution of liquid in the direction of gas flow. The evenness of distribution depends principally on the main propellant injector, film coolant injector system and conditions of the chamber surface. A poor distribution will require higher coolant flows in order to eliminate hot spots.

The process of vapor film cooling is similar to that of the liquid type except that the film and wall temperature vary as the coolant flows along the wall. However, the idea of interposing a colder fluid between the hot gas and the wall still exists. Reference 123 presents a useful model supported by experimental data which describes the process and provides an insight into the important parameters. By assuming that the coolant forms in a discrete layer with a low temperature profile in the flow direction and also normal to the wall and with no conduction along the wall a relationship was derived by making a heat balance on the film. This was the following:

$$\dot{W}_c \, C_p = \frac{h \, D \, \pi \, L}{- \ln n} \qquad (26)$$

where

h = Heat transfer coefficient of a smooth tube

D = Tube diameter

L = Cooled length

n = Temperature approach $= \dfrac{T_{ad\ wall} - T_{wall}}{T_{ad\ wall} - T_{coolant}}$

An experimental test program at NASA (Reference 123) obtained data for air and helium as coolant for a hot gas stream. The coolants were admitted by tangential slots. Temperatures, velocities, and slot heights were all varied for an 8-inch square duct. This data along with that of Reference 144 were correlated to the theoretical derivation Equation (26). Figure 79 shows a typical correlation. The final equation was as follows:

$$\dot{W}_c \, C_{pc} = h \pi D L \left[\frac{1}{\frac{-\ln n}{0.125} + 0.04} \right] \qquad (27)$$
$$\left(\frac{S \, V_g}{\alpha_c} \right) \qquad f \left(\frac{V_g}{V_c} \right)$$

where

S = Slot height

α_c = Thermal diffusivity of the coolant

V_g = Velocity of the main gas

V_c = Velocity of the coolant

and

$$f \left(\frac{V_g}{V_c} \right) = 1 + 0.4 \arctan \left(\frac{V_g}{V_c} - 1 \right) \text{ when } \frac{V_g}{V_c} \geq 1.0$$

and

$$f \left(\frac{V_g}{V_c} \right) = \frac{V_g}{V_c}^{1.5 \left(V_c / V_g - 1 \right)} \text{ when } \frac{V_g}{V_c} \leq 1.0$$

Follow-on work was reported in Reference 129 in which angled slots and normal holes were used as a means of injection. Essentially a series of experiments were run to obtain a correction factor for nontangential injection. The final equation showed the following:

$$\dot{W}_c \, C_{pc} = h \pi DL \left[\frac{1}{\frac{-\ln n + \ln \cos 0.8 \, i_{eff}}{0.125} + 0.04} \right] \qquad (28)$$
$$\left(\frac{S \, V_g}{\alpha_c} \right) \qquad f \left(\frac{V_g}{V_c} \right)$$

Where i_{eff} is the effective coolant injection angle $= \tan^{-1} \left(\frac{\sin i}{\cos i + \frac{(\rho V)_g}{(\rho V)_c}} \right)$

with i, the injection angle.

2. Recommended Design Calculations

a. Liquid Film

The mechanism of liquid film cooling has been well documented as evidenced from the discussion above. A number of experimenters have investigated the area of flow in a cylinder while little work has been done in the nozzle. Even in the work done on cylindrical flow the various investigators do not agree. The main dispute is the effective heat transfer coefficient. Reference 125 recommends a Stanton number of 0.002, Reference 124 shows coefficients twice as high as for a smooth tube. Reference 126 shows coefficients less than experimental coefficients taken upstream of the injection points. However, in this last case a number of runs were made with different coolants. On this basis it is recommended that the coefficient be taken for a smooth tube and that Equation (3) of Appendix C, as follows:

$$\frac{\dot{W}_c}{\dot{W}_g} = 2\,St_o\,\frac{L^*\,C_{p_g}\,(T_g - T_w)}{(C_r)^{3/2}\,\Delta Hc}\,\left(\frac{\pi C_F\,Po}{T}\right)^{1/2}$$

be used for design of the combustion chamber provided that the critical injection velocity as defined by Equations (21), (22), or (23) is not exceeded. Also, one should not stray far from the maximum dimensionless film coolant flow W+ as shown in Figure .

Data for liquid film cooling in the nozzle section is meager. The data from Reference 125 as plotted in Figure 75 shows a wide variation for Stanton numbers in the convergent section. Reference 145 reports film cooling requirements for ammonia of 19% of the total propellant flow and for water of 16% for completely cooling a convergent-divergent nozzle. No further detailed information was obtained except a high performance loss. The effect on film stability of adverse pressure gradients is not known. However, until further experimental data is forthcoming it is recommended that Equation (4) of Appendix C which is as follows:

$$\frac{d\dot{W}c}{\dot{W}g} = \frac{2\,St_o\,C_{p_g}\,(T_g - T_w)}{(A/A^*)^{1/2}\,\Delta H_c}\,\left(\frac{\pi C_F\,P_o}{T}\right)^{1/2}\,dL$$

be applied by using the Stanton number for smooth flow. The equation will need to be integrated over the section of interest. If the contour of the nozzle can be approximated by a series of conical sections, the equation can be integrated analytically. Otherwise, a step by step approach is required. It should be mentioned

that the above equations represent a conservative approach since the additional cooling ability of the cold vapor downstream from the point where the last drop of liquid existed was not considered. Only a limited amount of data and a questionable correlation (Equations (17) and (18)) are available at present. As further information becomes available, it may be possible to include this additional cooling effect. If one were to consider a coolant such as hydrogen which has a low heat of vaporization and a high vapor specific heat, the vapor cooling effect might be quite large.

b. Gas Film

The performance of gas film cooling has been well established by experiment, Reference 123. Data have to be correlated by assuming the heat transfer coefficient for a smooth tube. Therefore, for the combustion chamber design, it is recommended that Equation (6) of Appendix C, as follows:

$$\frac{\dot{W}_c}{\dot{W}_g} = \frac{2\,St_o\,L^*}{(Cr)^{3/2}} \left(\frac{\pi C_F P_o}{T}\right)^{1/2} \frac{C_{p_g}}{C_{p_c}} \left[\frac{1}{\frac{-\ln n}{\left(\frac{S\,Vg}{\alpha_c}\right)^{0.125} f\left(\frac{V_g}{V_c}\right)} + 0.04}\right]$$

be used with the Stanton number as that corresponding to smooth pipe flow. With regard to the nozzle section, no data seems to be available. Therefore, it was best to extrapolate the cylindrical tube data and use the following Equation (7) from Appendix C:

$$\frac{d\dot{W}c}{\dot{W}g} = \frac{2\,St_o}{(A/A^*)^{1/2}} \left(\frac{\pi C_F P_o}{T}\right)^{1/2} \frac{C_{p_g}}{C_{p_c}} \frac{dL}{\left[\frac{-\ln n}{\left(\frac{S\,Vg}{\alpha_c}\right)^{0.125} f\left(\frac{V_g}{V_c}\right)} + 0.04\right]}$$

with the Stanton number of a smooth pipe flow. This equation, of course, would have to be integrated from one end of the nozzle to the other.

3. Parameterization of Film Cooling Requirements

In order to understand the important factors to consider when contemplating the use of film cooling, a parametric study was made for some typical propellant combinations. A base condition with a thrust requirement of 4000 pounds, and a chamber pressure of 150 psia was selected. Also a contraction ratio of 1.5

MAC A 673

and a characteristic length of 30 inches was chosen. The motor was arbitrarily divided into four cylindrical or conical sections to make the calculations easier. These four sections were the combustion chamber, the convergent section, and the divergent section from an area ratio of 1:1 to 10:1, and the divergent section from an area ratio of 10:1 to 40:1.

Four propellant systems, N_2O_4/N_2H_4, N_2O_4/N_2H_4-UDMH, F_2/H_2, and OF_2/B_2H_6 were selected for comparison. Ideal assumptions were made such as uniform coolant flow distribution and thermal stability of the coolant. Also an adiabatic wall was assumed. Using the design procedures previously outlined, cooling requirements were calculated for the various sections of the motor and are listed in Table I. It can be seen that in each case the combustion chamber requires the most coolant. This is obvious since the small contraction ratio (1:5) gives high heat transfer coefficients and the length is of sufficient value to give reasonable heat transfer surface area. Although the convergent section has the highest heat transfer coefficient, the surface area is much smaller than any of the other sections. Thus the convergent part has the smallest coolant requirement. In comparing liquid film cooling, in which no advantage was assumed from the cold vapor downstream of the last drop of liquid, the main difference between the cooling requirements of the various propellant combinations is the heat flux and the heat of vaporization of the coolant. For these cases, the heat of vaporization is the controlling factor and thus the N_2O_4/N_2H_4 system has the lowest requirements.

For gas film cooling, the most important property is the specific heat of the coolant. Note that gaseous hydrogen has by far the lowest requirement for a gas. Liquid film cooling for hydrogen under the ground rules established looks less attractive because of its low heat of vaporization and low boiling point.

In estimating the liquid film requirements it is necessary to assure that a stable liquid film is established. By use of the stability criteria calculations were made to determine the maximum coolant flow at any one section in the motor. By knowing this along with the flow rate of coolant required, the minimum number of injection points may be determined. Figure 82 shows the injection scheme assumed. The OF_2/B_2H_6 system is not shown since it is similar to that for H_2/F_2.

Since there is no stability criteria for gas cooling, the injection was assumed to occur at the beginning of each section. The velocity of injection was arbitrarily assumed. Figure 83 shows typical injection conditions. These assumptions were by no means optimum and by proper variation of the number of injection points and the injection velocities it is possible to partly reduce the coolant requirement.

For the parametric studies made of film cooling in the nozzle, geometric similarity was assumed. In other words, the length of the nozzle was taken to be proportional to the throat diameter. Figure 84 shows the results of the parametric study. It is indicated that coolant requirements are independent of thrust for constant pressure. By increasing the thrust the throat area is increased proportionally. Hence, the throat diameter and the length are each increased by the square root, meaning the surface area is doubled. The heat transfer is held constant and so the heat duty is increased proportionally. Since the propellant requirement is increased proportionally, the coolant flow ratio is a constant.

By holding the thrust constant and increasing the pressure, the coolant requirement is reduced somewhat for the following reasons. Increasing the pressure causes the throat area to reduce proportionally. This gives a proportional reduction in surface area. Since the heat transfer coefficient is usually assumed to vary as P to the 0.8 power, a slight reduction in coolant requirement is the result.

The system, OF_2/B_2H_6, was examined in detail because of its special property of creating a very high heat flux at the nozzle throat. Although film cooling of the chamber does not appear attractive because of the large coolant flow required (see Table VI), it may be advantageous to use it locally such as at the throat, where the high heat flux creates problems with regenerative cooling. Figure 47 of Volume I, shows the accumulated liquid coolant requirement beginning at the chamber exit and ending at the nozzle exit. Figure 47 of Volume I includes requirements for gas cooling with a maximum wall temperature of 2200°R. From the latest Purdue data, the coolant requirements for liquid film including the vapor cooling effect is shown in Figure 47 of Volume I. By comparing this data with that of gas film cooling, the vapor cooling effect appears to be much greater. It is difficult to explain the large difference between the two. Probably the true coolant requirement for liquid cooling with the vapor cooling effect lies somewhere in between. The need for experimental verification in this case is obvious.

One further study with the OF_2/B_2H_6 system was made by varying the maximum wall temperature for adiabatic conditions for the convergent section. The result is plotted in Figure 85. Two effects are evident by the drop in coolant requirement with the increase in wall temperature. The rise in temperature reduces the heat flux and increases the heat content of the coolant since the maximum coolant temperature is taken to match the wall temperature. By coupling an additional cooling mechanism, such as radiation or regeneration, the coolant requirements will drop since the coolant temperature will be able to rise above the wall temperature.

4. Limitations of Film Cooling

Although film cooling does appear advantageous as a method of cooling since there are no apparent heat flux limitations as found with regenerative cooling or time limitations as with ablative cooling, or pressure limitations such as with radiation cooling, there is one important consideration that must be

evaluated. This is the amount of coolant that is required. From this point any flux and any total heat requirement can be met provided one is willing to pay the penalty resulting from the coolant flow rate and the temperature stratification. Ordinarily the fuel is used as the coolant in order to minimize the possibility of burning on the wall. Using the oxidizer introduces the possibility of burning at the surface. Inert coolants have been considered, but usually they produce a larger performance decrement (see Figure 76).

From a qualitative view, the effect of transient operation of film cooling does present some problems. If it is necessary to establish the film before ignition, hard start may result from a fuel rich mixture in the combustion chamber (Reference 125). Also a finite time may be required to establish the flow. For a pulse type operation a large expenditure of fuel may result. Starting the engine before the flow of coolant will result in a deposit of condensible combustion products on the wall, which will plug the coolant injector passages (Reference 125). To prevent this a small bleed of coolant could be allowed while starting the engine. To properly evaluate the restart problems it would be necessary to consider each particular coolant and its stability characteristics. Further search in the reference literature may reveal more pertinent information as to the starting and pulsing characteristics of film cooling.

The application of film cooling to a wide range of engine size presents no problem. The larger the engine, of course, the greater becomes the flow requirement since it is proportional to the total heat that would be transferred to the engine wall by the gas stream. Since this total heat is proportional to the surface area, it is proportional to the coolant film. Problems may be encountered in the application to very small motors when considered at the throat. The boundary layer buildup at the throat compared with A* may seriously effect the I_{sp}.

With regard to the process of film cooling under throttling conditions, Equation (3) of Appendix C indicates that the ratio of coolant flow to propellant flow is proportional to $(P_o/T)^{1/2}$. If under throttling conditions this ratio does not vary too much, the flow ratio should be essentially constant. Therefore, the coolant flow rate would be expected to throttle in proportion to the flow of fuel (assuming the fuel is the coolant). However, a change of O/F ratio would destroy the linear relationship to the propellant flow. Further literature search supported by experimental backup would bring to light the control problems of this process.

There is no limit to the duration of operation for film cooling since there will always be coolant available as long as there is propellant.

There are no storage problems involved with the coolant unless an inert coolant is selected which would require separate tankage and thus more weight.

The operation of film cooling in a high g field apparently has not been determined to date. One might expect a larger effect with the liquid film. A high g field exerted parallel to the axis of the motor would tend to thicken or thin the boundary layer of the liquid depending on the direction. This in turn would have an effect on the heat transfer rates, liquid film stability, and thus the coolant requirements. The g effect would be expected to have a lesser effect on gas cooling because of lighter density involved. It is interesting to note that the work of Reference 124 was performed with a water film coolant flowing in a horizontal tube without a large coolant flow length distribution (Figure 68). This indicates that a one g field normal to the surface is not detrimental. Theoretically, the high g condition could be analyzed for ideal conditions to indicate the approximate influence.

5. Transpiration Cooling

The process of transpiration cooling is similar to film cooling in that the sensible or latent heat of the coolant absorbs the heat from the working fluid of the rocket motor. However, there are some important differences. Unlike the film cooling principle, in which a cold film interposes itself between the hot gas stream and the structural wall and is injected through slots or holes, transpiration cooling utilizes a porous wall so that the coolant is in contact with a large surface area of the wall. In this manner, the coolant actually exchanges heat with the wall by means of the large surface area available so that the coolant, as it issues into the hot working fluid approaches the inner wall temperature. As this fluid enters the chamber or nozzle where it is being used, the momentum of the hot gas stream sweeps it along the wall. Therefore, an additional advantage is taken in that the coolant, at the temperature of the inner wall, essentially thickens the boundary layer and reduces the net heat flux to the wall. From a theoretical standpoint gaseous transpiration cooling should be equivalent to gaseous film cooling. However, the transpiration coolant reaches the maximum wall temperature before it comes in contact with the main gas stream, while the film coolant is in contact with the main gas stream as it reaches this temperature. Cooling efficiency is quite low in the latter case since some of the film will be torn away from the wall. As evidenced by sample calculations cooling is only about 20% efficient. Transpiration cooling can have an added advantage over liquid film cooling in that in theory the liquid can be thought to vaporize as it diffuses through the wall. In this manner the coolant can absorb more than the latent heat and thus reduce the amount of required coolant.

Reference 136 considered an ideal case of Couette flow with mass injection and by heat, mass and momentum balances derived an equation for the heat transfer coefficient between the main stream and the wall as a function of the coefficient without mass injection. The result was as follows:

$$\frac{h}{h_o} = \frac{\dfrac{G_g\ Cp_c}{St_o\ G_g\ Cp_g}}{\left[e^{\left(\dfrac{G_c\ Cp_c}{St_o\ G_g\ Cp_g}\right)} - 1\right]} \qquad (29)$$

MAC A673

where

h = Heat transfer coefficient with transpiration

h_o = Heat transfer coefficient without transpiration

St_o = Stanton number

G_g = Main bulk mass velocity

G_c = Coolant mass velocity

The above expression then, shows the effect of reduction in heat transfer by transpiration cooling.

Experiments have shown this derivation to be representative. Reference 146 considered a 7 by 1.5 inch porous flat plate constructed of sintered stainless steel wire 0.050 inch thick which would have sufficient pressure drop to produce uniform flow distribution. The roughness of the surface was apparent to the touch. The results shown in Figure 80 indicate good correlation with the film theory. Further work on transpiration cooling was reported in Reference 147 and essentially verify the results of Reference 146. Typical results are shown in Figure 81.

6. Transpiration Cooling Design Calculations

The theoretical derivation of transpiration cooling of a flat plate has been well documented by experiment (References 146 and 147). Therefore, one can have confidence in applying the results for a gaseous coolant. The use of liquids which vaporize as they diffuse through the wall has not been verified. As an ideal condition it may be postulated that this process is identical to the gaseous one except for the term which includes the enthalpy change of the coolant. This number should represent the change of temperature from that of the subcooled injected liquid to that of the wall temperature. Consequently, the combustion chamber cooling requirements can be determined by Equation (10) of Appendix C, which is as follows:

$$\frac{\dot{W}_c}{\dot{W}_g} = 2\,St_o \frac{L^*\,Cp_g\,(T_g - T_w)}{(C_r)^{3/2}\,\triangle He} \left(\frac{\pi C_F P_o}{T}\right) e^{\left(-1/2M^{0.57}\,\frac{G_c}{G_g\,St_o}\right)}$$

A question arises as to the application of this approach in the curved surfaces of the nozzle. Reference 127 considered the cooling effect downstream from a transpiration cooled section of the convergent area. The authors stated that the pressure gradient caused the departure of the results from the film theory and correlated the results for air and helium empirically. The question is still open

as to the applicability of these results to a more general case. Pending further experimental information in this area, it is recommended that the flat plate results be applied to the nozzle in the same manner as was done in the case of film cooling. Equation (11) in Appendix C shows the following:

$$\frac{\dot{W}_c}{\dot{W}_g} = \frac{2\ St_o\ Cp_g\ (T_g - T_w)}{(A/A^*)^{1/2}\ \Delta H_c} \left(\frac{\pi C_F\ P_o}{T}\right)^{1/2} e \left(-\ 1/2\ M^{0.57}\ \frac{G_c}{G_g\ St_o}\right) dL$$

which must be integrated over the areas to be cooled.

It is also recommended that in lieu of experimental data, the above equations be used for the liquid that is assumed to vaporize as it flows through the wall.

7. Limits to Transpiration Cooling

Theoretically, the requirements of transpiration cooling are less than those of film cooling. In general, the limitations are the same as for film cooling with the exception of a few additional ones.

There is no maximum heat flux which limits the use of transpiration cooling. The heat can be removed provided the coolant flow rate is available. The maximum pressure limitation would only be a function of the strength of the porous media through which the coolant diffuses. The loss in performance is similar to that of film cooling.

Perhaps the biggest problem involved in transpiration cooling is the selection and manufacture of the porous media. One prime requirement is that of uniformity. This is necessary to obtain uniform flow distribution; also sufficient pressure drop must be available to insure this uniformity. Ordinarily these materials are made of sintered metal, woven wire, perforated sheet, and fiber base porous materials. Reference 148 presents a limited discussion of materials and their problems. The author did indicate the importance of having a clean coolant which contains no foreign matter that will clog the pores. Also indicated was the lack of a deposition problem on the hot gas side because the flowing coolant will tend to prohibit any scale formation. Reference 149 considered the use of refractory metals as the most reasonable choices for fabrication of the porous media. A statement was made that fabrication of rocket nozzles with these materials would require a major development effort. In addition, the use of refractory metals introduces the problem of oxidation susceptability. In any event indications are that the materials problem must be solved before wide spread use can be made of transpiration cooling. Good heat transfer data obtained from a small test section leads one to believe that this can be accomplished.

MAC A673

The use of transpiration cooling may bring in a problem in the convergent or divergent section where a pressure gradient exists in the direction of the main gas flow. In order to obtain proper coolant distribution it may be necessary to taper the thickness of the porous media.

The use of transpiration cooling, aside from previously mentioned points depends strongly on the nature of the coolant. If it is a gas, it must be stable up to the operational temperature of the wall. If it decomposes somewhere along the way with formation of particles, plugging of the porous media will surely occur. The physical state of the coolant must also be considered. Reference 148 states that if a liquid coolant boils within the porous wall, coolant flow instability will occur. Reference 149 refers to an experiment in two-phase transpiration cooling in which a double wall section each 1/8-inch thick, of sintered stainless steel was used, with a thermocouple placed between the walls. The hot gas temperature was in excess of 2000°F and water was used to cool the section. Measurements made between the walls indicated that boiling occurred in the wall nearest the hot gas. Neither flow instabilities nor damage to the porous wall occurred. Until further experimental data is available on two-phase cooling the final conclusion on the matter must be reserved.

During transient operation some problems may occur. In order to prevent plugging of the pores, it is necessary to start the coolant flow first. This will require some throttling control since the back pressure has not been set by the working fluid. As combustion begins the throttling will need to be eased as the back pressure is built up. As in film cooling, the problem of hard starting in the combustion chamber may result from a fuel rich mixture (assuming the fuel is the coolant). If the coolant is a liquid, instability problems may result from a transient heat flux. Further analysis into these areas may indicate the magnitude of these problems.

In a similar manner to film cooling, a pulse operation may cause a large expenditure of propellant due to the requirement of flowing the coolant first. Development work along this line may establish a realistic quantitative penalty to the pulse type operation.

A throttling operation should not present a special problem since with small changes in thrust the coolant to propellant flow ratio is proportional to $(P_o/T)^{1/2}$. However, changing the O/F ratio does indicate the need for control.

Engine size does not present any problems to the application of transpiration cooling. Naturally, the larger the surface area of the engine, the larger will be the coolant flow requirements and the larger the decrement in I_{sp}.

There is no limit to the duration of operation of transpiration cooling since there will always be coolant available as long as there is propellant.

No storage problems will be encountered unless an inert coolant is selected which would require separate tankage.

The process of transpiration cooling has not been evaluated under high g fields. It would be expected that if the field is directed along the axis of the engine its major effect will be to thicken or thin the boundary on the wall depending on direction. Since the cooling process experimentally has agreed with the boundary layer assumptions, it seems reasonable that the effect of high g fields could be evaluated analytically and the increase or decrease in heat transfer rates indicated.

A vacuum environment should not pose a problem except for the startup case using a liquid coolant. The liquid will continue to flash at the surface or inside the porous media until the back pressure from the motor is brought in.

External environment effects outside the motor casing, of course, have no influence on the performance of transpiration cooling.

8. Parameterization of Transpiration Cooling

It has been shown that transpiration cooling is more efficient than film cooling because the coolant is protected from the shearing action of the main gas stream until it diffuses through the wall. Ineffeciencies occur in film cooling by the tearing from the wall cold portions of the film. From the sample calculations performed on the 4000-pound thrust engine, the advantages of transpiration cooling become evident. In comparing the results of an N_2O_4/N_2H_4 system with that of H_2/F_2, the advantage of the available enthalpy of the coolant becomes evident. However, the relationship is not linear as in the case of the film cooling calculations, since a higher coolant flow reduces the heat transfer coefficient and thus requires less coolant. Nevertheless, the same general trend of coolant requirements exists with transpiration cooling as shown by the similarity of the design equations.

Parameterization of the conditions would result in trends similar to that of film cooling. Effects of various factors will be somewhat different due to the influence of coolant flow ratio upon heat transfer coefficient.

E. Heat Sink Cooling

Combustion chamber and exit nozzle component temperatures may be held below structural limits while heat is being conducted away from the surface and absorbed in the chamber and nozzle walls. Heat sink components that are essentially inert, absorb heat as a function of the specific heat, mass, and temperature rise of the part. Heat sink capacity may be increased through the use of endothermoic heat sink materials. These materials such as subliming salts, lithium compounds and low melting point metals capable of absorbing large amounts of heat through a phase change from an initial solid state. The endothermic materials may be impregnated into porous refractory wall materials or used to back up the walls as an insulator as well as a heat sink.

The primary limitation on this concept is the run time available before a limiting surface temperature is reached. Two limiting temperatures are encountered: First, the melting, subliming or softening temperature at which the structural material would flow or erode rapidly. Second, the temperature at which the oxidation rate or reaction rate with the combustion gases would be excessive.

1. Inert Heat Sinks

Promising heat sink materials are those which have high heat capacity, high thermal conductivity, high structural temperature limits and compatibility with combustion gases. Figure 86 presents a plot of the surface temperature rise of a semi-infinite slab which is heated convectively at the surface. An examination of the parameter $h\sqrt{\alpha\theta}/k$ indicates that the initial heat sink surface temperature rise rate is proportional to the heat transfer coefficient and inversely proportional to the square root of the term $k C_p \rho$ (i.e., thermal conductivity and heat capacity per unit volume). Furthermore, the time for different materials to reach a given temperature under the same heating conditions is proportional to the product $k C_p \rho$. Hence, an approximate figure of merit for heat sink materials would be $k C_p \rho$. The exact solutions for the temperature response of cylindrical sections of finite wall thicknesses follow these relationships initially but the temperatures at later times become a function of radius ratio and wall thickness. These solutions have been worked out in a convenient graphical form in References 208 and 209. Since these reports are readily available, the solutions are not included here.

Values of $k C_p \rho$ for several materials are listed in Table VII as a comparison of heat sink potential. A further comparison of heat sink potential may be based on time required to reach a limiting temperature since these limits vary considerably for such materials as copper and tungsten. Table VII lists a reasonable temperature rise and the last column gives the time for a slab surface to reach this temperature for a heat transfer coefficient (h) of 500 and a gas temperature of 5000°F.

On this latter basis, edge oriented pyrolytic graphite washers represent the best heat sink material followed by tungsten and graphite. These materials also have the best thermal shock resistance. Oxidation is the critical problem with combustion gases containing CO_2 and H_2O. Graphite and tungsten oxidation resistant coating offers a partial solution for temperatures below 4000°F. In products containing primarily HF, the heat sink temperature limits may be in the 4000° to 6000°F range.

Typical run times to reach these high surface temperatures are shown in Figures 11 and 12 of Volume I for a nozzle throat insert (or chamber) with a 4-inch I.D. and an 8-inch O.D. with properties corresponding to graphite and pyrolytic graphite at chamber pressures up to 600 psia and gas temperatures to 2000°F.

The effect of a transient pulsing duty cycle on the temperature response of a graphite throat insert hot and cold sides is shown in Figures 87 and 88 . The thermal analyzer IBM 704 computer program was used to compare the difference between a 50% or 14% duty cycle with the approximation that the heat transfer coefficient could be assumed as 50% or 14% of the steady state value.

The combustion environment was as follows:

a. Throat insert size 0.85 inch I.D. and 2.75 inch O.D.

b. Propellants N_2O_4/0.5 N_2H_4 - 0.5 UDMH

c. Chamber pressure P_c = 100 psia

d. Combustion temperature = 4500 °F

e. Convective heat transfer coefficient h = 310 Btu/hr ft^2 °F

Duty Cycles:

a. 50% - 200 milli sec. on and 200 ms off

b. 14% - 200 ms on and 200 ms off followed by 10 sec off

Figure 87 compares in detail the transient temperature response for the 14% duty cycle with the 14% heating rate approximation.

The discussion of semi-infinite slabs indicates that a limiting surface temperature may be reached in a short time regardless of how thick the chamber walls are. Therefore, the first step in evaluating the feasibility of a heat sink component would be to calculate the run time available with infinitely thick walls. Then a calculation of chamber component weight versus run time may be made using the graphs available in References 208 and 209.

2. Endothermic Heat Sinks

Preliminary evaluation of endothermic heat sink materials may be made on the basis of the weight of material required to absorb all of the heat flux to a nozzle component at a specified wall temperature. Consider the following example which is worked out in round numbers to demonstrate the concept involved.

Example:

Thrust F	=	4000 lb
I_{sp}	=	400 sec
Flame temperature T_c	=	7000°F
Surface temperature T_w	=	4000°F
Heat transfer coefficient h	=	1000 Btu/hr ft^2 °F
Throat Diameter D*	=	2.5 inches
Surface area cooled A_s	=	30 $inches^2$
Propellant flow W_p	=	10 lb/sec
Heat flux	=	173.5 Btu/sec (30 $in.^2$)
Heat absorbed by sink material in phase change ΔH	=	1000 Btu/lb
Coolant utilization rate	=	0.17 lb/sec
Fraction of propellant rate	=	0.017 or 1.7%
Weight for 100-second run	=	17 lb

Some potential endothermic heat sink materials which sublime between room temperature and 4000°F are given in Table VIII. The temperatures of sublimation or dissociation for these materials vary from 800 to 6700 Btu per pound. Other potential endothermic materials would be metals which boil below 4000°F such as lithium, magnesium, and zinc, or materials which have a high heat of fusion such as lithium hydride (1065 Btu/lb).

The practical problems of controlling the nozzle component temperature and the utilization rate of the coolant are subjects of current research (References 205, 206 and 209). Results of uncooled nozzle tests (at NOTS, China Lake) with porous tungsten impregnated with copper and with brass as well as other heat sink materials are reported in Reference 205. Design studies on similar advanced cooling concepts for solid propellant application are reported in Reference 210.

IV. DESIGN DATA REFERENCE SECTION

A. Mission Requirements

The first part of the problem of determining the applicability of the various combustion chamber cooling methods to liquid propellant rocket engines used for space missions is to define the desired missions and the required rocket engine characteristics.

The following categories of space missions and maneuvers are considered representative of the various space activities which are currently undertaken or will be initiated in the foreseeable future:

1. Orbital corrections
2. Orbital rendezvous
3. Correction of injection errors, station keeping, and attitude control of a 24-hour satellite
4. Lunar and interplanetary trajectory corrections
5. Lunar and planetary orbiting maneuvers
6. Lunar and planetary landings and takeoffs

The basic study to determine the propulsion requirements and systems for these space missions was made by Aerojet-General under Contract NAS 5-915 (Reference 1) and by Rocketdyne (Reference 2). Other references were used to tailor the basic study toward establishing combustion chamber operating requirements.

Representative system characteristics in Table I of Volume I for the mission/system classifications were developed by considering a specific payload and vehicle size. The injected spacecraft weights were compatible with the capabilities of the Centaur, Saturn, and Nova Launch vehicles (References 2, 3, and 4). Most parameters are presented on the basis of per-unit initial mass, in order to allow direct scaling of the results with vehicle gross weight. The analyses of orbital maneuvers were generally based on impulsive thrusting assumptions. The characteristics evaluated as basic mission-related propulsion requirements were as follows:

1. Ideal velocity increment requirements
2. Desirable initial thrust-to-mass ratios
3. Required total impulse accuracy
4. Required thrust variability

5. Re-start requirements

6. Minimum service life requirements

7. Thrust programming

8. Storability requirements

The ideal velocity requirements were established directly from the nature and characteristics of the maneuver, whereas the required total impulse accuracy is normally determined by the accuracy with which the maneuver must be completed. The desirable initial thrust-to-mass ratios were established from the following:

1. Maximum acceleration tolerance of payload

2. Required cutoff impulse accuracy

3. Increase of propulsion system weight with thrust

4. Variations in ΔV requirement with thrust level (such as those due to gravity and drag losses)

5. Effects of maneuver duration on guidance complexity (as for orbital maneuvers)

6. Effects of accelerometer bias errors on monitoring accuracy for the maneuver

The requirements for thrust variability, re-start requirements, minimum service life, thrust programming, and storability were established directly from the characteristics of the maneuvers.

The propulsion requirements for the representative systems fall into propulsion capability groups which are as follows:

1. Systems in low thrust range capable of multiple re-starts and thrust variability

2. Systems with a nominal constant thrust of 2000 to 20,000 lbs capable of multiple re-starts and using thrust vector control

3. Systems with constant thrust on the order of 1 by 10^6 lb_f with multiple re-start capability.

The various space missions considered and the associated propulsion system requirements were summarized in Table IX (Table I, Volume I). A review of this table reveals the wide range of system parameters under consideration. Thrust requirements vary almost continuously from one pound to over one million pounds, the number of restarts vary from none to hundreds, the burning times vary from less than one minute to several minutes. Studies are continuing to evaluate further detailed operating requirements for the various missions, such as thrust transients and lunar landing thrust programming techniques.

Further detailed considerations of the space mission maneuvers and how they affect the propulsion requirements are as follows:

1. Thrust-Time Requirements

Four different types of thrust-time plots for space engines which affect the cooling system selection and performance are presented in Figure 2 of Volume I. Although it seems obvious that regenerative cooling would be more applicable to long, steady state firing than to pulse rocket application, other limitations on various cooling techniques require a more detailed study to define the cooling technique limitations imposed by the thrust-time restart requirements.

Figure 89 illustrates the relationship between engine thrust level and total burning time in the case of a constant thrust soft lunar landing with a spacecraft of a typical weight that could be launched by Saturn type boosters. The vehicle energy (in terms of unbraked impact velocity) and propellant effective exhaust velocity are fairly representative and are used only as examples. A curve showing the tradeoff between thrust level and burning time is desirable because of the probability of different chamber cooling techniques being applicable for different portions of the curve. The near optimum point from the standpoint of the maximum landed usable weight (not considering cooling techniques) is shown in this plot. This point and the resultant engine design configuration may change with chamber cooling considerations.

Figure 90 is a plot similar to Figure 89 for the case of landing with a constant deceleration descent. The conditions of vehicle weight, effective exhaust velocity, and total energy are the same. The required thrust levels at the initiation of combustion and at the end of combustion are given as functions of the total combustion period. The two curves in Figure 90 are meant to be used together with total burning time being the independent parameter. A linear thrust decrease with time during any particular landing is indicated on the plot. This is not precisely true, but is sufficient for determining chamber cooling requirements. Again, the near optimum conditions indicated may change with cooling considerations.

Figure 91 is a plot of the relationship between thrust level and total burning time for taking off from the lunar surface. The vehicle weight has been chosen to be compatible with the landed weight of the vehicles discussed in Figures 89 and 90. Again, the near optimum condition is indicated. For long burn times in a gravity field, the total impulse requirement increases imposing a weight penalty to be considered in the choice of engine size.

The concept of landing with a constant thrust engine with more than one burning period is being studied. In considering a typical thrust-time program for a thrust to initial weight ratio of 5 (a thrust of 20,000 lbs for a vehicle weight of 25,000 earth lbs), the time sequence would be approximately 240 seconds of burning, 128 seconds off, 15 seconds of burning, 40 seconds off, and 3 seconds of burning.

The concept of a pulse rocket burning cycle is limited primarily to low thrust precise corrections of vehicle attitude.

Two thrust-time considerations which enter directly into the cooling system choice are the thrust transient requirements at ignition and shutdown. Regenerative cooling requires pressurization and filling of the cooling passages and may delay thrust buildup. Also, at engine shut down, a large volume of propellant is trapped in the lines which may produce an unacceptable residual thrust. Even in an ablative engine, some residual thrust is produced by outgassing of the heated thrust chamber wall.

2. Engine Configuration and Location

From the mission studies of References 1 and 2, a number of promising spacecraft configurations have been proposed. Engine sizes and locations for various lunar missions are shown in Figures 92 to 94 . Spacecraft engine configurations proposed for earth orbit rendezvous and docking missions are shown in Figure 95.

Some of the thrust chamber design considerations related to the engine configuration and location are listed below:

a. Spacecraft Envelope

The spacecraft envelope may limit engine size or exit nozzle expansion ratio. Reference 1 provides the following vehicle envelope restrictions for Centaur, Saturn, and Nova vehicles:

Vehicle Envelope Restrictions	Centaur	Saturn	Nova
Maximum diameter ins.	120	220	260
Minimum diameter ins.	--	154	154

The diameter of the Apollo spacecraft for some missions is 154 inches.

b. Soak-Back Limitations

Heat stored in the thrust chamber walls at shutdown must be dissipated by radiation and conduction to the adjacent structure or to space. During firing, this heat may have been contained within the chamber or absorbed by the flowing propellants. After shutdown, the outside of the chamber walls may continue to rise in temperature and also the heat may be absorbed by the stagnant propellants. When considered in terms of the long storage times required of propulsion systems to be used on extended space missions, the conduction heat transfer

between the propellant tanks and the thrust chamber through feed lines and supporting structure may be the critical factor in limiting the storability of certain propellants (cryogenics).

3. Space Environments

The spacecraft engine will be subject to both operation and storage in the space environment. The elements of the space environment which most directly concern the thrust chamber design are as follows:

1. Zero gravity
2. Vacuum effects
3. Meteoroid penetration
4. Ionizing radiation
5. Solar radiation
6. Heat transfer to space
7. Re-entry from space

A great amount of information is becoming available on how the space environment affects both materials and physical phenomena (References 10 through 28). The success of the satellite programs indicates that these space effects are not prohibitively detrimental. Space effects are much more critical in crew survival, mechanical, optical, electrical, and electronic component performance, and propellant storage. The more important effects of space environment on thrust chamber design have been covered in the sections on cooling method applicability.

4. Space Mission Maneuvers

a. Orbital Corrections

In determining the propulsion requirements for orbital corrections, most of the orbital maneuvers which it might be desirable to accomplish have been considered. These include the following:

1. Control of orbital perturbations
2. Control of orbit eccentricity
3. Orbital plane changes
4. Orbital altitude variation and control
5. Orbital epoch changes
6. Correction of injection errors (References 5 and 6).

MAC A 673

(1). Control of Orbital Perturbations

(a). Atmospheric Drag

The most significant disturbance, from the standpoint of absorption of orbital energy, that confronts a satellite that must pass over the earth at low altitudes is atmospheric drag. The propulsion requirements to overcome atmospheric drag, and still allow the satellite to remain at its established altitude, is best satisfied by the use of the attitude control system rather than the propulsion itself.

(b). Earth's Oblateness Effect

For a satellite in orbit with eccentricities of 0.05 or less, the earth's oblateness effects four elements of motion as follows:

1. The period of revolution
2. The rate of rotation of the orbital plane
3. The rate of rotation of the major axis of the orbit
4. The oscillation in the radial distance.

The most practical of these to require correction is the rotation of the orbit plane. The propulsion requirements to compensate for the rotation of the orbital plane due to the earth's oblateness are presented in Table IX.

(c). Solar Radiation Pressure

A variation in altitude of satellites with large surface to mass ratios can be caused by solar radiation pressure. However, the corrections are small and they could be made with a system which combined attitude control and station keeping.

(d). Satellite Perturbations Due to Lunar and Solar Gravities

The only effects of solar and lunar gravities which significantly change the motion of the satellite are the regression of the nodes and the oscillation of the orbit-inclination angle. These effects can also be controlled by a combined attitude control and station keeping system.

(2). Orbit Eccentricity Control

Operational requirements may make it necessary to change the eccentricity of satellite orbits so that large spatial coverage can be obtained with one satellite. Propulsion requirements necessary to effect these changes are presented in Table IX.

(3). Orbital Plane Changes

Plane changing maneuvers may be required to perform various functions required of an earth satellite, such as correction of regression of the nodes due to the earth's oblateness, interception and rendezvous, and varying spatial coverage. The propulsion requirements to cover both circular and elliptical orbits and rotation angles to 45° for orbital altitudes between 300 and 19,310 nautical miles are presented in Table IX.

(4). Orbital Altitude Variation

Propulsion requirements to transfer from one circular orbit to another coplanar, circular, orbit of different altitude were determined for both impulsive and continuous thrust assumptions, and are presented in Table IX. Thrust modulation will generally not be required; different velocity requirements at perigee and apogee can be achieved by two different burning times. Also, a zero g, restartable propulsion system will be required to perform the perigee and apogee operations unless a continuous, low thrust propulsion system is used.

(5). Orbital Epoch Change

(a). Types of Maneuvers

Three types of maneuvers for achieving an epoch change are 1. The use of continuous thrust, 2. Impulsive transfer to a new path for a fast or emergency transfer, and 3. A special case of the fast transfer in which the satellite is required to achieve the epoch change in one orbital revolution.

(b). Continuous Thrust

When an epoch change is made using continuous thrust, velocity is increased during the first half of the transfer, and decreased during the second half, or vice versa, depending on whether the epoch change is "leading" or "lagging". The original circular orbit path is maintained during the maneuver by directing an appropriate thrust component along the radial axis. The radial thrust component is directed inward, when the velocity is greater than that for the normal circular orbit, and outward when the velocity is below orbital. Generally, the application is in the terminal phase of a normal rendezvous maneuver.

(c). Fast or Emergency Transfer

Fast or emergency transfers require transfer by impulsive thrust to new trajectories. If the desired position leads the satellite, the new trajectory is either elliptical or hyperbolic, depending on the magnitude of the change required. If the desired position lags the satellite, the new trajectory is elliptical. The new trajectory intersects the original circular orbit in such a manner that the satellite achieves the epoch transfer at the time of intersection. At this instant, a velocity increment, equal to that applied to transfer it to a new trajectory, returns the satellite to the original circular orbit.

MAC A 658

(d). Special Case of the Fast Transfer

In the special case of the fast transfer, the satellite is transferred by impulsive thrust to an elliptical path in such a manner that it takes one revolution of the satellite to reach its desired position in the orbit.

The propulsion requirements to achieve an epoch change dictate two general types of systems. The small changes can be made with a continuous thrust system. However, the change requiring greater capability must use the impulsive system. The basic requirements are presented in Table I.

(6). Correction of Injection Errors

The two methods which could be used to correct injection errors are: 1. Correction of the errors in each orbital parameter separately, termed the three-impulse transfer, and 2. Correction of the errors simultaneously by one maneuver by selecting a point in the desired orbit and then utilizing continuous thrust to attain that position.

In the three-impulse transfer method, errors in eccentricity and perigee altitude can be corrected simultaneously, and errors in the orientation of the orbit plane can be corrected by an additional impulse. The propulsion requirements to correct anticipated nominal injection errors, using the three-impulse transfer, are presented in Table IX. The continuous thrust method is a rendezvous technique which is discussed in the following section.

b. Orbital Rendezvous

Three basically different techniques of rendezvous are presented. The first assumes that rendezvous is composed of two operations: a course injection maneuver and a fine correction of the injection errors. The second, making also a plane change, is called a dogleg maneuver, and the third, which used not only the phases of the above two, but further employs an orbital epoch change, and it is termed emergency rendezvous (References 7, 8, and 9).

(1). Rendezvous with Nominal Injection Errors

It was assumed that out-of-plane errors are small compared to in-plane errors and the resulting two-dimensional rendezvous determines the propulsion requirements. The basic propulsion requirements necessary when the satellites are in the same orbit were determined in connection with the orbital epoch change. The general propulsion requirements for the terminal phase of the rendezvous are presented in Table IX.

(2). Rendezvous with the Dogleg Maneuver

Rendezvous with the dogleg maneuver is generally comprised of two separate maneuvers, the first to make the orbital plane change and injection, and the second to make the final rendezvous. With the final rendezvous requirements previously tabulated, the first portion of the rendezvous requirements are presented in Table IX under "Dogleg Maneuver."

(3). Emergency Rendezvous

An emergency rendezvous may include any or all of the following operations: 1. Injection with the dogleg maneuver, 2. Orbital epoch change, and 3. Final rendezvous. Thus, the velocity requirements for emergency rendezvous are the sum of the individual maneuvers. The propulsion requirements are summarized in Table IX.

c. Satellite 24-hour Mission

Propulsion requirements are presented for three basic operations which the satellite propulsion system will be required to perform. These operations are: 1. Orbit correction for the elimination of injection errors and for the achievement of the desired longitudinal position, 2. Station keeping to maintain orbit velocity and angular position of the orbit plane, and 3. Attitude control to correct the effects of solar pressure, thrust misalignment, initial rates, and undisturbed limit cycle. The propulsion requirements are shown in Table IX.

d. Lunar and Interplanetary Trajectory Corrections

The propulsion requirements necessary to perform lunar and interplanetary trajectory corrections were established by error analysis for the nominal trajectories and particular missions considered. Midcourse corrections are presented for Earth-Moon flights and Earth-Mars flights. Terminal corrections are presented for outbound lunar and Mars flights and return flights from the Moon and Mars.

(1). Midcourse Corrections

Midcourse correction capability will be required on ballistic space flights where the uncorrected trajectory results in miss distances which are excessively large for terminal phase correction. The propulsion requirements for midcourse correction are affected by: 1. The initial burnout-velocity-vector accuracy, 2. The allowable miss distance at the target body, 3. The accuracy of midcourse navigation and guidance equipment, 4. The accuracy with which the corrective maneuvers are carried out, and 5. Any significant inaccuracies in astrophysical data.

Propulsion requirements for midcourse correction for Earth-Moon flights and Earth-Mars flights are presented in Table IX.

(2). Terminal Corrections

Terminal corrections are classed as the impulses applied to correct the final perigee distance after the target body's gravitational effects have become predominant. Correction of position error in determining the final perigee distance as the target is approached is also a terminal maneuver.

Propulsion requirements for terminal correction are presented in Table IX for outbound lunar and Mars flights and return lunar and Mars flights.

e. Lunar and Planetary Orbiting Maneuvers

In determining the propulsion requirements for orbiting the Moon and Mars, the perigee altitude established by the terminal trajectory corrections will form one apsis point for orbiting maneuvers of the target body.

(1). Lunar Orbiting Maneuvers

Lunar approach trajectories with approach velocities ranging between 4000 and 7000 fps were considered. The propulsion requirements under these conditions are presented in Table IX.

(2). Mars Orbiting Maneuvers

Propulsion requirements are tabulated in Table I for Mars orbiting maneuvers both with and without the use of atmospheric deceleration. The range of hyperbolic approach velocities varied between 8000 and 27,000 fps.

Without atmospheric deceleration, approach perigee radii vary from 200 to 2000 nautical miles with apsidal radius ratio ranging from 0.70 to 3.8.

Atmospheric braking can be utilized to reduce considerably the propulsion requirements for Mars orbiting maneuvers. One technique is to make several grazing passes to reduce the apogee altitude to that desired and then add the required velocity increment to raise the perigee altitude to establish the required orbit. The only propulsion requirement provided for this type of maneuver is to vary the perigee altitude.

f. Lunar and Planetary Landings

(1). Lunar Landings

Four methods for landing on the moon were considered: 1. Direct radial approach and landing, 2. Injection into circular orbit and a gravity turn from orbit to landing; 3. Injection into circular orbit, transfer to lower orbit, deceleration to zero velocity at low orbit altitude, and vertical descent to the surface, and 4. Injection into circular orbit, transfer to ellipsical orbit with a perigee altitude of 50,000 feet, deceleration to zero velocity and descent to 100 feet, and hover above surface.

Errors in measured quantities and operational parameters were considered in the first three cases but not in the fourth. The upper circular orbits considered ranged from 50 to 200 nautical miles and the lower circular orbit was 5 nautical miles.

(a). Direct, Radial Landing

A direct, radial landing on the moon from a 66-hour trajectory with no errors in ignition altitude, requires an ideal velocity increment of 9000 pps. When an error in ignition altitude and an assumed error of 0.33% in measured quantities is considered, the velocity increment totals 9800 to 9900 fps. The propulsion requirements for direct landing is presented in Table IX, and the sample thrust-time program is shown in Figure 96.

(b). Gravity Turn from Circular Orbit

The velocity increment required for injection into circular orbits from 50 to 200 nautical miles is 3200 fps. The velocity increment to land (zero velocity at 5 nautical mile altitude) is 5700 to 6000 fps. The propulsion requirement for this phase is presented in Table IX.

To let down from 5 nautical miles, the velocity increment is 1100 fps. The thrust time program for these maneuvers is presented in Figure 97.

(c). Transfer to Low Circular Orbit

This method considered coplanar transfer from either the 50 or 200 nautical mile circular orbit to a 5 nautical mile circular orbit, deceleration to zero velocity at constant altitude, and letdown to the surface of the moon. An additional penalty of from 2 to 4% is also paid in transfer to the lower orbit and the resulting errors in this approach.

(d). Transfer to Elliptical Orbit

A fourth approach to landing on the surface of the moon considered similar phases of the above examples (References 7 and 8). The establishing of a 200 nautical mile circular orbit permits initial survey of the surface and location of the landing area. A transfer is then made into an elliptical orbit which has a perigee altitude of 100,000 feet over the landing area. Deceleration to zero velocity and descent to an altitude of 100 feet is then made. The additional requirement to hover at this altitude is also given.

(2). Mars Landings

The propulsion requirements for landing on Mars are presented in Table IX for both a direct, radial landing and a landing from orbit.

MAC A673

(a). Direct, Radial Landing

Due to the extremely high approach velocities, between 18,000 and 31,000 fps, direct entry into the atmosphere cannot be made by a single retrothrust before landing. Excessive aerodynamic heating and extremely high deceleration rates would be experienced unless retrorocket firing began hundreds of miles above the surface. The total propulsion requirements, including the error effects associated with the high ignition altitude, are presented in Table IX.

(b). Landing from Mars Orbit

The propulsion requirements to land on Mars on a gravity turn from orbit are higher than for the direct approach when atmospheric braking is not used. However, the technique of entering an elliptical orbit, employing atmospheric braking and then landing has orbit-landing propulsion requirements comparable to the direct approach (Table IX.)

g. Lunar and Planetary Takeoffs

(1). Lunar Takeoff

Propulsion requirements for lunar takeoff with ascent trajectories into lunar orbits and direct injection on return flights to the Earth assumed constant thrust and specific impulse, a gravitational constant, nonrotation of the moon, and optimum thrust to mass ratio. (Table IX.)

(2). Mars Takeoff

Propulsion requirements for Mars takeoff were similar in nature to those of the moon with the additional consideration of the Martian atmosphere. Single stage vehicle configurations were assumed adequate for takeoff into a Mars orbit. However, the velocity increment for ascent trajectories for direct flights to the Earth requires staging. The propulsion requirements for both cases are presented in Table IX.

B. Propellants

Heat transfer analyses and design studies in this report have been limited to consideration of a group of liquid propellants considered typical of three classes of currently interesting propellants for spacecraft engines. These groups were:

1. Earth storable hypergolics
2. Cryogenic (hydrogen fuel)
3. Space storable

The propellants for which physical and thermodynamic properties are presented include the following oxidizers and fuels: Figures 98 through 121.

Oxidizers	Fuels
O_2	H_2
F_2	N_2H_4
OF_2	0.5 N_2H_4 - 0.5 UDMH
N_2O_4	B_2H_6

Rocket performance analyses were made and are presented in Figures 122 through 141 for space operation at an expansion ratio of 40:1. These graphs present the following parameters:

I_{sp} vs. O/F, P_c (shifting equilibrium)

Combustion temperature (T_c vs. O/F, P_c

Characteristic velocity (C*) vs. O/F, P_c

Combustion products vs. O/F at constant P_c

The propellant combinations for which these analyses are presented are:

N_2O_4/N_2H_4	Figures 122, 123, 124
N_2O_4/0.5 N_2H_4 - 0.5 UDMH	Figures 125, 126, 127
O_2/H_2	Figures 128, 129, 130
F_2/H_2	Figures 131, 132
OF_2/H_2	Figures 133, 134, 135
OF_2/B_2H_6	Figures 136, 137, 138
OF_2/CH_4	Figures 139, 140, 141

C. Material Properties

Several different classes of available thrust chamber materials may be defined with respect to applications and physical characteristics.

MAC A 673

Characteristics of each group may be defined and compared with available materials and their properties. The groups considered in this section are

a. Heat resistant alloys readily fabricated

b. High temperature refractory metals

c. High temperature refractory nonmetals

d. Ablative materials

e. Insulation

The materials considered under these headings are those with particular application to the thrust chamber fabrication including cooled and uncooled components. The properties discussed are those which define the limits of its applicability and facilitate completion of preliminary thrust chamber designs.

The ablative materials and their properties have been discussed separately in Section III-D.

1. Heat Resistant Alloys

The nickel and cobalt base alloys have met technological demands very well up to about 1800°F, but usually require special techniques to satisfy higher temperature requirements. There appears to be little hope of extending the usefulness of these superalloys much beyond 2200°F. The thorium dispersed nickel (TD-Nickel) is reported (Figure 142, 143 and 144) to have usable strengths to 2400°F, but degrades beyond that range to its melting point of 2650°F.

Typical properties of the nickel and cobalt alloys and TD-Nickel are presented in Figures 142, 143, 144 and 145.

Fabrication operations on the nickel and cobalt alloys are considered routine. Cutting, machining, and forming are conducted at room temperature. Welding can be conducted by both manual and automatic operation with weld joint efficiencies in excess of 85%. TD-Nickel is available only as bar stock at this time, but some experimental sheet has been made. It is reported that cutting, forming, and machining present no problems. Welding of this material is being investigated by DuPont Metal Center, Baltimore, Maryland.

The titanium alloys are usable at temperatures below 1000°F. The superalpha alloys are weldable and have high creep strength in the 700 to 1000°F temperature range. It is anticipated that these alloys will be usable at low temperatures (<0°F). Selected mechanical properties of these alloys are given in Table X.

2. High Temperature Refractory Metals

Although there is no exact definition of refractory materials, by common usage this term is limited to materials with a melting point above 3400°F. A listing of refractory materials would include the metals listed in Table XI and the materials in Figure 148. There is considerable research in the development of refractory metal alloys. Table XII is a listing of molybdenum, columbium, tantalum, tungsten, and vanadium alloys which are in production. Figures 146, 147, 148, and 149 indicate ultimate tensile strength/density to test temperature relationships for some of the refractory metals. Table XII lists the producers of the various refractory metals.

a. Molybdenum

Typical molybdenum alloys are TZM and 0.5% titanium-molybdenum. These alloys have usable strengths up to 3500°F, but available oxidation resistance coatings limit their use in oxidizing environments to temperatures below 3200°F.

Since molybdenum was the first of the refractory metals to be applied to aerospace use, more experience has been obtained with it. All conventional forming methods have been used, but hot working is generally necessary. Forgings of molybdenum and its alloys are being produced in commercial quantities.

A study of the mechanism to improve the high temperature strength of Mo-0.5 percent Ti-C alloy indicated that both nitrogen and carbon strengthens this alloy with carbon being the more effective.

Climax Molybdenum Corporation has fabricated ring sections of Mo-0.15 percent Ti-0.003C alloy with a low transition temperature and high temperature strength. Stock of this alloy displayed 16% elongation in tension at -100°F and absorbed more than 60 ft/lb in room temperature unnotched Izod and Charpy tests.

b. Columbium (Niobium)

Typical columbium alloys are Fansteel FS82 and Wah Chang C103. These and other alloys have usable strengths up to 3100°F but must be coated for oxidation resistance. The coatings available are similar to those for molybdenum as discussed in a following section on coatings.

Commercially pure columbium is ductile and may be formed cold by any conventional technique including spinning. Sheets of C103 as thin as 0.040 inch thick have been spun down to 0.020 inch without wrinkling (Reference 222). Columbium and its alloys may be welded and brazed, and chemically milled. These alloys are new and many of these fabrication techniques are still in the development stage. Mechanical properties of columbium alloys are presented in Figures 149 and 150.

c. Tantalum

A typical alloy is 90% tantalum 10% tungsten. This alloy has exhibited usable strength at 5000°F (Figure 151). However, no satisfactory oxidation resistant coating has been developed for operation above 3300°F.

Commercially pure tantalum sheet is ductile and readily fabricated by any conventional method and heating is not required. The 90Ta-10W alloy is more difficult to fabricate and frequent intermediate anneals are needed. Explosive forming has not been applied to tantalum and its alloys, but the method appears feasible. Some work has been done in forging commercially pure tantalum and the 90Ta-10W alloy. Work in extruding tantalum and its alloys by both conventional and high energy rate methods appears promising. Ductile welds may be obtained in either commercially pure tantalum or 90Ta-10W alloy using conventional techniques. Machining is fairly good.

Tantalum is available in all forms including foil. Sheet widths are available up to 24 inches.

d. Tungsten

Very few alloys of tungsten are commercially available at the present time and even these are still in the development stage. The 85W-15Mo forging study (Reference 223) has reached its preliminary feasibility goal. Pure tungsten sheet has exhibited usable strengths up to 5000°F (Figure 151). Some work has been done on developing oxidation resistant coatings for tungsten (Figures 152 and 153), but all this work is in the development stage.

Most of the work done to date in forming sheet tungsten has been done by spinning and drop hammer forming. For any forming operation, including shearing and bending, hot working is necessary. Fairly complex nozzle configurations have been fabricated by spinning tungsten manually in the case of sheet less than 0.125 inch thick, and by hydrospinning or spin forging for thicker sheet.

Slip casting, plasma spraying, and vapor deposition promise to be important means of fabricating tungsten shapes in cases where properties obtained by working are not needed. Machining of tungsten is difficult and abrasive wheels offer the best means of metal removal. Chemical milling is an effective alternate, and electrical discharge machining is also being used. Welding tungsten by conventional methods results in an embrittled joint. However, where this can be tolerated, arc welding and spot welding may be used. Work is being done on tungsten using electron beam welding and offers some promise. Little work has been done on brazing but limited work at Marquardt on diffusion bonding (similar to brazing in technique) has resulted in joint remelt (Reference 224) temperatures near that of the tungsten sheets.

An inhouse program at Marquardt-Ogden on the possibilities of explosive forming of tungsten has met with some success. Also, some extrusion work, both conventional and high energy rate, has been done and the results have been promising.

Massive nozzle components of cast and forged tungsten are in production for large solid rockets. Pressed and sintered porous tungsten impregnated with metals such as silver and copper has been in use for many years and is currently being evaluated for nozzle throat insert application (Reference 205).

e. Coatings for Refractory Metals

The refractory metals oxidize rapidly at elevated temperatures in the presence of oxygen (Figure 154). The oxides of the more common refractory metals melt or sublime at lower temperatures than the metal. To fully utilize the capabilities of the refractory metals at high temperature, a protective coating is required. Figures 152 and 153 and Table XIV give a graphical presentation of coating capabilities.

3. High Temperature Refractory Nonmetals

These nonmetallic materials which include those having the very highest melting temperatures, the greatest high temperature strength (Figure 155) and those which have the greatest resistance to oxidation are also subject to the most severe restrictions in their application because of brittleness and poor thermal shock resistance. Also, except for the oxides, they are subject to oxidation in a liquid rocket environment. The book, "High Temperature Technology", Reference 212), gives an excellent review of these materials.

Table XI lists the materials which have melting points above 4000°F. Of these materials, graphite in its various forms is the most generally adaptable to high temperature rocket application even though the carbides of hafnium, tantalum and zirconium melt at slightly higher temperatures.

Graphite has structural strength up to near its sublimation temperature of 6650 to 6700°F. The available grades and forms of graphite are constantly being improved for rocket and high temperature applications. Protective coatings have been developed to operate in the 3000 to 4000°F range depending upon the exact environment and time required. Handbooks and data sheets on many grades of graphite are available from the vendors, References 225 and 226). Graphites may be tailored for many specific requirements by varying such parameters as the following:

a. Structure

(1). Fine grain flour base (ATJ)

(2). Coarse grain (HLM)

(3). Anisotropic (Pyrolytic graphite)

(4). Fibrous (Pluton, carbon and graphite cloth)

(5). Porous Carbon

(6). Graphite hollow spheres

(7). Pyrofoam (expanded pyrolytic graphite)

(8). Powder, as lubricant or insulation

MAC A 679

b. Density

Density varies from 1.0 lb/ft^3 (Pyrofoam) to 140 lb/ft^3 (pyrolytic graphite). ATJ grade averages 109 lb/ft^3.

c. Thermal Conductivity

Thermal conductivity varies by a factor of two in extruded grades in directions parallel and normal to the direction of extrusion. In pyrolytic graphite the ratio may be 200 (Reference 177). The powdered and foamed graphites are effective high temperature insulators.

d. Thermal Expansion

Thermal expansion may be varied to match available surface coatings. A state of the art survey of high temperature materials and their applications is presented in several feature articles in the January 1963 issue of "Aerospace Engineering" (Reference 206).

4. Insulation

For many reasons including envelope restrictions and aerodynamic considerations, spacecraft engines may have to be buried within the vehicle during operation. As noted in Volume I, the exterior temperature of the engine may vary during operation from 300°F for regeneratively cooled structures to 4000°F for radiation cooled or heat sink engines. If the effective exterior temperature of the engine must be limited, it can be done in at least the following three ways:

a. Increased heat sink capacity

b. Liquid cooled shielding

c. High temperature, low density insulation blanket.

Design data on insulations suitable for high temperature application are presented in terms of insulation weight required to drop the external thrust chamber temperature to 250°F at a heat flux of 350 Btu/hr-ft^2 (Figures 156 and 157). Heat fluxes through different insulation compositions are presented in Figure 158.

Available high temperature insulations with their compositions and temperature limits are given in Table XV. References 215 through 221 provide additional sources of design data.

V. BIBLIOGRAPHY AND REFERENCES

Mission Analysis

1. Aerojet-General Corporation, Report No. 2150, Vols. I, IIa, and IIb, "Research Study to Determine Propulsion Requirements and Systems for Space Missions", December 1961.

2. Rocketdyne, Report No. 3208, Vols. I, II, and III, "Propulsion Requirements for Space Missions", May 1961. CONFIDENTIAL.

3. NASA TN-D-81, National Aeronautics and Space Administration, "Methods and Velocity Requirements for the Rendezvous of Satellites in Circumplanetary Orbit", W. E. Brunk, et al, October 1959.

4. NASA TN-D-437, National Aeronautics and Space Administration, "A Two-Impulse Plan for Performing Rendezvous on a Once-A-Day Basis", J. D. Bird and D. F. Thomas, Jr., November 1960.

5. IAS Paper No. 61-206-1900, Institute of the Aerospace Sciences, "Terminal Maneuvers for Satellite Ascent and Rendezvous", P. W. Soule and A. T. Kidd, June 1961.

6. ARS Preprint 1228-60, American Rocket Society, "Propulsion Requirements for Controllable Satellites", T. N. Edelbaum.

7. Marquardt Report S-212, "Propulsion Requirements for Lunar Excursions", dated 15 June 1961.

8. Marquardt Report S-227, "Lunar Landing Propulsion Analysis", dated October 1961.

9. Marquardt Report No. S-228, "Maneuverable Satellite Velocity Change Requirements", dated October 1961.

Space Environments

10. ARS Journal, "Behavior of Materials in Space Environments", Jaffe and Rittenhouse, March 1962.

11. ARS Space Flight Report to the Nation, "Zero Gravity Problems in Space Powerplants - A Status Survey", Unterberg and Congelliere, 1961.

12. General Dynamics/Astronautics, "Hydrostatics in Various Gravitational Fields", T. Li.

13. General Dynamics/Astronautics, "Cryogenic Liquids in the Absence of Gravity", T. Li, 1961.

MAC A-673

14. WADC Technical Note 58-282, ASTIA No. AD 203527, "Orbital Storage of Cryogenic Fluids", K. R. Cramer, October 1958.

15. ARS Report No. 1087-60, "Liquid Hydrogen Transport Time Limits in Space", C. C. Love, Jr., April 1960.

16. NASA Contract No. NAS 5-664, First Quarterly Report, "Liquid Propellant Losses During Space Flight", Arthur D. Little, Inc., January 1960.

17. IAS Paper No. 60-23, "Cryogenic Propellant Storage for Round Trips to Mars and Venus", January 1960.

18. ARS 1123-60, "High Energy Propellant Comparison for Space Missions", Burry, Jortner and Rosemary.

19. Rand RM-2332, "Estimated Damage to Space Vehicles by Meteoroids", R. L. Bjork and C. Gasley, 20 February 1959.

20. Rand S-103, "Numerical Solutions of the Axially Symmetric Hypervelocity Impact Process Involving ION", R. L. Bjork, 16 December 1958. CONFIDENTIAL.

21. University of Utah, VV-E, QR-6, Sixth Quarterly Report, "Penetration and Cratering Studies", E. P. Palmer and R. W. Grow, 1 June to 31 August 1959.

22. Aerospace Engineering, May 1960.

23. MIT 052e, "An Experimental Investigation in Lead of the Whipple Meteor Bumper", A. E. Olshaker, August 1960.

24. NASA - Industry Apollo Technical Conference, "Impact Resistance of Space Vehicle Structure", J. Summers and R. Nysmith, 1961.

25. Journal of the Aerospace Sciences, "Space Vehicle Environment", Gazley, Kellogg, and Vestine, December 1959.

26. The Ohio State University, WADD Phase Technical Note 4, "Natural Environment of Interplanetary Space", J. W. Shaw, Department of Physics and Astronomy, January 1960.

27. USAF Specification Bulletin Number 523, "Space Environment Criteria for Aerospace Vehicles", 28 November 1960.

28. Lockheed Missiles and Space Division Report LMSD-895006, "Satellite Environment Handbook", December 1960.

Propellant Properties

29. Product Data Sheet, Allied Chemical, General Chemical Division.

30. Aerojet-General Corporation, "Performance and Properties of Liquid Propel- nts lants", Liquid Rocket Plant.

31. Astronautic Data Sheets - Compiled by Stanley Sayner for various propellant combinations.

32. Applied Physics Laboratory, The John Hopkins University, "Liquid Propellant Manual".

33. Callery Chemical Company, "Diborane, Space Storable Fuel", January 1962.

Regenerative Cooling

34. NASA TN-D-66, "Analysis of Effects of Rocket-Engine Design Parameters on Regenerative-Cooling Capabilities of Several Propellants", by A. N. Curren, dated September 1959.

35. ASME Paper 58-Ht-11, "Heat Transfer to a Boiling Liquid", by K. Foster and R. Greif, dated June 1958.

36. CITJPL-TR 32-109, "Experimental Investigation of Heat Transfer of Hydrazine", by M. B. Noel, dated June 1961.

37. U. S. Naval Air Rocket Test Station, "Ninety Percent Hydrogen Peroxide as a Regenerative Coolant in a 350-Pound-Thrust Rocket Motor", A. H. Blessing, dated 20 August 1959. CONFIDENTIAL.

38. NACA TN 4 382, "Investigation of Boiling Burnout and Flow Stability for Water Flowing in Tubes", by W. H. Lowdermilk, dated September 1958.

39. Jet Propulsion, "A Simple Equation for Rapid Estimation of Rocket Nozzle Convective Heat Transfer Coefficients", by D. R. Bartz, January 1957.

40. United Kingdom of Great Britain and Northern Ireland Explosives Research and Development Establishment, "Heat Transfer and Performance Studies on the Propellant Combination Gaseous Hydrogen/Gaseous Oxygen: Part I - Some Computed Thermodynamic Data for 10, 30, 60, and 100 Atm. Combustion Pressure", by L. S. Herbert and H. Ziebland, dated November 1958.

41. Bernath, L., "A Theory of Local Boiling Burnout and Its Application to Existing Data", Paper Presented at the Third National Heat Transfer Conference ASME-AICHE, for E. I. DuPont deNemours and Company, August 1959.

42. AFOSR TN 59-488, "High Temperature Heat Transfer from Gases to Cylinders and Nozzles", by I. E. Kanter, General Electric Company Flight Propulsion Laboratory Department, February 1959.

43. RAE TN No. RPD 147, "Failures of Regeneratively Cooled Rocket Engine Combustion Chambers-Results and Recommendations from Metallurgical Investigations", by P. Bradley and D. Bunting, October 1956. CONFIDENTIAL.

44. Bartz, D. R., ARS Paper 417-57, "Factors Which Influence the Suitability of Liquid Propellants as Rocket Motor Regenerative Coolants", 1957.

45. Dean, L. E., and L. A. Shurley, ARS Paper 460-57, "Analysis of Regenerative Cooling in Rocket Thrust Chambers", 1957.

46. Aerojet General Corporation Report ID 0-28007, "Determination of Burnout Limits of Polyphenyl Coolants", by T. C. Core and K. Sato, 14 February 1958.

47. CITJPL Publication 111, "Evaluation of Hydrazine as a Regenerative Coolant", by D. R. Bartz, M. B. Noel and A. F. Grant, Jr., 15 October 1957.

48. Curtiss Wright Corporation Monthly Progress Report 2, 31 May 1960; Monthly Progress Report 4, CI-83101, "Rocket Engine Nozzles Cooled by Liquid Metals in Forced Convection". CONFIDENTIAL.

49. NASA TN D765, "Experimental Heat Transfer and Pressure Drop of Liquid Hydrogen Blowing through a Heated Tube", by R. C. Hendricks, et al, dated May 1961.

50. General Electric Company KAPL-M-DRM-1, "Comparison of Coolants", by D. R. Miller, dated October 1946.

51. Purdue University Jet Propulsion Center Report Number F-57-1, "Experimental Rocket Motor Performance and Heat Transfer of the WFNA-Ammonia and the RFNA-Ammonia Propellant Systems at Combustion Pressure of 1000 psia and 1500 psia", by D. G. Elliot and R. K. Rose, June 1957.

52. NRCC MT-37, "The Cooling of a Hot Surface by Drops Boiling in Contact with It", by P. Savic, April 1958.

53. USAF, Air University, Institute of Technology, GA/ME/60-7, "Performance Evaluation of Reverse-Flow Cooling Combustion Chamber", by J. F. Heye, August 1960.

54. JPL TR No. 32-78, "Experimental Investigation of Heat Flux at the Upper Limit of Nucleate Boiling for Two Mixtures of Hydrazine and Unsymmetrical Dimethylhydrazine", A. B. Witte.

55. Callery Chemical Company, "Forced Convection Heat Transfer Characteristic of Liquid Pentaborane", J. P. Cherenko.

56. Gambill, W. R., "Generalized Prediction of Burnout Heat Flux for Flowing, Subcooled, Wetting Liquids", Oak Ridge National Laboratory AIChE preprint Autust 5-8, 1962.

57. Wolf, H., and J. R. McCarthy, "Heat Transfer to Hydrogen and Helium with Wall-to-Fluid Temperature Ratios to 11:09", paper presented at AIChE Annual Meeting, 4-7 December 1960.

58. Hendricks, R. C., R. W. Graham, Y. Y. Hsu, and A. A. Mederios, "Correlation of Hydrogen Heat Transfer in Boiling and Supercritical Pressure States", paper presented at ARS Meeting 26-28 April 1961.

59. Rocketdyne Division of North American Aviation, Inc., R-2600-4, "J-2 Program Quarterly Progress Report for Period Ending 31 August 1961", CONFIDENTIAL.

60. CIT JPL M-30-8, "On the Mechanism of Subcooled Nucleate Boiling", S.G. Bankoff.

61. NASA TN D-131, "Comparison of Hydrazine-Nitrogen Tetroxide and Hydrazine-Chlorine Trifluoride in Small Scale Rocket Engines", J. Rollbuhler, W. A. Tomazic.

62. Aerojet General Corp., Report Nr. 0106-01-4, "Feasibility Investigation of a Storable Propellant Rocket Engine", Ellis, Kreig and McFarland.

63. Knolls Atomic Power Laboratory M S36 RES22, "Correlation of Subcooled and Quality Burnout Data for Tubes and Ducts", R. Hoe, L. Senghaus.

Ablative Cooling

64. WADD TR 60-101, "The Effects of Material Parameters on Ablation Characteristics", Halle and Nicolosi, Chicago Midway Laboratories, (ASTIA AD 247 100L), 16 February 1960.

65. WADD TR 60-101, "The Effects of Thermal Environment Parameters on Ablation Characteristics", Manos and Taylor, Chicago Midway Laboratories, (ASTIA AD 247 100L), 16 February 1960.

66. WADD TR 60-101, "Structural and Insulative Characteristics of Ablating Plastics", Vassallo, Wahl, Sterbutzel and Beal, Cornell Aeronautical Laboratory, (ASTIA AD 247 100L), 16 February 1960.

67. WADD TR 60-101, "A Brief Review of the ABMA Ablation Materials Program", Lucas and Kingsbury, Army Ballistic Missile Agency, (ASTIA AD 247 100L), 16 February 1960.

68. ASD, WADD TR 60-101, "Thermal Diffusivity - Its Significance and a Method of Determination", R. W. Farmer, (ASTIA AD 247 100L), 16 February 1960.

69. ASD, WADD TR 60-101, "Studies of Plastics Exposed to High Mass Flow Thermal Environments", Schwartz and Farmer, (ASTIA AD 247 100L), 16 February 1960.

70. Aerojet General Corp., RD-R60-70, "Thermal Properties of Phenolic Composites", W. J. McLaughlin, 21 July 1960.

71. WADC TR-59-368, "The Study of Ablation of Structural Plastic Materials", Vassallo, Wahl, Sterbutzel and Beal, Cornell Aeronautical Laboratory, (Part I, ASTIA AD 234779; Part II, ASTIA AD 240-636), May 1959, April 1960.

72. WADD TR 59-668, Part I, "A Study of the Mechanisms of Ablation of Reinforced Plastics", Stanford Research Institute, Mixer and Marynowski, (ASTIA AD 237242), February 1960.

73. Avco Corporation, "Analysis of the Ablation of Plastic Heat Shields That Form a Charred Layer", Barreautt and Yos, Published in ARS Journal Vol. 30, No. 9., September 1960.

74. WADC TR-59-229, "Strength Properties of Reinforced Plastic Laminates at Elevated Temperatures", Boller and Kimball, Forest Products Laboratory, U.S. Dept. of Agriculture, (ASTIA AD 229442), September 1959.

75. WADD TR 59-668, Part II, "A Study of the Mechanism of Ablation of Reinforced Plastics", Chamberlain, Van Sickle and Marynowski, Stanford Research Institute, (ASTIA AD 256558), February 1960.

76. WADD TR 60-697, "Study of Thermal Radiation within Solids and Study of Internally Ablating Composites", Vasallo, Camnitz and Kirchner, Cornell Aeronautical Laboratory, (ASTIA AD 259648), May 1961.

77. Avco Corporation, TM 2-TM-58-103, "A Study of the Ablation Process with Variable Thermal Properties in a Semi-Infinite Slab", J. V. Beck, 30 January 1959.

78. Army Ballistic Missile Agency, "The ABMA Reinforced Plastic Ablation Program", Published in Modern Plastics, Vol. 38, No. 2, October 1960.

79. Aeronutronics Division, Ford Motor Company, U-702, "Experimental Ablation Rates in a Turbulent Boundary Layer", Denison and Bartlett, (ASTIA AD 230168), 1 November 1959.

80. National Research Corporation, "Ablation Mechanism in Plastics with Inorganic Reinforcement", Beecher and Rosenweig, Published in ARS Journal, Vol. 31, No. 4, April 1961.

81. Aerojet General Corp., "Plastic in Rocket Nozzle Environments", Epstein, Cecca and Robbins, Presented at 2nd Symposium on Materials and Design for Rocket Insulation and Nozzles, March 1960.

82. Aerojet General Corp., SP-TP-16, "Evaluation of Plastics for Rocket Motor Nozzles (Phase I)", Epstein and King, July 1959.

83. Wright Air Development Center TR 59-268, "Vacuum Volatility of Organic Resins", G. F. Matacek, September 1959.

84. ASD-TDR-62-261, "Thermal Stability of Plastics", G. F. L. Ehlers, April 1962.

85. WADD TR 60-125, "The Effects of High Vacuum and Ultraviolet Radiation on Plastic Materials", Cornell Aeronautical Laboratory, Wahl and Lapp, July 1960.

86. WADD TR 60314, "The Thermal Diffusivity of a Structural Plastic Laminate at Elevated Temperatures", R. W. Farmer, September 1960.

87. ASD TR 61-650, "Ablation of Plastics", Donald L. Schmidt, February 1962.

88. ASD-TD-61-439, "Part I, Criteria for Plastic Ablation Materials as Functions of Environmental Parameters", McFarland, Joerg and Taft, Aerojet General Corporation, May 1962.

89. AFFTC TR 61-7, "Research and Development on Components for Pressure-Fed LO_2/LH_2 Upper Stage Propulsion Systems, Ablative Thrust Chamber Feasibility Firings", Lonon and Olcott, February 1961. CONFIDENTIAL.

90. ASD TDR 62-629, "Effect of Elevated Temperatures on Strength Properties of Reinforced Plastic Laminates, Final Report", October 1962.

91. NASA TM X476, Lewis Research Center, "Experimental Investigation of the Effectiveness of an Ablation-Produced Film in Cooling a Rocket Nozzle", R. R. Cullom, July 1961. CONFIDENTIAL.

92. Avco Corp., RAD TM 61-14, "The Mechanism of Silica Phenolic Ablation", Ihnat, McCafferty, Phanenf and Walters, May 1961.

93. Aerojet General Corp., Contract AF 33(657)-8890, "Phase I, Effects of Process Variables on the Performance and Properties of Fiberite MX2625", July 1962 - September 1962.

94. Aerojet General Corp., Contract AF 33(657)-8890, "Phase I, A Preliminary Evaluation of the Mechanical, Physical and Thermal Properties of Thirteen Reinforced Plastic Materials", July 1962 - September 1962.

95. Aeronutronics, Contract AF 04(611)-7443, Publication No. C-1544, "Feasibility Investigations of Uncooled Thrust Chamber and Nozzle Designs, 2nd Quarterly Progress Report", January 1962.

96. Avco Corp., ASTIA AD 250 724 TM RAD-9-TM-60-83, "Calculation of Transient Ablation", Zlotnick and Nordquist, January 1961.

97. Avco Corp., ARS Paper 2099-61, "Ablation Measurements in Turbulent Flow", Offenbartz and Rose, October 1961.

98. Moog Servocontrols, Inc., ER-41, "Supplemental Final Report on Moog Variable Thrust Injector and Ablative Liner Evaluations, MJL Test 2981", J. Walsh, December 1961.

99. Aerojet General Corp., Report No. 0496-01-4, "Thermal Erosion of Ablative Materials Under Simulated Propulsion Conditions, Quarterly Report for Period Covering 1 June through 31 August 1962", D. L. Robbins.

100. ASD WADD TR 60-856, "Microstructure of Ablative Plastic Chars", S. A. Marolo, August 1961.

101. WADD TN 60-286, "Properties of Thermally Degraded Ablative Plastics", Schwartz, Schmidt, Marolo and Starks, January 1961.

102. Aerojet General Corp., ASD TR 61-307, "Thermal Erosion of Ablative Materials", D. Robbins, Final Report, April 1962.

103. Aeronutronics, Div. Ford Motor Co., Publication C 1145, "Study Program of Improved Thrust Chamber Cooling Methods, Final Report", Kaufman, Green, Armour and Mitchell, January 1961. CONFIDENTIAL.

104. Aeronutronics, Div. Ford Motor Co., Publication C 1150, "Thermal Protection of Uncooled Rocket Thrust Chambers", Special Report, E. P. Bartlett, January 1961.

105. Aeronutronics, Div. Ford Motor Co., Publication C 1779, "Feasibility Investigations of Uncooled Thrust Chamber and Nozzle Designs; Fourth Quarterly Report", Bartlett, Blaes and Dougham, July 1962.

106. Aeronutronics, Div. Ford Motor Co., Publication C 1640, "Feasibility Investigation of Uncooled Thrust Chamber and Nozzle Designs; 3rd Quarterly Report", Bartlett, Dougham and Jeffries, April 1962.

107. Aerojet General Corp., AD No. 286218, "Plasma Arc Evaluation of Reinforced Plastics, Contract AF 33(657)-8890, Phase I, 1st Quarterly Progress Report", 15 October 1962.

108. Beecher, N., and R. E. Rosensweig, "Ablation Mechanisms in Plastics with Inorganic Reinforcement", ARS Journal, April 1961.

109. WADD TR 60-649, "Comparative Erosion Resistance of Plastic Materials in a Supersonic Rocket Exhaust and Subsonic Air Arc Plasma", by H. S. Schwartz, September 1960.

110. Journal of Aero-Space Sciences, Volume 27, "Ablation of Reinforced Plastics", G. W. Sutton, 1960.

111. NASA TM X418, "Experimental Investigation of the Feasibility of Ablation-Cooling a Rocket Nozzle with Possible Application to Solid-Propellant Engines", by R. R. Cullom, March 1961. CONFIDENTIAL.

112. CIT JPL, Astronautics Information: Literature Search No. 102, "Theoretical Studies and Experimental Techniques Used in Ablative Heat Transfer", by L. Kalvinskas, May 1959. CONFIDENTIAL.

113. Aerojet General Corporation, Progress Report 0401-01-1, "Plastic Ablation Materials", October 31, 1961 - January 8, 1962.

114. WADC TR 58-452, "Metal Fiber Reinforced Ceramics", U. S. Department of Commerce, by J. J. Sevica, et al, January 1960.

115. WADD TR 60-491, "Development of Reinforced Ceramic Material Systems", by L. M. Stejskal, et al, Boeing Airplane Company, January 1961.

116. WADD TR 60-244, "Continuous Filament Ceramic Fibers", by W. A. Lambertson, et al, June 1960.

117. CIT JPL, "Astronautics Information: Ablation and Associated Subjects", Literature Search No. 280, October 1960.

118. NACA RM L58 B17, "Investigation of Lithium Hydride and Magnesium as High Temperature Internal Coolants with Several Skin Materials", by J. L. Modisett, May 1958. CONFIDENTIAL.

119. Ford Motor Company Aeronutronic Division Quarterly Progress Reports 1-3. July-December 1959; Final Report, 30 January 1960, "Study of Improved Thrust Chamber Cooling Methods", by J. Neustein, et al. CONFIDENTIAL.

120. Redstone Division, Thiokol Chemical Corporation Report Number 37-57, "Ceramic Nozzle Evaluation Program (Phase III)", by M. J. Kemp and U. E. Garrison, December 1957. CONFIDENTIAL.

121. Naval Ordnance Laboratory Quarterly Report, January - March 1960; Quarterly Report, April-June 1960; "High Temperature Resistant Materials for Missile Propulsion Systems". CONFIDENTIAL.

122. JPL Space Programs Summary No. 37-10, Volume II, August 1, 1961. CONFIDENTIAL.

Film and Transpiration Cooling

123. NASA Report TN D-130, "Use of a Theoretical Model to Correlate Data for Film Cooling or Heating an Adiabatic Wall by Tangential Injection of Gases of Different Fluid Properties", J. E. Hatch and S. S. Papell, November 1959.

124. NACA Report 1087, "Internal Liquid Film Cooling Experiments with Air-Stream Temperatures to 2000°F in 2 and 4 inch Diameter Horizontal Tubes", Kinney, Abramso, and Sloop, 1952.

125. JPL Report TR 32-58, "Review of Results of an Early Rocket Engine Film Cooling Investigation at the Jet Propulsion Laboratory", W. E. Welsh, Jr., March 1961.

126. Jet Propulsion Center, Purdue University Report I-62-2, "Effects of Selected Gas Stream Parameters and Coolant Physical Properties on Liquid Film Cooling" D. L. Emmons and C. F. Warner, January 1962.

127. MIT Naval Supersonic Laboratory Report TR 447, "An Experiment with a Transpiration Cooled Nozzle", R. P. Bernicker, July 1960.

128. JPL Progress Report No. 1-74, "An Investigation of Film Cooling in a Flame Tube", G. A. Schurman, 30 June 1948.

129. NASA Report TN D-299, "Effects on Gaseous Film Cooling of Coolant Injection through Angled Slots and Normal Holes", S. S. Papell, September 1960.

130. Purdue University Rocket Laboratory Report TM 57-3, "Film Cooling, Its Theory and Application", A. R. Graham and M. J. Zucrow, October 1957.

131. Sellers, J. P., "Effectiveness of RP-1 Film Cooling in a Large Rocket Motor", ARS Journal, September 1962.

132. Zucrow, M. J., and J. P. Sellers, "Experimental Investigation of Rocket Motor Film Cooling", ARS Journal, May 1961.

133. Sellers, J.P., "Experimental and Theoretical Study of the Application of Film Cooling to a Cylindrical Rocket Thrust Chamber", Ph D Thesis, Purdue University, 1958.

134. Purdue University Report No. F-57-3, "An Experimental and Theoretical Investigation of Film Cooling of Rocket Motors", A. R. Graham, October 1957.

135. NACA Report RM E52 B20, "Internal Film Cooling Experiments with 2 and 4 Inch Smooth-Surface Tubes and Gas Temperatures to 2000°F", by G. R. Kinney, 29 April 1952.

136. Eckert and Drake, "Heat and Mass Transfer", McGraw Hill Book Co., Inc., 1959.

137. Graham, A. R., "Film Cooling of Rocket Motors", Ph D Thesis, Purdue University, January 1958.

138. Berghley, C. M., "Physical Characteristics of Flow Issuing from a Slot into a Moving Air Stream as Related to Transpiration Cooling", M. S. Thesis, Purdue University, August 1949.

139. Knuth, E. L., "The Introduction of Fluids into a Moving Gas Stream through Parallel Disks as Related to Film Cooling", M. S. Thesis, Purdue University, 1950.

140. Greenberg, A. B., "The Stability and Flow of Liquid Film Injected into an Air Duct through Spaced Parallel Disks in the Two and Three Dimensional Cases", M. S. Thesis, Purdue University, August 1952.

141. Louden, R. K., "The Effect of Air Duct Diameter Upon the Stability of Liquid Films Injected Radially into an Air Duct through Spaced Parallel Disks", M. S. Thesis, January 1954.

142. JPL 20-85, "The Mechanics of Film Cooling", E. L. Knuth, 21 September 1953.

143. NACA Report RM E50F19, "Internal Film Cooling Experiments in 4-inch Duct with Gas Temperatures to 2000°F", G. R. Kinney and Sloop, 21 September 1950.

144. ASME Paper 58-A-107, "Adiabatic Wall Temperature Downstream of a Single, Tangential Injection Slot", J. H. Chin, S. C. Skirvin, L. E. Hayes and A. H. Silver, 1958.

145. NACA Report RM E52C26, "Investigation of Internal Film Cooling of Exhaust Nozzle of a 1000-Pound Thrust Liquid Ammonia-Liquid Oxygen Rocket", A. E. Ahramson, 17 June 1952.

146. University of Minnesota Research Report No. 126, "Measurement of Recovery Factors and Heat Transfer Coefficient with Transpiration Cooling in a Turbulent Boundary Layer at M = 3 Using Air and Helium as Coolants", B. M. Leadon and C. J. Scott, February 1956.

147. NASA Report TN D-721, "Exploratory Investigation of Transpiration Cooling of a 40° Double Wing Using Nitrogen and Helium as Coolants at Stagnation Temperatures from 1295° to 2910°F", Bernard Rashis, May 1961.

148. Grootenhus, P., "The Mechanism and Application of Effusion Cooling", Journal of the Royal Aeronautical Society, No. 578, Vol. 63, Page 73, February 1959.

149. United Nuclear Corporation, "Transpiration and Film Cooling for Solid Propellant Rocket Nozzles", by Hyman, Kuo, Israel, Minushkin, Cooper, and Hawkins, February 1961.

150. Jet Propulsion Center, Purdue University Report TM-62-5, "Effects of Selected Gas Stream Parameters and Coolant Physical Properties on Film Cooling of Rocket Motors", by D. L. Emmons, August 1962.

151. AFOSR TN 60-1484, "An Experiment with a Transpiration-Cooled Nozzle", by R. P. Bernicker, July 1960.

152. U.S.A.F. Air University Institute of Technology, GAE/ME/60-4, "An Evaluation of a Reverse-Flow Film Cooled Rocket Engine", by R. N. James, August 1960.

153. U.S.A.F. Air University Institute of Technology, GA/ME/60-12, "An Evaluation of a Film Cooled Gaseous Hydrogen and Oxygen Rocket Engine of 100 Pound Thrust", by G. Y. W. Ow, August 1960.

154. Aeronutronic, First Quarterly Progress Report, AF 04 (611)-7443, "Feasibility Investigation of Uncooled Thrust Chamber and Nozzle Designs", 30 October 1961. CONFIDENTIAL.

155. NACA RME51E04, "Investigation of Internal Film Cooling of 1000 Pound Thrust Liquid-Ammonia-Liquid-Oxygen Rocket Engine Combustion Chamber", G. Morrell, 17 July 1951. CONFIDENTIAL.

156. NASA TN-D-9, "Experimental Investigation of Air Film Cooling Applied to an Adiabatic Wall by Means of an Axially Discharging Slot", S. S. Papell and A. M. Trout, August 1959.

157. Jet Propulsion Laboratory, California Institute of Technology, Progress Report No. 1-75, "Preliminary Experiments of Gaseous Transpiration Cooling of Rocket Motors", R. B. Canright, 24 November 1948.

158. Knuth and Eldon, "The Mechanics of Film Cooling - Part I", Jet Propulsion, Page 359, November-December 1954.

159. Knuth and Eldon, "The Mechanics of Film Cooling - Part II", Jet Propulsion, Page 16, January 1955.

160. Friedman, J., "A Theoretical and Experimental Investigation of Rocket-Motor Sweat Cooling", ARS Journal No. 79, pp. 147-154, December 1949.

161. JPL Progress Report No. 9-17, "Sweat Cooling with the 50-Pound Thrust Rocket Motor", by G. Zima and H. L. Wheeler, Jr., 22 July 1947.

162. Zurcow, M. J., and A. R. Graham, "Some Considerations of Film Cooling for Rocket Motors", Jet Propulsion, Volume 27, pp 650-656, 1957.

163. ARS Paper 42051, "An Approximate Theory of Porous, Sweat or Film Cooling with Reactable Fluids", by L. Crocco, 1951.

164. CIT JPL PR 1-79, "A Study of the Mechanics of Liquid Films as Applied to Film Cooling", by E. L. Knuth, 21 November 1951.

165. NACA RM E9L09, "Cooling of Ramjets and Tailpipe Burners-Analytical Method for Determining Temperatures of a Combustion Chamber Having Annular Cooling Passage", by W. K. Koffel, et al, 21 March 1950.

166. Boden, R. H., "Heat Transfer in Rocket Motors and the Application of Film and Sweat Cooling", ASME Transactions, Volume 73, pp 385-390, 1951.

167. Duewy, P., and H. R. Wheeler, "Experimental Study of Cooling by Injection of a Fluid Through a Porpus Material", Journal of the Aeronautical Sciences, Volume 15, pp 509-521, 1948.

168. CIT JPL Report 1-35, "An Evaluation of Transpiration Cooling in a Rocket Motor Chamber", 16 June 1952.

169. Arde-Portland, Inc., Summary Report No. 1, "Cooled Solid Propellant Rocket Nozzles", 20 June to 30 September 1961.

170. Massachusetts Institute of Technology, AFOSR-TN-59-873, Technical Report No. 393, "An Investigation of Porous Wall Cooling", R. P. Bernicker, June 1959.

171. Curtiss-Wright Corporation, Monthly Progress Report No. 2., "Design, Fabrication and Static Firing of a Full Scale Lithium Cooled Rotating Nozzle", 14 July 1961. CONFIDENTIAL.

172. Hercules Powder Company, Allegany Ballistics Laboratory, "Status of Advanced Research Projects", 1 July 1961 through 31 October 1961. CONFIDENTIAL.

Thrust Chamber Cooling, General

173. Marquardt Report S-188, "Materials Evaluation for Uncooled Separation Nozzles", by J. G. Campbell and C. D. Coulbert, dated 25 January 1961.

174. Unterberg, W., "An Analysis of Heating Problems in Supersonic Ramjet Tailpipes", Jet Propulsion, Volume 27, No. 5, pp 514-521, May 1957.

175. Marquardt Report 5840, "Hypersonic Air-Breathing Engine Research Program, Annual Report (1960), Volume IV, Structural Design", dated 31 March 1961. CONFIDENTIAL.

176. Marquardt Report M-1808, "Investigations of Non-Regeneratively Cooled Rocket Thrust Chambers and Nozzles", 20 June 1961. UNCLASSIFIED.

177. Marquardt Report 5907, "Final Report Pyrolytic Graphite Thrust Chamber Development", dated 31 July 1962. UNCLASSIFIED.

178. Marquardt Report 5865, "Radiation Cooled Ultra-Low Pressure Rocket Thrust Chamber, Theoretical Studies", dated 15 October 1961. CONFIDENTIAL.

179. Marquardt Report 5848, "Summary of Development Tests of the 1/10 Scale Model, Gaseous Propellant Rocket Propulsion System Marquardt Model MA 80-XAA", dated 19 April 1961. UNCLASSIFIED.

180. Marquardt Report S-154, "An Experimental Investigation of the Suitability of JP-4 Fuel for the Regenerative Cooling of a Hypersonic Ramjet Engine", dated 1960. UNCLASSIFIED.

181. NASA TN D-596, "An Analysis of Thermal Radiation Heat Transfer in a Nuclear-Rocket Nozzle", by W. H. Robbins, dated January 1961.

182. NASA TN D-62, "Analysis of the Transient Radiation Heat Transfer of an Uncooled Rocket Engine Operating Outside Earth's Atmosphere", by W. H. Robbins, dated December 1959.

183. General Electric Quarterly Progress Report No. 2, "Analytical and Experimental Investigation of Uncooled Nozzles and Thrust Chambers", General Electric Company Flight Propulsion Laboratory Department, dated September-December 1960. CONFIDENTIAL.

184. WADC TN 58-218, "The Ultra-Low Pressure Liquid Propellant Space Propulsion System", by D. R. Hast, dated June 1958. CONFIDENTIAL.

185. Jack, J. R., "Regenerative and Radiation Cooling of Electro-Thermal Thrust Generators", IAS AND ARS Paper 61-97-1791, dated June 1961.

186. Aerojet General Corporation First Quarterly Report 0406-01-1, October 1961; Second Quarterly Report 0406-01-2, February 1961; Third Quarterly Report 0406-01-3, May 1961; "Ultra Low Chamber Pressure Systems".

187. Aeronutronics Systems, Inc., Second Quarterly Progress Report on Thrust Chamber Cooling, "Heat Transfer from Notched Walls in Subsonic and Supersonic Flow", January 1959. CONFIDENTIAL.

188. Allison Division, GMC, EDR 1835, May-July 1960; EDR 1894, November 1960; EDR 2029, March 10, 1961; "Quarterly Progress Report on Nozzle Cooling for Solid Propellant Rocket Motors". CONFIDENTIAL.

189. Sellers, J. P., Jr., "Effect of Carbon Deposition on Heat Transfer in a LOX/RP-1 Thrust Chamber", ARS Journal No. 5, pp 662-663, May 1961.

190. Bartz, D. R., "A Simple Equation for Rapid Estimation of Rocket Nozzle Convective Heat Transfer Coefficients", Jet Propulsion, Volume 27, pp 49-51, 1957.

191. American Gas Assoc. Labs. Res. Report 1255, "Study of Combustion and Heat Transfer Fundamentals in Small Diameter Tubes", by F. G. Hammaker and T. E. Hampel, August 1956.

192. A,E,R,E. R/R 2153 AD 127690, "Thermodynamic Aspects of Coolant Choice for Gas Cooled Reactors", by P. Fortescue, 1957.

193. Lohner, K., and G. Chone, "Heat Transmission through Fins and Finned Cylinders", Engineers Digest, Volume 19, pp 111-114, 1958.

194. Matsunaga, S., "On Radiation from Combustion Gas", Jet Propulsion, Volume 28, pp 125-126, 1958.

195. WADC TN56-14, "Partial Vaporization of Unsymmetrical Dimethylhydrazine at Low Ambient Pressure", by J. S. Gordon, 22 November 1955.

196. ERDE 13/M/56, "Some Experimental Observations Regarding the Convective Heat Transfer from Highly Dissociated Combustion Gases to Cooled Walls of Rocket Engines", by H. Ziebland, August 1956.

197. Gordon, R., "Heat Transfer Problems in Liquid Propellant Rocket Motors", ARS Journal No. 81, pp 65-78, 1950.

198. Ellion, M. E., "New Techniques for Obtaining Heat Transfer Parameters of the Wall and Combustion Gas in a Rocket Motor", ASME Transactions, Volume 73, pp 109-114, 1951.

199. CIT JPL PR 20-166, "Radiation of Rocket-Motor Combustion Gases" by T. T. Omori and W. B. Powell, 15 January 1953.

200. Topper, L., "Radiant Heat Transfer from Flames in a Turbojet Combustor", IEC. Volume 46, pp 2551-2558, 1954.

201. Naval Ordnance Test Station, Memo No. 1471, "Gas-Film Conductance at a Rocket Motor Wall", by P. K. Chung, 9 March 1954. CONFIDENTIAL.

202. Royal Aircraft Establishment (Great Britain), "Measurement of Heat Transfer in a Rocket Nozzle", W. S. Long. CONFIDENTIAL.

203. Bulletin of the 16th Meeting, JANAF Solid Propellant Group, Volume II, June 14 to June 16, 1960, "Recent Advances in Nozzle Cooling Techniques for Solid Propellant Rockets", by D. P. Hug, et al. CONFIDENTIAL.

204. Jet Propulsion Laboratory Research Summary No. 36-2, Volume I, Part 2, 1 February 1960 to 1 April 1960.

205. Robinson, A. T., et al., "Transpiration Cooling with Liquid Metals", AIAA Journal, Vol. I., No. 1, January 1963.

206. Bartlett, Eugene P., "Thermal Protection of Rocket-Motor Structures", Aerospace Engineering, January 1963.

207. Kaufman, W. F., W. H. Armour, and L. Green, "Thermal Protection of Fluorine-Hydrogen Thrust Chambers by Carbonaceous Materials", ARS Journal, October 1962.

208. Medford, J. E., "Transient Radial Heat Transfer in Uncooled Rocket Nozzles", Aerospace Engineering, October 1962.

209. NASA TR R-56, "Graphical Presentation of Difference Solutions for Transient Radial Heat Conduction in Hollow Cylinders with Heat Transfer at the Inner Radius and Finite Slabs with Heat Transfer at One Boundary", J. E. Hatch, et al, 1960.

210. Ford Motor Company Aeronutronic Division, Publication No. C-1869, "Applied Research for Advanced Cooled Nozzles" First Quarterly Report, 15 October 1962, by W. H. Armour. CONFIDENTIAL.

211. NASA TN D-944, "Configuration Factors for Exchange of Radiant Energy Between Axisymmetrical Sections of Cylinders, Cones, and Hemispheres and their Bases", Albert J. Buschman, Jr., and Claude M. Pittman, October 1961.

Material Properties

212. Campbell, I. E., "High Temperature Technology", John Wiley & Sons, Inc., New York, 1956.

213. Jaffee, Robert I., and D. A. Maykuth, "Refractory Materials, Part I - Technology and Low Temperature Behavior", Aero-Space Engineering, June 1960. "Part II - High Temperature Behavior", July 1960.

214. Chance Vought Aircraft, Report AST-E9R-12073, "Thermal Properties of Solids", by V. L. Arne and G. W. Wolfe, September 1939.

215. Arthur D. Little, "Advances in Thermal Insulating Materials for Thermal Protection Systems", by Peter E. Glaser, October 1961.

216. Aviationote No. 55 (Aviation Products Specific Heats), Johns-Manville, January 1961.

217. Johns-Manville, "Insulation Product Information IN-150A", (Thermoflex), June 1959.

218. Johns-Manville, "Insulation Product Information IN-254A", (Min-Klad), October 1959.

219. Johns-Manville, "Insulation Product Information IN-330A", (Micro-Quartz and Micro-Fibers), February 1961.

220. "Fiberfrax Ceramic Fiber CFB1-0160-2", Carborundum, 1960.

221. Products Bulletin, 1-2A (HITCO Refrasil Materials for High Temperature Application), H. I. Thompson, April 1961.

222. Marquardt Report 5952, "Final Report, Development of Radiation Cooled, Ultra-Low Pressure Rocket Thrust Chamber", (RTD-TDR-63-4), Dated 19 January 1963. CONFIDENTIAL.

223. Metalworking News, "Tungsten Alloy Forging Process Redirected by Air Force to Test", March 1962, p. 14.

224. Albom, M. J., "Diffusion Bonding Tungsten", Welding Journal, November 1962.

225. National Carbon Co., "The Industrial Graphite Engineering Handbook".

226. Society of Aerospace Materials and Process Engineers (SAMPE), "Symposium on Ceramics and Composites, Coatings and Solid Bodies", November 14-15, 1961, Dayton, Ohio.

TABLE I

EFFECTS OF MIXTURE RATIO ON HEAT SINK CAPACITY OF COOLANT FUELS

N_2O_4/N_2H_4		
Mixture Ratio (O/F)	Variation of Local Heat Flux	Variation of Heat Sink Potential
1.0	0.972	1.12
1.2	1.0	1.0
1.5	1.02	0.89
2.0	1.022	0.79
N_2O_4/50% UDMH-50% N_2H_4		
1.5	0.965	1.222
2.0	1.0	1.0
2.5	1.01	0.88
O_2/H_2		
Mixture Ratio (O/F)	Variation of Local Heat Flux	Variation of Wall Temperature
4.0	0.88	0.79
5.0	1.0	1.0
6.0	1.075	1.23

MAC A 673

TABLE II

HIGH TEMPERATURE DEGRADATION OF LAMINATED REFRASIL PHENOLIC MATERIAL IN A VACUUM ENVIRONMENT

Run No.	Environment	Run Time	Lamina Orientation	Maximum Surface Temperature (°F)	Maximum Back Face Temperature (°F)	Weight Loss (%)	Length Change (%)	Outer Diameter Change (%)	Inner Diameter Change (%)
1	Vacuum	4 Min	Perpendicular to Axis	2340	--	12.0	+2.4	-1.96	-1.94
2	Vacuum	4 Min	Parallel to Axis	2580	--	13.3	-2.02	-0.25	+5.5
3	Ambient Pressure	4 Min	Parallel to Axis	2440	--	11.8	-0.45	+0.3	-0.2
4	Ambient Pressure	4 Min	Perpendicular to Axis	2580	--	11.4	+0.077	-1.04	-0.75
5 (Rerun Sample 1)	Vacuum	3 Min	Perpendicular to Axis	--	1143	1.67	0	-0.05	+0.1
6 (Rerun Sample 4)	Ambient Pressure	3 Min	Perpendicular to Axis	--	1155	1.3	+0.31	0.25	+0.6

Samples: Laminated Refrasil phenolic cylinders, approx. 2 in. OD, 1 in. ID and 1.25 in. length.

Maximum Vacuum: 10^{-3} mm Hg; all samples were soaked in environment for 2 hrs after firing.

Remarks: Large dimensional change in Run 2 was due to cracking of sample.

TABLE III

NARMCO ABLATIVE AND INSULATING MATERIALS CHART

PRODUCT			CURE CYCLES				PHYSICAL PROPERTIES						THERMAL PROPERTIES				MECHANICAL PROPERTIES			
Reinforcement	Resin Type	Product Number	Pressure (psi)	Temp (°F)	Time (min)	Post Cure Min. at °F	Hardness (Barcol)	Resin Content (%)	Volatile Content (%)	Flow (Williamson) (%)	Bulk Factor	Cured Density (lbs/cu ft)	Specific Heat (Btu/lb/°F) (Cp)	Thermal Conduct (Btu/hr/ft^2) (K)	Thermal Diffusivity	Emissivity	Ultimate Compression (10^3 psi)	Ultimate Flexural (10^3 psi)	Flexural Modulus (10^3 psi)	Ultimate Tensile (10^3 psi)
High Silica	Phenolic	525-T4-VA	3000	350	60	None	65	26	5	8	(6) See note	109			(7)	0.85	17.0	10.0	2.72	3.1
		525-T2	30	350	60	None	65	24	5	12	(6) See note	104			2.25		20.5	24.0	2.5	13.1
		525-T4	30	350	60	None	66	24	5	7	(6) See note	105			(7)		25.9	24.8		15.1
		548-T4	2000	300	60	60 at 350°F	70	33	6	40	(6) See note	103	0.23	1.51	(7)		9.4	9.9	1.75	3.1
			6000	300	60								0.22	1.92						
		4012	2000	300	60	60 at 350°F	66	29	3	32	10.8	105	0.23	1.90	(7)		24.0	12.0	2.42	4.0
			6000	300	60								0.22	1.62						
		4014	2000	300	60	60 at 350°F	64	30	3	12	4.0	102	0.21	0.77	(7)		13.5	8.7	1.87	1.9
Glass	Phenolic	506	6000	300	60															
		506 (4)	30	350	60	None	60	33	6		(6) See note	122			2.4	0.81	46.0	74.0	3.66	60.0
			3000	300	60							102					26.0	24.0	3.25	6.0
	Epoxy	533	50	310	60	None	72	33	3		(6) See note	114			(7)	0.79	54.0	78.0	3.47	59.0
		4008	1500	350	60	None		40	3		(6) See note	120			(7)		25.0	32.0	2.70	
	Phenyl-Silane	534	2000	250	60	(2) See note	76	32			(6) See note	112	0.24	1.11	(7)		50.0	74.0	3.72	45.0
	Silicon	523	30	350	60	(3) See note	55	35	11	23	5.9	59	0.24	1.56	1.6	0.83	24.0	47.0	3.19	36.0
Asbestos	Phenolic	538-A1	2000	300	60		59	55							(7)		15.0	21.0	2.89	1.7
			6000	300	60															
	Silicone		2000	300	60	(3) See note	55	40	3			97								
Graphite	Phenolic	546-C1	2000	300	60	None	24	50	14	23	3.2	83	0.24	4.22						
			6000	300	60							90	0.22	4.48						
		4024	2000	300	60	None	17	35	6	22	4.1		0.18	4.90	(7)		10.0	8.0	1.30	2.70
			6000	300	60							70	0.24	4.24						
	Elastomer Phenolic	542-C1	2000	300	60	None	16	38	6	13	4.1		0.23	5.18	(7)		8.0	8.4	1.92	2.20
			6000	300	60								0.24	4.60						
	Silicon	552	2000	30	60	(3) See note	17	33	3			72			(7)		6.5	7.5	0.78	3.0
Synthetic Organics	Phenolic	4016	6000	350	60	None	10	100	None											
		4018	2000	300	60	None	19	48	8	23	3.4	76	0.35	1.09	(7)		2.0	4.0	3.22	2.5
Liner Materials			6000	300	60								0.34	1.16	(7)		16.0	7.0	3.84	2.0
		4501	750	350	60	None	92 (5)		100% solids						(7)					
															(7)					
		4502	750	350	60	None	92 (5)		100% solids											
															(7)					

(1) The mechanical and thermal properties may be upgraded by curing at temperatures of 325°F to 350°F.

(2) Post cures. 24 hrs at 250°F
24 hrs at 300°F
24 hrs at 350°F
8 hrs at 400°F
48 hrs at 500°F

(3) Post cures as follows:
1/2 hr at 200°F
1/2 hr at 275°F
1/2 hr at 350°F
1/2 hr at 400°F
1/2 hr at 450°F
1/2 hr at 485°F

(4) Available in plain fabric, chopped squares (1/2" x 1/2") and macerated form.

(5) Shore hardness.

(6) Bulk factor is dependent upon the form, i.e., chopped, macerated.

(7) The thermal diffusivity may be calculated from the thermal conductivity and specific heats.

(8) The information listed indicates typical performance for the types of products shown and are not to be considered as guaranteed values, each designer should establish allowable values for his requirements.

TABLE IV

HI - SILICA PRE - PREGS

Test Method		U.S. POLY		U.S. POLY		TM I		COAST		FIBERITE	W.B.	
		FM 5027A	FM 5067	FM-5083 Hi-Sil M.C.	FM-5063 Carbon	SL-530	SL-511	8P048-8	8P048-9	MX 2600	2214	8P048-8 Re-Run
D792	Specific Gravity	1.68	1.66	1.74	1.37	1.58	1.77	1.66		1.79	1.64	
7061	Resin Content % - Raw	32.76	31.20	26.88	26.54	27.38	31.70	29.95	27.74	30.13	19.95	
	Resin Content % - Cured	23.29	26.34			30.12	30.29	27.58	23.68	24.17		28.66
	Vols Content % 325°/15M.	4.45	4.50	1.94	5.28	2.47	2.90	5.47	3.44	4.29	6.82	4.75
	Flow % 500 psi/300°F	20.40	12.87	6.93	11.42	0.24	3.95	13.96	12.31	11.94	3.68	7.70
D955	Mold shrinkage											
	THK/PLY - 500 psi	0.025	0.026	NA	0.014	0.023	0.020	0.020	0.020	0.021	0.021	
D695	Compression - psi											
	11 to M.P. - R.T.	45,981								47,138	33,018	
	11 to M.P. - 550°F	27,969								37,166	17,222	
	1 to M.P. - R.T.	42,695								15,645	10,688	
	1 to M.P. - 550°F	7,560								15,356	2,330	
D638	Tensile - psi											
	11 to Warp - R.T.	13,579	8,939	6,743*	16,042	14,429	15,383	8,667	11,732	14,286	9,548	18,125
	11 to Warp - 550°F	6,090	6,751	1,896*	10,566	8,800	10,333	6,498	8,498	9,987	5,324	11,559
	45° to Warp - R.T.	12,250	9,450	NA	9,631	7,961	8,903	7,323	6,644	5,033	6,667	15,778
	45° to Warp - 550°F	4,913	6,076	NA	6,477	2,800	6,498	4,656	4,373	4,045	1,755	7,102
D256	Izod Impact - ft/lb/in. notch											
	11 to Warp		0.54							1.41	1.22	
	45° to Warp	3.27	0.78							1.42	1.32	
C177	Thermal Cond. - 300°F											
D695	Thermal Exp. to 350°F											
	Vendor Lot #											
	Carbon Type				CCA-1							
	Hi-Silica Type											

* Dog-Bone

THE Martin Marietta Corporation
VAN NUYS, CALIFORNIA
REPORT 5981 VOL. II

TABLE V

HIGH TEMPERATURE SWELLING INVESTIGATION OF LAMINATED REFRASIL PHENOLIC MATERIAL

Temperature (°F)	Maximum Expansion During Run (%)	Stabilized Expansion During Run (%)	Contraction on Cooldown (%)	Accumulative Length Change (%)	Accumulative Weight Change (%)
400	+0.19	+0.09	-0.122	-0.122	-1.98
600	+0.304	+0.171	-0.127	-0.254	-3.3
800	+0.342	+0.228	-0.019	-0.273	-5.92
1000	+0.344	+0.0412	-0.268	-0.524	-15.2
	Above values are based on condition of the sample preceding each run.			Above values are based on initial condition of sample	

Sample: Laminated refrasil phenolic, 7/8 in. by 2 5/8-in. by 6 5/16-in., Weight = 0.76 lbs. Orientation of lamina approx. 20° with respect to longitudinal axis.

Test Procedure: One hour soak to indicated temperatures at ambient pressure followed by cooldown to ambient temperature. Sample was weighed and measured before proceeding to next soak temperature.

Remarks: Sample delaminated at end of 1000°F soak period and char was silver-black throughout. Much of the carbon residue had been oxidized.

TABLE VI

COOLANT FLOW RATIO REQUIREMENTS

Conditions:

L* = 30 inches

T = 4000 lbs

CR = 1.5

P_o = 150 psia

Maximum Wall Temperature = 2200°R

PROPELLANT (N_2O_4/N_2H_4)	$\dot{W}_c/\dot{W}_p$			
Cooling Method	Combustion Chamber	Nozzle Convergent	Divergent A/A* 1→10	Divergent A/A*10→40
Liquid Film	0.134	0.0067	0.041	0.045
Gas Film	0.416	0.025	0.155	0.194
Transpiration				
Liquid to 2200°R	0.0245	0.0014	0.008	0.009
Liquid to Sat. Vapor	0.052	0.0030	0.017	0.018
Sat. Vapor to 2200°R	0.036	0.0020	0.013	0.014
PROPELLANT (H_2/F_2)				
Liquid Film	1.15	0.052	0.356	0.39
Gas Film	0.066	0.0022	0.0148	0.016
Transpiration				
Liquid to 2200°R	0.0072	0.0005	0.0035	0.0037
Liquid to Sat. Vapor	0.083	0.0028	0.016	0.018
Sat. Vapor to 2200°R	0.0072	0.0005	0.0035	0.0037

MAC A673

TABLE VI (Continued)

Cooling Method	Combustion Chamber	Nozzle Convergent	Divergent A/A* 1→10	Divergent A/A* 10→40
PROPELLANT OF_2/B_2H_6		$\dot{W}_c/\dot{W}_p$		
Liquid Film	1.24	0.0511	0.451	0.54
Liquid Film	--	0.0047	0.026	0.029
With vapor cooling				
Gas Film	0.305	0.0121	0.108	0.12
Transpiration				
Liquid to 2200°R	0.0515	0.00264	0.0227	0.0237
Liquid to Sat. Vapor	0.170	0.00855	0.091	0.0984
Vapor 540°R to 2200°R	0.0576	0.00294	0.0255	0.0266
PROPELLANT N_2O_4/N_2H_4 - UDMH				
Liquid Film	0.252	0.0102	0.0717	0.082
Gas Film	0.525	0.0211	0.1152	0.174
Transpiration				
Liquid to 2200°R	0.0405	0.00211	0.0156	0.015
Liquid to Sat. Vapor	0.080	0.00416	0.0317	0.030
Sat. Vapor to 2200°R	0.0604	0.00315	0.0236	0.023

TABLE VII

CAPABILITY COMPARISON OF HEAT SINK MATERIALS

Material	$k C_p \rho$ (Relative Value)	ΔT (Above 100°F)	Time to Reach ΔT (sec)
Pyrolytic Graphite (Edge oriented)	68.5	3000°F	126 sec
Tungsten	35.6	3000°F	65.5
Graphite	28.2	3000°F	51.9
Molybdenum	24.8	3000°F	45.6
Tantalum Carbide	23.2	3000°F	42.7
Copper	117.0	1700°F	29.7
Silicon Carbide	14.4	3000°F	26.5
Tantalum	12.0	3000°F	22.1
Beryllium	52.5	2000°F	21.2
Silver	81.0	1000°F	5.39
Steel (4130)	13.4	1500°F	2.38
Stainless Steel	5.8	2000°F	2.35
Aluminum (Pure)	38.6	800°F	1.46

TABLE VIII

MATERIALS WHICH SUBLIME BETWEEN ROOM TEMPERATURE AND 2000°C*
(3632°F)

Substance	Specific Gravity	Melting Point (°C)	Boiling Point (°C)	Heat of Sublimation or Dissociation** (Btu/lb)
ALN	3.26	>2200	Sublimes at 2000	6700
Si_3N_4	3.44	1900 (pressure)	Sublimes	5040
Mg_3N_2	--	--	Decomposes at 1500	3830
NH_4F	1.315	--	Sublimes	2310
NH_4CL	1.527	--	Sublimes at 335	1790
ALF_3	3.07	--	1270 (760 mm)	1630
KCNO	2.048	--	Decomposes 700 to 900	1600
SiS_2	--	--	Sublimes	1250
CdO	6.95	>1426	Decomposes 900 to 1000	1250
ZnO	5.606	>1800	Sublimes at 1800	1000
Na_2O	2.27	--	Sublimes at 1275	1000
Teflon	2.2	--	Sublimes at 730	800
GeO	--	--	Sublimes at 710	790

* Reference 206
Primary source of data, Handbook of Chemistry & Physics, 40th Edition, pp. 526-687, Chemical Rubber Publishing Company, Cleveland, Ohio, 1958.

** Computed from thermodynamic data.

MAC A673

TABLE IX

SUMMARY OF SPACECRAFT MISSIONS AND PROPULSION SYSTEM REQUIREMENTS

Space Mission and Maneuver	Basic Mission Requirements: Range of Ideal ΔV Requirements (fps)	Range of Desirable F / M_o (lb_f / lb_m)	Allowable Impulse Cutoff Accuracy $\Delta I_t / M_f$ $(lb_f\text{-sec}/lb_m)$	Required Thrust Variability	Restart Requirements	Typical Minimum Service Life (sec)	Thrust Program	Storability Requirements (Max.)	Representative System Characteristics: Small Payload (Centaur or Saturn Launch) M_{P_L} (lb_m)	M_o (lb_m)	F (lb_f)	I_t $(lb_f$ - sec)	Large Payload (Saturn or Nova Launch) M_{P_L} (lb_m)	M_o (lb_m)	F (lb_f)	I_t $(lb_f$ - sec)	Possible Space Engine Configuration: Thrust Required for Largest Nova H-S Payload (lb_f)	Type Engine Used For Mission	Engine Location	Engine Attachment	Number of Engines	Thrust Level percent/ per type Main/Vernier	Mode of Thrust Correction
	1	2	3	4	5	6	7	8	9	10	11	12	13	14	15	16	17	18	19	20	21	22	23
I. 300 N. Mi. Orbit																							
A. Orbital Correction																							
1. Orbital Perturbation	100 to 1,000	0.05 to 1.0	1.5	None	Multiple	240	1/3	Months	7100	8000	1000	0.24×10^6	36,000	40,000	5,000	1.2×10^6	60,000	M / V	M - E / V - E	M - F / V - G	1 - M / 4 - V	80 - M / 20 - V	V
2. Eccentricity Control	100 to 5,000	0.05 to 1.0	2.5	None	None	60	1	Months	7100	8000	4000	0.24×10^6	36,000	40,000	20,000	1.2×10^6	230,000	M / V	M - E / V - E	M - F / V - G	1 - M / 4 - V	80 - M / 20 - V	V
3. Orbital Plane Change	200 to 19,000	0.15 to 2.0	1.0	None	None	60	1	Months	7100	8000	4000	0.24×10^6	36,000	40,000	20,000	1.2×10^6	230,000	M / V	M - E / V - E	M - F / V - G	1 - M / 4 - V	80 - M / 20 - V	V
4. Orbital Altitude Variation	200 to 14,000	0.1 to 2.0	1.0	None	1 to 2	60	1/3	Months	7100	8000	4000	0.24×10^6	36,000	40,000	20,000	1.2×10^6	230,000	M / V	M - E / V - E	M - F / V - G	1 - M / 4 - V	80 - M / 20 - V	V
5. Orbital Epoch Change	100 to 20,000	0.1 to 2.0	0.5	None	1 to 2	60	1/3	Months	7100	8000	4000	0.24×10^6	36,000	40,000	20,000	1.2×10^6	230,000	M / V	M - E / V - E	M - F / V - G	1 - M / 4 - V	80 - M / 20 - V	V
6. Corr. of Injection Error	50 to 1,000	0.01 to 0.5	0.03	None	1 to 2	124	1/3	5 Days	7500	8000	1000	0.12×10^6	37,600	40,000	5,000	0.62×10^6	60,000	M	E	F	1 - M	100 - M	A
B. Orbital Rendezvous																							
1. Nominal Injection Errors	50 to 1,000	0.01 to 1.5	0.15 to 0.5	100 : 1	0 to 2	38	2/3	5 Days	7900	8500	4250	0.16×10^6	42,000	45,000	22,500	0.84×10^6	230,000	M	E	F	2 - M	100 - M	A
2. Dog-leg Maneuver	500 to 18,000	0.01 to 3.0	0.15 to 0.5	1,000 : 1	1 to 2	85	2/3	5 Days	3700	8500	25,500	1.3×10^6	20,700	45,000	135,000	7×10^6	1.4×10^6	M / V	M - E / V - E	M - F / V - G	4 - M / 4 - V	90 - M / 10 V	V
3. Emergency Rendezvous	1,000 to 25,000	0.01 to 3.0	0.15 to 0.5	1,000 : 1	1 to 2	105	2/3	1 Day	2000	4650	14,000	1×10^6	10,000	23,300	70,000	5.1×10^6	1.4×10^6	M / V	M - E / V - E	M - F / V - G	4 - M / 4 - V	90 - M / 10 V	V
II. 24 - Hour Orbit (19,310 N. Mi.)																							
A. Correction of Injection Errors	100 to 450	0.0004 to 0.2	2.0 to 15	None	Multiple	--	1/3	1 Month	5650	6000	60	90,000	26,400	28,000	200	420,000	1,700	A	E	F	1 - A	100 - A	A
B. Station Keeping	50 to 130	0.0002 to 0.02	0.55 to 3.25	None	Multiple	--	1/3	2 Years	5850	6000	40	19,500	27,300	28,000	150	91,000	1,400	A	E	F	2 - A	100 - A	A
C. Attitude Control	--	--	--	None	Multiple	--	1/3	2 Years	5850	6000	1	15,600	27,300	28,000	10	84,400	100	A	E	F	12 - A	100 - A	A
III. Lunar Flights																							
A. Trajectory Correction																							
1. Midcourse - Flt.	25 to 250	0.025 to 0.25	0.02	None	3	62	1/3	3 Days	2470	2500	125	7,750	98,500	100,000	5,000	0.31×10^6	5,000	M	E	F	2 - M	100 - M	A
2. Terminal - Flt.	25 to 500	0.020 to 0.5	0.03	None	2	62	1/3	3 Days	2470	2500	125	7,750	98,500	100,000	5,000	0.31×10^6	5,000	M	E	F	2 - M	100 - M	A
3. Terminal - Return	50 to 500	0.015 to 1.0	0.15 to 0.30	None	3	62	1/3	Months	490	500	25	1,550	19,800	20,000	1,000	62,000	1,000	M	E	F	2 - M	100 - M	A
B. Lunar Orbit	2,000 to 5,500	1.0 to 2.0	0.15 to 1.0	None	None	110	1	3 Days	1550	2500	2500	0.26×10^6	72,500	100,000	100,000	11×10^6	100,000	M / V	M - E / V - E	M - F / V - G	1 - M / 4 - V	80 - M / 20 - V	V
C. Lunar Landing																							
1. Direct	9,800 to 9,900	1.0	--	6 : 1	None	330	2	3 Days	700	2300	2300	0.45×10^6	43,000	95,000	95,000	21×10^6	95,000	M / V	M - E / V - E	M - F / V - G	1 - M / 4 - V	80 - M / 20 - V	V
2. From Orbit	5,700 to 6,000	1.0	--	6 : 1	1	200	2/3	3 Days	740	1500	1500	0.21×10^6	45,000	72,000	72,000	11×10^6	72,000	M / V	M - E / V - E	M - F / V - G	1 - M / 4 - V	80 - M / 20 - V	V
D. Lunar Take-off																							
1. To Orbit	6,000 to 6,500	1.0 to 1.6	0.15	None	1	140	1/3	Weeks	1500	3000	3000	0.42×10^6	21,200	40,000	40,000	5.6×10^6	40,000	M / V	M - E / V - E	M - F / V - G	1 - M / 4 - V	80 - M / 20 - V	V
2. Direct to Earth	9,000 to 11,000	1.0 to 1.5	0.30	None	None	130	1	Weeks	930	3000	4500	0.59×10^6	13,600	40,000	60,000	7.8×10^6	60,000	M / V	M - E / V - E	M - F / V - G	1 - M / 4 - V	80 - M / 20 - V	V
IV. Mars Flights																							
A. Trajectory Correction																							
1. Midcourse - Flt.	50 to 1,000	0.025 to 0.50	0.05	None	6	300	1/3	250 Days	9470	10,000	500	0.15×10^6	23,750	25,000	1,250	0.38×10^6	1,250	A	E	F	2 - A	100 - A	A
2. Terminal - Flt.	100 to 1,000	0.020 to 1.0	0.3	None	3	62	1/3	250 Days	9880	10,000	500	31,000	24,700	25,000	1,250	78,000	1,250	A	E	F	2 - A	100 - A	A
3. Midcourse - Return	50 to 1,000	0.025 to 0.50	0.05	None	6	310	1/3	3 Years	2840	3,000	150	45,600	8,000	8,500	425	0.13×10^6	425	A	E	F	2 - A	100 - A	A
4. Terminal - Return	200 to 1,500	0.03 to 1.0	0.1 to 0.25	None	3	62	1/3	3 Years	2960	3,000	150	9,300	8,380	8,500	425	26,400	425	A	E	F	2 - A	100 - A	A
B. Mars Orbit																							
1. No Atmospheric Braking	5,000 to 20,000	1.0 to 3.0	0.5 to 2.0	None	None	104	1	250 Days	3200	9000	18,000	1.6×10^6	8,500	23,500	47,000	4.2×10^6	47,000	M / V	M - B / V - B	M - F / V - F	1 - M / 4 - V	80 - M / 20 - V	V
2. With Atmospheric Deceleration	≈ 1,000	0.5 to 1.0	0.03	None	5 to 10	30	1/3	250 Days	7900	9000	9,000	0.28×10^6	20,600	23,500	23,500	0.73×10^6	23,500	M	M - B	M - F	1 - M	100 - M	A
C. Mars Landing																							
1. Direct	13,000 to 21,000	1.0 to 2.0	--	10 : 1	0 to 1	300	2/3	250 Days	1450	9000	18,000	2.2×10^6	3,800	23,500	47,000	5.75×10^6	47,000	M / V	M - B / V - B	M - F / V - F	1 - M / 4 - V	80 - M / 20 - V	V
2. From Orbit	11,000 to 15,000	2.0 to 4.0	--	10 : 1	1	140	2/3	250 Days	630	3500	14,000	0.79×10^6	1,500	8,500	34,000	1.9×10^6	34,000	M / V	M - B / V - B	M - F / V - F	1 - M / 4 - V	80 - M / 20 - V	V
D. Mars Take-off																							
1. To Orbit	15,000 to 17,000	0.7 to 1.0	0.30	None	1	167	1/3	Years	1600	10,000	15,000	2.4×10^6	4,000	25,000	37,500	6.2×10^6	37,500	M / V	M - E / V - E	M - F / V - G	1 - M / 4 - V	80 - M / 20 - V	V
2. Direct to Earth	20,000 to 35,000	--	0.30	None	None	--	1	Years	--	--	--	--	--	--	--	--	--	M / V	M - E / V - E	M - F / V - G	1 - M / 4 - V	80 - M / 20 - V	V
a. 1st Stage	--	1.5 to 2.0	--	--	--	100	--	--	8300	25,000	50,000	5×10^6	--	--	--	--	50,000	--	--	--	--	--	--
b. 2nd Stage	--	1.0 to 2.0	--	--	--	120	--	--	1600	8,300	16,600	2×10^6	--	--	--	--	16,600	--	--	--	--	--	-

NOTES FOR EACH COLUMN:

1. Estimated range of ideal velocity increments for each maneuver (Reference A-1).
2. The thrust and acceleration requirements for the various operations (Reference A-1).
3. The allowable total impulse error per unit mass at cutoff (Reference A-1).
4. Control of thrust level or total impulse per unit time (Reference A-1).
5. Possible number of restarts required (Reference A-1).
6. Typical burning time required for a fixed thrust level and total impulse maneuver (Reference A-1).
7. Typical thrust program for mission (Reference A-1). 1 = Constant, 2 = Variable, 3 = Pulse.
8. Propellant space storability requirements (Reference A-1).
9 - 12. Representative system requirements for a small payload (usually unmanned) using the Atlas-Centaur or Saturn launch vehicle (Reference A-1).
13 - 16. Representative system requirements for a large payload (potentially manned) using the Saturn or Nova launch vehicle (Reference A-1).
17. Maximum thrust requirements for a payload and given mission launched with the Nova H-8 vehicle.
18. Type engine used for mission / maneuver. M = Main, V = Vernier, A = Attitude.
19. Possible configuration installation of engines, B = Buried, E = Exposed.
20. Possible configuration attachment of engines, F = Fixed, G = Gimballed.
21. Typical cluster arrangement
22. Distribution of thrust levels between engines to accomplish thrust variability and control.
23. Mode of thrust correction and control in boost phase. V = Vernier, A = Attitude control.

TABLE X

SELECTED PROPERTIES[a] OF SUPER-ALPHA ALLOY SHEET

(A variety of heat treatments are represented. Longitudinal Tests)

Property	Ti-8Al-1Mo-1V	Ti-7Al-12Zr	Ti-5Al-5Sn-5Zr	Ti-5Al-2.5Sn	DOD Target[b] Range
RT, UTS, ksi	150 (150)	146 (120)	129 (120)	125-133	120-150
RT, YS (0.2%), ksi	142 (135)	140 (110)	123 (110)	120-123	110-135
RT, EL (2"), %	16 (12)	18 (10)	18 (12)	15-18	10-12
RT, MBR, T	2.6-4 (4)	3.0-5 (5)	2.5-5 (5)	3-4	4-5
800 F, UTS, ksi	111	111 (85)	85 (80)	82	80-85
800 F, YS (0.2%), ksi	86	94 (75)	63 (60)	63	60-75
800 F, EL (2"), %	14	22	24	16	--
800 F, 150 hour creep def., % (Stress specified)	0.22 (65) [155-149-16 156-142-15][c]	(65)	(50)	[0.1% (~35 ksi)][d]	0.1 (50-65)
1000 F, UTS, ksi	90	105 (80)	82 (75)	75	75-80
1000 F, YS (0.2%), ksi	72	82 (70)	62 (55)	58	55-70
1000 F, EL (2"), %	20	20	24	18	--
1000 F, 150 hour creep def., % (25-ksi stress)	0.18 to 0.73 [146-136-18 149-140-16][c]	0.018 to 0.03 [139-129-21 143-133-20][c]	0.000 to 0.06 [124-113-20 126-113-21][c]	[0.1% (~4 ksi)][d]	0.1 (25)

(a) The properties were selected without regard to comparable heat-treatment relationships between kind of tests or between alloys.

(b) Target properties vary for individual alloys and are shown in parentheses beside the data.

(c) Room-temperature tensile properties (UTS-YS-EL) before (above) and after (below) the creep exposure are given between the brackets.

(d) Stress to give 0.1% creep deformation is shown.

TABLE XI

SOME SOLIDS THAT MELT ABOVE 4000°F

Class	Solid	Chemical Formula	M.P. (°F)	B.P. (°F)	Specific Gravity (Dense Form)
Pure Metals	Tungsten	W	6170	10,600	19.3
	Rhenium	Re	5755	8,700	20.0
	Tantalum	Ta	5430	7,400	16.6
	Osmium	Os	4890	9,600	22.5
	Molybdenum	Mo	4750	6,700	10.2
	Ruthenium	Ru	4530	4,900	12.2
	Iridium	Ir	4445	8,700	22.5
	Niobium	Nb	4380	6,000	8.6
Oxides	Thoria	ThO_2	5970	7,950	9.7
	Magnesia	MgO	5070	5,115	3.6
	Hafnia	HfO_2	5020		9.7
	Zirconia	ZrO_2	4850	7,800	5.6
	Ceria	CeO_2	4710		7.1
	Calcia	CaO	4710	5,160	3.3
	Beryllia	BeO	4620	7,700	3.01
	Strontia	SrO	4380	5,430	4.7
	Yttria	Y_2O_3	4370	7,800	4.9
	Lanthana	L_2O_3	4180	7,600	6.5
	Urania	UO_2	4140	7,450	11.0
	Chromia	Cr_2O_3	4115	5,430	5.2
Complex Oxides	Thorium Zirconate	ThO_2ZrO_2	5070		
	Strontium Zirconate	$SrOZrO_2$	4890		5.5
	Barium Zirconate	$BaOZrO_2$	4890		6.3
	Beryllium Zirconate	$3BeO2ZrO_2$	4590		
	Zirconium Silicate	ZrO_2SiO_2	4390		4.6
	Calcium Zirconate	$CaOZrO_2$	4240		4.8
Carbides	Hafnium Carbide	HfC	7025		12.2
	Tantalum Carbide	TaC	7015		14.5
	Zirconium Carbide	ZrC	6890	9,200	6.7
	Niobium Carbide	NbC	6330		7.8
	Tantalum Carbide	Ta_2C	6150		15.0
	Titanium Carbide	TiC	5680	7,900	4.8
	Tungsten Carbide	WC	5190	11,000	15.5
	Tungsten Carbide	W_2C	5170	11,000	17.2
	Vanadium Carbide	VC	5730	7,050	5.4
	Aluminum Carbide	Al_4C_3	5070		3.0
	Molybdenum Carbide	Mo_2C	4860		8.9
	Molybdenum Carbide	MoC	4870		8.5
	Thorium Carbide	ThC_2	4810		9.6
	Thorium Carbide	ThC	4760	9,050	10.6
	Boron Carbide	B_4C	4440		2.5
	Silicon Carbide	SiC	4350		3.2
	Uranium Carbide	UC_2	4260	7,900	11.3

MAC A673

TABLE XI (Continued)

Class	Solid	Chemical Formula	M.P. (°F)	B.P. (°F)	Specific Gravity (Dense Form)
Borides	Chrome Nickel Boride	Cr_2NiB_4	4000		6.0
	Tantalum Boride	TaB_2	5440		12.60
	Niobium Boride	NoB_2	5250		7.21
	Chromium Boride	CrB_2	5000		5.6
	Tungsten Boride	W_2B	5020		16.7
	Hafnium Boride	HfB_2	5540		11.2
	Zirconium Boride	ZrB_2	5430		6.1
	Tungsten Boride	WB	5290		16.0
	Titanium Boride	TiB_2	4710		4.5
	Thorium Boride	ThB_2	4530		8.45
Silicides	Tungsten Silicide	W_3Si_2	4250		
	Tantalum Silicide	Ta_9Si_2	4550		12.7
	Tantalum Silicide	Ta_5Si_3	4530		11.6
	Zirconium Silicide	Zr_6Si_5	4080		
Nitrides	Hafnium Nitride	HfN	5990		
	Boron Nitride	BN	5430		2.2
	Tantalum Nitride	TaN	5400		
	Zirconium Nitride	ZrN	5390		6.9
	Titanium Nitride	TiN	5340		5.4
	Scandium Nitride	ScN	4800		
	Uranium Nitride	UN	4765		14.32
	Thorium Nitride	ThN	4280		
	Aluminum Nitride	AlN	4050		
Miscellaneous	Cerium Sulfide	CeS	4440		6.0
	Carbon Graphite	C	6800		
	Uranium Monocarbide	UC	4490		13.63
	Beryllium Nitride	Be_3N_2	4000	Dissoc.	

TABLE XII

ALLOYS OF MOLYBDENUM, COLUMBIUM, TANTALUM, TUNGSTEN, AND VANADIUM

Alloy	Nominal Alloy Composition, Weight Percent (Balance Refractory-Metal Base)									
	W	Mo	Ta	Cb	Hf	Ti	Zr	V	C	Other
Molybdenum-Base Alloys										
Mo-0.5 Ti						0.5			0.02-0.05	
TZM						0.5	0.08		0.02-0.08	
TZC						1.25	0.15		0.15	
Mod. TZC						1.27	0.29		0.3	
Mo-0.05 Zr							0.054		0.024	
Mo-0.5 Zr							0.5		0.02	
Mo-1.5 Cb				1.5					0.25	
Mo-25 W	25						0.11		0.05	
Mo-0.5 TiO_2										0.5 TiO_2
Columbium-Base Alloys										
F-48	15	5					1		0.1	
F-50	15	5				5	1		0.05	
Cb-7	28					7				
Cb-16	20					10		3		
Cb-65						7	0.8		0.075	0.11 O, 0.02 N
Cb-74	10						5		0.03	0.12 O, 0.02 N
FS-80							0.75			
FS-82			33				0.75			
D-31		10				10			0.06	0.05 O, 0.07 N
D-41	20	6				10				
15-20	15		20							
20-20	20		20							
Cb-Ta-W-Zr	10		24				1			
C-103					10	1	0.5			
Cb-Mo-Hf		5			5					
Cb-W-Zr	10						5			
Cb-Ti						8				
Cb-V-Al								3		3Al
Tantalum-Base Alloys										
Ta-10W	10									
Ta-10Hf-5W	5				10					
Ta-30Cb-7.5V				30				7.5		
Tungsten-Base Alloys										
W-1ThO_2										1 ThO_2
W-2ThO_2										2 ThO_2
W-10Mo		10								
W-15Mo		15								
W-25Mo		25								
W-0.38 TaC										0.38 TaC
Vanadium-Base Alloys										
V-50Cb				50						
V-20Cb-5Ti				20		5				

MAC A 673

TABLE XIII

PRINCIPAL PRODUCERS OF REFRACTORY METALS

Primary Producers of Refractory Metals	Tungsten	Molybdenum	Tantalum	Columbium	Chromium	Vanadium	Hafnium	Platinum	Palladium	Osmium	Ruthenium	Rhodium	Iridium	Rhenium
Anaconda Co., New York								X	X					
Bishop, J. & Co., Malvern, Pa.								X	X	X	X	X	X	
Carborundum Metals Co., Akron, N. Y., div. Carborundum Co.							X							
Chase Brass & Copper Co., Waterbury, Conn.														X
Cleveland Tungsten, Inc., Cleveland, sub. Molybdenum Corp. of America	X													
Climax Molybdenum Co. of Michigan, Inc., Detroit, div. American Metal Climax		X												
Du Pont de Nemours & Co., Inc., E. I., Wilmington, Del.				X										
Elmet Div. Lewiston, Maine, North American Phillips Co., Inc.	X	X												
Engelhard Industries, Inc. Newark, N. J.								X	X	X	X	X	X	
Fansteel Metallurgical Corp., North Chicago, Ill.	X	X	X	X										
Firth Sterling Inc., Pittsburgh	X													
Foote Mineral Corp., Philadelphia							X							
General Electric Co., Schenectady, N. Y.	X	X		X										
Goldsmith Bros., Chicago, div. National Lead Co.								X	X	X	X	X	X	
International Nickel Co., New York								X	X		X	X	X	
Johnson-Matthey & Co., Limited London								X	X	X	X	X	X	
Kawecki Chemical Co., Inc. New York			X	X										
Kennametal Inc., Latrobe, Pa.	X		X	X										
Metals & Controls Division Attleboro, Mass., Texas Instruments, Inc.								X						
Metals & Residues, Inc., Springfield, N. J.	X	X												
Molybdenum Corp. of America Pittsburgh		X												
National Research Corp., Metals Division Cambridge, Mass.			X											
Oregon Metallurgical Corp., Albany, Oregon	X	X				X								
Phelps Dodge Corp., New York								X	X					
Reactive Metals Inc., Niles, Ohio			X	X			X							
Reduction & Refining Co., Kenilworth, N. J.	X	X												
Shield Alloy Corp., Newfield, N. J.					X									
Stauffer Chemical Co., Metals Div. Richmond, California	X	X	X	X										
Sylvania Electric Products, Inc., Chemical and Metallurgical Div., Towanda, Pa.	X	X												
Temescal Metallurgical Corp., Berkeley, California		X	X	X										
Union Carbide Metals Co., div. of Union Carbide Corp., New York	X		X	X	X	X								
Universal-Cyclops Steel Corp. Bridgeville, Pa.	X	X												
University of Tennessee Department of Chemistry, Knoxville, Tenn.														X
Vanadium Corp. of America New York						X								
Wah Chang Corp., New York	X	X	X	X			X							
Westinghouse Electric Corp., Pittsburgh		X												

MAC A673

TABLE XIV

TIME-TEMPERATURE CAPABILITY OF VARIOUS REFRACTORY METAL COATINGS
(See Figures 152 and 153 for Data)

Ident.	Coating	Metal	Coated by	Tested by
1	Zinc, Hot-dipped and Conditioned at 1800°F	Columbium	Naval Research Laboratory	Naval Research Laboratory
2	W-2	CP Molybdenum	Chromizing Corp.	Chromizing Corp.
3	Cr-50Ti vac. dist. 0.001" + Si vac. dist. 0.001"	F-48 Columbium	Thompson-Ramo Wooldridge	Thompson-Ramo Wooldridge
4	Aluminide or Beryllide	Tantalum	Sylcor	Sylcor
5	Pack Silicide	Tantalum Alloy (experimental)	Battelle	Battelle
6	Pack Silicide	Tantalum	Battelle	Battelle
7	Cr-50Ti vac. dist. 0.001" + Si vac. dist. 0.001"	D-31 Columbium	Thompson-Ramo Wooldridge	Thompson-Ramo Wooldridge
8	W-2	CP Molybdenum	Chromizing Corp.	Chromizing Corp.
9	W-2	CP Molybdenum	Martin Co.	Martin Co.
10	CR-ZrO_2 Electrodep.	Tantalum	Value Engr.	Value Engr.
11	Cr-ZrB_2 Electrodep.	Tantalum	Value Engr.	Value Engr.
12	Sprayed 50Sn-50Al	Tantalum and Tantalum-tung.	Sylcor	Sylcor
13	Modified W-2	Columbium + 10Mo + 10Ti	Bell	Bell
14	T-1	Tungsten	Bell	Bell
15	Flame Sprayed Rokide Z (0.027")	0.5 Ti-Mo	Bell	Bell
16	Electroplated Cr (0.005") CPA 1800	0.5 Ti-Mo	Bell	Bell
17	Detonation Sprayed LM-5 (Mo, Cr, Si 0.008 to 0.016")	0.5 Ti-Mo	Bell	Bell
18	Thermomet T-55 Pack silicide	0.5 Ti-Mo	Thermomet	Marquardt

MAC A673

TABLE XIV (Continued)

Ident.	Coating	Metal	Coated by	Tested by
19	Al-Cr-Si 0.005" Flame Sprayed	CP Molybdenum	Climax	Climax
20	Al-Cr-Si 0.005" Flame Sprayed	CP Molybdenum	Marquardt	Marquardt
21	Hot-dip in Molten Copper Silicon Bath	CP Molybdenum	Metalwork Plansee	Metalwork Plansee
22	Chrome Plate 0.001"	Fansteel 82 Columbium	Fansteel	Fansteel
23	Chrome Plate 0.002"	Fansteel 82 Columbium	Fansteel	Fansteel
24	Si-Co Co-Deposited, Single Cycle Pack Diffusion, 0.0025 inch thick	0.5 Ti-Mo	Pfaudler	Pfaudler
25	Cr, Si, Co Separate Layers, Pack Diffusion 0.0015 inch thick	0.5 Ti-Mo	Pfaudler	Pfaudler
26	Cr + Si Co-Deposited then Co on top, Pack Diffusion 0.0035 inch thick	0.5 Ti-Mo	Pfaudler	Pfaudler
27	Si + Cb Co-Deposited Single -Cycle Pack Diffusion 0.0035 inch thick	0.5 Ti-Mo	Pfaudler	Pfaudler
28	Cr, then Si + Co Co-Deposited on top Pack Diffusion, 0.0025 inch thick	0.5 Ti-Mo	Pfaudler	Pfaudler
29	Cr, Co, Si Separate Layers, Pack Diffusion 0.0035 inch thick	0.5 Ti-Mo	Pfaudler	Pfaudler
30	Mo-Cr-Al-Si-B Alloy Pack Diffusion	CP Columbium	WADD	WADD
31	Thermomet 254B Pack Silicide	C-103 Columbium	Thermomet	Marquardt
32	Thermomet 259B Pack Silicide	CP Tungsten Sheet	Thermomet	Marquardt
33	Durak MG-F	Slip-cast Tungsten	Chromizing Corp.	Marquardt

MAC A673

TABLE XIV (Continued)

Ident.	Coating	Metal	Coated by	Tested by
34	Durak MG	CP Mo. sheet	Chromizing Corp.	Marquardt
35	PFR-1	D-31 Columbium	Pfaudler	Pfaudler
36	AMFKOTE-3	Columbium	AMF	AMF
37	AMFKOTE-2	Molybdenum	AMF	AMF
38	Durak B	Molybdenum	Chromizing	Chromizing
39	W-2	Molybdenum	Chromalloy	NASA, Langley
40	PFR-5	Molybdenum	Pfaudler	Pfaudler
41	$MoSi_2$ in a Continuous Matrix of An-Si Alloy (Paint & Sinter)	Molybdenum	G.E.	G.E.
42	G.E. System 400 (Flame Spray Al_2O_3 then spray glass frit and sinter at 2700°F)	Columbium or Tantalum	G.E.	G.E.
43	Zirconium Diboride (0.010 inch thick)	Molybdenum	Picatinny Arsenal	Picatinny
44	Undercoat of ZrO_2 + Metal (metal rich); overcoat of ZrO_2 + Metal (ZrO_2 rich)	Molybdenum	Picatinny Arsenal	Picatinny
45	70% Pt-30% Rh (0.002-0.005 inch)	Molybdenum or Tungsten	AMF	AMF
46	G.E. System 300 (Flame sprayed Al_2O_3 over Chrome plate)	Molybdenum	G.E.	G.E.
47	G-14 Al-5Cr-5Ti $CbAl_3$ (dip coat) (0.002-0.004 inch)	Columbium	Sylcor	Sylcor
48	Paint & Sinter Mo-Si-Ni or vapor plate (+ Cr, Al, Mn, etc.)	Molybdenum	Narmco	Narmco
49	$MoSi_2$ + Ni-Cr Electrophoretic coating (0.005-0.010 inch)	Molybdenum or Tungsten	Thiokol	Thiokol

MAC A673

TABLE XIV (Continued)

Ident.	Coating	Metal	Coated by	Tested by
50	$MoSi_2$+6% Ni Electrophoretic (0.001-0.003 inch)	Molybdenum	Vitro	Vitro
51	Vought II, IX Multi-cycle pack cementation	Molybdenum F-48 Columbium FS82 Columbium	Chance-Vought	Chance-Vought
52	Al-Si Flame sprayed	Molybdenum or Tantalum	National Research	National Research
53	Simultaneous Electroplate and electrophoresis of ceramic and cermet (0.002 to 0.005 inch)	Molybdenum Tantalum Columbium Tungsten	American Machine & Foundry	American Machine & Foundry
54	Beryllide Pack Cementation or plasma spray or paint and sinter	Molybdenum Tantalum Columbium	Brush-Beryllium Co.	Brush-Beryllium Co.
55	PFR-6	0.5 Ti Molybden	Pfaudler	Pfaudler
56	Aluminide	CP Cb	Gen. Telephone & Electronics	Thompson-Ramo Wooldridge
57	Aluminide	D-14 Cb	Gen. Telephone & Electronics	Thompson-Ramo Wooldridge
58	Aluminide	F-48	Gen. Telephone & Electronics	Thompson-Ramo Wooldridge
59	Pack Disilicide + Cb	FS 82	Boeing	Thompson-Ramo Wooldridge
60	Pack disilicide (modified)	C-103 D-14 D-31 F-48	Pfaudler	Thompson-Ramo Wooldridge
61	PFR-1	FS 82	Pfaudler	Thompson-Ramo Wooldridge
62	PFR-1	D-21	Pfaudler	Thompson-Ramo Wooldridge
63	Cr-Ti-Si 3-cycle vacuum deposition	FS 85	Thompson-Ramo Wooldridge	Thompson-Ramo Wooldridge
64	Pack disilicide, dual cycle + Cr + Mo	FS 85	Pfaudler	Thompson-Ramo Wooldridge
65	Aluminide	90TA-10W	Marquardt	Marquardt

MAC A673

TABLE XV

HIGH TEMPERATURE INSULATORS

Insulation	Vendor	Composition	Form	Temperature Limit
Fiberfrax	Carborundum	Alumina-silica fiber	Bulk, chopped, washed, or long staple fibers, block, board, paper, blanket, roving, wicking, yarn, rope, cloth, tape, cord, braid, castable shapes, coating cement, tubes and laminates	2300°F (steady state)
Kaowool	Babcock & Wilcox	Mineral alumina-silica (kaolin fibers)	Bulk fiber and blanket	2300°F (steady state)
Micro-Quartz	Johns-Manville	Quartz fibers	Bulk fiber, felt, mat and web	2000°F (steady state)
Min-K	Johns-Manville		Mat, block, and cast shapes	1300°F (200 hr, Min-K 1301) 2000°F (steady, Min-K 2000)
Pyrolytic Graphite	High Temperature Materials	Anistropic graphite	Plates, tubes, Pyrofoil, and Pyrofoam	5000°F (in non-oxidizing gas)
Super-insulation	Linde	Fiberglas and aluminum foil, quartz fiber and copper foil	Multi-layer blankets	1000°F (steady state) 1700°F (steady state)
Thermoflex	Johns-Manville	Alumina-silica fiber	Bulk fiber and felts	2000°F (steady state)
Typersil	DuPont	Potassium titanate fibers	Bulk fiber, felt, paper, block, and coating cement	2200°F (steady state)
Refrasil	H. I. Thompson	Vitreous silica (leached fiberglas)	Bulk fiber, cloth, tape, sleeving, yarn, cordage, and flakes	2000°F (steady state)

HEAT FLUX AT UPPER LIMIT OF NUCLEATE BOILING vs. BULK TEMPERATURE OF COOLANT

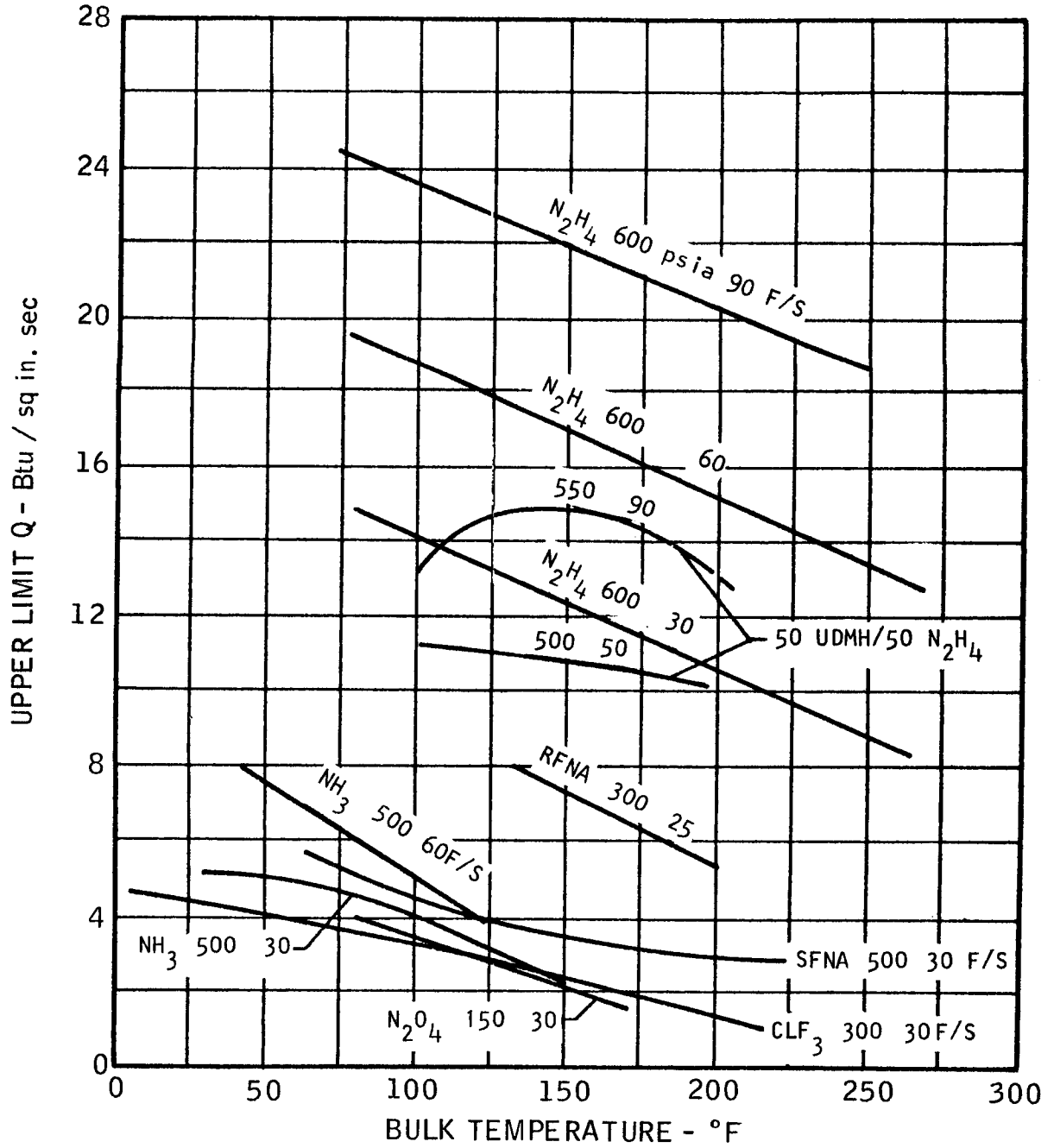

MAC A673

FIGURE 1

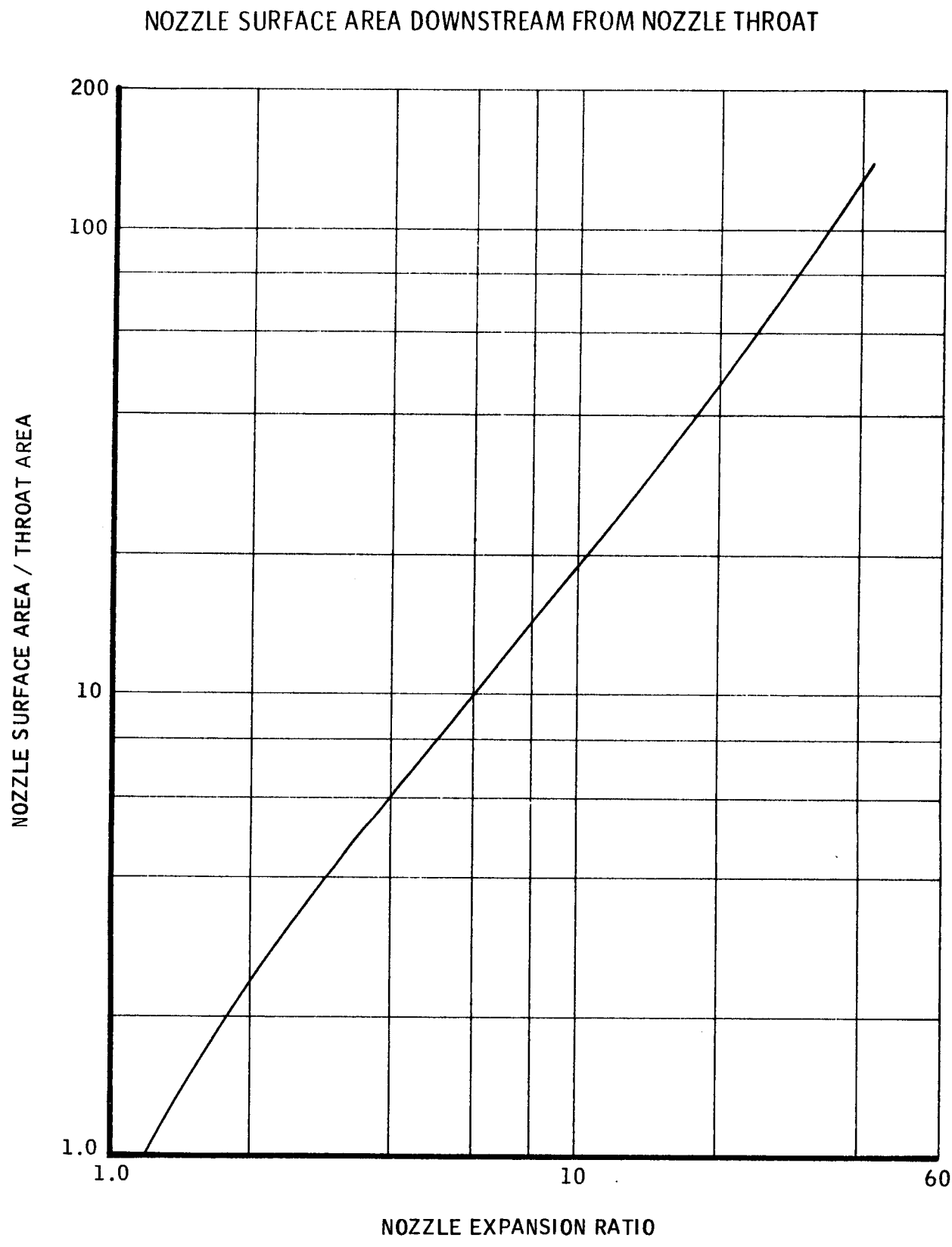

MAC A673

FIGURE 2

SURFACE AREA UPSTREAM FROM NOZZLE THROAT AS A FUNCTION OF CONTRACTION RATIO AND NOZZLE THROAT AREA

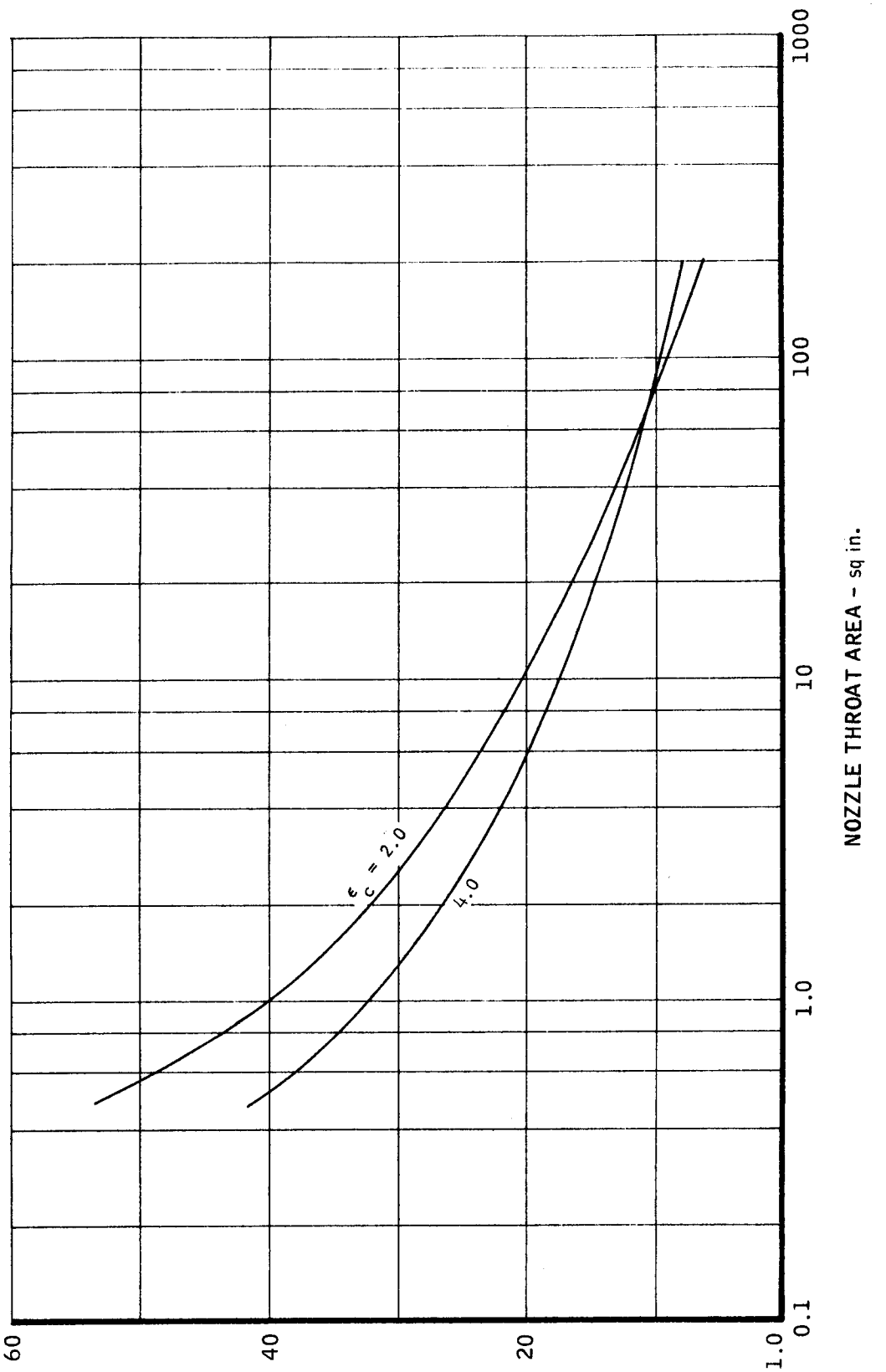

MAC A673

FIGURE 3

VELOCITY HEAD FOR ESTIMATION OF COOLING JACKET PRESSURE DROP

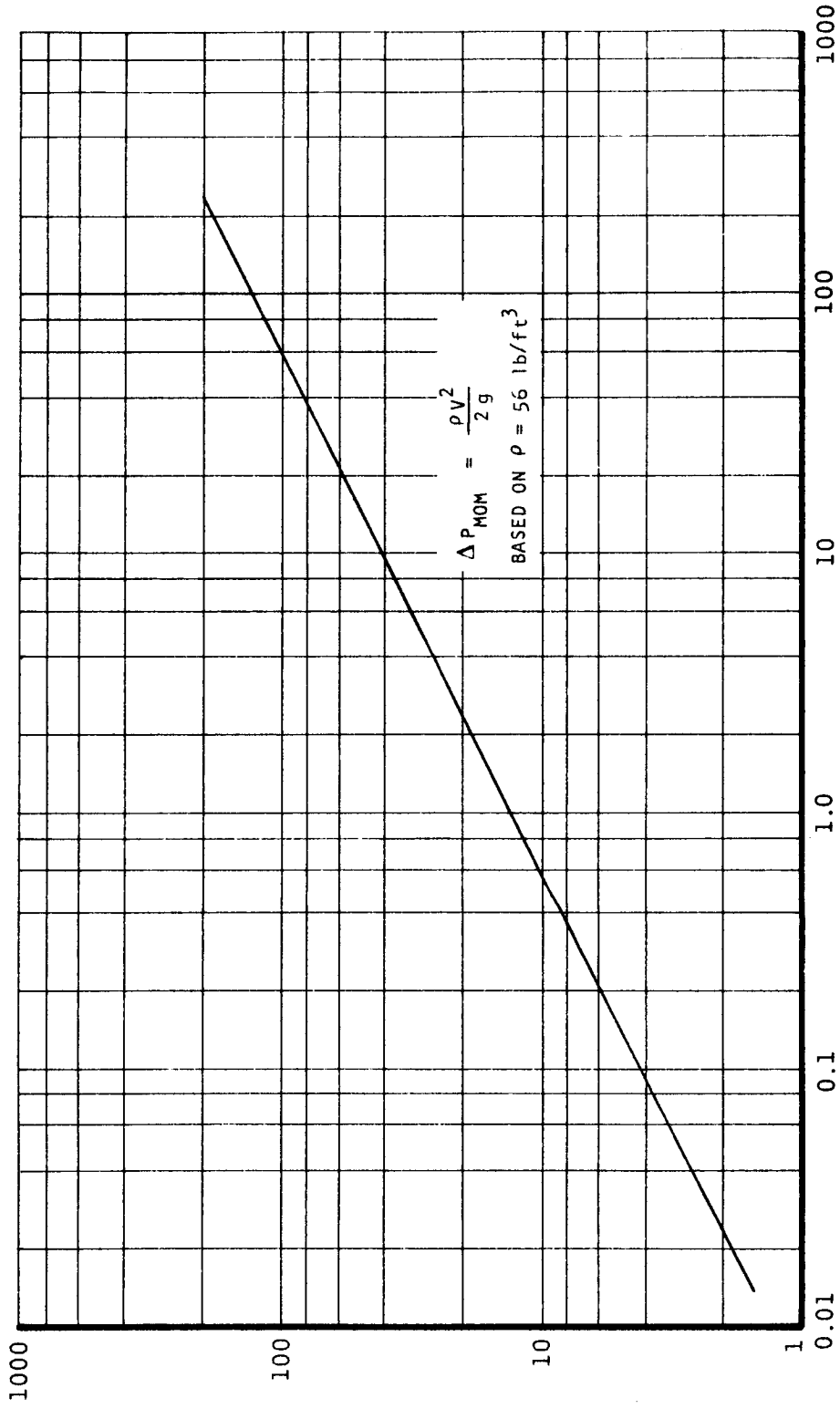

MAC A673

FIGURE 4

MAXIMUM COOLABLE NOZZLE EXPANSION RATIO
AS A FUNCTION OF THRUST AND CHAMBER PRESSURE

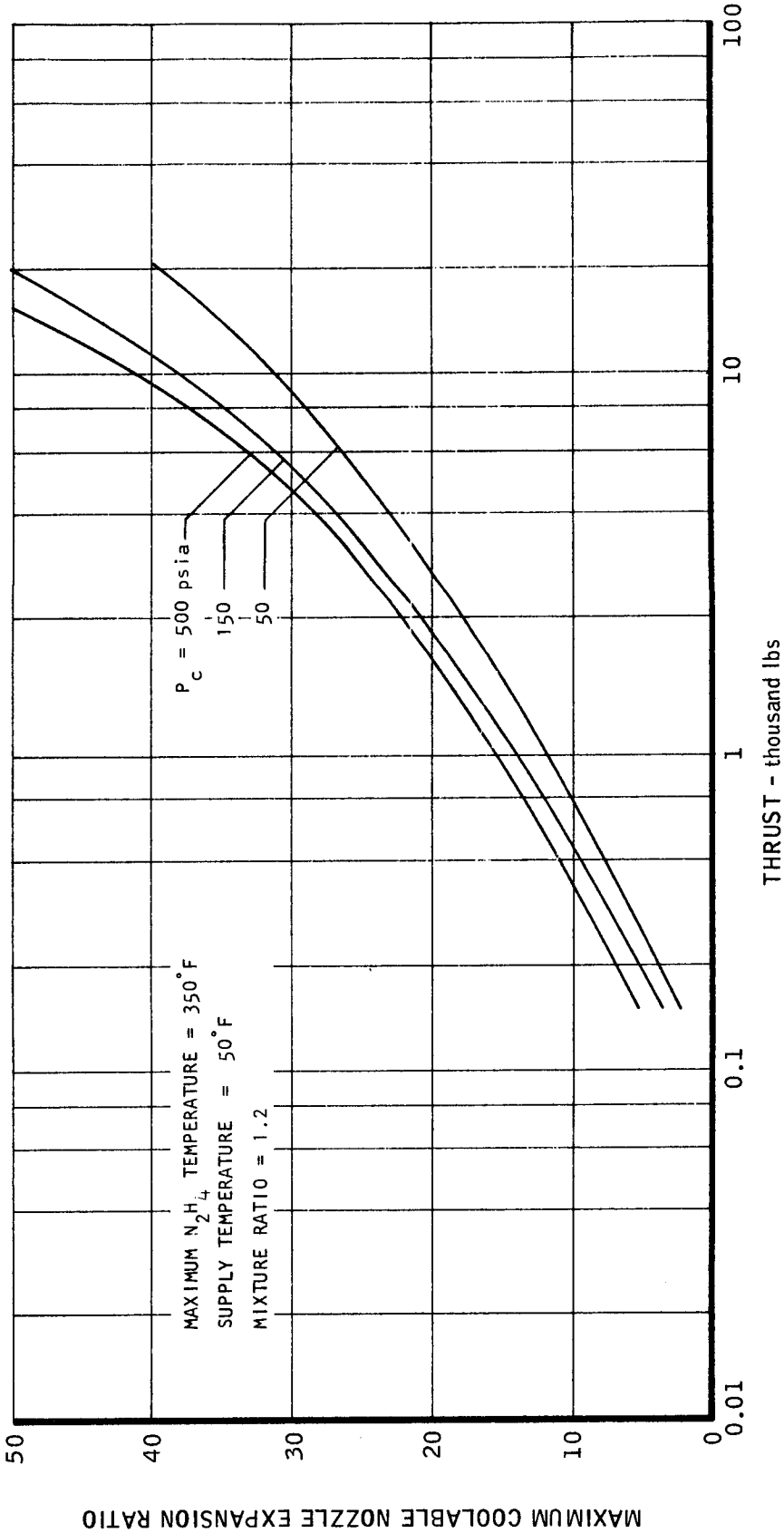

MAC A673

FIGURE 5

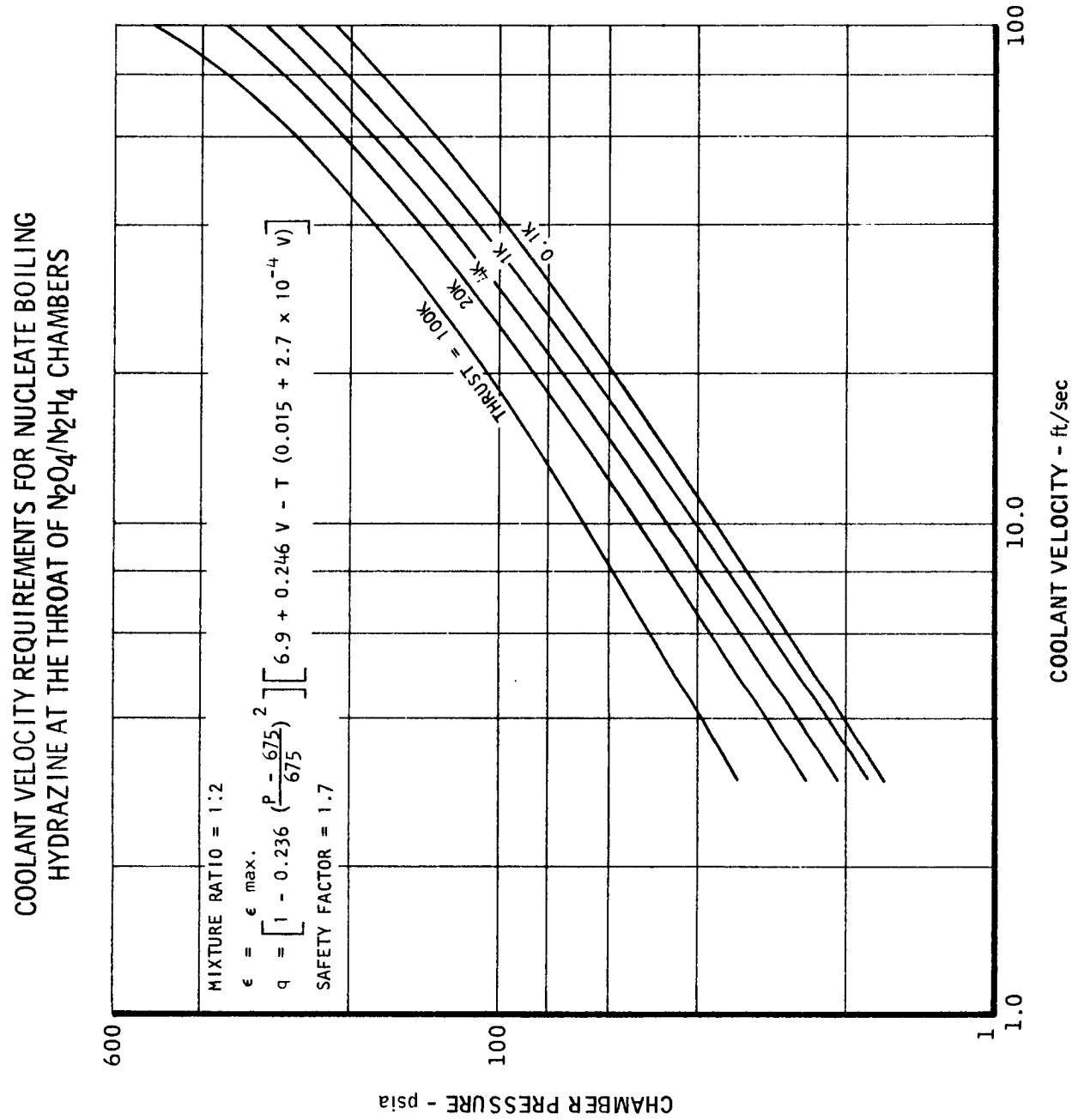

MAC A 673

FIGURE 6

COOLANT PRESSURE REQUIREMENTS FOR N_2O_4 / N_2H_4 CHAMBERS

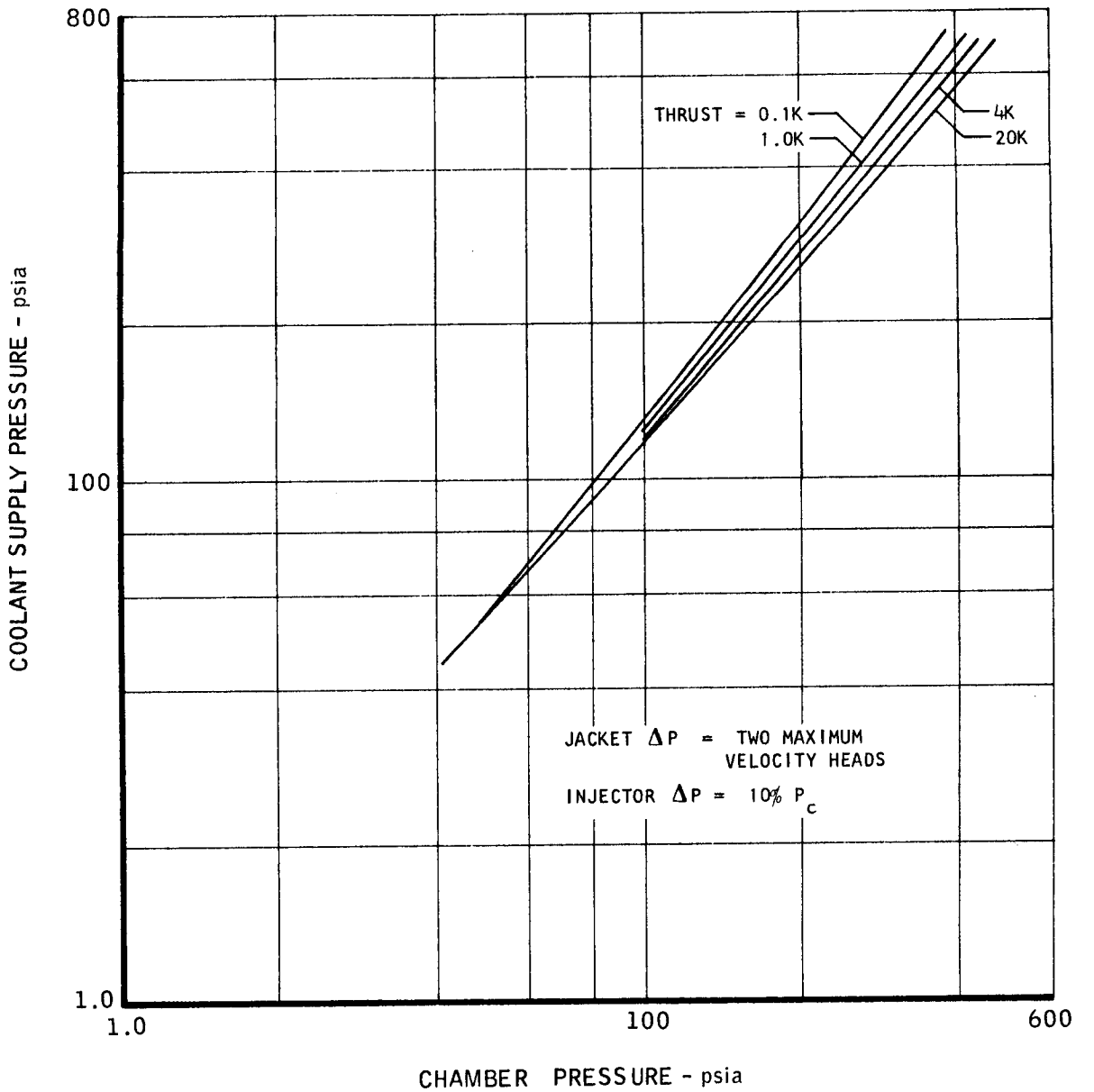

MAC A 673

FIGURE 7

MAXIMUM AND MINIMUM DIMENSIONS FOR
LONGITUDINAL AND RECTANGULAR PASSAGES
AS AFFECTED BY PASSAGE FACTOR

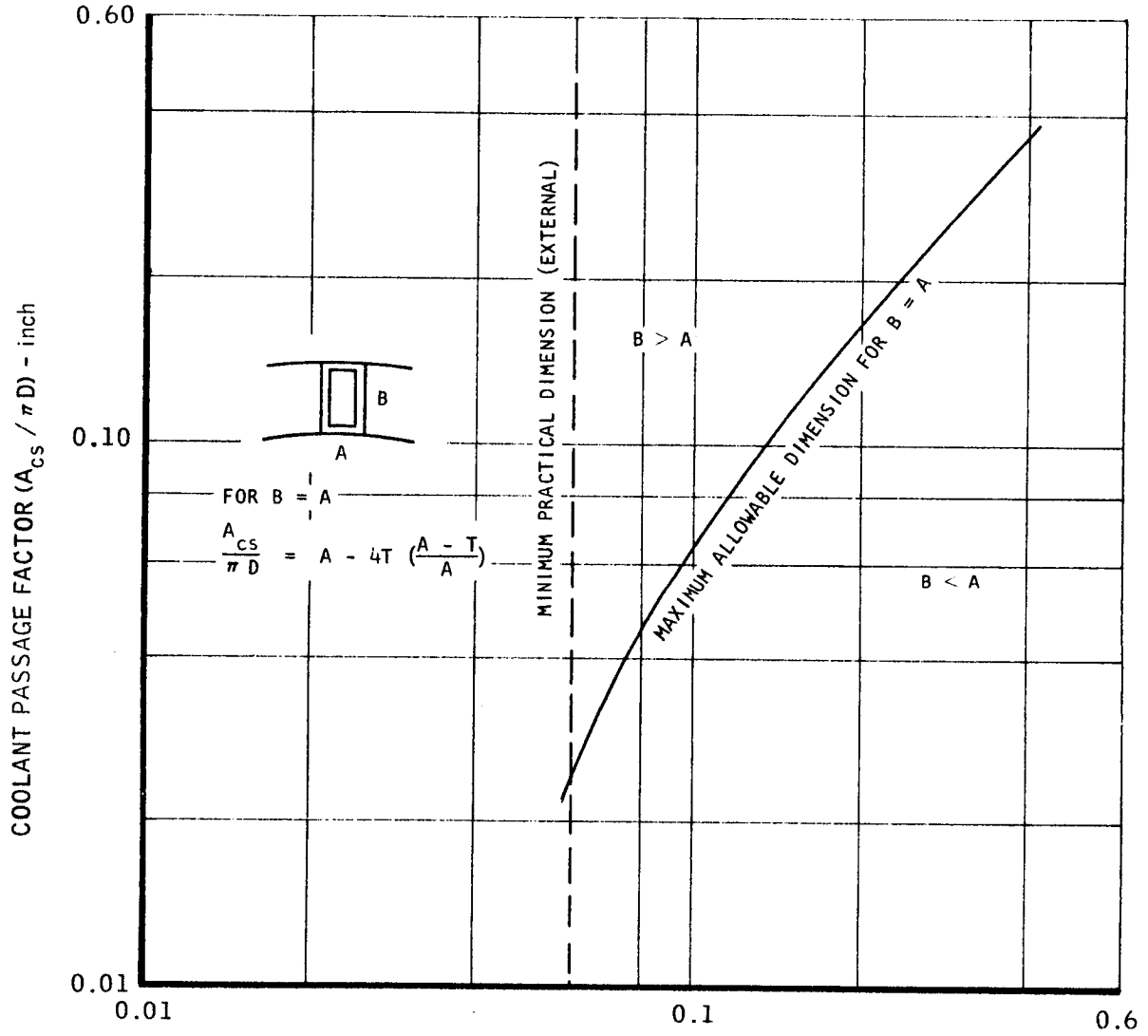

CORRELATION OF PASSAGE FACTOR WITH THRUST AND CHAMBER PRESSURE FOR HYDRAZINE COOLING

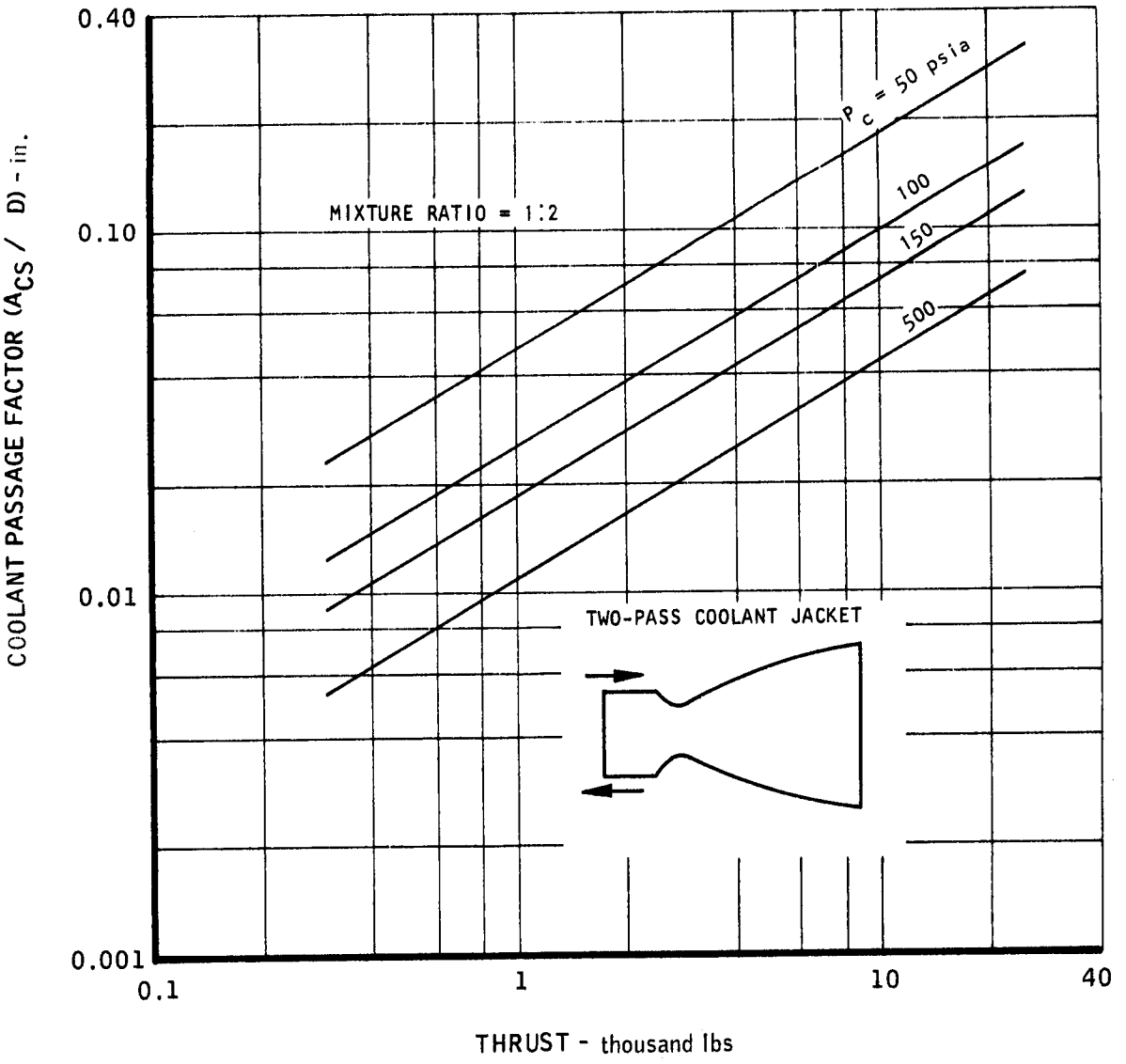

EFFECT OF EXPANSION RATIO ON COOLANT VELOCITY

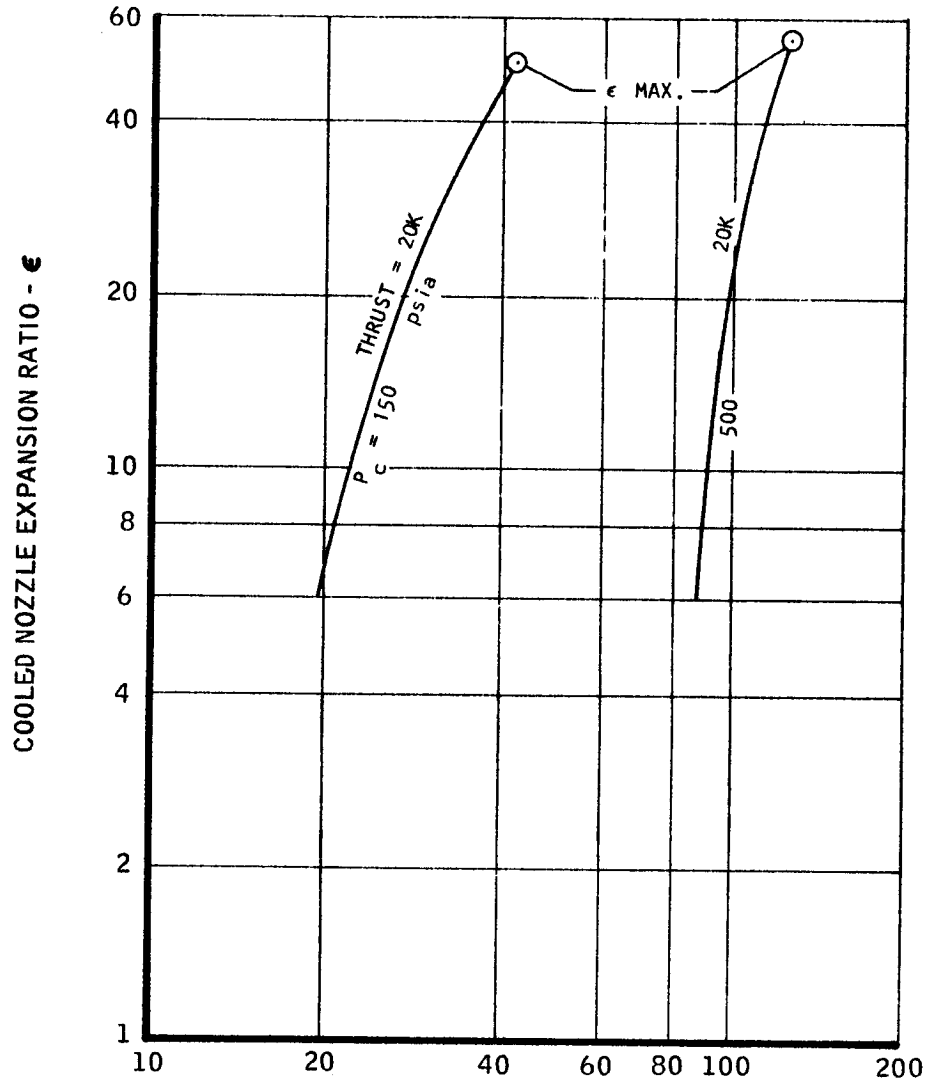

MAC A673

FIGURE 10

COMBINED EFFECT OF LIMITING PARAMETERS ON THE APPLICATION OF REGENERATIVE COOLING TO N_2O_4 / N_2H_4 THRUST CHAMBERS

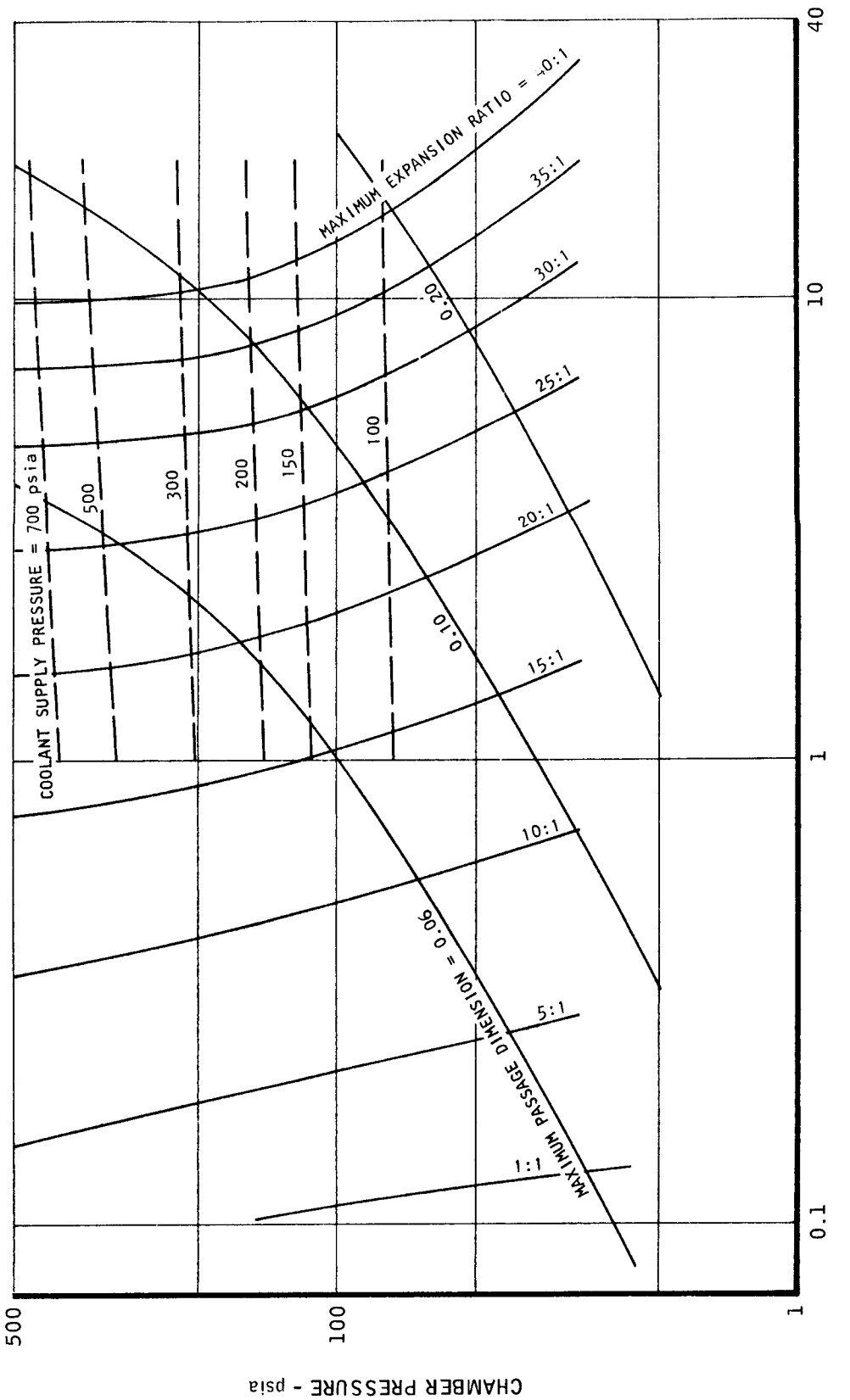

MAC A673

FIGURE 11

THROTTLING POTENTIAL OF N_2O_4 / N_2H_4
REGENERATIVELY COOLED THRUST CHAMBERS
BASED ON ALLOWABLE INCREASE IN PRESSURE

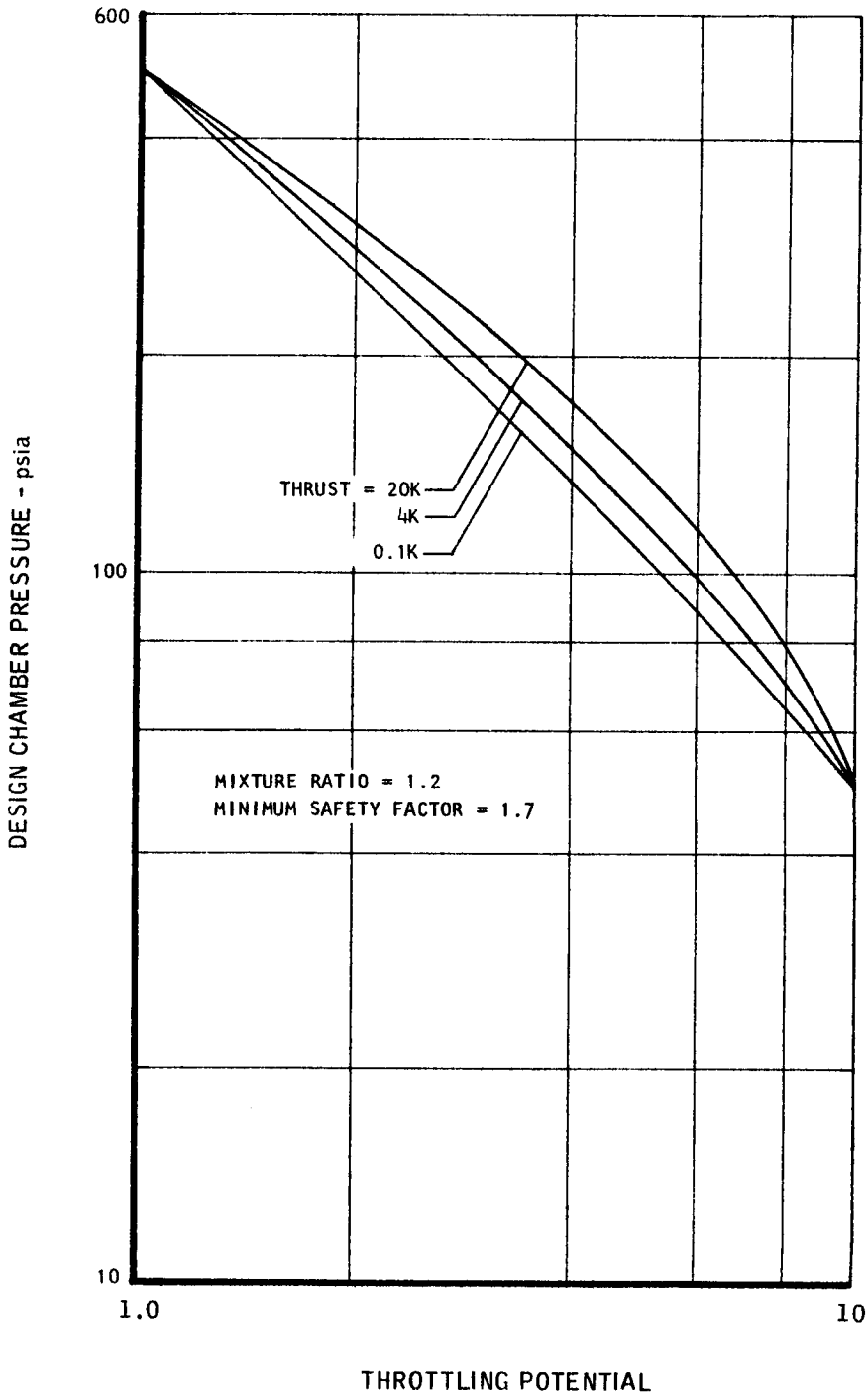

MAC A673

FIGURE 12

COOLANT SUPPLY PRESSURE REQUIREMENTS AS A FUNCTION OF CHAMBER PRESSURE AND THROTTLING FACTOR

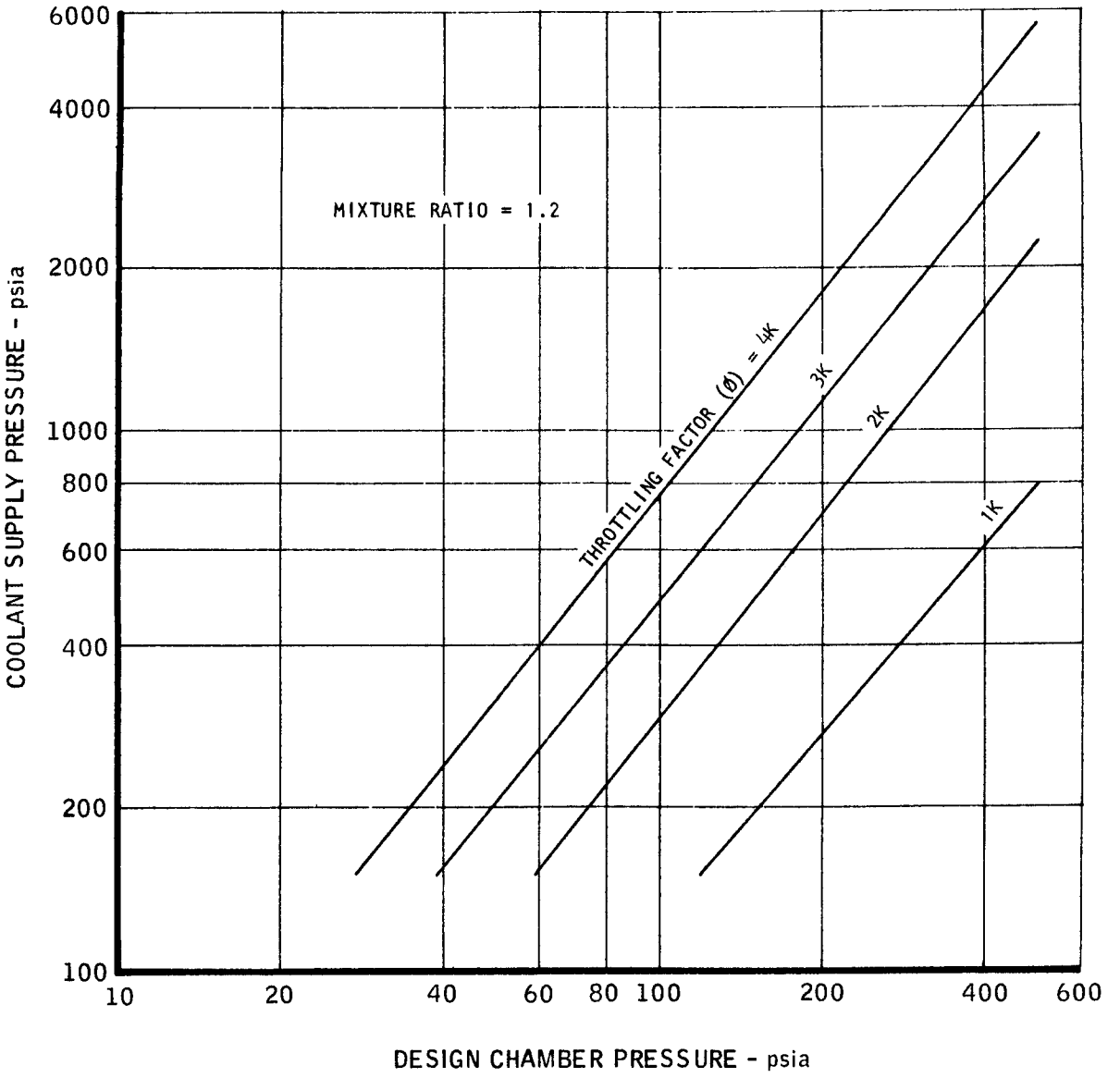

MAC A673

COOLING POTENTIAL LIMITS FOR AEROZINE 50 EXPRESSED AS NOZZLE AREA RATIO FOR N_2O_4 / AEROZINE 50 CHAMBERS

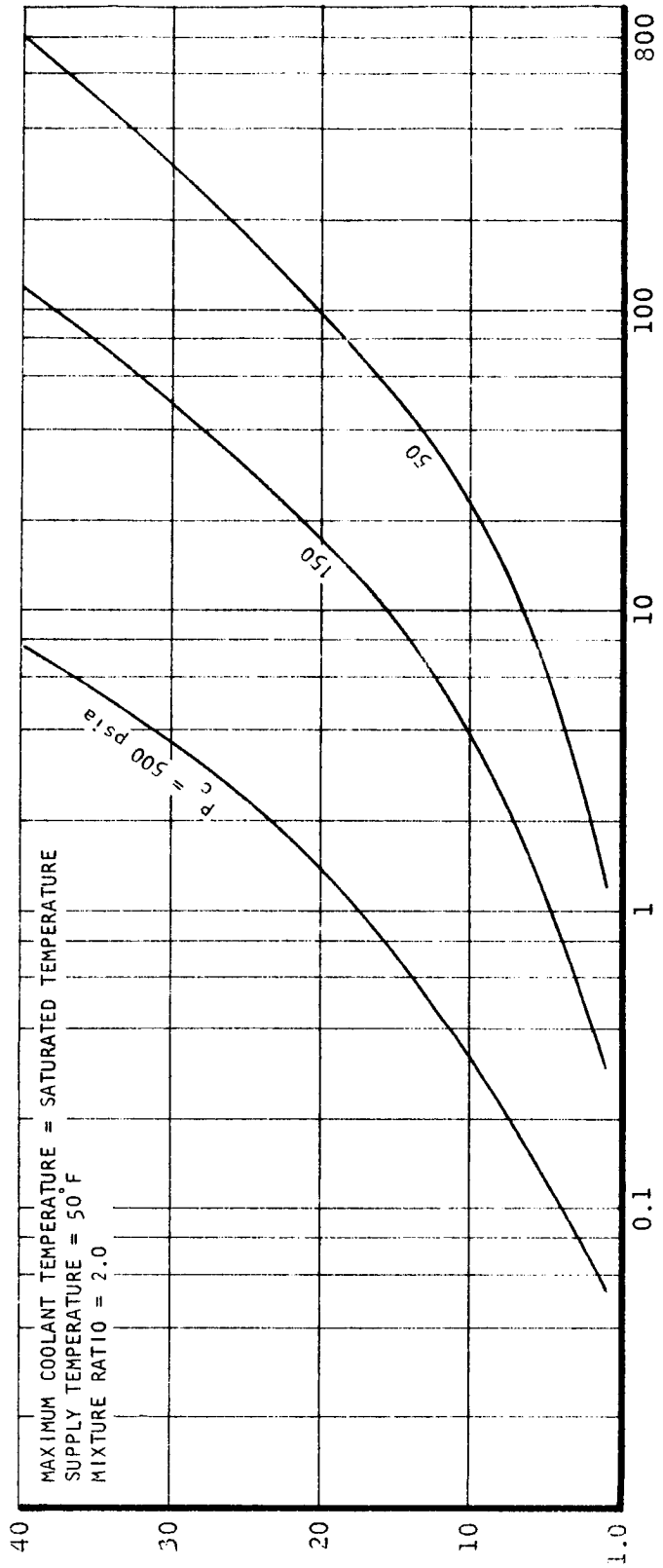

MAC A 673

FIGURE 14

COOLANT VELOCITY REQUIREMENTS FOR NUCLEATE BOILING AEROZINE 50 AT THE THROAT OF N_2O_4 / AEROZINE 50 CHAMBERS

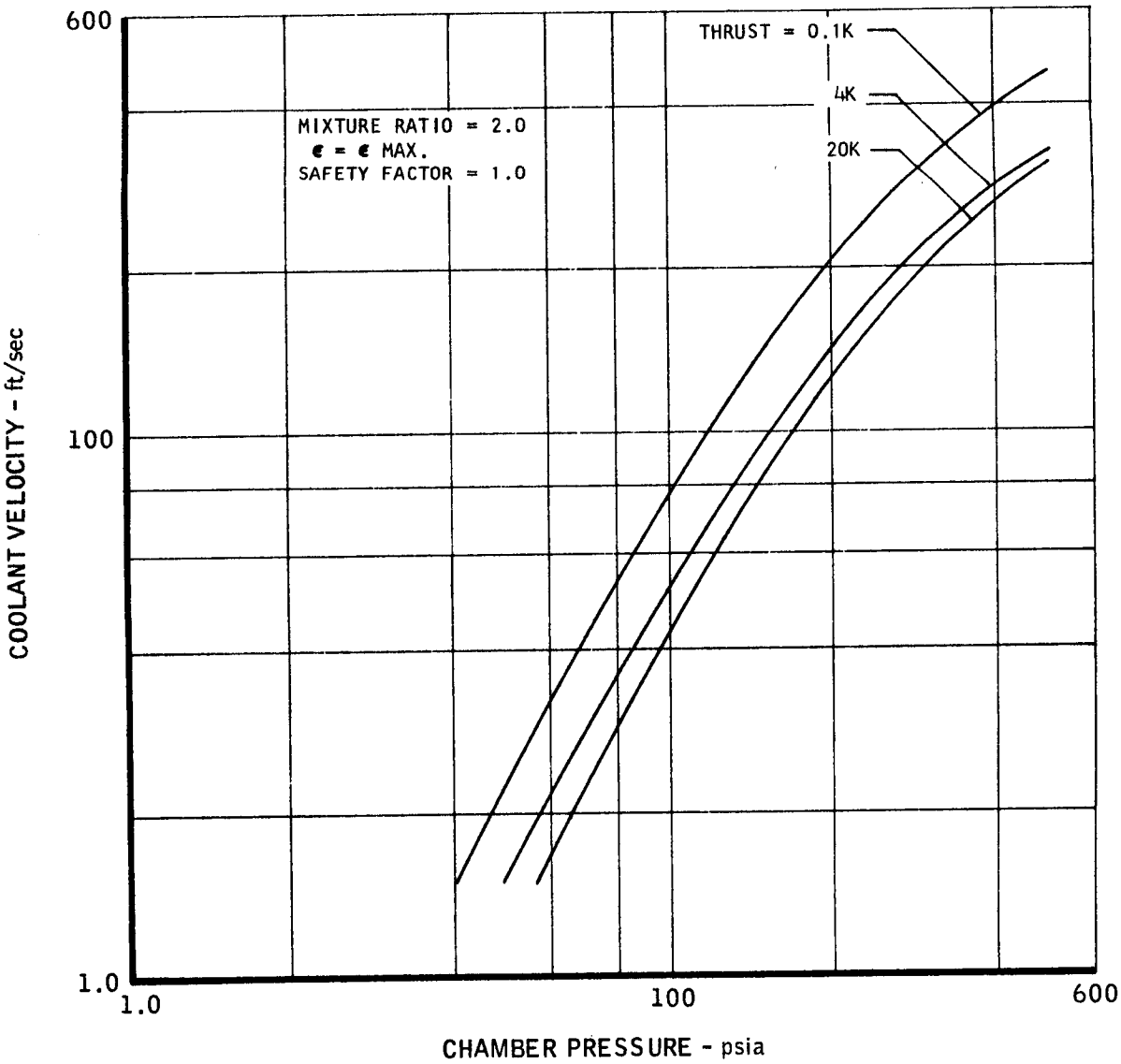

MAC A673

FIGURE 15

COOLANT PRESSURE REQUIREMENTS FOR N_2O_4 / AEROZINE 50 CHAMBERS

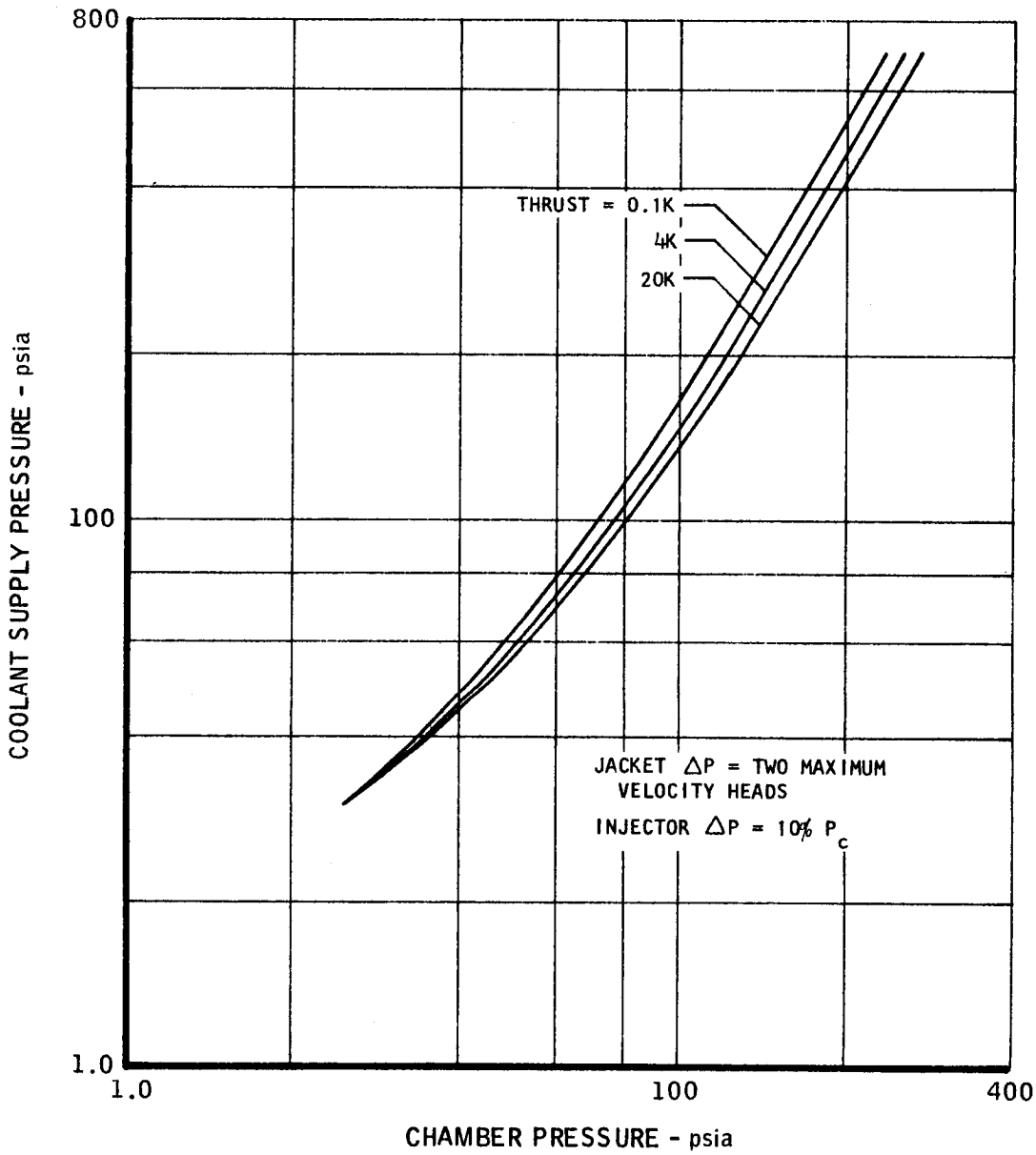

MAC A673

FIGURE 16

CORRELATION OF COOLANT PASSAGE FACTOR WITH THRUST AND CHAMBER PRESSURE FOR NUCLEATE BOILING AEROZINE - 50

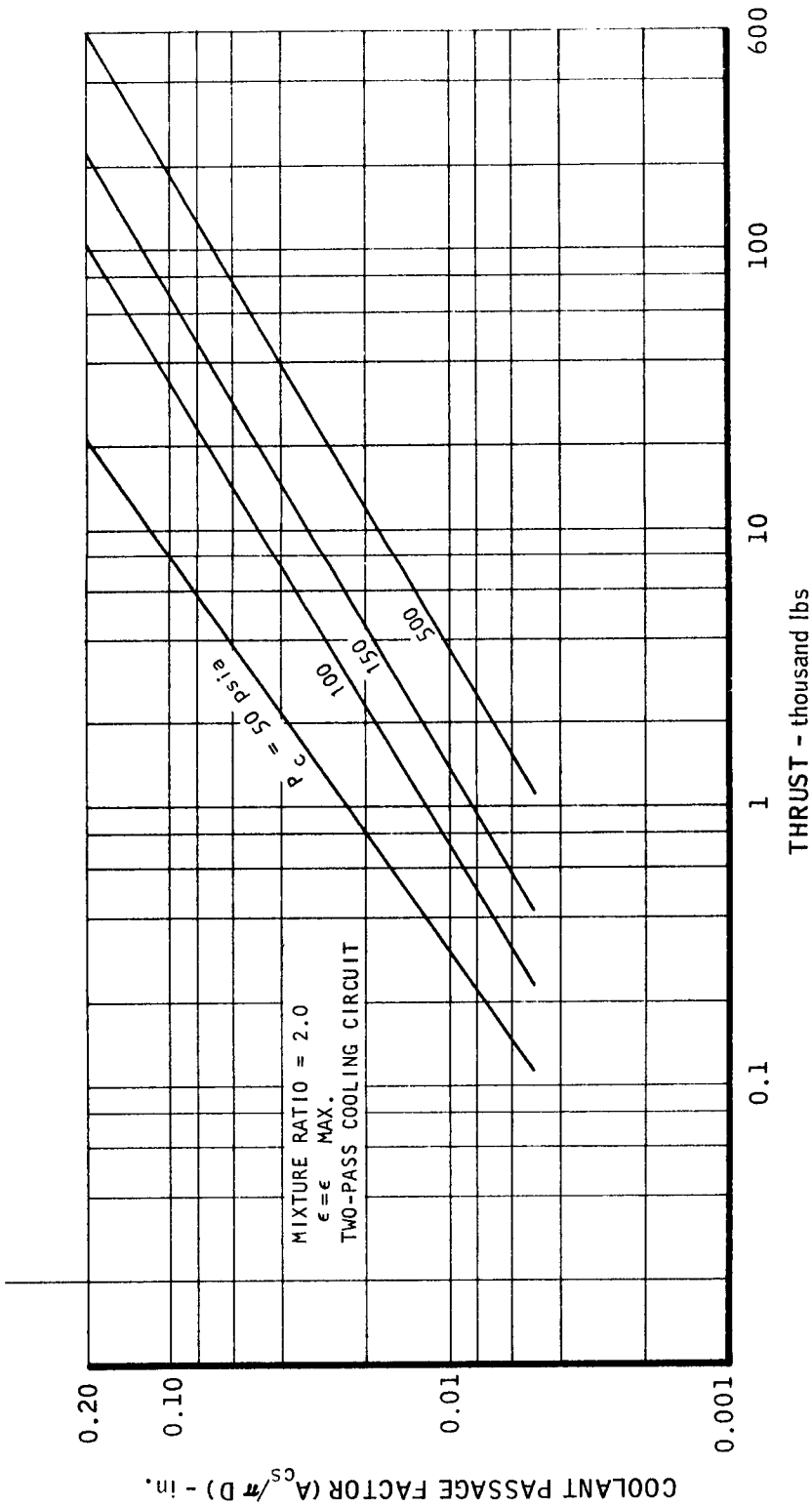

MAC A673

FIGURE 17

APPLICABILITY MAP FOR REGENERATIVE COOLING WITH N_2O_4 / AEROZINE 50

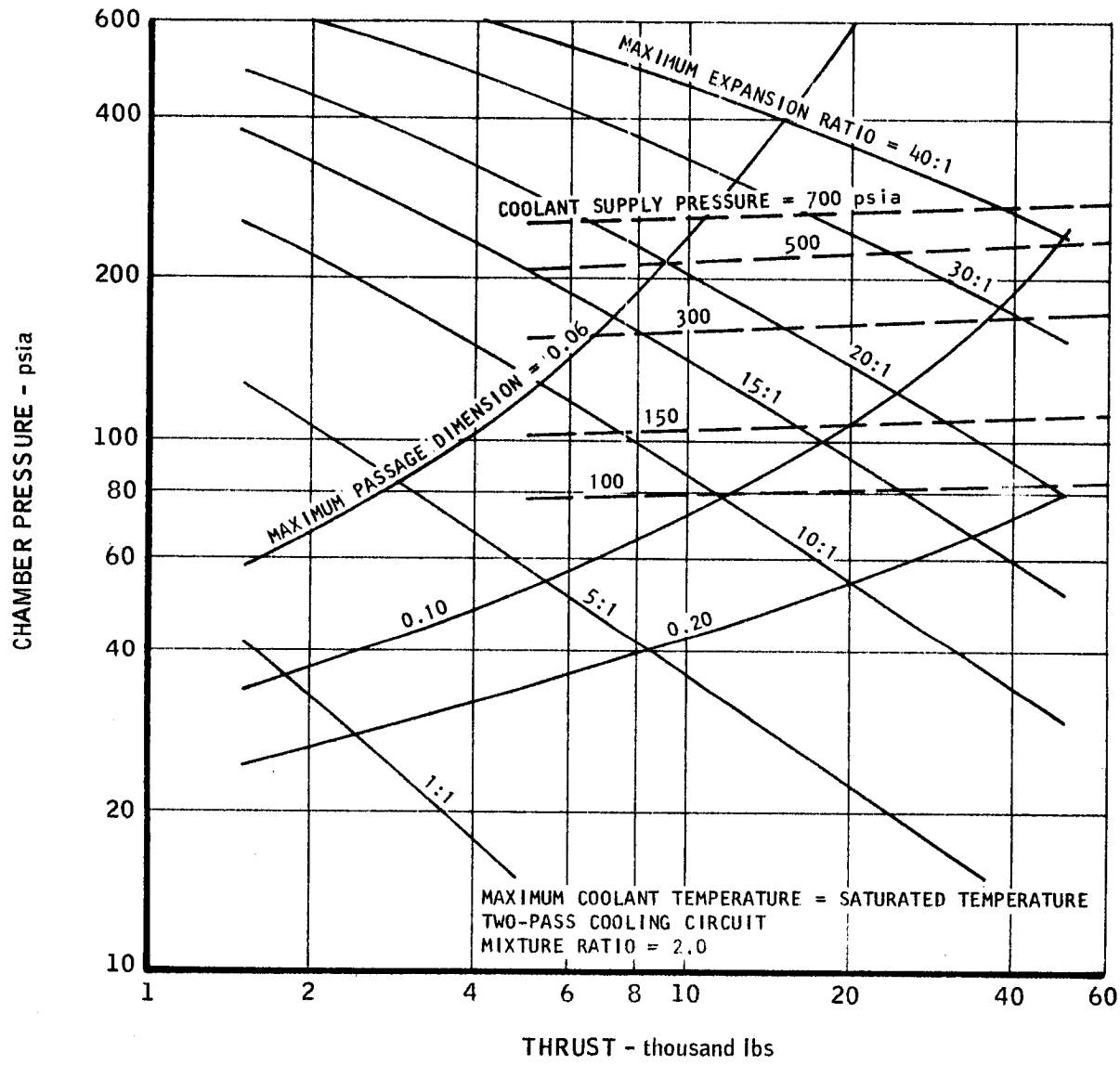

MAC A673

FIGURE 18

TYPICAL EFFECT OF NOZZLE EXPANSION RATIO ON NOZZLE WALL TEMPERATURE FOR HYDROGEN REGENERATIVE COOLING

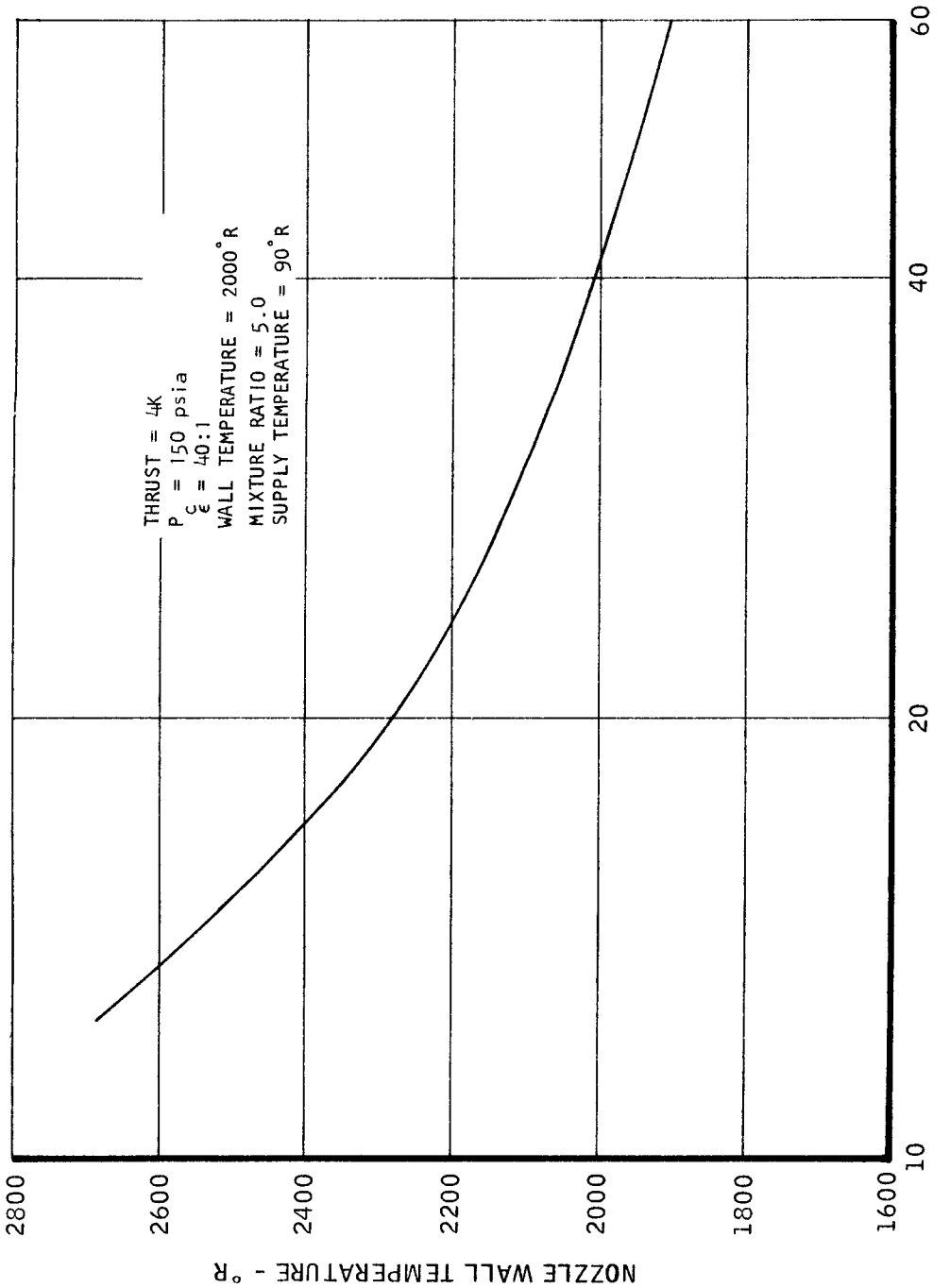

MAC A 673

FIGURE 19

COOLANT MASS VELOCITY REQUIREMENTS FOR
REGENERATIVE COOLING WITH HYDROGEN
(NOZZLE THROAT)

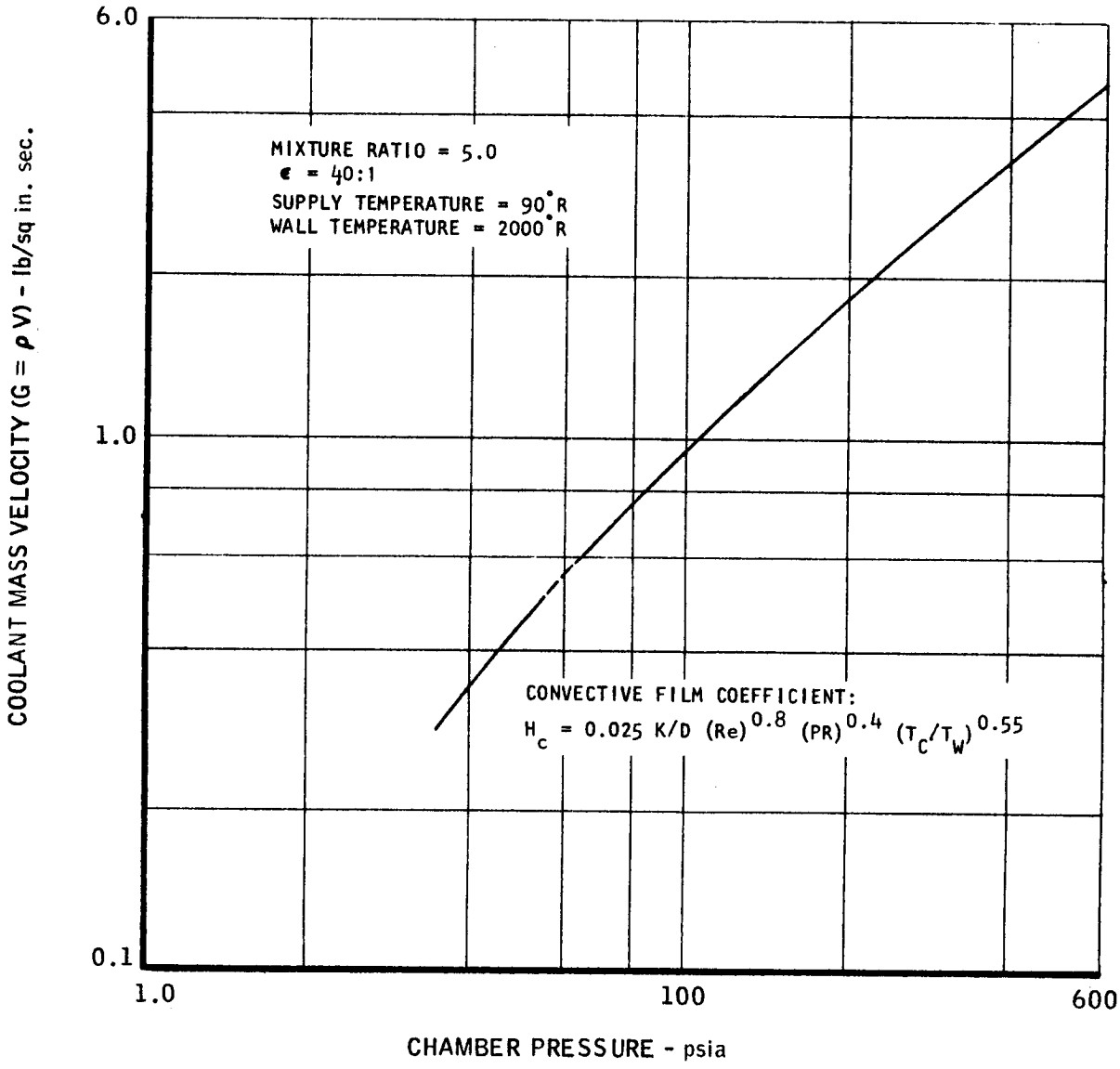

MAC A673

FIGURE 20

HYDROGEN SUPPLY PRESSURE REQUIREMENTS AS A FUNCTION OF CHAMBER PRESSURE AND THRUST

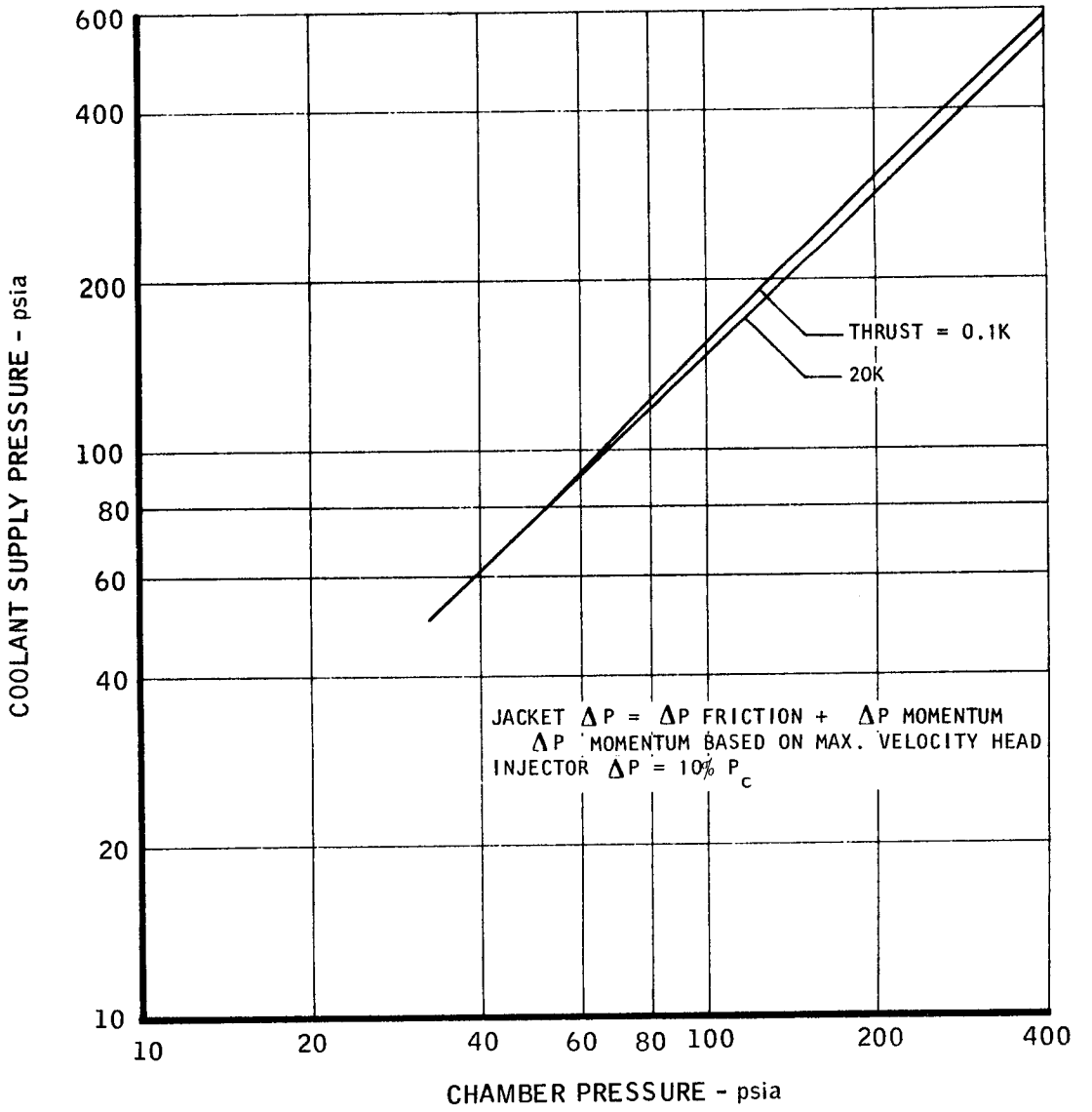

CORRELATION OF PASSAGE FACTOR WITH THRUST AND CHAMBER PRESSURE FOR HYDROGEN COOLING

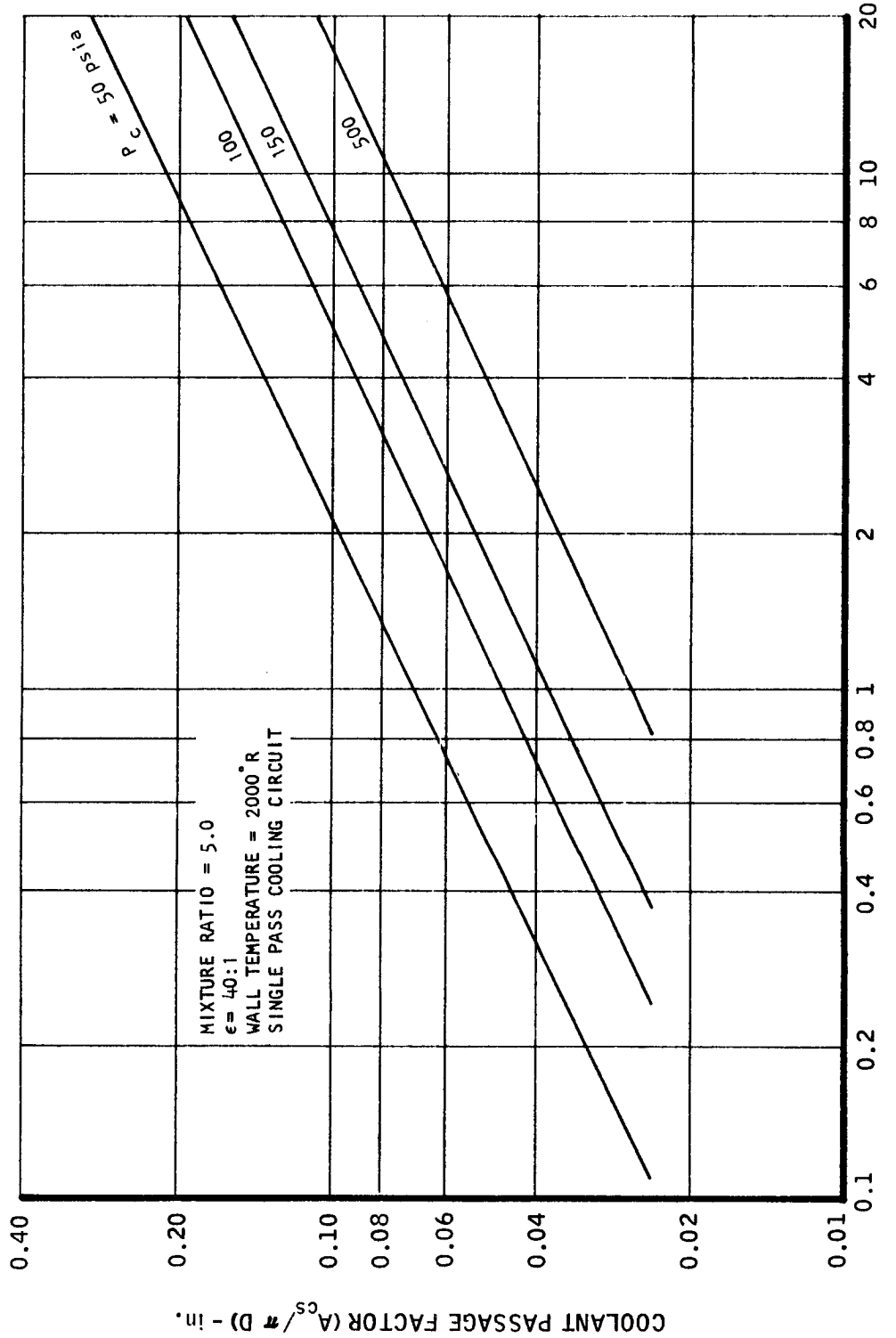

MAC A 673

FIGURE 22

EFFECTS OF LIMITING PARAMETERS ON REGENERATIVE COOLING OF O_2/H_2 THRUST CHAMBERS

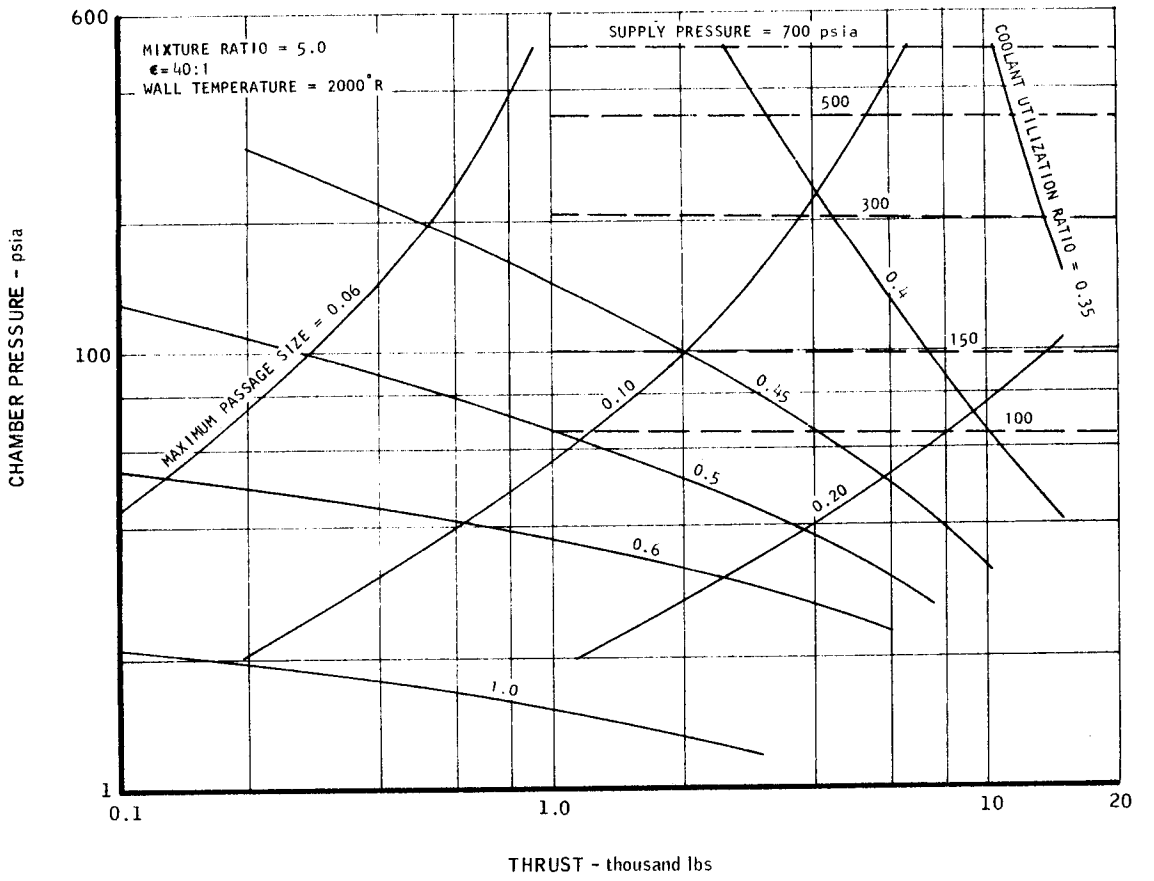

VARIATION OF CHAMBER PRESSURE WITH TEMPERATURES FOR A TYPICAL HYDROGEN COOLED THRUST CHAMBER

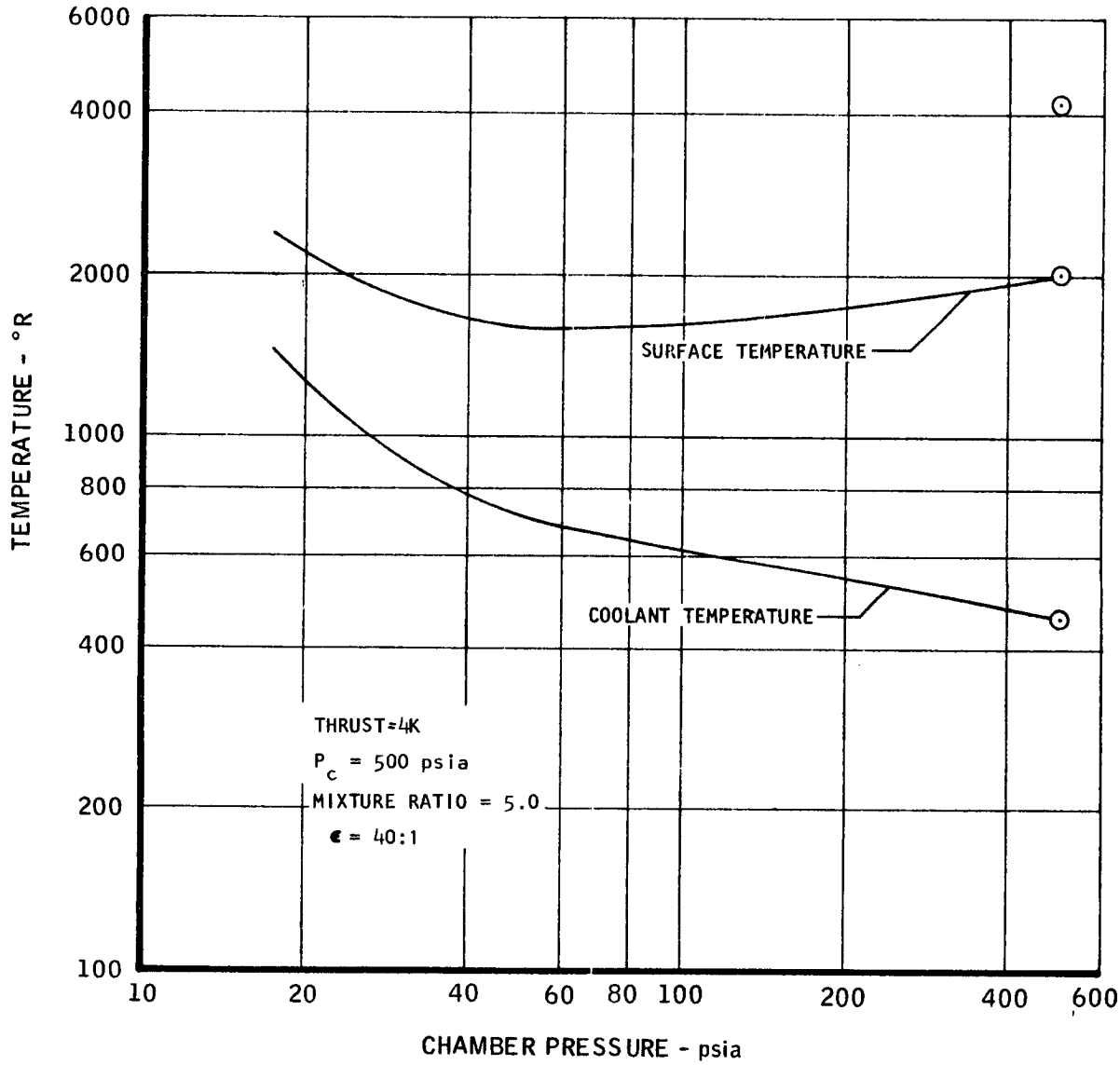

EFFECT OF THROTTLING ON SEVERAL O_2/H_2 REGENERATIVELY COOLED THRUST CHAMBERS

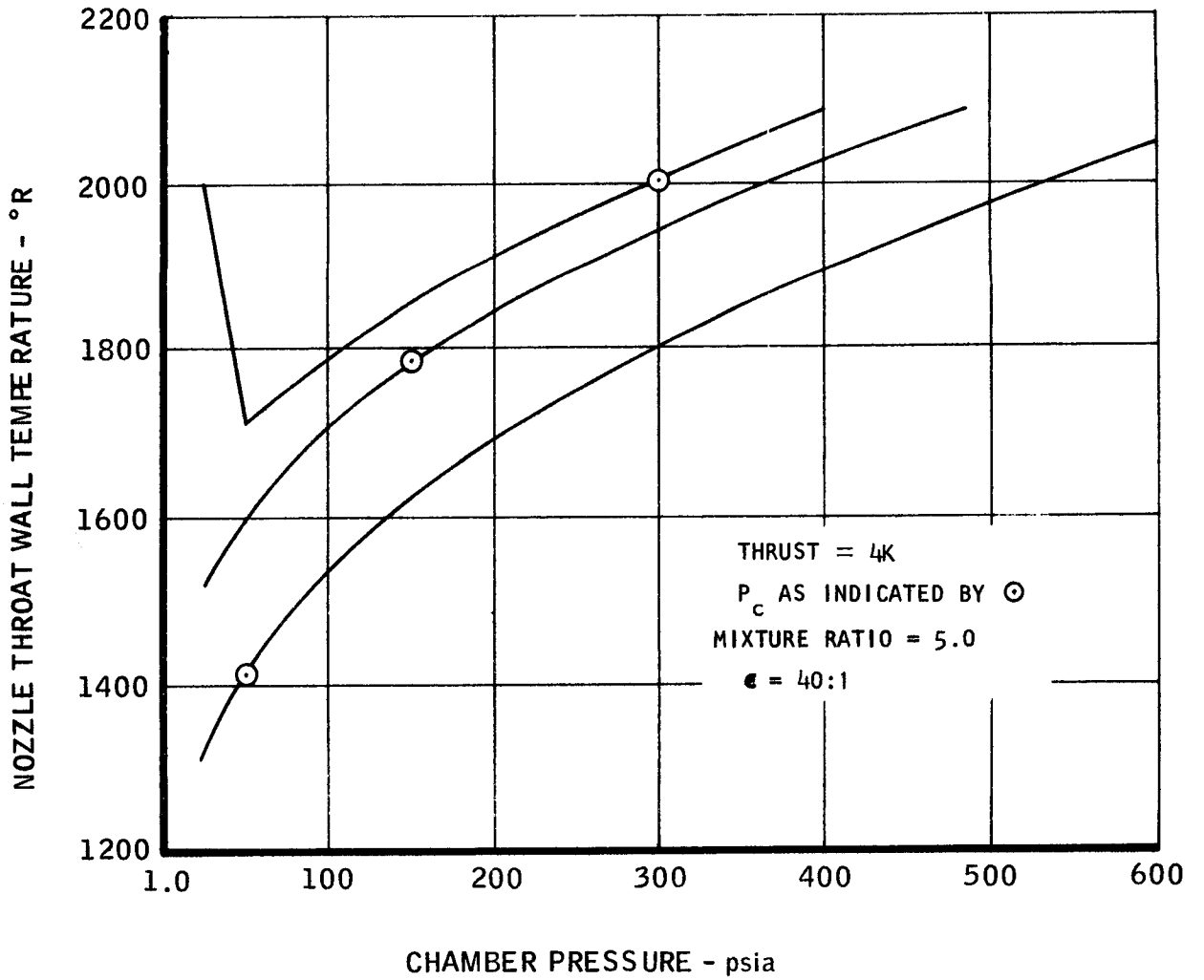

COMPARISON OF HEAT FLUX WITH WALL TEMPERATURE
N_2O_4/0.5 N_2H_4 - 0.5 UDMH
P_c = 20 psia

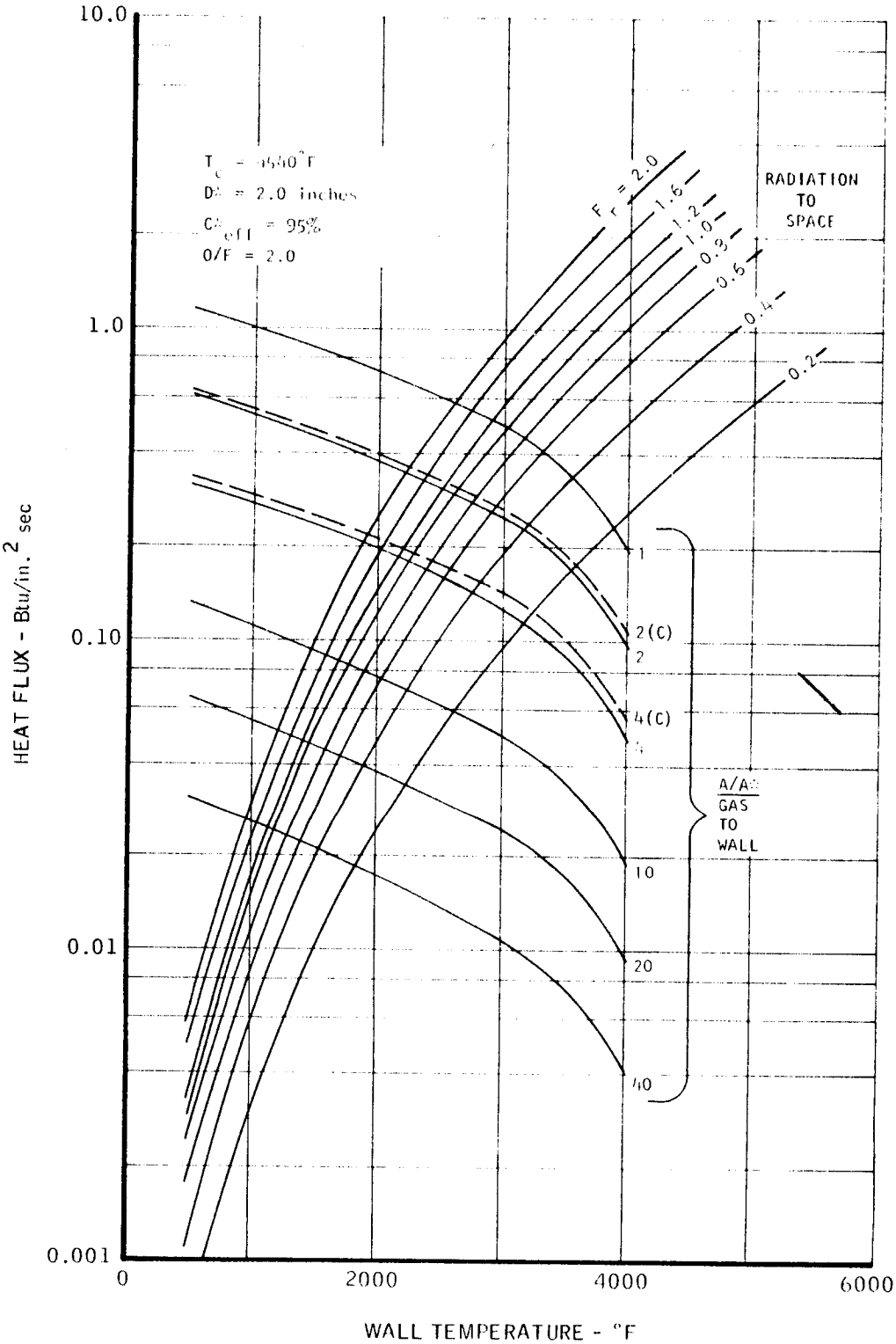

MAC A673

FIGURE 26

COMPARISON OF HEAT FLUX WITH WALL TEMPERATURE
$N_2O_4/0.5\ N_2H_4 - 0.5$ UDHM
$P_C = 50$ psia

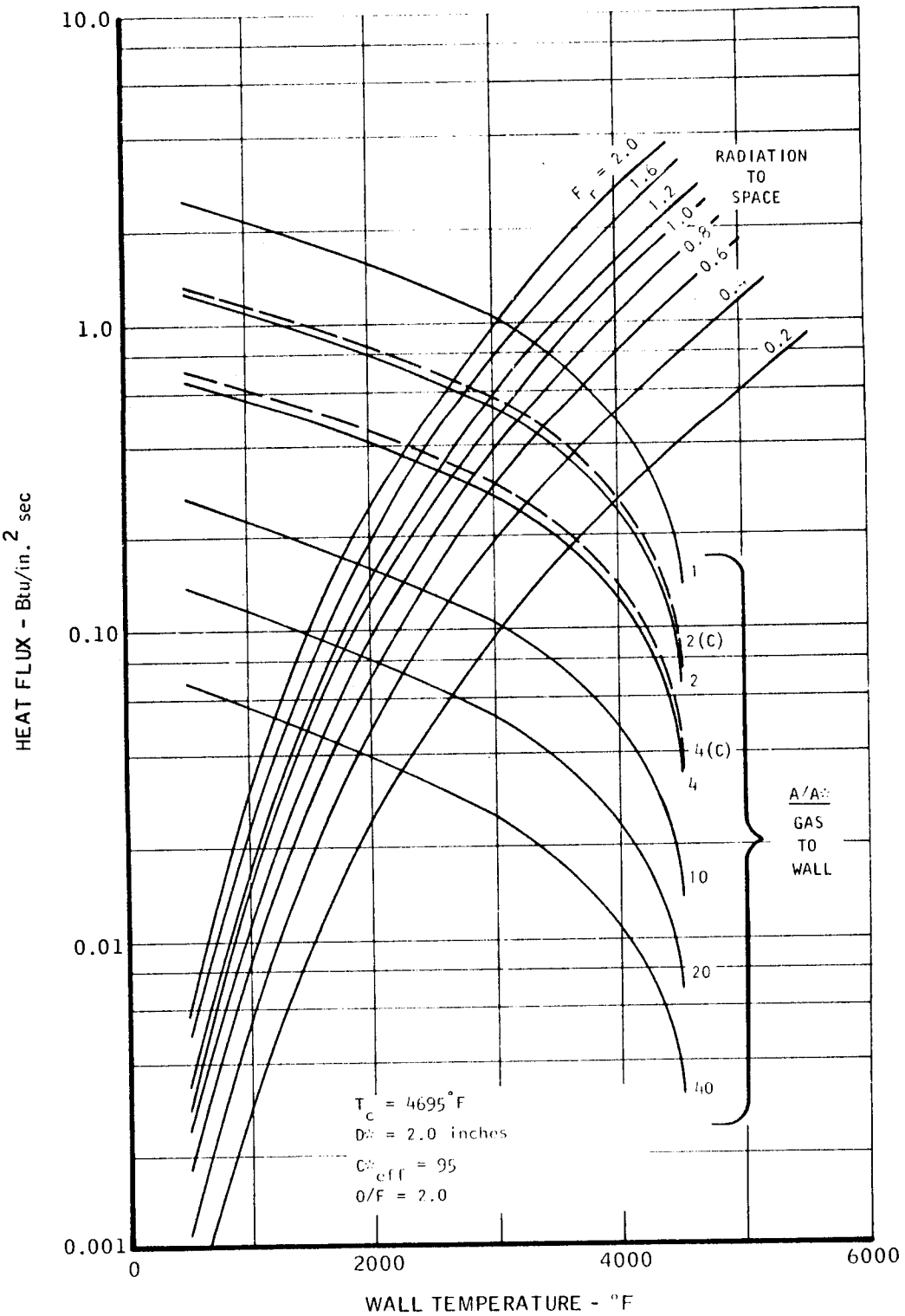

FIGURE 27

COMPARISON OF HEAT FLUX WITH WALL TEMPERATURE
$N_2O_4/0.5\ N_2H_4$ - 0.5 UDHM
P_c = 100 psia

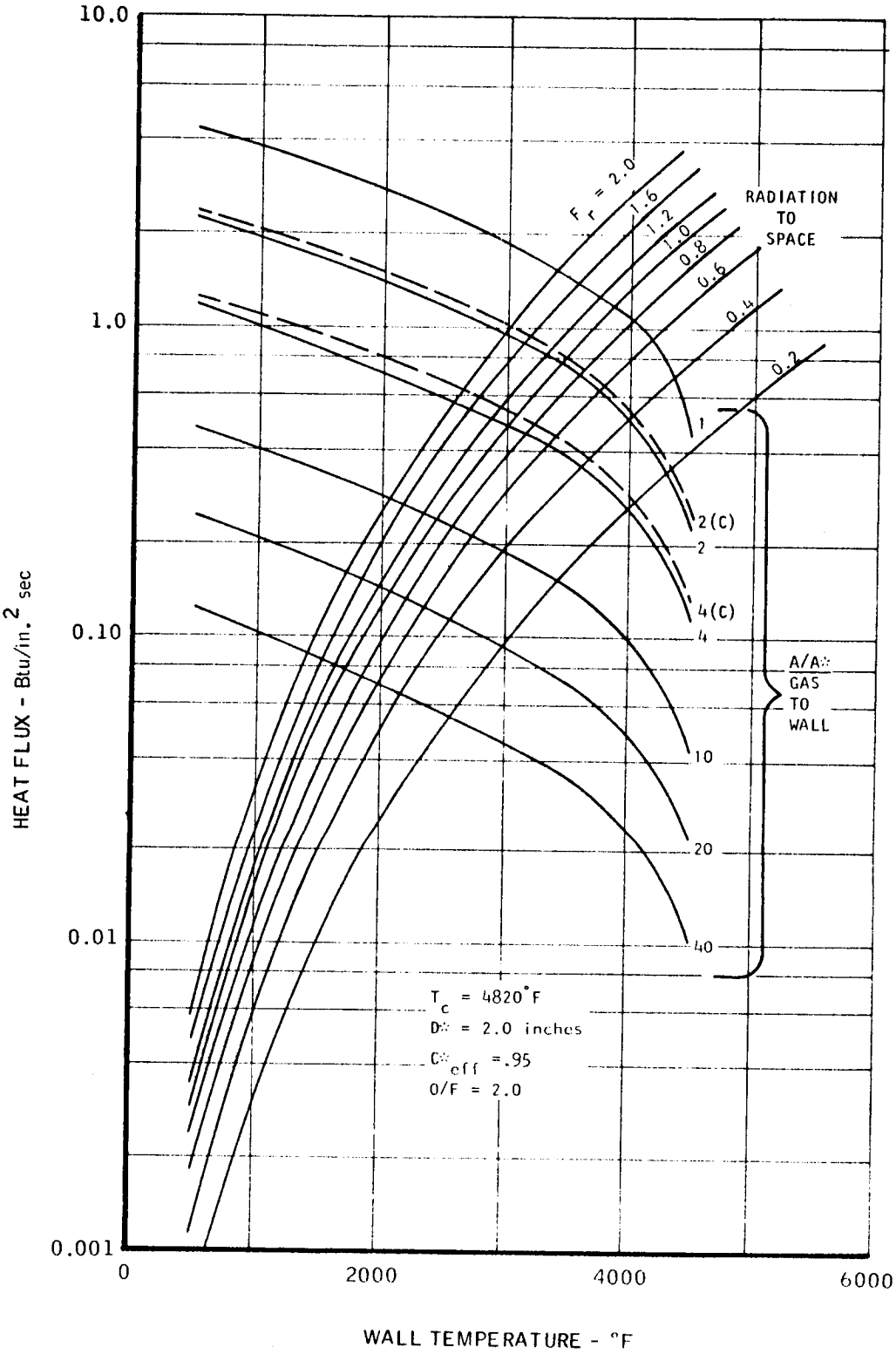

MAC A673

COMPARISON OF HEAT FLUX WITH WALL TEMPERATURE
N_2O_4/0.5 N_2H_4 - 0.5 UDHM
P_c = 150 psia

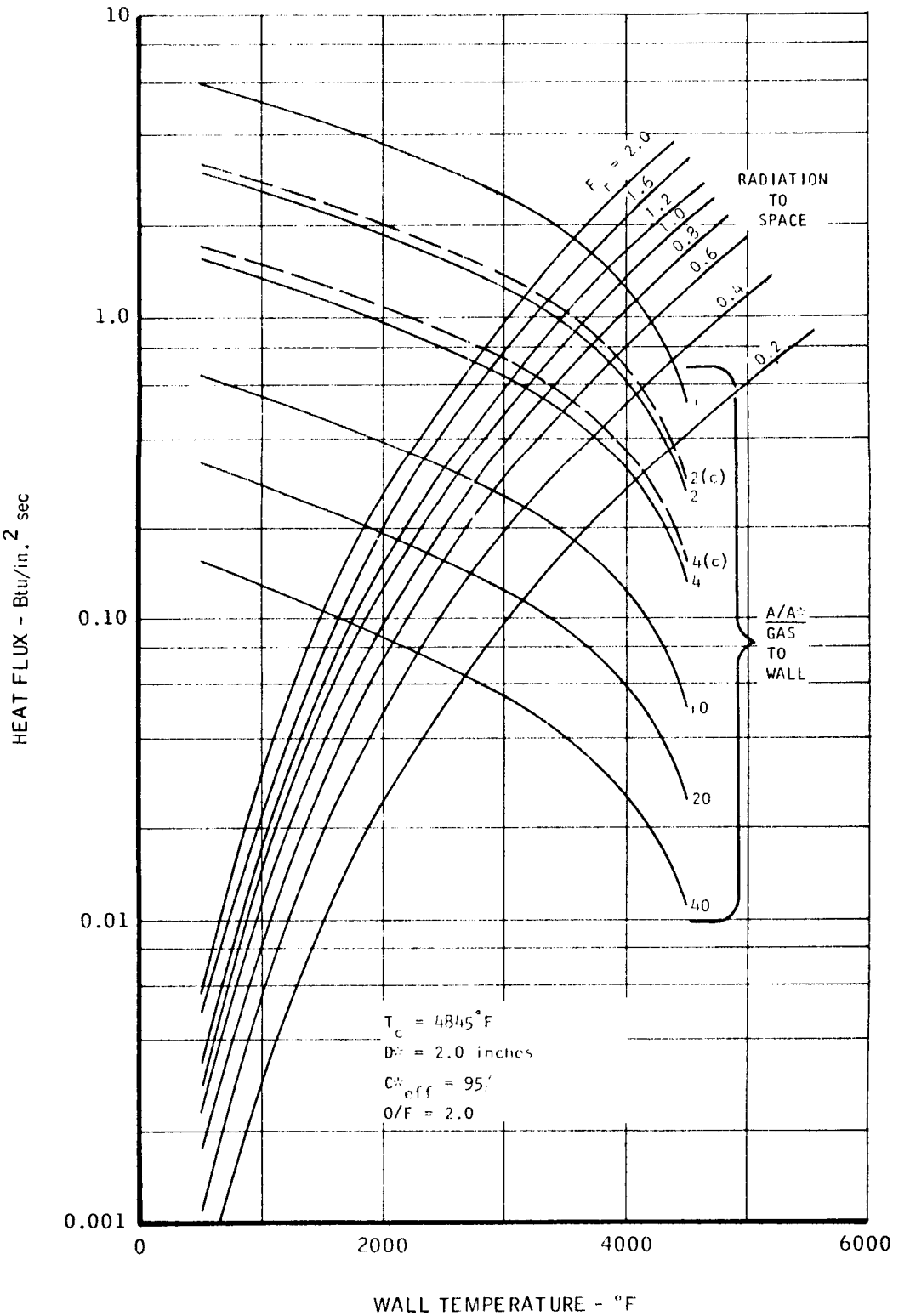

COMPARISON OF HEAT FLUX WITH WALL TEMPERATURE
O_2 / H_2
P_C = 20 psia

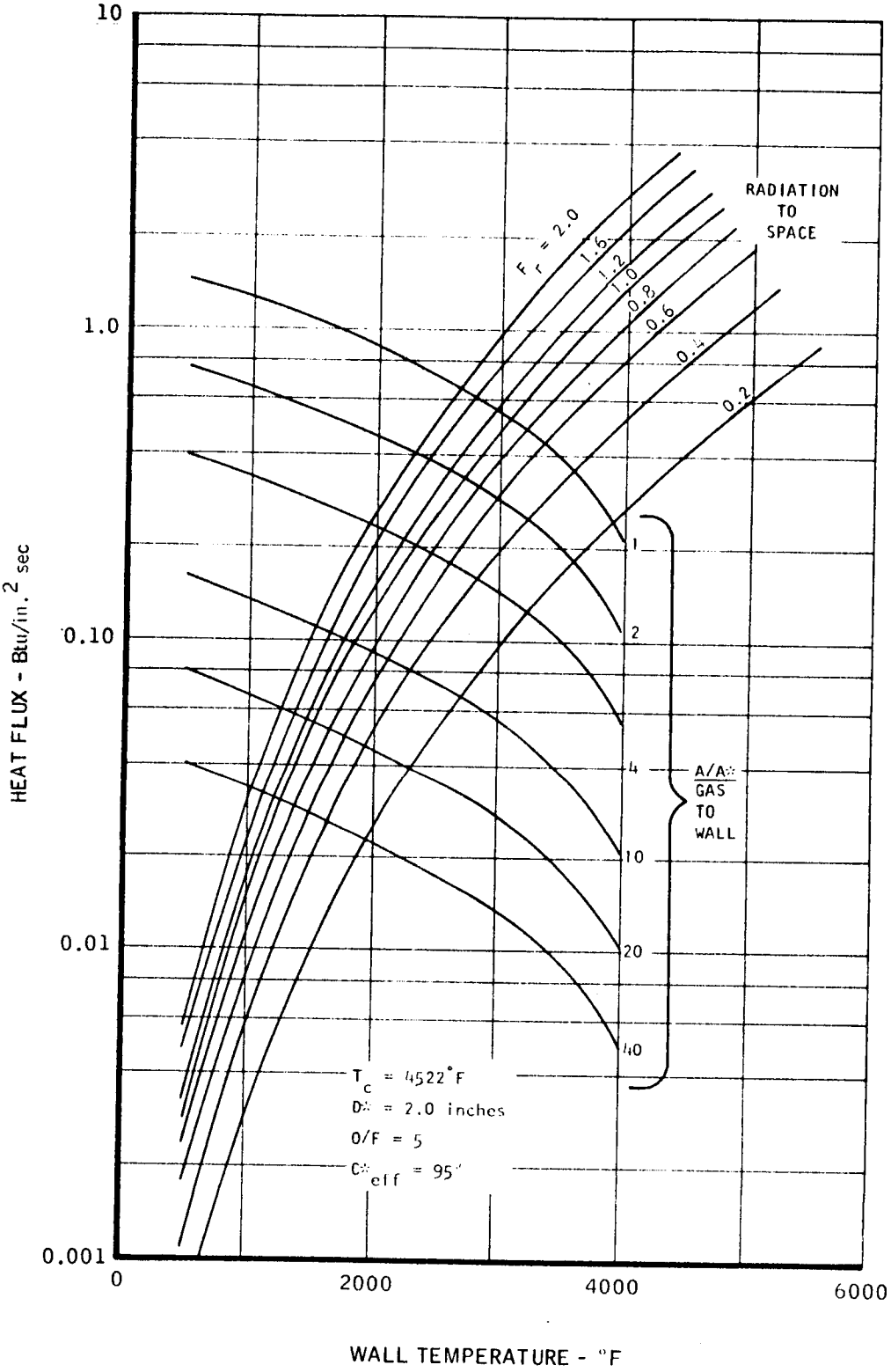

MAC A673

FIGURE 30

COMPARISON OF HEAT FLUX WITH WALL TEMPERATURE
O_2 / H_2
P_c = 50 psia

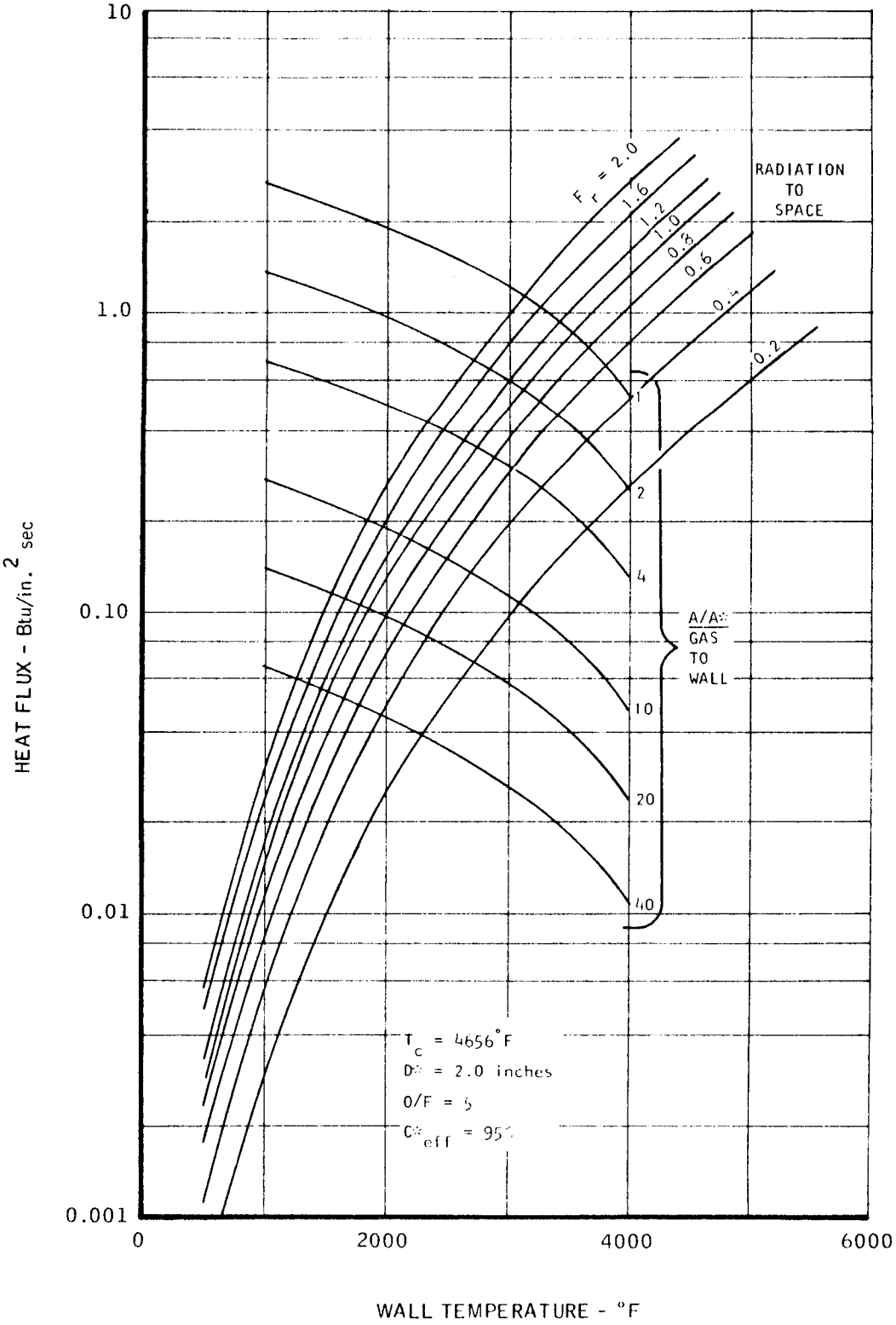

FIGURE 31

COMPARISON OF HEAT FLUX WITH WALL TEMPERATURE
O_2 / H_2
P_c = 100 psia

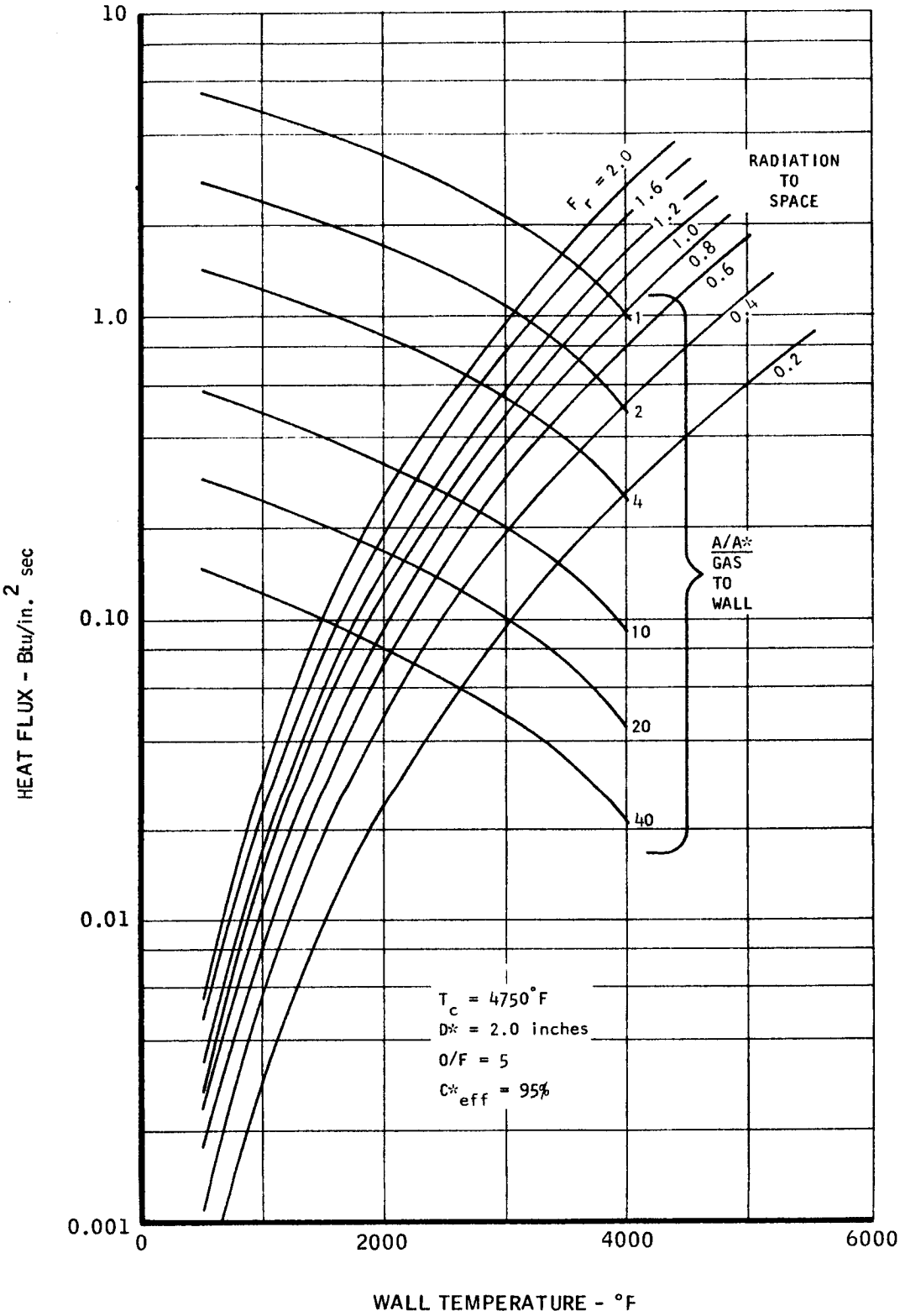

COMPARISON OF HEAT FLUX WITH WALL TEMPERATURE
O_2 / H_2
P_c = 150 psia

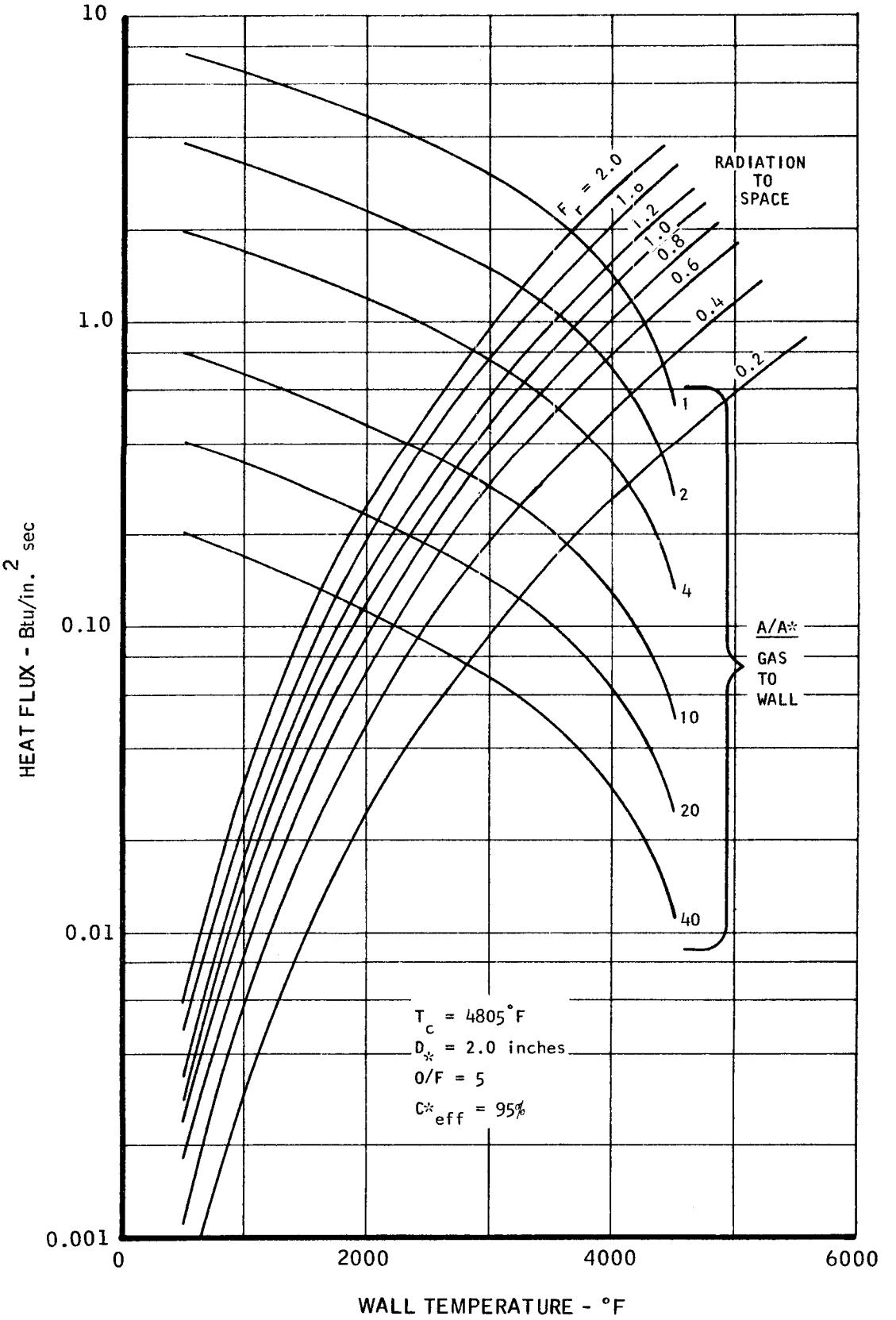

MAC A673

FIGURE 33

COMPARISON OF HEAT FLUX WITH WALL TEMPERATURE
O_2 / H_2
P_c = 300 psia

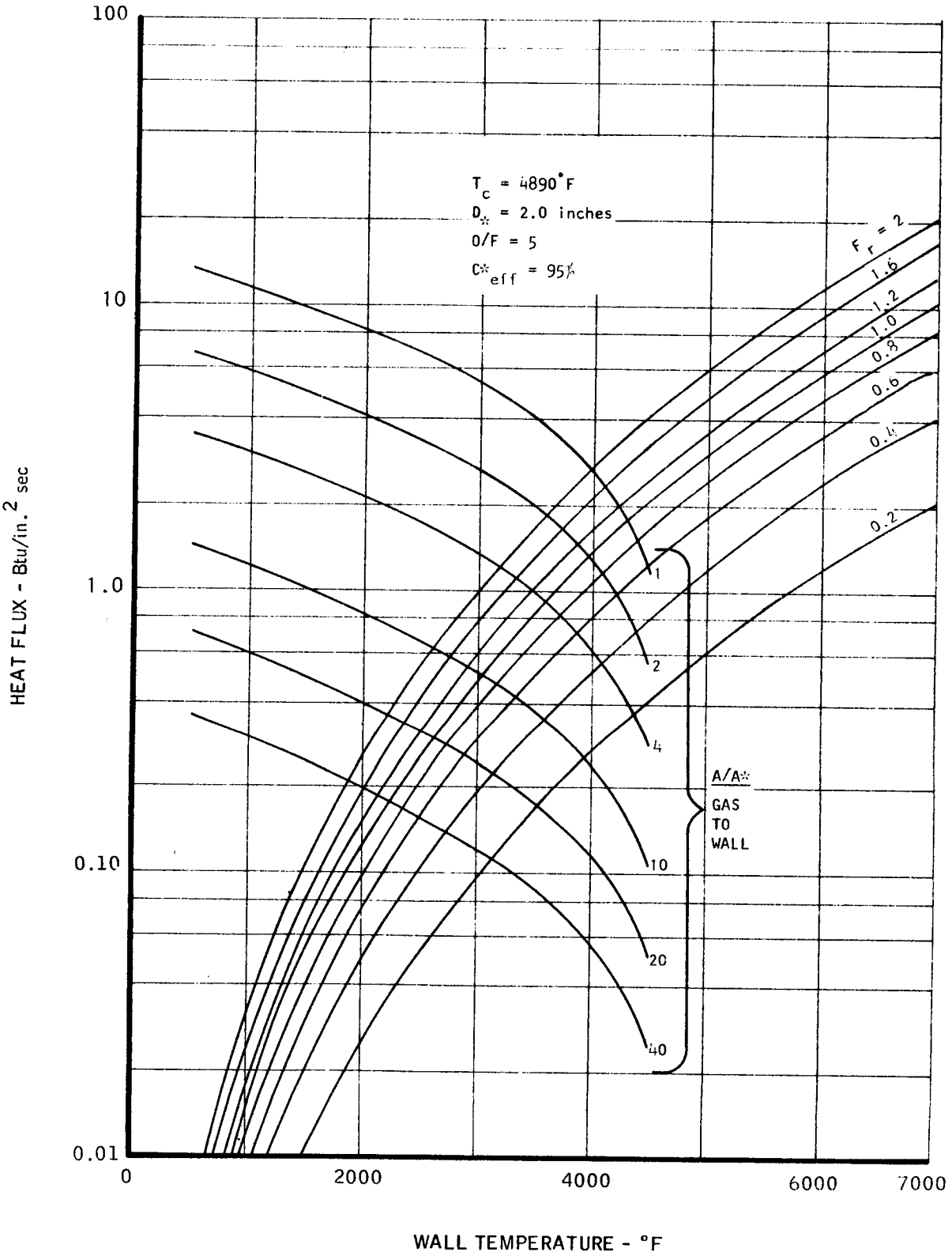

MAC A 673

COMPARISON OF HEAT FLUX WITH WALL TEMPERATURE

O_2/H_2

P_c = 500 psia

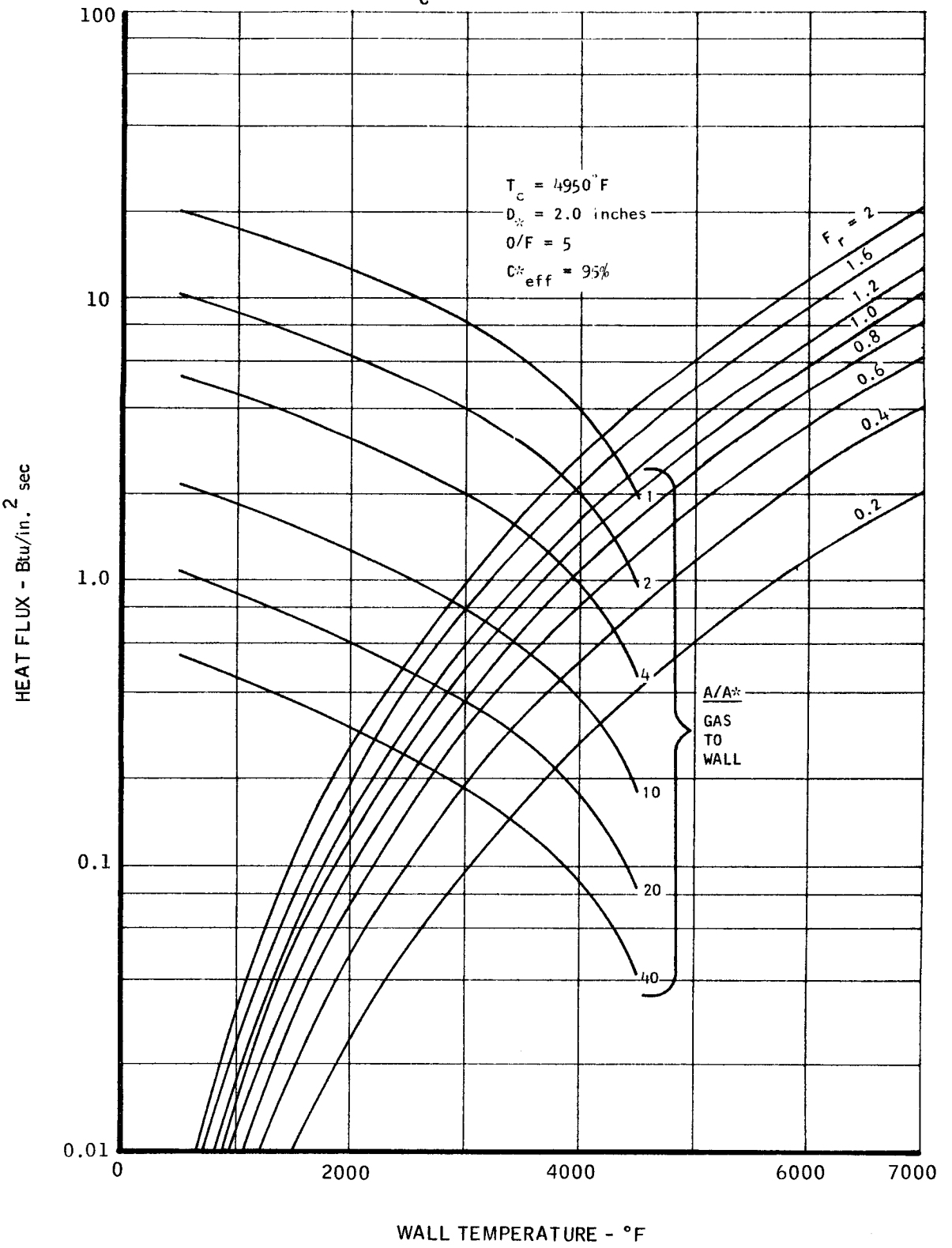

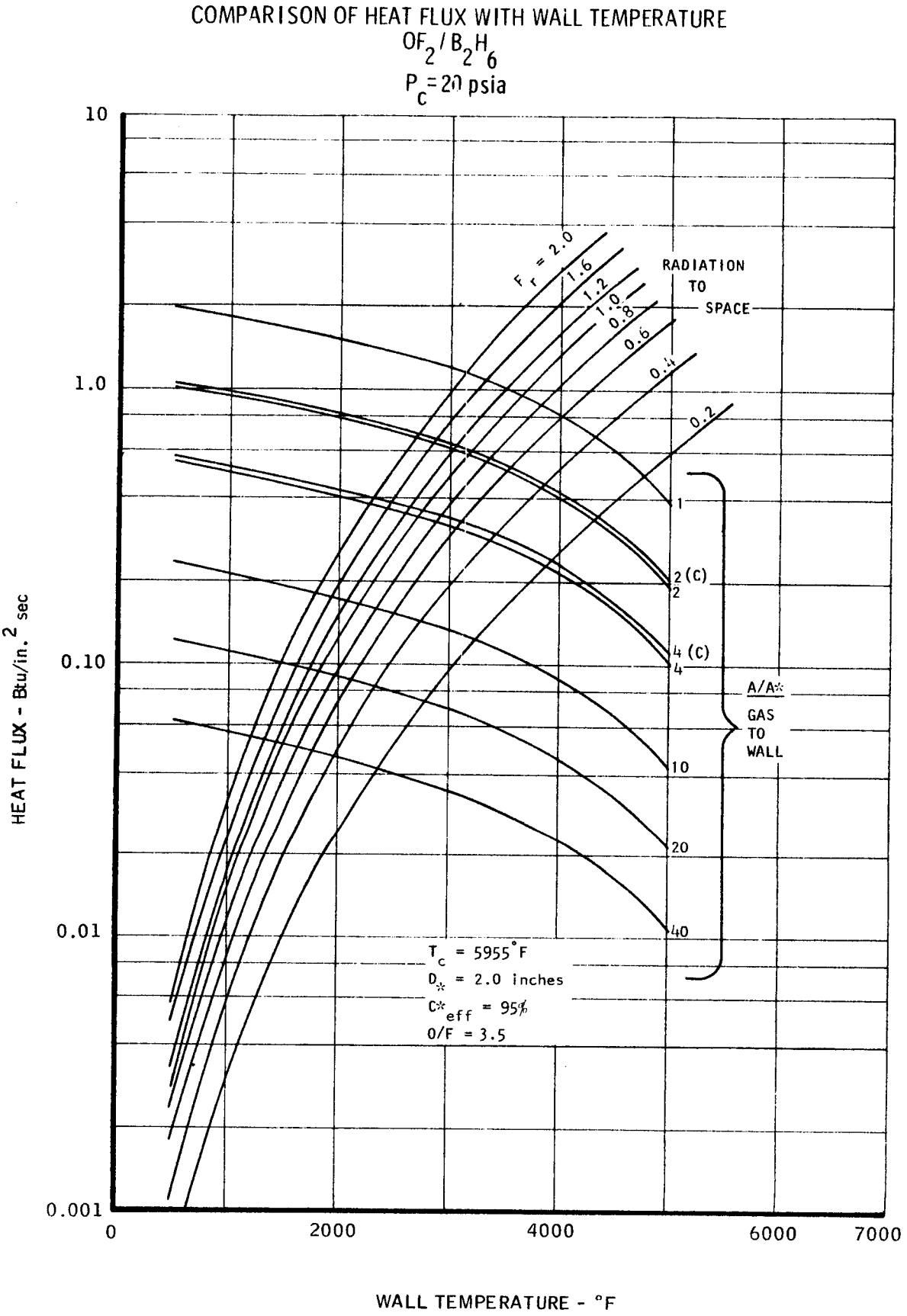

MAC A673

FIGURE 36

COMPARISON OF HEAT FLUX WITH WALL TEMPERATURE
OF_2/DIBORANE
P_c = 50 psia

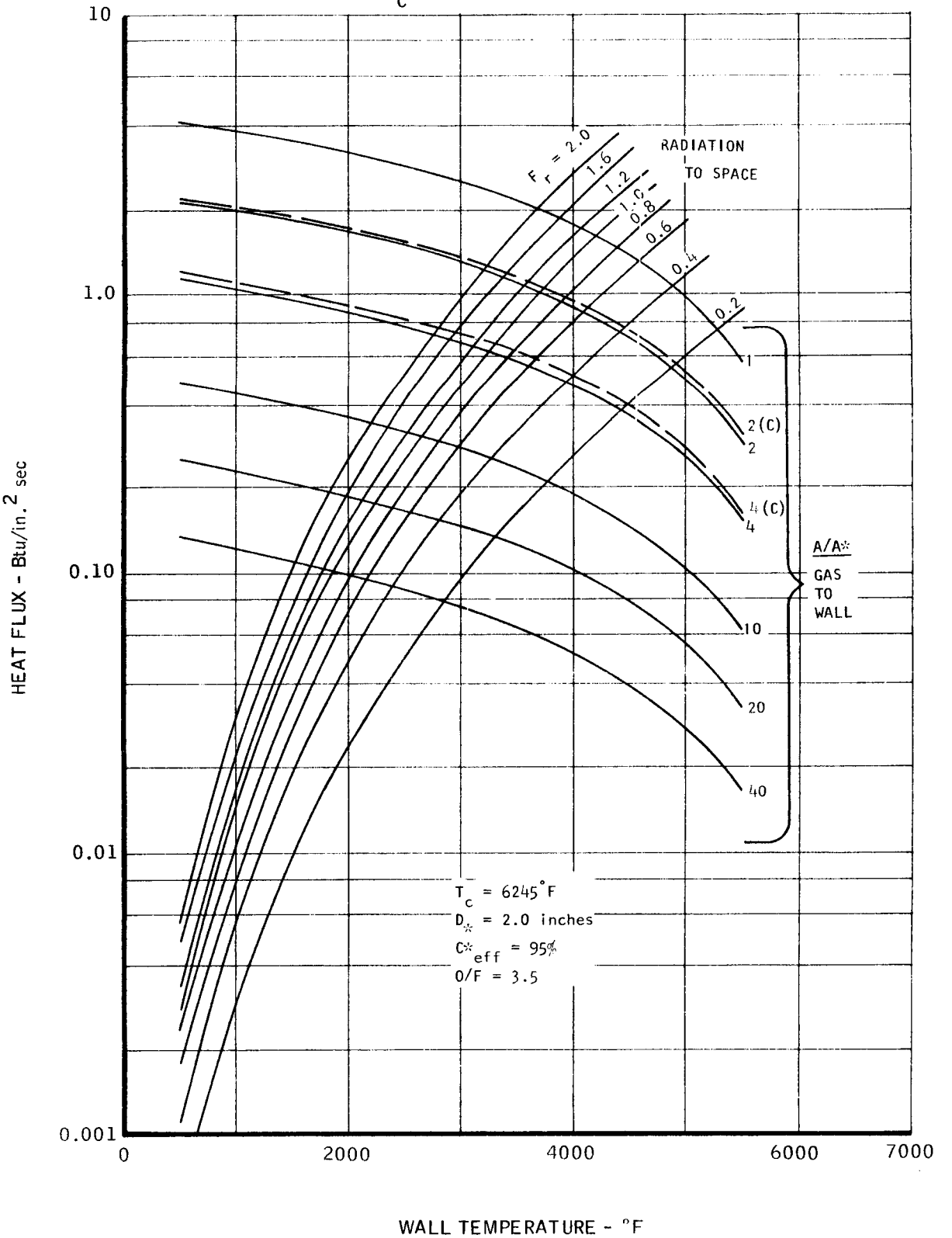

COMPARISON OF HEAT FLUX WITH WALL TEMPERATURE
OF_2/DIBORANE
P_c = 100 psia

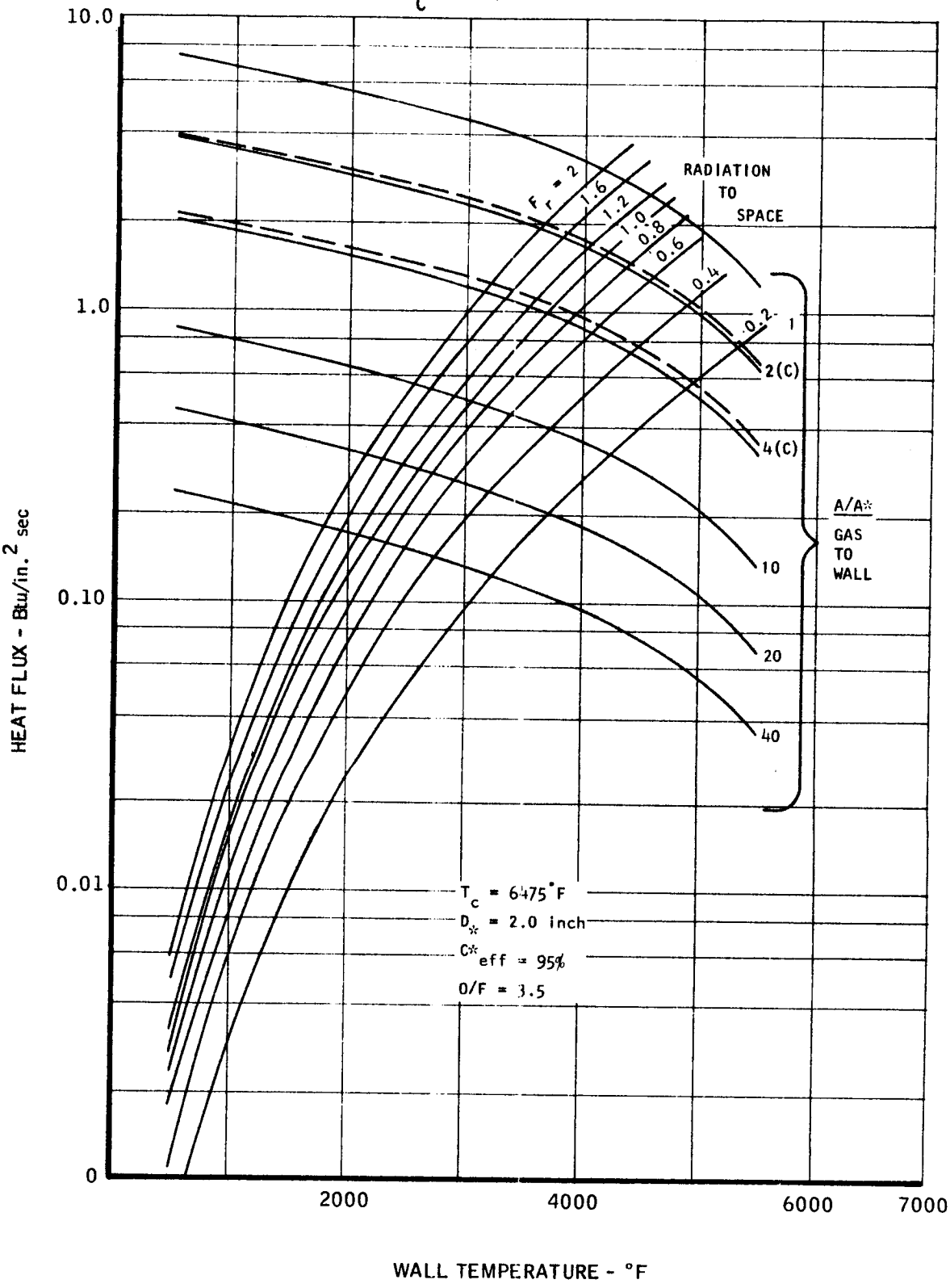

MAC A678

FIGURE 38

COMPARISON OF HEAT FLUX WITH WALL TEMPERATURE
OF_2/DIBORANE
P_c = 150 psia

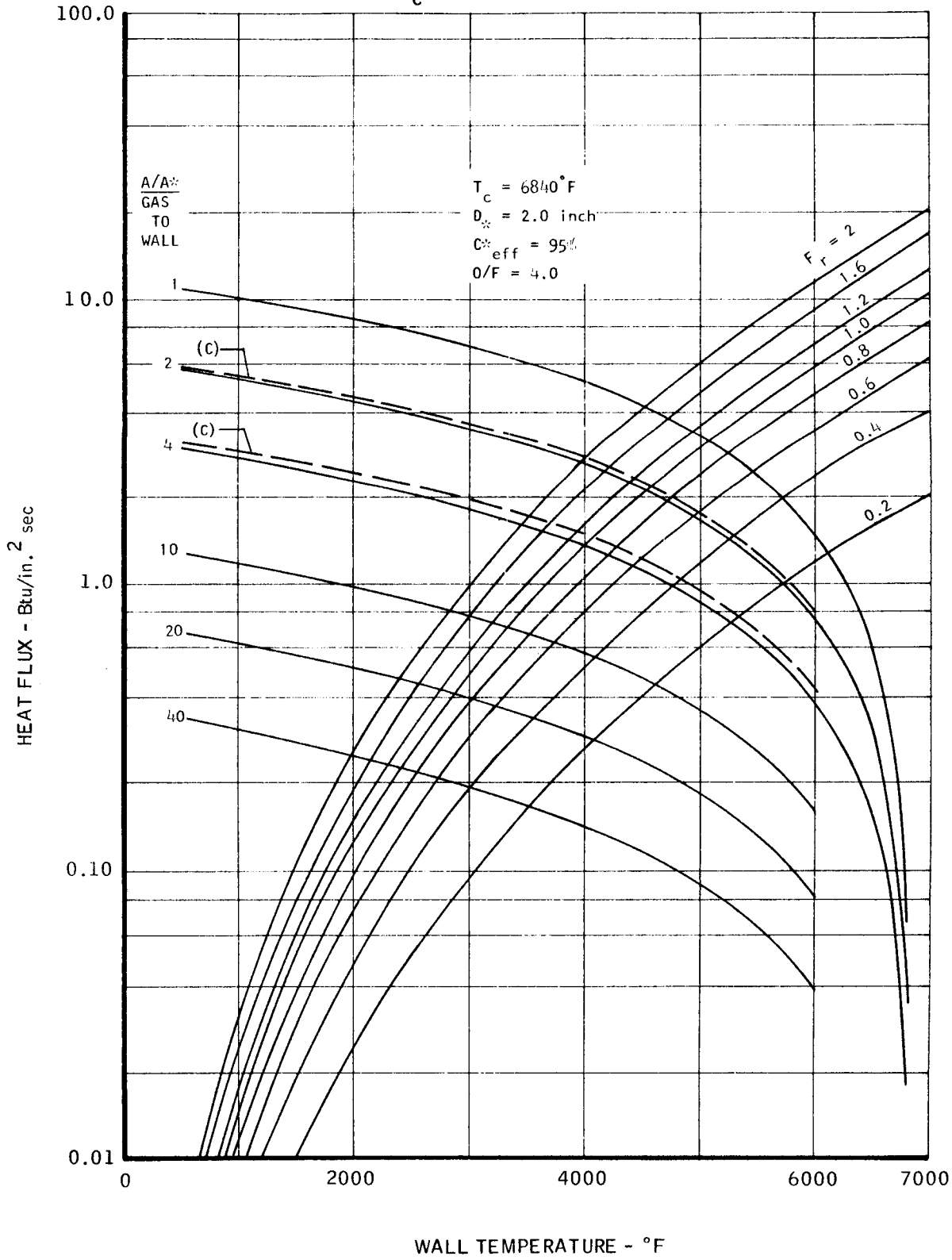

THRUST CHAMBER CROSS SECTIONS
25 - POUND THRUST, RADIATION COOLED MOTOR

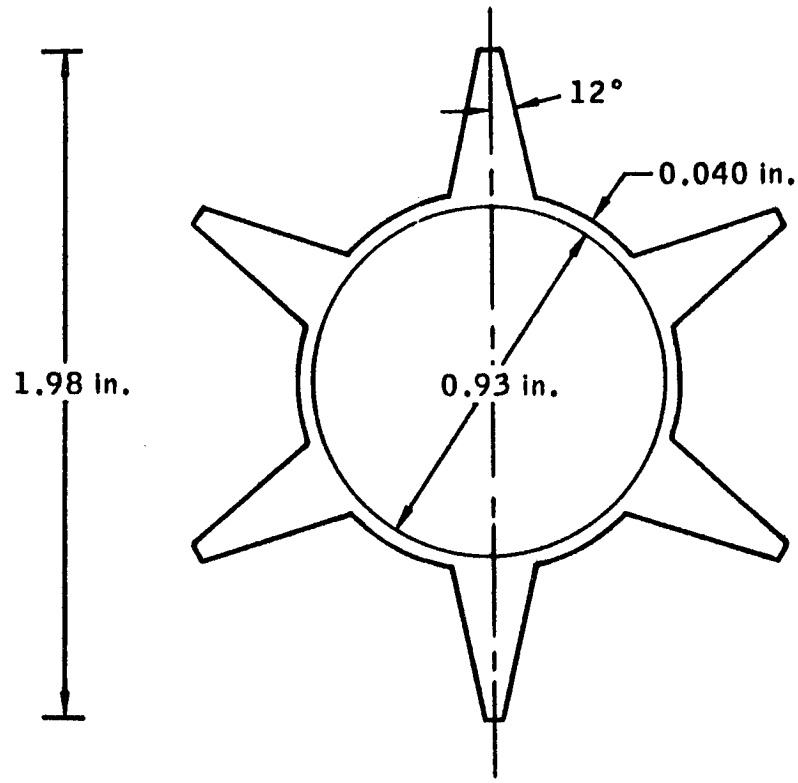

FIN CONFIGURATION NO. 1

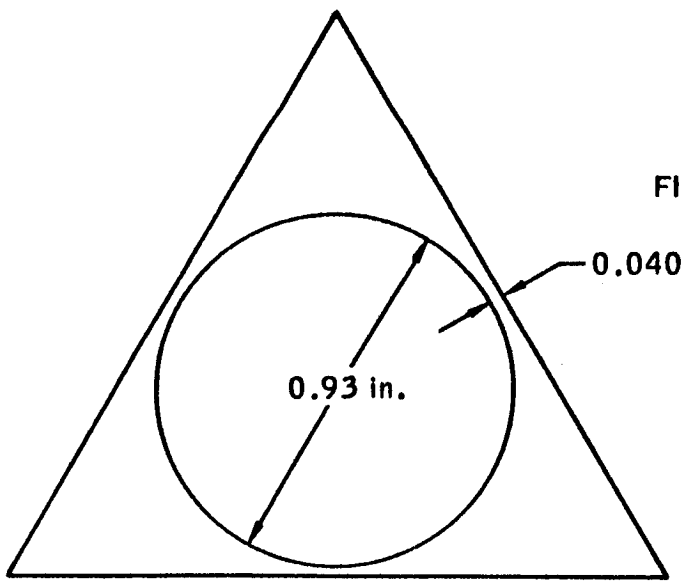

FIN CONFIGURATION NO. 2

MAC A 673

FIGURE 40

THROAT WALL CONFIGURATIONS FOR A 100 - lb THRUST MOTOR

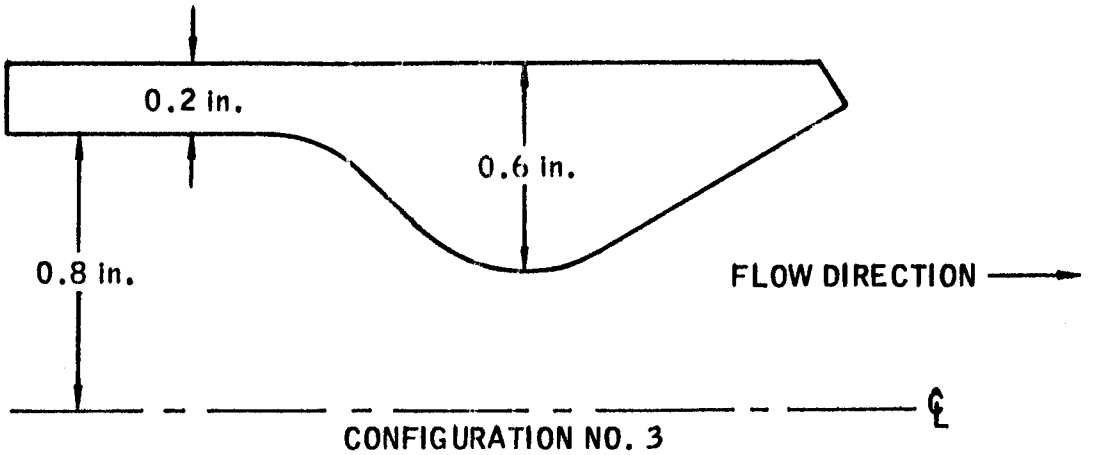

CONFIGURATION NO. 3

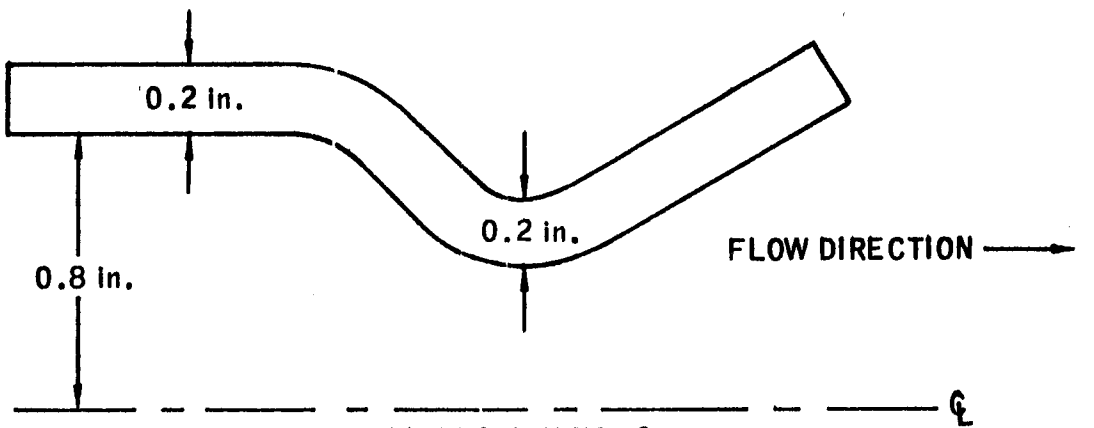

CONFIGURATION NO. 2

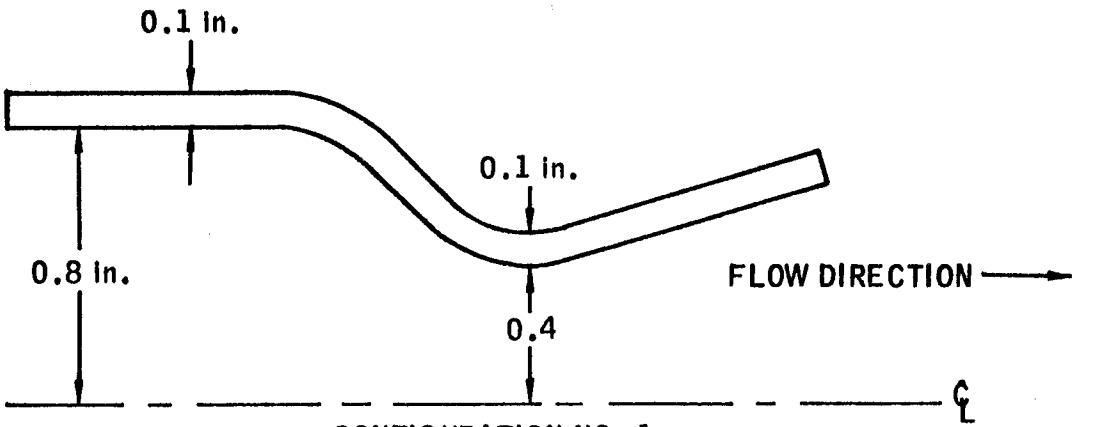

CONFIGURATION NO. 1

MAC A673

FIGURE 41

MAXIMUM TEMPERATURE vs. WALL THICKNESS AT THROAT FOR A 100-lb THRUST RADIATION COOLED MOTOR

P_c = 100 PSIA

N_2O_4 / 25% MMH - 75% N_2H_4

O / F = 1.4

C*EFF = 89.6%

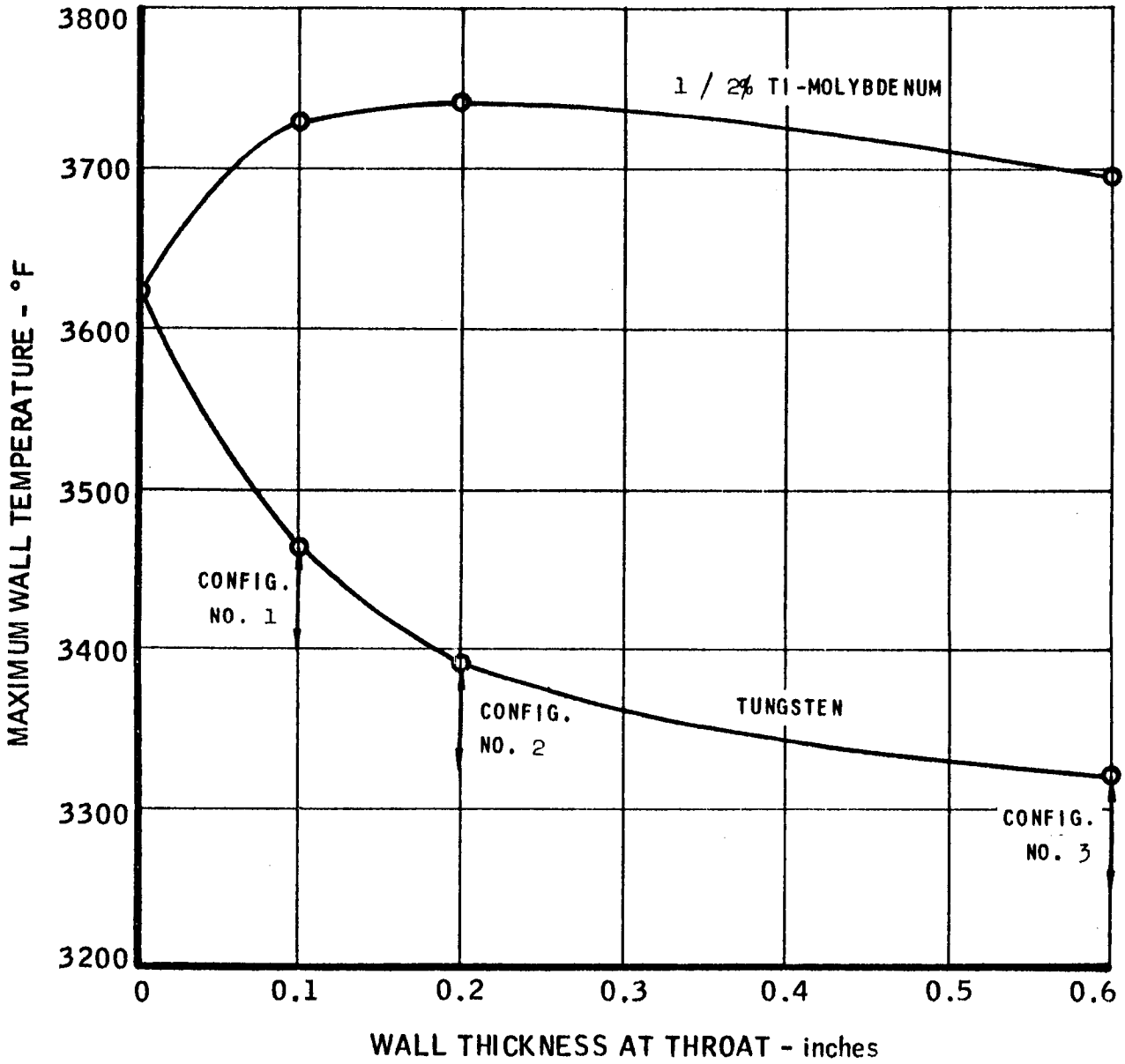

MAC A623

FIGURE 42

TWO - DIMENSIONAL FLOW MOTOR

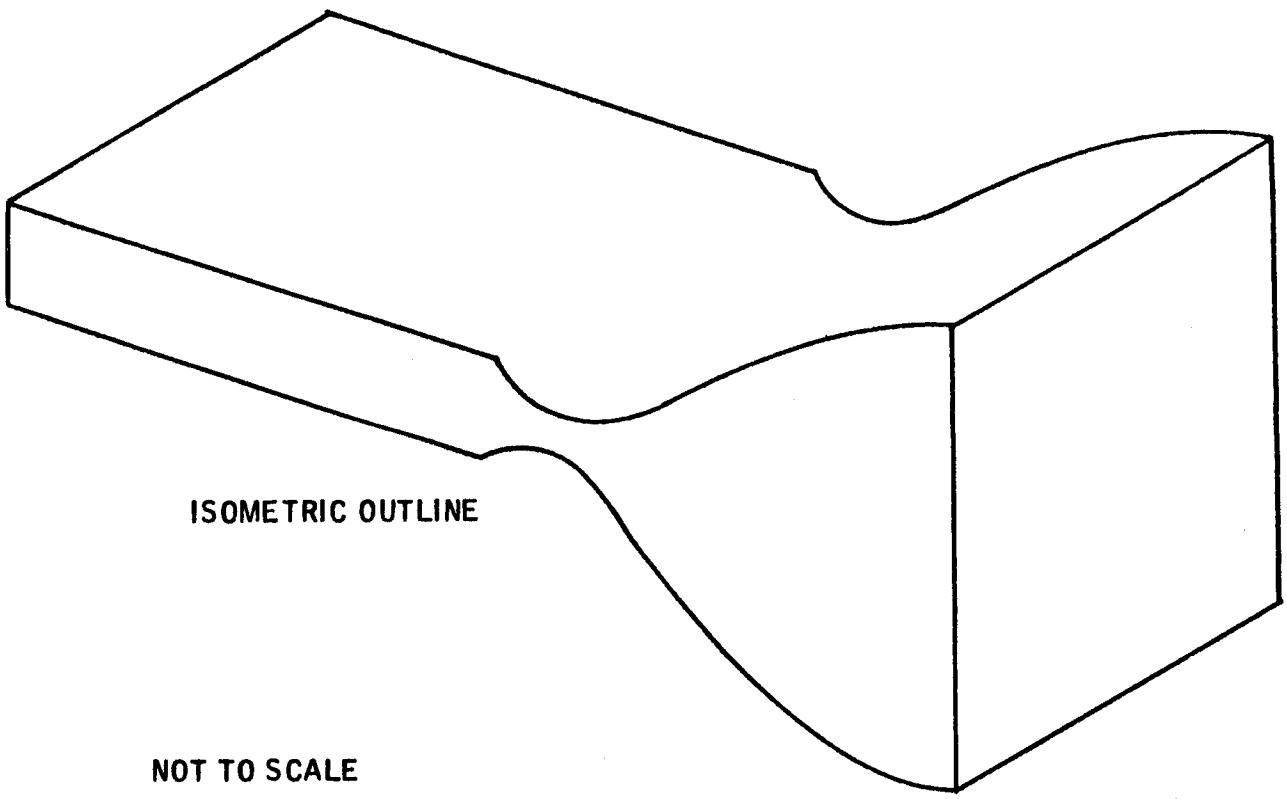

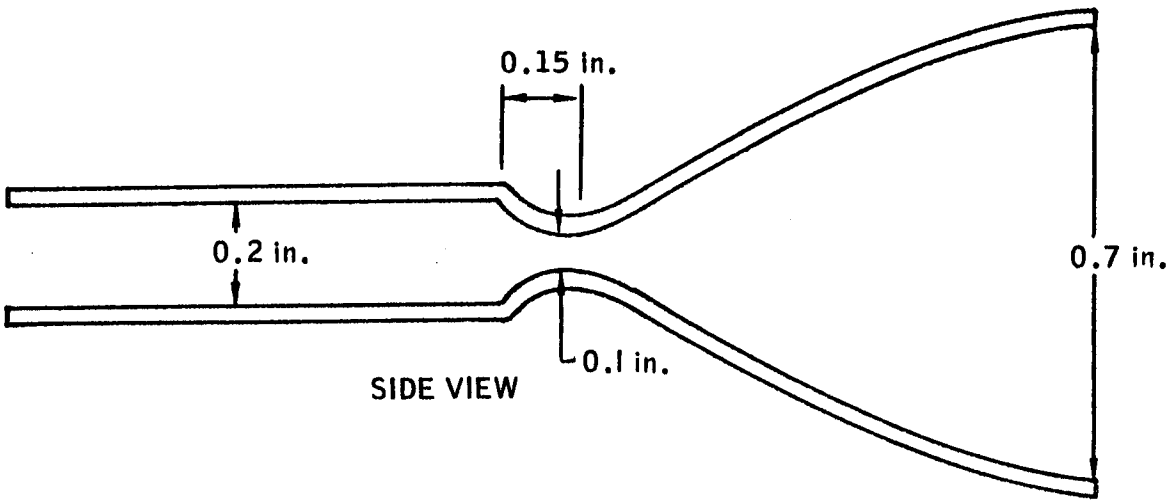

MAC A673

FIGURE 43

TYPICAL THRUST CHAMBER CONFIGURATIONS OF SAME VOLUME AND EXPANSION RATIO
$A_e / A_t = 40$

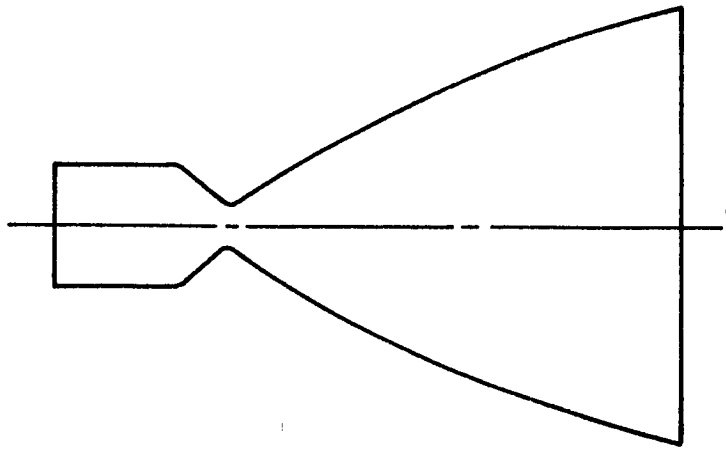

CONVERGENT-DIVERGENT
(C-D) NOZZLE

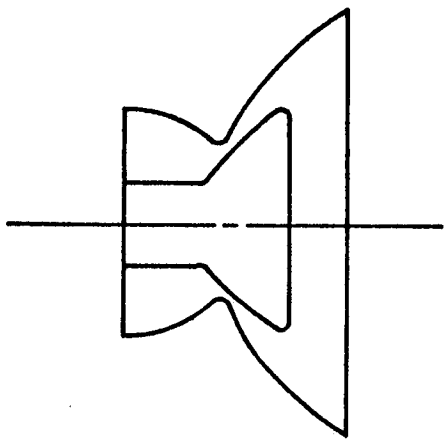

EXPANSION-DEFLECTION
(E-D) NOZZLE

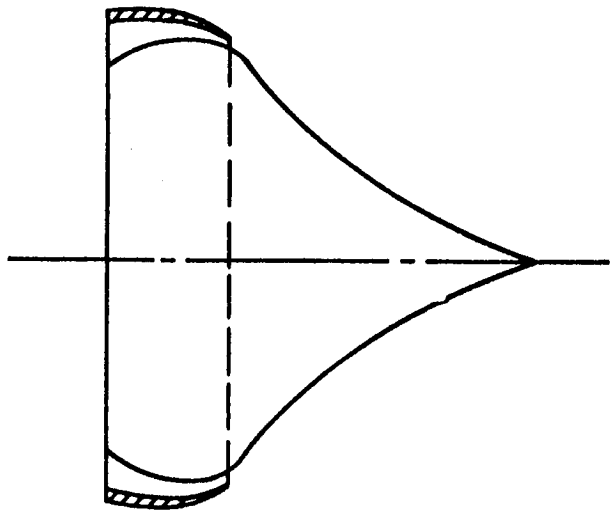

PLUG NOZZLE

MAC A673

FIGURE 44

VARIATION OF NOZZLE AREA RATIO WITH EFFECTIVE RADIATION SHAPE FACTOR

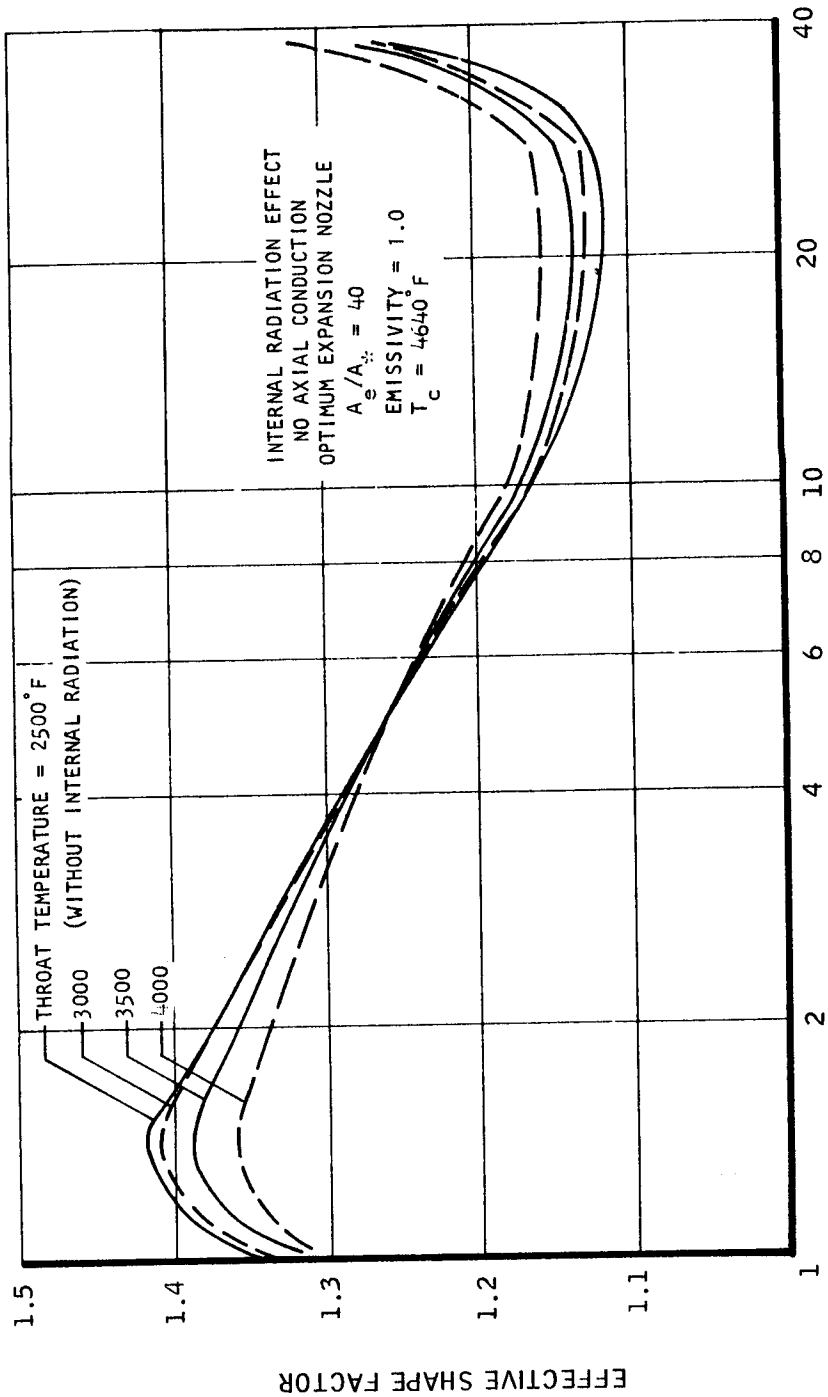

FIGURE 45

WALL TEMPERATURE AS A FUNCTION OF NOZZLE AREA RATIO
AND INTERNAL RADIATION EFFECT
NO AXIAL CONDUCTION
OPTIMUM EXPANSION NOZZLE

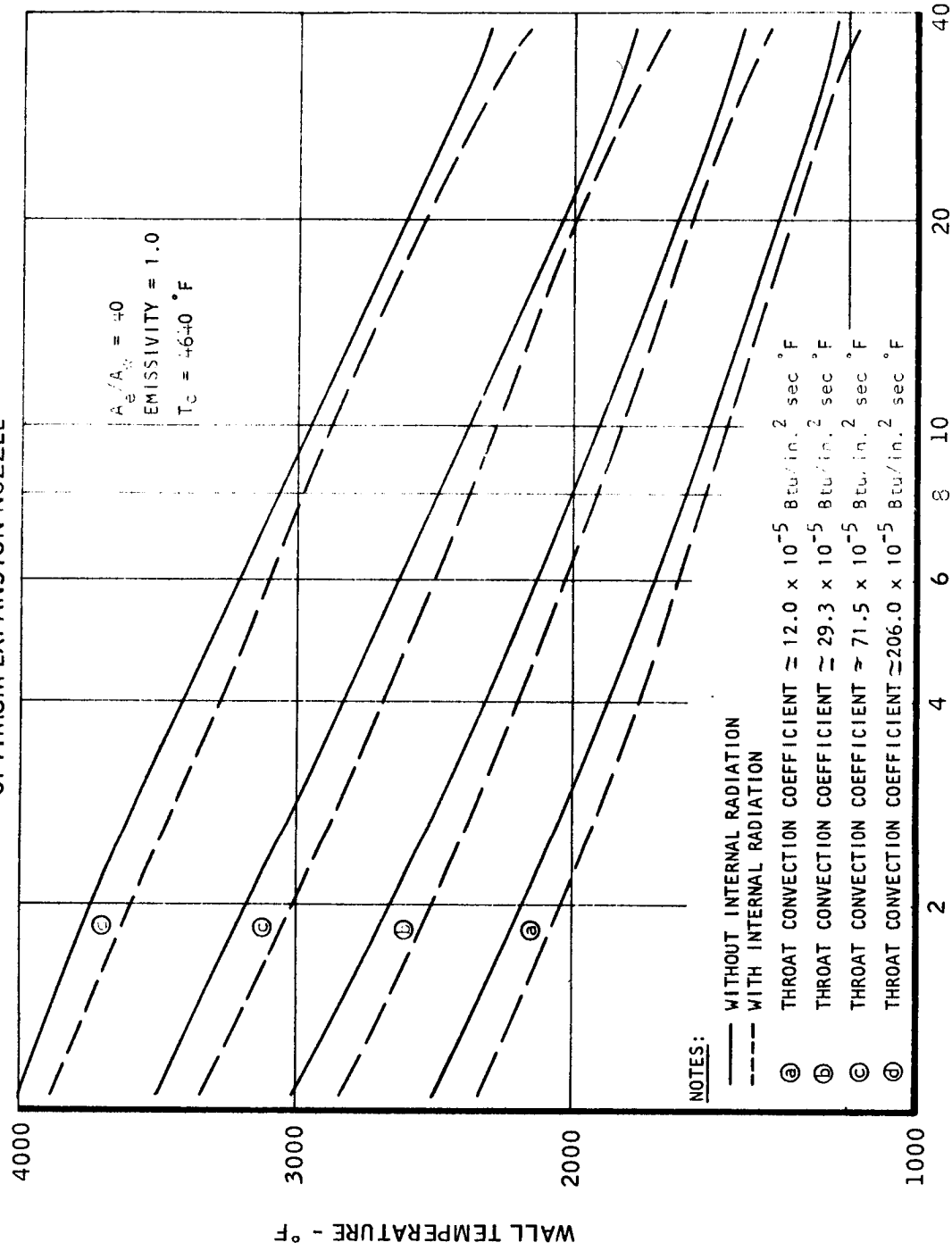

MAC A673

FIGURE 46

WALL TEMPERATURE AS A FUNCTION OF NOZZLE AREA RATIO
AND INTERNAL RADIATION EFFECT
NO AXIAL CONDUCTION
OPTIMUM EXPANSION NOZZLE

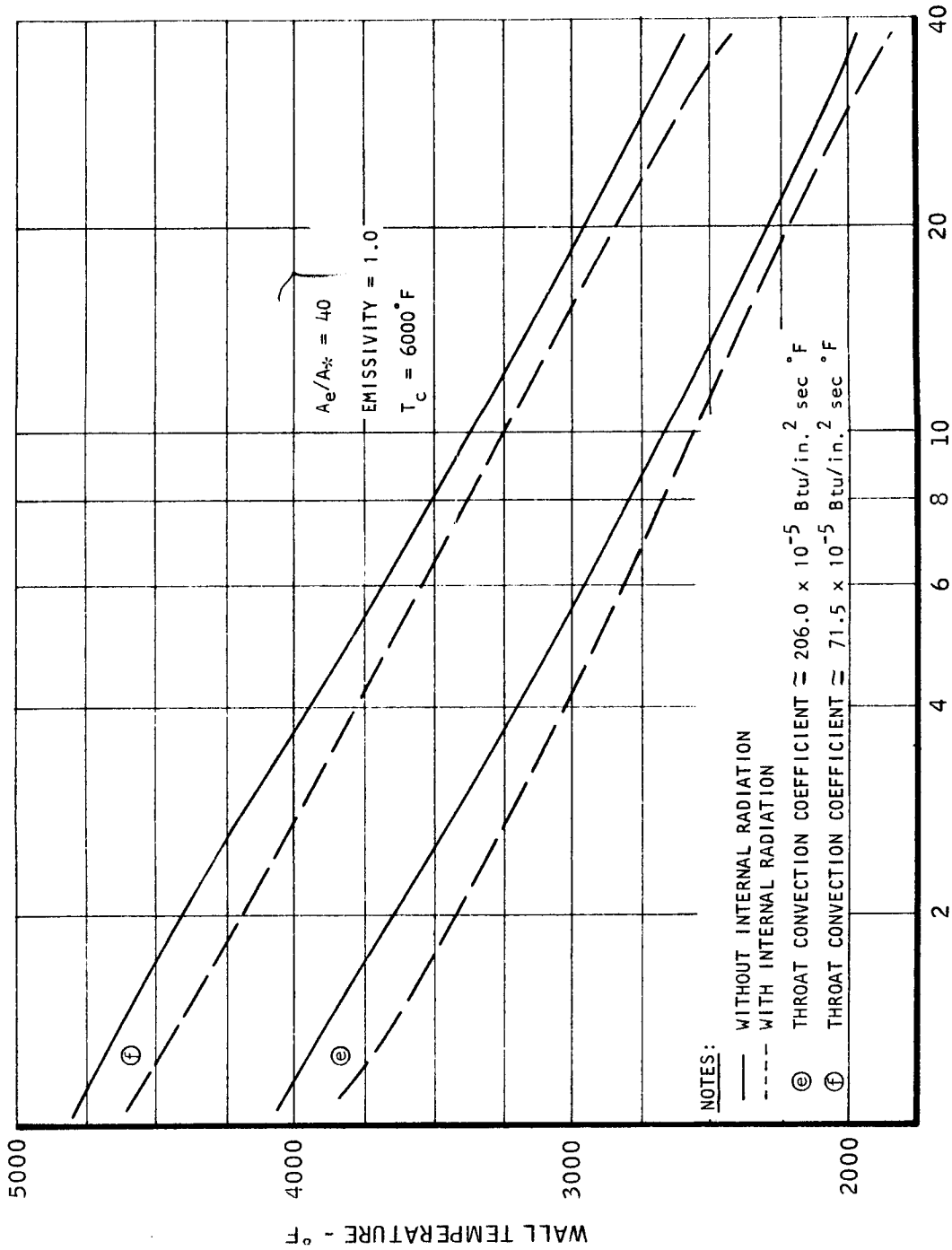

FIGURE 47

THEORETICAL AND EXPERIMENTAL TEMPERATURES
FOR A RADIATION COOLED MOTOR

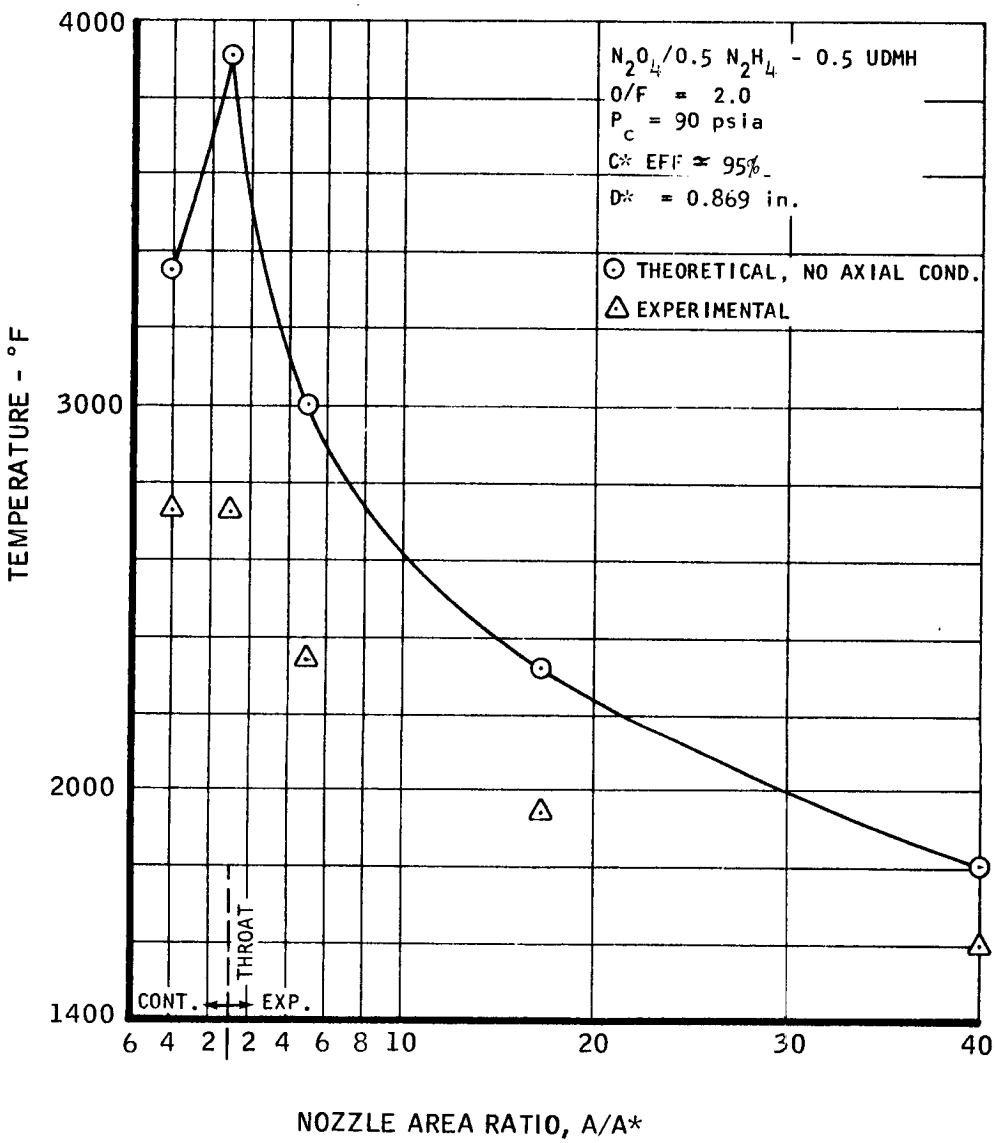

EFFECT OF THROAT SIZE ON ABLATION RATE OF
REFRASIL CLOTH - PHENOLIC RESIN LAMINATES IN A ROCKET NOZZLE

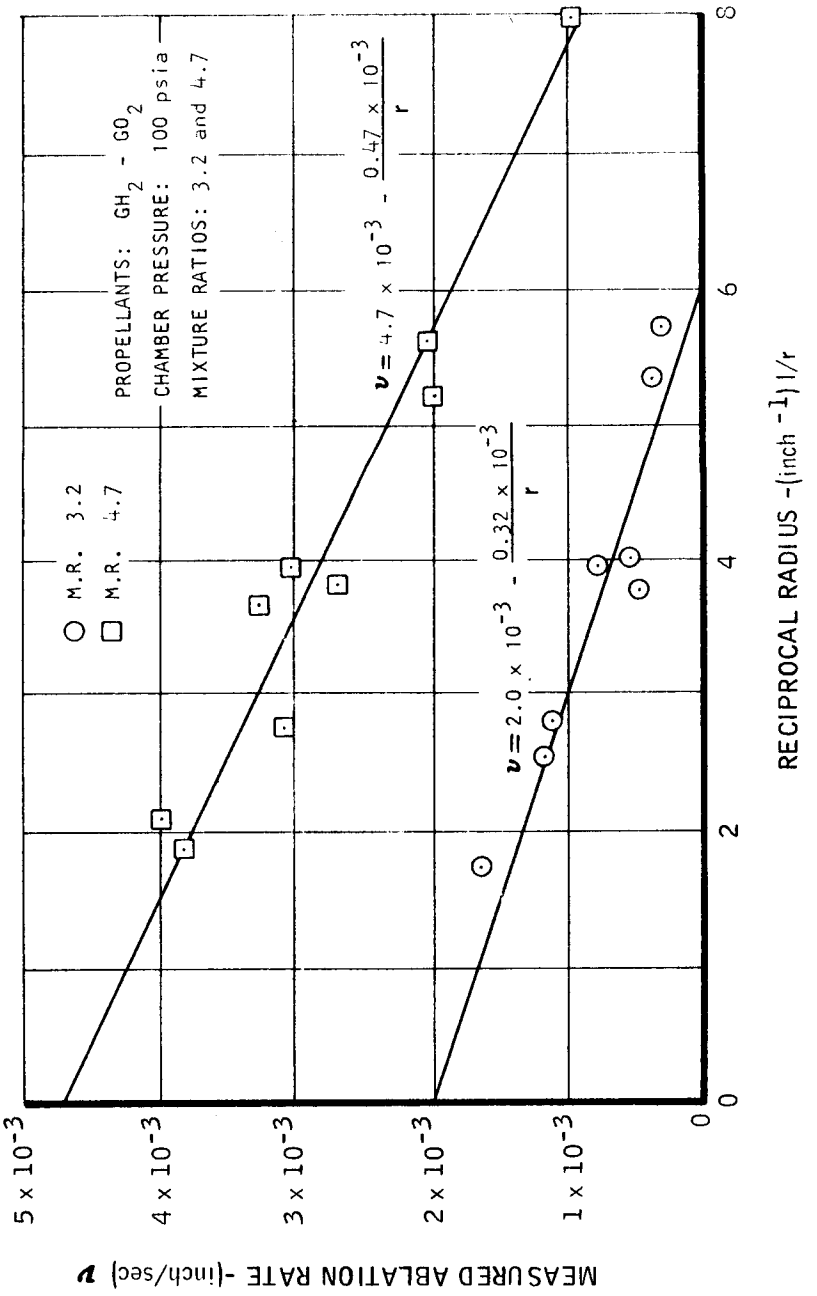

FIGURE 49

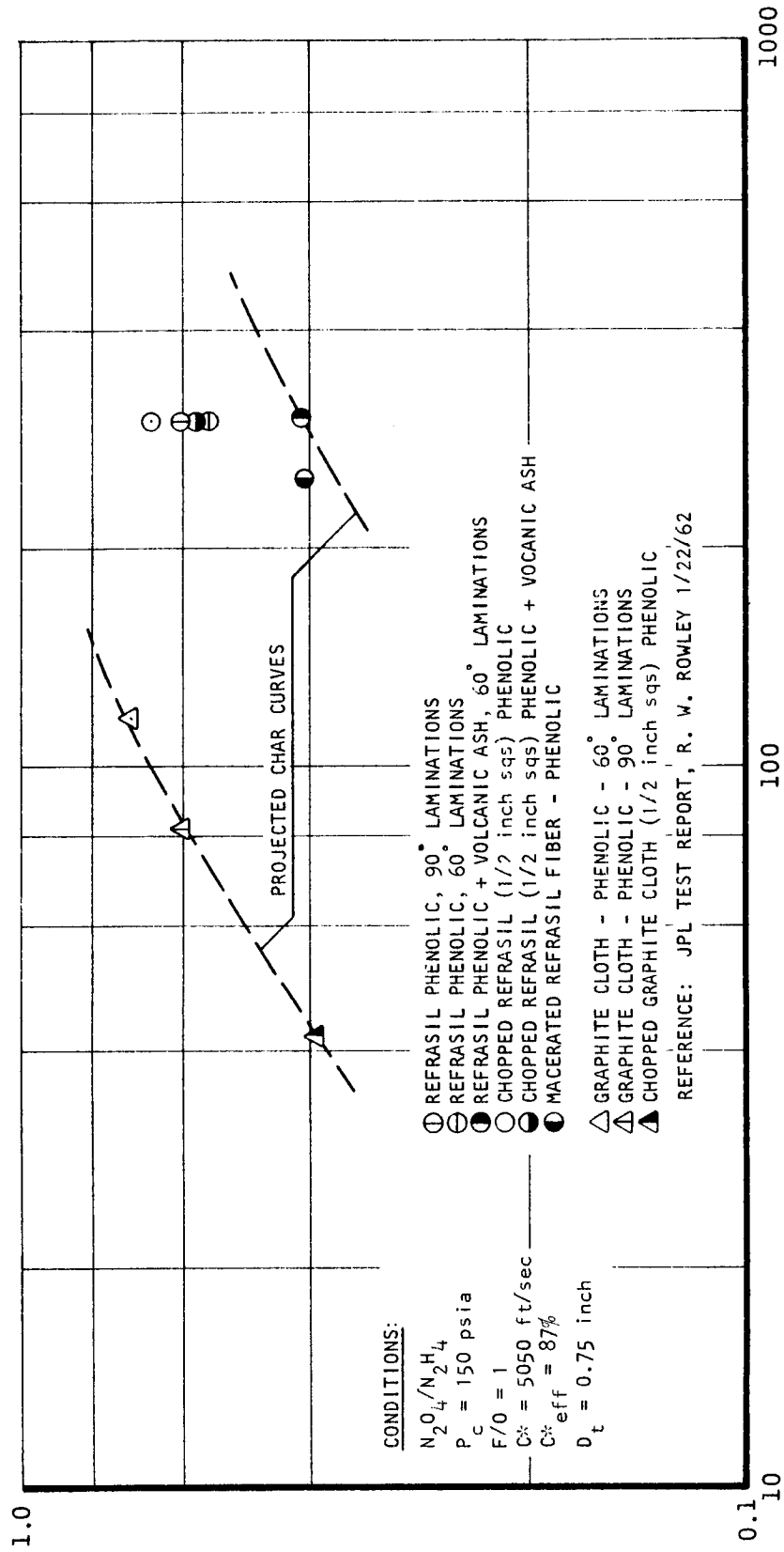

MAC A673

FIGURE 50

MARQUARDT ABLATIVE TEST DATA

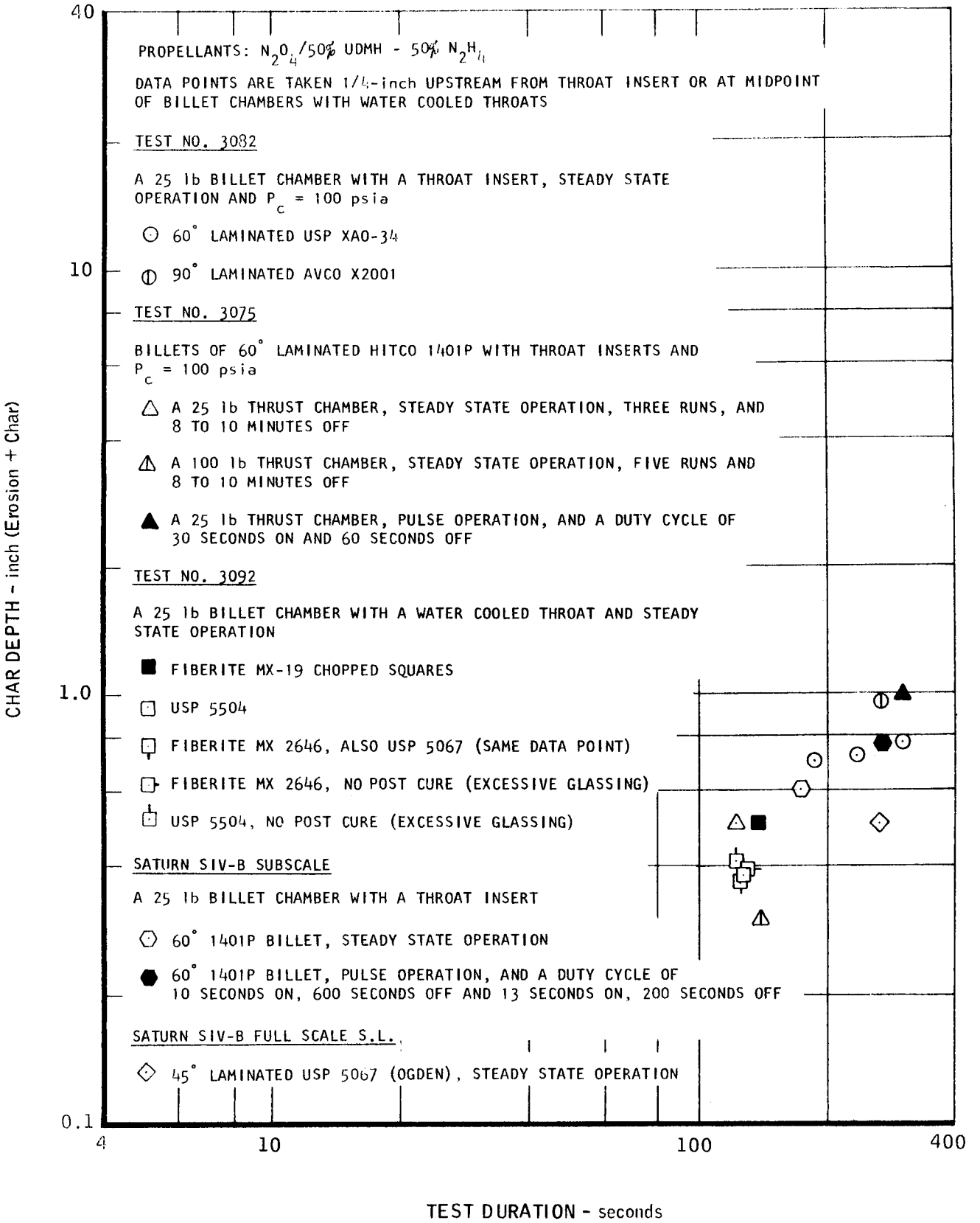

MAC A673

FIGURE 51

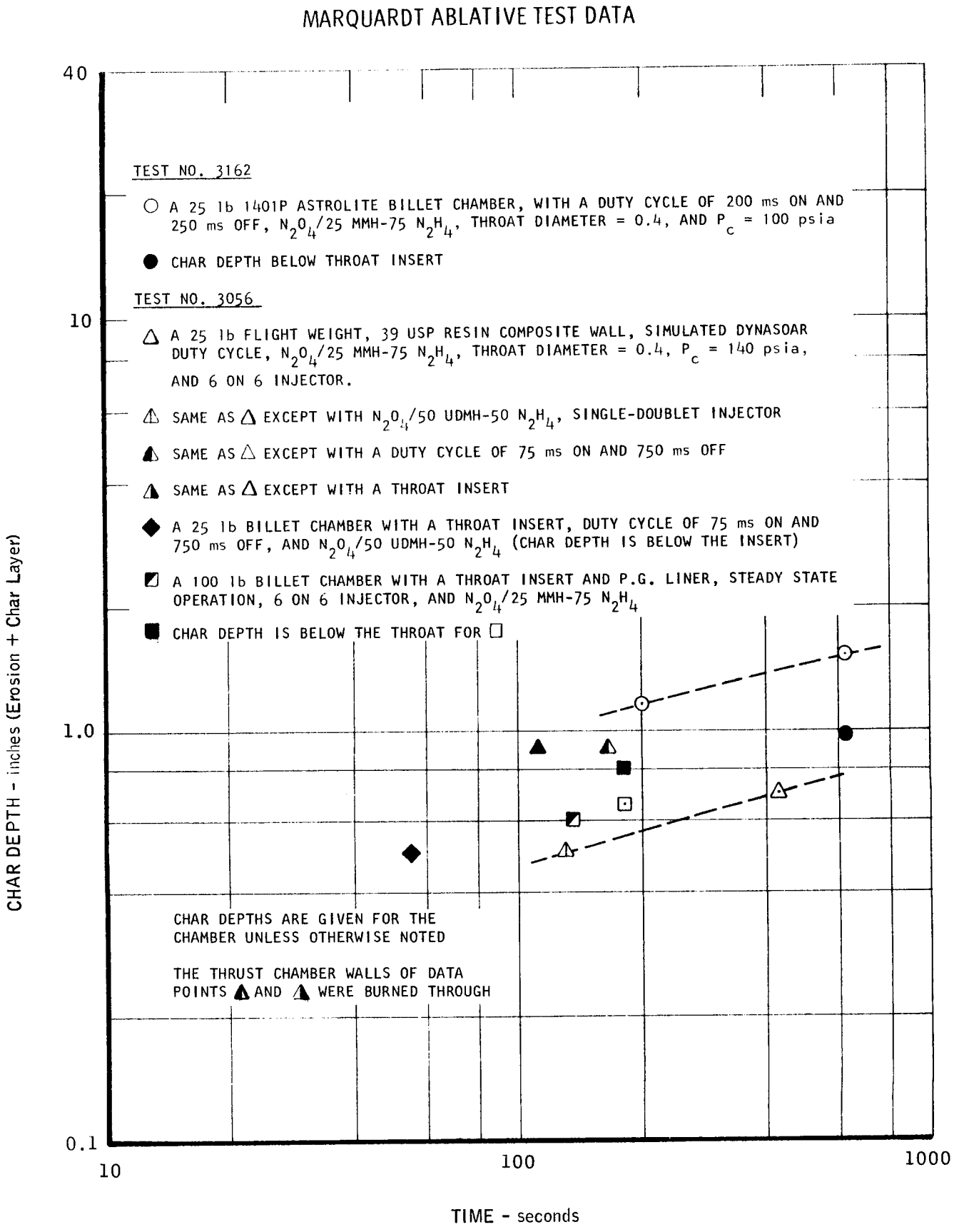

MAC A673

FIGURE 52

RESULTS OF MARQUARDT 100 POUND THRUST ABLATIVE MOTOR TEST
TOTAL RUNNING TIME - 190 seconds

TEST INFORMATION:

THOMPSON 1401 P ASTROLITE
TMC RM005 THROAT INSERT
RUN NO. 1451-1455, TEST ENG. EM-3-3101-1
P_c = 90 psia (NOMINAL), SINGLE-DOUBLET INJECTOR
DUTY CYCLE:
1. 90 RUNS - 10 CYCLES OF 200 ms ON AND 200 ms OFF 10 SECONDS OFF
2. 2 RUNS - 2 SECONDS EACH
3. 3 RUNS - 2 SECONDS EACH
TOTAL ABLATED MATERIAL (EROSION + CHAR)
THROAT = NEGLIGIBLE
CHAMBER (MAX.) = 0.8 inch AT INSERT
1.4 inch JUST UPSTREAM FROM INSERT

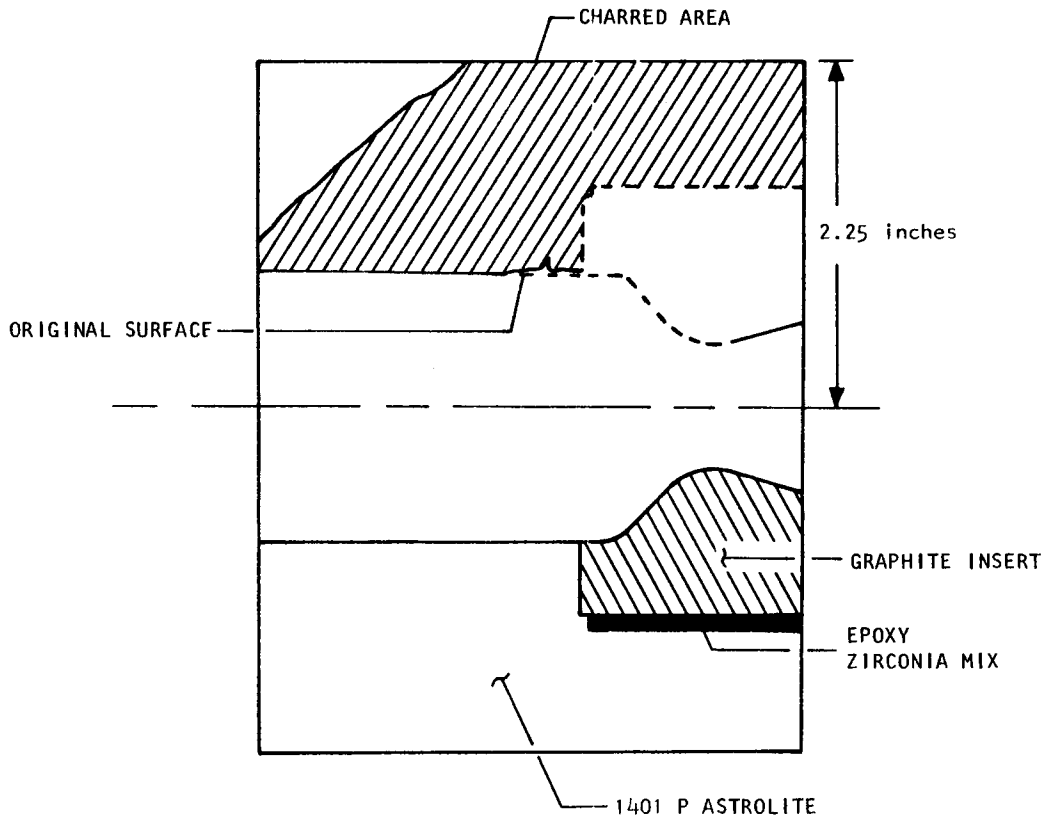

FIGURE 53

RESULTS OF MARQUARDT 100 POUND THRUST ABLATIVE MOTOR TEST
TOTAL RUNNING TIME - 200 seconds

TEST INFORMATION:

THOMPSON 1401 P ASTROLITE
TMC RM005 THROAT INSERT
RUN NO. 1450, TEST ENG. EM-3-3101-1
P_c = 90 psia (NOMINAL), SINGLE-DOUBLET INJECTOR
DUTY CYCLE:
1. 1 RUN - 5 SECONDS
2. 1 RUN - 195 SECONDS
TOTAL ABLATED MATERIAL (EROSION + CHAR)
THROAT - NEGLIGIBLE
CHAMBER (MAX.) - 0.46 inch AT INSERT
0.95 inch JUST UPSTREAM FROM INSERT

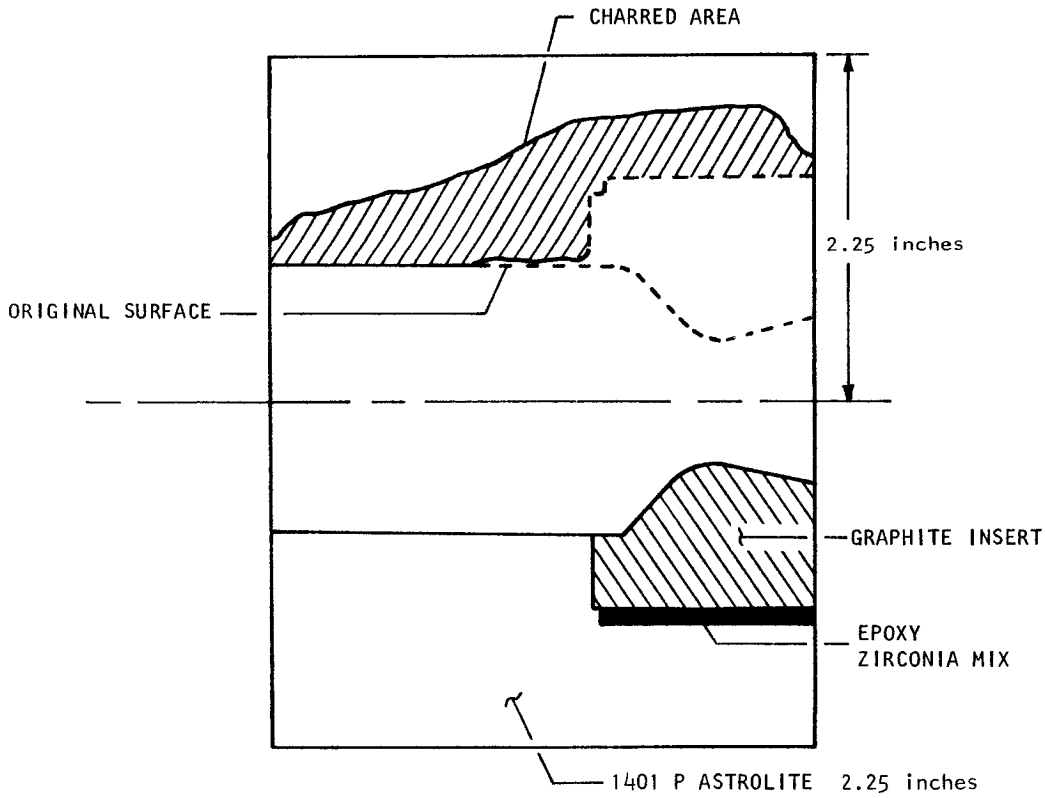

MAC A673

FIGURE 54

CHAR DEPTH RESULTS OF SIV-B SUBSCALE TEST 3093
CONTINUOUS vs. PULSE COMBUSTION

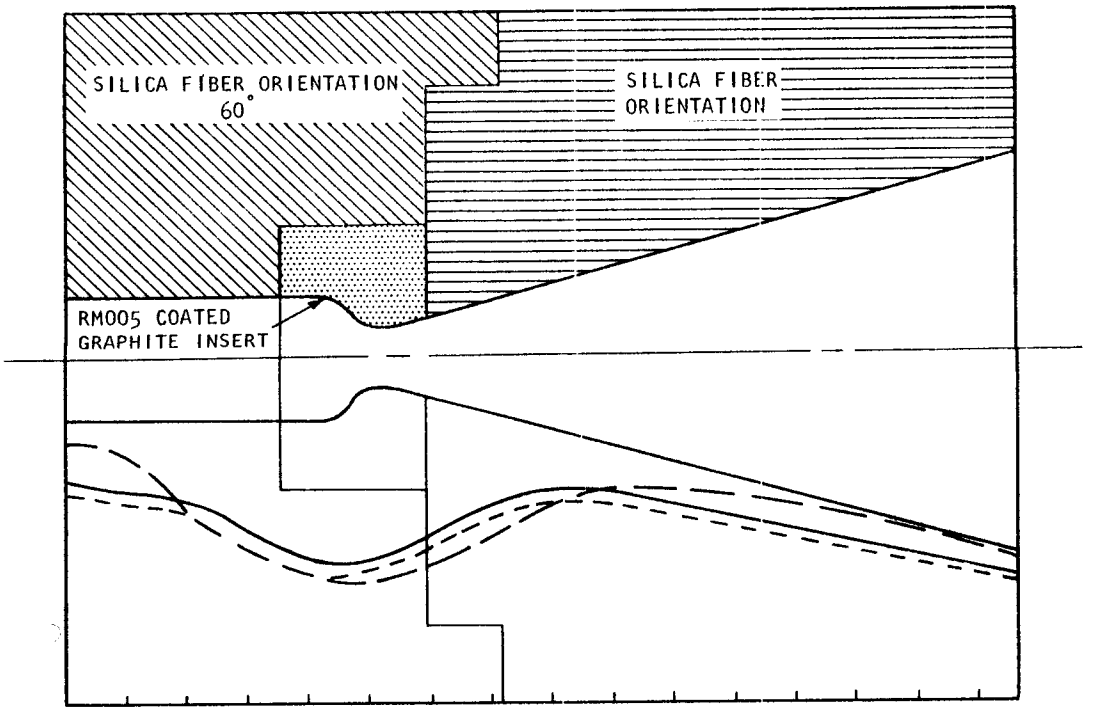

NOTES:

1. 1401P RESIN USED IN BOTH S/N1 AND S/N2 ENGINE FABRICATION
2. ——DENOTES CHAR DEPTH OF S/N1 ENGINE AFTER CONTINUOUS COMBUSTION FOR 168 SECONDS
3. — — DENOTES CHAR DEPTH OF S/N2 ENGINE AFTER PULSE COMBUSTION FOR 270 SECONDS
4. S/N2 ENGINE DUTY CYCLE: 10 SECONDS ON, 600 SECONDS OFF AND 20 CYCLES AT 13 SECONDS ON, 200 SECONDS OFF
5. ———DENOTES ESTIMATED CHAR DEPTH AFTER 250 SECONDS OF CONTINUOUS COMBUSTION
6. TEST INFORMATION:

		S/N1	S/N2
PROPELLANTS - MMH/N_2O_4	P_e	= 0.35 psia	0.035 psia
	P_c	= 143 psia	151 psia
	I_{SP}	= 303 seconds	303 seconds
	O/F	= 1.58	1.60

COMPOSITE WALL DESIGNS

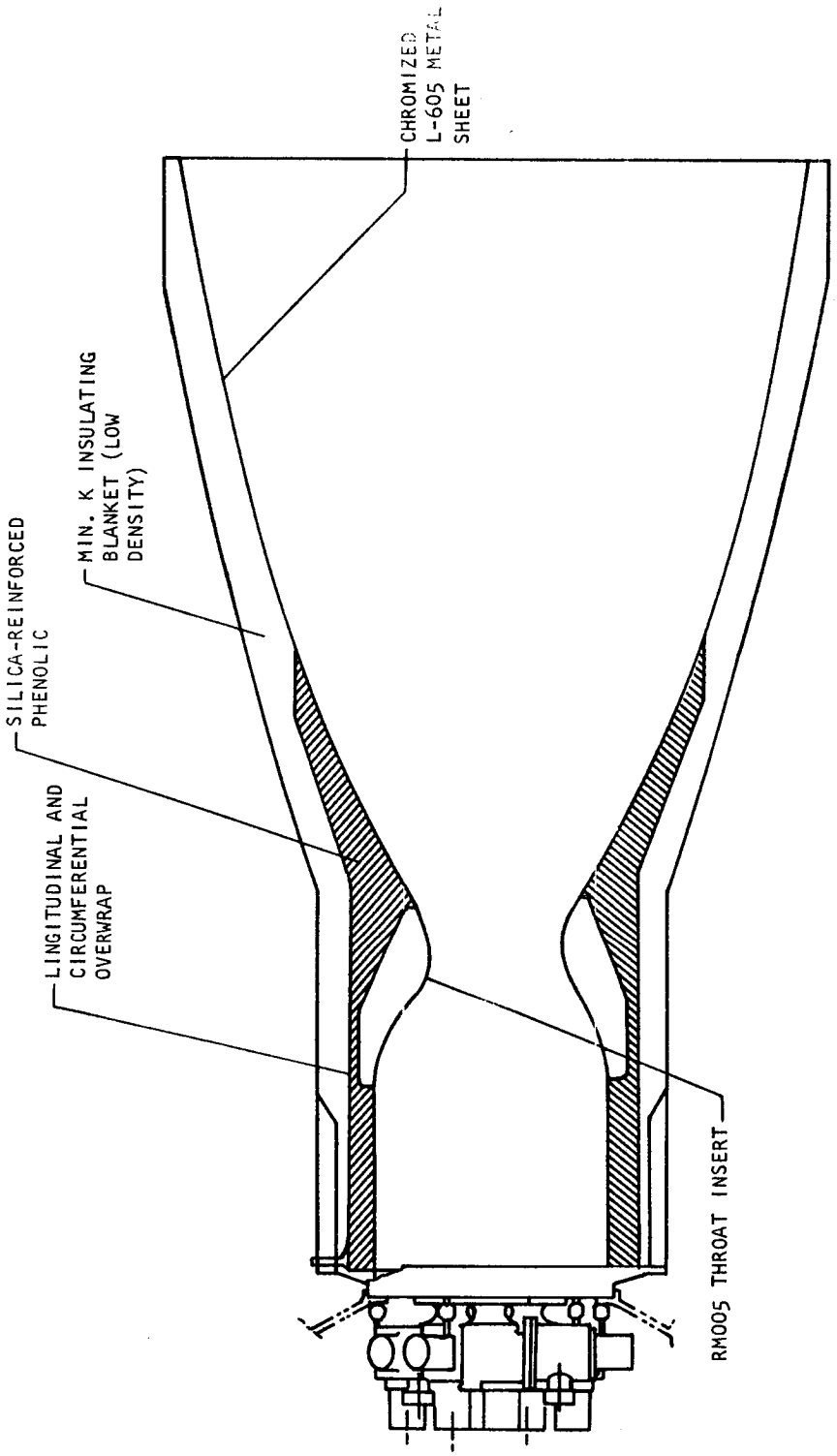

MAC A673

ANALYTICALLY DETERMINED TEMPERATURE HISTORY OF REFRASIL-PHENOLIC SLAB AT SEVERAL DEPTHS

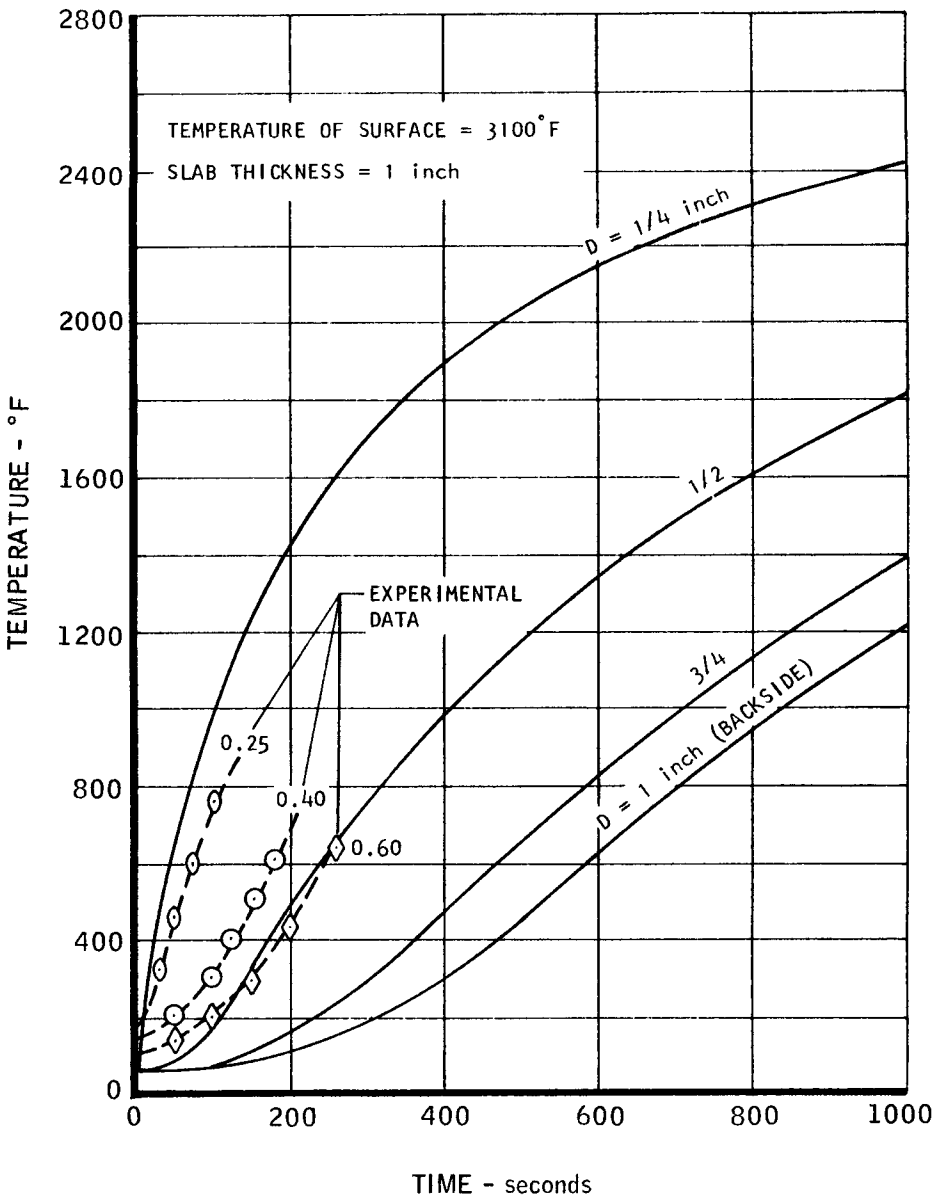

ANALYTICALLY DETERMINED TEMPERATURE HISTORY
LAMINATED REFRASIL - PHENOLIC (BACK FACE)
$T_{surface}$ 3100° F

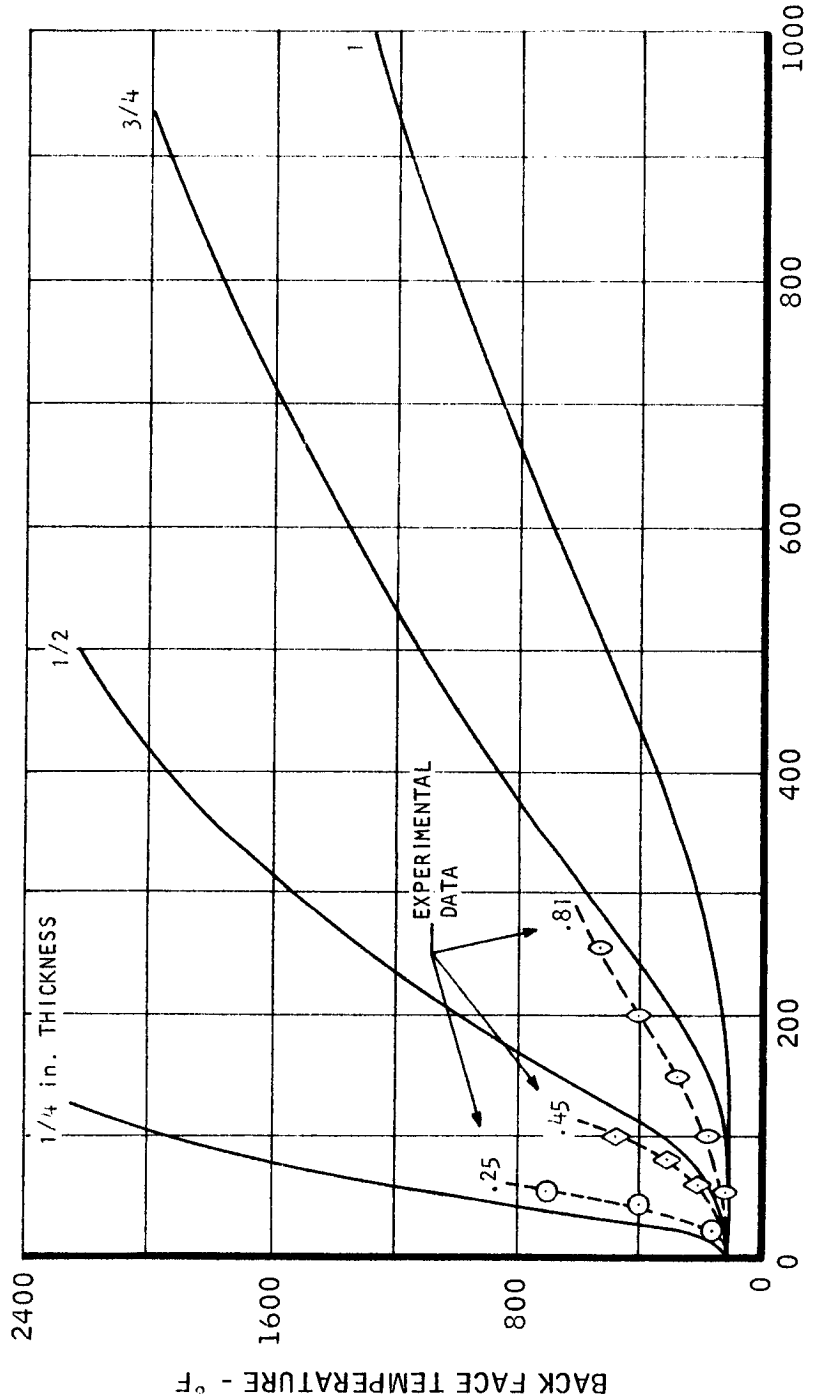

MAC A673

FIGURE 58

DECOMPOSITION OF PHENOLIC IN VACUUM vs. SAMPLE TEMPERATURE

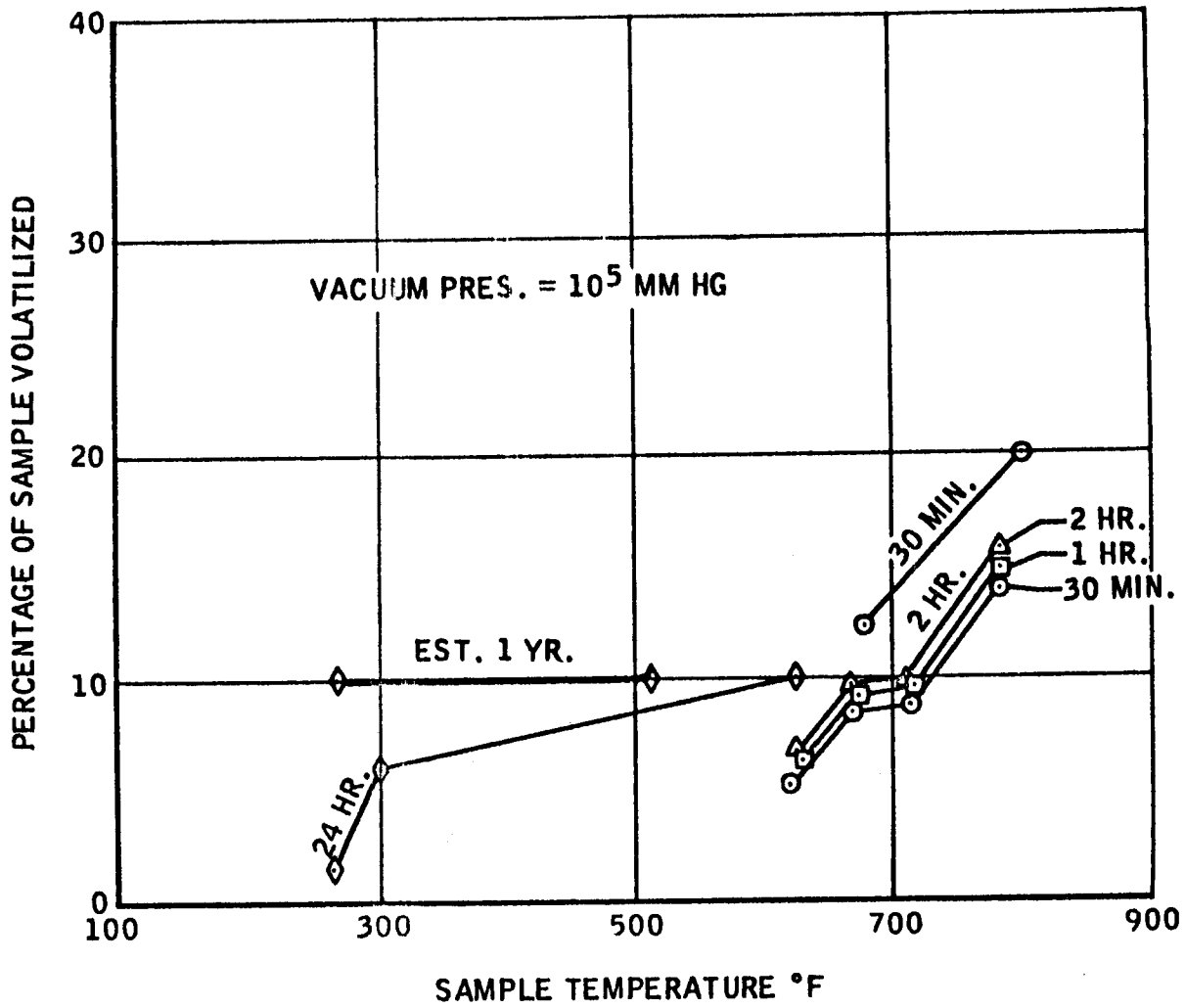

FIGURE 59

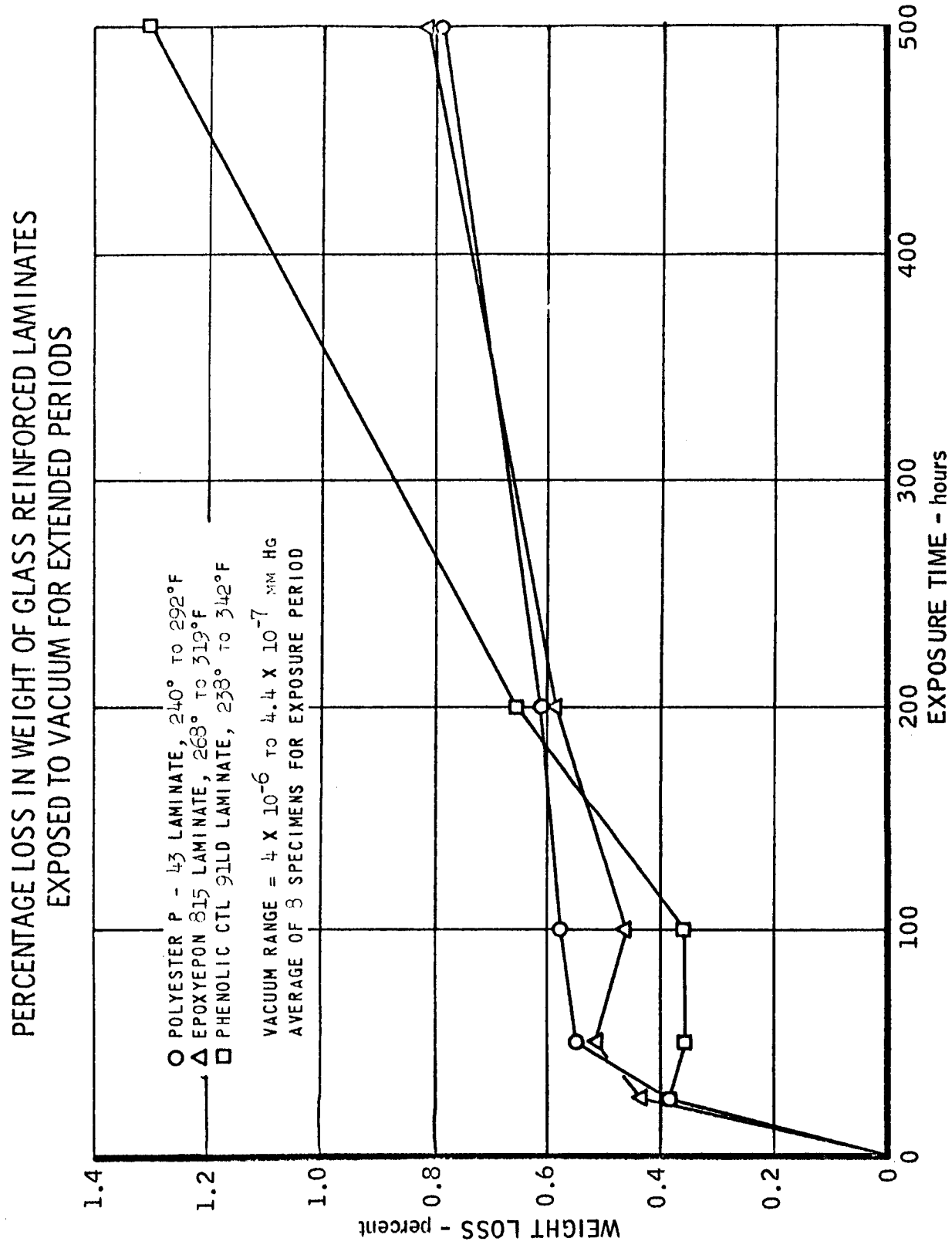
PERCENTAGE LOSS IN WEIGHT OF GLASS REINFORCED LAMINATES
EXPOSED TO VACUUM FOR EXTENDED PERIODS
O POLYESTER P - 43 LAMINATE, 240° TO 292°F
Δ EPOXYEPON 815 LAMINATE, 268° TO 319°F
□ PHENOLIC CTL 91LD LAMINATE, 238° TO 342°F
VACUUM RANGE = 4 X 10⁻⁶ TO 4.4 X 10⁻⁷ MM HG
AVERAGE OF 3 SPECIMENS FOR EXPOSURE PERIOD
WEIGHT LOSS - percent
1.4
1.2
1.0
0.8
0.6
0.4
0.2
0
0
100
200
300
400
500
EXPOSURE TIME - hours

FIGURE 60

TIME - TEMPERATURE FLEXURAL STRENGTH OF A PHENOLIC-GLASS LAMINATE

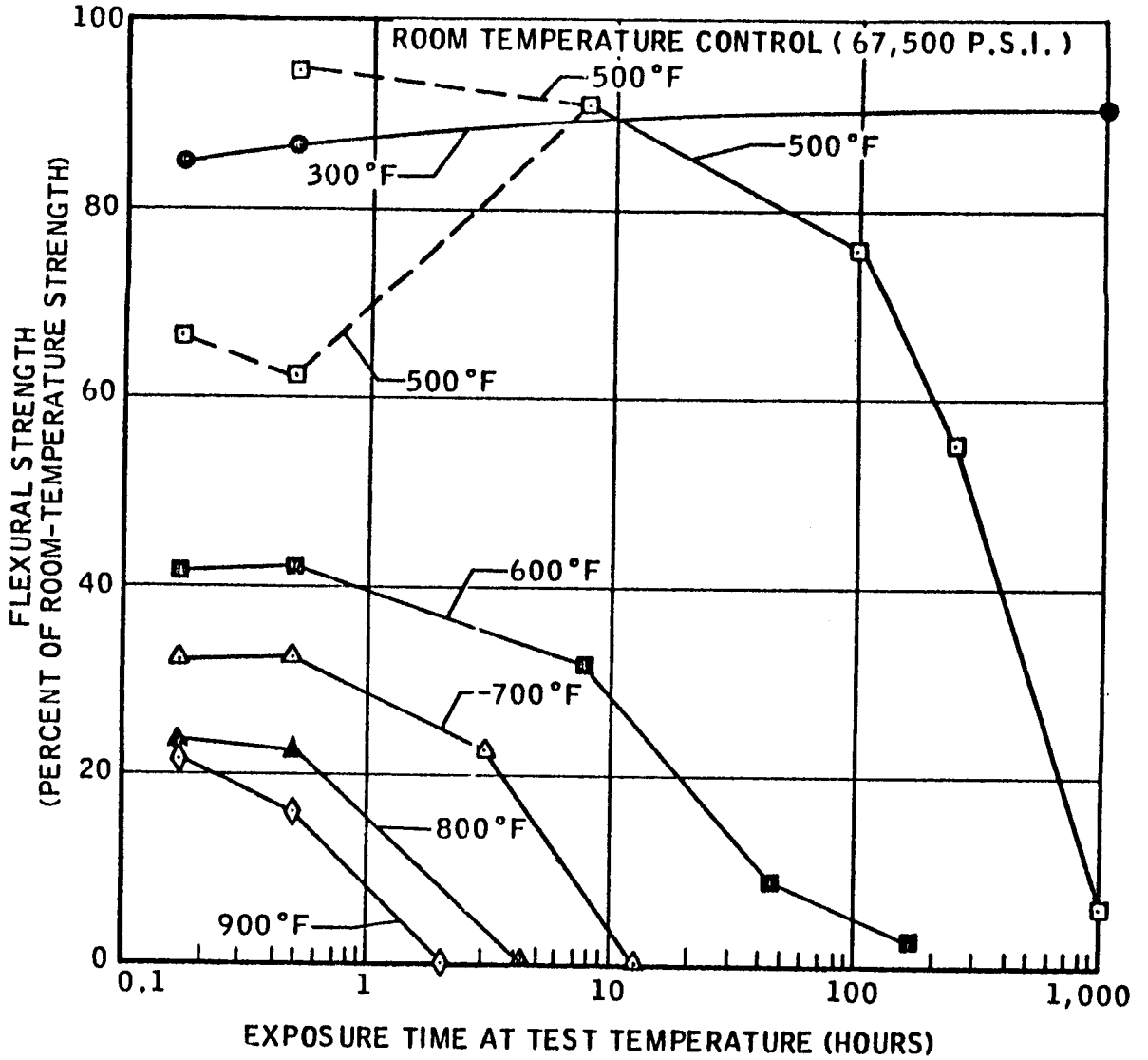

THERMOGRAVIMETRICAL ANALYSIS OF HEATED THERMOSETTING RESINS

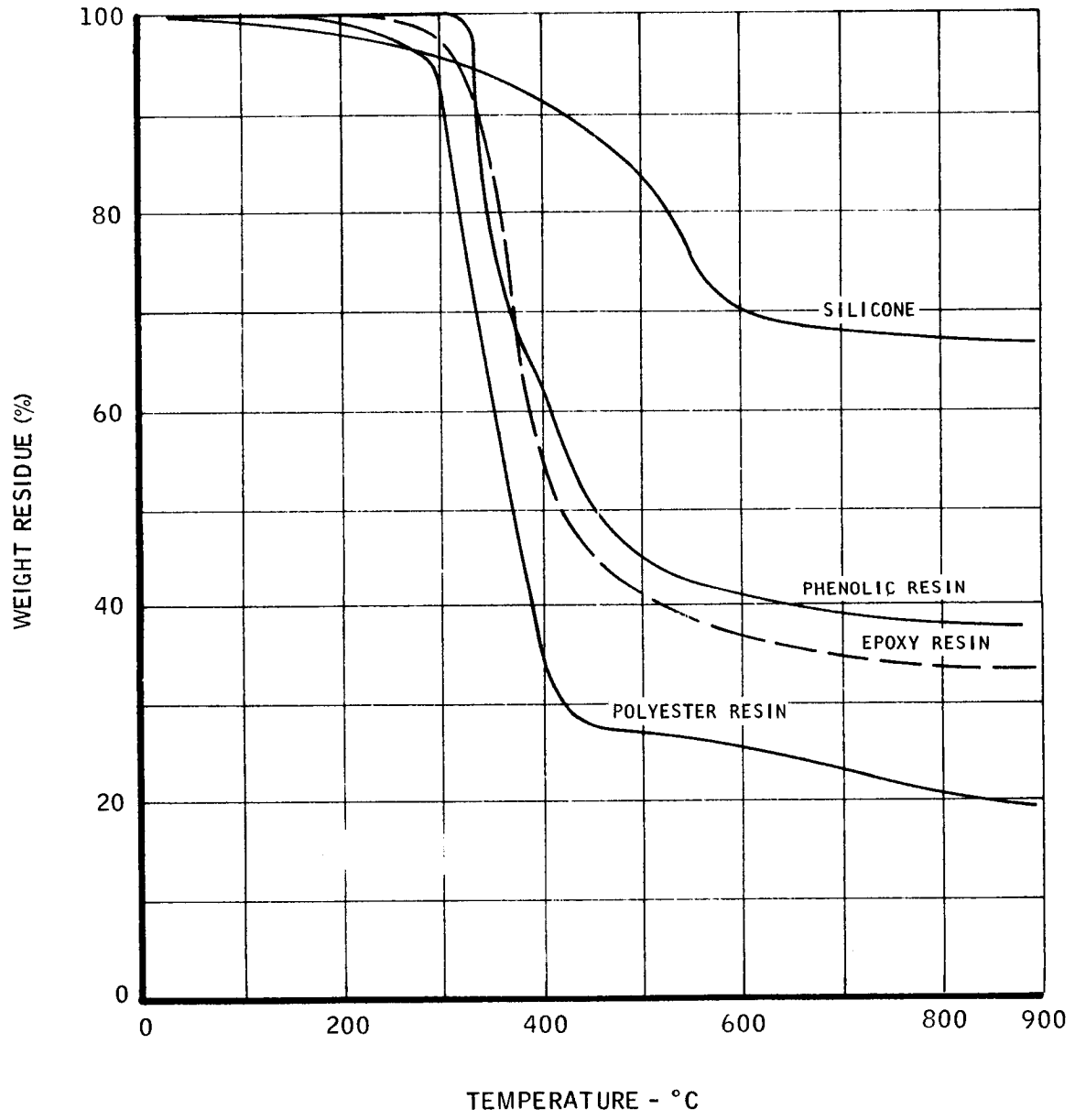

MAC A673

FIGURE 62

THERMAL CONDUCTIVITY OF ASTROLITE

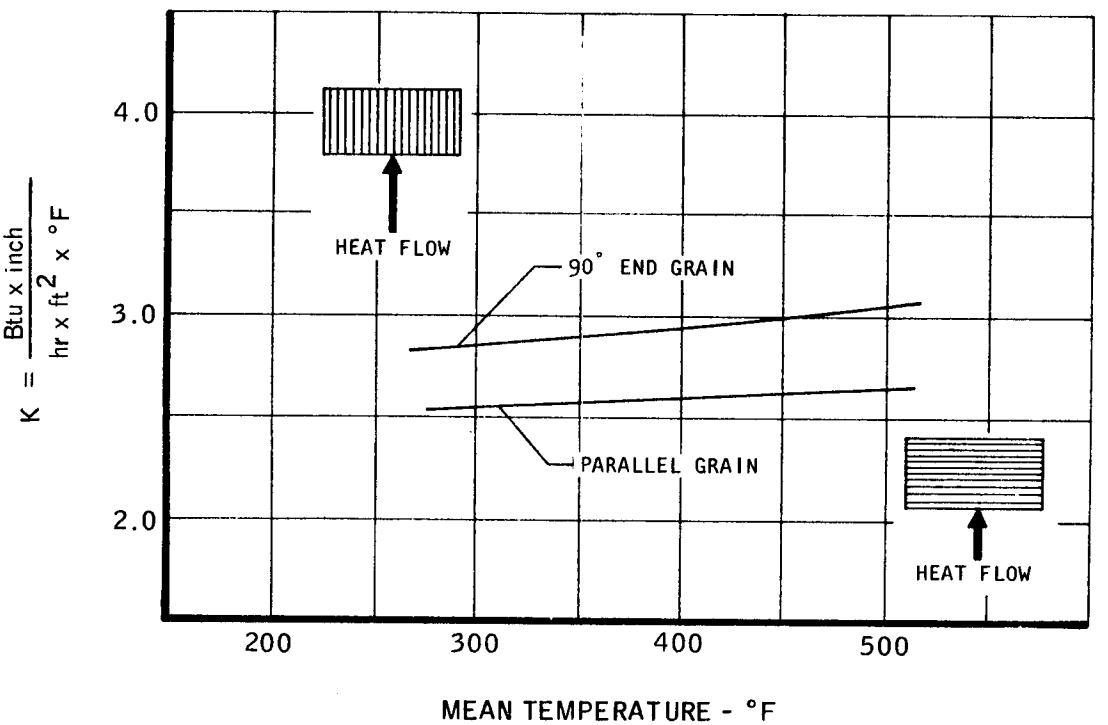

EFFECT OF RESIN CONTENT ON THERMAL CONDUCTIVITY
OF PHENOLIC-GLASS FIBER LAMINATE

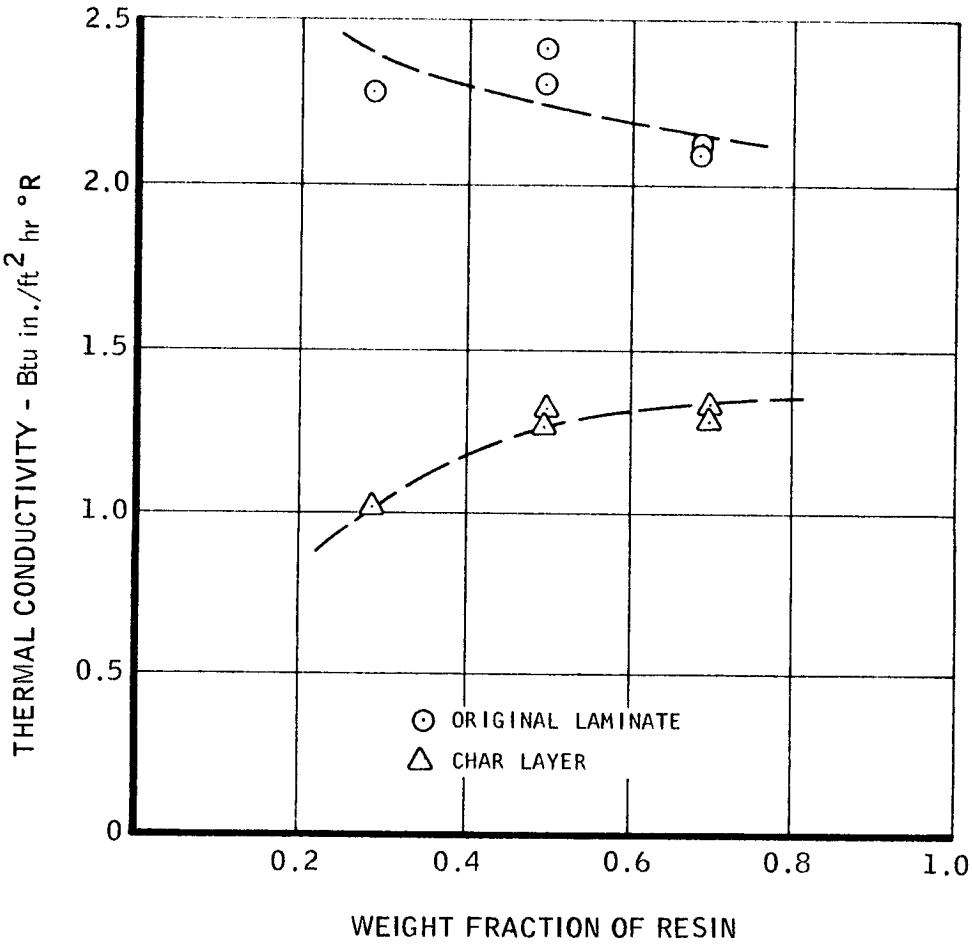

MAC A673

FIGURE 64

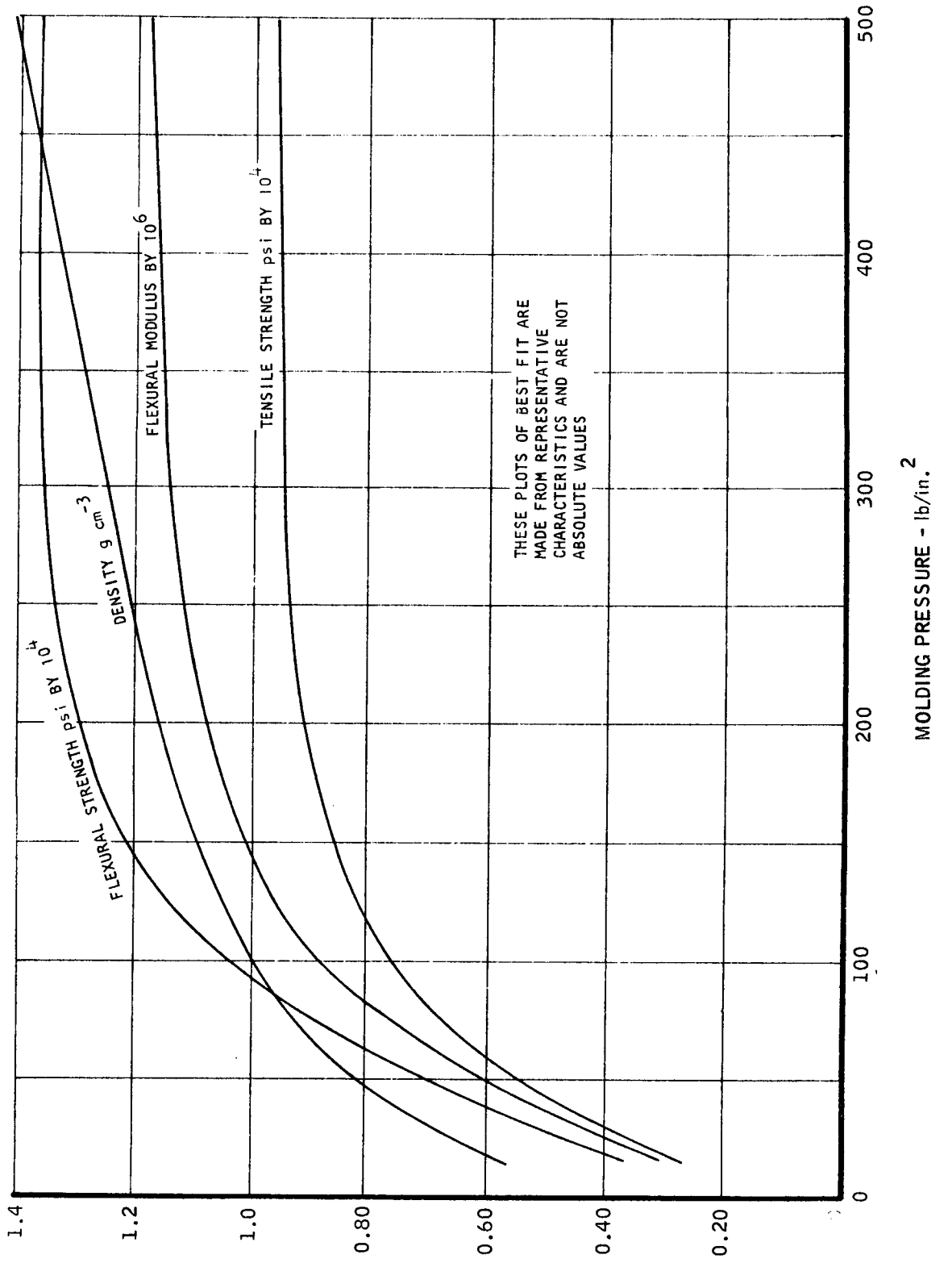
EFFECT OF MOLDING PRESSURE ON PHYSICAL PROPERTIES ASBESTOS-PHENOLIC
FLEXURAL STRENGTH psi BY 10^4
DENSITY g cm^{-3}
FLEXURAL MODULUS BY 10^6
TENSILE STRENGTH psi BY 10^4
THESE PLOTS OF BEST FIT ARE MADE FROM REPRESENTATIVE CHARACTERISTICS AND ARE NOT ABSOLUTE VALUES
1.4
1.2
1.0
0.80
0.60
0.40
0.20
0
100
200
300
400
500
MOLDING PRESSURE - $lb/in.^2$

FIGURE 65

NEG. 4283-3

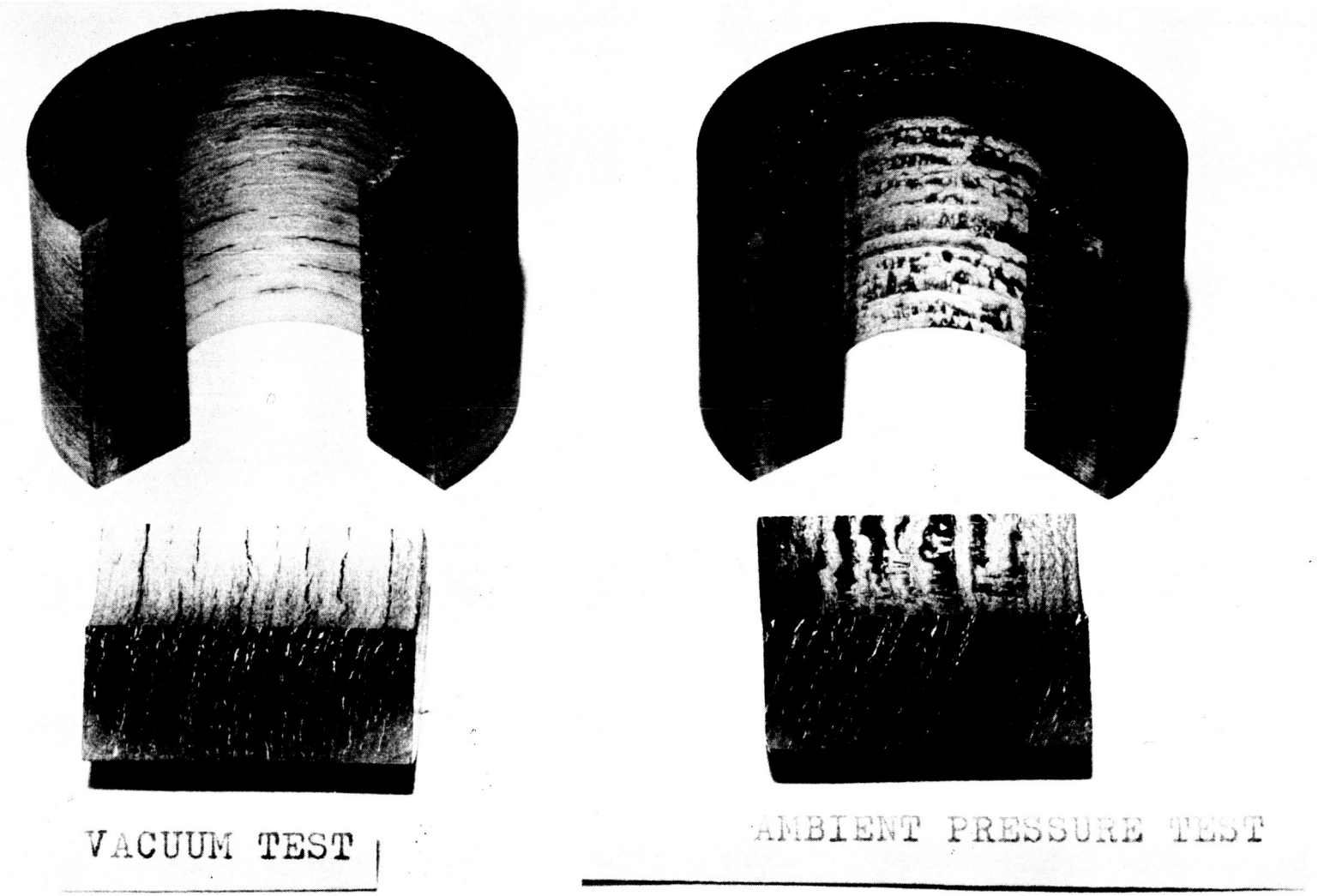

Figure 66 - High Temperature Degradation of Refrasil Phenolic 39 USP Resin System

DEFLECTION vs. TEMPERATURE FOR A REFRASIL - PHENOLIC LAMINATE

ORIENTATION OF GRAIN APPROXIMATELY
30° WITH RESPECT TO LONGITUDINAL AXIS

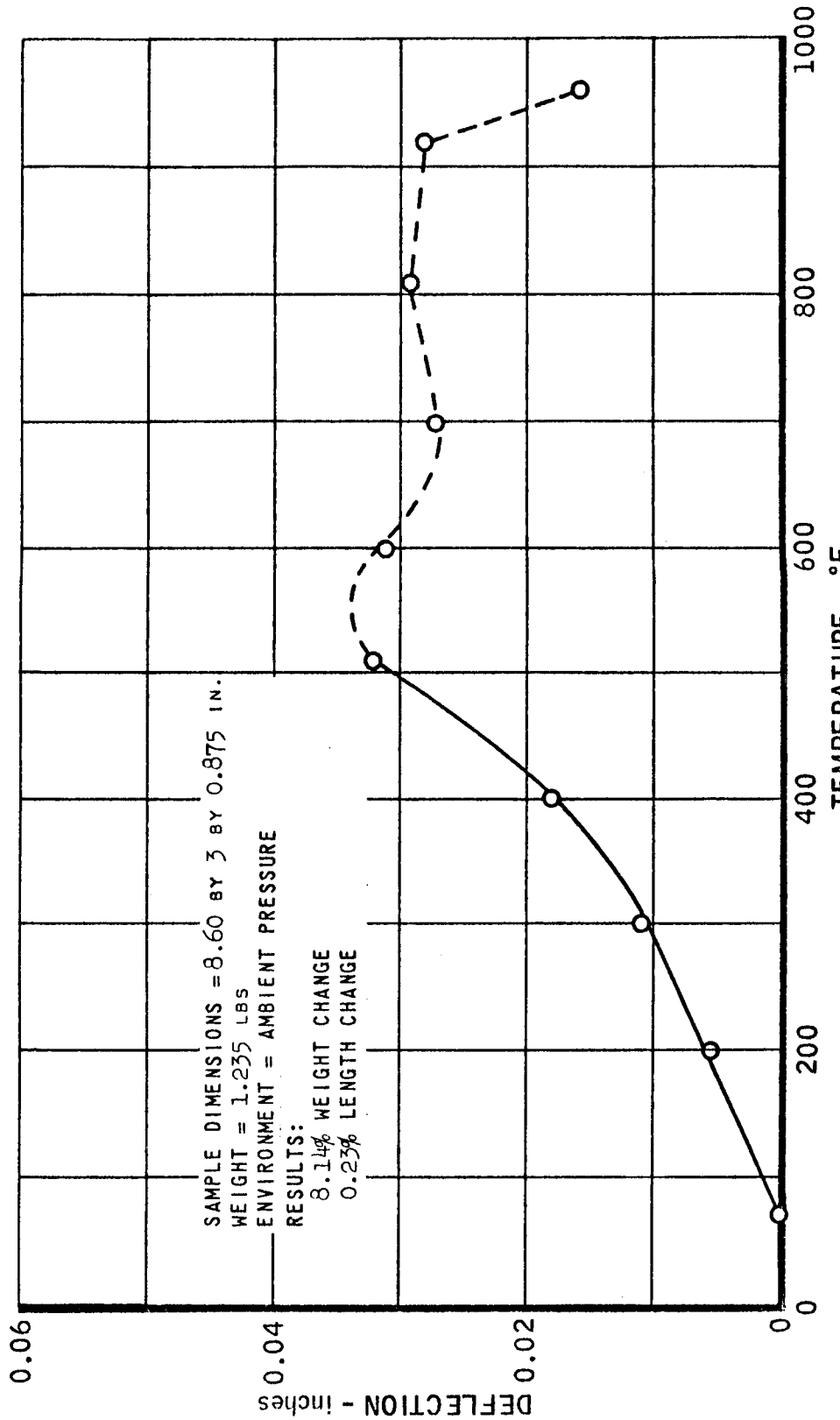

MAC A673

FIGURE 67

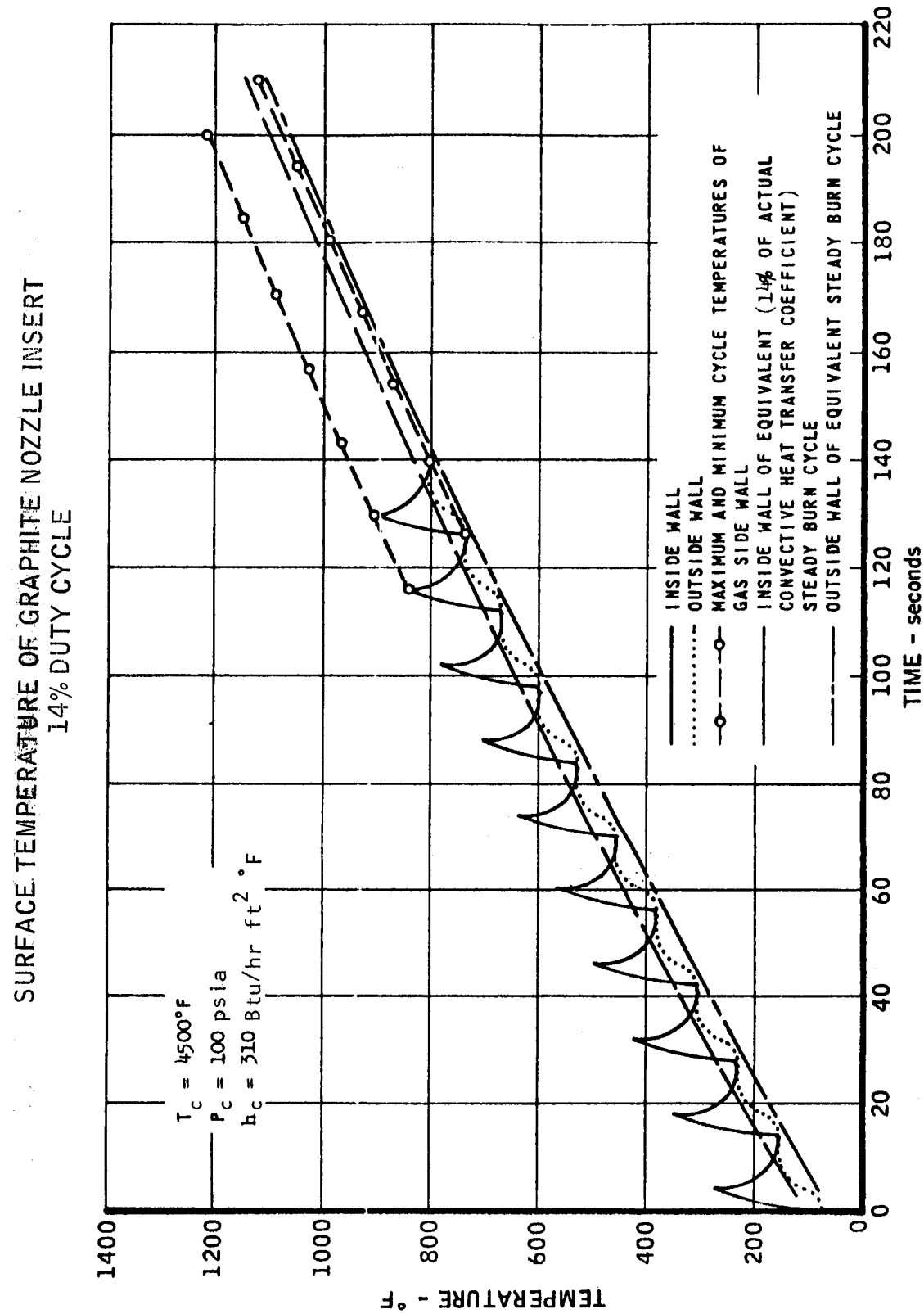

MAC A673

FIGURE 68

CORRELATION OF HEAT TRANSFER FROM AIR STREAM TO WATER FILM

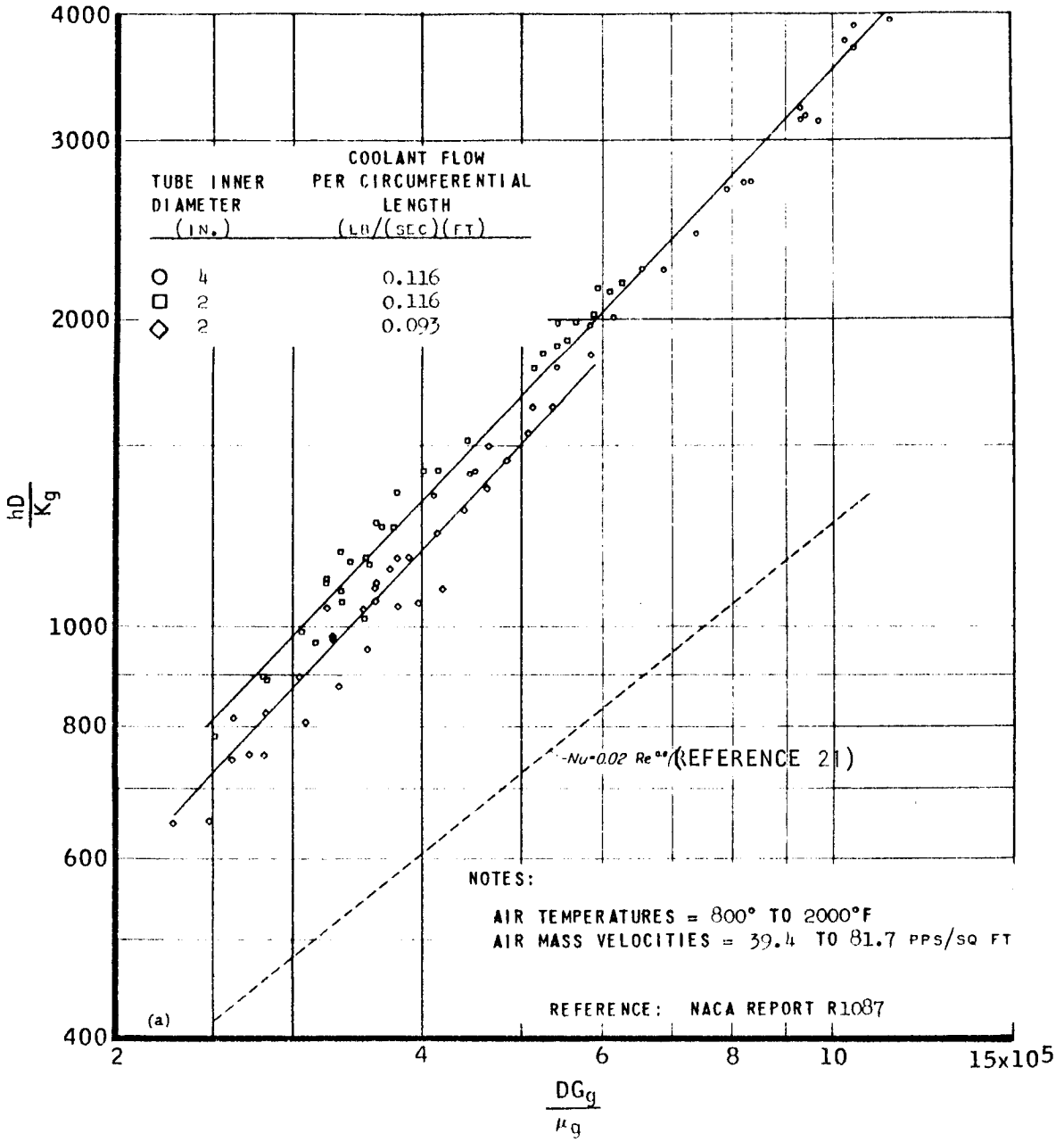

FIGURE 69

VARIATION OF AVERAGE TEST SECTION TEMPERATURE WITH FILM COOLANT FLOW RATE FOR DIFFERENT FILM COOLANTS

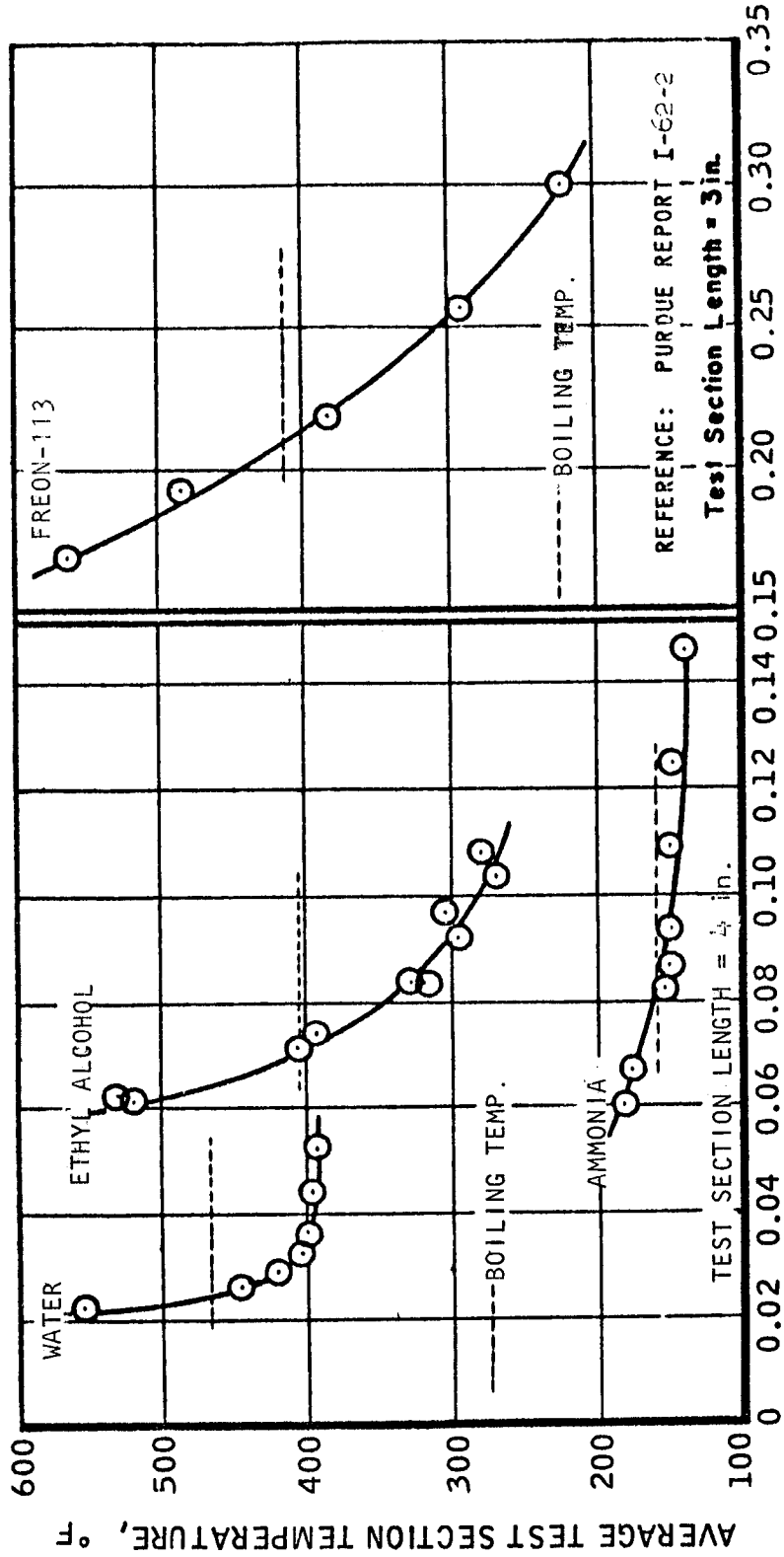

FIGURE 70

VARIATION OF FILM-COOLED LENGTH WITH FILM COOLANT FLOW RATE FOR DIFFERENT FILM COOLANTS

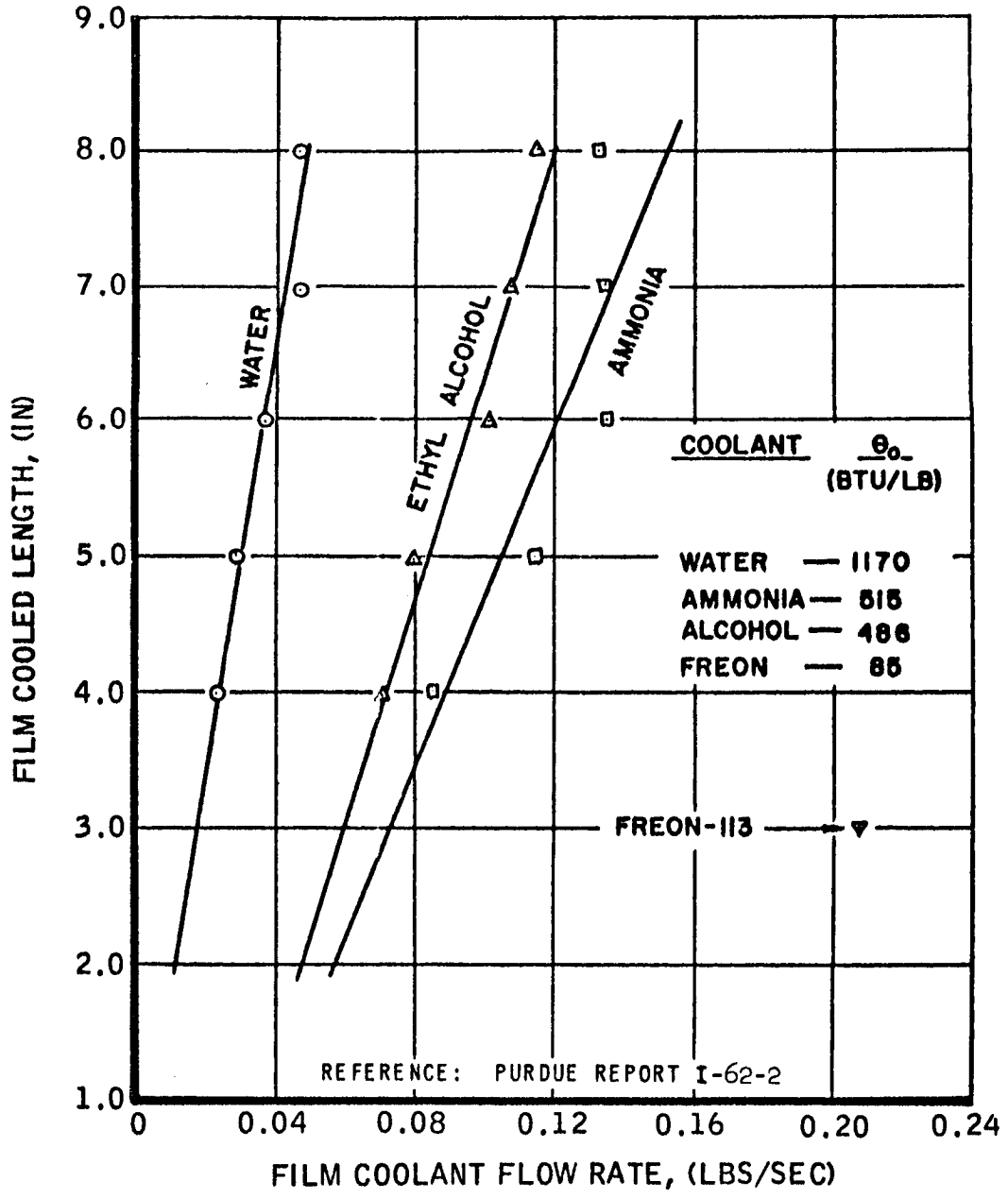

TEMPERATURE RATIO PARAMETER AS A FUNCTION
OF THE LENGTH PARAMETER FOR AMMONIA FILM
COOLANT - GAS STREAM REYNOLDS NO. = 0.55 (10^5)

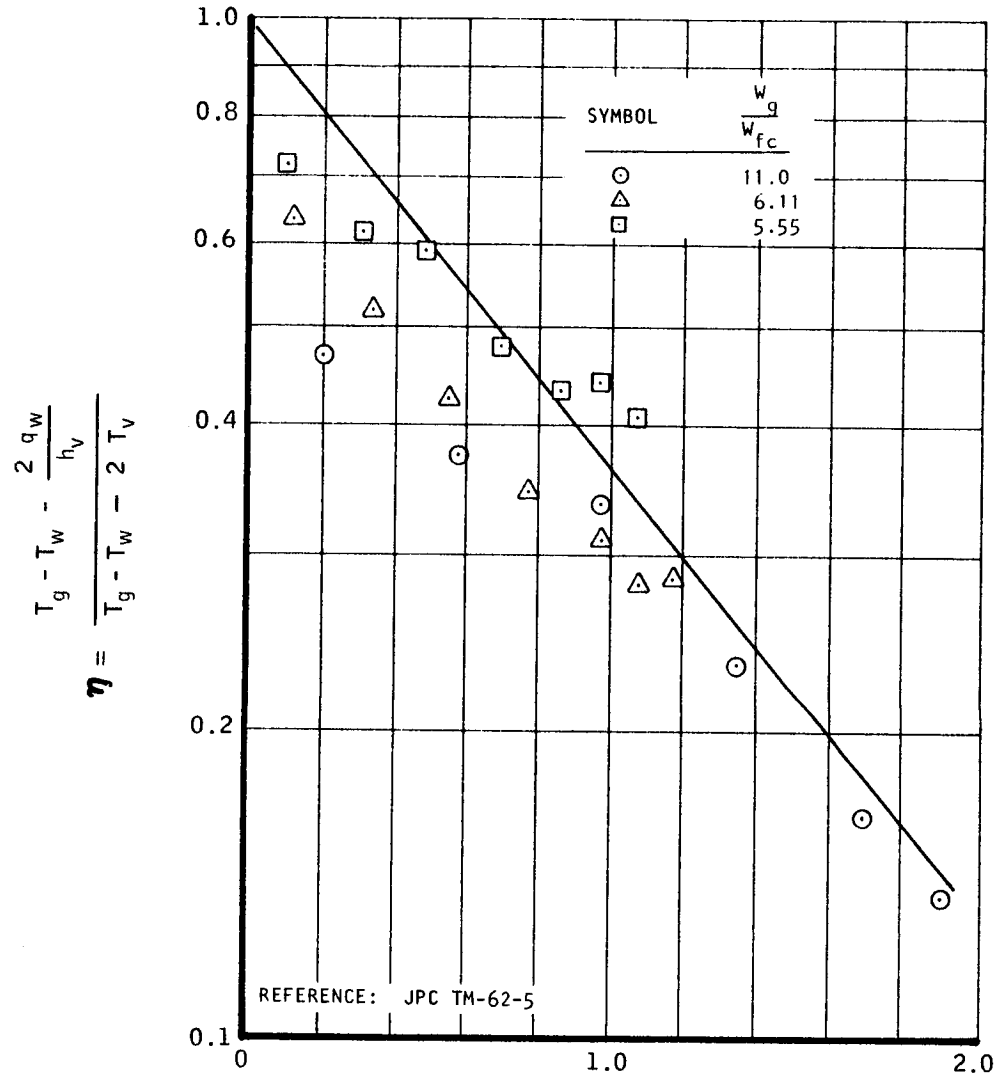

TEMPERATURE RATIO PARAMETER AS A FUNCTION OF THE LENGTH PARAMETER FOR COMBINED FILM AND CONVECTIVE COOLING

$$\beta = \frac{\frac{h_f}{h_w}(T_g - T_v) + \frac{\dot{W}_{fc}\ \Delta H_v}{\pi D L h_w} - \frac{q_w}{h_w}}{\frac{h_f}{h_w}(T_g - T_v) + \frac{\dot{W}_{fc}\ \Delta H_v}{\pi D L h_w} + T_w - T_o}$$

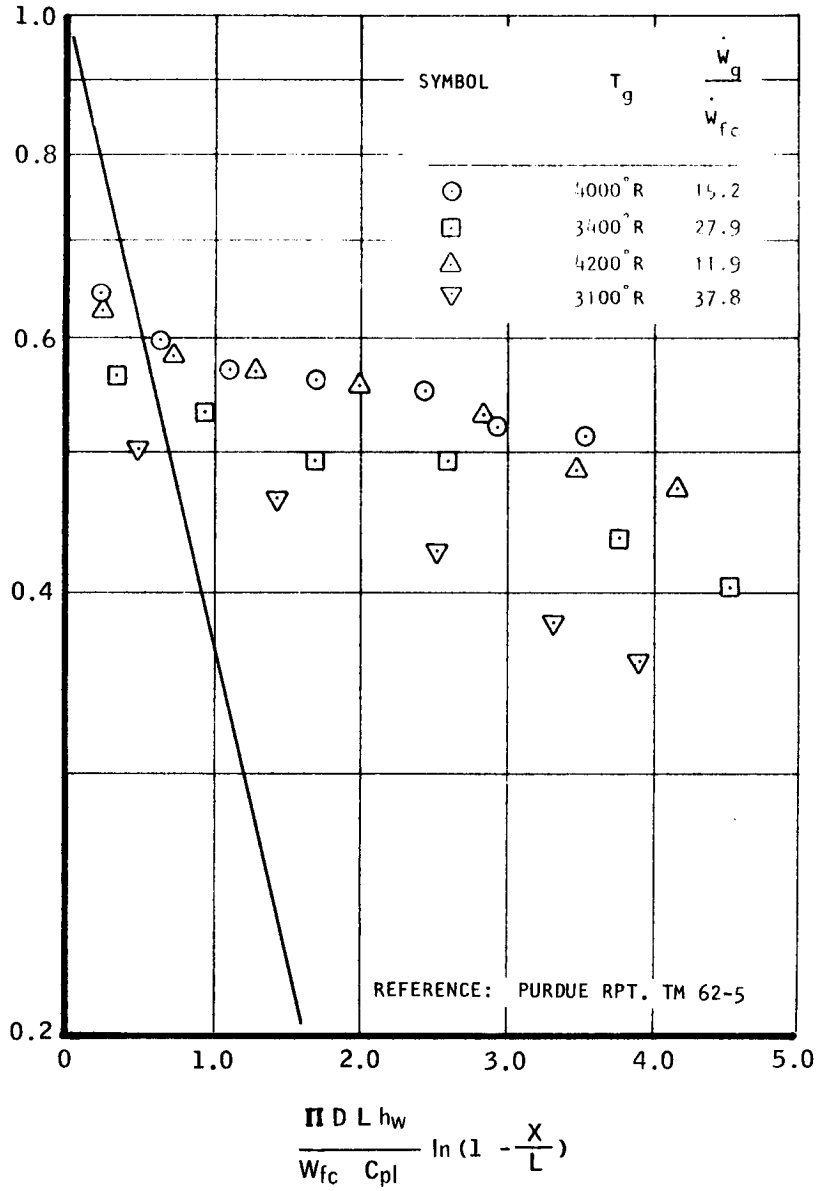

TEMPERATURE RATIO PARAMETER AS A FUNCTION OF THE MODIFIED LENGTH PARAMETER FOR COMBINED FILM AND CONVECTIVE COOLING

$$\beta = \frac{\frac{h_f}{h_w}(T_g - T_v) + \frac{\dot{W}_{fc}\,\Delta H_v}{\pi D L h_w} - \frac{q_w}{h_w}}{\frac{h_f}{h_w}(T_g - T_v) + \frac{\dot{W}_{fc}\,\Delta H_v}{\pi D L h_w} + T_w - T_o}$$

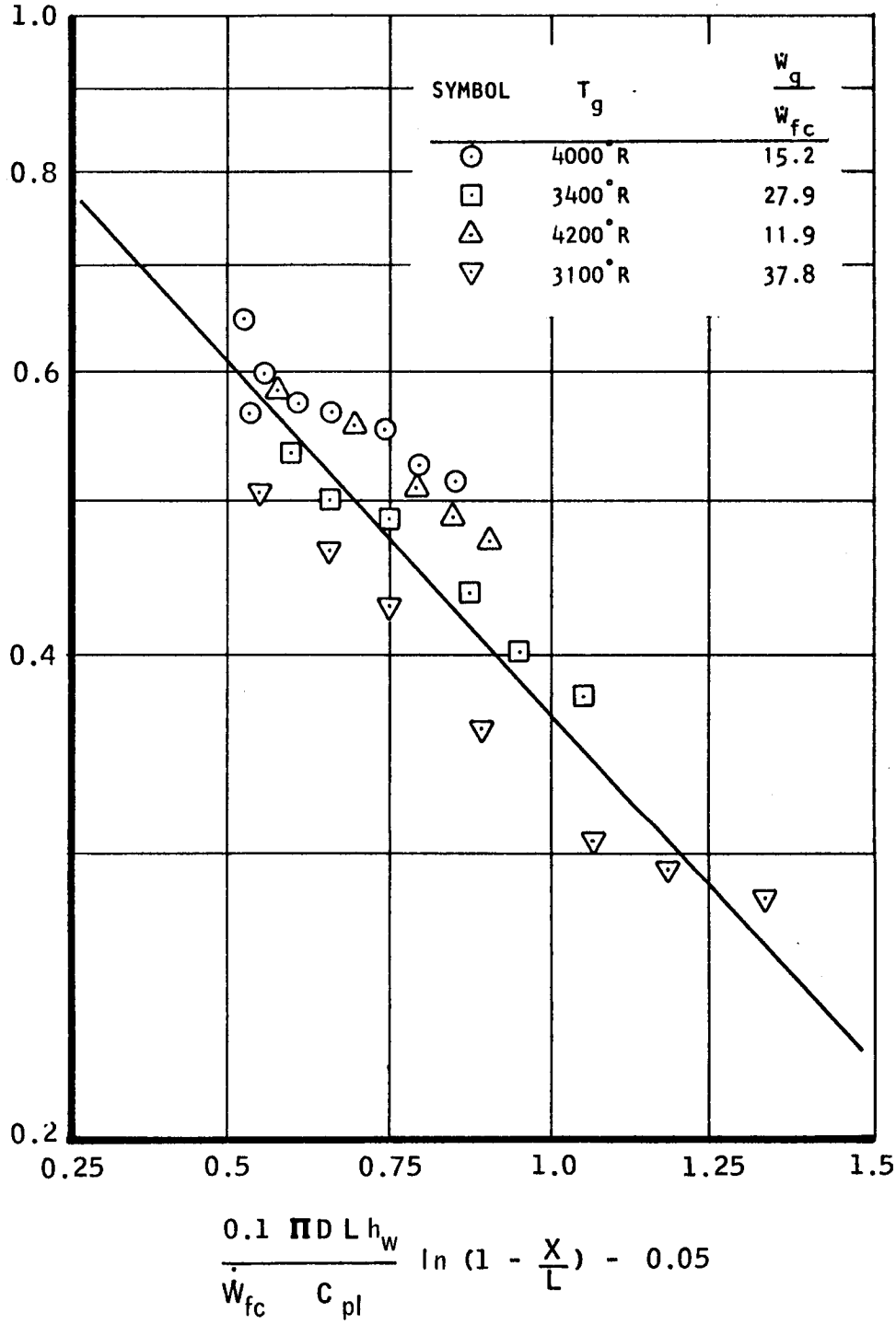

MAC A 673

STANTON NUMBER COMPARISON WITH NACA RESULTS

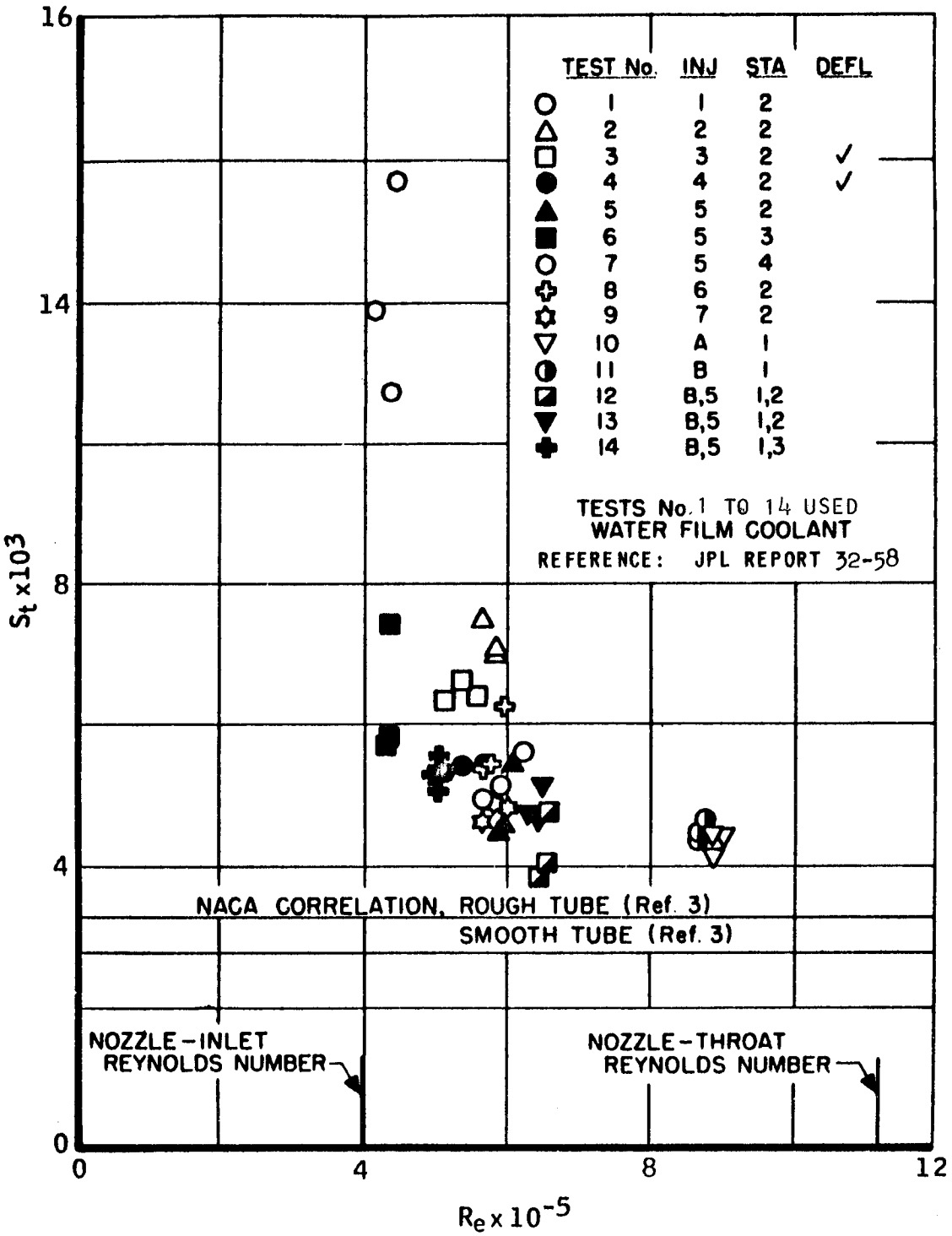

MAC A673

FIGURE 75

MOTOR PERFORMANCE DECREASE WITH FILM COOLING

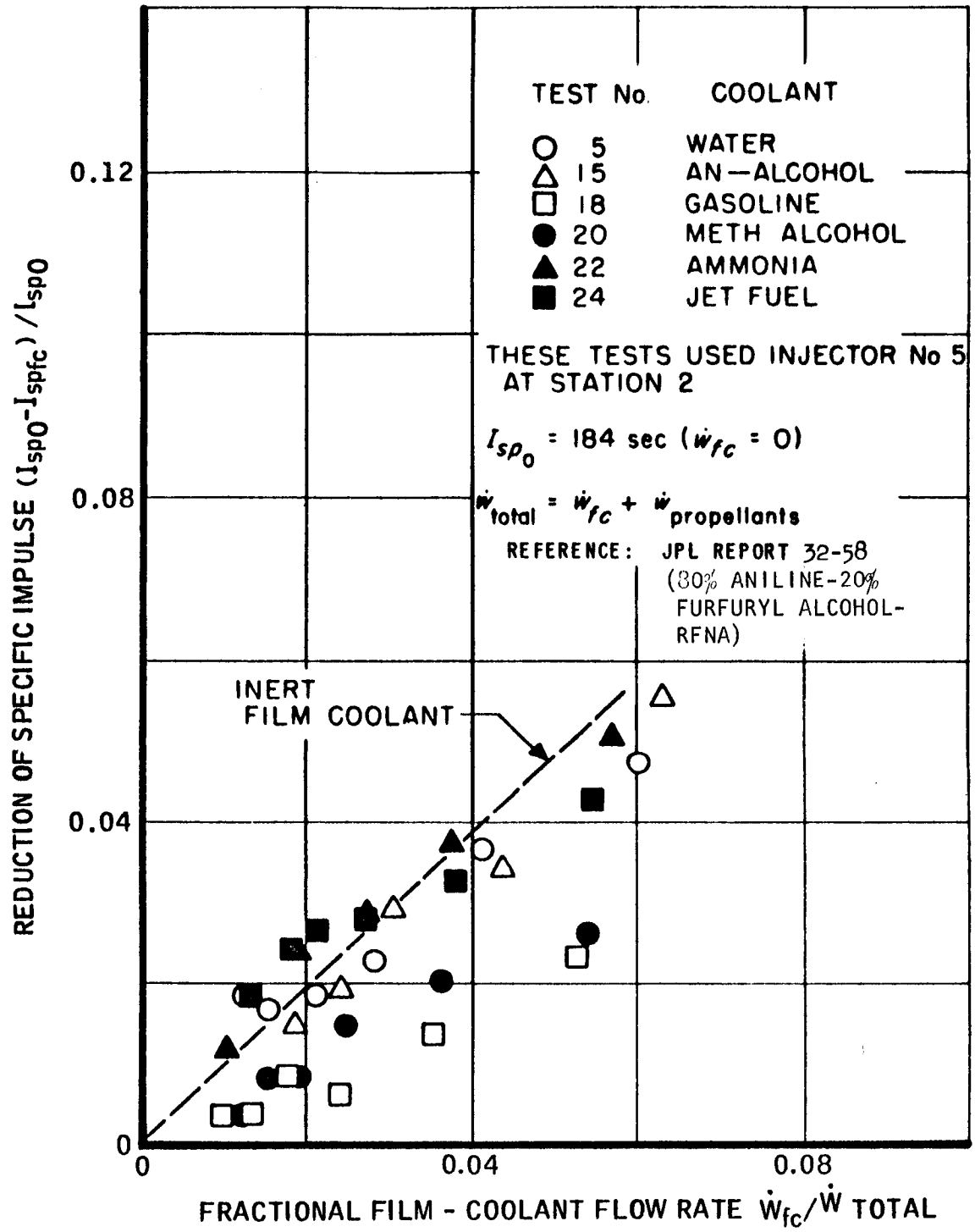

MAC A673

FIGURE 76

STABILITY EFFECTIVENESS vs. DIMENSIONLESS FILM COOLANT FLOW

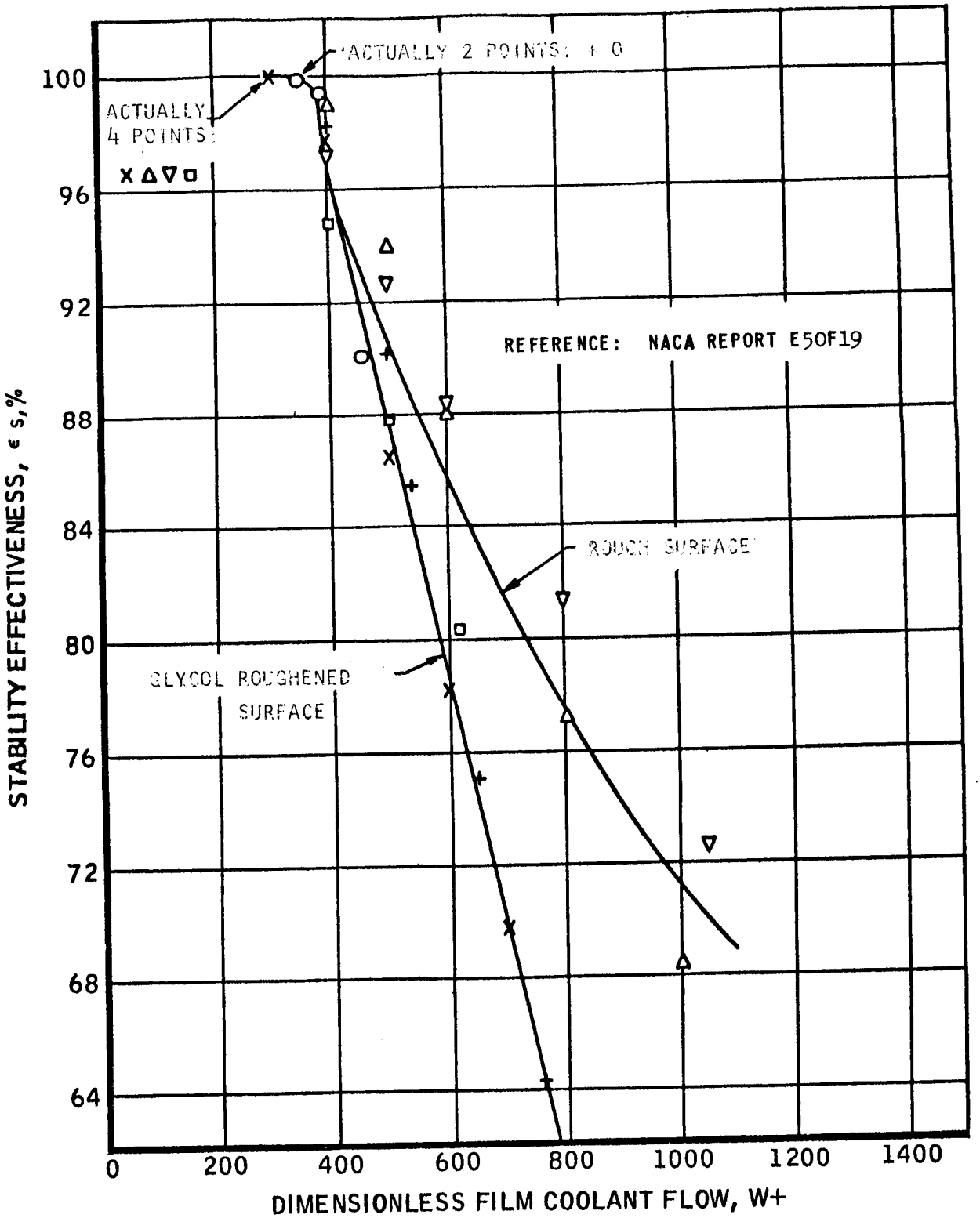

VARIATION OF FILM COOLED LENGTH WITH FILM COOLANT FLOW RATE

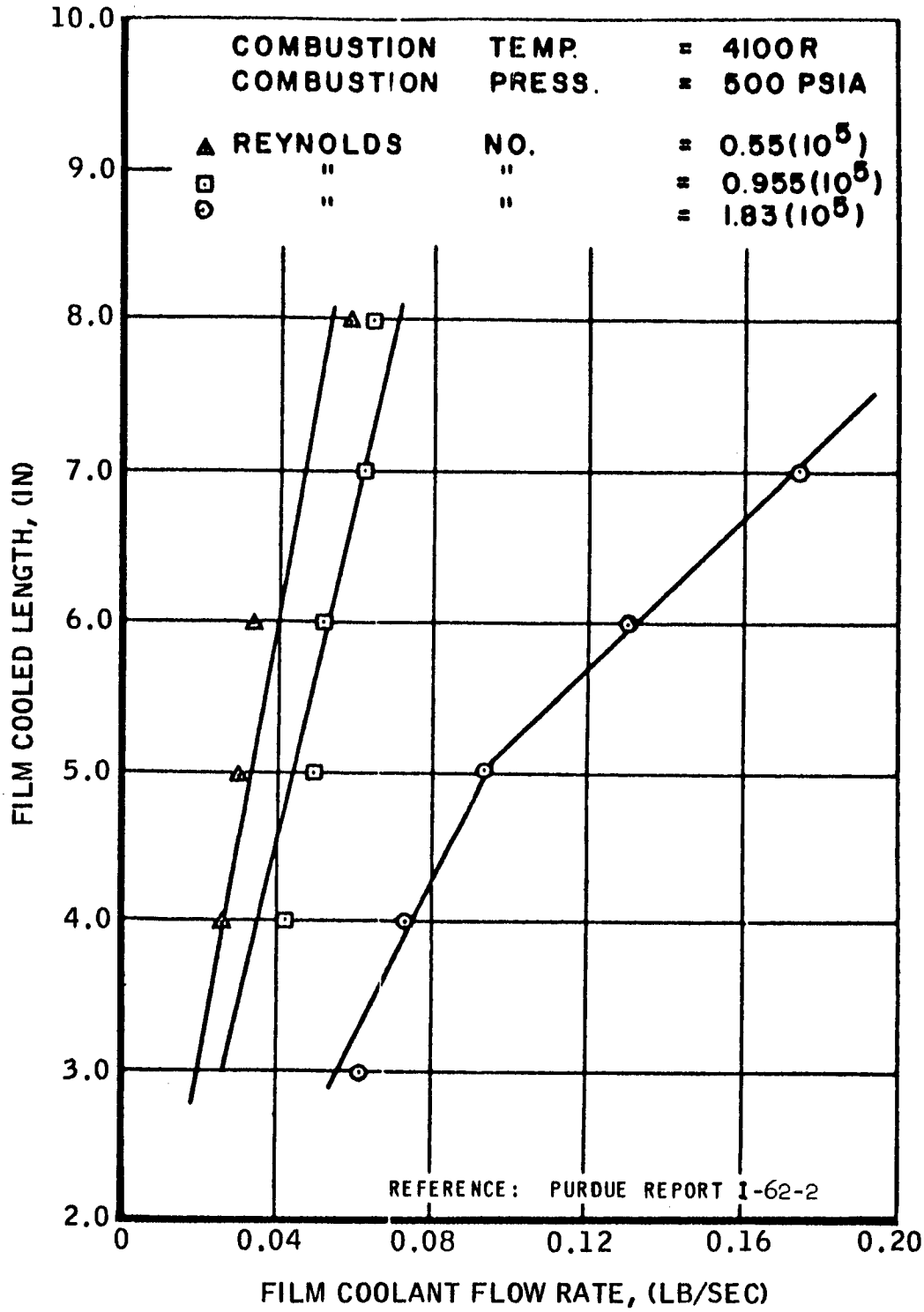

MAC A673

NASA HELIUM COOLANT DATA FOR SLOT HEIGHT OF 1/8 inch

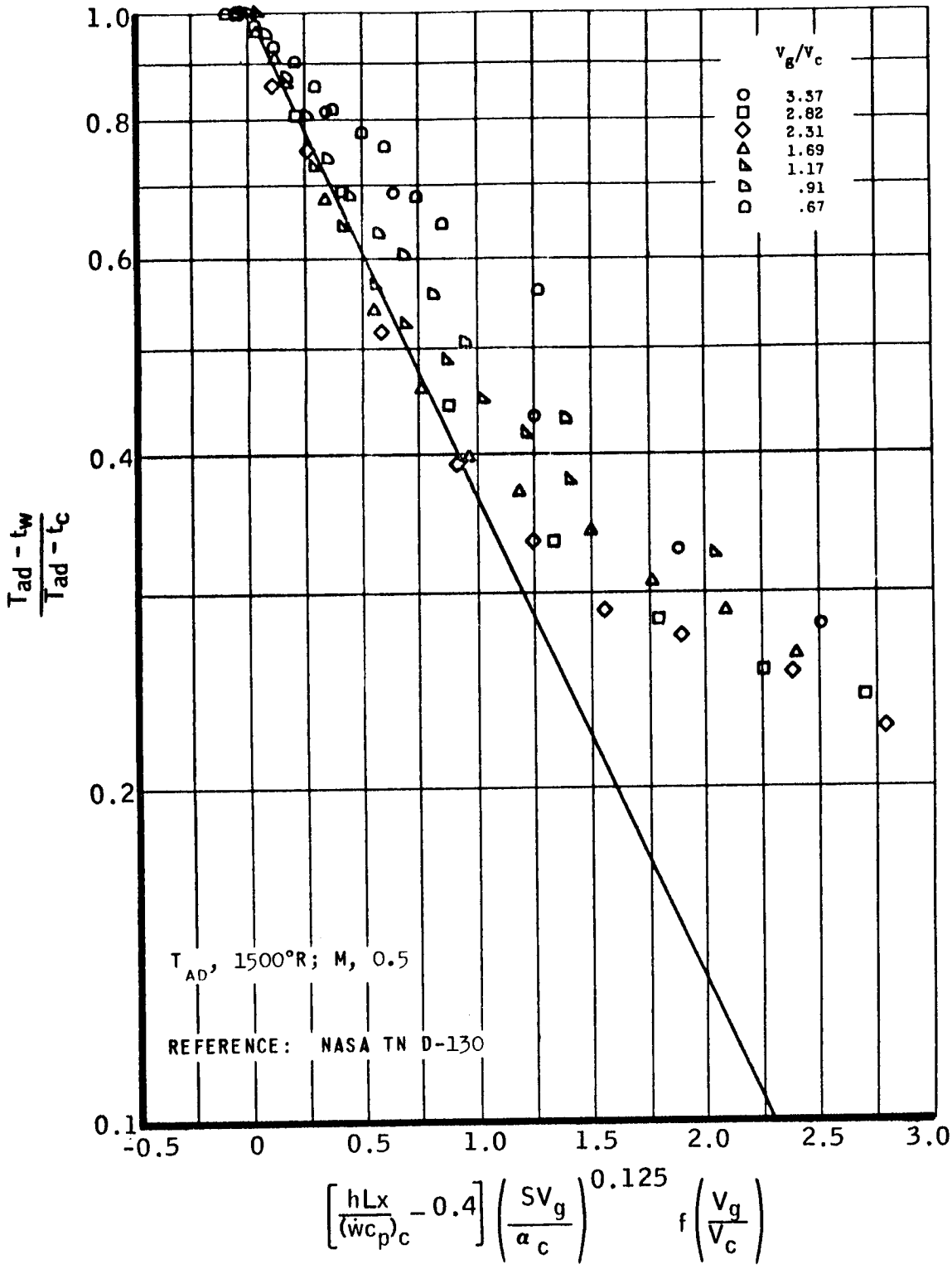

COMPARISON OF MEASURED TURBULENT STANTON NUMBERS WITH AVAILABLE THEORIES

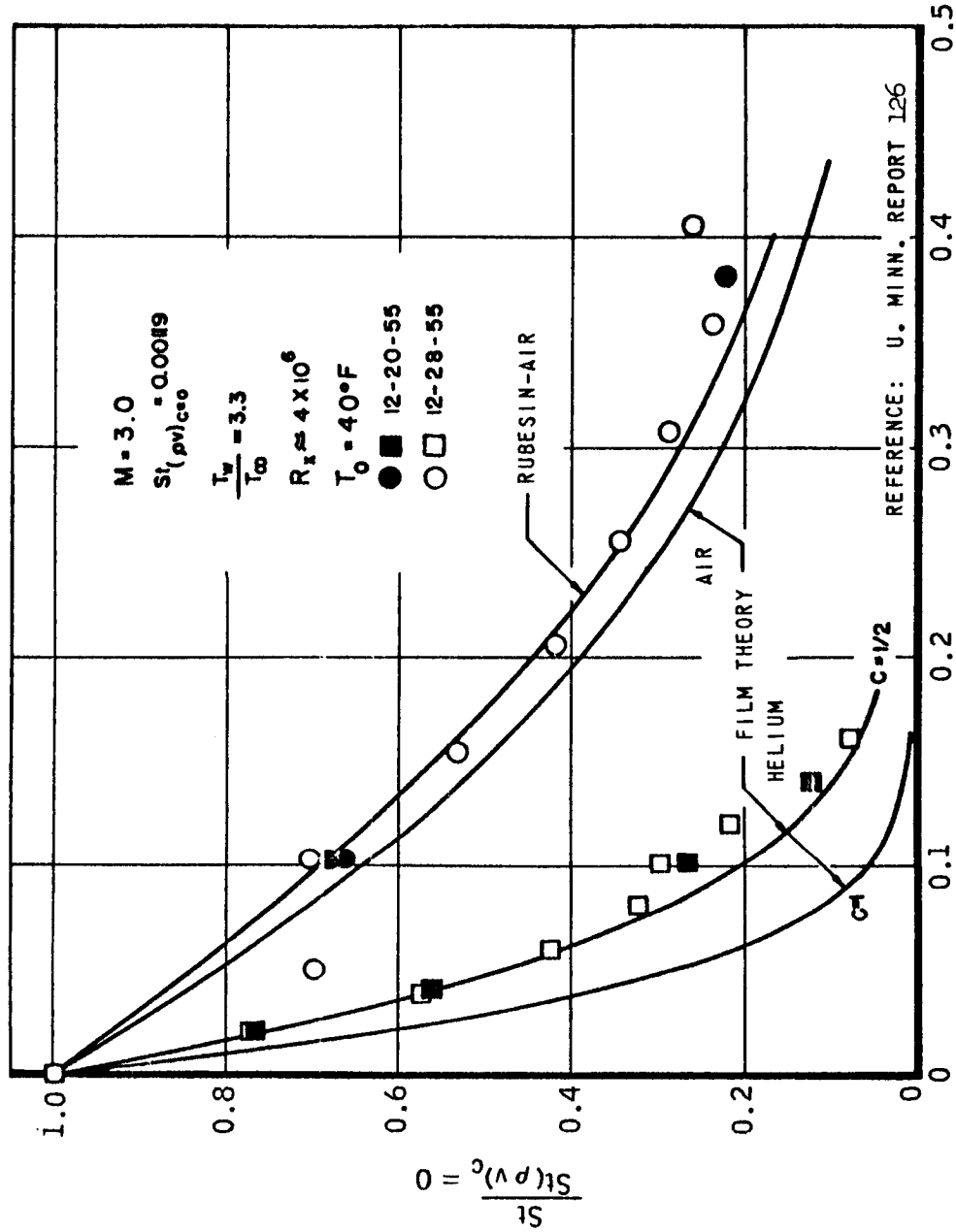

MAC A673

FIGURE 80

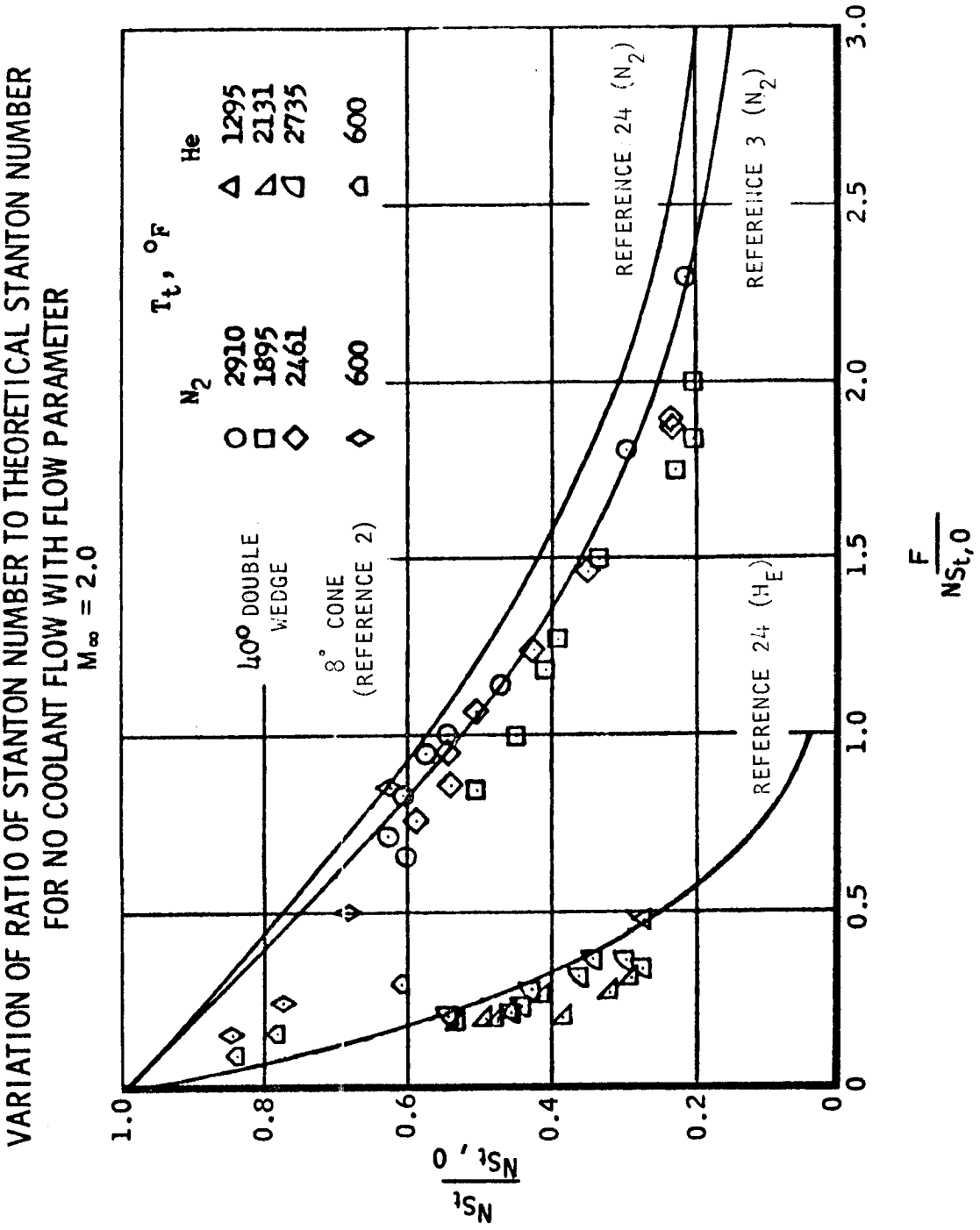
VARIATION OF RATIO OF STANTON NUMBER TO THEORETICAL STANTON NUMBER FOR NO COOLANT FLOW WITH FLOW PARAMETER
$M_\infty = 2.0$
T_t, °F
N_2
2910
1895
2461
600
He
1295
2131
2735
600
40° DOUBLE WEDGE
8° CONE (REFERENCE 2)
REFERENCE 24 (N_2)
REFERENCE 3 (N_2)
REFERENCE 24 (H_E)
$\frac{N_{St,0}}{N_{St}}$
$\frac{F}{N_{St,0}}$
1.0
0.8
0.6
0.4
0.2
0
0
0.5
1.0
1.5
2.0
2.5
3.0

FIGURE 81

LIQUID FILM COOLING THRUST CHAMBER DESIGN LAYOUT

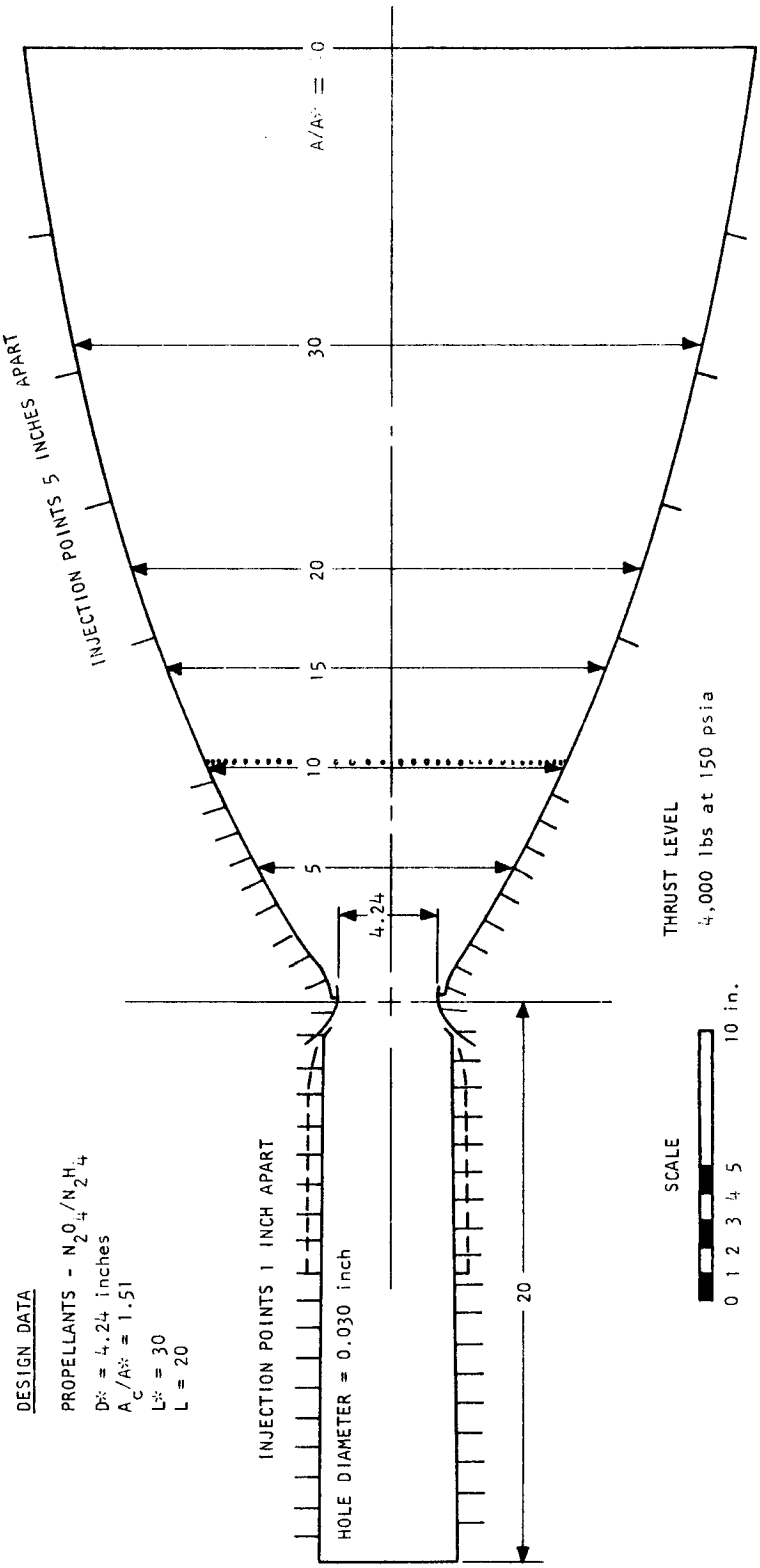

MAC A673

FIGURE 82

GAS FILM COOLING THRUST CHAMBER DESIGN LAYOUT

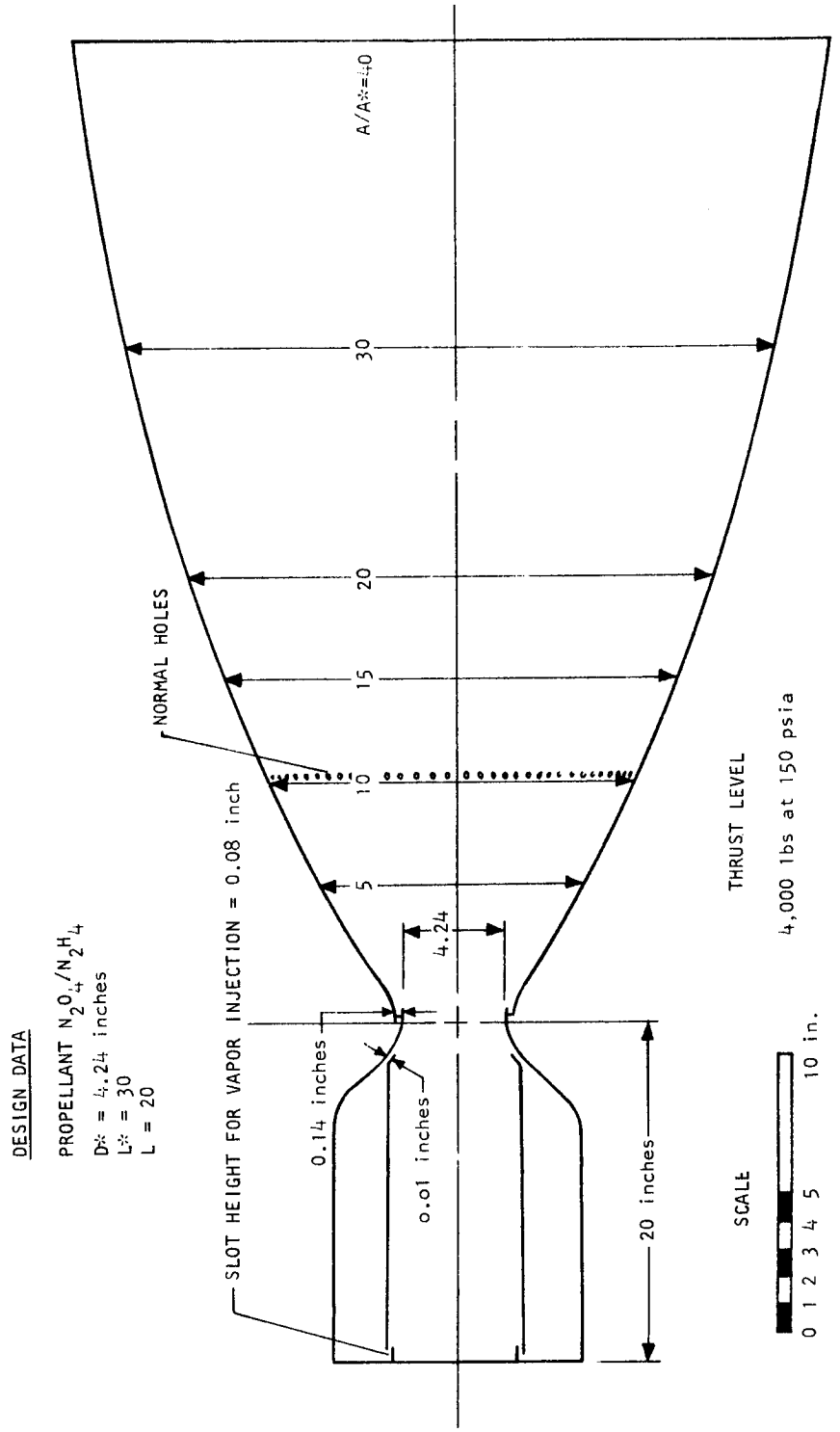

LIQUID FILM COOLING REQUIREMENTS FOR THE DIVERGENT AND CONVERGENT NOZZLE SECTIONS

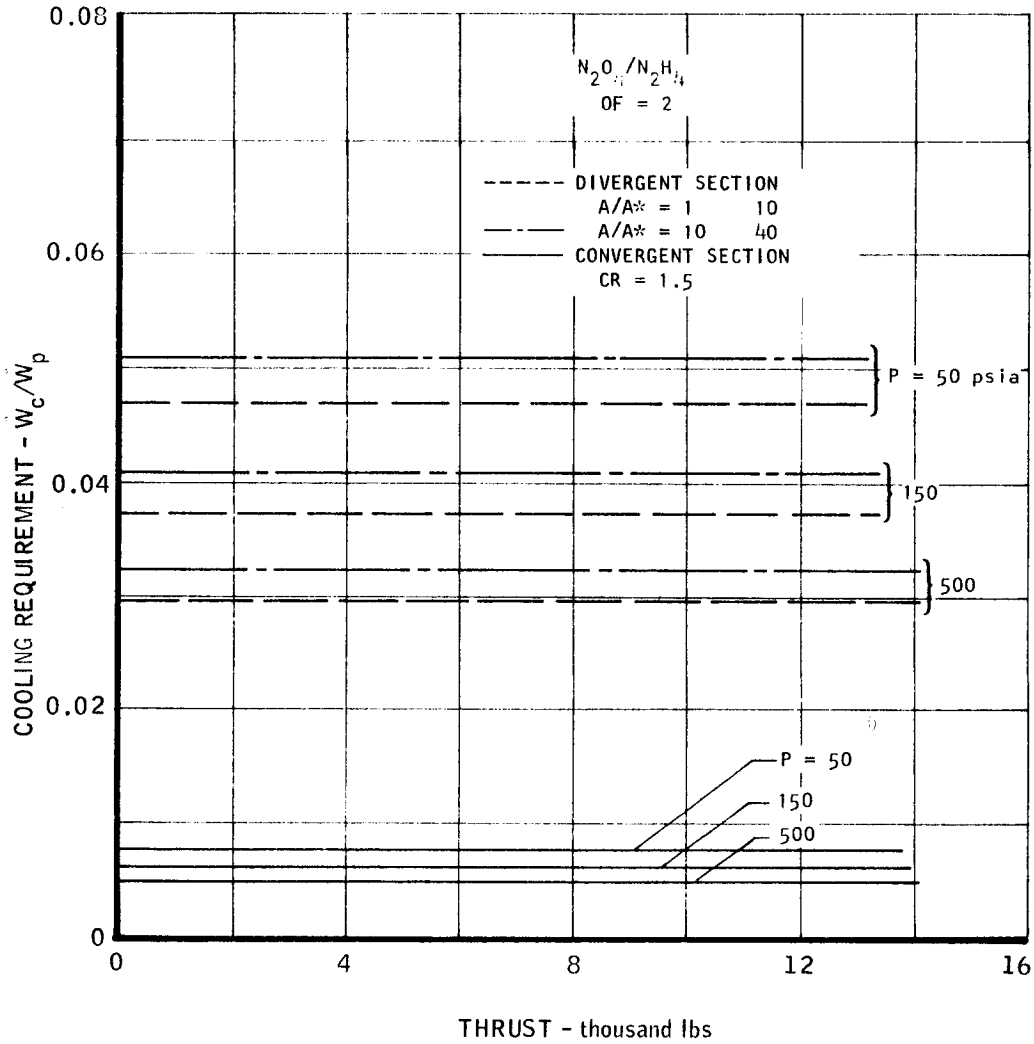

GAS FILM COOLING REQUIREMENTS FOR THE CONVERGENT NOZZLE SECTION

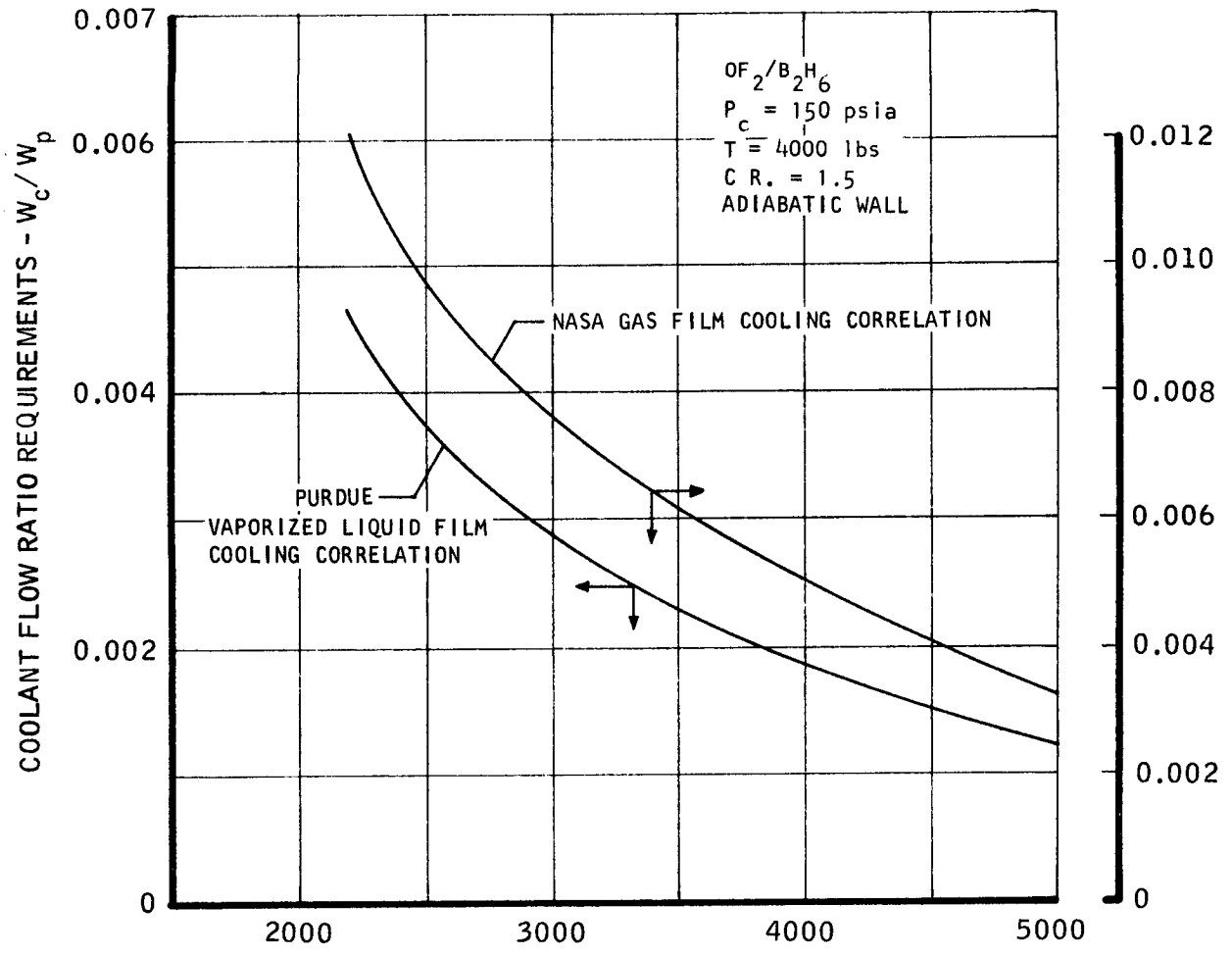

MAC A673

FIGURE 85

SURFACE TEMPERATURE OF SEMI - INFINITE SOLID WITH FORCED SURFACE CONVECTION

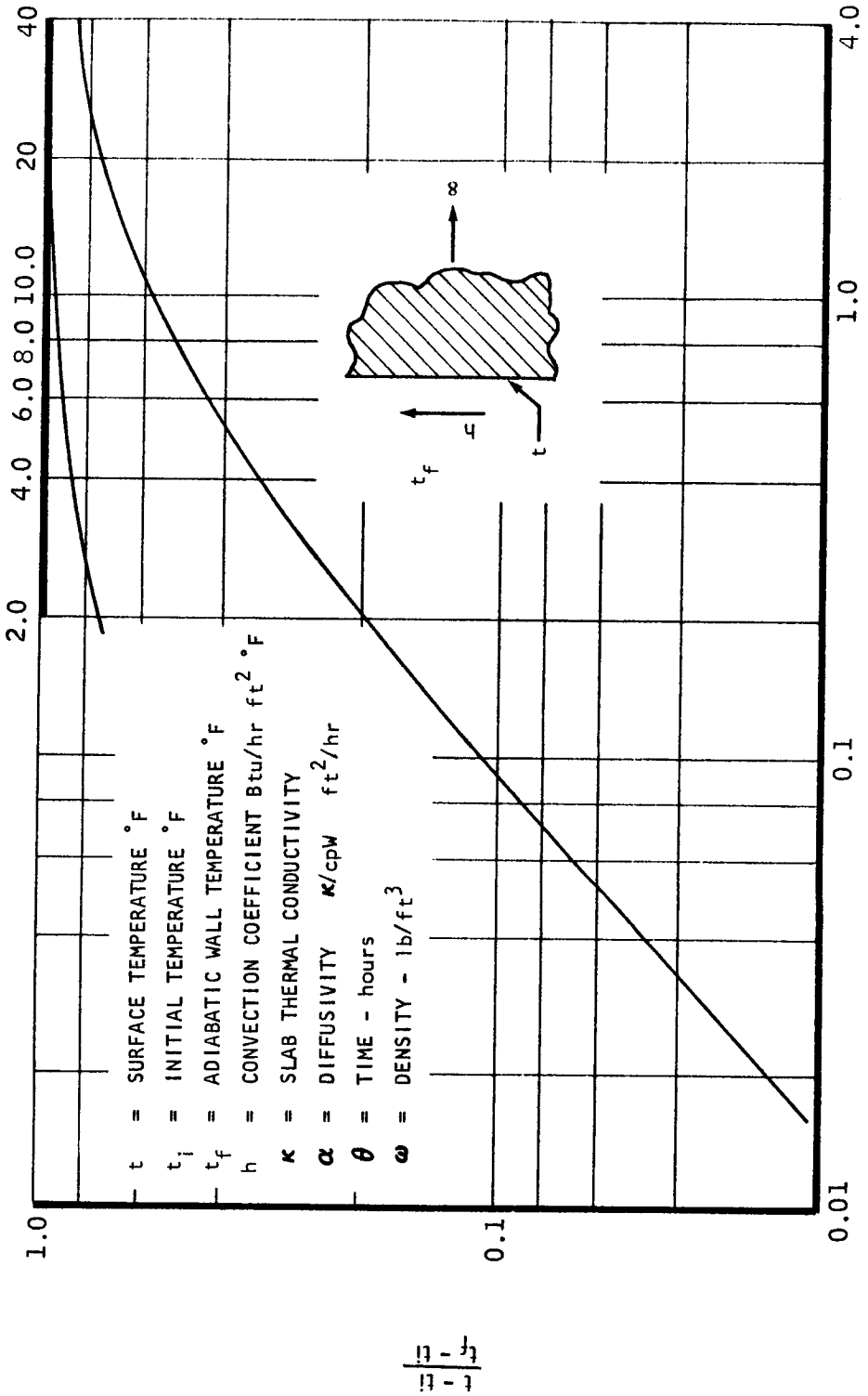

MAC A673

FIGURE 86

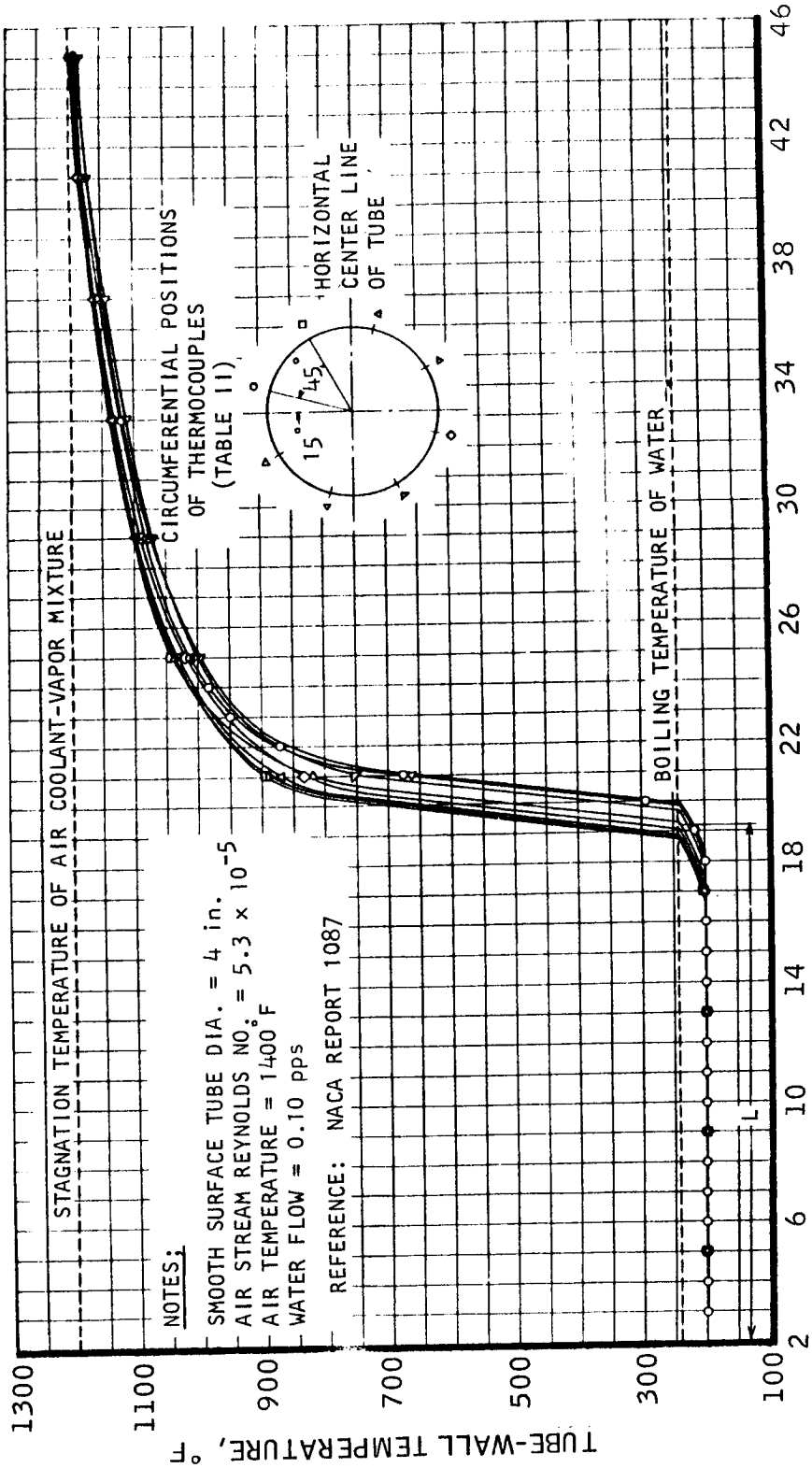

MAC A673

FIGURE 87

SURFACE TEMPERATURE VERSUS TIME
CONTINUOUS, 50%, AND 14% OPERATION OF GRAPHITE NOZZLE INSERT
CASE I CONFIGURATION

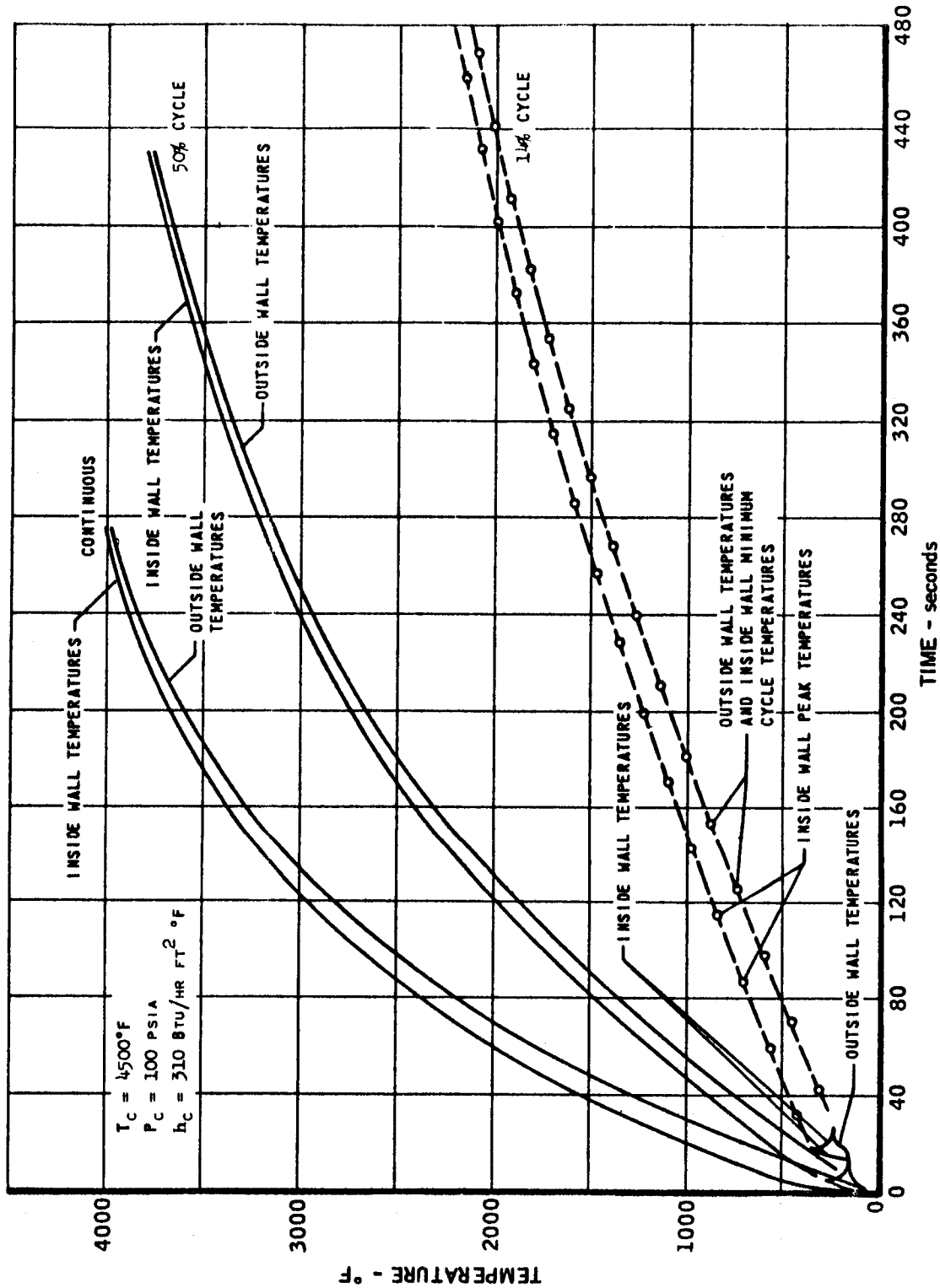

MAC A673

FIGURE 88

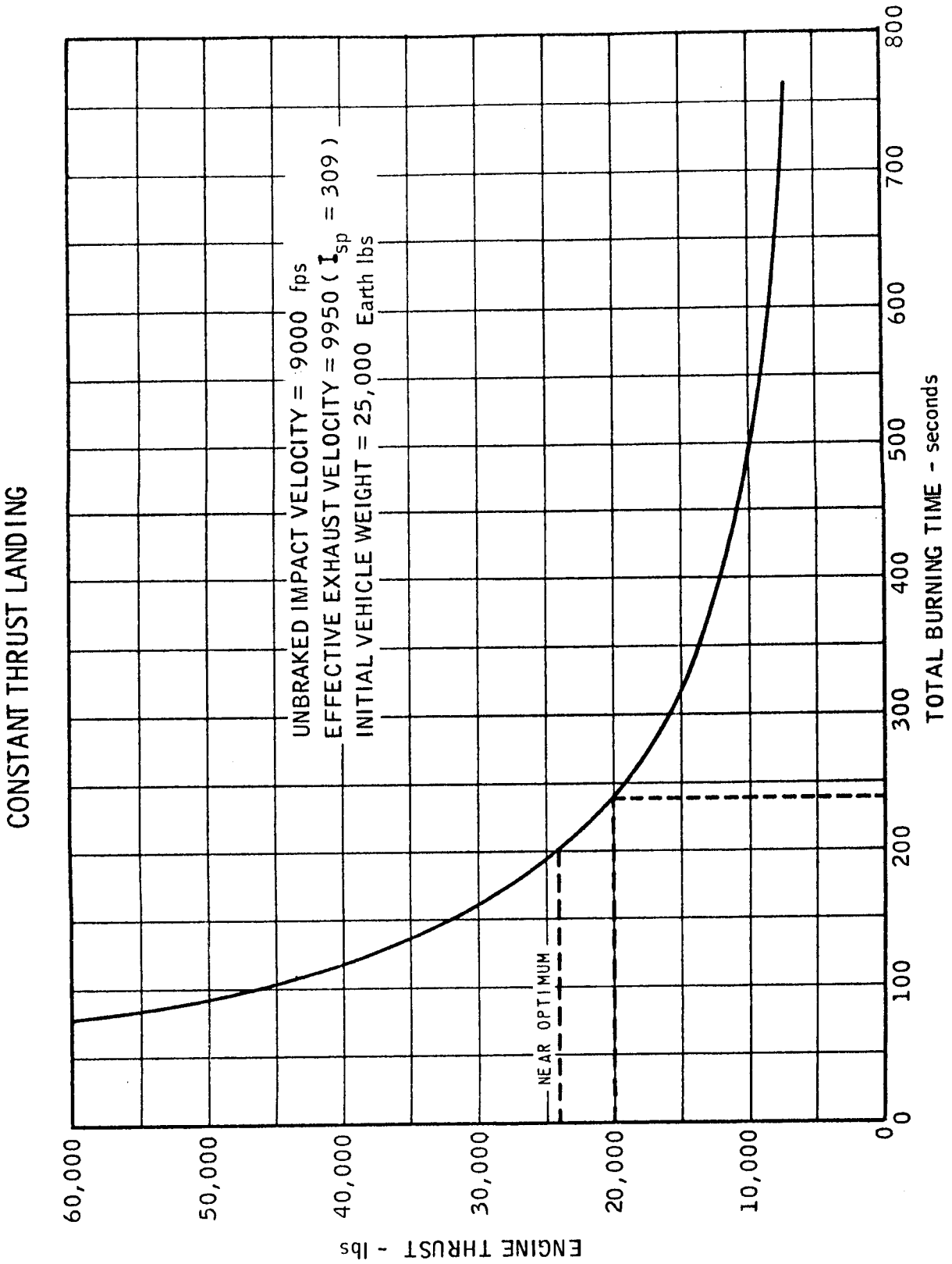
CONSTANT THRUST LANDING
UNBRAKED IMPACT VELOCITY = 9000 fps
EFFECTIVE EXHAUST VELOCITY = 9950 (I_{sp} = 309)
INITIAL VEHICLE WEIGHT = 25,000 Earth lbs
NEAR OPTIMUM
ENGINE THRUST - lbs
60,000
50,000
40,000
30,000
20,000
10,000
0
TOTAL BURNING TIME - seconds
0
100
200
300
400
500
600
700
800

FIGURE 89

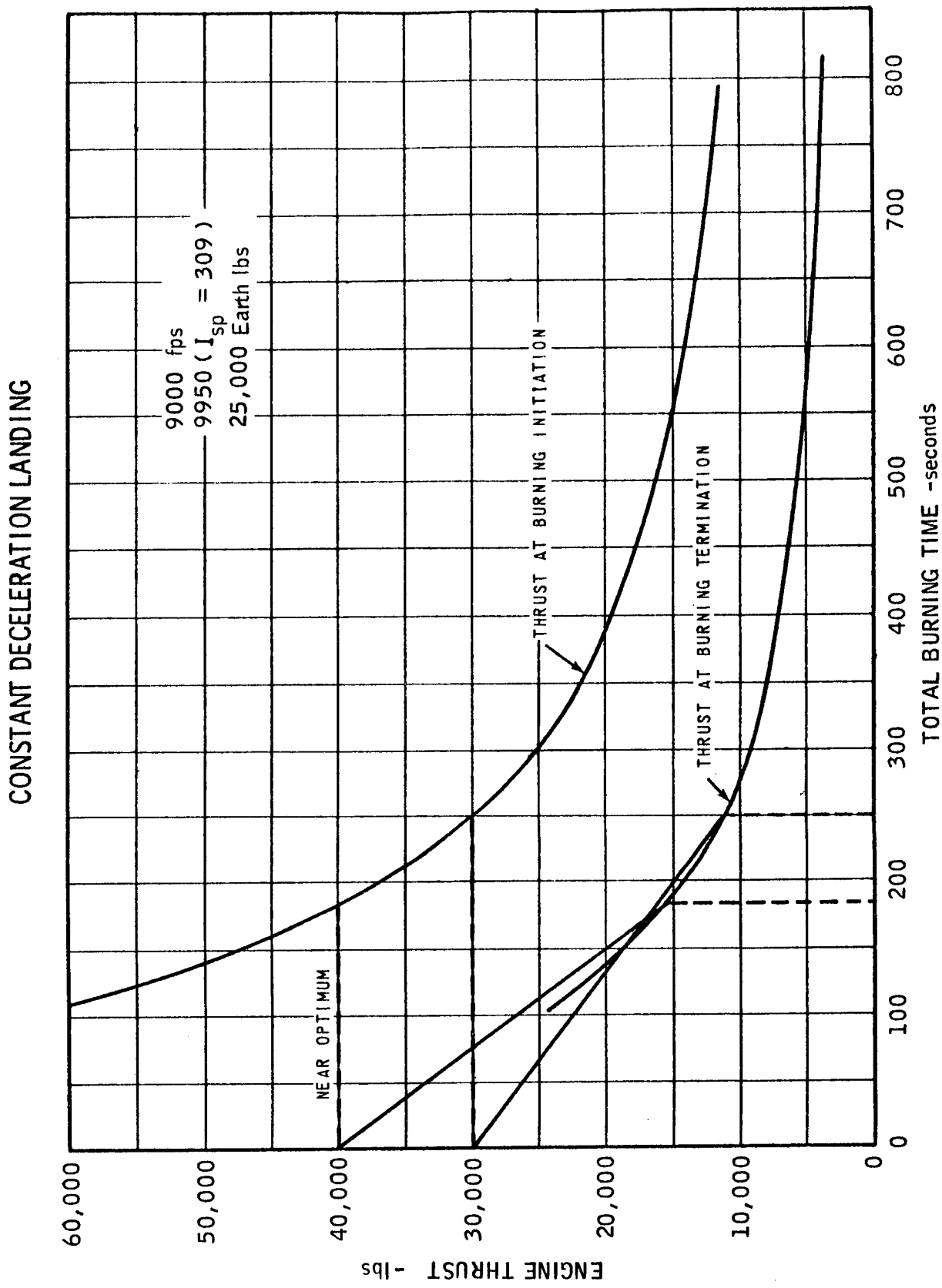

MAC A678

FIGURE 90

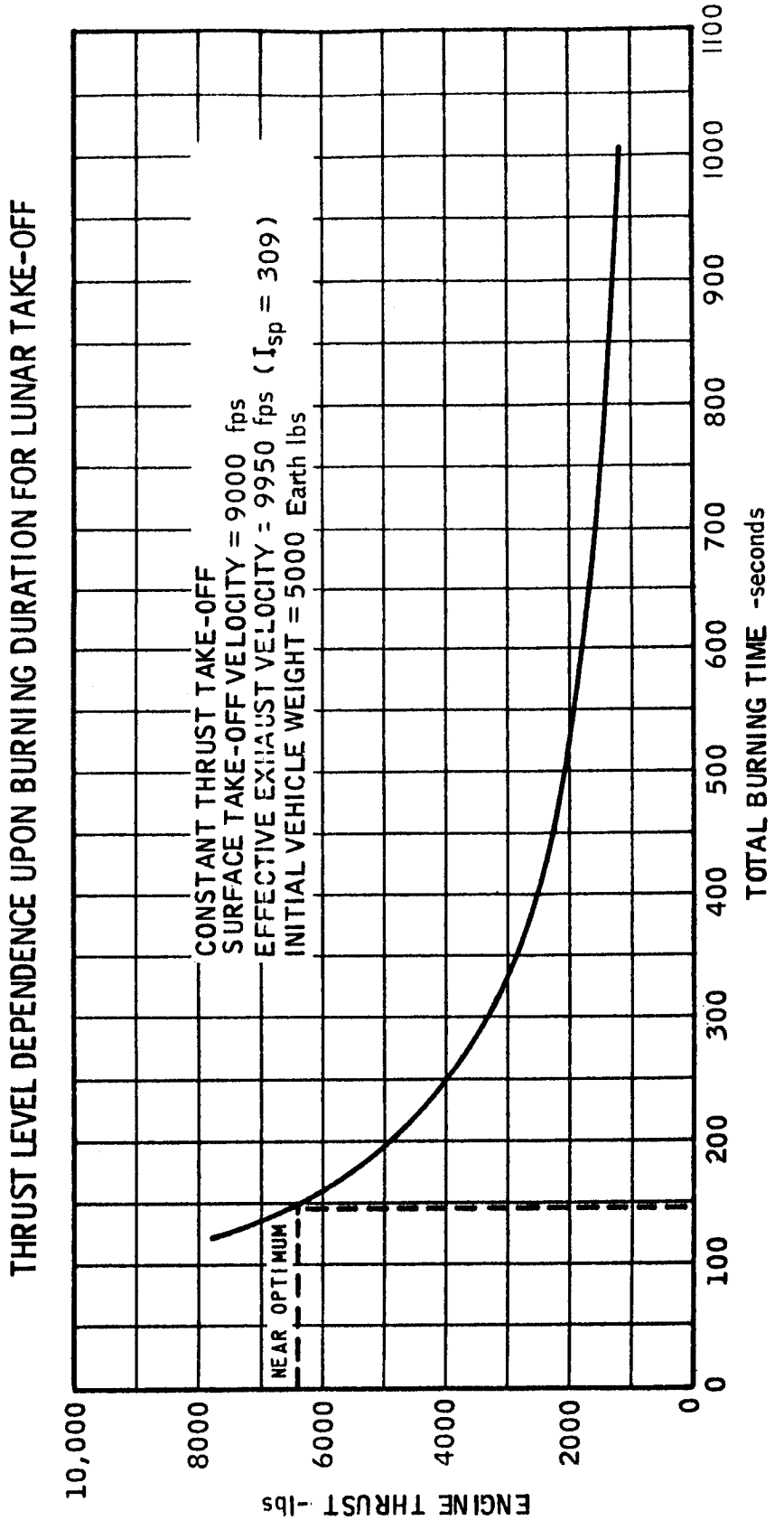
THRUST LEVEL DEPENDENCE UPON BURNING DURATION FOR LUNAR TAKE-OFF
CONSTANT THRUST TAKE-OFF
SURFACE TAKE-OFF VELOCITY = 9000 fps
EFFECTIVE EXHAUST VELOCITY = 9950 fps (I_{sp} = 309)
INITIAL VEHICLE WEIGHT = 5000 Earth lbs
NEAR OPTIMUM
ENGINE THRUST -lbs
10,000
8000
6000
4000
2000
0
TOTAL BURNING TIME -seconds
0
100
200
300
400
500
600
700
800
900
1000
1100

APOLLO SPACECRAFT CONFIGURATION FOR LUNAR LANDING
(TYPICAL ENGINE LOCATIONS)

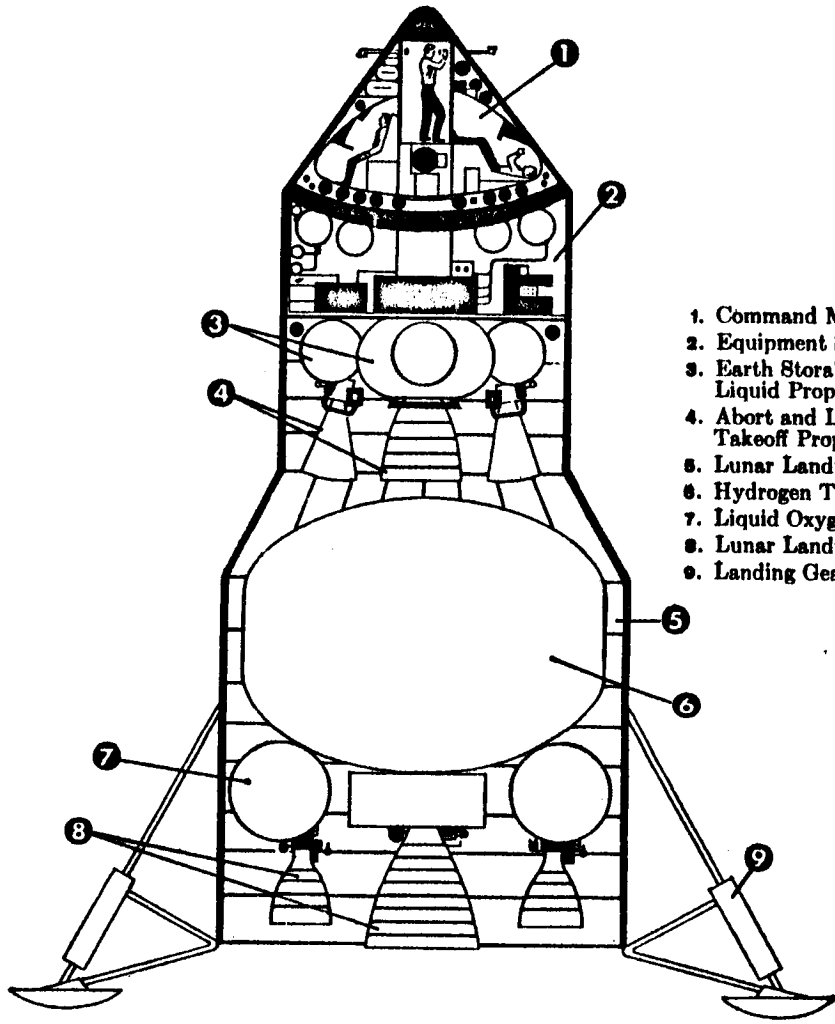

MAC A 673

NOVA LUNAR ORBITING AND RETURN MISSION CONFIGURATION, SELECTED ALTERNATE 3 - C_1

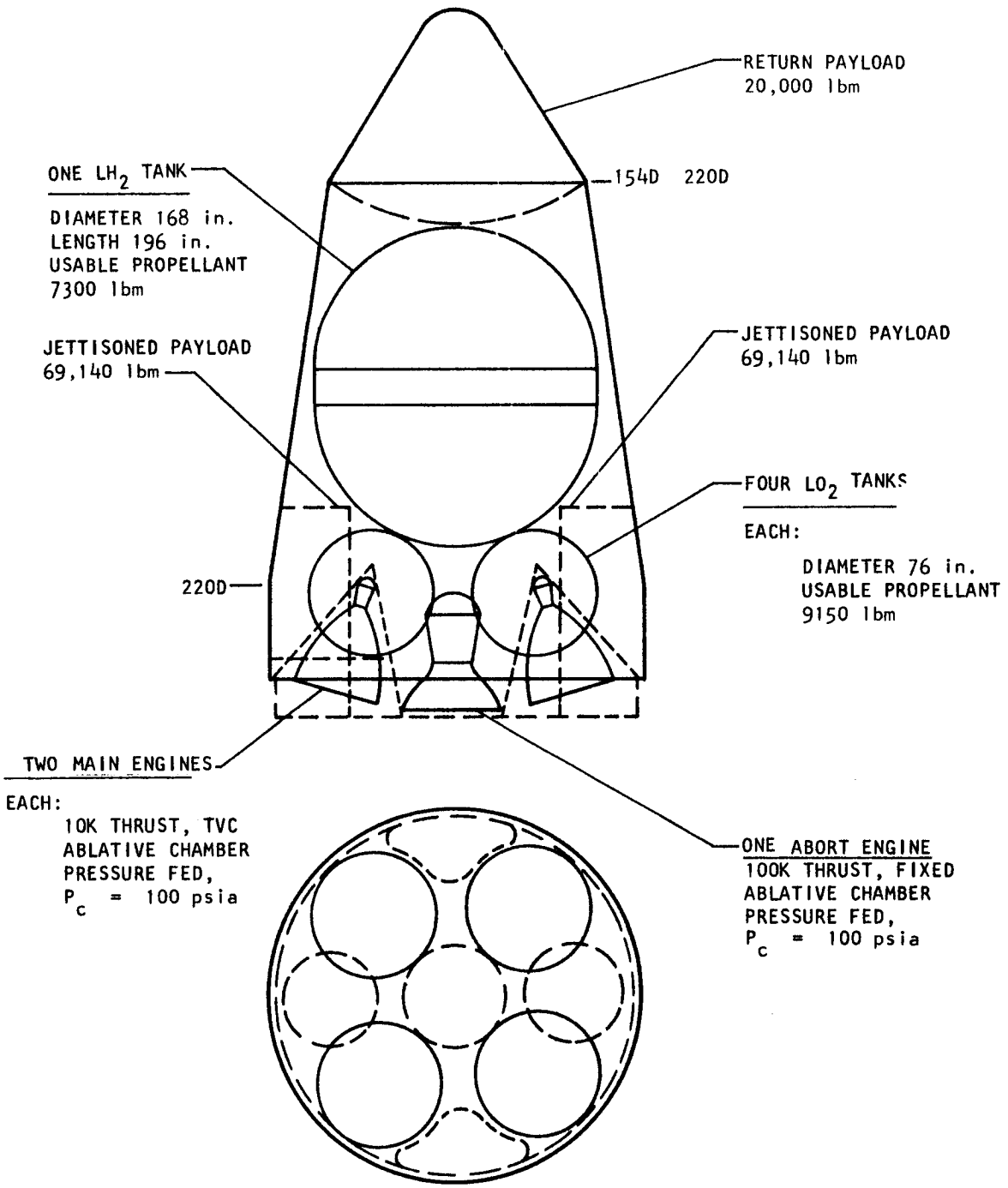

FIGURE 93

NOVA CIRCUMLUNAR MISSION CONFIGURATION, ALTERNATE 5 - A

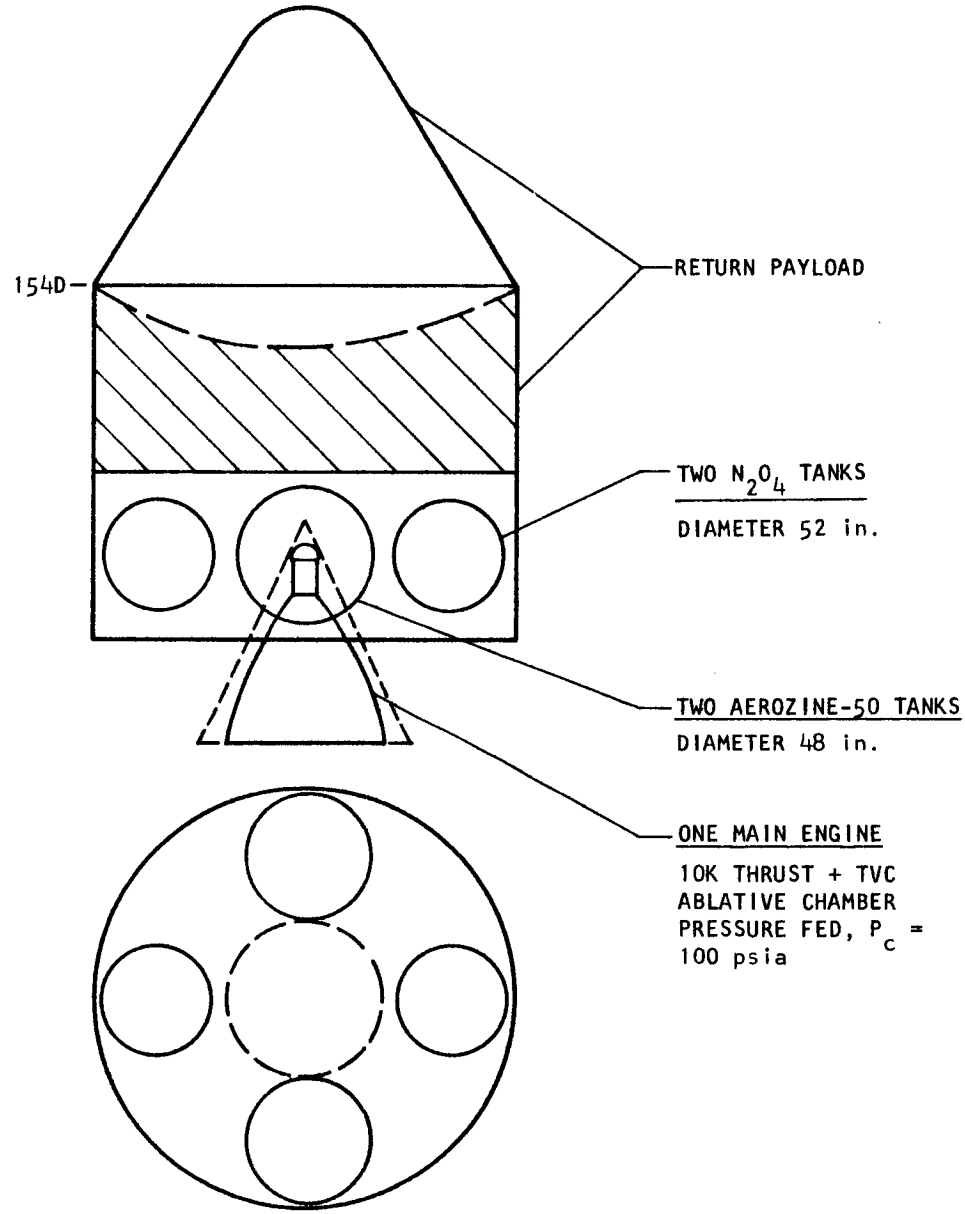

MAC A673

FIGURE 94

SPACECRAFT ENGINE CONFIGURATIONS FOR RENDEZVOUS MISSIONS

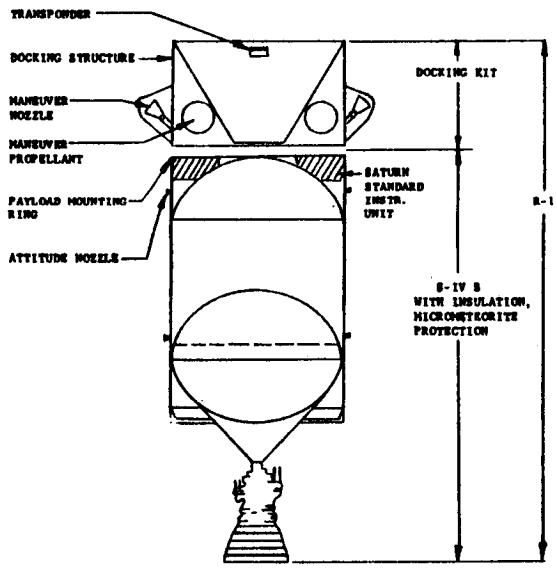

Concept for Saturn S-IVB/R1 Docking Kit

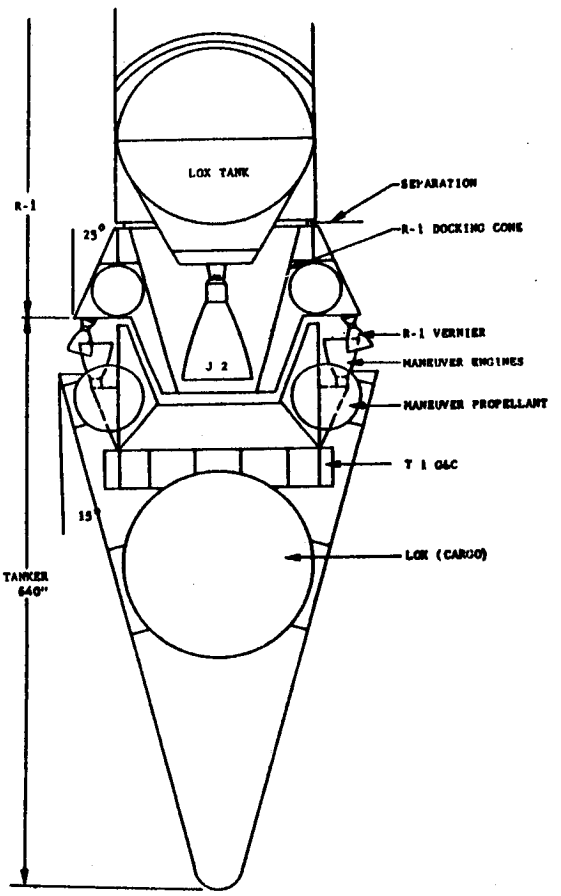

Concept for Docking with a Tanker

TYPICAL SINGLE THRUST - TIME PROGRAM
DIRECT LUNAR LANDING

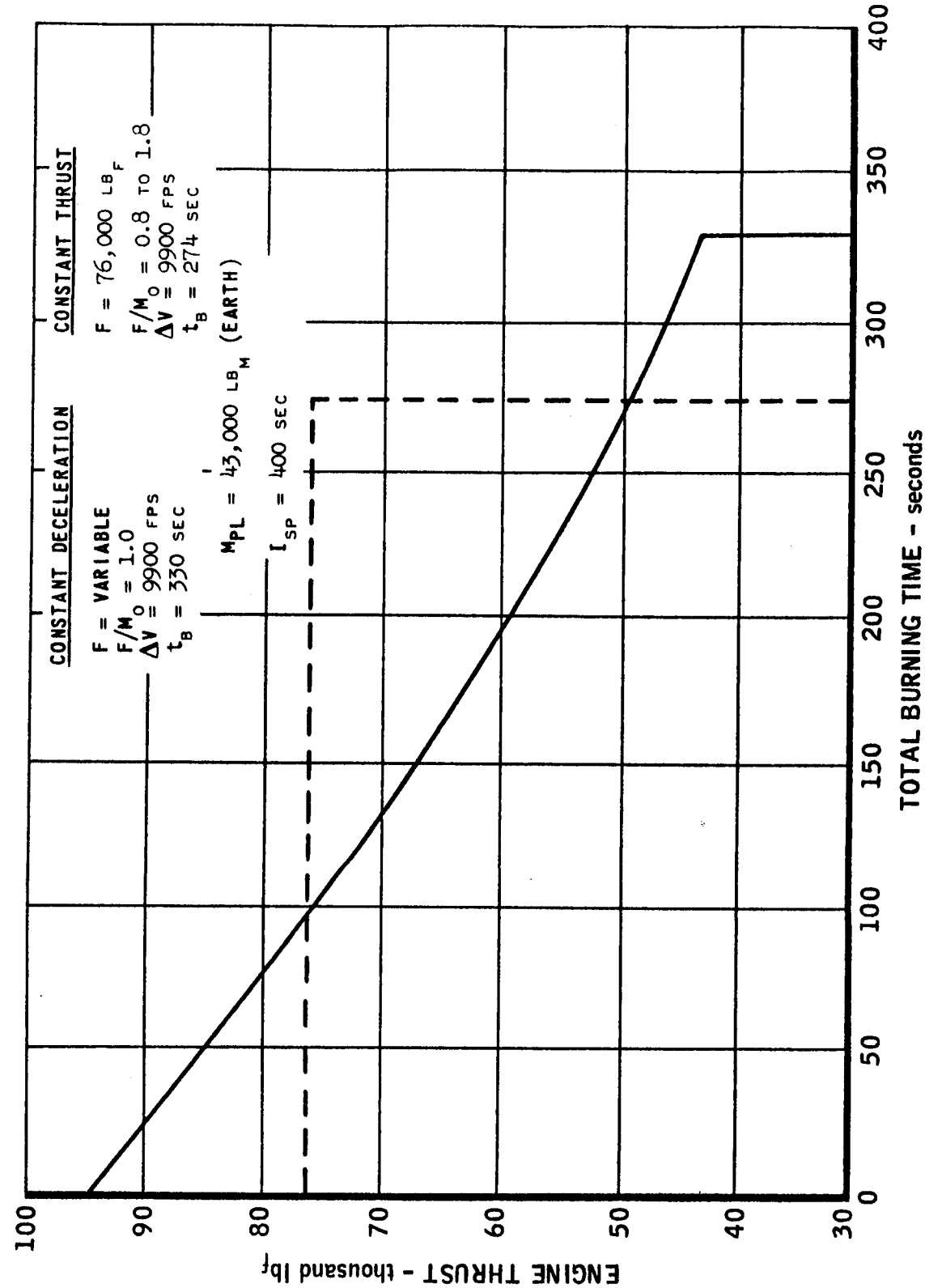

TYPICAL DUAL THRUST - TIME PROGRAM
LUNAR LANDING FROM ORBIT

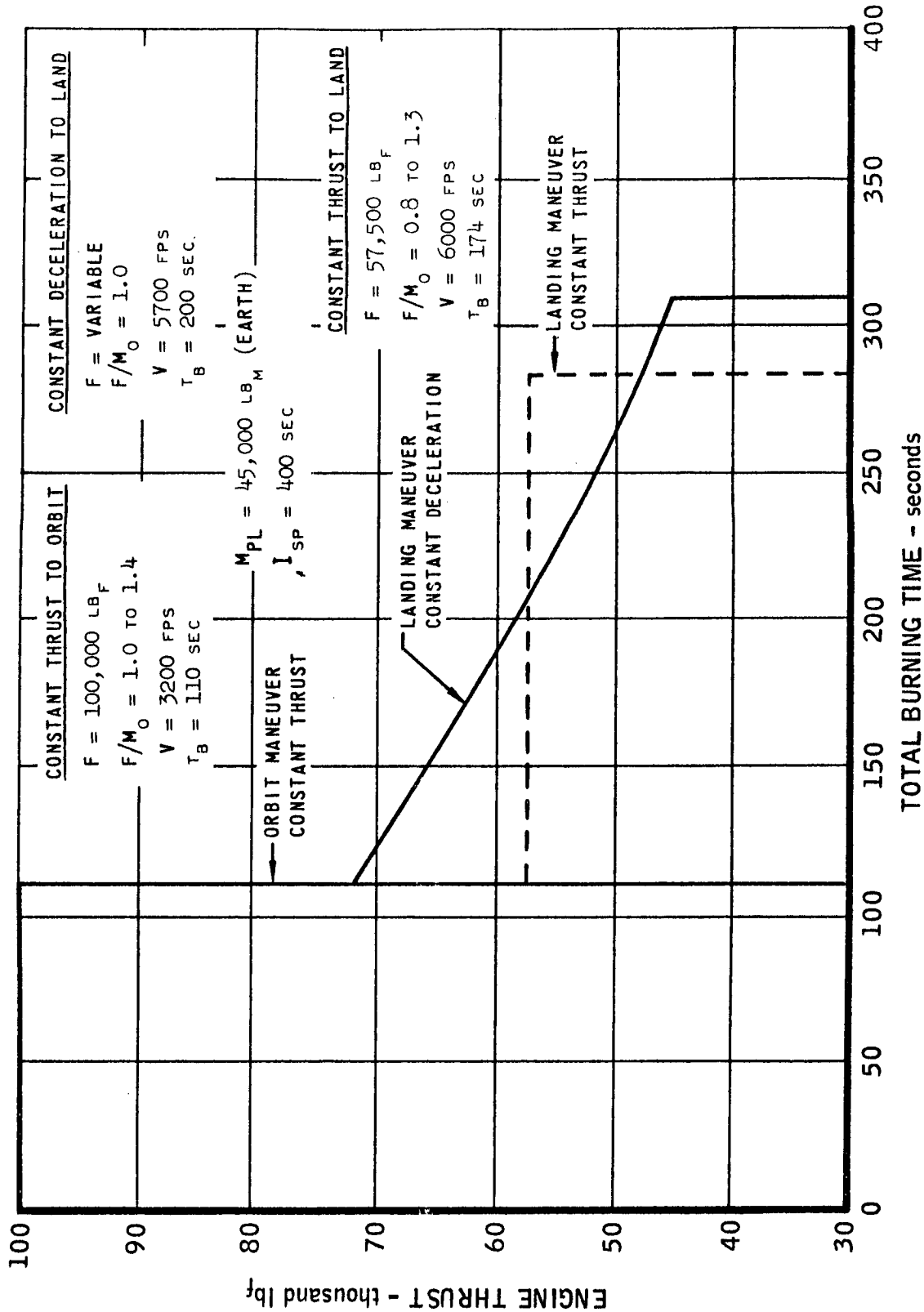

MAC A678

FIGURE 97

PHYSICAL AND CHEMICAL PROPERTIES OF OXYGEN

PROPERTIES		REFERENCE
Freezing Point, °F at 1 atm	-361.9	32
Boiling Point, °F at 1 atm	-297.45°F	32
Vapor Pressure in °R, atm	log P = -419.31 T + 5.2365 - 0.00648T	32
Density, gm/cc	11.4 g/cc at -297°F	32
Viscosity Centipoise	0.241 x 10^{-8} Centipoise at -297°F	32
Critical Temperature, °F	-181.08°F	32
Critical Pressure, psia	736.9 psia	32
Molecular Weight	32.00	32
Thermal Conductivity, Btu/hr ft °F	0.4696 x 10^{-2} Btu/hr ft °F at -298°F	32
Heat of Formation, Kcal/mole	-3.109 Kcal/mole at -297.45 °F	31
Heat Capacity, Btu/pound	0.405 Btu/pound °F at -297°F	31
Toxicity, Maximum Allowable Concentration, ppm, 8 hr.	Not Toxic	32
Stability to Temperature	Stable	32
Stability to Shock	Stable	32
AVAILABILITY		
Types of Containers	Insulated Containers	32
Cost	1.8 to 11.4 cents/lb	31

MAC A 633

PROPELLANT PROPERTIES OF OXYGEN

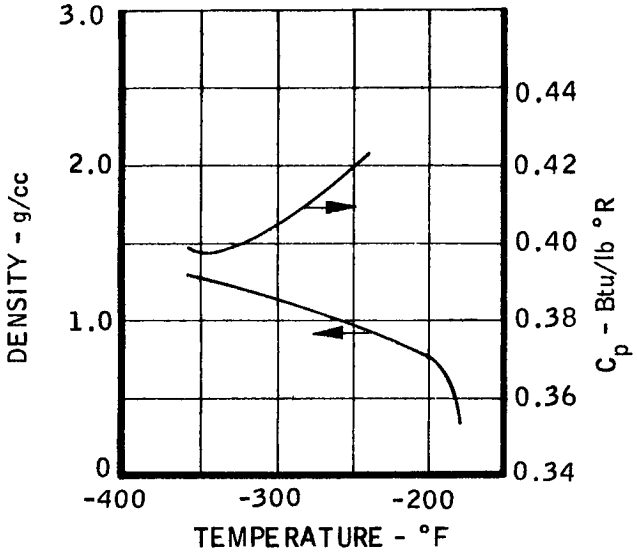

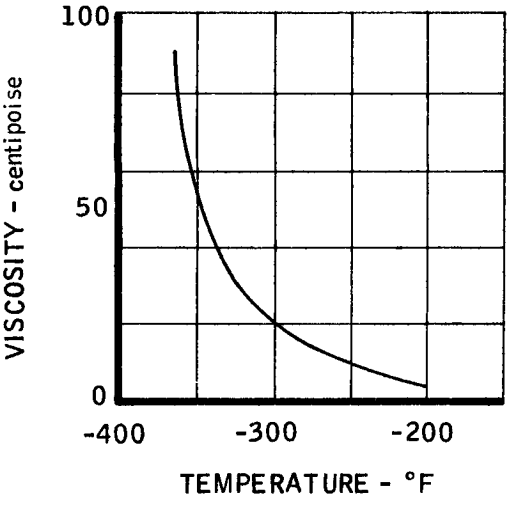

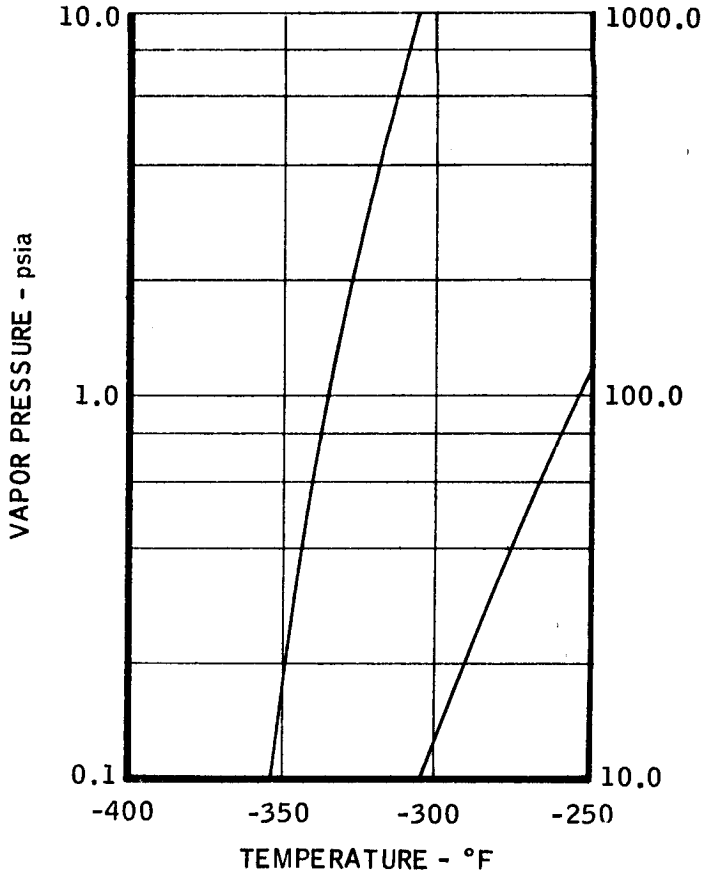

FIGURE 99

PHYSICAL AND CHEMICAL PROPERTIES OF FLUORINE

PROPERTIES		REFERENCE
Freezing Point, °F at 1 atm	-363.21°F	32
Boiling Point, °F at 1 atm	-306.55°F	32
Vapor Pressure, psia	5.4 psia at -320.4°F	32
Density, gm/cc	1.505 g/cc at -306.55°F	32
Viscosity Centipoise	2.82 Centipoise at -315.4°F	32
Critical Temperature, °F	-200.38°F	32
Critical Pressure, psia	808.5 psia	32
Molecular Weight	38.00	32
Thermal Conductivity, Btu/hr ft °F	14.3×10^{-3} Btu/ft hr °F at 32°F	32
Heat of Formation, Kcal/mole	-2.874 Kcal/mole at -306.55°F	31
Heat Capacity, Btu/pound	0.363 Btu/pound°R at -312°F	32
Toxicity, Maximum Allowable Concentration, ppm, 8 hr.	--	--
Stability to Temperature	Stable	
Stability to Shock	Stable	
AVAILABILITY		
Types of Containers	Cylinders and Tankcars	
Cost, $/lb	$4	31

MAC A673

PROPELLANT PROPERTIES OF LIQUID FLUORINE

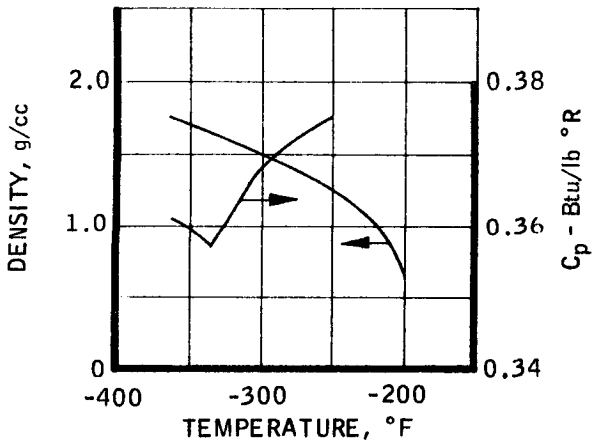

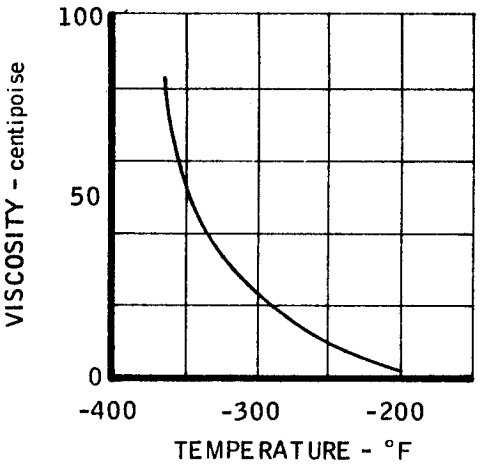

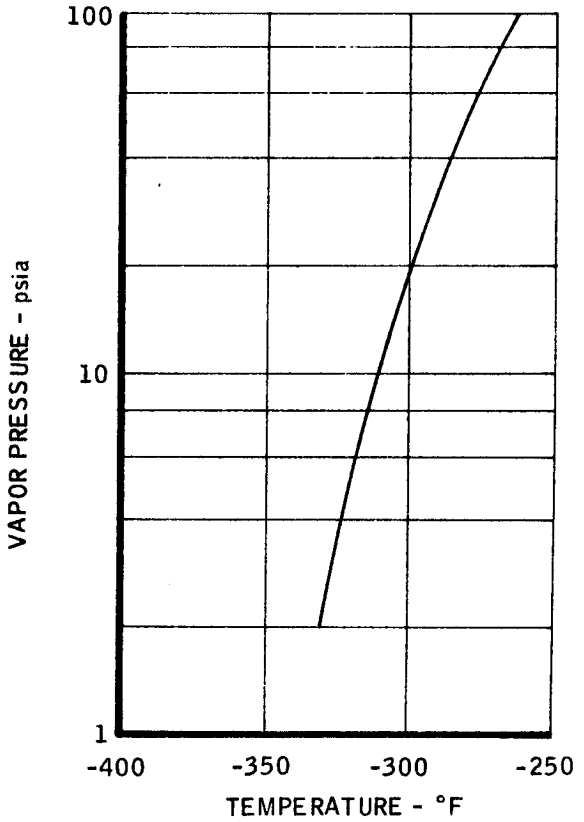

MAC A673

FIGURE 101

PHYSICAL AND CHEMICAL PROPERTIES OF OXYGEN DIFLUORIDE

PROPERTIES		REFERENCE
Freezing Point, °F at 1 atm	-370.8°F	31
Boiling Point, °F at 1 atm	-228.6°F	31
Vapor Pressure, psia	174.7 psia at -148°F	31
Density, gm/cc	1.519 g/cc at -229°F	31
Viscosity Centipoise	0.2852 Centipoise at -262.4°F	31
Critical Temperature, °F	72.4°F	31
Critical Pressure, pais	718.8 psia	31
Molecular Weight	54.00	31
Thermal Conductivity, Btu/hr ft °F	--	--
Heat of Formation, Kcal/mole	7.62 Kcal/g mole at 273.16°K	31
Heat Capacity, Btu/pound	0.186 Btu/pound °F at 32°F	31
Toxicity, Maximum Allowable Concentration, ppm, 8 hr	0.005	29
Stability to Temperature	Stable	29
Stability to Shock	Stable	29
AVAILABILITY		
Types of Containers	Steel Containers	29
Cost	1-lb Cylinders - $110 9-lb Cylinders $55/lb	29

MAC A673

FIGURE 102

PROPELLANT PROPERTIES OF OXYGEN DIFLUORIDE

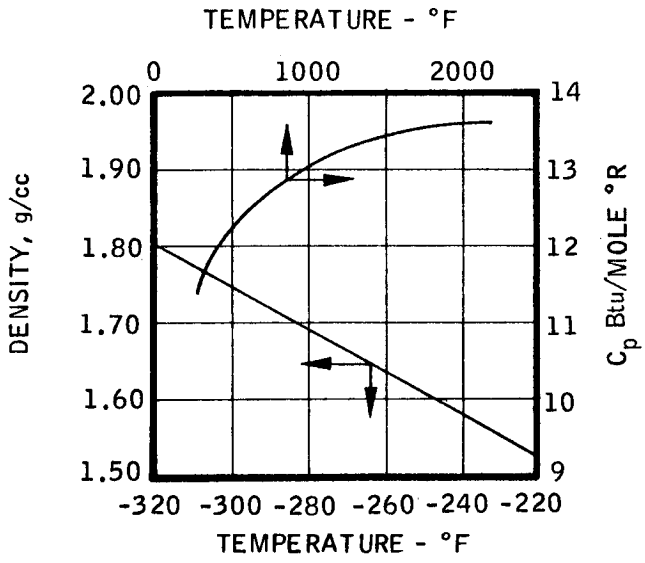

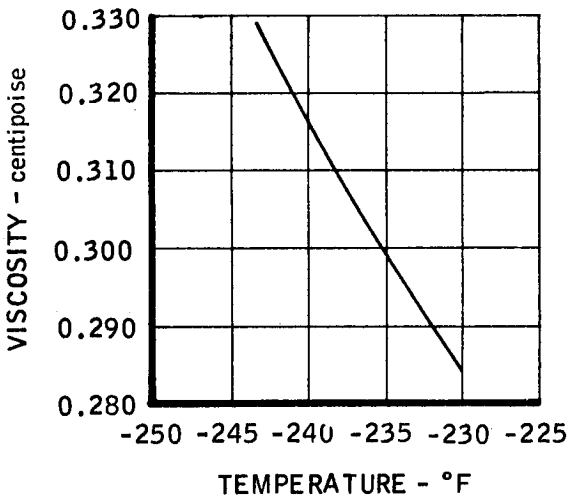

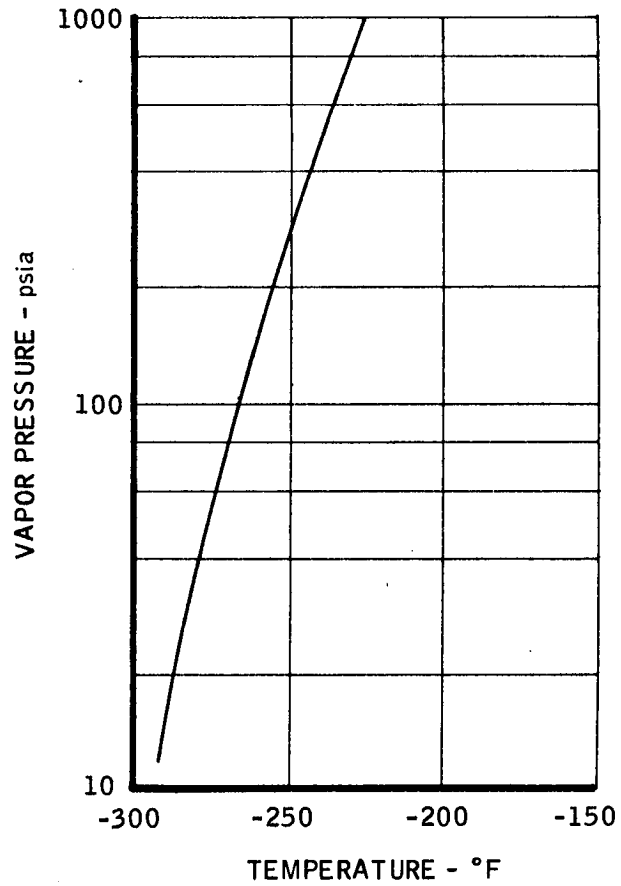

FIGURE 103

PROPELLANT PROPERTIES OF NITROGEN TETROXIDE

PROPERTIES		REFERENCE
Freezing Point, °F at 1 atm	11.8	32
Boiling Point, °F at 1 atm	70.1	32
Vapor Pressure at 77°F, psia	17.7	32
Density at 77°F, gm/cc	89.34 lb/ft^3	32
Viscosity at 77°F Centipoise	0.410	32
Critical Temperature, °F	316.8	32
Critical Pressure, psia	1469	32
Molecular Weight	92.016	32
Thermal Conductivity Btu/hr ft °F	0.0755	32
Heat of Formation, Kcal/mole	-6.8	31
Heat Capacity, Btu/lb-°F	0.374	32
Toxicity, Maximum Allowable Concentration, ppm, 8 hr.	25	31
Stability to Temperature	Stable	31
Stability to Shock	Stable	31
AVAILABILITY		
Types of Containers	Tankcars and Cylinders	31
Cost, $/lb.	0.065 to 0.075	31

MAC A673

PROPELLANT PROPERTIES OF NITROGEN TETROXIDE

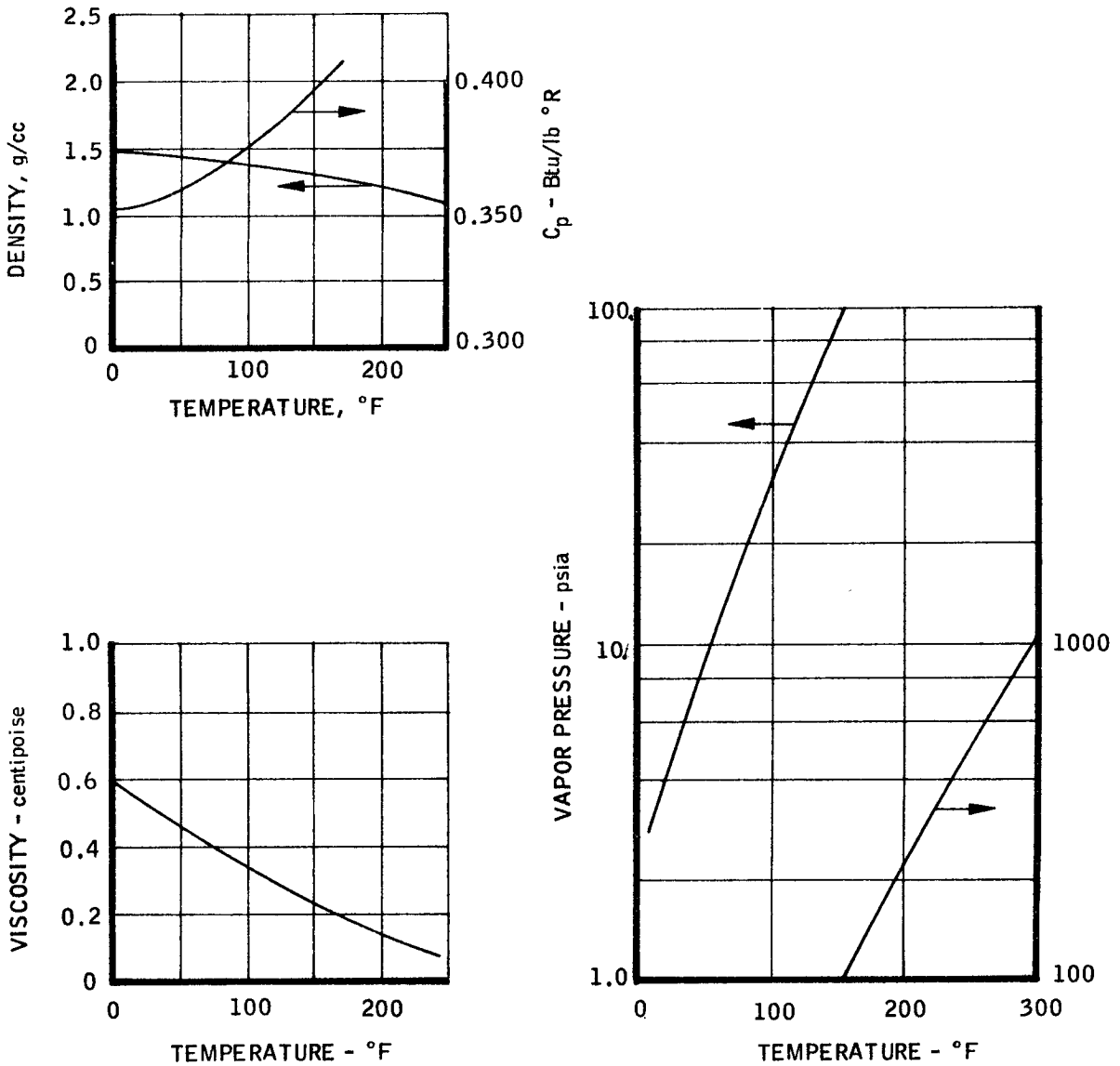

PHYSICAL AND CHEMICAL PROPERTIES OF LIQUID HYDROGEN

PROPERTIES		REFERENCE
Freezing Point, °F at 1 a tm.		
Boiling Point, °F at 1 a tm.	-423°F	32
Vapor Pressure, psia	13.06 psia at -394.6°F	32
Density, gm/cc	0.0012 g/cc at -423.3°F	32
Viscosity Centipoise	1.344×10^{-2} centipoise at -423.4°F	32
Critical Temperature, °F	-399.7°F	32
Critical Pressure, psia	190.8 psia	32
Molecular Weight	2.016	32
Thermal Conductivity Btu/hr ft °F	673 Btu/ft-hr-F at 136°F and 1 atm	32
Heat of Formation, Kcal/mole	-1.92 Kcal/mole	31
Heat Capacity, Btu/pound °R	1.45 Btu/lb °R at 36°R	32
Toxicity, Maximum Allowable Concentration, ppm, 8 hr.	None Required	32
Stability to Temperature	Stable	32
Stability to Shock	Stable	32
AVAILABILITY		
Types of Containers	Insulated Tanks	32
Cost, $/lb.	$1.75	32

MAC A673

PROPELLANT PROPERTIES OF LIQUID HYDROGEN

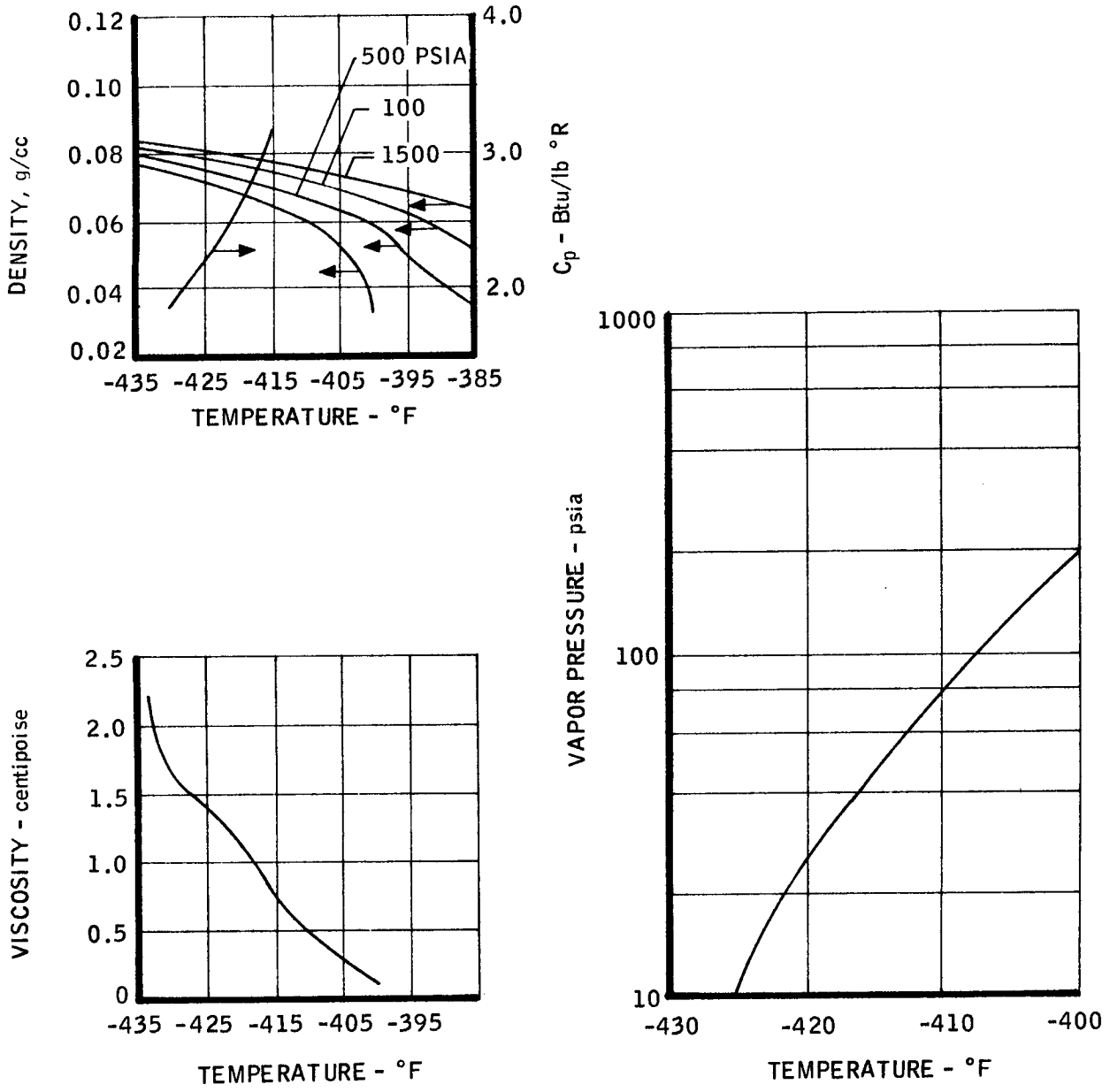

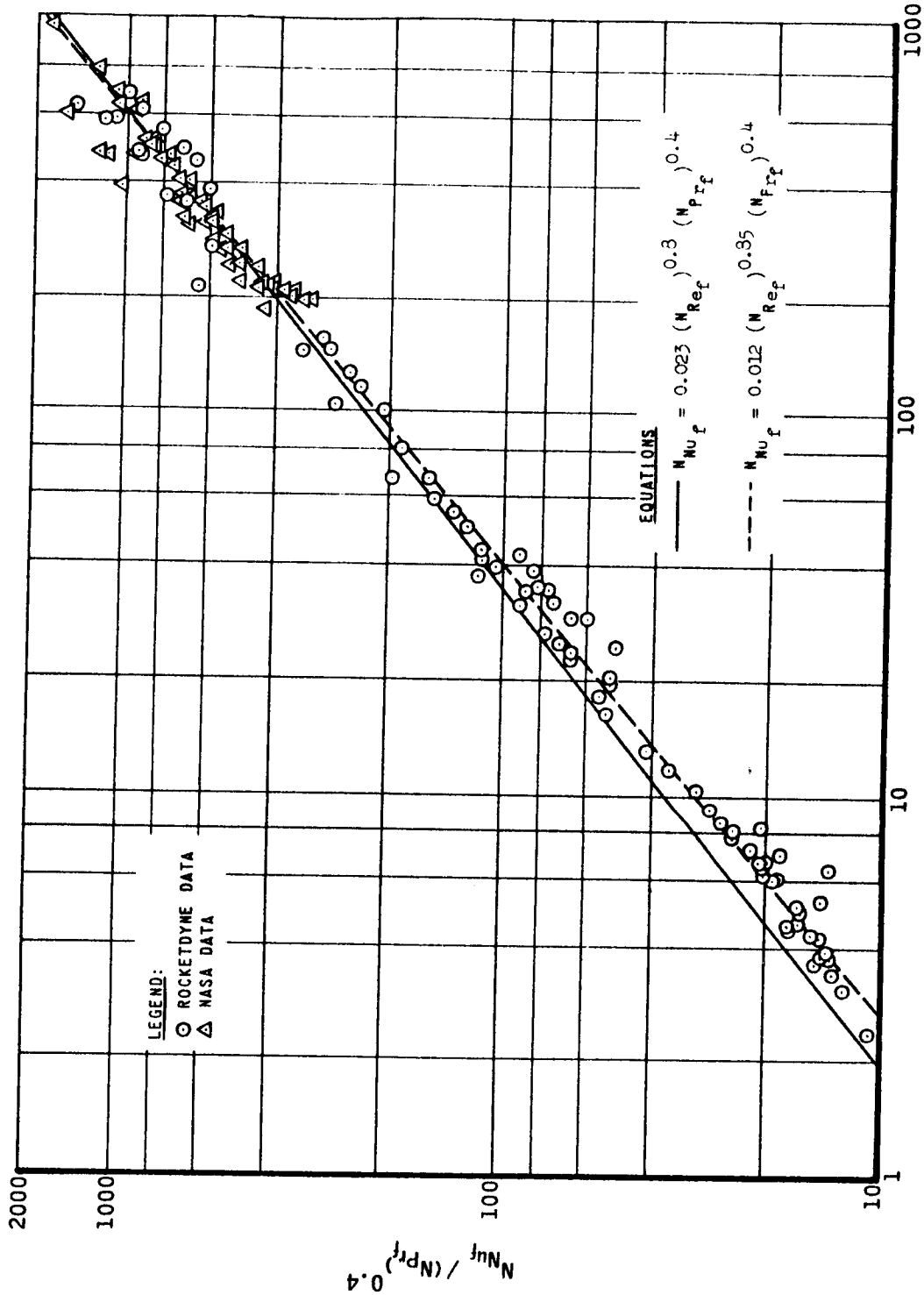

MAC A673

FIGURE 108

ROCKETDYNE CORRELATION OF GASEOUS HYDROGEN HEAT TRANSFER DATA

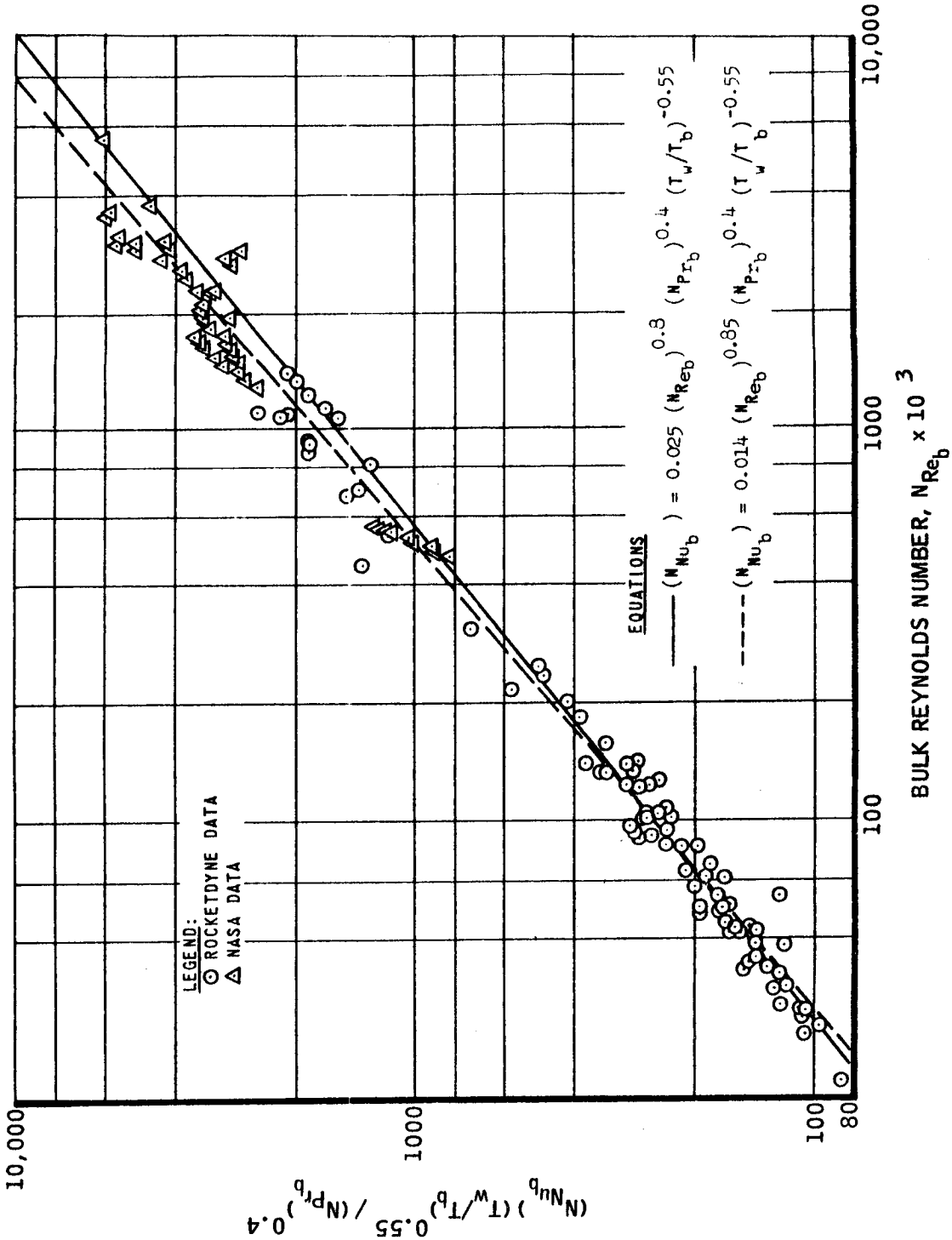

MAC A673

FIGURE 109

THERMAL CONDUCTIVITY OF HYDROGEN

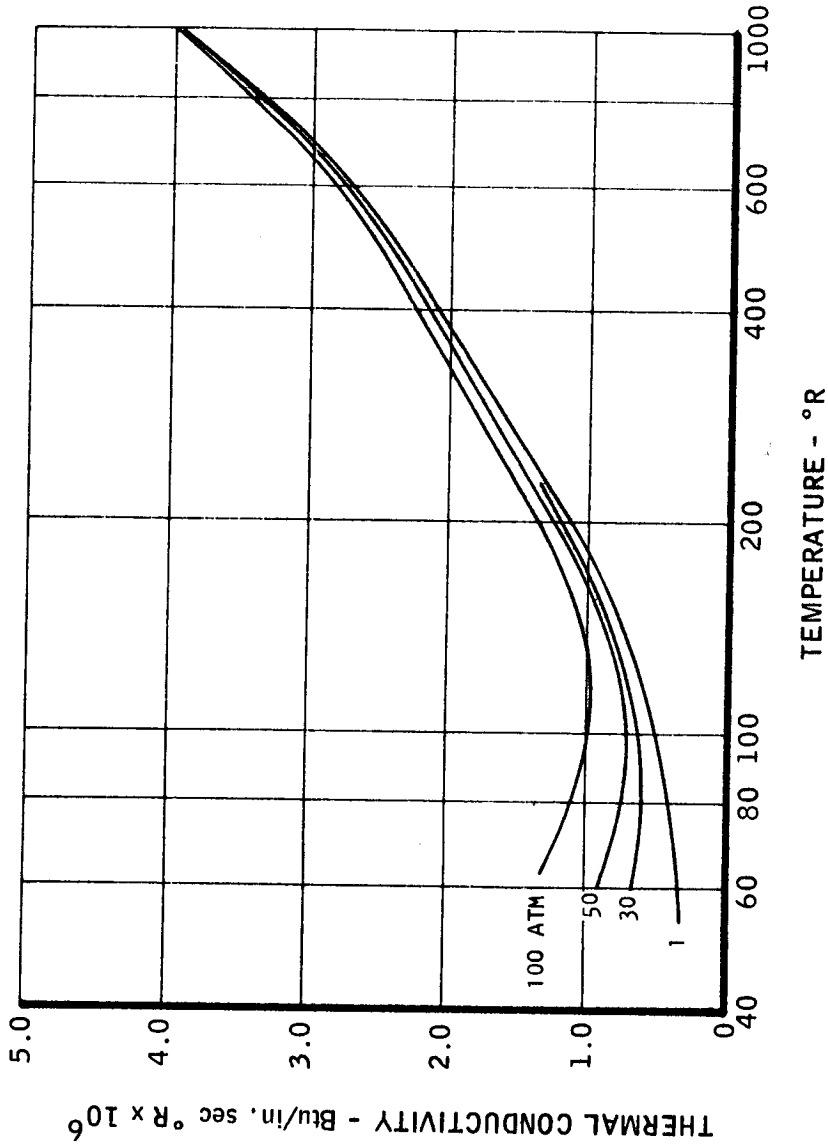

MAC A673

FIGURE 110

SPECIFIC HEAT OF PARAHYDROGEN

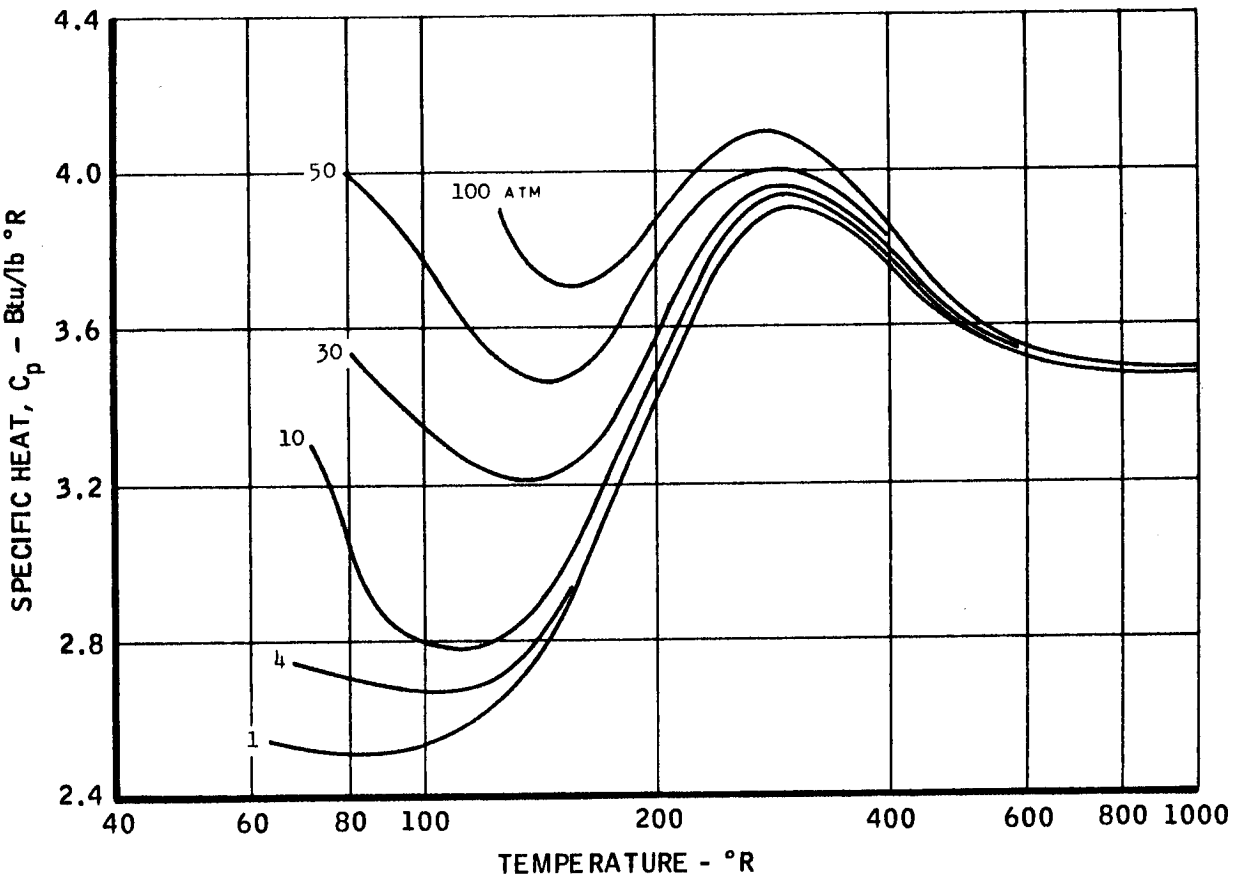

FIGURE 111

VISCOSITY OF HYDROGEN

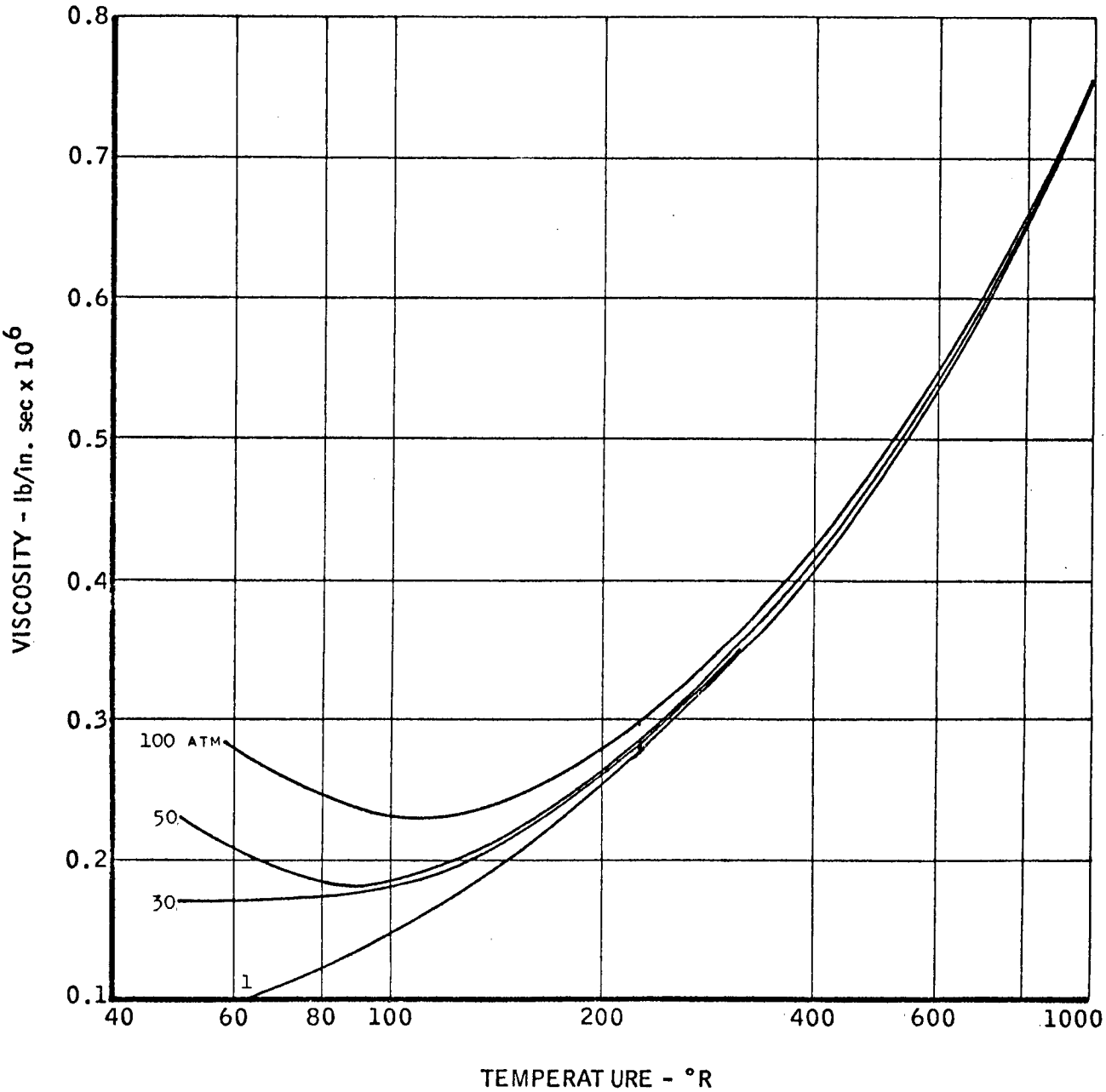

FIGURE 112

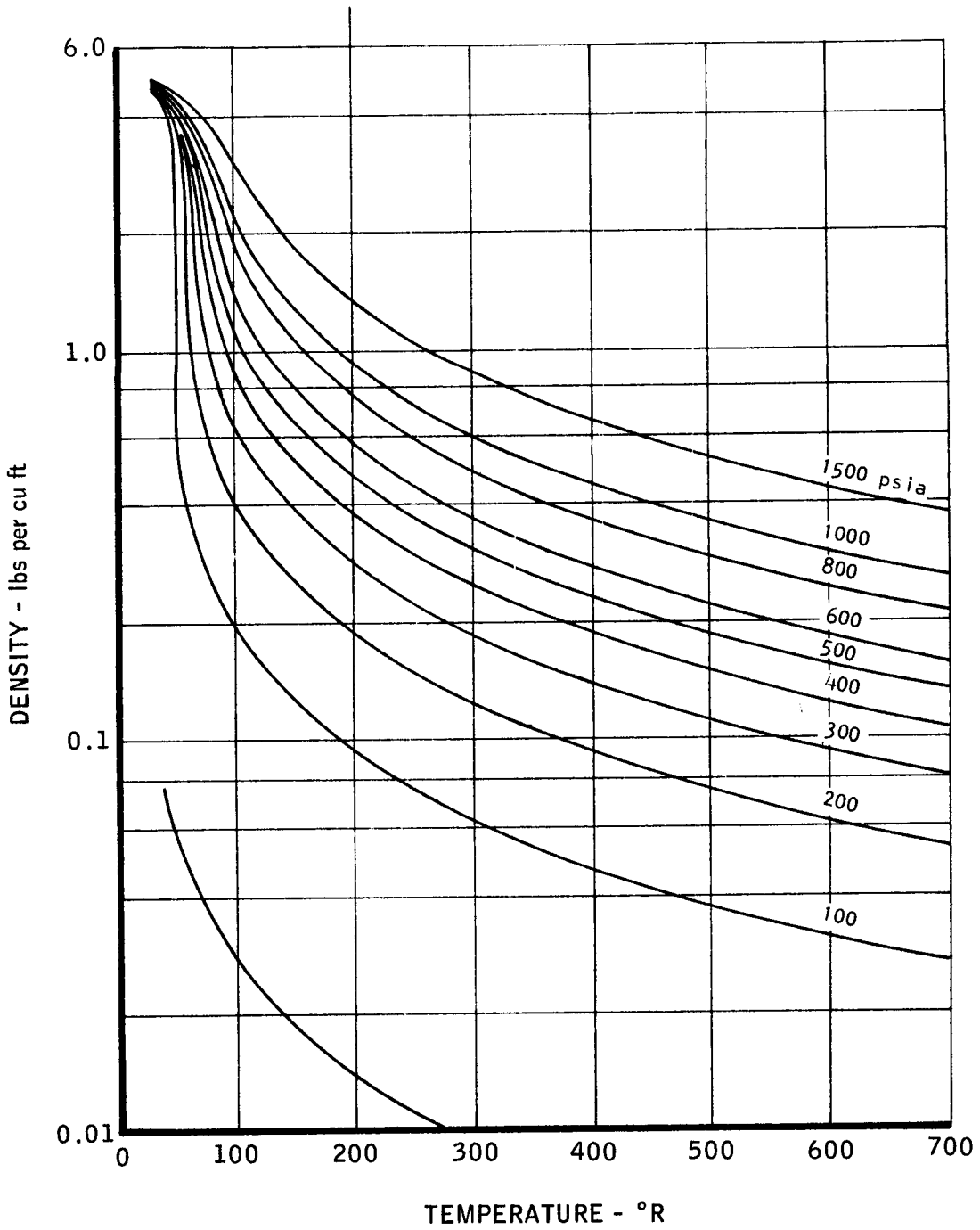
DENSITY OF PARAHYDROGEN
DENSITY - lbs per cu ft
6.0
1.0
0.1
0.01
0
100
200
300
400
500
600
700
TEMPERATURE - °R
1500 psia
1000
800
600
500
400
300
200
100

FIGURE 113

PHYSICAL AND CHEMICAL PROPERTIES OF HYDRAZINE

PROPERTIES		REFERENCE
Freezing Point, °F at 1 atm	34.7	31
Boiling Point, °F at 1 atm	236.3	31 and 32
Vapor Pressure at 77°F, psia	0.27	30
Density at 77°F, gm/cc	1.0073	31
Viscosity at 77°F Centipoise	0.90	32
Critical Temperature, °F	716	32 and 31
Critical Pressure, psia	2231	31
Molecular Weight	32.048	31
Thermal Conductivity Btu/hr ft °F	0.205	30
Decomposition Rate	1.5-2% at 390°F Violently Explosive 490°F	
Heat of Formation, Kcal/mole	+12.05	31
Heat Capacity, Btu/lb-°F	0.737	32
Toxicity, Maximum Allowable Concentration, ppm, 8 hr.	0.5 to 1	31
Stability to Temperature	Vapor is explosive	31
Stability to Shock	Vapor is shock sensitive	31
AVAILABILITY		
Types of Containers	Tankcars	31
Cost, $/lb.	1.20	31

MAC A 673

FIGURE 114

PROPELLANT PROPERTIES OF HYDRAZINE

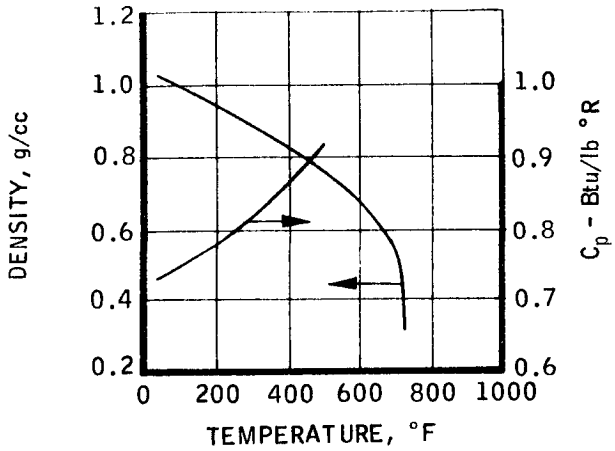

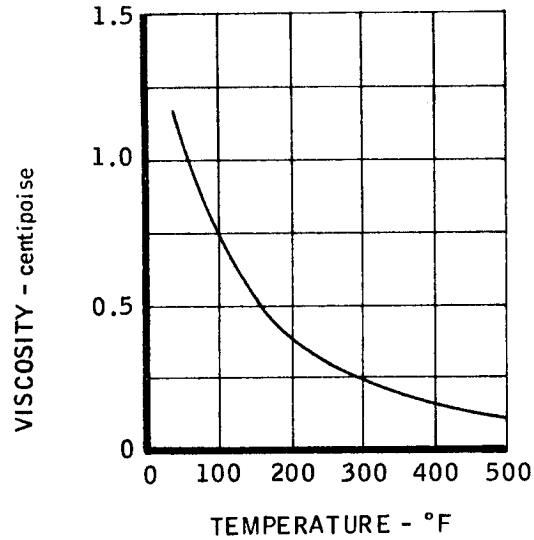

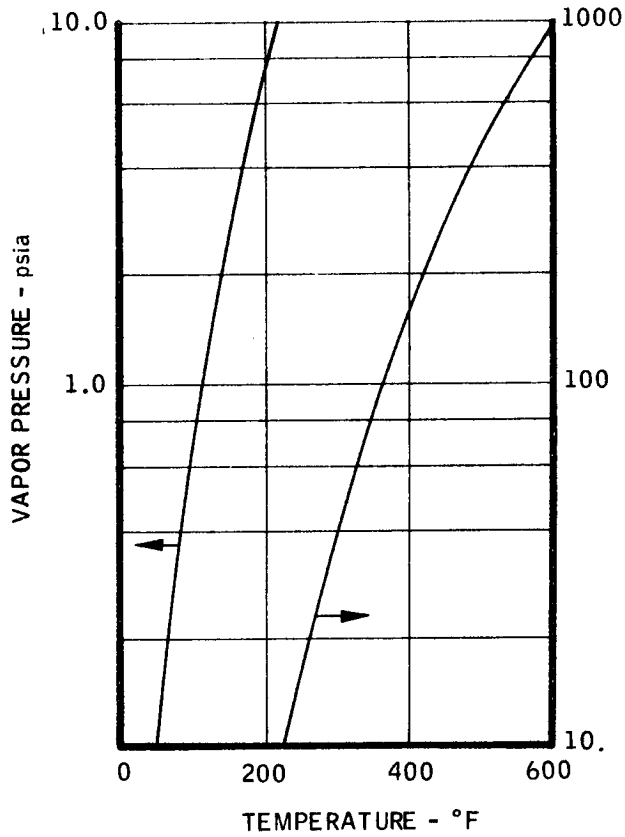

PHYSICAL AND CHEMICAL PROPERTIES OF 50% UDMH/50% N_2H_4

PROPERTIES		REFERENCE
Freezing Point, °F at 1 atm	18 to 21	32
Boiling Point, °F at 1 atm	170	30
Vapor Pressure at 77°F, psia	2.20	30
Density at 77°F, gm/cc	0.898	32
Viscosity at 77°F Centipoise	0.817	32
Critical Temperature, °F	634	32
Critical Pressure, psia	1696	32 and 30
Molecular Weight	41.797	30
Thermal Conductivity Btu/hr ft °F	0.1505	30
Heat of Formation, Kcal/mole	12.251	32
Heat Capacity, Btu/lb-°F	0.694	32
Toxicity, Maximum Allowable Concentration, ppm, 8 hr.	0.5	32
Stability to Temperature	Vapor is explosive	32
Stability to Shock	Stable	32
AVAILABILITY		
Types of Containers	Tanks and Drums	32
Cost, $/lb.	0.975	32

MAC A678

FIGURE 116

PROPELLANT PROPERTIES OF 50% UDMH/50% N_2H_4

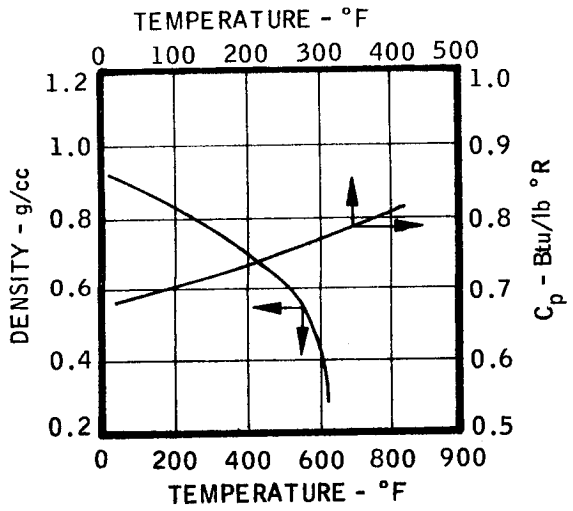

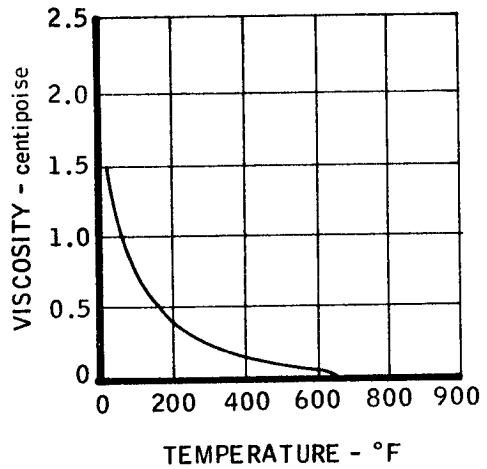

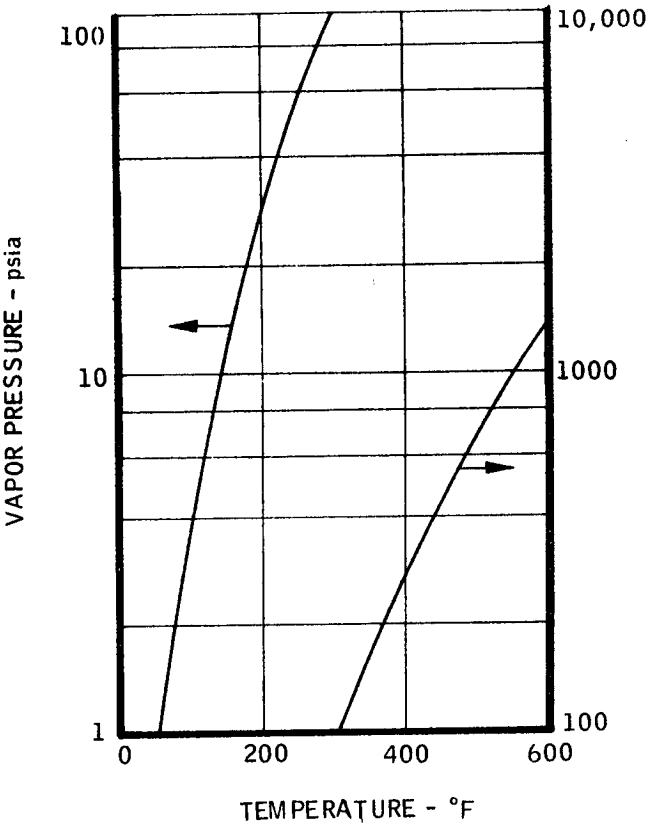

MAC A673

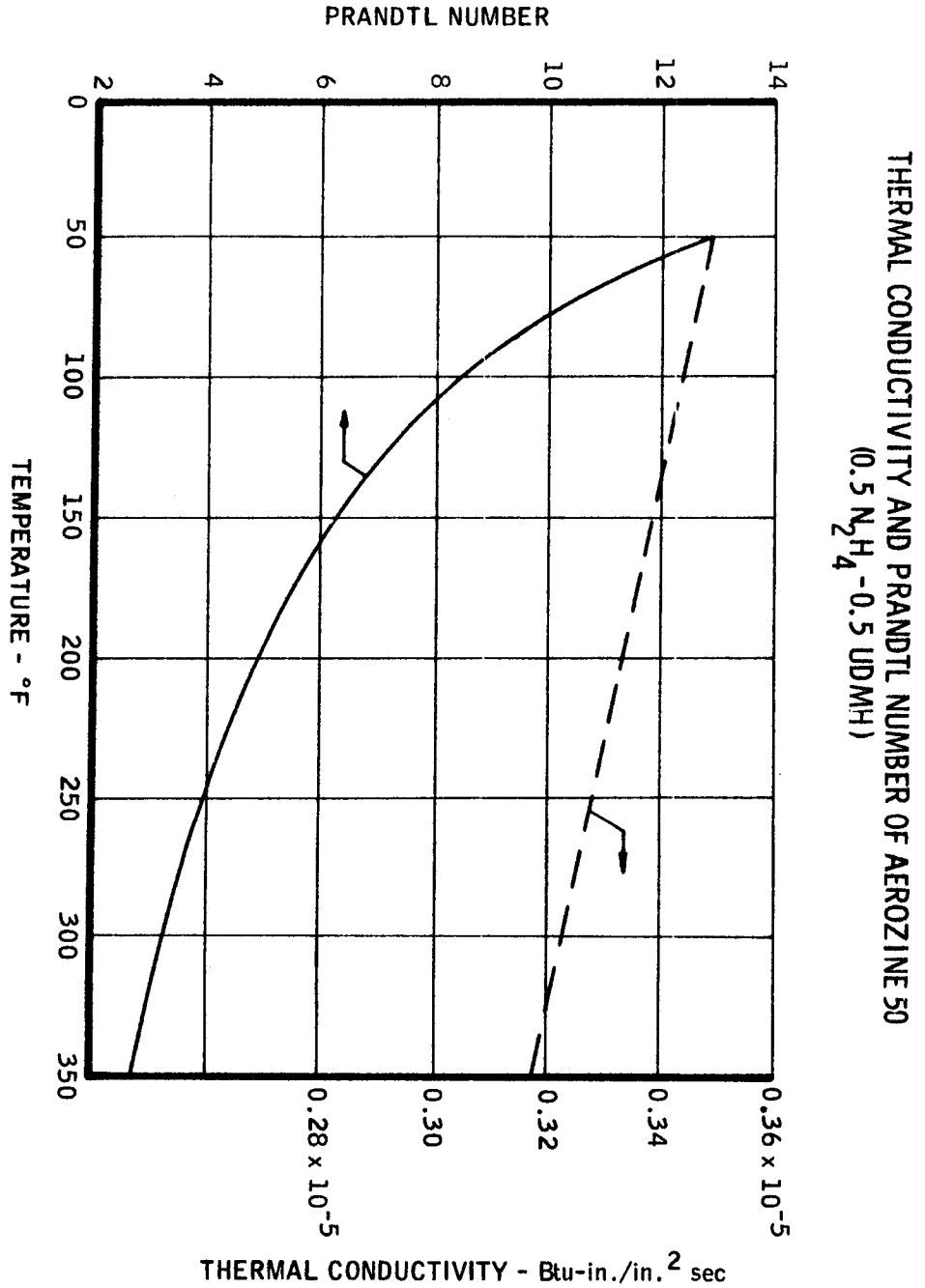

THERMAL CONDUCTIVITY AND PRANDTL NUMBER OF AEROZINE 50
(0.5 N_2H_4-0.5 UDMH)

MAC A673

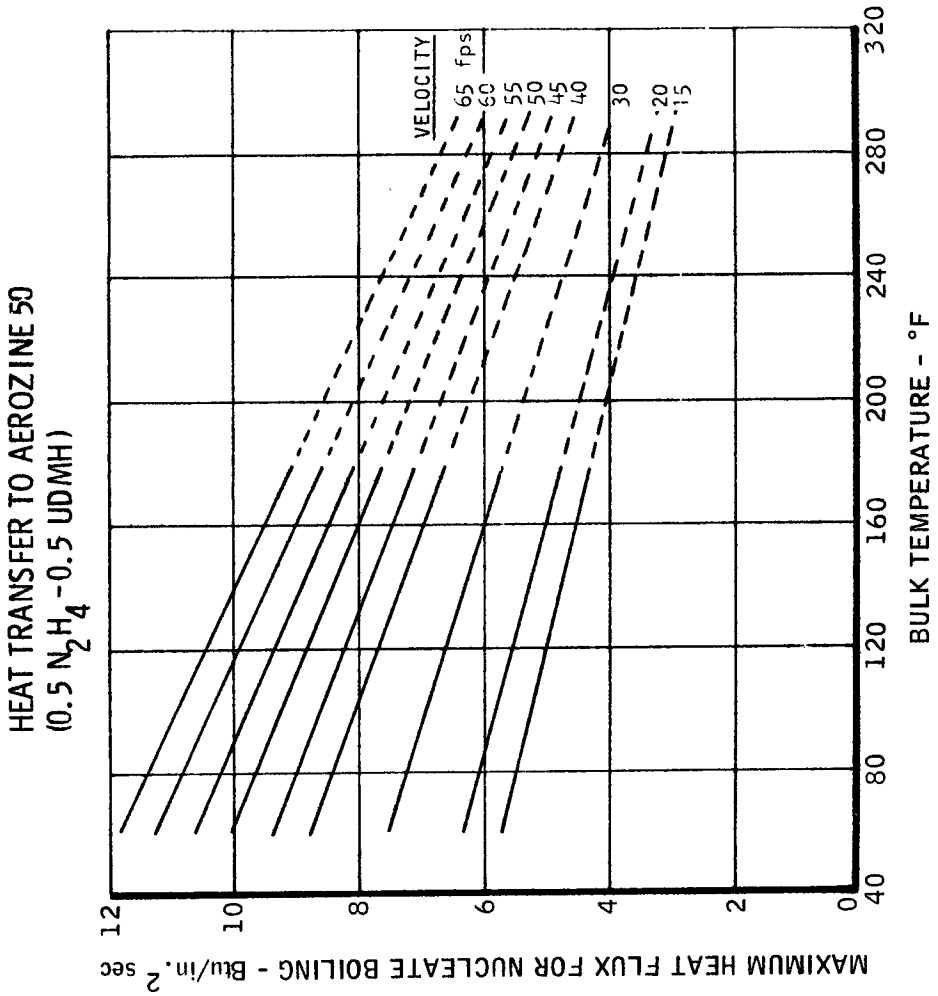
HEAT TRANSFER TO AEROZINE 50
(0.5 N_2H_4 - 0.5 UDMH)
MAXIMUM HEAT FLUX FOR NUCLEATE BOILING - Btu/in.^{2} sec
BULK TEMPERATURE - °F
VELOCITY fps
65
60
55
50
45
40
30
20
15
12
10
8
6
4
2
0
320
280
240
200
160
120
80
40

FIGURE 119

PHYSICAL AND CHEMICAL PROPERTIES OF DIBORANE

PROPERTIES		REFERENCE
Freezing Point, °F at 1 atm.	-266.	33
Boiling Point, °F at 1 atm.	-134.5	33
Vapor Pressure at 77°F, psia	See Figure 121	33
Density at 77°F, gm/cc	See Figure 121	33
Viscosity at 77°F Centipoise	0.775	33
Critical Temperature, °F	62.	33
Critical Pressure, psia	581.	33
Molecular Weight	27.69	33
Thermal Conductivity Btu/hr ft °F	0.061	30
Heat of Formation, Kcal/mole	2.93 at -134.5	33
Heat Capacity, Btu/pound	See Figure 121	30
Toxicity, Maximum Allowable Concentration, ppm, 8 hr.	0.10	33
Stability to Temperature	Indefinitely stable at -80°C	33
Stability to Shock	Stable	33
AVAILABILITY		
Types of Containers	Cylinders	33
Cost, $/lb.	$80.0	33

MAC A 633

PROPELLANT PROPERTIES OF DIBORANE

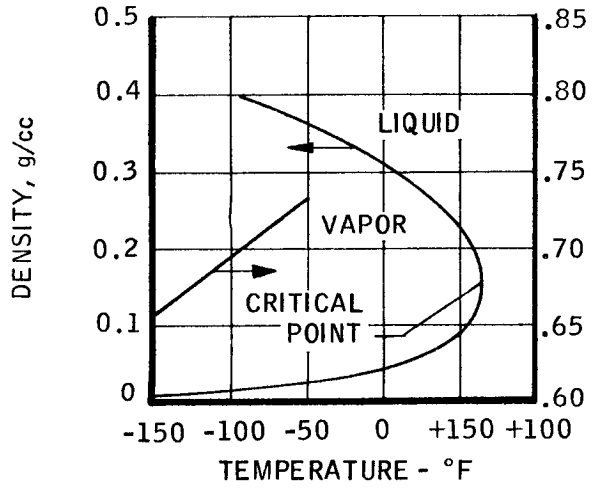

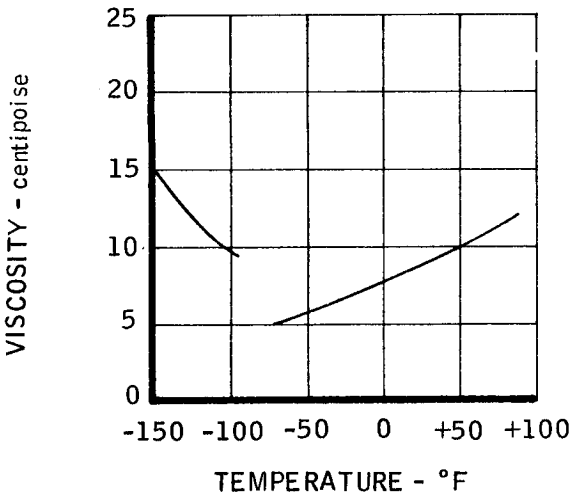

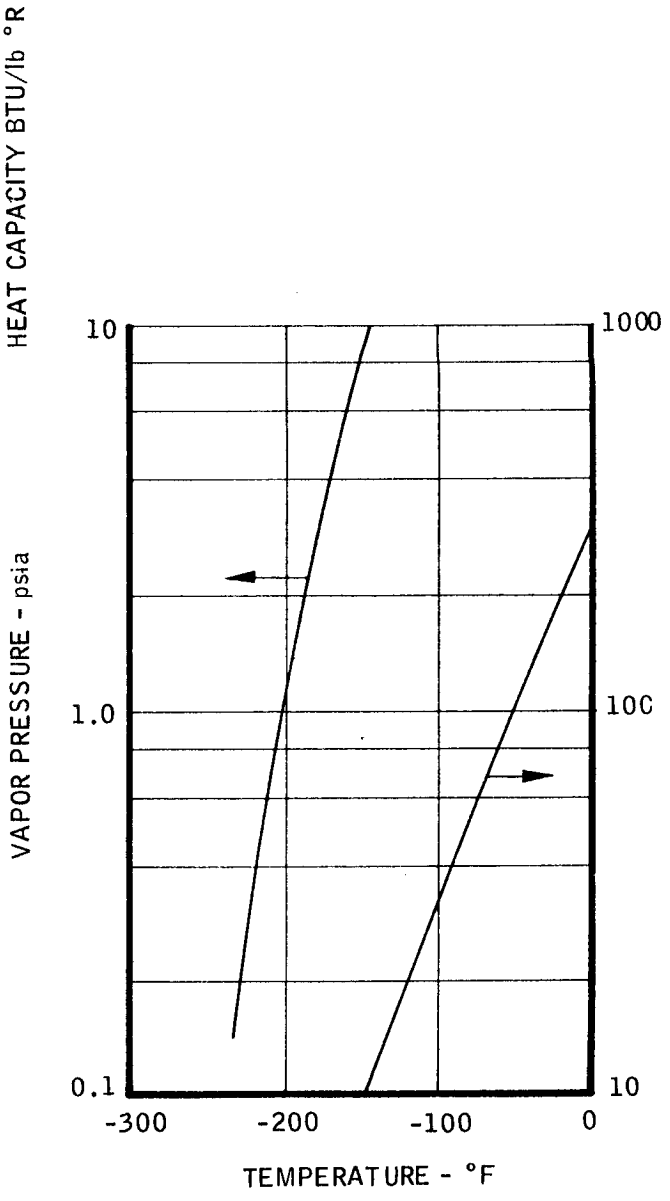

ROCKET ENGINE THEORETICAL SPECIFIC IMPULSE WITH N_2H_4 / N_2O_4

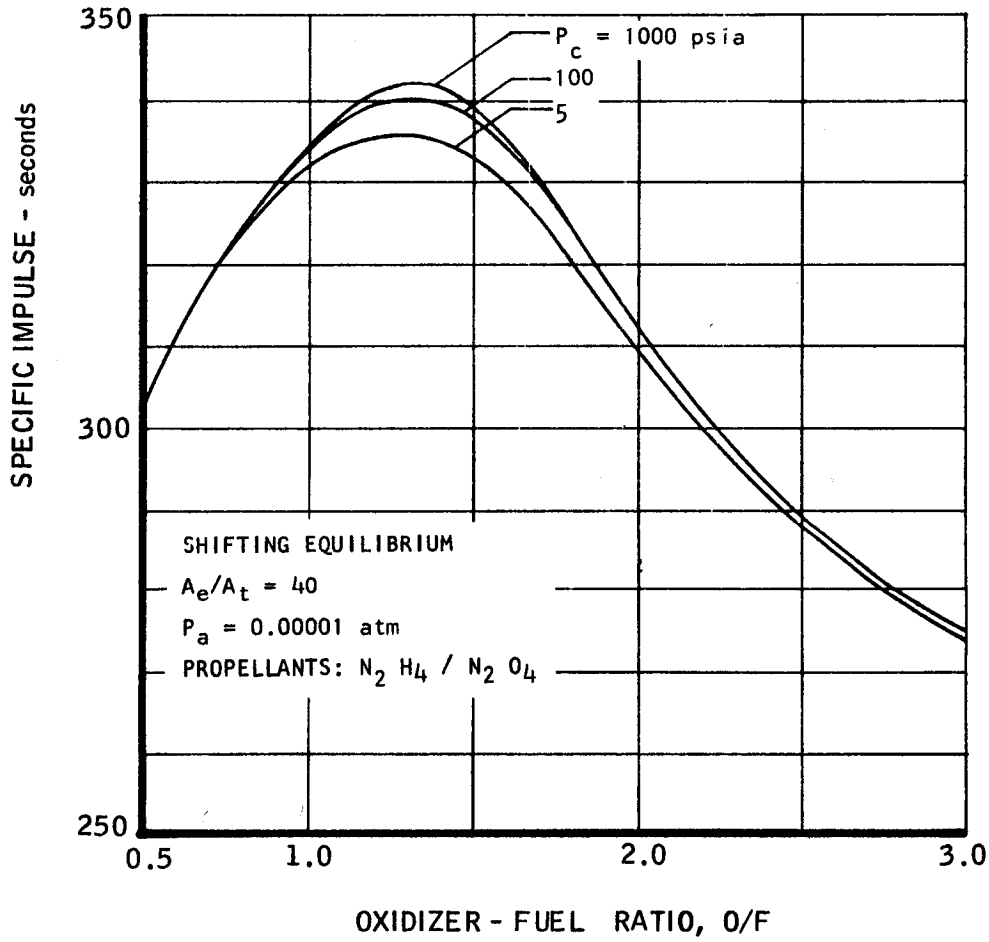

COMBUSTION TEMPERATURE AND CHARACTERISTIC VELOCITY OF N_2H_4/N_2O_4

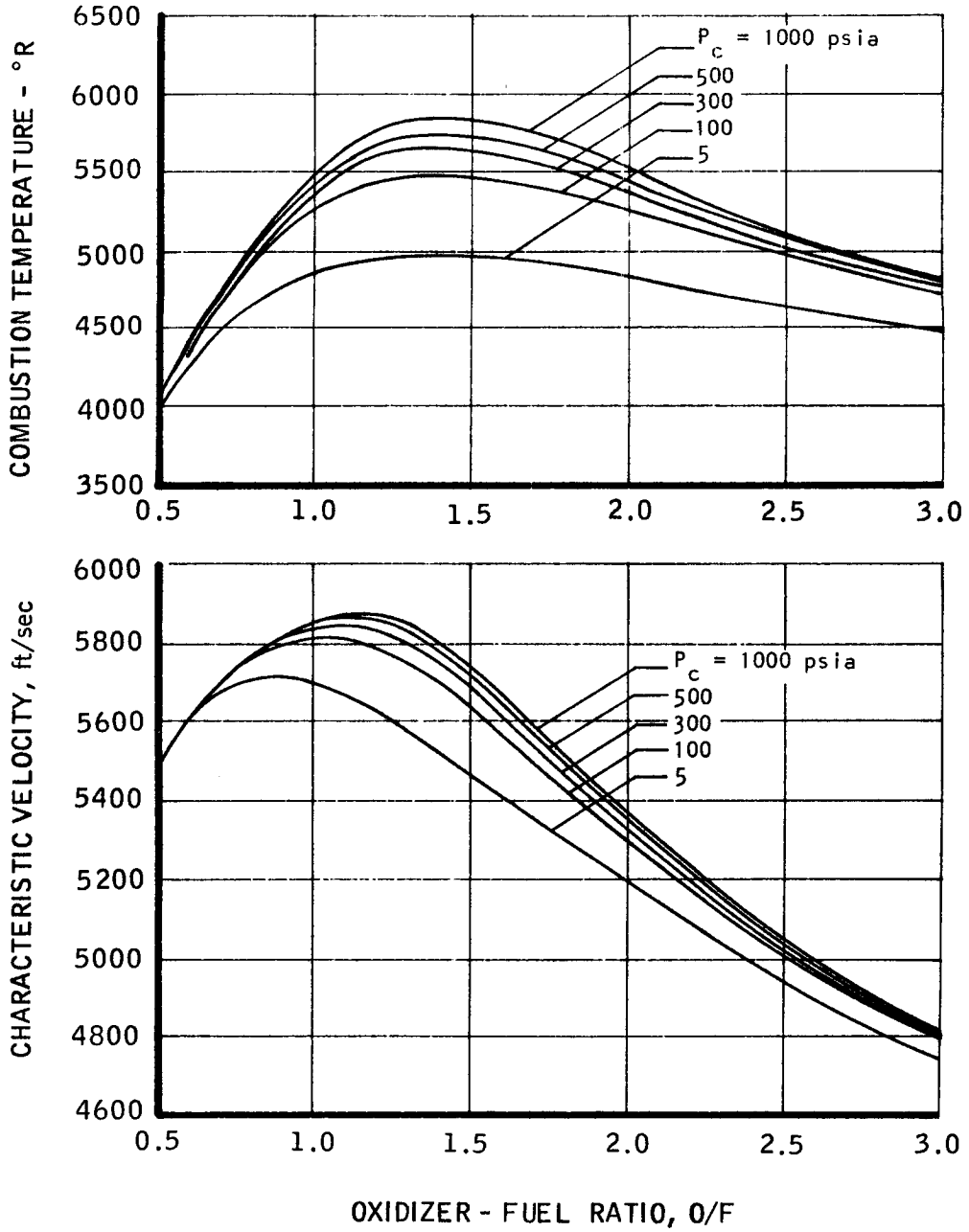

MAC A673

FIGURE 123

COMBUSTION PRODUCTS OF
N_2O_4/N_2H_4 IN COMBUSTION CHAMBER

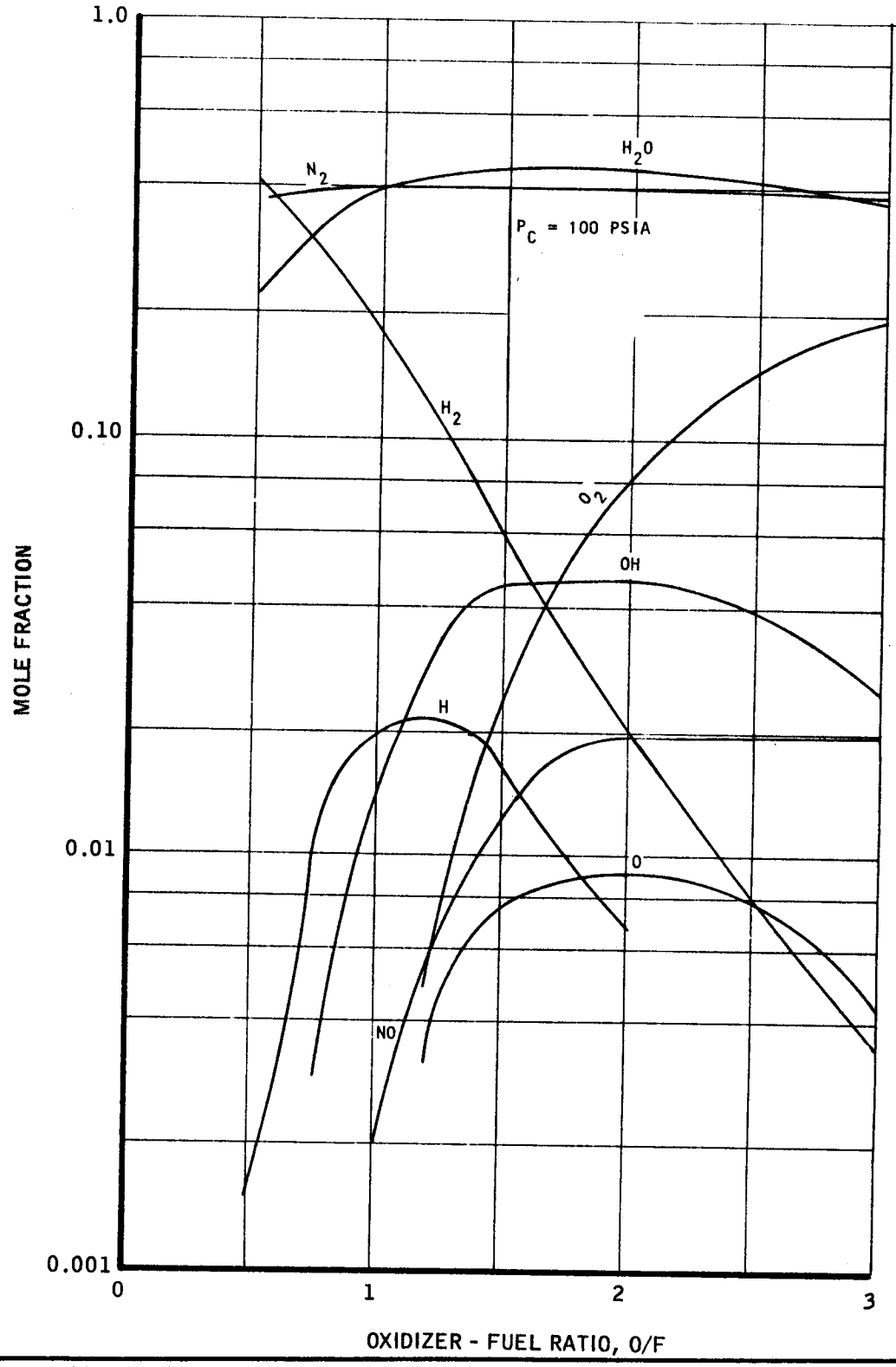

MAC A678

FIGURE 124

ROCKET ENGINE THEORETICAL SPECIFIC IMPULSE WITH N_2O_4/0.5 N_2H_4-0.5 UDMH

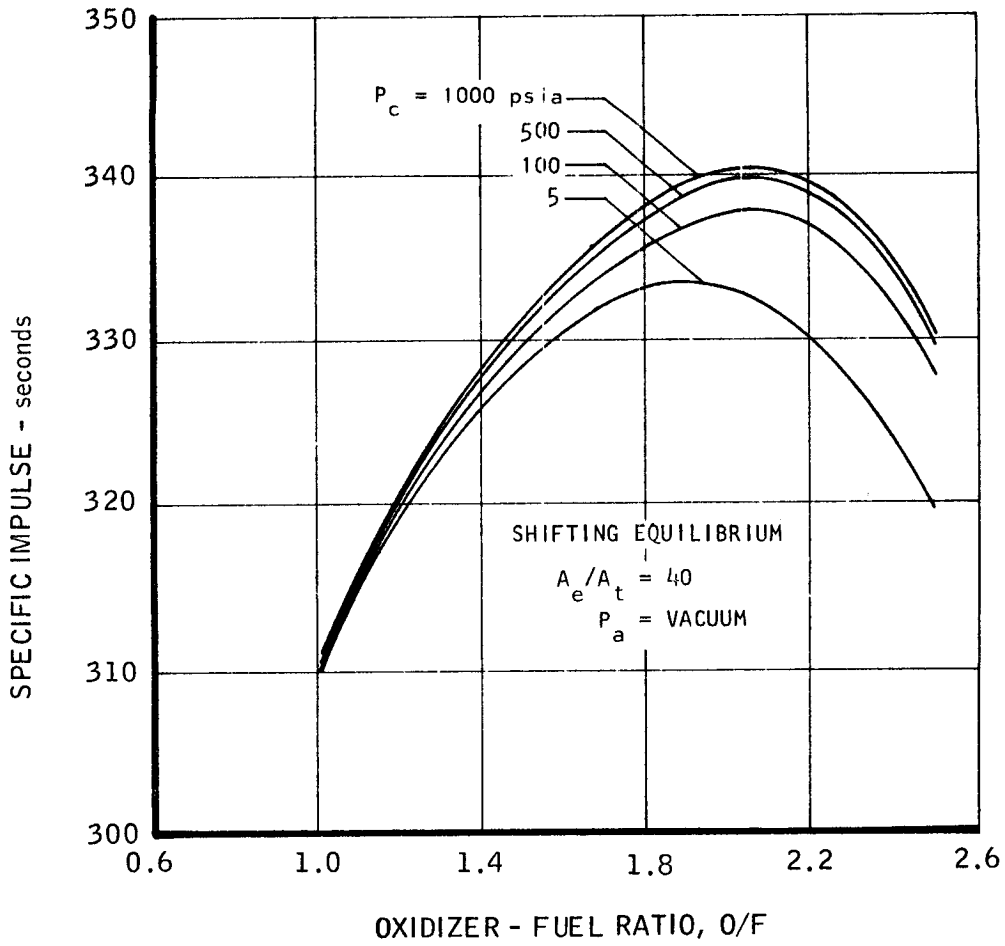

FIGURE 125

COMBUSTION TEMPERATURE AND CHARACTERISTIC VELOCITY OF N_2O_4/0.5 N_2H_4-0.5 UDMH

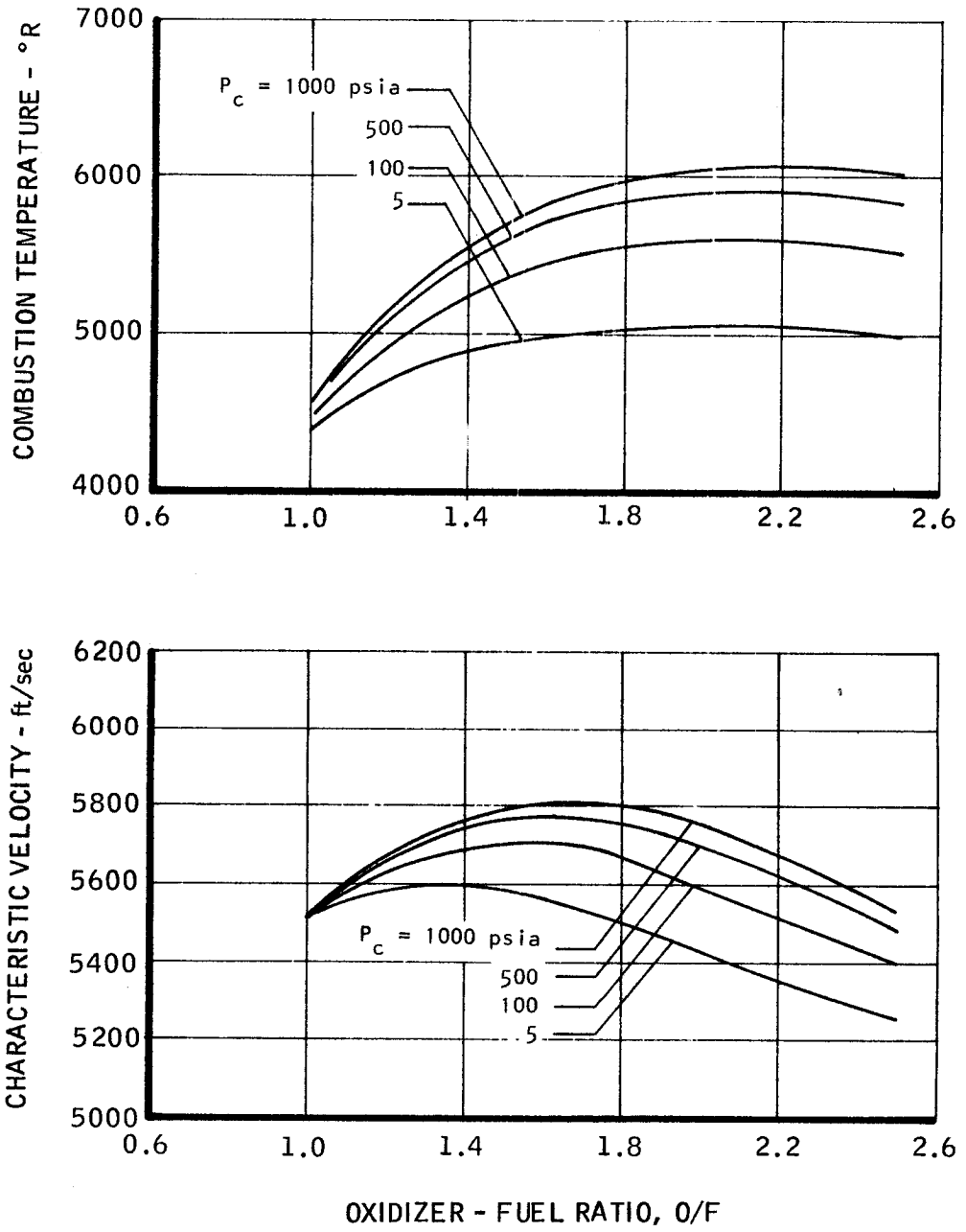

MAC A673

COMBUSTION PRODUCTS OF N_2 O_4 /0.5 N_2 H_4 - 0.5 UDHM
IN COMBUSTION CHAMBER

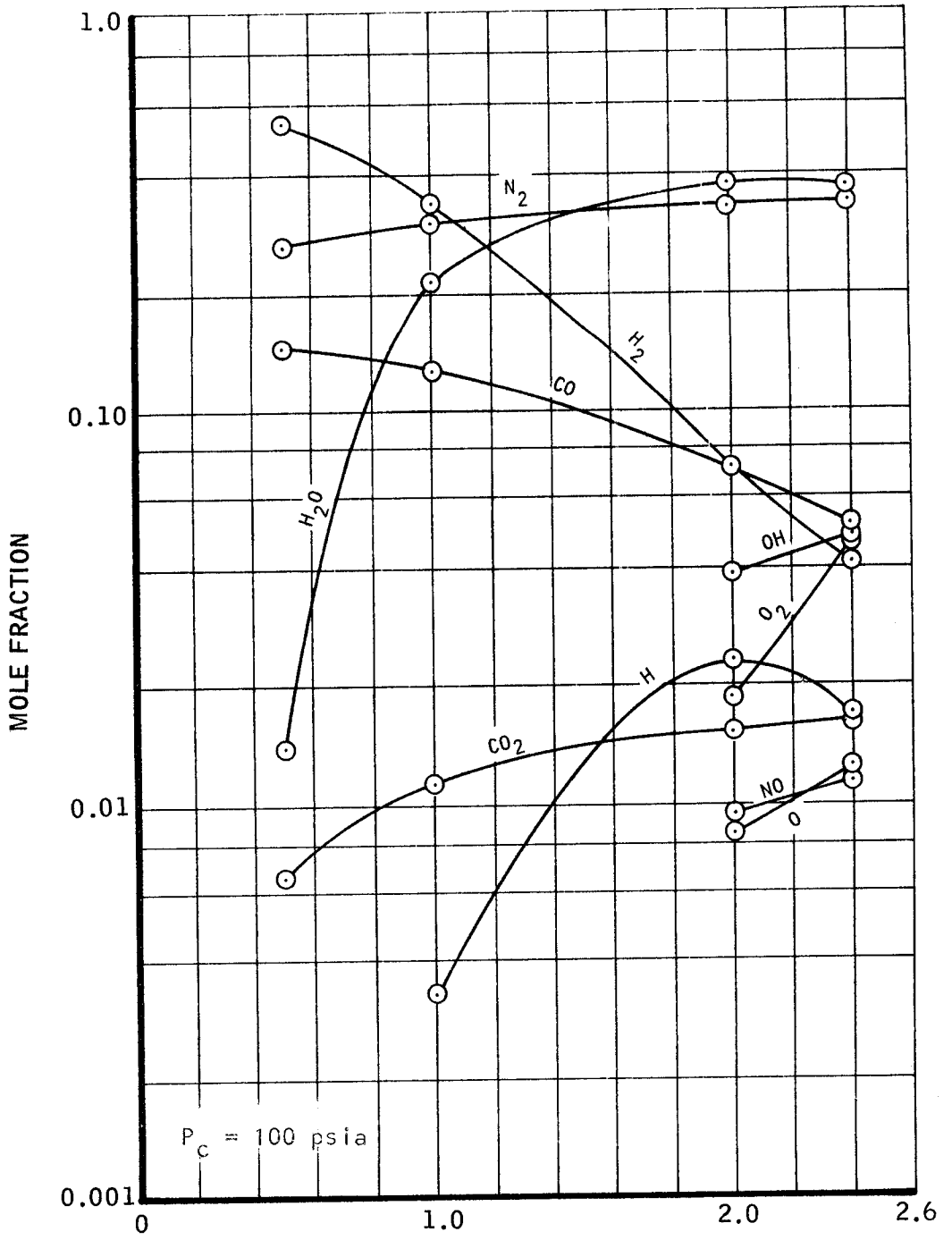

MAC A673

FIGURE 127

ROCKET ENGINE THEORETICAL SPECIFIC IMPULSE WITH LOX/LH_2

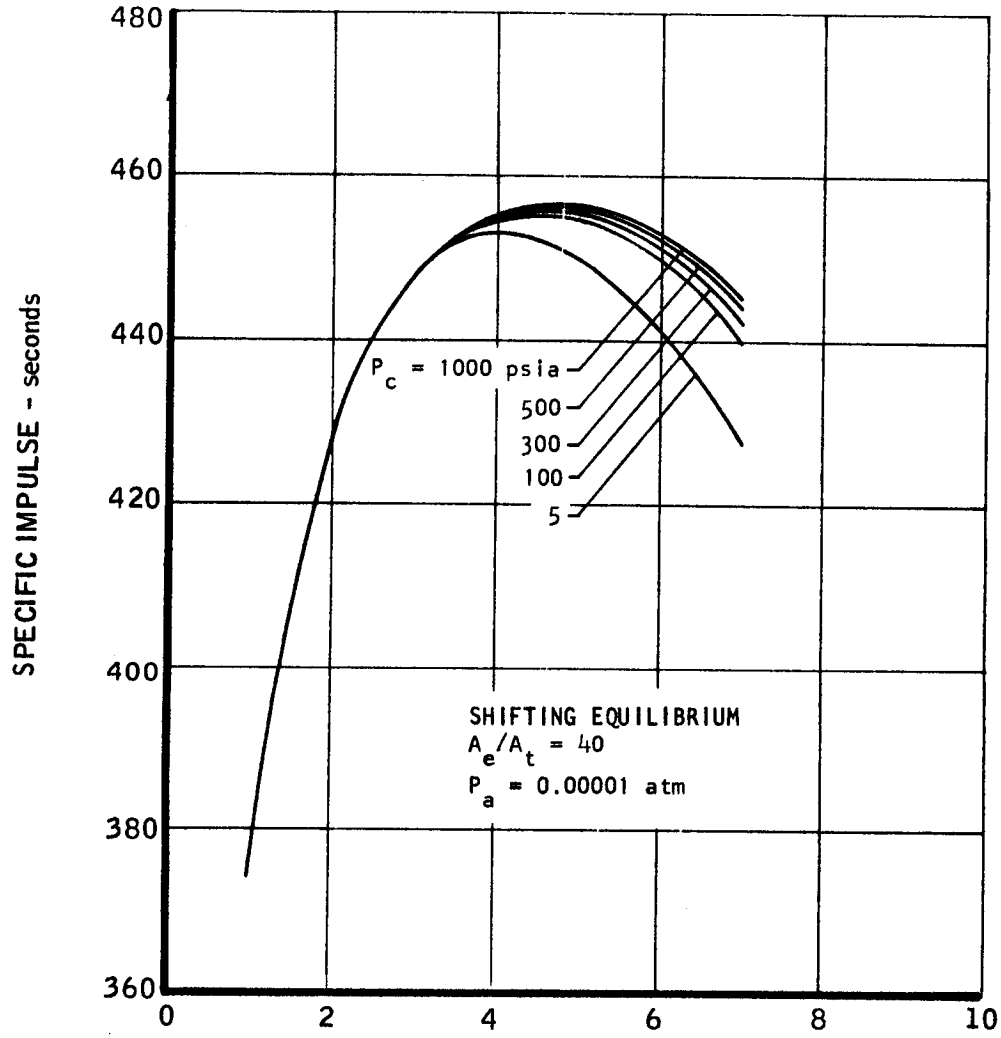

COMBUSTION TEMPERATURE AND CHARACTERISTIC VELOCITY OF LOX/LH_2

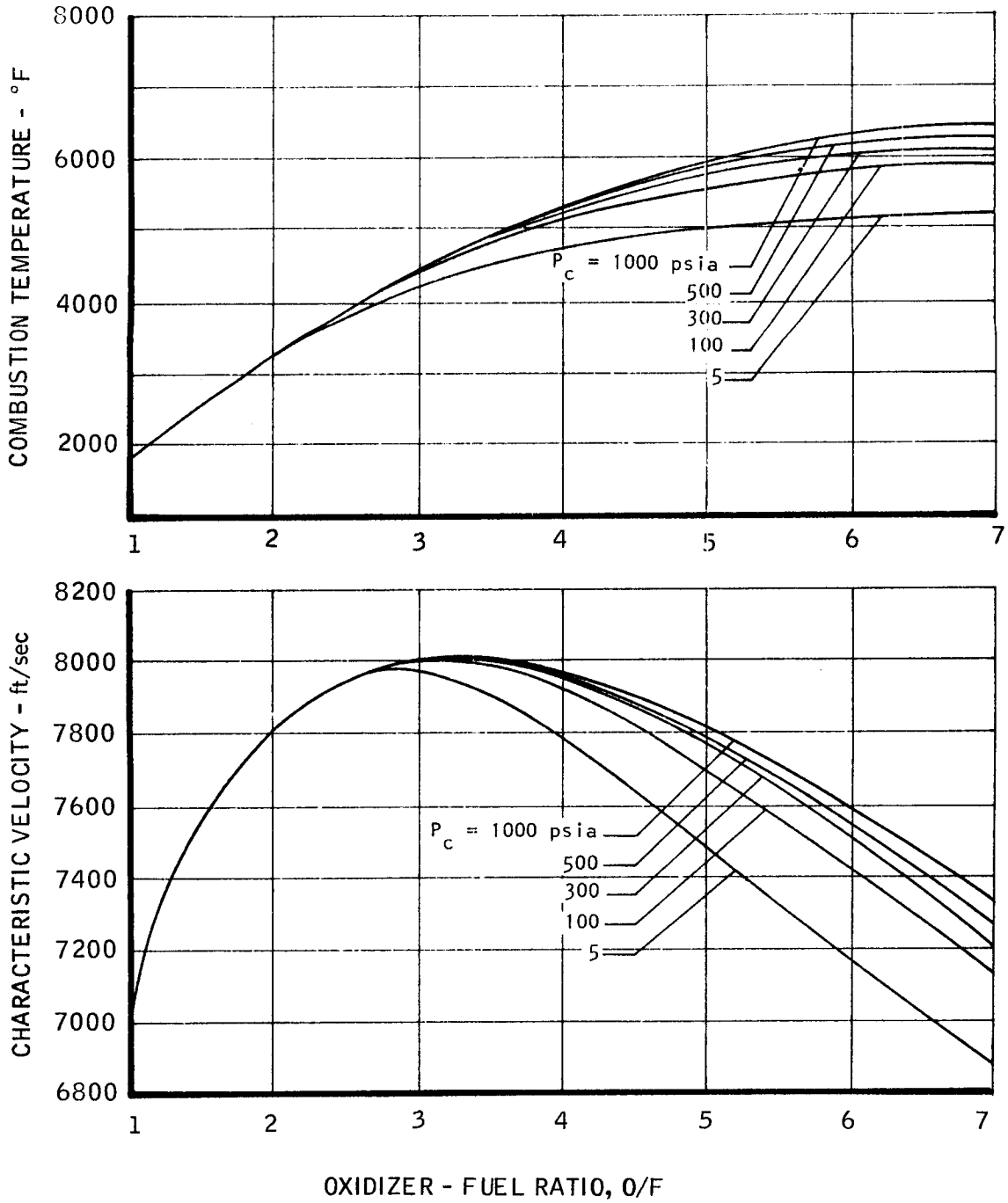

COMBUSTION PRODUCTS OF LH_2/LO_2 IN COMBUSTION CHAMBER

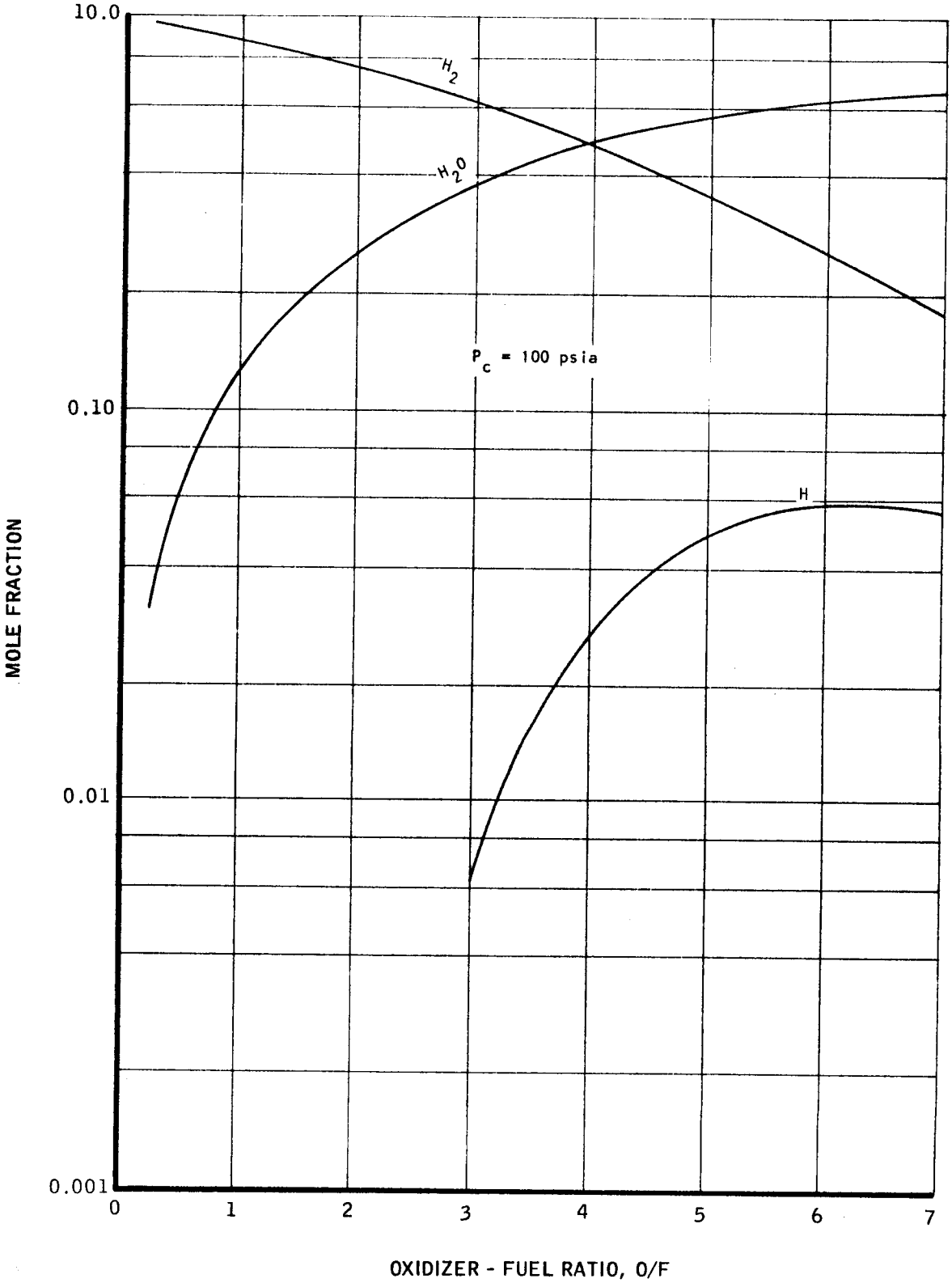

MAC A673

FIGURE 130

ROCKET ENGINE THEORETICAL SPECIFIC IMPULSE WITH LH_2 / LF_2

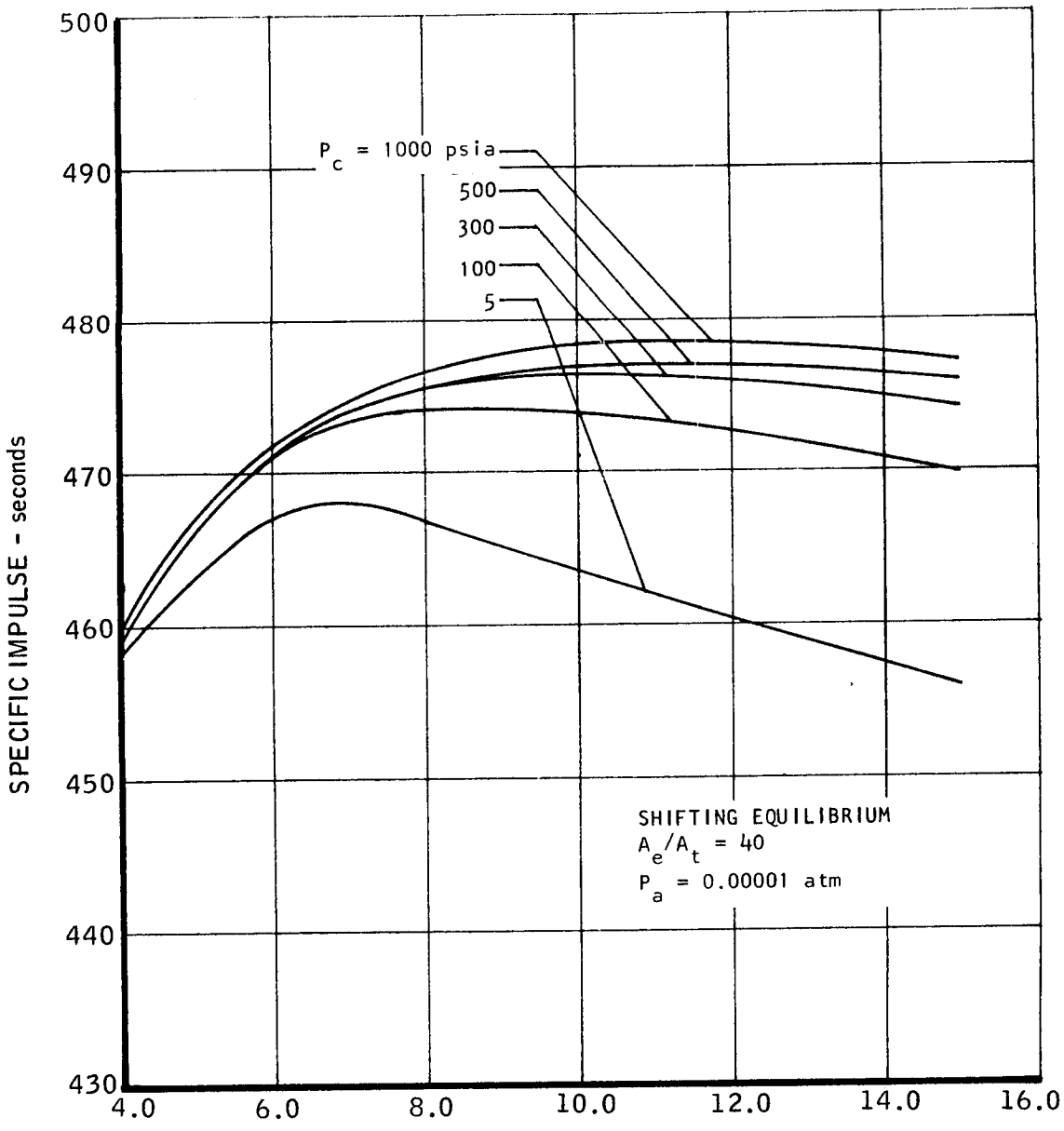

COMBUSTION TEMPERATURE AND CHARACTERISTIC VELOCITY OF LH_2/LF_2

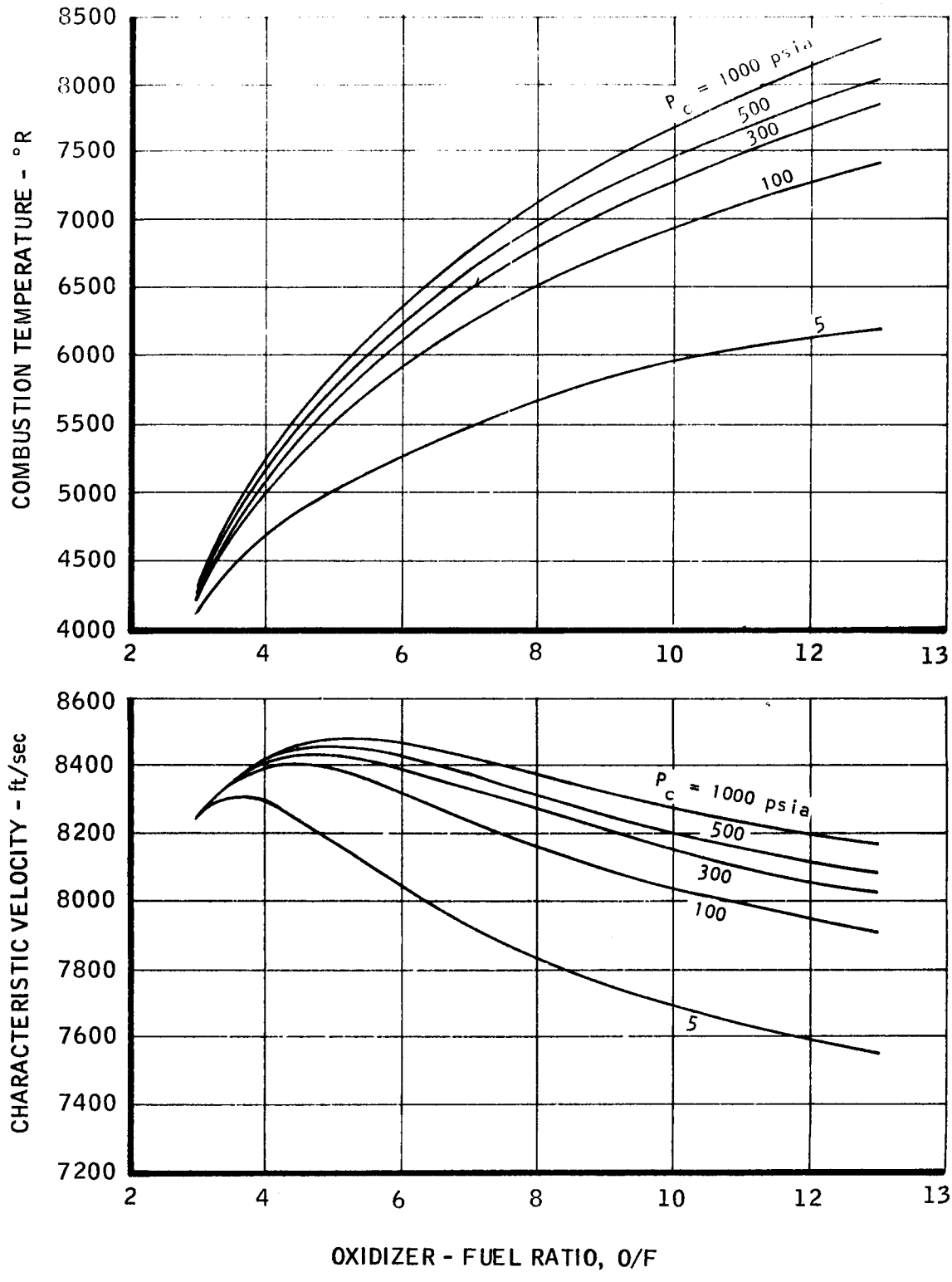

MAC A673

FIGURE 132

ROCKET ENGINE THEORETICAL SPECIFIC IMPULSE WITH OF_2 / H_2 (LIQUID)

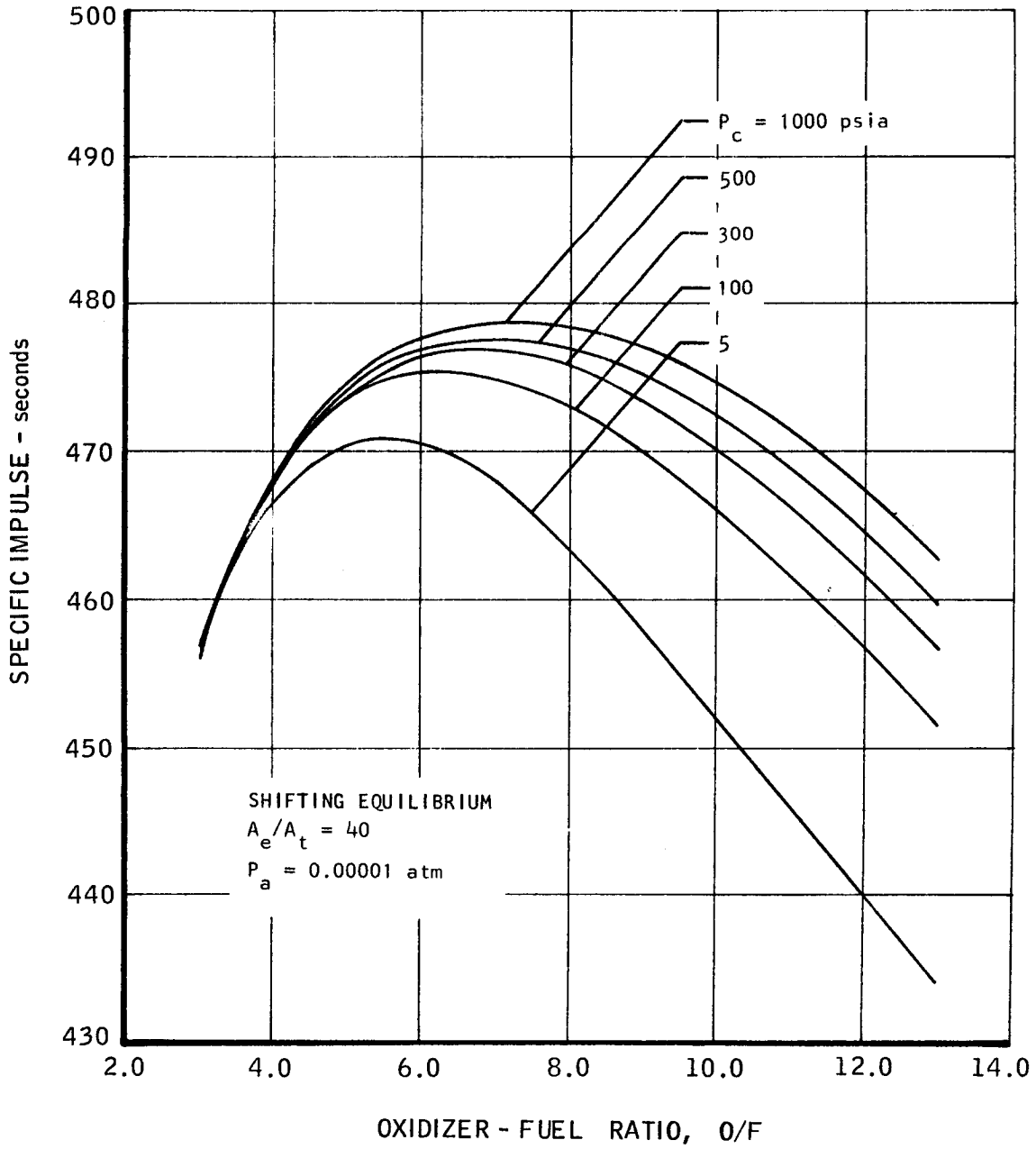

MAC A673

FIGURE 133

COMBUSTION TEMPERATURE AND CHARACTERISTIC VELOCITY OF OF_2/H_2 (LIQUID)

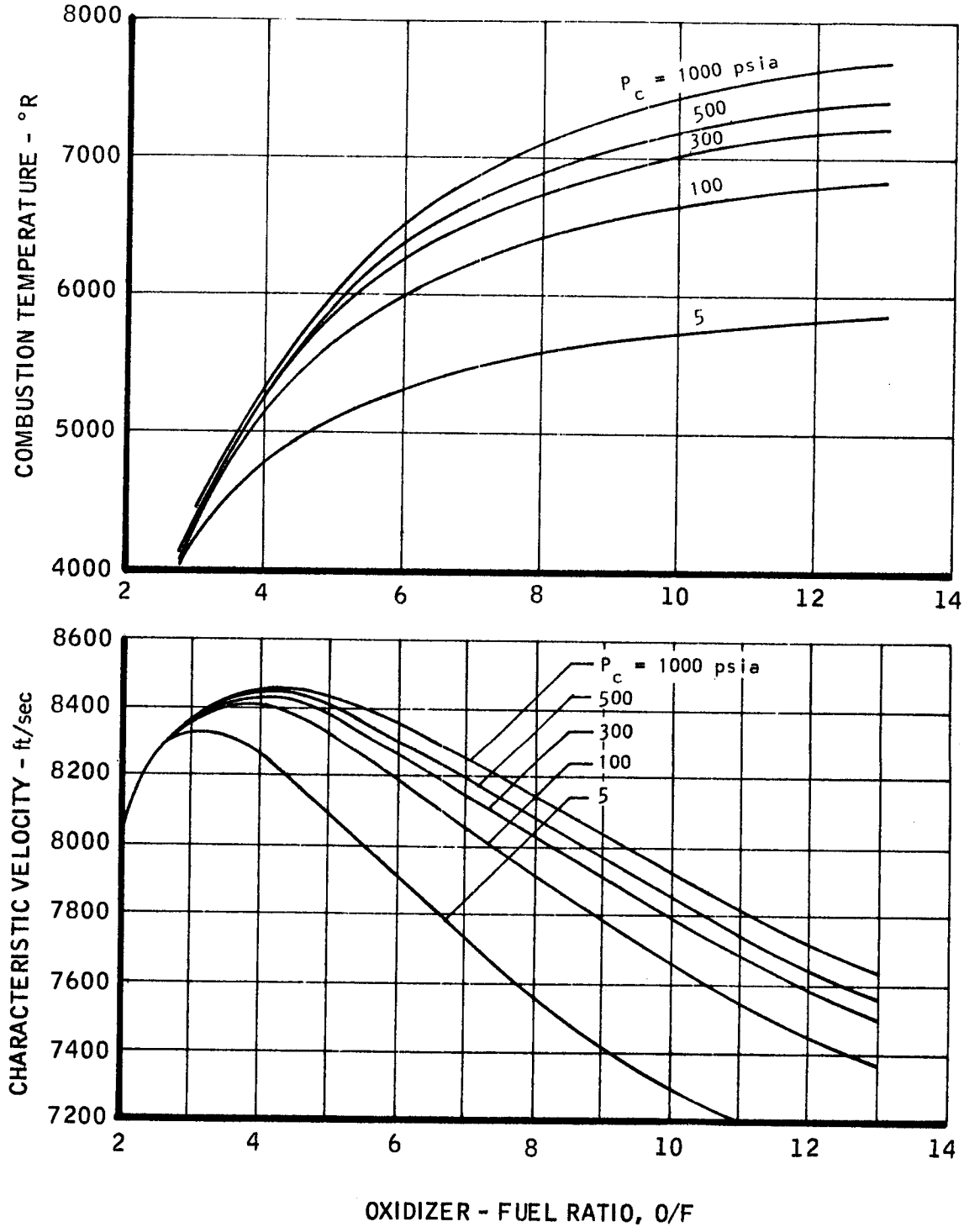

COMBUSTION PRODUCTS OF OF_2/H_2 IN COMBUSTION CHAMBER

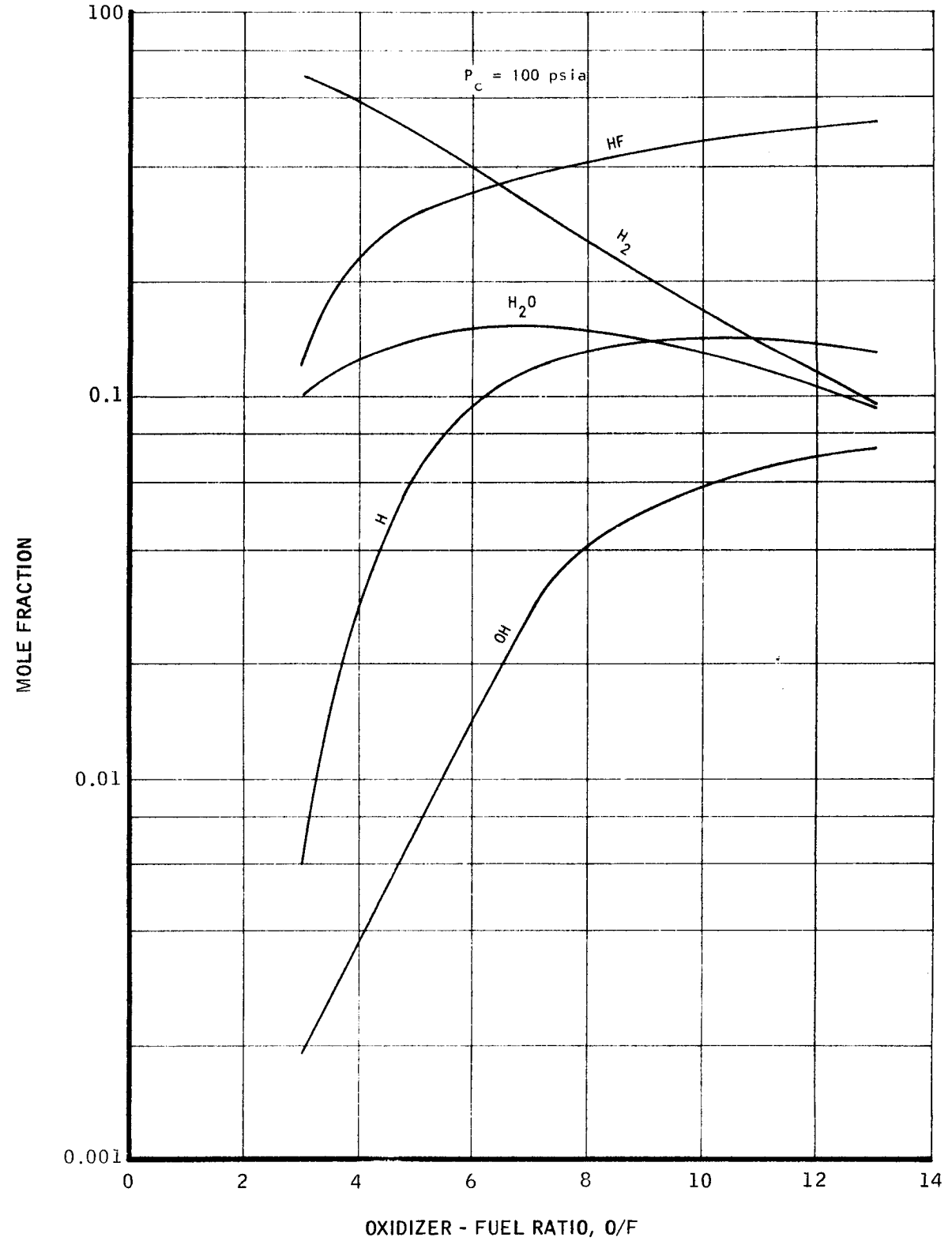

MAC A673

FIGURE 135

ROCKET ENGINE THEORETICAL SPECIFIC IMPULSE WITH OF_2/DIBORANE

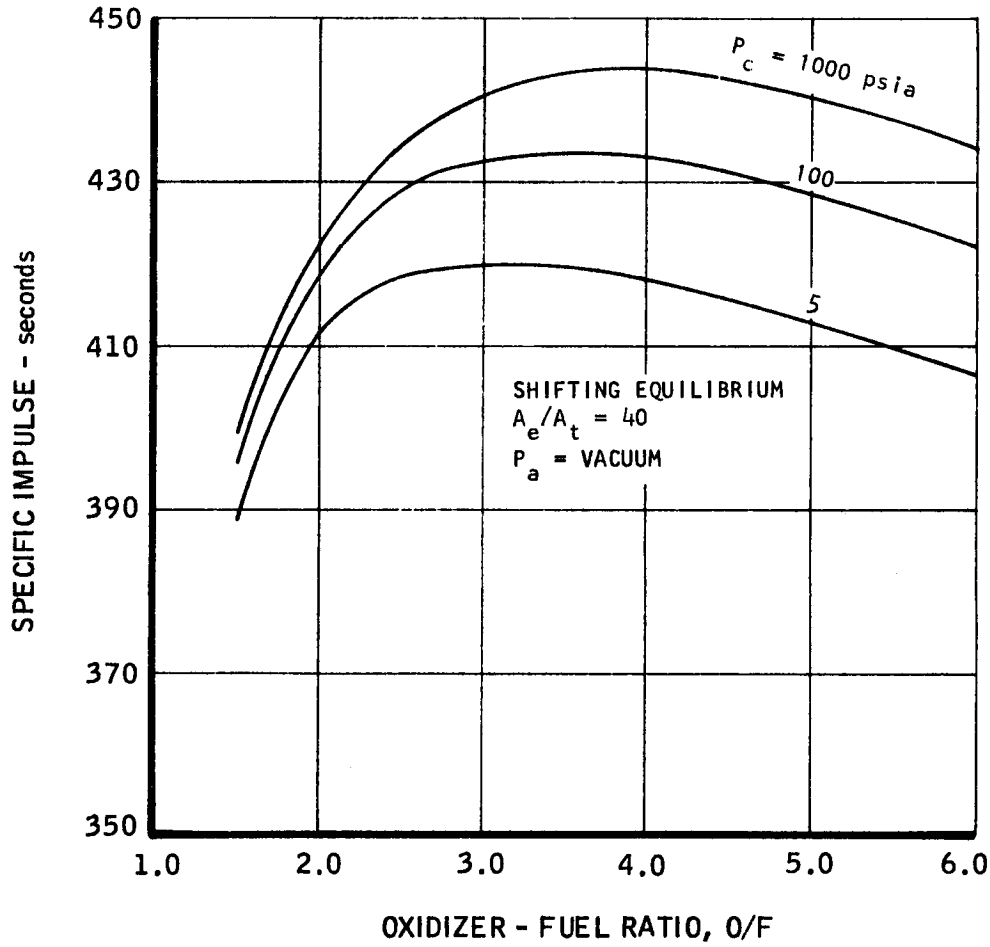

COMBUSTION TEMPERATURE AND CHARACTERISTIC VELOCITY OF OF_2/DIBORANE

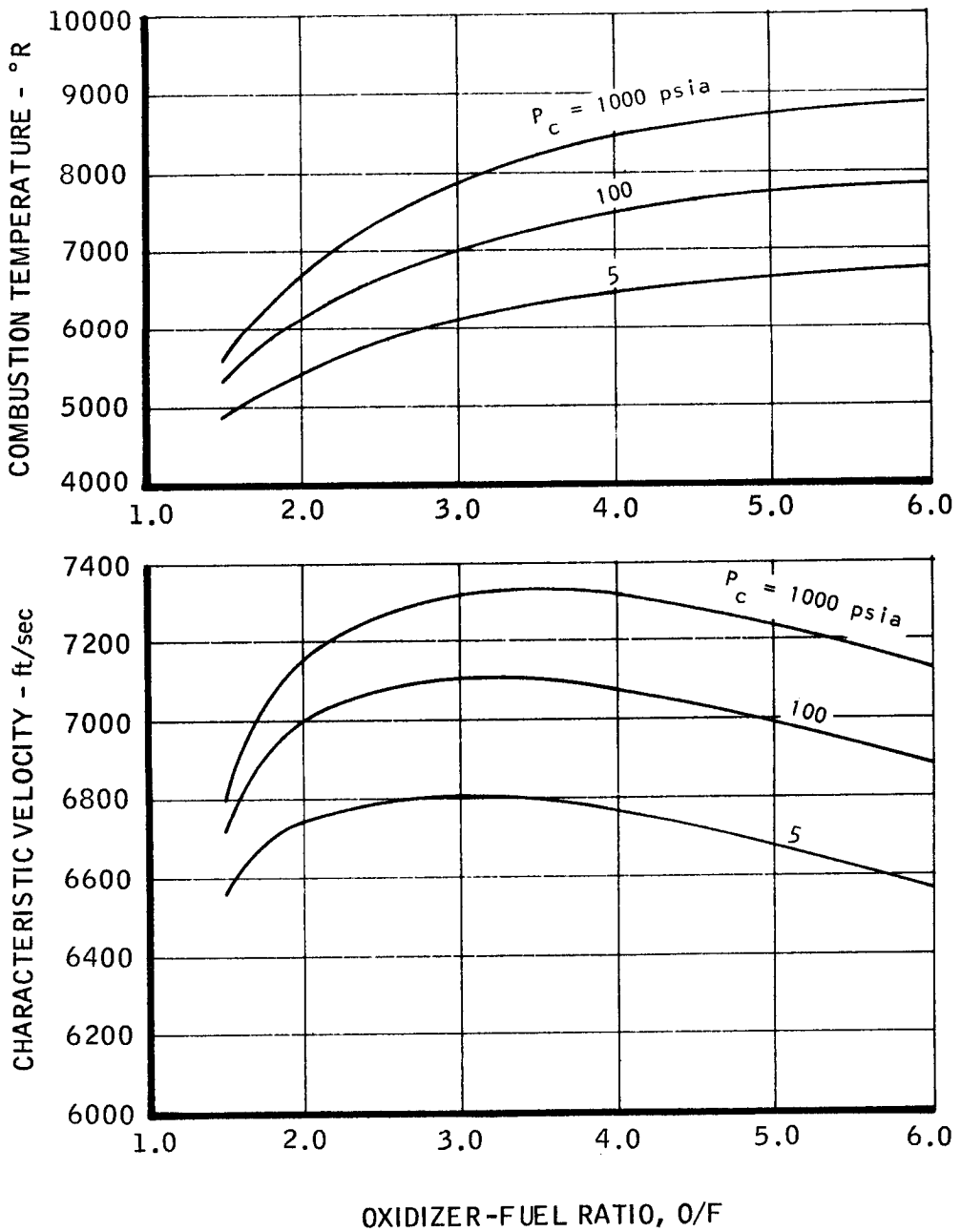

COMBUSTION PRODUCTS OF OF_2/DIBORANE IN COMBUSTION CHAMBER

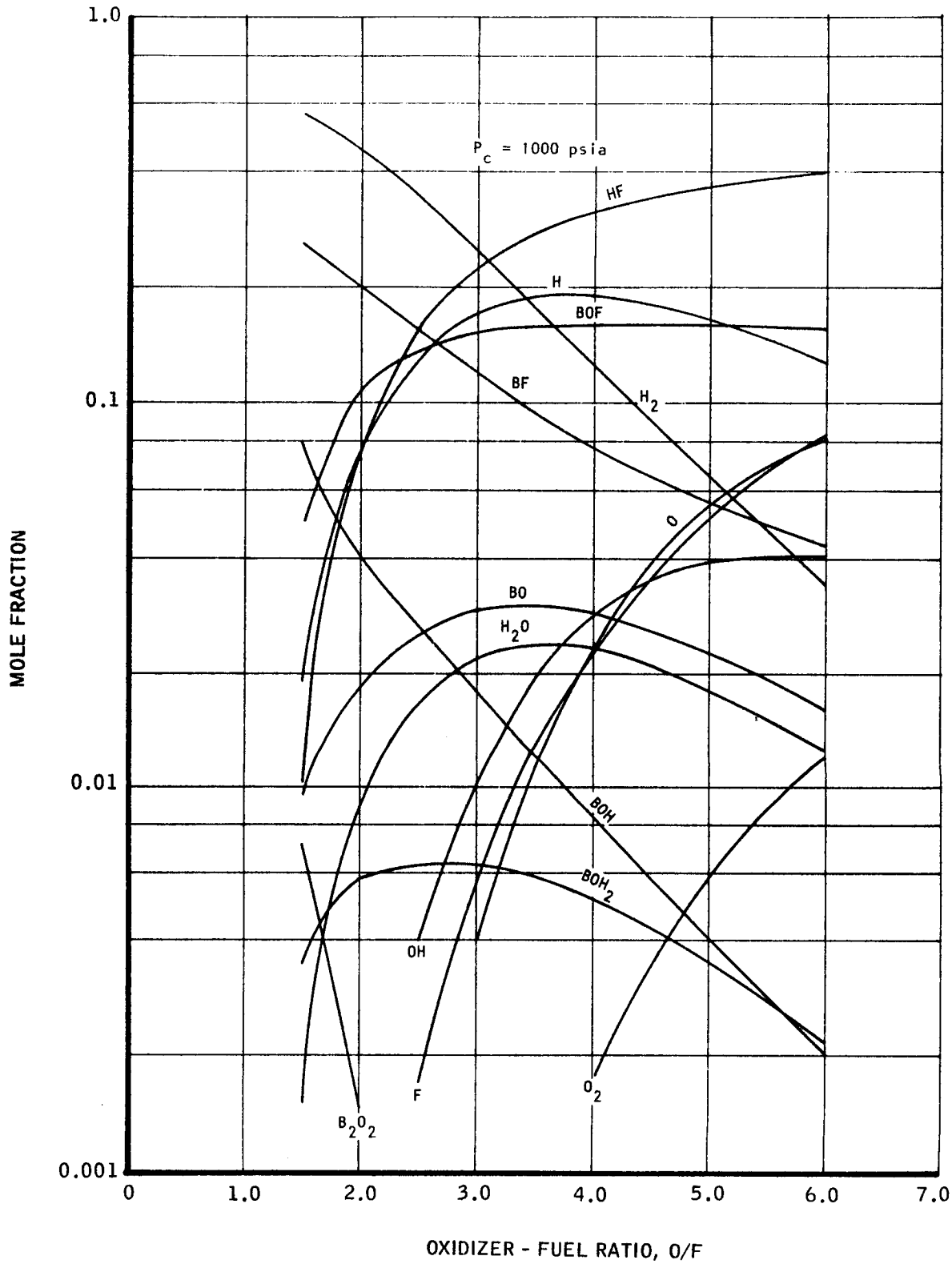

MAC A673

FIGURE 138

ROCKET ENGINE THEORETICAL SPECIFIC IMPULSE WITH OF_2/METHANE

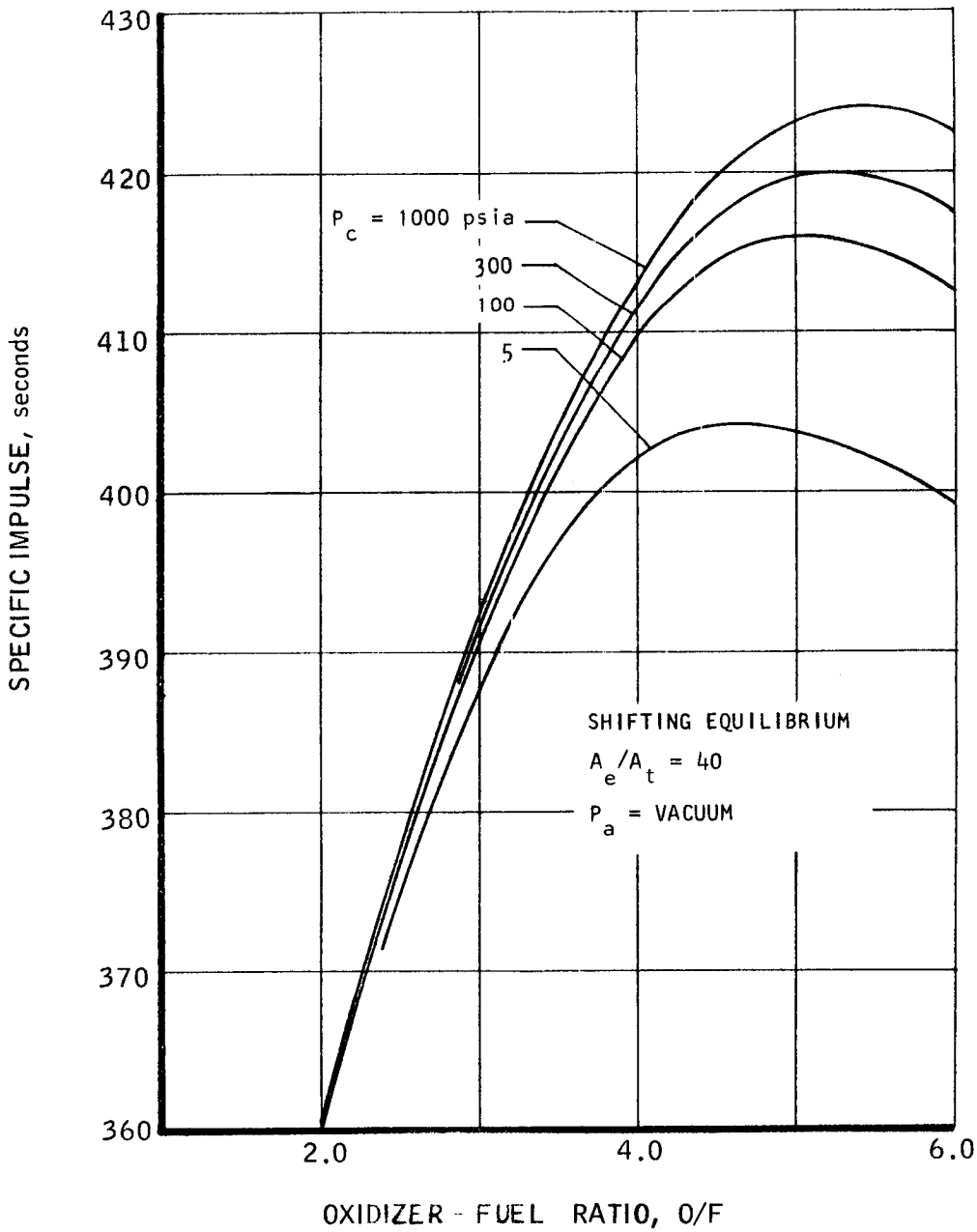

FIGURE 139

COMBUSTION TEMPERATURE AND CHARACTERISTIC VELOCITY OF OF_2/METHANE

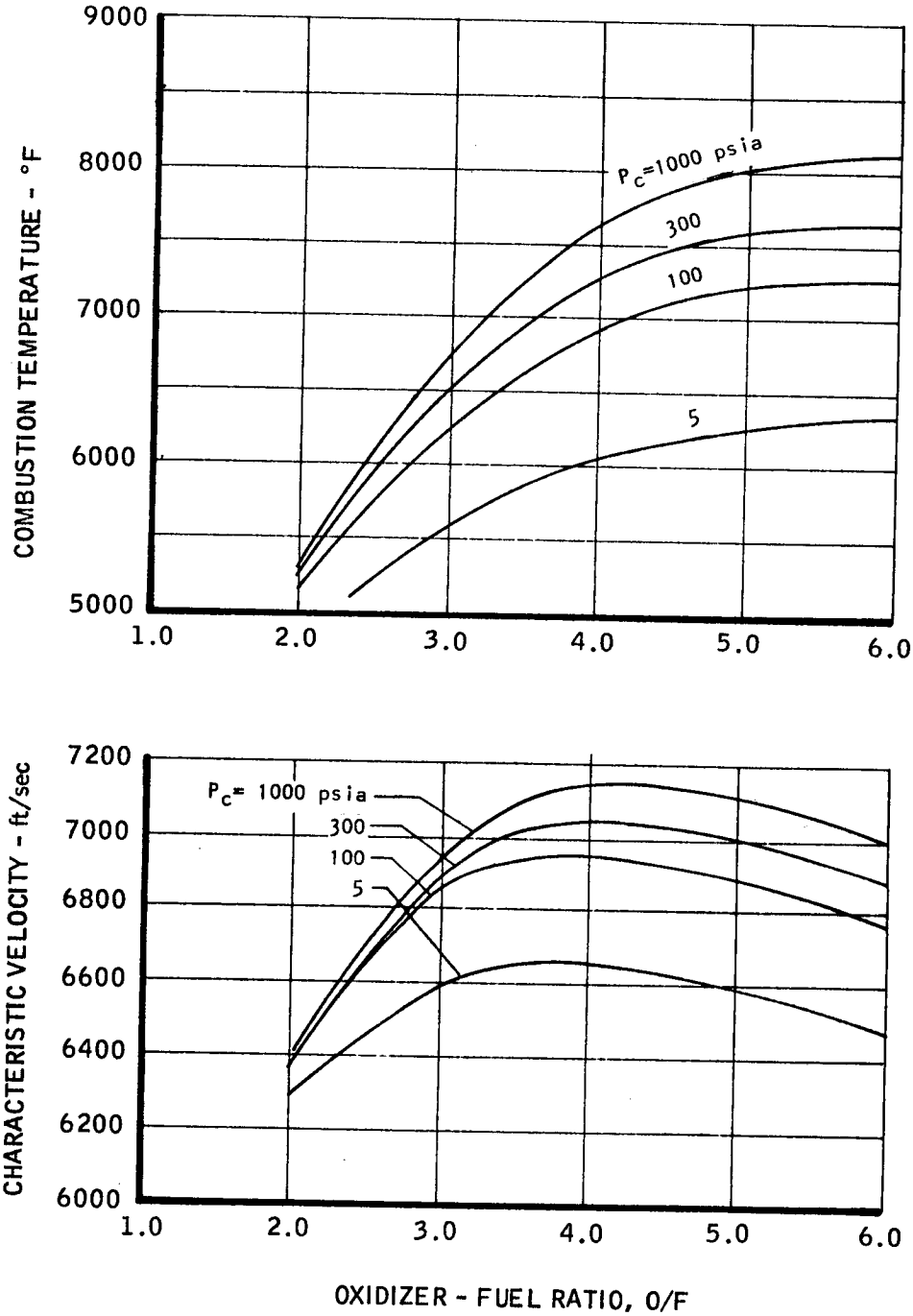

COMBUSTION PRODUCTS OF OF_2/METHANE IN COMBUSTION CHAMBER

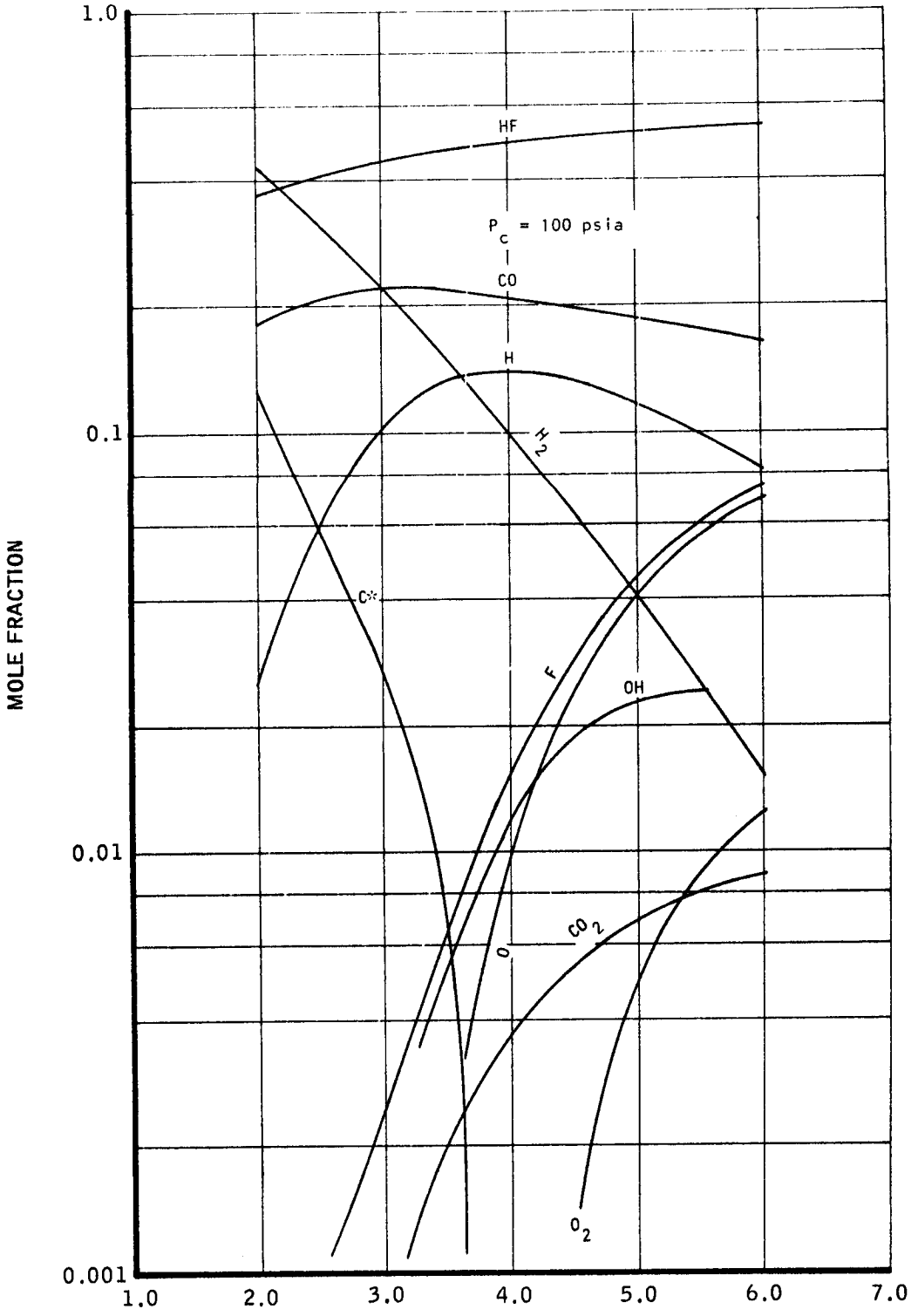

MAC A 673

FIGURE 141

OXIDATION RESISTANCE OF ALLOYS
(2000° F, STATIC AIR)

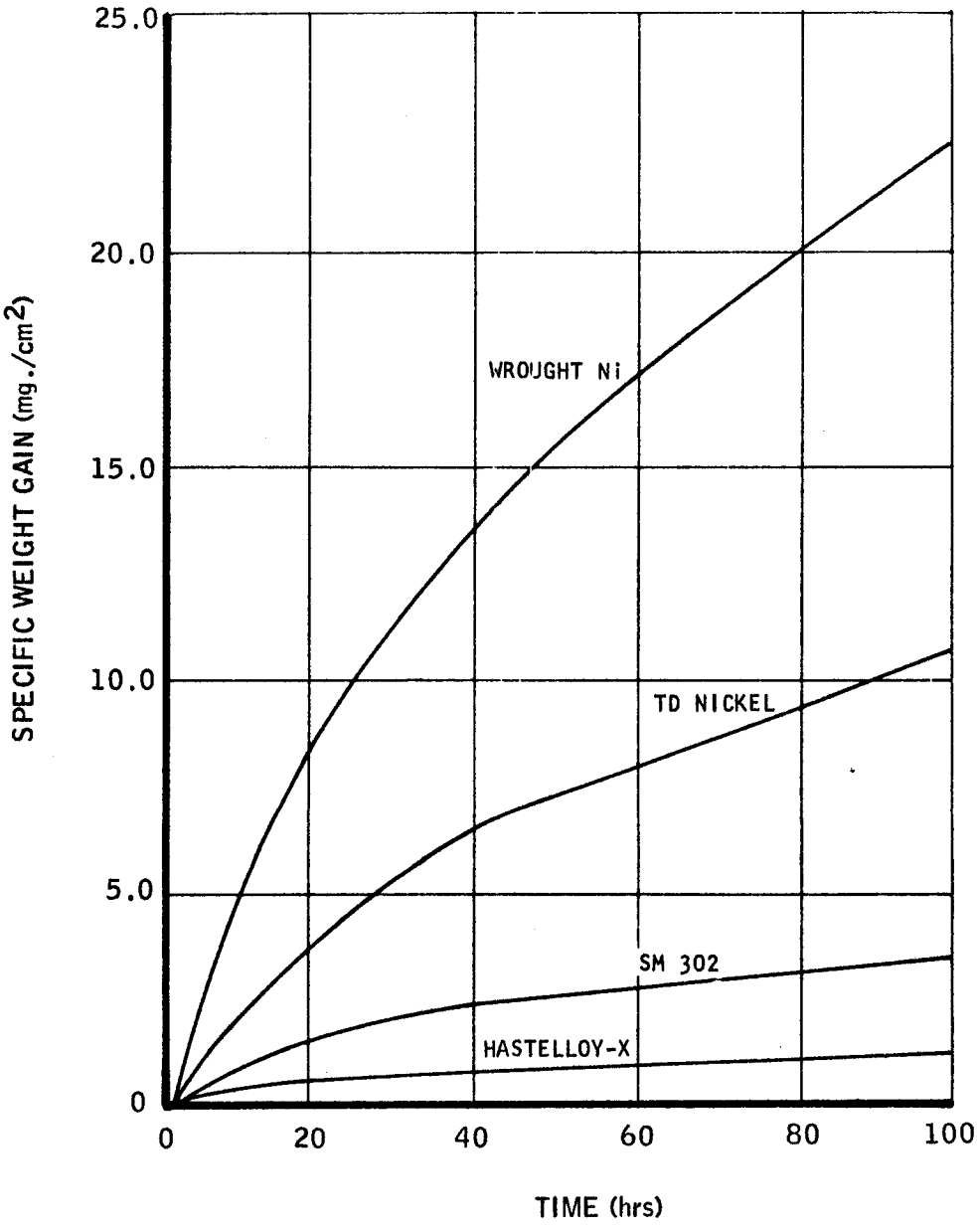

MAC A673

COMPARATIVE ULTIMATE TENSILE STRENGTH OF ALLOYS AT HIGH TEMPERATURES

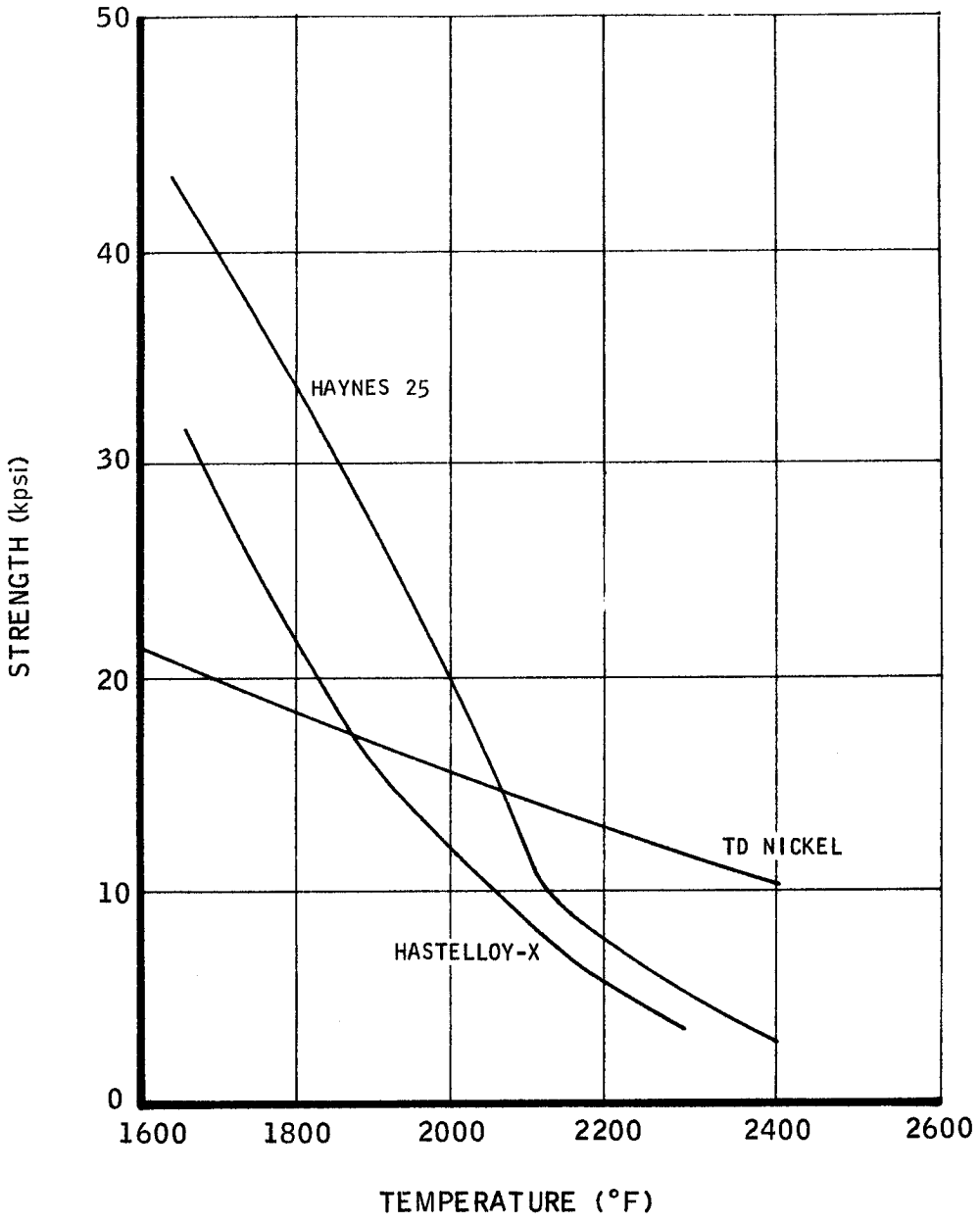

MAC A673

FIGURE 143

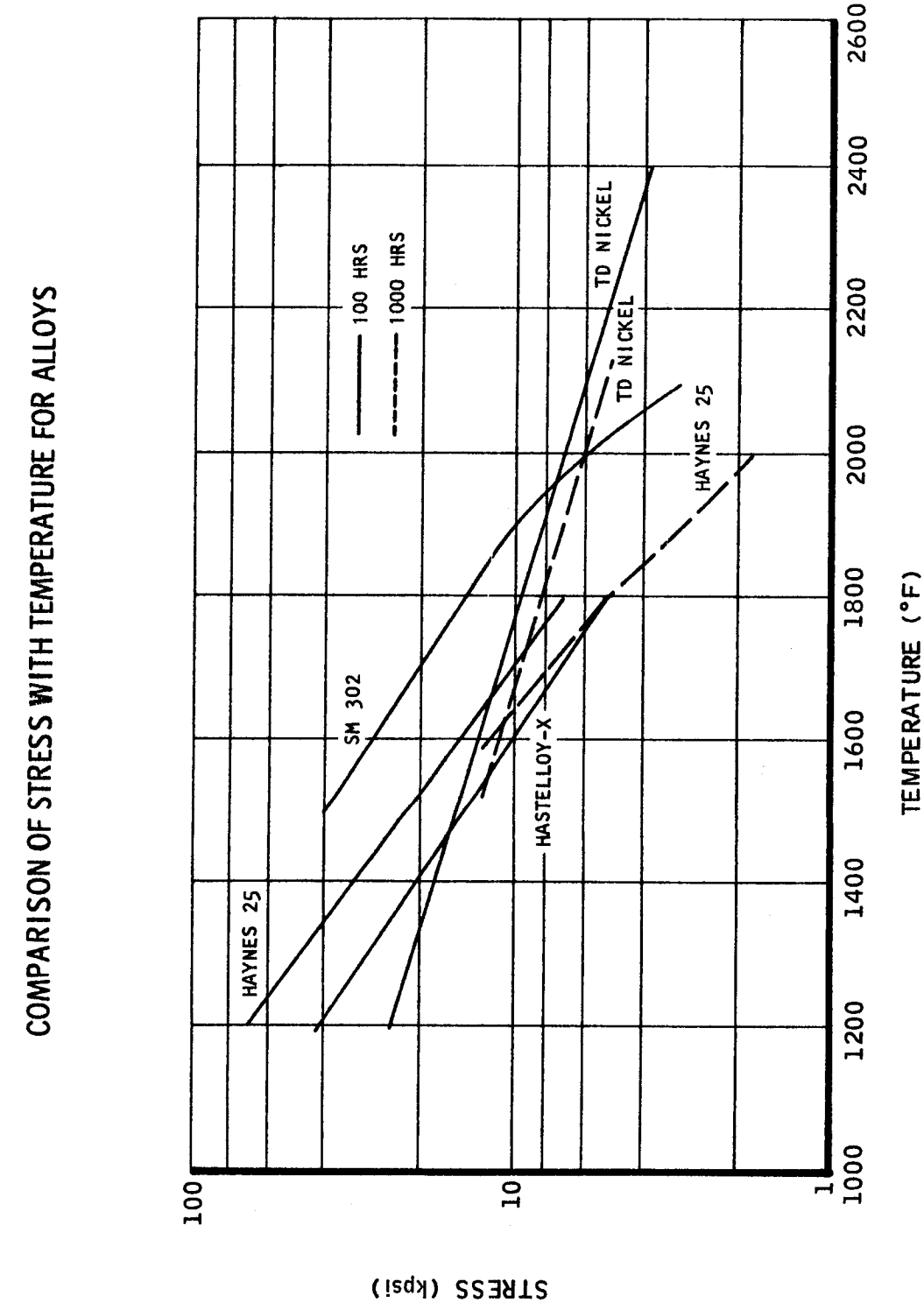

MAC A673

FIGURE 144

INCREASED STRENGTH OF TYPICAL HIGH TEMPERATURE STRUCTURAL ALLOYS SINCE 1958

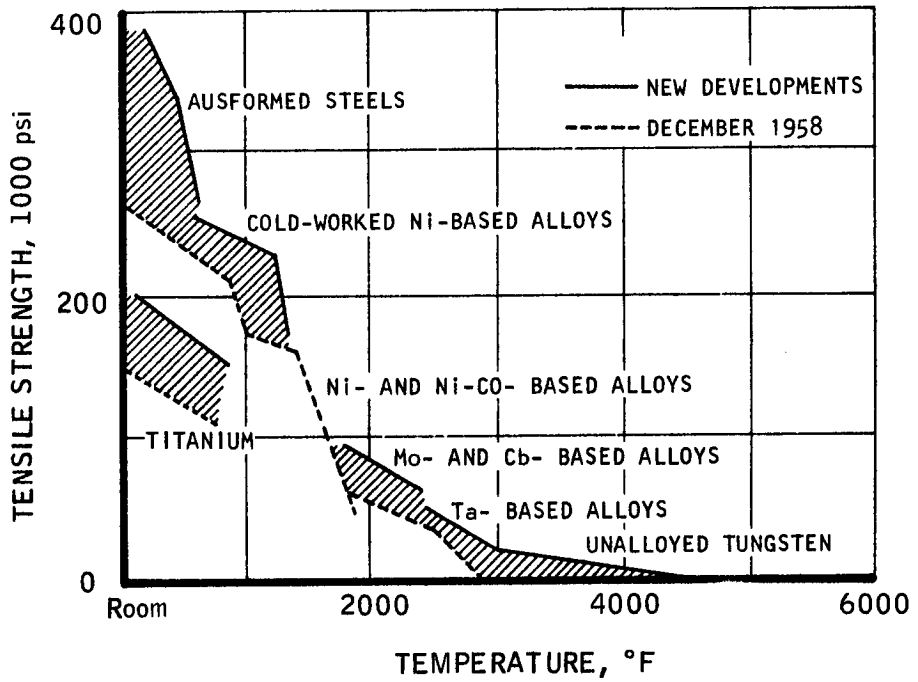

NOTE

SHADED AREAS INDICATE THE EXTENT OF THE INCREASE AS MEASURED BY TENSILE STRENGTH

MAC A63

STRENGTH - TO - WEIGHT RATIO OF UNALLOYED TUNGSTEN
AND THREE TUNGSTEN - MOLYBDENUM ALLOYS

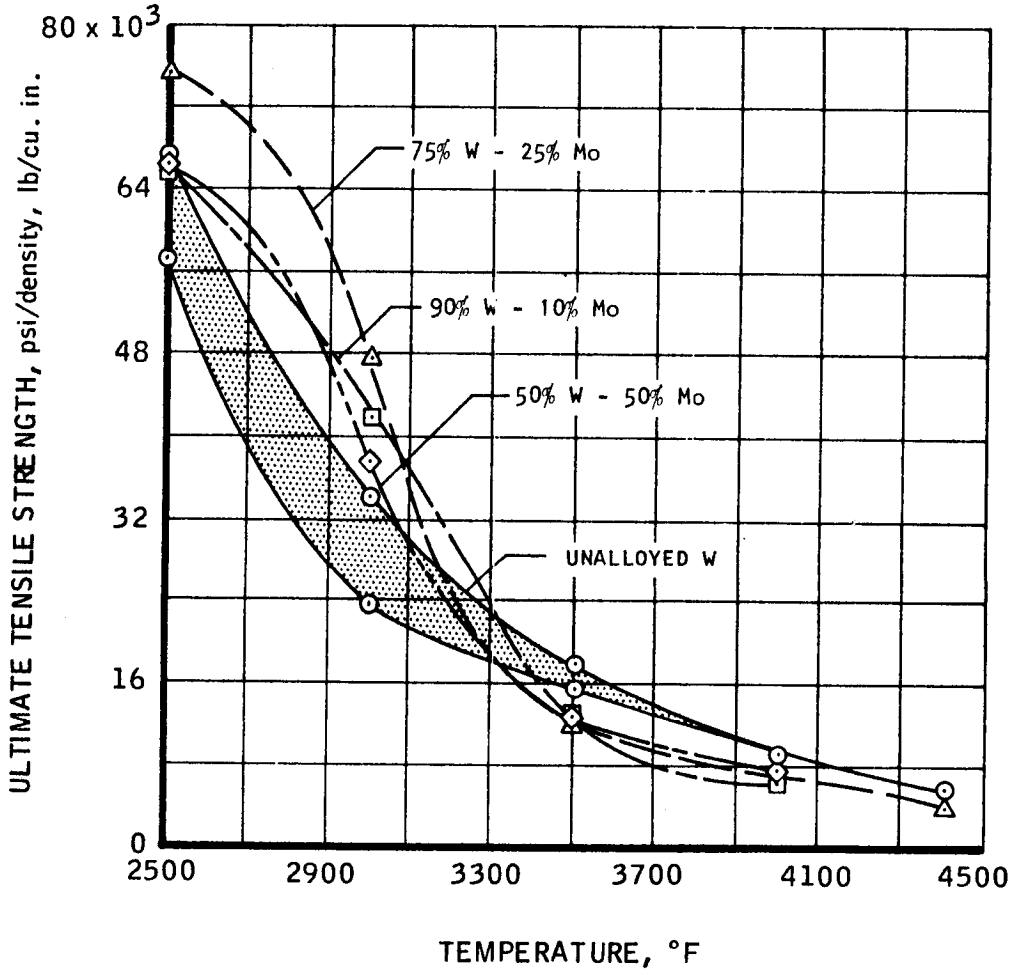

EFFECT OF ALLOYING TUNGSTEN WITH MOLYBDENUM ON ULTIMATE TENSILE STRENGTH AND THE STRENGTH-TO-WEIGHT RATIO

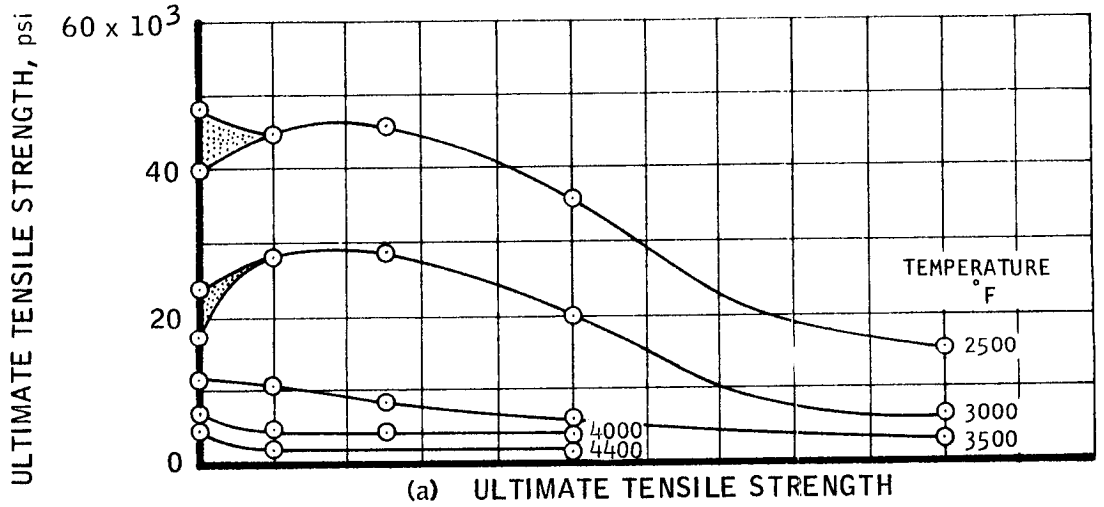

(a) ULTIMATE TENSILE STRENGTH

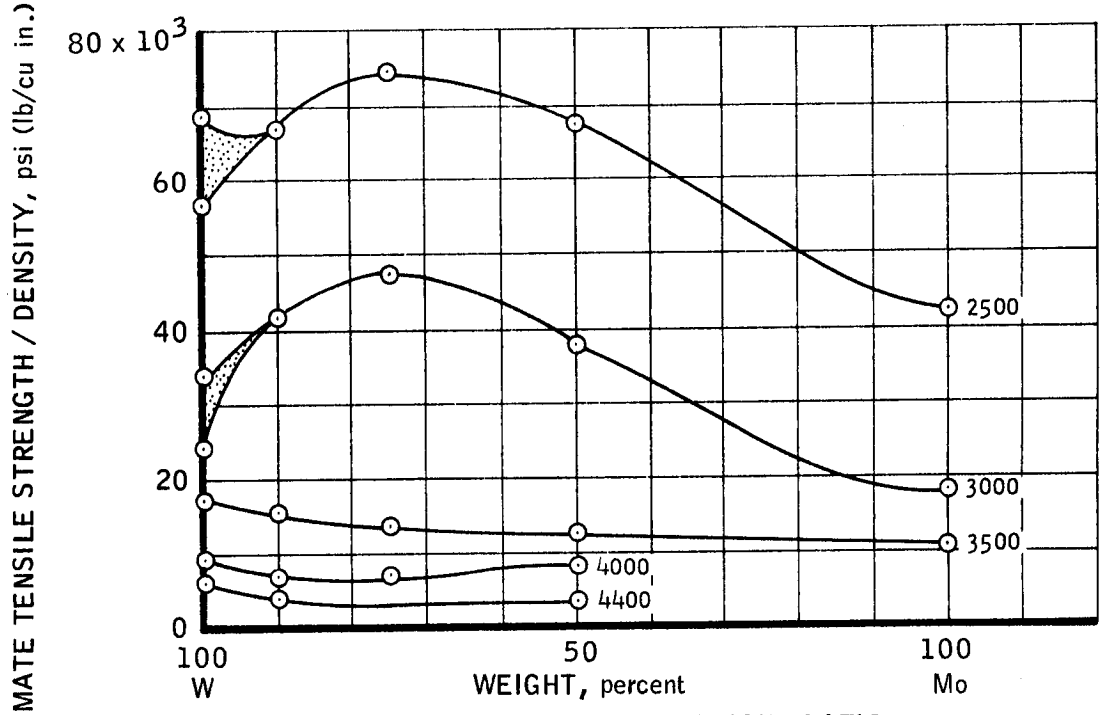

(b) STRENGTH-TO-WEIGHT RATIO

FIGURE 147

COLUMBIUM TENSILE STRENGTH / DENSITY RATIO vs. TEMPERATURE

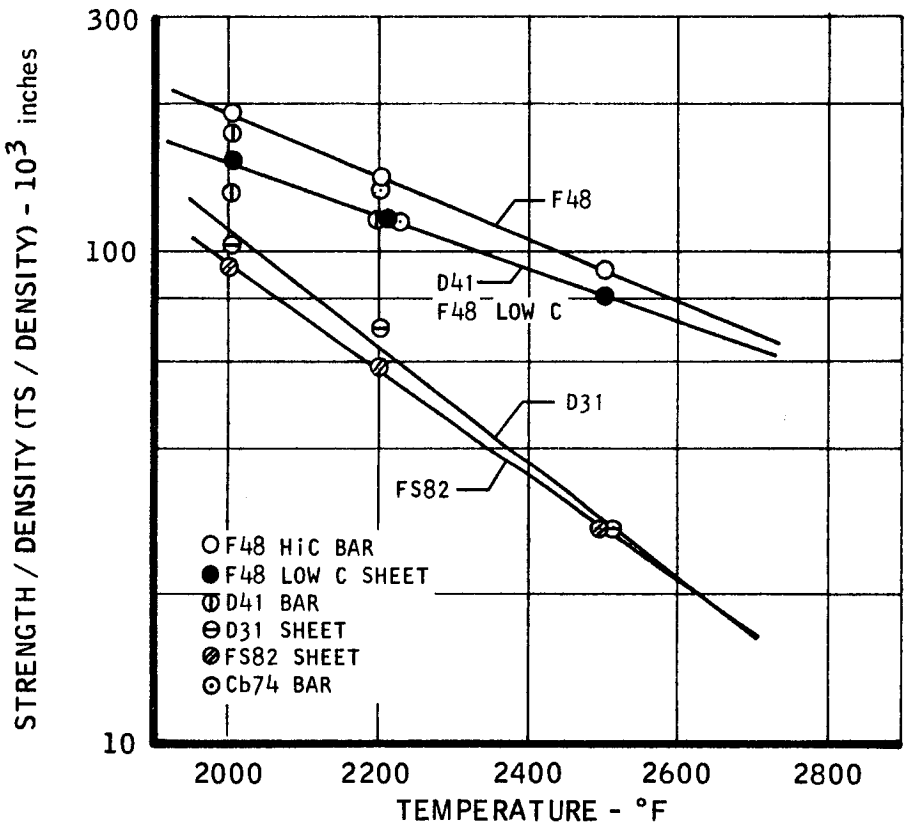

FIGURE 149

0.2% YIELD STRENGTH TO WEIGHT RATIOS FOR VARIOUS REFRACTORY METAL ALLOYS

TEST CONDITIONS:

MACHINE - E.T.T.M.
METHOD OF HEATING - RESISTANCE
TIME TO TEST TEMPERATURE - 200°F/sec
HOLD TIME AT TEMPERATURE - 5 min
STRAIN RATE TO Y.S. - 0.001 in./in./sec
STRAIN RATE FROM Y.S. TO U.T.S. -
0.01 in./in./sec
ATMOSPHERE - INERT
MATERIAL - SHEET AND UNCOATED

*BATTELLE MEMORIAL INSTITUTE

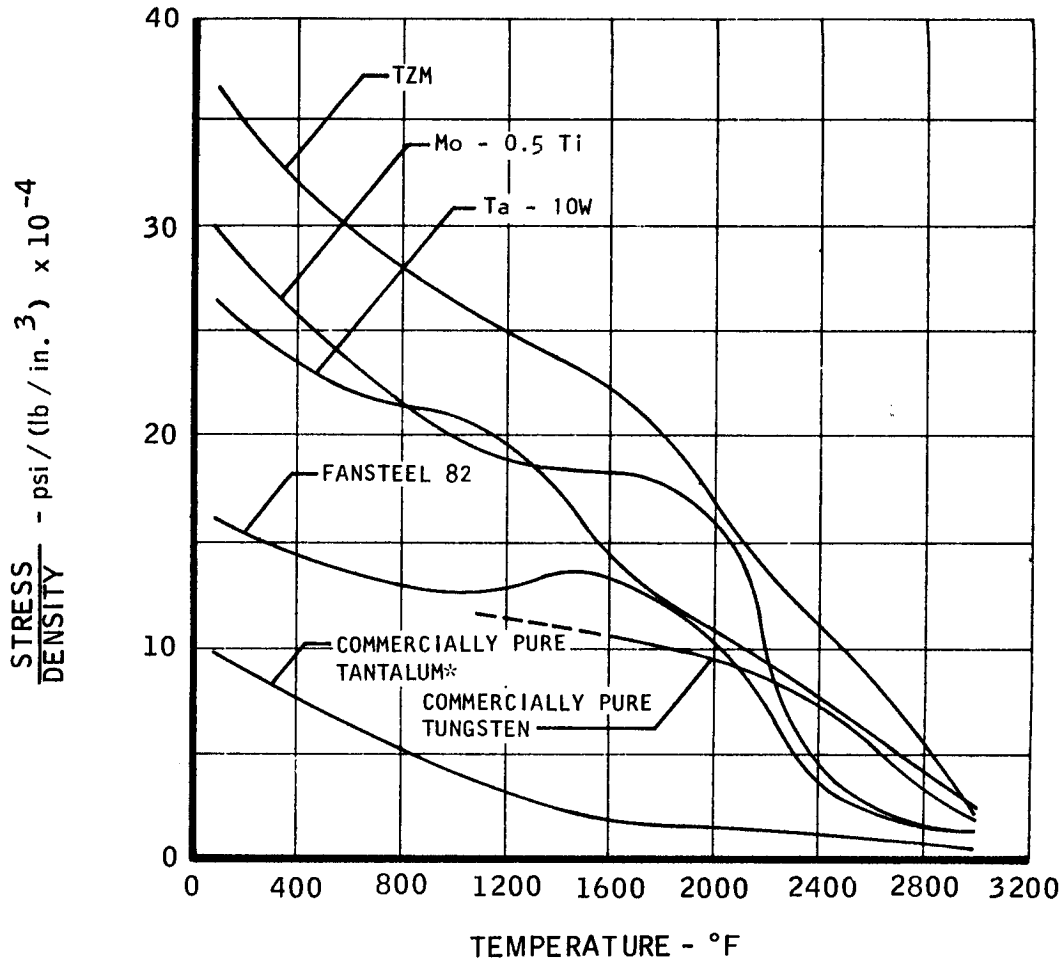

MAC A673

CREEP STRENGTH / DENSITY RATIO FOR SEVERAL MATERIALS
0.2% CREEP, 10 MINUTES

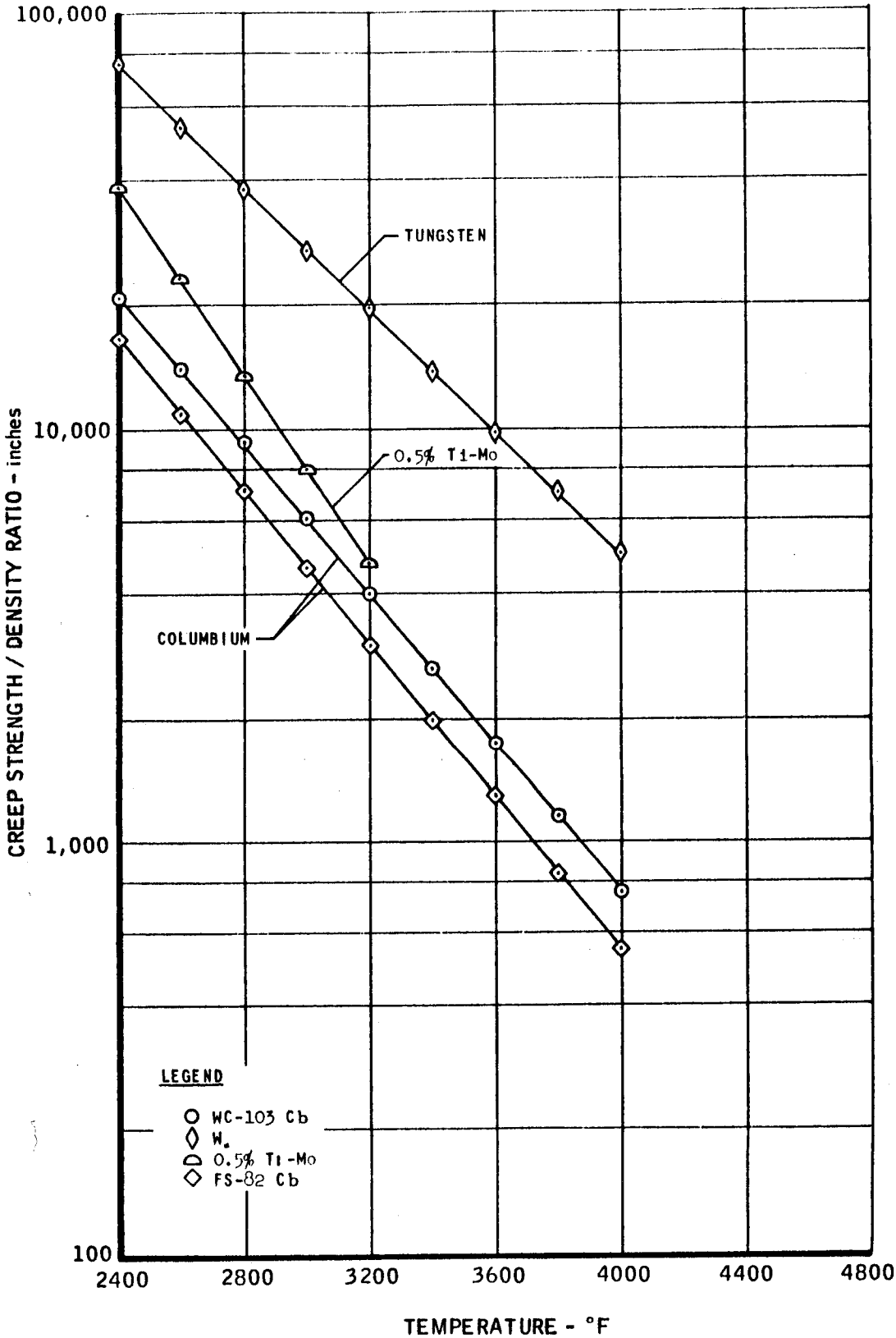

FIGURE 150

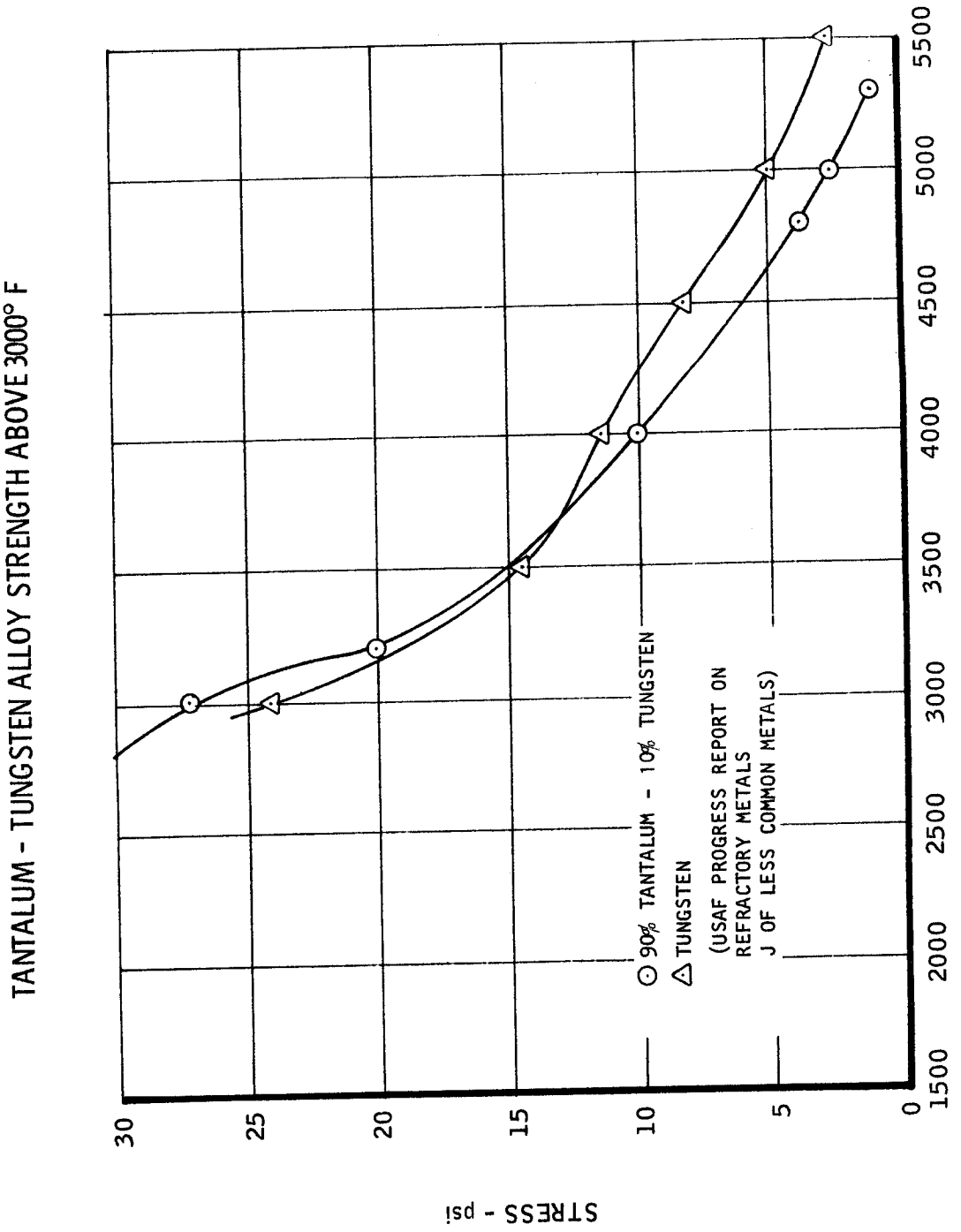

MAC A673

FIGURE 151

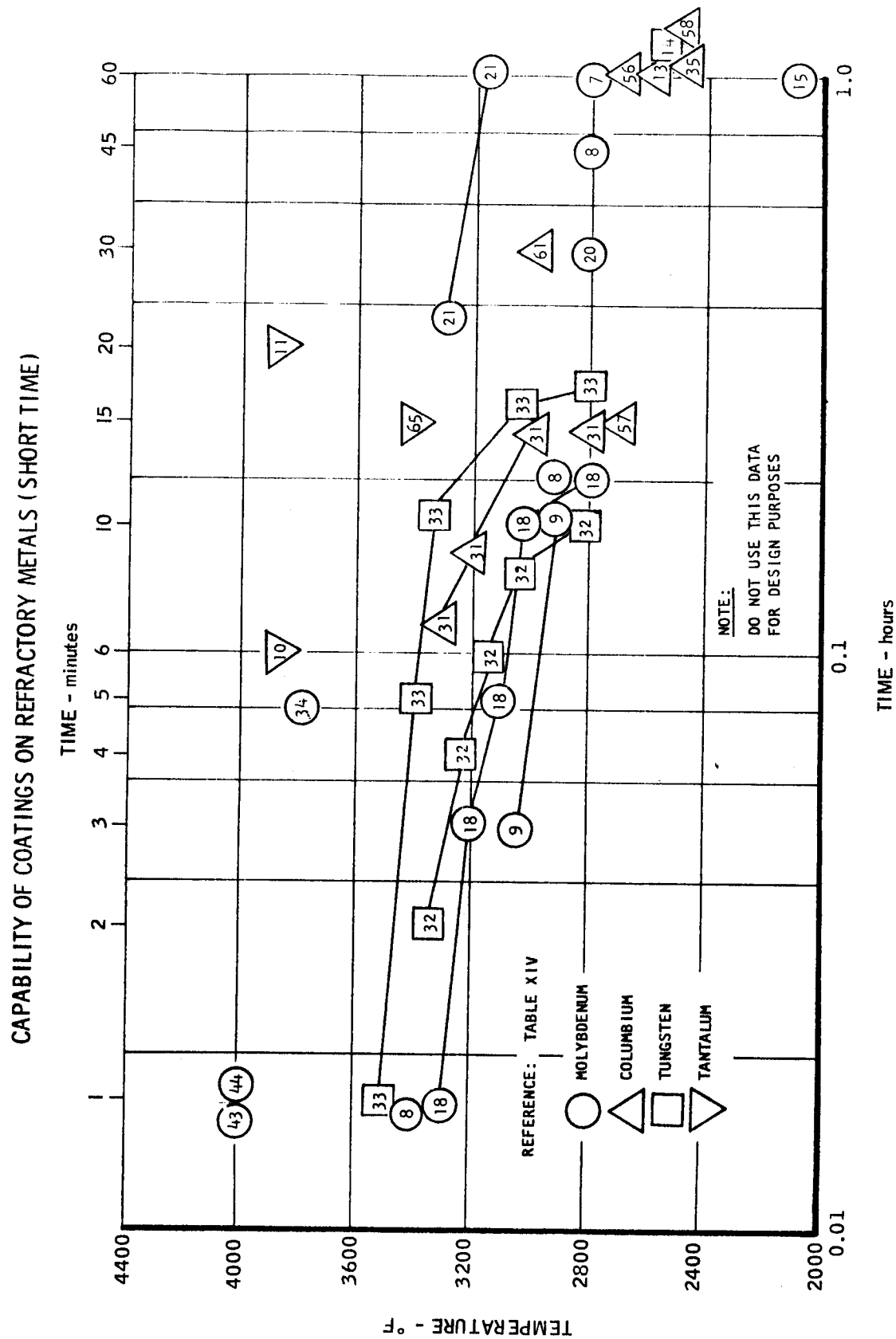

MAC A673

FIGURE 152

CAPABILITY OF COATINGS ON REFRACTORY METALS (LONG TIME)

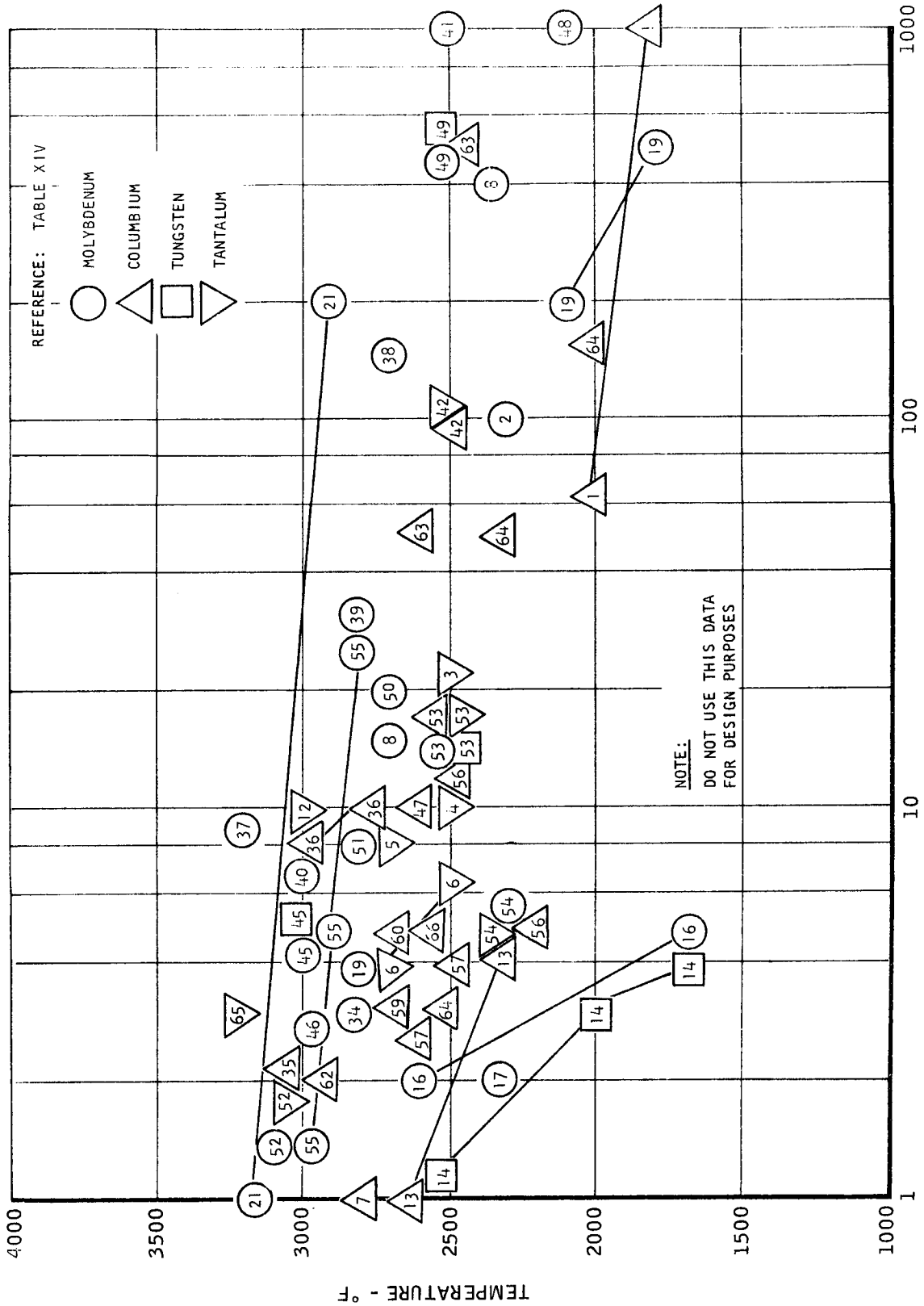

MAC A673

FIGURE 153

CHANGES IN OXIDATION RATE OF REFRACTORY METALS IN RELATION TO TEMPERATURE

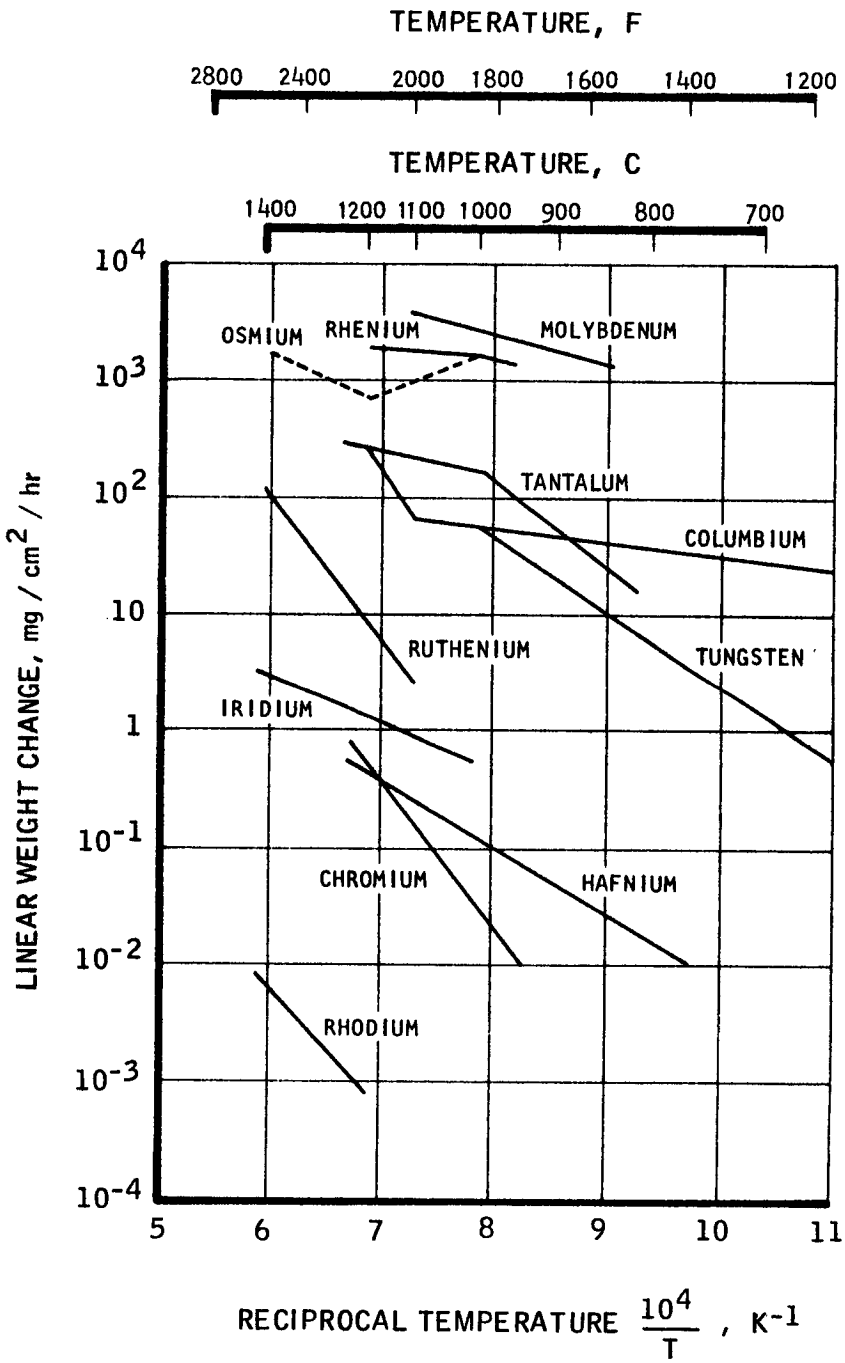

MAC A673

FIGURE 154

VARIATION OF STRENGTH-TO-WEIGHT RATIO WITH TEMPERATURE FOR PYROLYTIC GRAPHITE AND SELECTED MATERIALS

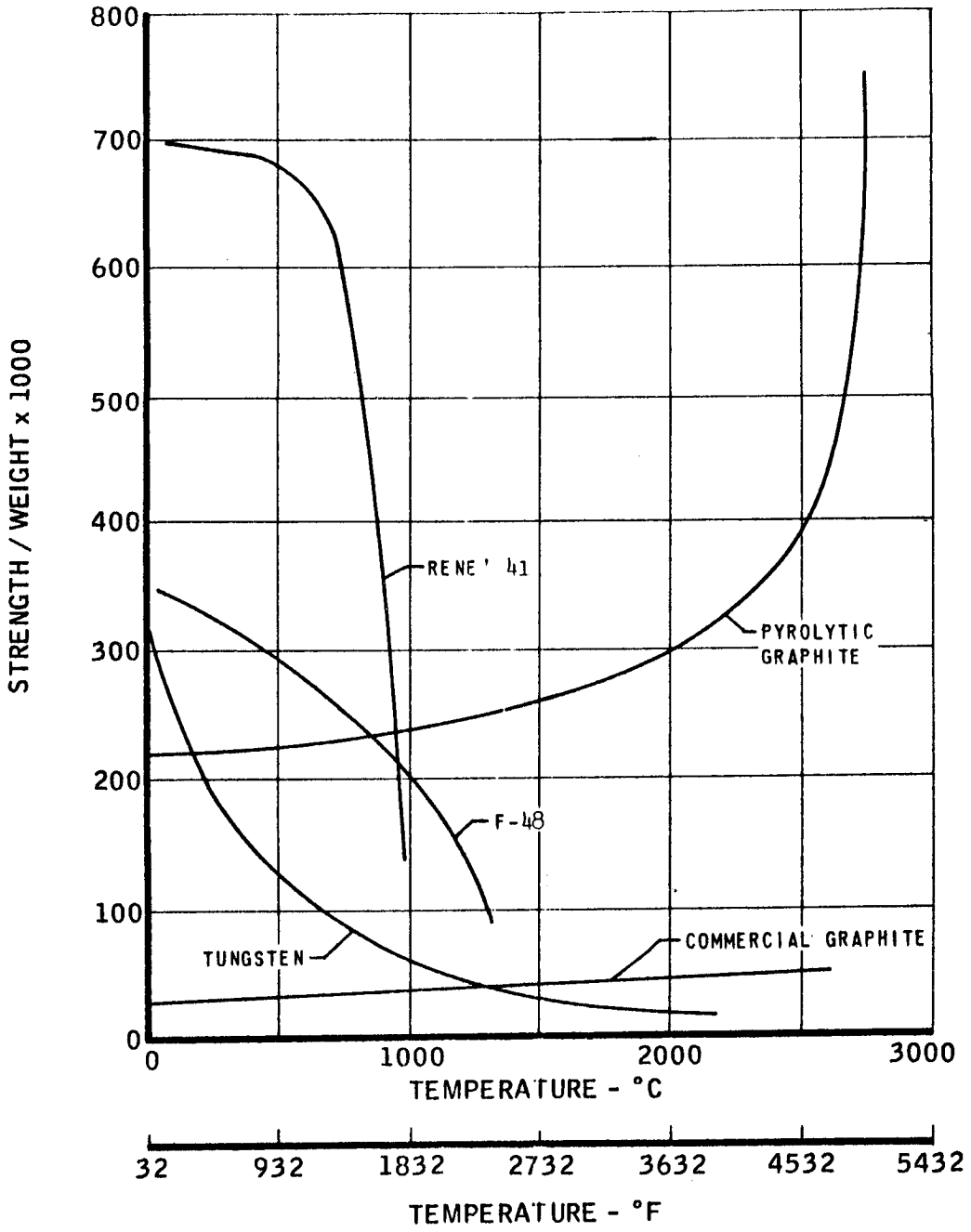

FIGURE 155

INSULATION SYSTEM WEIGHT REQUIRED TO LOWER TEMPERATURE
TO 250 ° F WITH 350 Btu/hr. sq. ft. HEAT FLUX

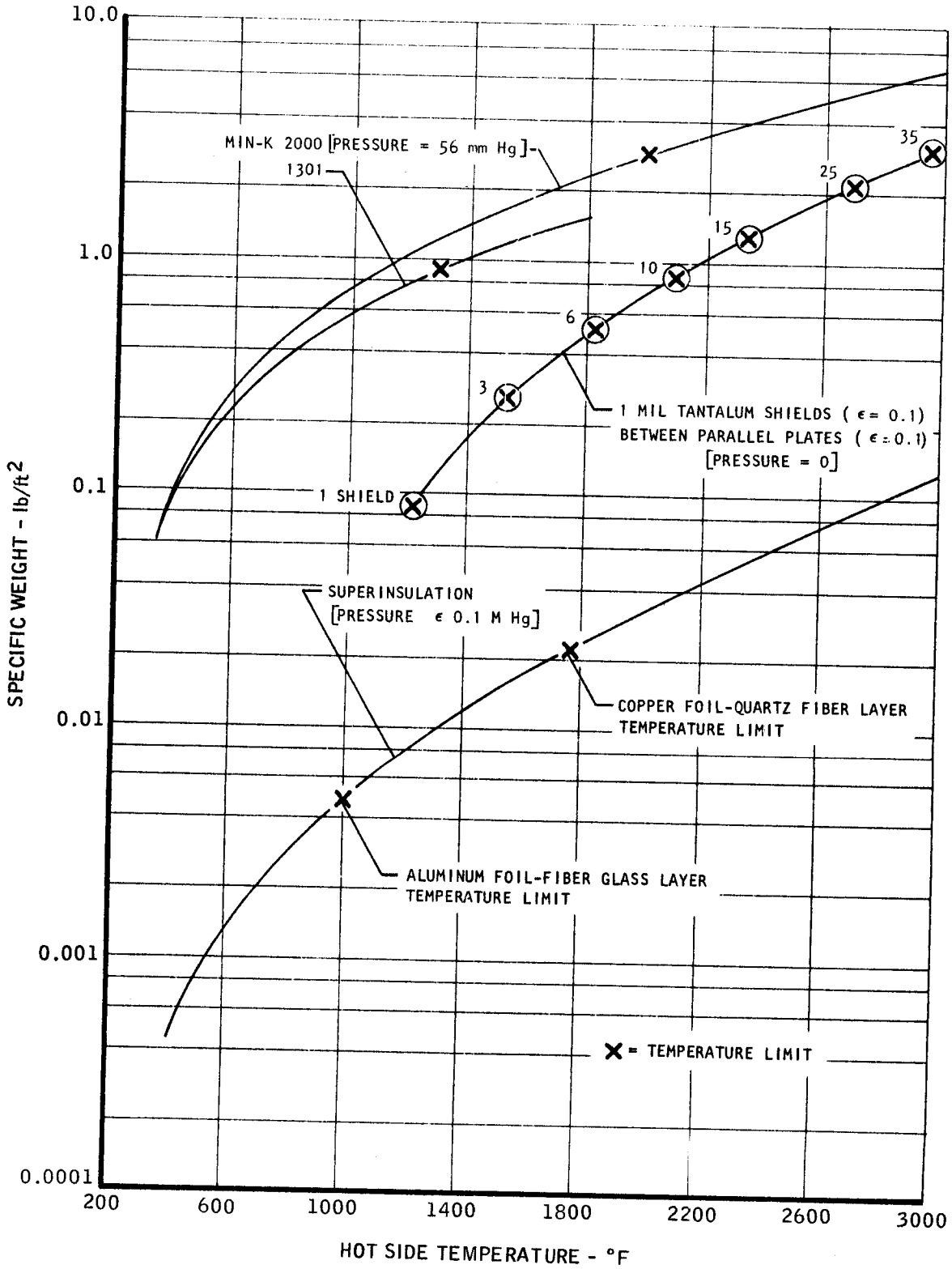

MAC A673

FIGURE 156

INSULATION REQUIRED TO LOWER THRUST CHAMBER TEMPERATURE TO 250 ° F

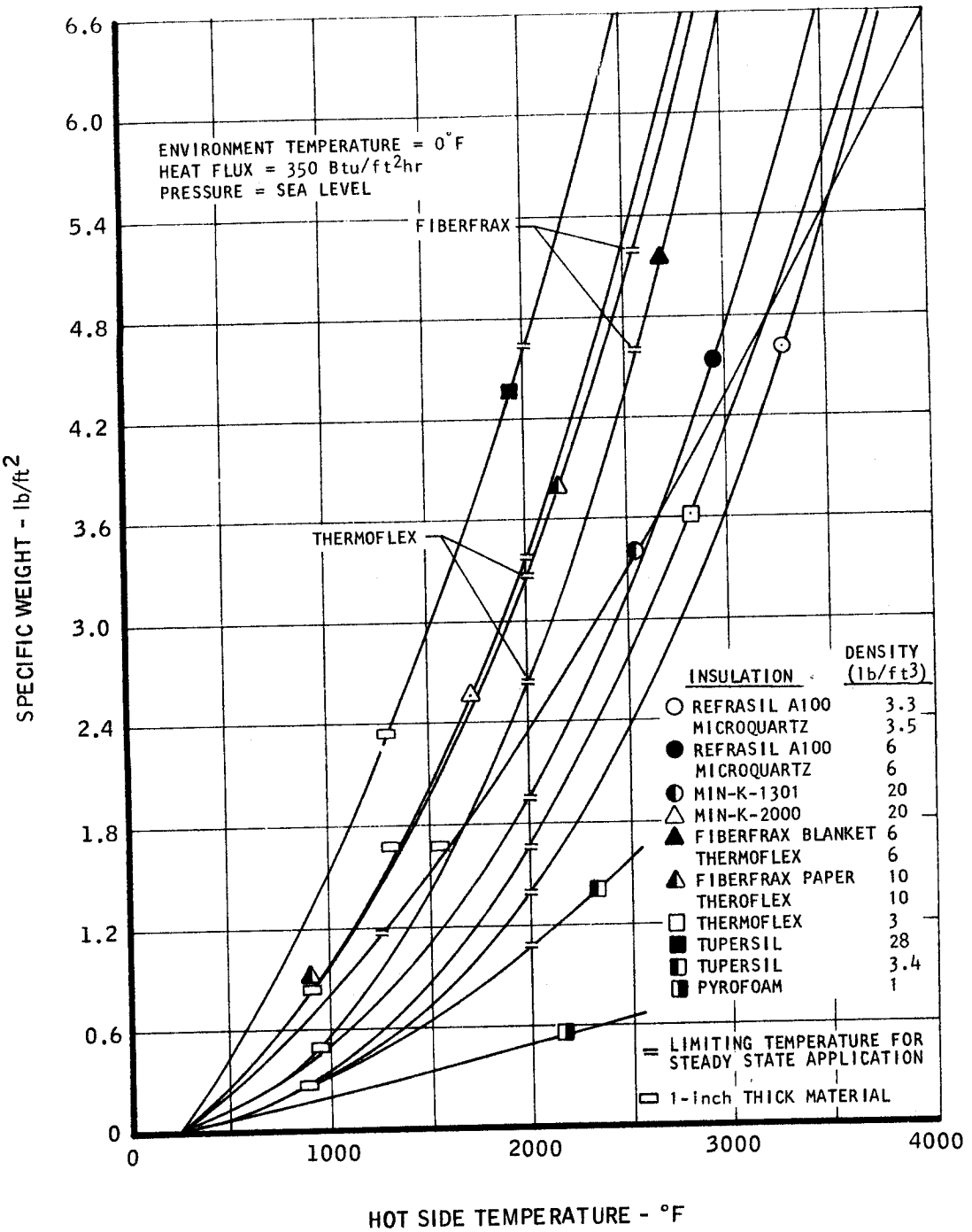

MAC A673

FIGURE 157

HEAT FLUX BETWEEN INFINITE PARALLEL PLATES SEPERATED BY A ONE-INCH GAP

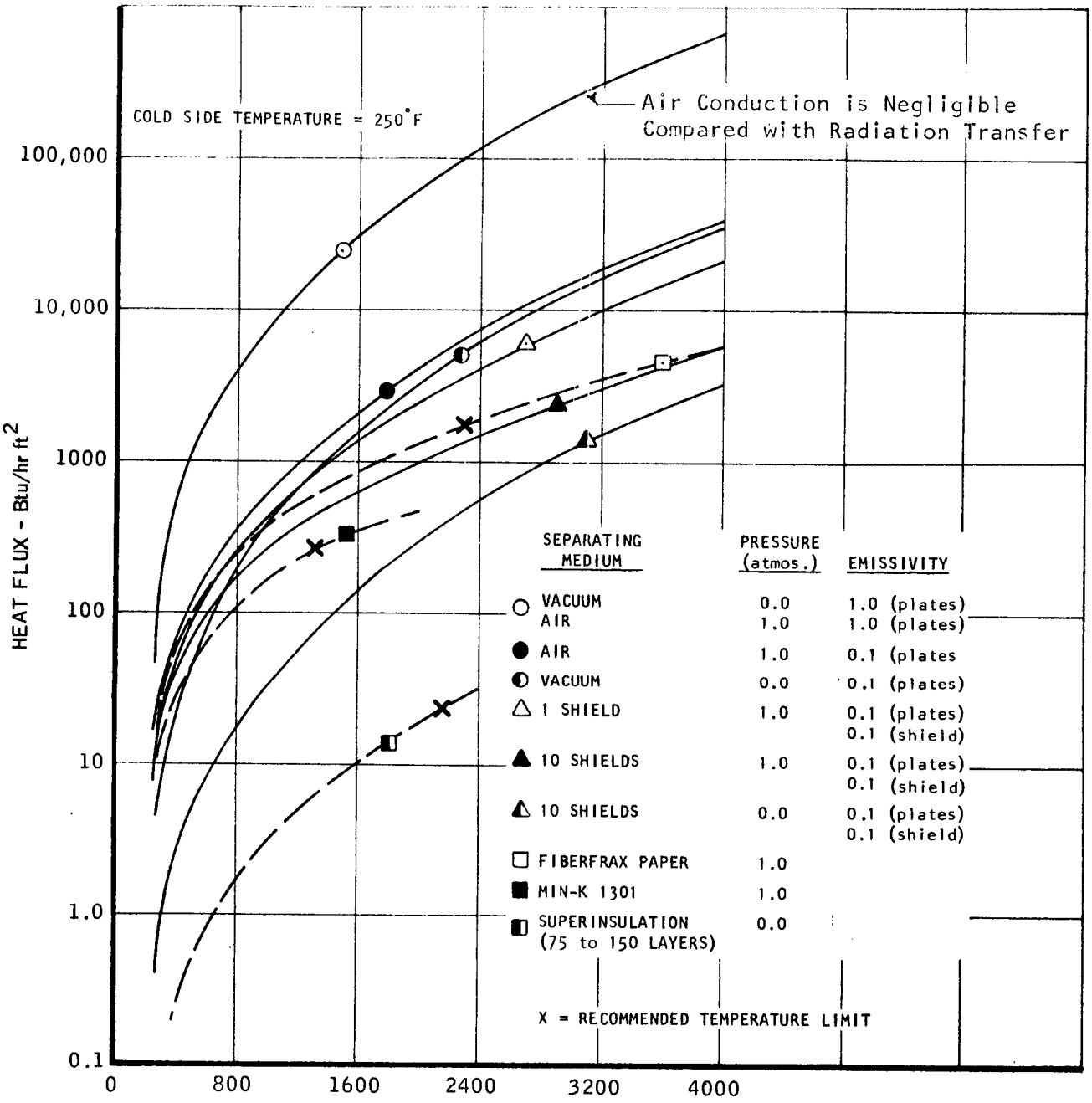

MAC A673

THERMAL CONDUCTIVITIES OF SEVERAL REFRACTORY METALS

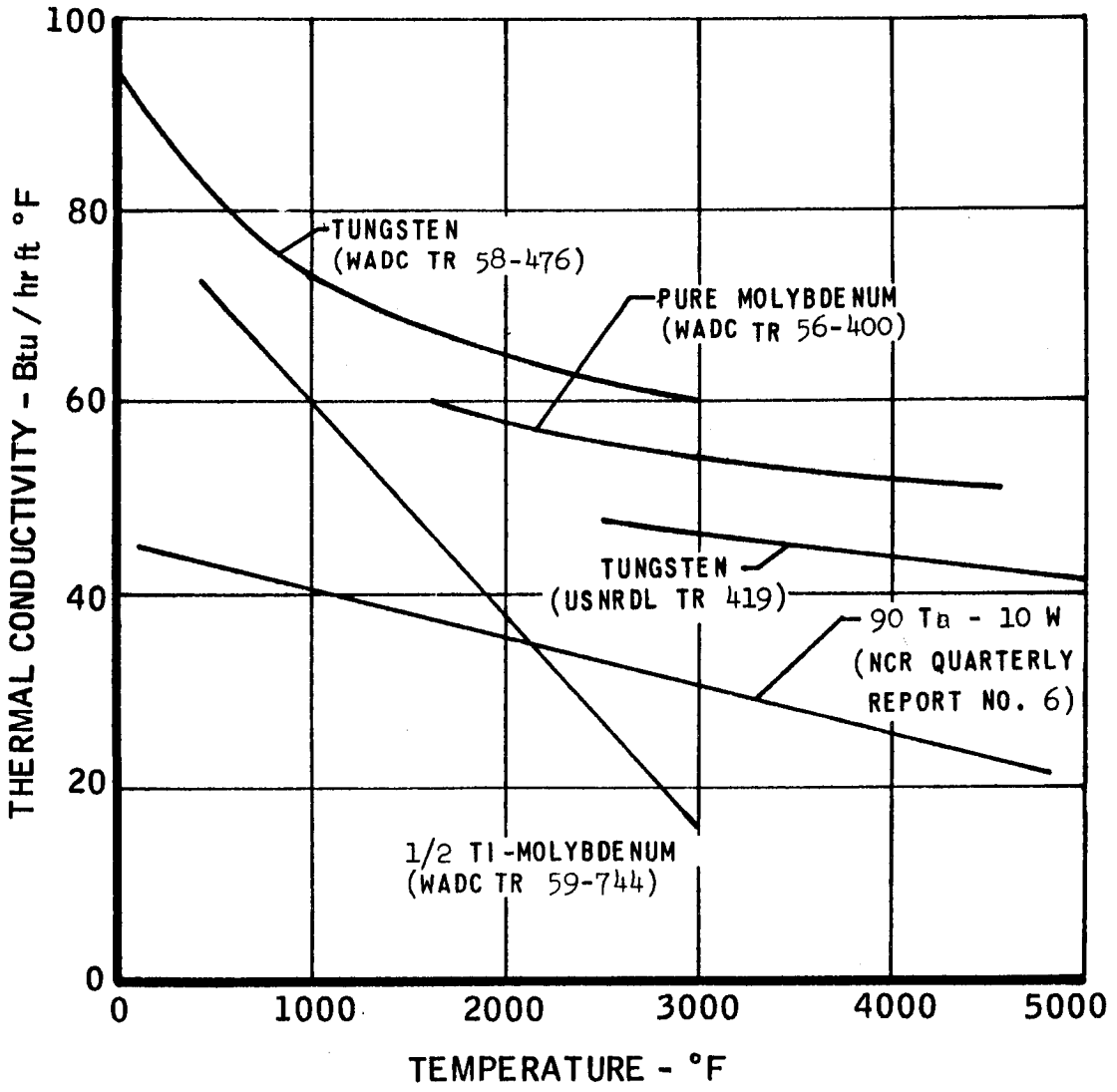

APPENDIX A

SUMMARY OF NOMENCLATURE

Symbol	Description (Note context in case of duplication)	Units
A	Area	sq in.
A_c	Combustion chamber cross section area	sq in.
A_{c_j}	Coolant jacket cross-sectional flow area	sq in.
b	Slot width	in.
C*	Characteristic velocity	ft/sec
C_F	Rocket nozzle thrust coefficient	--
C_p	Specific heat at constant pressure	Btu/lb °F
C_r	Contraction ratio	--
C_D	Orifice discharge coefficient	--
D	Diameter (or hydraulic diameter)	in.
D*	Nozzle throat diameter	in.
F	Rocket engine thrust (pounds force) (kilo-pounds)	lbf K
F_r	Radiation factor (see context)	--
F_e	Emissivity factor	--
F_a	Effective shape factor	--
G	Mass flow rate per unit area	lb/ft^2 hr
g	Gravitational constant	ft/sec^2
H	Total enthalpy	Btu/lb
ΔH	Total enthalpy change	Btu/lb
h	Static enthalpy	Btu/lb
h	Heat transfer coefficient	Btu/hr ft^2 °F
I_{sp}	Specific impulse $F/\dot{W}_p$	$\frac{\text{lbf-sec}}{\text{lbm}}$

MAC A673

APPENDIX A (Continued)

Symbol	Description (Note context in case of duplication)	Units
I_t	Total impulse	lbf-sec
J	Joule's constant	ft-lb/Btu
k	Thermal conductivity	Btu/hr ft °F
L	Length	in.
L*	Characteristic combustion chamber length $L^* = V_c/A^*$	in.
L_n	Exit nozzle length from throat to exit	in.
M	Mach number	--
M_o	Initial mass	lb
M	Molecular weight ratio, main to coolant gas	--
$\dot{m}$	Mass flow parameter q	$°R^{1/2}/sec$
M_{P_L}	Mass of payload	lbs
Nu	Nusselt number	--
P_c	Chamber pressure	psia
P	Pressure	psia
Pr	Prandtl number	--
Q, q	Heat flow	Btu/hr
R	Resistance to heat transfer R = 1/h or L/k	--
Re	Reynolds number	--
R	Radius	in.
R	Gas constant	ft/°R
S	Slot height	in.
St	Stanton number	--

MAC A673

APPENDIX A (Continued)

Symbol	Description (Note context in case of duplication)	Units
T	Temperature	°F or °R
T_g	Gas temperature	°F or °R
T_c	Temperature of combustion gas or coolant (refer to context)	°F or °R
t	Time	sec
U	Overall value of heat conductance	Btu/hr ft^2 °F
U_b	Gas stream velocity	ft/sec
V	Velocity	ft/sec
V_c	Combustion chamber volume	$in.^3$
$\dot{W}$	Flow rate	lb/sec
$\dot{W}$	Flow rate	lb/sec
$\dot{W}+$	Critical flow rate (film cooling)	lb/sec
α	Thermal diffusivity	ft^2/hr
γ	Ratio of specific heats	--
Δ	Incremental change	--
δ	Coolant film thickness	in.
ρ	Density	lb/ft^3
μ	Viscosity	--
ε	Emissivity	--
ε	Exit nozzle expansion ratio	Ae/A*
ε_s	Effectiveness ratio	--
η	Temperature ratio	--
π	Pi	--

MAC A673

APPENDIX A (Continued)

Symbol	Description (Note context in case of duplication)	Units
Subscript		
*	Condition at nozzle throat	
a	Ambient	
ave	Average	
b	Bulk value or free stream value	
C	Combustion chamber	
c	Coolant	
e	Exit plane	
g	Main gas stream	
w	Wall	
r	Recovery value	
v	Vapor	
o	Initial or base	
f	Film	
i	Ideal	
Inj	Injection	
p	Primary	
p	Propellant	
t	Throat	
T	Total	
s	Surface	
x	Local value	

MAC A673

APPENDIX B

THEORETICAL VARIATION OF ROCKET MOTOR PERFORMANCE DUE TO HEAT TRANSFER, PROPELLANT STRATIFICATION EFFECTS, AND NOZZLE THROAT EROSION

B-I. INTRODUCTION

Rocket engine performance degradation resulting from heat loss, propellant stratification, and cooling passage pressure drop as expressed in terms of specific impulse is computed. The assumptions and derivations used throughout the analysis are presented along with results of sample calculations. To simplify the analysis, the effects of the various cooling methods on motor performance were determined separately. The effects of combined cooling methods can easily be evaluated by combining the analytical methods presented.

B-II. ANALYSIS

A. Effects of Heat Loss

The criterion of rocket motor performance is the specific impulse efficiency, that is, the ratio of the specific impulse attained in a practical system and the specific impulse attainable in a theoretical or perfect system. Symbolically (symbols used are defined in Section B-IV),

$$\eta = \frac{I_{sp}}{I_{sp_i}} \tag{1}$$

By definition, the specific impulse (I_{sp}) is the thrust output per pound of propellant flow per second, or

$$I_{sp} = \frac{F}{\dot{w}} \tag{2}$$

The thrust (F) is

$$F = \frac{\dot{w}}{g} V_e + A_e (P_e - P_a) \tag{3}$$

and the propellant weight flow at the nozzle exit is

$$\dot{w} = \rho_e A_e V_e \text{ and } \rho_e = \frac{P_e}{R_e T_e} \tag{4}$$

Substituting Equations (3) and (4) into Equation (2) and simplifying

$$I_{sp} = \frac{V_e^2 g + R_e T_e}{V_e} - \frac{P_a A_e}{\dot{w}} \tag{5}$$

MAC A673

APPENDIX B (Continued)

The exhaust velocity (V_e) can be expressed in terms of the total and static enthalpies as

$$V_e = \sqrt{2gJ\ (H-h)_e} \tag{6}$$

and the gas constant (R_e), which is a point function, is

$$R_e = JC_{p_e}\ \frac{\gamma_e - 1}{\gamma_e} \tag{7}$$

Substituting Equations (6) and (7) into Equation (5) yields

$$I_{sp} = \frac{2J(H-h)_e + C_{p_e} J\ T_e\ \frac{\gamma_e - 1}{\gamma_e}}{\sqrt{2gJ\ (H-h)_2}} - \frac{P_e A_e}{\dot{w}} \tag{8}$$

By defining enthalpy as

$$h = C_p T = \int_{T=o}^{T} C_p dT$$

where recognition must be given the fact that C_p is not a constant at high temperatures but depends upon integrated path

$$C_p = \frac{\int_{T=o}^{T} C_p dT}{T}$$

Equation (8) can be expressed as

$$I_{sp} = \frac{JH_e \left[2\left(1 - \frac{h}{H}\right)_e + \left(\frac{h}{H}\right)_e \left(\frac{\gamma_e - 1}{\gamma_e}\right)\right]}{\sqrt{2gJH\ (1-h/H)_e}} - \frac{P_e A_e}{\dot{w}} \tag{9}$$

From the basic thermodynamic relations

$$\frac{h}{H} = \frac{C_p T}{C_{p_T} T_t} = \frac{C_p}{C_{p_T}} (P/P_T)\ \frac{\gamma_{ave} - 1}{\gamma_{ave}}$$

where once again a high temperature γ is a path function between the stagnation and static conditions, which, when substituted into Equation (9) yields

MAC A678

APPENDIX B (Continued)

$$I_{sp} = \sqrt{JH_e}\left\{\frac{2\left[1-\left(\frac{C_p}{C_{p_T}}\right)_e (P/P_t)_e^{\frac{\gamma'-1}{\gamma'_{ave}}}\right] + \frac{\gamma'-1}{\gamma_e}\left(\frac{C_p}{C_{p_T}}\right)_e (P/P_t)_e^{\frac{\gamma'-1}{\gamma'_{ave}}}}{2g\left[1-\left(\frac{C_p}{C_{p_T}}\right)_e (P/P_t)_e^{\frac{\gamma'-1}{\gamma'_{ave}}}\right]}\right\}^{1/2} - \frac{P_e A_e}{\dot{w}} \qquad (10)$$

This equation shows that for a given expansion ratio the specific impulse is dependent only upon the square root of the total enthalpy. Consequently, any heat loss due to chamber cooling will produce a corresponding loss in specific impulse. Comparing a cooled rocket motor with an adiabatic system (and noting that the last term is small or approaches zero in most practical cases), the specific impulse efficiency of Equation (1) can be written as

$$\eta = \sqrt{\frac{H_c - \Delta H}{H_c}} = \sqrt{1 - \frac{\Delta H}{H_c}} \cong 1 - \frac{1}{2}\frac{\Delta H}{H_c} \text{ (since } \frac{\Delta H}{H_c} \text{ is small compared to one.)} \qquad (11)$$

where H_c represents the total enthalpy of the adiabatic system, and ΔH represents the heat loss to the cooled rocket motor. Therefore the effect of heat loss on impulse efficiency is only one-half of the ratio of the heat loss to total enthalpy.

B. Effects of Gas Temperature Stratification

Gas temperature stratification in the throat and divergent portion of the exhaust nozzle, due to film or transpiration cooling, degrades the performance of a rocket motor. (A sketch of the two models used in this analysis are presented in Figure B-1.) Since by definition the specific impulse is the ratio of thrust to the propellant weight flow,

$$I_{sp} = \frac{F}{\dot{w}_p + \dot{w}_f} \qquad (12)$$

where $\dot{w}_f$ represent the coolant flow rate.

In Case I, it was assumed that the coolant was completely vaporized and/or decomposed at the nozzle throat. The resultant physical change in throat primary gas flow area produces a change in the chamber pressure and primary propellant flow rate in the manner analytically described as follows.

1. The flow through the injectors is generally expressed as

$$\dot{w}_\rho = C_p A_{inj} \sqrt{2\rho g (P_{inj} - P_c)}$$

APPENDIX B (Continued)

2. The flow at the throat can be written as

$$\dot{w} = \frac{P_c A^* \rho_o}{C^*}$$

Representing the uncooled system with subscript (o), the ratio of the total mass flows between a cooled and uncooled system is

$$\frac{\dot{w}_p}{\dot{w}_{p_o}} = \sqrt{\frac{P_{inj} - P_c}{P_{inj} - P_{c_o}}}$$

for a constant injection pressure (P_{inj}). Rearranging the equation and dividing through by P_{c_o} yields

$$\frac{P_c}{P_{c_o}} = \frac{P_{inj}}{P_{c_o}} - \left(\frac{\dot{w}_p}{\dot{w}_{p_o}}\right)^2 \left(\frac{P_{inj}}{P_{c_o}} - 1\right) \tag{13}$$

The mass flow ratio can also be expressed as

$$\frac{\dot{w}_p}{\dot{w}_{p_o}} = \frac{P_c \, A_p^*}{P_{c_o} \, A_t} \tag{14}$$

By assuming a change in mass flow rate, the change in chamber pressure and effective throat area can be determined. The variations of the primary propellant flow rate and the chamber pressure with film thickness which is representative of the change in primary gas throat area are plotted in Figure B-2.

Before any performance calculation could be made of a gas temperature stratified system, it was necessary to determine the expansion ratios of the primary gas and the coolant. In order to compute the expansion ratios, a few simplifying assumptions were employed which were as follows:

1. The integrity of the gases is maintained throughout the divergent portion of the nozzle, i.e., the flows are isentropic and the gases do not mix.

2. The process specific heats ratios and gas constants are fixed.

3. The total pressure of the coolant gas is equal to the total pressure of the primary gas.

4. The total temperature of the coolant gases does not change in the divergent portion of the nozzle.

APPENDIX B (Continued)

The area relationships of a nozzle with stratified gases are expressed as

$$A_{T_e} = A_{P_e} + A_{f_e} \qquad \text{Exit plane} \qquad (15a)$$

and

$$A_t = A_P^* + A_f^* \qquad \text{Throat} \qquad (15b)$$

By simple algebraic manipulation, the expansion ratio of the coolant can be expressed as

$$(A/A^*)_f = \frac{A_{T_e}/A_t - (A/A^*)_P \, (A_P^*/A_t)}{A_f^*/A_t} \qquad (15)$$

The thrusts produced by the coolant and primary gases are

$$F_f = P_{f_e} A_{f_e} (1 + \gamma_f M_f^2)_e - P_a A_{f_e} \qquad (16a)$$

and

$$F_P = P_{P_e} A_{P_e} (1 + \gamma_P M_P^2)_e - P_a A_{P_e} \qquad (16b)$$

respectively. However, the static pressures of both streams are equal. Consequently, using P_e as the static pressure at the exit, the total thrust can be expressed as

$$F_T = P_e A_{f_e} (\gamma_f M_f^2)_e + P_e A_{P_e} (\gamma_P M_P^2)_e + A_{T_e} (P_e - P_a) \qquad (16)$$

and the thrust coefficient is

$$C_F = \left(\frac{P_e}{P_c}\right)\left(\frac{A}{A^*}\right)_f \left(\frac{A_f^*}{A_t}\right) (\gamma_f M_f^2)_e + \left(\frac{P_e}{P_c}\right)\left(\frac{A}{A^*}\right)_P \left(\frac{A_P^*}{A_t}\right) (\gamma_P M_P^2)_e + \left(\frac{A_{T_e}}{A_t}\right)\left(\frac{P_e - P_a}{P_c}\right) \qquad (17)$$

APPENDIX B (Continued)

To resolve this equation, the following parameters must be known: the area ratio of the nozzle, the coolant film thickness at the throat, and the ratio of the specific heats of the gases. If these parameters are known, the expansion ratios of the gases can be defined by an iterative process. This is due to the fact that for a given nozzle area ratio there is only one combination of expansion ratios that will satisfy Equations (15a) and (15b). To prove this it is first necessary to divide Equation (15a) by the throat area (A_t) or

$$\frac{A_{T_e}}{A_t} = \frac{A_{P_e}}{A_t} + \frac{A_{f_e}}{A_t} \tag{15a1}$$

By a simple algebraic manipulation, this equation becomes

$$A_{T_e}/A_t = (A/A^*)_P \, (A_P^*/A_t) + (A/A^*)_f \, (A_f^*/A_t) \tag{15a2}$$

The expansion ratio (A/A*) can be expressed in terms of the pressure ratio (P_e/P_c) in the following manner

$$A/A^* = \left[\frac{2}{\gamma-1}\left\{(P_e/P_c)^{\frac{-\gamma-1}{\gamma}} - 1\right\}\right]^{1/2} \left[\frac{2}{\gamma+1}\,(P_e/P_c)^{\frac{-\gamma-1}{\gamma}}\right]^{\frac{\gamma+1}{2(\gamma-1)}}$$

Substituting this equation into Equation (15a2) results in

$$\begin{aligned} A_{T_e}/A_t = {} & (A_P^*/A_t)\left[\frac{2}{\gamma_P-1}\left\{(P_e/P_c)_P^{\frac{\gamma_P-1}{\gamma_P}} - 1\right\}\right]^{1/2}\left[\frac{2}{\gamma_P+1}\,(P_e/P_c)_P^{-\frac{\gamma_P-1}{\gamma_P}}\right]^{\frac{\gamma_P+1}{2(\gamma_P-1)}} \\ & + (A_f^*/A_t)\left[\frac{2}{\gamma_f-1}\left\{(P_e/P_c)_f^{-\frac{\gamma_f-1}{\gamma_f}} - 1\right\}\right]^{1/2}\left[\frac{2}{\gamma_f+1}\,(P_e/P_c)^{-\frac{\gamma_f+1}{\gamma_f}}\right]^{\frac{\gamma_f+1}{2(\gamma_f-1)}} \end{aligned} \tag{18}$$

Since the pressure ratios (P_e/P_c) of the coolant and primary gases are equal, it is obvious that for a given film thickness, one and only one pressure ratio will yield the required nozzle area ratio. Establishing the expansion ratios of the coolant and primary gases, the resolution of Equations (16), (12), and (1) (in that order) can easily be accomplished.

APPENDIX B (Continued)

The results of sample calculations for a rocket motor with an expansion ratio of 40, a chamber pressure of 300 psia, and combustion temperature of 5750°F are presented in Figures B-3 and B-4. The ratio of specific heats assumed for the primary gas was 1.22 and for the coolant was 1.30. Figure B-3 represents the mass flow variations and Figure B-4 represents the performance variations with coolant film thickness at the nozzle throat.

In Case II the effect of gas stratification considered, it was assumed that all of the coolant at the throat was in a liquid state with zero effective thickness. Further assumptions were as follows:

1. The coolant is vaporized and/or decomposed completely before it reaches the nozzle exit plane.

2. The gases do not mix.

3. The velocity of the coolant at the exit throat is sonic.

4. The chamber pressure and the primary propellant flow rate is unaffected by the liquid film in the throat.

5. The heat lost by the primary stream to the coolant is negligible and therefore the total temperature and pressure of the primary gas remains constant.

As in Case I it is necessary to determine the expansion ratio of the primary gas before the performance parameter can be computed. The area relationships are

$$A_{T_e} = A_{P_e} + A_{f_e} \tag{19a}$$

as in Equation (15a). However,

$$A_t = A_P^* \tag{19b}$$

in this case. The coolant flow rate at the exit can be expressed as

$$\dot{w}_f = \frac{P_e \, A_{f_e} \, m_{m^*}}{\sqrt{T_{T_f}}} \tag{20a}$$

and the primary gas flow rate as

$$\dot{w}_P = \frac{P_c \, A_P^* \, (P/P_T \, \dot{m})_{m^*}}{\sqrt{T_c}} \tag{21a}$$

MAC A-073

APPENDIX B (Continued)

If both flow rates are assumed to be known, the expansion ratio of the primary gas can be determined for various coolant temperatures (T_{t_f}) by an iterative process.

By assuming an exit static pressure, the area occupied by the coolant is calculated by

$$A_{f_e} = \frac{\dot{w}_f \sqrt{T_{T_f}}}{P_e \, \dot{m}_{m*}} \qquad (20b)$$

From this and Equations (19a) and (19b), the expansion ratio $(A/A^*)_p$ is determined. The pressure ratio, obtained from this area ratio, multiplied by the chamber pressure must be equal to the assumed exit static pressure. Following establishment of the expansion ratio the performance parameters can be calculated by using Equations (16), (12), and (1), in that order.

Results of sample performance calculations for Case II are graphically illustrated in Figure B-5. The same rocket motor operating conditions and assumptions as used in the first case were used in these calculations. Neither of the two cases, i.e., an all liquid or an all vapor phase film, exist at the throat in an actual system but by considering the extreme cases, a means of comparison has been established.

C. Effects of Pressure Losses in a Regenerative Cooling Passage

A pumping or pressure loss generally occurs in a regeneratively cooled system. This loss is usually compensated by increasing the pumping energy. In evaluating the effect of the pumping loss on the performance of a rocket motor, the increased pumping energy must be charged to the energy loss of the system. Mathematically stated,

$$\Delta H_{loss} = H_{H.L.} + H_{P.E.}$$

Where

$H_{H.L.}$ = Enthalpy loss due to heat loss

$H_{P.E.}$ = Enthalpy loss due to pumping loss

The pumping loss is defined as

$$H_{P.E.} = \frac{\Delta P}{\rho J}$$

MAC A 673

APPENDIX B (Continued)

In a regenerative cooling system where the coolant is one of the propellants, the energy losses due to heat losses are negligible. The major portion of the heat absorbed by the walls is transferred to the propellant and is therefore not wasted. It actually augments the heat content of the propellant prior to combustion. Consequently, the enthalpy loss due to heat loss can be neglected in a regenerative cooling system and the impulse efficiency of Equation (11) can be written as

$$\eta = \sqrt{\frac{H_c - H_{P.E.}}{H_c}}$$

D. Effect of Nozzle Throat Erosion on Rocket Motor Performance

An analysis was conducted to determine the effect of nozzle throat erosion on rocket motor performance for constant propellant flow and varying propellant flow. The derivations of the equations used in this analysis are presented along with the results of calculations for a specific heat ratio (γ) of 1.24. The results are based on the following simplifying assumptions which may be unattainable in practice:

1. The flow is isentropic.
2. The nozzle efficiency is unaffected by the erosion.
3. The characteristic velocity (C*) remains constant and is independent of the chamber pressure, i.e., the O/F ratio is constant and, consequently, the combustion temperature is constant.
4. The gases are in frozen equilibrium, i.e., the ratio of specific heats is constant.

In order to maintain generality, the equations were derived as dimensionless ratios. The basic relations used are well known (They can be found in any text book dealing with rocket performance). The symbols are defined in Section B-IV.

1. Mass Flow Through the Injectors

$$\dot{w} = C_D A_{inj} \sqrt{2g\rho(P_{inj} - P_c)} \qquad (21)$$

2. Characteristic Velocity

$$C^* = P_c A_t \frac{g}{\dot{w}} \qquad (22)$$

MAC A-63

APPENDIX B (Continued)

3. Engine Thrust

$$F = C_F P_c A_t \tag{23}$$

Where

$$C_F = \left\{ \frac{2\gamma^2}{\gamma - 1} \left(\frac{2}{\gamma + 1} \right)^{\frac{\gamma+1}{\gamma-1}} \left[1 - (P_e/P_c)^{\frac{\gamma-1}{\gamma}} \right] \right\}^{1/2} + \frac{P_e - P_a}{P_c} \quad (A_e/A_t)$$

Combining Equations (21) and (22), and rearranging the resultant equation yields

$$P_c = K_1 \sqrt{\frac{P_{inj} - P_c}{A_t}}$$

Where

$$K_1 = C^* C_D A_{inj} \sqrt{\frac{2\rho}{g}}$$

Designating the initial values with sub-subscript o, the change in the chamber pressure can be expressed in terms of the initial conditions.

$$P_c/P_{c_o} = \sqrt{\frac{P_{inj} - P_c}{P_{inj} - P_{c_o}}} \frac{A_{t_o}}{A_t}$$

Solving this equation for the pressure ratio yields

$$P_c/P_{c_o} = -1/2 \left[\frac{(A_{t_o}/A_t)^2}{(P_{inj}/P_{c_o} - 1)} \right] + 1/2 \left\{ \left[\frac{(A_{t_o}/A_t)^2}{(P_{inj}/P_{c_o} - 1)} \right]^2 + 4 \frac{(P_{inj}/P_{c_o})(A_{t_o}/A_t)^2}{(P_{inj}/P_{c_o} - 1)} \right]^{1/2} \tag{24}$$

This equation represents the nondimensionalized change of the chamber pressure as a function of the change in throat area and accounts for any change in propellant flow due to the change of the pressure differential across the injectors.

APPENDIX B (Continued)

For constant mass flow, the change in the chamber is inversely proportional to the change in throat area. From Equation (22)

$$P_c/P_{c_o} = A_{t_o}/A_t \tag{25}$$

The expression representing the thrust variation can also be derived in a similar manner. Letting

$$K_2 = \frac{2\gamma^2}{\gamma - 1}\left(\frac{2}{\gamma + 1}\right)^{\frac{\gamma + 1}{\gamma - 1}}$$

and rewriting Equation (23)

$$F = P_c A_t \left\{ K_2 \left[1 - (P_e/P_c)^{\frac{\gamma - 1}{\gamma}} \right] \right\}^{1/2} + A_e(P_e - P_a)$$

then

$$F/F_o = \frac{P_c A_t \left\{ K_2 \left[1 - (P_e/P_c)^{\frac{\gamma - 1}{\gamma}} \right] \right\}^{1/2} + A_e(P_e - P_a)}{P_{c_o} A_{t_o} \left\{ K_2 \left[1 - (P_e/P_c)_o^{\frac{\gamma - 1}{\gamma}} \right] \right\}^{1/2} + A_e(P_{e_o} - P_a)}$$

With simple algebraic manipulation, the expression becomes

MAC A673

APPENDIX B (Continued)

$$F/F_o = \left\{ \frac{A_t/A_{t_o}\sqrt{K_2\left[1-(P_e/P_c)^{\frac{\gamma-1}{\gamma}}\right]} + \left(\frac{A_e}{A_t}\right)_o\left[(P_e/P_c) - \frac{P_a/P_{c_o}}{P_c/P_{c_o}}\right]}{\sqrt{K_2\left[1-(P_e/P_c)_o^{\frac{\gamma-1}{\gamma}}\right]} + \left(\frac{A_e}{A_t}\right)_o\left[(P_e/P_c)_o - P_a/P_{c_o}\right]} \right\}(P_c/P_{c_o}) \quad (26)$$

If the ambient pressure (P_a) is zero (space conditions), the equation simplifies to

$$F/F_o = \left\{ \frac{A_t/A_{t_o}\sqrt{\left[K_2\,1-(P_e/P_c)^{\frac{\gamma-1}{\gamma}}\right]} + (A_e/A_t)_o\,(P_e/P_c)}{\sqrt{K_2\left[1-(P_e/P_c)_o^{\frac{\gamma-1}{\gamma}}\right]} + (A_e/A_t)\;(P_e/P_c)_o} \right\}(P_c/P_{c_o} \quad (26a)$$

Although the pressure ratio (P_e/P_c) is dependent only upon the area ratio (A_e/A_t), the pressure ratio, and consequently the thrust ratio of Equation (26), cannot be expressed explicitly in terms of the area ratio. This can easily be established in the following manner:

From the basic relation

$$P_e/P_c = \left[1 + \frac{\gamma-1}{2} M_e^2\right]^{-\frac{\gamma-1}{\gamma}}$$

the Mach number, in terms of P_e/P_c, can be expressed as

$$M_e = \left[\frac{2}{\gamma-1}\left\{(P_e/P_c)^{-\frac{\gamma-1}{\gamma}} - 1\right\}\right]^{1/2}$$

APPENDIX B (Continued)

Substituting this expression into the basic relation

$$A_e/A_t = \frac{1}{M_e}\left[\frac{2 + (\gamma - 1) M_e^2}{\gamma + 1}\right]^{\frac{\gamma + 1}{2(\gamma - 1)}}$$

results in

$$A_e/A_t = \left[\frac{2}{\gamma - 1}\left\{(P_e/P_c)^{-\frac{\gamma - 1}{\gamma}} - 1\right\}\right]^{1/2}\left[\frac{2}{\gamma + 1}(P_e/P_c)^{-\frac{\gamma - 1}{\gamma}}\right]^{\frac{\gamma + 1}{2(\gamma - 1)}}$$

Inspection of this equation shows that the pressure ratio (P_e/P_c) cannot be expressed explicitly in terms of the area ratio (A_e/A_t).

Numerical computations show that the thrust ratio of Equation (26) is for practical purposes independent of the initial nozzle expansion ratio. The mathematical proof is beyond the scope of this presentation.

The mass flow variation, obtained from Equation (22), is

$$\frac{\dot{w}}{\dot{w}_o} = \left(\frac{P_c}{P_{c_o}}\right)\left(\frac{A_t}{A_{t_o}}\right) \tag{27}$$

Then, from the definition of specific impulse

$$I_s/I_{s_o} = (F/F_o)\left(\frac{\dot{w}}{\dot{w}_o}\right)^{-1} = \frac{F}{F_o}\frac{1}{P_c/P_{c_o}\ A_t/A_{t_o}} \tag{28}$$

which is independent of initial injection pressure ratio (P_{inj}/P_{c_o}) and, for practical purposes, initial nozzle expansion ratio $(A_e/A_t)_o$.

MAC A633

APPENDIX B (Continued)

To effectively demonstrate the effects of nozzle throat erosion on the performance of a rocket motor operating in space, Equations (24) through (28) were numerically resolved for various initial injection pressure ratio and nozzle expansion ratios. The results are graphically depicted in Figures B-6 through B-8. Both Figures B-6 and B-7 are applicable to any rocket motor, the only restriction being that assumption (3) is not exactly correct. The characteristic velocity is affected by the chamber pressure to some extent, but the effect is almost negligible and may be ignored.

The performance parameters, i.e., thrust and specific impulse ratios, are presented in Figure B-8. The increased thrust is due to the increased mass flow caused by the increased pressure differential across the propellant injector orifices. However, the specific impulse decreases because the increase in thrust is proportionately less than the increase in mass flow. The total increase in thrust may not be attainable in practice because erosion of the throat will not be smooth and even. This haphazard erosion will have an adverse effect on the nozzle efficiency.

In carrying out the numerical evaluation of these relationships it is shown, as plotted in Figures B-6, B-7, and B-8, that the following amplified relationships apply in most cases:

a. Chamber pressure decreases with throat erosion. At constant propellant flow rate it is simply,

$$\frac{P_c}{P_{c_o}} = \frac{A_{t_o}}{A_t}$$

b. For fixed area propellant injection orifices at various injection pressure ratios, the propellant flow rate increases appreciably, with a nearly corresponding increase in thrust in the case of low orifice pressure drops.

c. The loss in thrust at constant propellant flow and isentropic expansion is due only to the change in C_F, which in turn is a function of the change in expansion ratio A_e/A_t.

d. In any case the loss in I_s is related simply to the change in C_F as a first approximation.

$$\frac{I_s}{I_{s_o}} = \frac{C_F}{C_{F_o}}$$

MAC A673

APPENDIX B (Continued)

B-III. CONCLUSIONS

Evaluation of the effects of chamber cooling on rocket motor performances has shown that the degree of system performance degradation is,

1. Least with regeneratively or radiation cooled motors. The losses of a radiation cooled chamber can be made to approach that of a regeneratively cooled system by using a fuel cooled, radiant heat absorber system. This system is defined here as a cooling unit in which the radiated heat from the chamber is absorbed by a fuel cooled absorber.

2. Greater with a transpiration or film cooled system. This is primarily due to temperature stratification, mixing losses, coolant pump requirements, and the necessary propellant mass for cooling purposes.

3. Possibly high with ablative cooling at the throat. The mass of the ablative material, greater propellant requirement for a given total impulse, mixing losses, losses due to haphazard erosion of the ablative material, and temperature stratification all contribute to the degradation of the system performance.

B-IV. NOMENCLATURE

Symbol	Description	Unit
A	Area	sq in.
C*	Characteristic velocity	fps
C_F	Thrust coefficient	--
C_p	Specific heat at constant pressure	Btu/lb °F
C_D	Injection orifice discharge coefficient	--
F	Thrust	lbs
g	Gravitational acceleration	ft/sec^2
H	Total enthalpy	Btu/lb
h	Static enthalpy	Btu/lb

MAC A673

APPENDIX B (Continued)

Symbol	Description	Unit
I_{sp}	Specific impulse	second
J	Joule's constant	ft-lb/Btu
$\dot{m}$	Mass flow parameter	--
M	Mach number	--
P	Pressure	psia
R	Radius	in.
R	Gas constant	--
T	Temperature	°R
V	Gas velocity	fps
$\dot{w}$	Weight flow rate	pps
δ	Film thickness	in.
ρ	Density	lb/cu in.
γ	Ratio of specific heats	--
Superscript		
*	Sonic condition	
Subscript		
a	Ambient	
ave	Average	
c	Chamber	
e	Exit	
f	Film (coolant)	
i	Ideal	
Inj.	Injection	
o	Initial (no coolant flow)	
p	Primary	
t	Throat	
T	Total	

MAC A673

GAS TEMPERATURE STRATIFICATION

CASE 1

GAS FILM AT THROAT

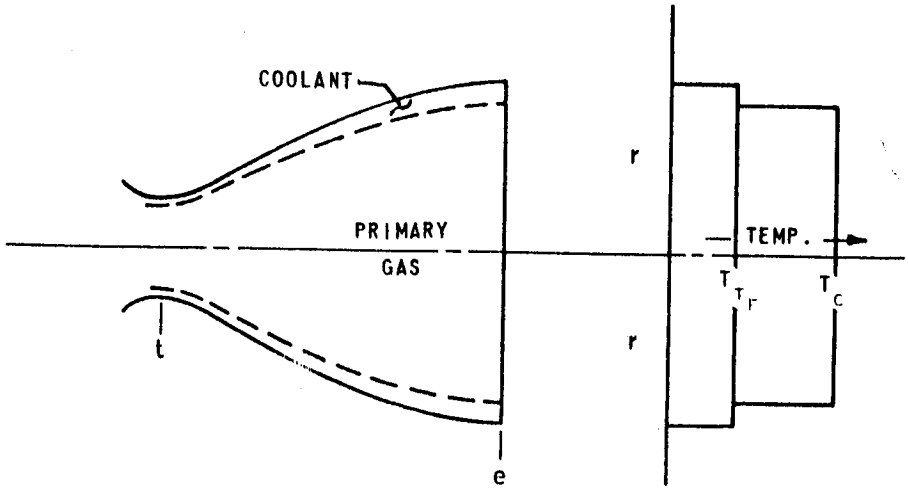

CASE 2

LIQUID FILM AT THROAT

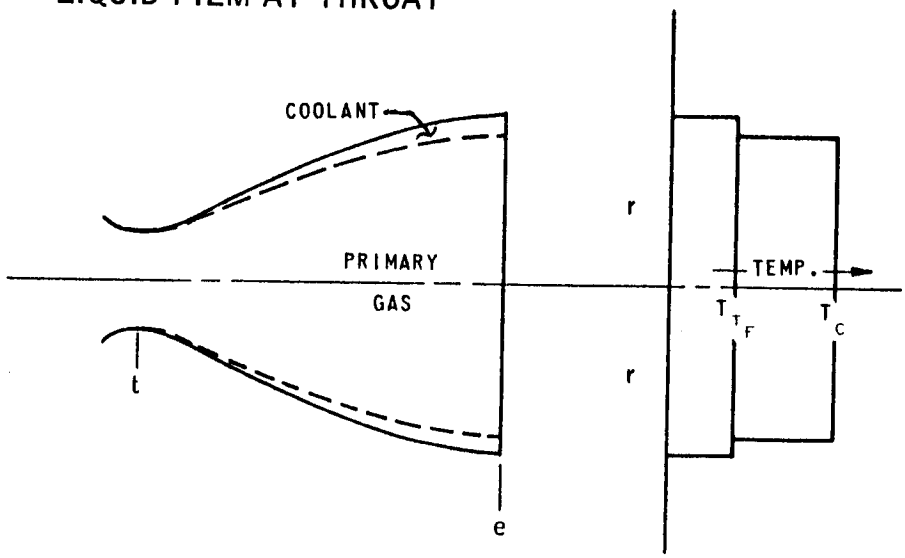

MAC A 673

FIGURE B-1

CHAMBER PRESSURE AND PRIMARY MASS FLOW VARIATION WITH COOLANT FILM THICKNESS
CASE I

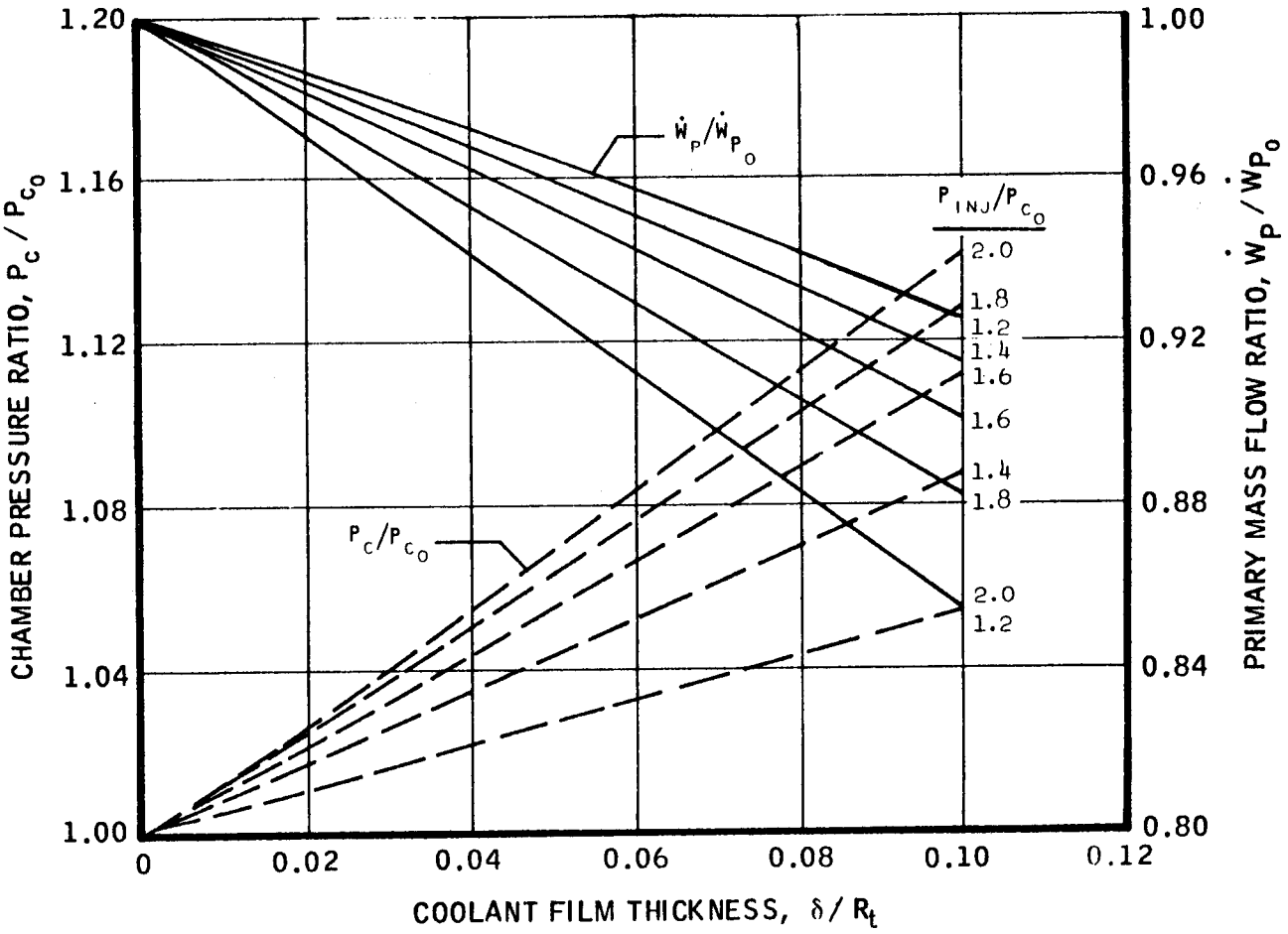

FIGURE B-2

MASS FLOW VARIATION WITH COOLANT FILM THICKNESS
CASE I

PRIMARY $\gamma = 1.22$
COOLANT $\gamma = 1.30$

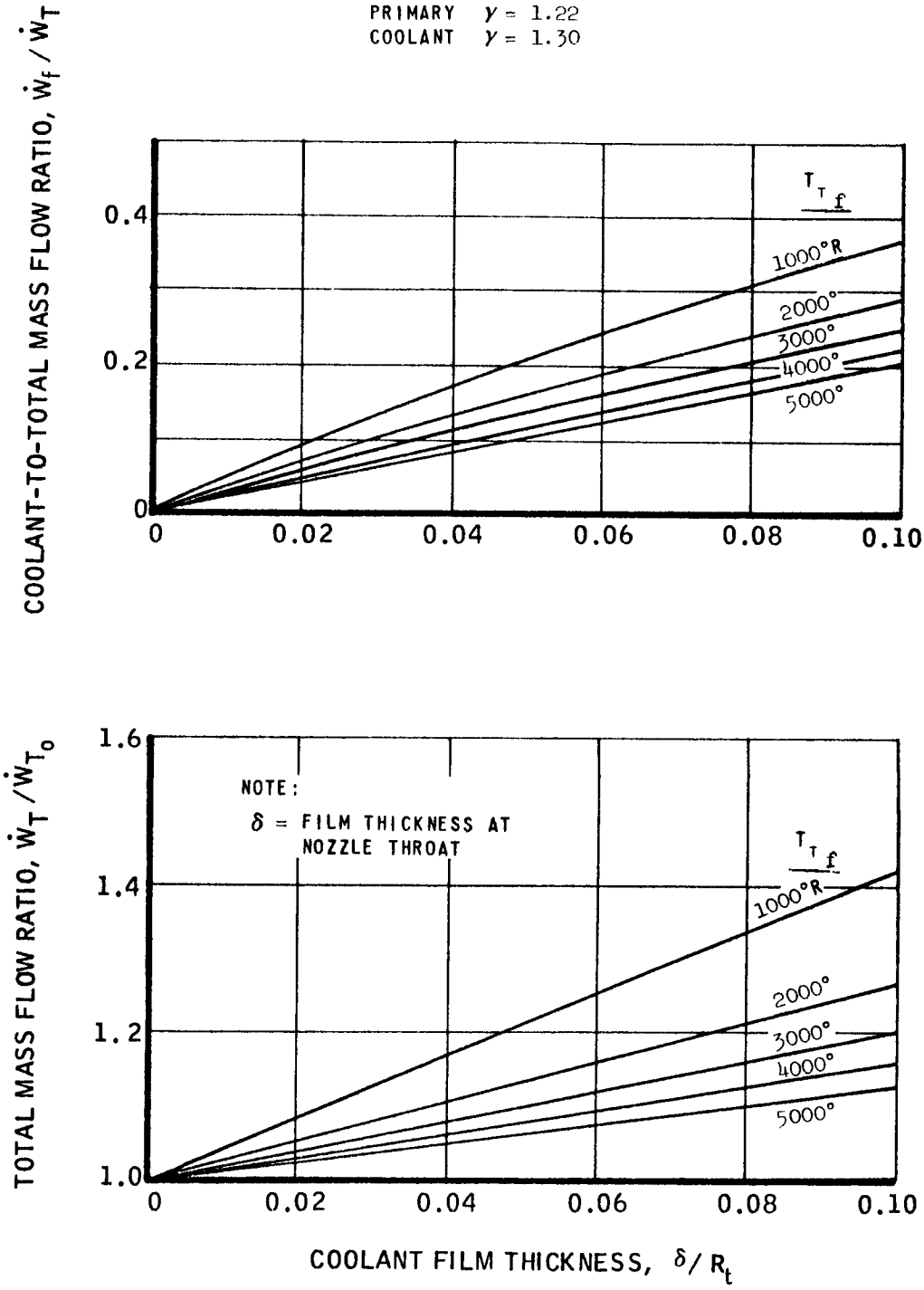

MAC A673

FIGURE B-3

PERFORMANCE VARIATION WITH COOLANT FILM THICKNESS
CASE I

PRIMARY γ = 12.2
COOLANT γ = 1.30

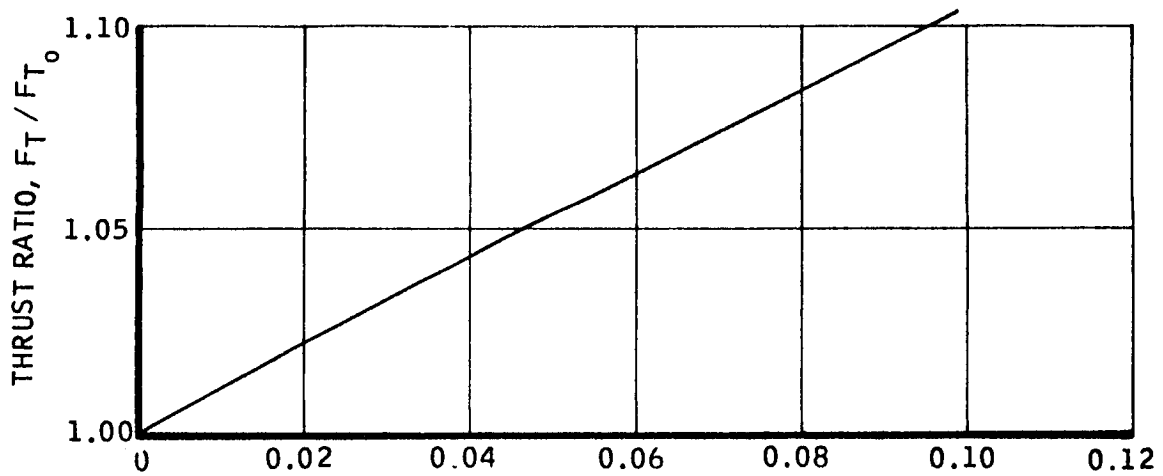

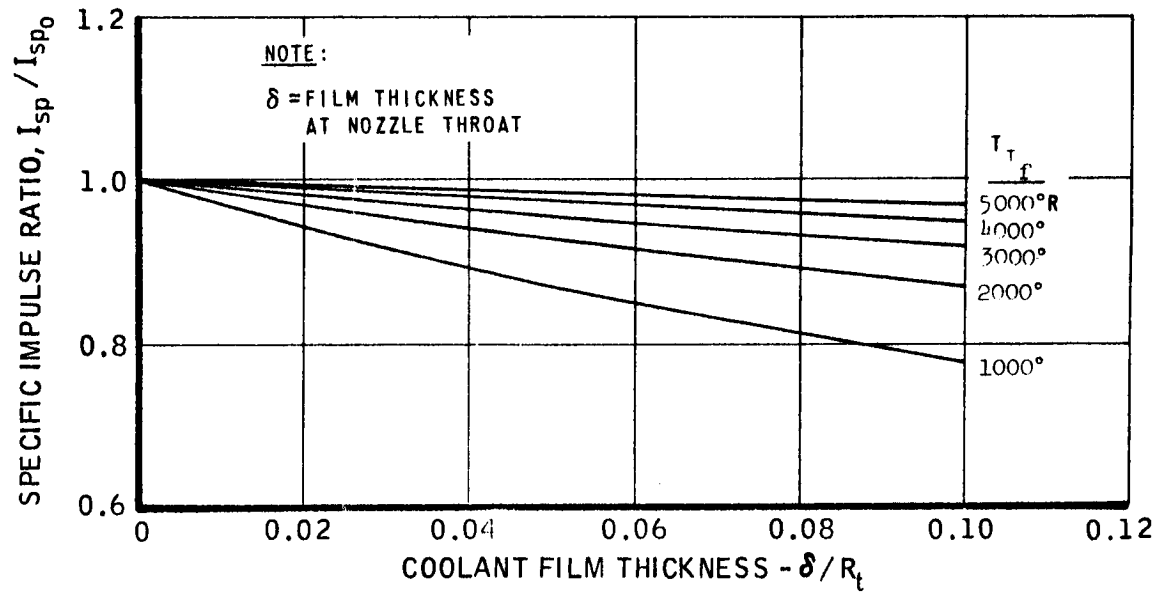

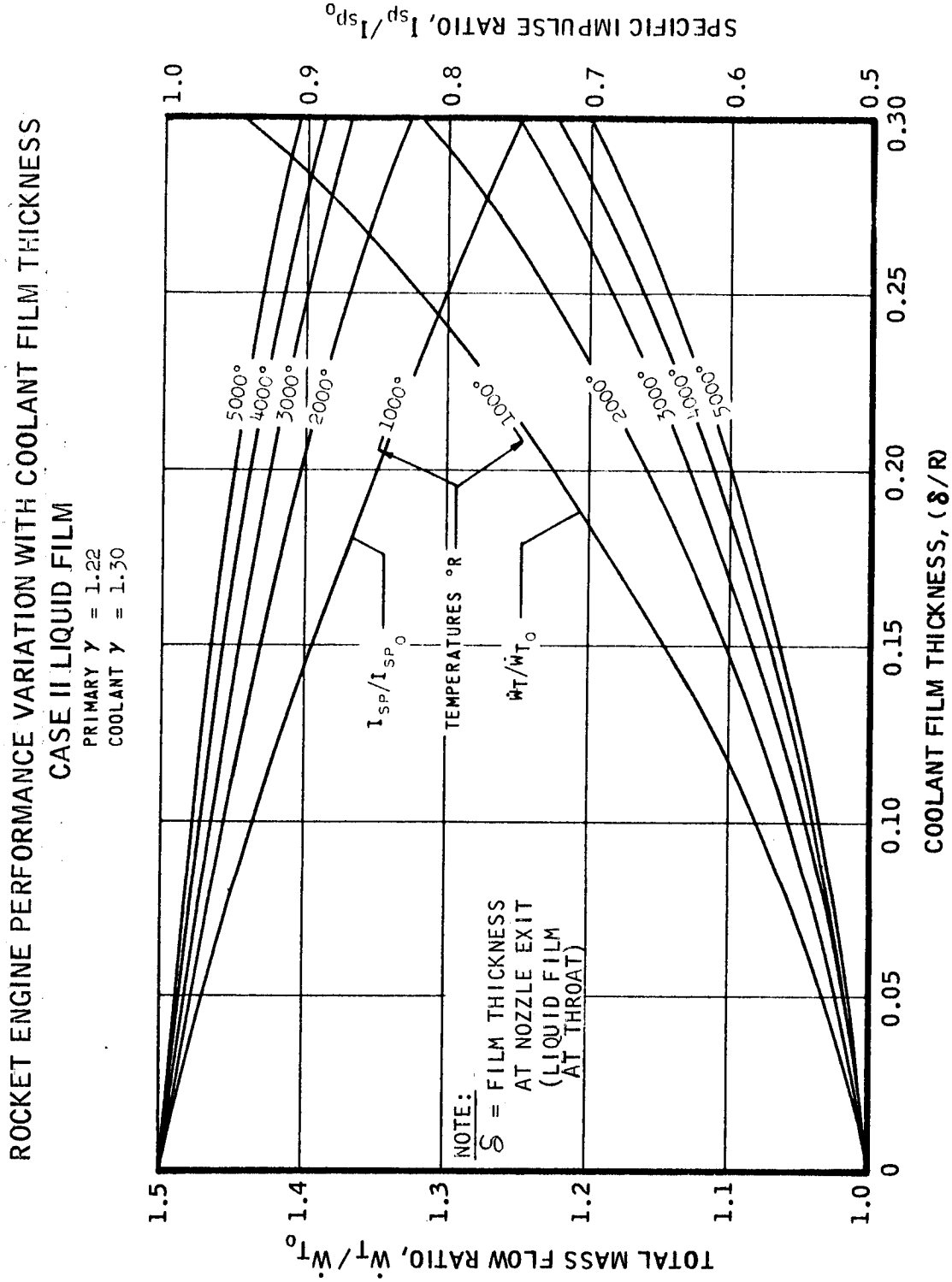
ROCKET ENGINE PERFORMANCE VARIATION WITH COOLANT FILM THICKNESS
CASE II LIQUID FILM
PRIMARY γ = 1.22
COOLANT γ = 1.30
SPECIFIC IMPULSE RATIO, I_{sp}/I_{sp_o}
TOTAL MASS FLOW RATIO, $\dot{W}_T/\dot{W}_{T_o}$
COOLANT FILM THICKNESS, (δ/R)
TEMPERATURES °R
5000°
4000°
3000°
2000°
1000°
1000°
2000°
3000°
4000°
5000°
I_{SP}/I_{SP_o}
$\dot{W}_T/\dot{W}_{T_o}$
NOTE:
δ = FILM THICKNESS AT NOZZLE EXIT (LIQUID FILM AT THROAT)
1.0
0.9
0.8
0.7
0.6
0.5
1.5
1.4
1.3
1.2
1.1
1.0
0.30
0.25
0.20
0.15
0.10
0.05
0

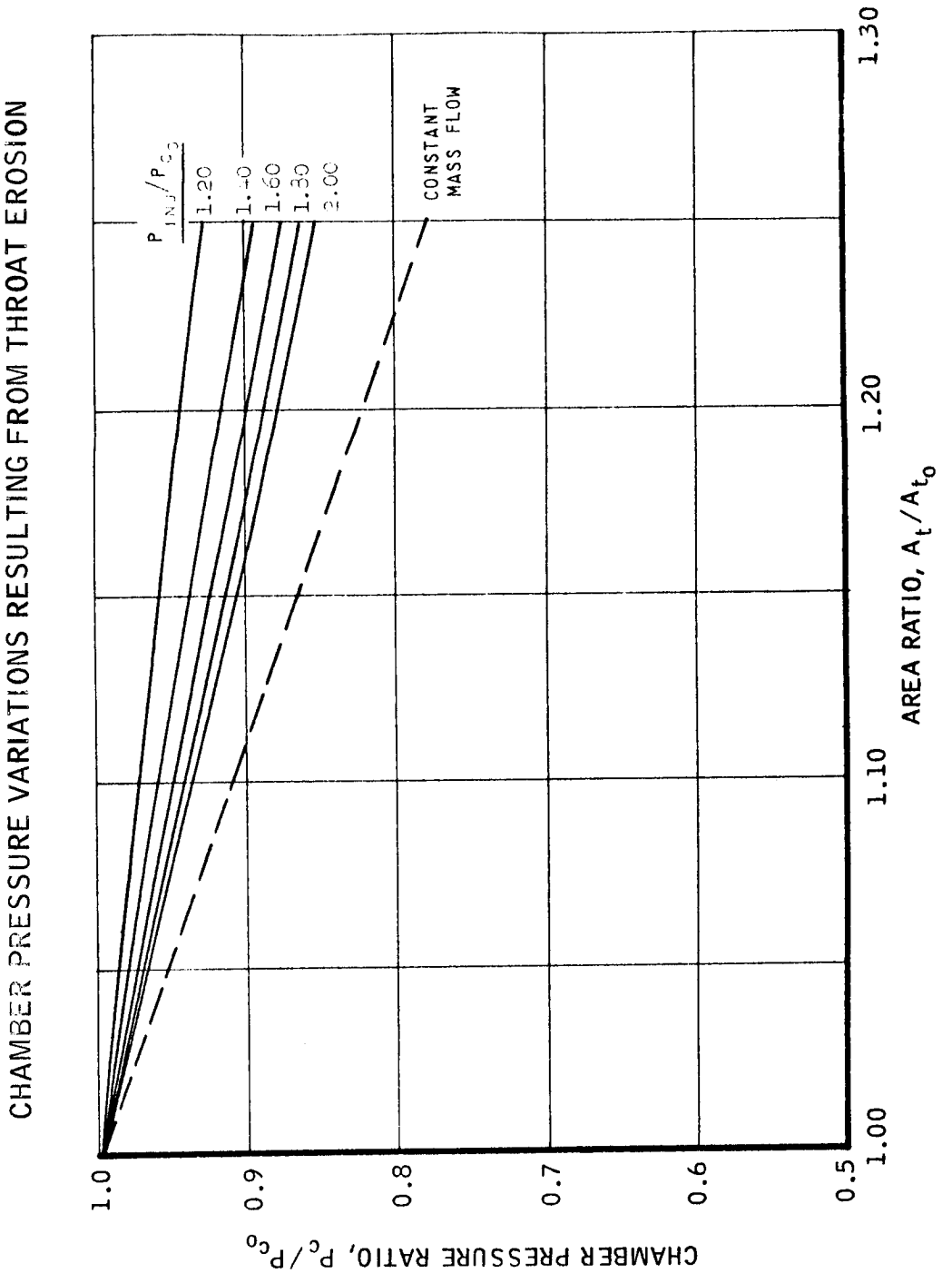
CHAMBER PRESSURE VARIATIONS RESULTING FROM THROAT EROSION
P_{INJ}/P_{C_o}
1.20
1.40
1.60
1.80
2.00
CONSTANT MASS FLOW
AREA RATIO, A_t/A_{t_o}
1.30
1.20
1.10
1.00
CHAMBER PRESSURE RATIO, P_c/P_{c_o}
1.0
0.9
0.8
0.7
0.6
0.5

FIGURE B-6

MASS FLOW VARIATIONS RESULTING FROM THROAT EROSION

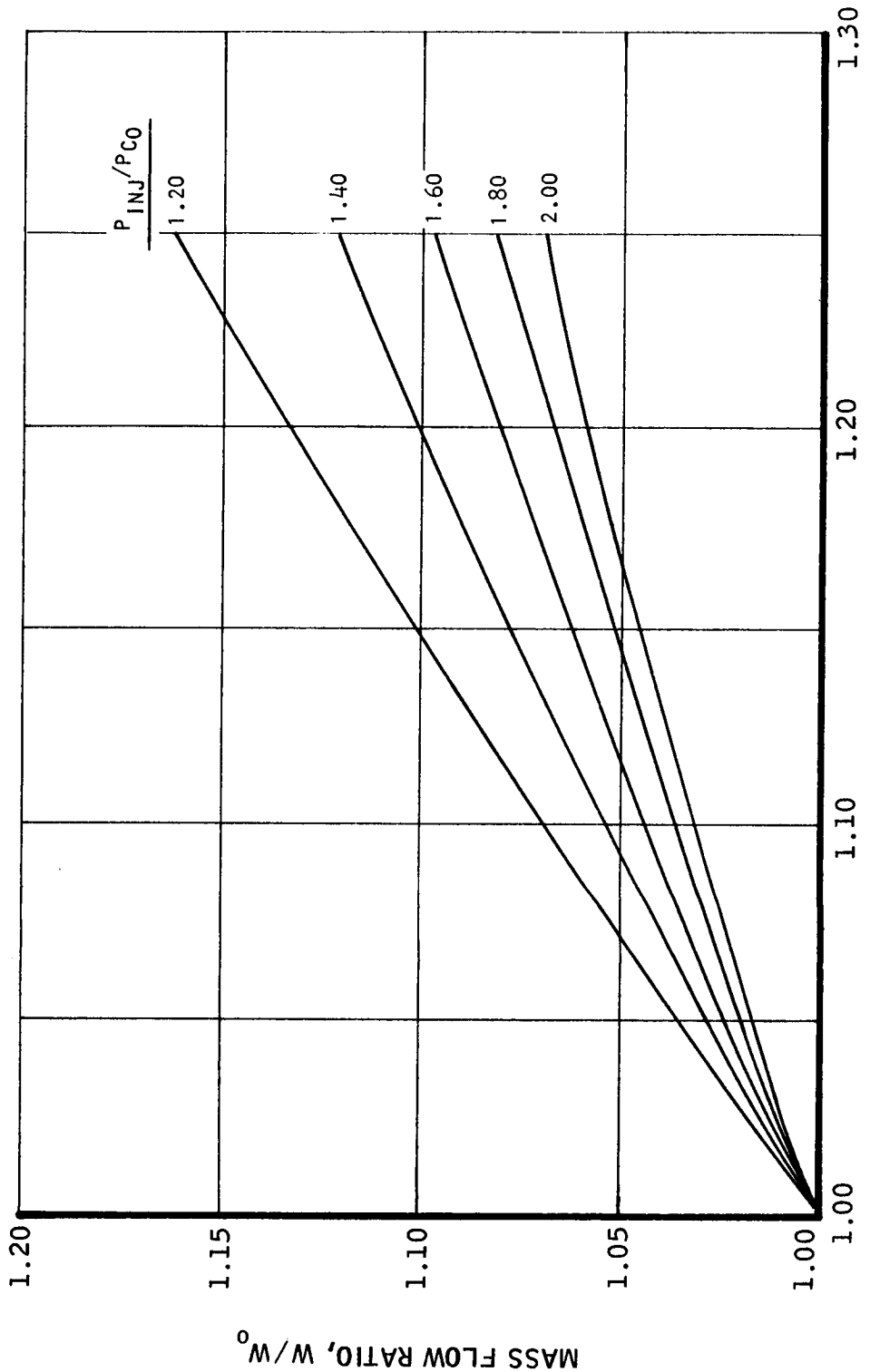

MAC A673

FIGURE B-7

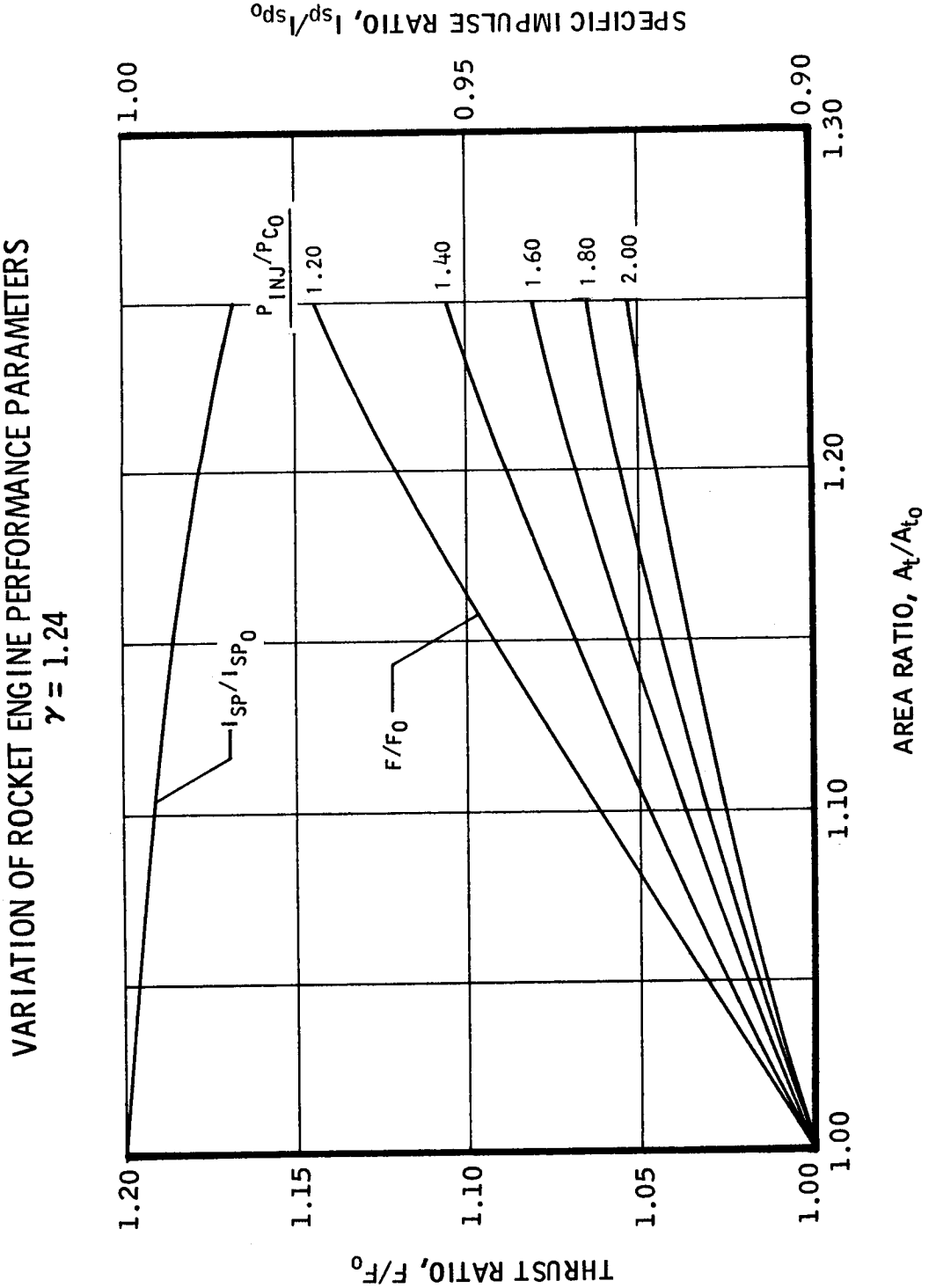
VARIATION OF ROCKET ENGINE PERFORMANCE PARAMETERS
γ = 1.24
SPECIFIC IMPULSE RATIO, I_{sp}/I_{sp_o}
1.00
0.95
0.90
P_{INJ}/P_{C_o}
1.20
1.40
1.60
1.80
2.00
1.30
1.20
1.10
1.00
I_{SP}/I_{SP_o}
F/F_o
AREA RATIO, A_t/A_{t_o}
1.20
1.15
1.10
1.05
1.00
THRUST RATIO, F/F_o

FIGURE B-8

APPENDIX C

FILM COOLING DESIGN EQUATIONS FOR LIQUID ROCKET MOTORS

A. Liquid Film Cooling

From Reference 124 a heat balance on the liquid film shows

$$h = \frac{\dot{W}_c \ \Delta H_c}{(T_g - T_w)\ \pi DL} \tag{1}$$

or

$$\dot{W}_c = \frac{h\ (T_g - T_w)\ \pi DL}{\Delta H_c} \tag{2}$$

dividing by

$$\dot{W}_g = G_g \frac{\pi D^2}{4}$$

$$\frac{\dot{W}_c}{W_g} = \frac{4\ h\ \pi DL\ (T_g - T_w)}{G_g\ \pi D^2\ \Delta H_c}$$

$$\frac{\dot{W}_c}{\dot{W}_g} = \frac{4\ h\ L\ (T_g - T_w)}{G_g\ D\ \Delta H_c}$$

Since $St_o = \frac{h}{G_g\ C_{pg}}$ for $Pr \approx 1$

$$\frac{\dot{W}_c}{\dot{W}_g} = 4\ St_o\ Cp_g\ \frac{L\ (T_g - T_w)}{D\ \Delta H_c}$$

Since $D = \sqrt{\frac{4A}{\pi}}$

$$\frac{\dot{W}_c}{\dot{W}_g} = \frac{2\ St_o\ L\ Cp_g\ (T_g - T_w)}{(A/\pi)^{1/2}\ \Delta H_c}$$

MAC A 673

APPENDIX C (Continued)

For a combustion chamber

$$L^* = \frac{A}{A^*} L = (C_r) L$$

or

$$\frac{\dot{W}_c}{\dot{W}_g} = \frac{2 St_o L^* Cp_g (T_g - T_w)}{C_r (A/\pi)^{1/2} \Delta H_c}$$

and

$$A = C_r A^* = C_r \frac{T}{P_o C_F}$$

$$\frac{\dot{W}_c}{\dot{W}_g} = \frac{2 St_o L^* Cp_g (T_g - T_w)}{(C_r)^{3/2} \Delta H_c} \left(\frac{\pi C_F P_o}{T}\right)^{1/2} \qquad (3)$$

From the nozzle section a differential approach must be taken since the L/D ratio is not constant.

$$d\frac{\dot{W}_c}{\dot{W}_g} = \frac{2 St_o Cp_g (T_g - T_w) dL}{\Delta H_c (A/\pi)^{1/2}}$$

or

$$d\frac{\dot{W}_c}{\dot{W}_g} = \frac{2 St_o Cp_g (T_g - T_w)}{(A/A^*)^{1/2} \Delta H_c} \left(\frac{\pi C_F P_o}{T}\right)^{1/2} dL \qquad (4)$$

APPENDIX C (Continued)

B. Gas Film Cooling

From Reference 123

$$\dot{W}_c \, Cp_c = h \, \pi \, D \, L \left[\frac{1}{\frac{-\ln n}{\left(\frac{S \, V_g}{\alpha_c}\right)^{0.125} f\left(\frac{V_g}{V_c}\right)} + 0.04} \right] \tag{5}$$

$$\frac{\dot{W}_c}{\dot{W}_g} = \frac{St_o \, Cp_g \, L}{Cp_c \, D} \left[\frac{1}{\frac{-\ln n}{\left(\frac{S \, V_g}{\alpha_c}\right)^{0.125} f\left(\frac{V_g}{V_c}\right)} + 0.04} \right]$$

For the combustion chamber

$$\frac{\dot{W}_c}{\dot{W}_g} = \frac{2 \, St_o \, L^*}{(C_r)^{3/2}} \left(\frac{\pi C_F \, P_o}{T}\right)^{1/2} \frac{Cp_g}{Cp_c} \left[\frac{1}{\frac{-\ln n}{\left(\frac{S \, V_g}{\alpha_c}\right)^{0.125} f\left(\frac{V_g}{V_c}\right)} + 0.04} \right] \tag{6}$$

For the nozzle

$$\frac{d\dot{W}_c}{\dot{W}_g} = \frac{2 \, St_o}{(A/A^*)^{1/2}} \left(\frac{\pi C_F \, P_o}{T}\right)^{1/2} \frac{Cp_g}{Cp_c} \left[\frac{d \, L}{\frac{-\ln n}{\left(\frac{S \, V_g}{\alpha_c}\right)^{0.125} f\left(\frac{V_g}{V_c}\right)} + 0.04} \right] \tag{7}$$

MAC A673

APPENDIX C (Continued)

C. Transpiration Cooling Design Equations for Liquid Rocket Motors

From Reference 136 from theory

$$\frac{h}{h_o} = \frac{\frac{G_c\ Cp_c}{G_g\ Cp_g\ St_o}}{\left[e^{\frac{G_c\ Cp_c}{G_g\ Cp_g\ St_o}} - 1\right]} \tag{8}$$

a curve fit of the data of Reference 146 shows

$$\frac{h}{h_o} = e^{-\left(1/2\ M^{0.57}\ \frac{G_c}{G_g\ St_o}\right)}$$

where M is the molecular weight ratio of the main gas to the coolant. From Section A of this appendix, it was shown by heat balance across the film

$$\frac{\dot{W}_c}{W_g} = \frac{2\ St_o\ L\ Cp_g\ (T_g - T_w)}{(A/\pi)^{1/2}\ \Delta H_c}$$

Since for transpiration cooling there is a reduction in St we can write

$$\frac{\dot{W}_c}{\dot{W}_g} = \frac{2\ St_o\ L\ Cp_g\ (T_g - T_w)}{(A/\pi)^{1/2}\ \Delta H_c}\ e^{-\left(1/2\ M^{0.57}\ \frac{G_c}{G_g\ St_o}\right)} \tag{9}$$

or for the combustion chamber

$$\frac{\dot{W}_c}{\dot{W}_g} = \frac{2\ St_o\ L^*\ Cp_g\ (T_g - T_w)}{(C_r)^{3/2}\ \Delta H_c}\left(\frac{\pi C_F\ P_o}{T}\right)^{1/2}\ e^{-\left(1/2\ M^{0.57}\frac{G_c}{G_g\ St_o}\right)} \tag{10}$$

APPENDIX C (Continued)

for the nozzle

$$\frac{\dot{dW_c}}{\dot{W}_g} = \frac{2\ St_o\ Cp_{\dot{g}}\ (T_g - T_w)}{(A/A^*)^{1/2}\ \Delta H_c} \left(\frac{\pi C_F\ P_o}{T}\right)^{1/2} e^{-(1/2\ M^{0.57}\ \frac{G_c}{G_g\ St_o})}\ dL \quad (11)$$

DISTRIBUTION

Copy No.	Transmitted to
1.	NASA Western Operations Office 150 Pico Boulevard Santa Monica, California Attn.: Office of Technical Information
2.	NASA Western Operations Office 150 Pico Boulevard Santa Monica, California Attn.: Contracting Officer
3.	NASA Western Operations Office 150 Pico Boulevard Santa Monica, California Attn.: Patent Office
4 to 7.	NASA Headquarters 400 Maryland Ave., S.W. Washington 25, D. C. Attn.: Chief, Liquid Propulsion Systems, RPL Mr. Henry Burlage, Jr.
8.	NASA Headquarters 400 Maryland Ave., S.W. Washington 25, D.C. Attn.: Asst. Director for Propulsion, MLP Mr. A. O. Tischler
9.	Jet Propulsion Laboratory California Institute of Technology 4800 Oak Grove Drive Pasadena, California Attn.: Propulsion Division, Mr. Bruce Johnson
10, 11.	NASA Ames Research Center Moffett Field, California Attn.: Technical Librarian (Designee: H. Hornby)
12, 13.	NASA Goddard Space Flight Center Greenbelt, Maryland Attn.: Technical Librarian (Designee: M. Moseson)
14, 15.	Jet Propulsion Laboratory California Institute of Technology 4800 Oak Grove Drive Pasadena, California Attn.: Technical Librarian (Designee: R. Rose)

MAC A633

DISTRIBUTION (Continued)

Copy No.	Transmitted to
16, 17.	NASA Langley Research Center Langley Field, Virginia Attn.: Technical Librarian (Designee: F. L. Thompson)
18, 19.	NASA Lewis Research Center 21000 Brookpark Road Cleveland 35, Ohio Attn.: Technical Librarian (Designee: A. Silverstein)
20, 21.	NASA Marshall Space Flight Center Huntsville, Alabama Attn.: Technical Librarian (Designee: H. Weidner)
22, 23.	NASA Manned Spacecraft Center Houston, Texas Attn.: Technical Librarian (Designee: A. Gilruth)
24.	Advanced Research Projects Agency The Pentagon, Room 3D154 Washington 25, D. C. Attn.: Technical Librarian (Designee: D. E. Mock)
25.	Aeronautical Systems Division Air Force Systems Command Wright-Patterson AF Base, Ohio Attn.: Technical Librarian (Designee: D. L. Schmidt Code ASRCNC-2)
26.	AF Missile Development Center Holloman AF Base, New Mexico Attn.: Technical Librarian (Designee: Maj. R. E. Bracken Code MDGET)
27.	AF Missile Test Center Patrick AF Base, Florida Attn.: Technical Librarian (Designee: L. J. Ullian)
28.	AF Systems Command, Dyna-Soar AF Unit Post Office Los Angeles 45, California Attn.: Technical Librarian (Designee: Col. Clark Tech. Data Center)

MAC A673

DISTRIBUTION (Continued)

Copy No.	Transmitted to
29.	Army Ordnance Missile Command Redstone Arsenal, Alabama Attn.: Technical Librarian (Designee: Dr. W. Wharton)
30.	Armed Services Technical Information Agency Arlington 12, Virginia Attn.: Technical Librarian (Designee: J. Biel)
31.	Arnold Engineering Development Center A.E.O.R. Tullahoma, Tennessee Attn.: Technical Librarian (Designee: H. K. Doetsch)
32.	Bureau of Naval Weapons Department of the Navy Washington 25, D.C. Attn.: Technical Librarian (Designee: R. L. Little)
33.	Central Intelligence Agency 2430 E Street, N.W. Washington 25, D.C. Attn.: Technical Librarian (Designee: E. Kernan)
34.	Headquarters, U.S. Air Force Washington 25, D.C. Attn.: Technical Librarian (Designee: Col. Stambaugh)
35.	Office of Naval Research Washington 25, D.C. Attn.: Technical Librarian (Designee: F. Bertlan)
36.	Picatinny Arsenal Dover, New Jersey Attn.: Technical Librarian (Designee: I. Forsten, Chief, Liquid Prop. Laboratory)
37.	Rocket Research Laboratories Edwards AF Base, California Attn.: Technical Librarian (Designee: Col. H. W. Norton)
38.	U.S. Naval Ordnance Test Station China Lake, California Attn.: Technical Librarian (Designee: E. Vim, Jr., Chief Missile Prop. Div. Code 451)

MAC A673

DISTRIBUTION (Continued)

Copy No.	Transmitted to
39.	U. S. Atomic Energy Commission Technical Information Services P.O. Box 62, Oak Ridge, Tennessee Attn.: Technical Librarian
40.	Chemical Propellant Information Agency Johns Hopkins University Applied Physics Laboratory 8621 Georgia Avenue Silver Spring, Maryland Attn.: Technical Librarian (Designee: N. Safeer)
41.	Aerojet-General Corporation P.O. Box 296, Azusa, California Attn.: Technical Librarian (Designee: L. F. Kohrs)
42.	Aerojet-General Corporation P.O. Box 1947, Sacramento 9, California Attn.: Technical Librarian (Designee: R. Stiff)
43.	Aeronutronic Division, Ford Motor Company Ford Road Newport Beach, California Attn.: Technical Librarian (Designee: D. A. Carrison)
44.	Aerospace Corporation 2400 East El Segundo Boulevard El Segundo, California Attn.: Technical Librarian (Designee: E. Perchonak)
45.	Arthur D. Little, Inc. Acorn Park Cambridge 40, Massachusetts Attn.: Technical Librarian (Designee: A. C. Tobey)
46.	Astropower, Inc., Subsidiary of Douglas Aircraft Co., Inc. 2968 Randolph Avenue Costa Mesa, California Attn.: Technical Librarian (Designee: G. Moe)
47.	Astrosystems, Inc. 82 Naylor Avenue Livingstone, New Jersey Attn.: Technical Librarian (Designee: A. Mendenhall)

MAC A633

DISTRIBUTION (Continued)

Copy No.	Transmitted to
48.	Atlantic Research Corporation Edsall Road and Shirley Highway Alexandria, Virginia Attn.: Technical Librarian (Designee: A. Scurlock)
49.	Beech Aircraft Corporation Boulder Facility P.O. Box 631, Boulder, Colorado Attn.: Technical Librarian (Designee: J. H. Rodgers)
50.	Bell Aerosystems Company P.O. Box 1, Buffalo 5, New York Attn.: Technical Librarian (Designee: W. M. Smith)
51.	Bendix Systems Division Bendix Corporation Ann Arbor, Michigan Attn.: Technical Librarian (Designee: J. M. Brueger)
52.	Boeing Company P.O. Box 3707, Seattle 24, Washington Attn.: Technical Librarian (Designee: J. D. Alexander)
53.	Convair/Astronautics P.O. Box 2672, San Diego 12, California Attn.: Technical Librarian (Designee: F. Dore)
54.	Curtiss-Wright Corporation Wright Aeronautical Division Wood-Ridge, New Jersey Attn.: Technical Librarian (Designee: G. Kelley)
55.	Douglas Aircraft Company, Inc. Missile and Space Systems Division 3000 Ocean Park Boulevard Santa Monica, California Attn.: Technical Librarian (Designee: C. J. Dorenbacher)
56.	Fairchild Stratos Corporation Aircraft Missiles Division Hagerstown, Maryland Attn.: Technical Librarian (Designee: J. R. Farrow)

MAC A633

DISTRIBUTION (Continued)

Copy No.	Transmitted to
57.	General Electric Company Missile and Space Vehicle Department P.O. Box 855J, Philadelphia, Pennsylvania Attn.: Technical Librarian (Designee: L. S. Beers)
58.	General Electric Company Rocket Propulsion Units, Bldg. 300 Cincinnati 15, Ohio Attn.: Technical Librarian (Designee: D. Suichu)
59.	Grumman Aircraft Engineering Corporation Bethpage, Long Island, New York Attn.: Technical Librarian (Designee: J. Gavin)
60.	Walter Kidde and Company, Inc. Kidde Aerospace Division 675 Main Street Belleville 9, New Jersey Attn.: Technical Librarian (Designee: J. Marcinek)
61.	Lockheed Aircraft Corporation Missile and Space Division Sunnyvale, California Attn.: Technical Librarian (Designee: H. Zwerner)
62.	Lockheed Propulsion Company P.O. Box 111, Redlands, California Attn.: Technical Librarian (Designee: H. L. Thackwell)
63.	Martin-Marietta Corporation Martin Division Baltimore 3, Maryland Attn.: Technical Librarian (Designee: W. P. Sommers)
64.	Martin-Marietta Corporation Martin Denver Division Denver, Colorado Attn.: Technical Librarian (Designee: J. D. Goodletti, A-241)
65.	McDonnell Aircraft Corporation P.O. Box 6101, Lambert Field, Missouri Attn.: Technical Librarian (Designee: R. A. Herzmark)

MAC A673

DISTRIBUTION (Continued)

Copy No.	Transmitted to
66.	North American Aviation, Inc. Space and Information Systems Division Downey, California Attn.: Technical Librarian (Designee: H. Storms)
67.	Northrop Corporation 1001 East Broadway Hawthorne, California Attn.: Technical Librarian (Designee: W. E. Gasich)
68.	Pratt and Whitney Aircraft Corporation Florida Research and Development Center West Palm Beach, Florida Attn.: Technical Librarian (Designee: R. J. Coar)
69.	Radio Corporation of America Astro-Electronics Division Defense Electronics Products Princeton, New Jersey Attn.: Technical Librarian (Designee: S. Fairweather)
70.	Thiokol Chemical Corporation Reaction Motors Division Denville, New Jersey Attn.: Technical Librarian (Designee: A. Sherman)
71.	Republic Aviation Corporation Farmingdale, Long Island, New York Attn.: Technical Librarian (Designee: W. O'Donnell)
72.	Rocketdyne Division North American Aviation, Inc. 6633 Canoga Avenue Canoga Park, California Attn.: Technical Librarian (Designee: E. B. Monteath)
73.	Space-General Corporation 9200 Flair Avenue El Monte, California Attn.: Technical Librarian (Designee: C. E. Roth)
74.	Space Technology Laboratories P.O. Box 95001, Airport Station Los Angeles 45, California Attn.: Technical Librarian (Designee: G. W. Elverum)

MAC A673

DISTRIBUTION (Continued)

Copy No.	Transmitted to
75.	Stanford Research Institute 333 Ravenswood Avenue Menlo Park, California Attn.: Technical Librarian (Designee: T. Smith)
76.	Thompson-Ramo-Wooldridge, Inc. Tapco Division 23555 Euclid Avenue Cleveland 17, Ohio Attn.: Technical Librarian (Designee: P. T. Angell)
77.	Thiokol Chemical Corporation Redstone Division Huntsville, Alabama Attn.: Technical Librarian (Designee: W. L. Berry)
78.	United Aircraft Corporation East Hartford Plant 400 Main Street Hartford, Connecticut Attn.: Technical Librarian (Designee: E. Martin)
79.	United Technology Corporation 587 Mathilda Avenue Sunnyvale, California Attn.: Technical Librarian (Designee: B. Abelman)
80.	Vought Aeronautics P.O. Box 5907, Dallas 22, Texas Attn.: Technical Librarian (Designee: W. C. Trent)

MAC A673